MICROBIOLOGY OF EXTREME AND HUMAN-MADE CONFINED ENVIRONMENTS (SPACECRAFT, SPACE STATIONS, CLEANROOMS, AND ANALOGOUS SITES)

EDITED BY: Rakesh Mogul and Ralf Moeller
PUBLISHED IN: Frontiers in Microbiology

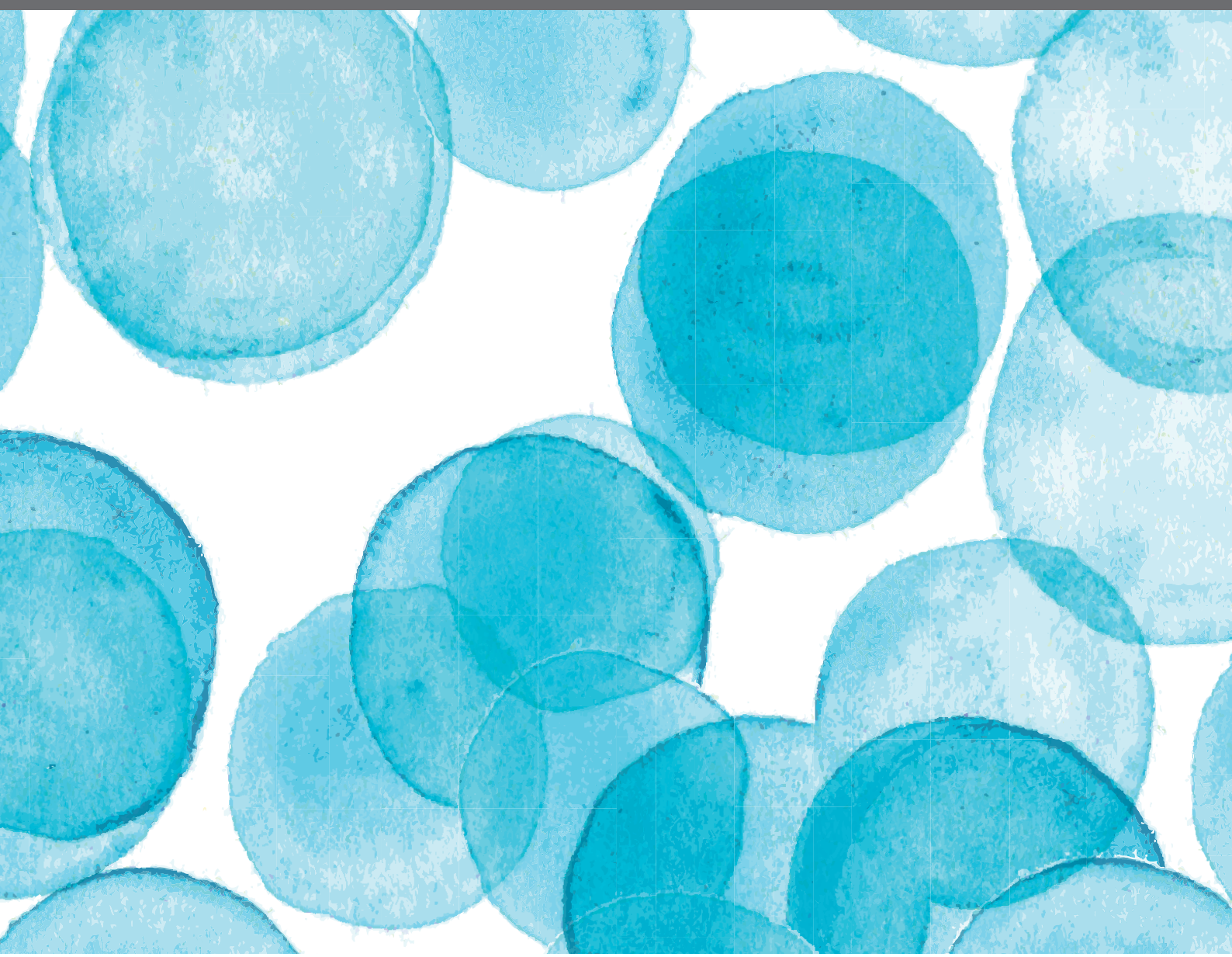

frontiers Research Topics

frontiers

ISSN 1664-8714
ISBN 978-2-88976-359-7
DOI 10.3389/978-2-88976-359-7

About Frontiers

Frontiers is more than just an open-access publisher of scholarly articles: it is a pioneering approach to the world of academia, radically improving the way scholarly research is managed. The grand vision of Frontiers is a world where all people have an equal opportunity to seek, share and generate knowledge. Frontiers provides immediate and permanent online open access to all its publications, but this alone is not enough to realize our grand goals.

Frontiers Journal Series

The Frontiers Journal Series is a multi-tier and interdisciplinary set of open-access, online journals, promising a paradigm shift from the current review, selection and dissemination processes in academic publishing. All Frontiers journals are driven by researchers for researchers; therefore, they constitute a service to the scholarly community. At the same time, the Frontiers Journal Series operates on a revolutionary invention, the tiered publishing system, initially addressing specific communities of scholars, and gradually climbing up to broader public understanding, thus serving the interests of the lay society, too.

Dedication to Quality

Each Frontiers article is a landmark of the highest quality, thanks to genuinely collaborative interactions between authors and review editors, who include some of the world's best academicians. Research must be certified by peers before entering a stream of knowledge that may eventually reach the public - and shape society; therefore, Frontiers only applies the most rigorous and unbiased reviews.
Frontiers revolutionizes research publishing by freely delivering the most outstanding research, evaluated with no bias from both the academic and social point of view. By applying the most advanced information technologies, Frontiers is catapulting scholarly publishing into a new generation.

What are Frontiers Research Topics?

Frontiers Research Topics are very popular trademarks of the Frontiers Journals Series: they are collections of at least ten articles, all centered on a particular subject. With their unique mix of varied contributions from Original Research to Review Articles, Frontiers Research Topics unify the most influential researchers, the latest key findings and historical advances in a hot research area! Find out more on how to host your own Frontiers Research Topic or contribute to one as an author by contacting the Frontiers Editorial Office: frontiersin.org/about/contact

MICROBIOLOGY OF EXTREME AND HUMAN-MADE CONFINED ENVIRONMENTS (SPACECRAFT, SPACE STATIONS, CLEANROOMS, AND ANALOGOUS SITES)

Topic Editors:
Rakesh Mogul, California State Polytechnic University, Pomona, United States
Ralf Moeller, German Aerospace Center (DLR), Germany

Citation: Mogul, R., Moeller, R., eds. (2022). Microbiology of Extreme and Human-Made Confined Environments (Spacecraft, Space Stations, Cleanrooms, and Analogous Sites). Lausanne: Frontiers Media SA.
doi: 10.3389/978-2-88976-359-7

Table of Contents

frontiers in Microbiology

ORIGINAL RESEARCH
published: 31 March 2020
doi: 10.3389/fmicb.2020.00525

Microbial Monitoring in the EDEN ISS Greenhouse, a Mobile Test Facility in Antarctica

Jana Fahrion[1,2], Carina Fink[1], Paul Zabel[3], Daniel Schubert[3], Mohamed Mysara[4], Rob Van Houdt[4], Bernhard Eikmanns[2], Kristina Beblo-Vranesevic[1] and Petra Rettberg[1]*

[1] Institute of Aerospace Medicine, German Aerospace Center (DLR), Cologne, Germany, [2] Institute of Microbiology and Biotechnology, Faculty of Natural Sciences, University of Ulm, Ulm, Germany, [3] Institute for Space Systems, German Aerospace Center (DLR), Bremen, Germany, [4] Microbiology Unit, Belgian Nuclear Research Centre (SCK CEN), Mol, Belgium

The EDEN ISS greenhouse, integrated in two joined containers, is a confined mobile test facility in Antarctica for the development and optimization of new plant cultivation techniques for future space programs. The EDEN ISS greenhouse was used successfully from February to November 2018 for fresh food production for the overwintering crew at the Antarctic Neumayer III station. During the 9 months of operation, samples from the different plants, from the nutrition solution of the aeroponic planting system, and from diverse surfaces within the three different compartments of the container were taken [future exploration greenhouse (FEG), service section (SS), and cold porch (CP)]. Quantity as well as diversity of microorganisms was examined by cultivation. In case of the plant samples, microbial quantities were in a range from 10^2 to 10^4 colony forming units per gram plant material. Compared to plants purchased from a German grocery, the produce hosted orders of magnitude more microorganisms than the EDEN ISS plants. The EDEN ISS plant samples contained mainly fungi and a few bacteria. No classical food associated pathogenic microorganism, like *Escherichia* and *Salmonella*, could be found. Probably due to the used cultivation approach, Archaea were not found in the samples. The bioburden in the nutrition solutions increased constantly over time but never reached critical values like 10^2–10^3 cfu per 100 mL in irrigation water as it is stated, e.g., for commercial European plant productions. The surface samples revealed high differences in the microbial burden between the greenhouse part of the container and the SS and CP part. However, the numbers of organisms (bacteria and fungi) found in the planted greenhouse were still not critical. The microbial loaded surfaces showed strong temporal as well as spatial fluctuations. In samples of the nutrition solution and the surface, the amount of bacteria exceeded the amount of fungi by many times. For identification, 16S rRNA gene sequencing was performed for the isolated prokaryotic organisms. Phylogenetic analyses revealed that the most abundant bacterial phyla were Firmicutes and Actinobacteria. These phyla include plant- and human-associated bacterial species. In general, it could be shown that it is possible to produce edible fresh food in a remote environment and this food is safe for consumption from a microbiological point of view.

Keywords: EDEN ISS, greenhouse, bacteria, plants, surfaces, phyllosphere, space exploration

OPEN ACCESS

Edited by:
Rakesh Mogul, California State Polytechnic University, Pomona, United States

Reviewed by:
Tatiana A. Vishnivetskaya, The University of Tennessee, Knoxville, United States
David Anthony Pearce, Northumbria University, United Kingdom

****Correspondence:***
Kristina Beblo-Vranesevic
Kristina.beblo@dlr.de

Specialty section:
This article was submitted to Extreme Microbiology, a section of the journal Frontiers in Microbiology

Received: *19 November 2019*
Accepted: *11 March 2020*
Published: *31 March 2020*

Citation:
Fahrion J, Fink C, Zabel P, Schubert D, Mysara M, Van Houdt R, Eikmanns B, Beblo-Vranesevic K and Rettberg P (2020) Microbial Monitoring in the EDEN ISS Greenhouse, a Mobile Test Facility in Antarctica. Front. Microbiol. 11:525. doi: 10.3389/fmicb.2020.00525

INTRODUCTION

Manned missions to other planets like Mars or to the Moon, as well as stays on the International Space Station (ISS), have to be well planned in advance. For a successful mission, the expertise of many different scientific and technical fields needs to be combined. One important part that has to be considered is the food supply of the crew. From the beginning of space flight, astronauts had to bring everything with them. For example, lots of water and food have to be packed and brought to the ISS (Perchonok et al., 2012). Because flights to other planets or the Moon take much longer than to the ISS and also require longer stays in space, it is of high importance to find technical solutions to secure food production and water recycling in-flight as well as in future extraterrestrial habitats. So-called bio-regenerative life support systems not only provide fresh food but can also be used for oxygen production, recycling of carbon dioxide, water recycling, and waste management (Zabel et al., 2015). One approach to develop such a bio-regenerative life support system was the EDEN ISS project (Evaluation and Design of Environmentally closed Nutrition-sources; funded by the European Union's Research and Innovation Action program Horizon 2020; grant agreement ID: 636501). In 2015, the main goal of the project was defined as "the adaptation, integration, fine-tuning, and demonstration of higher plant cultivation technologies and operation procedures for safe food production on-board ISS and for future human space exploration missions" (Zabel et al., 2015). The EDEN ISS greenhouse is a mobile test facility at the Neumayer III station in Antarctica. It was designed, tested, and operated by a team of 14 international companies, institutes, and universities between March 2015 and April 2019, including a test phase in Antarctica from December 2017 to December 2018. At first, the EDEN ISS greenhouse was assembled, integrated, and tested in Bremen, Germany, in order to investigate its functionality in a laboratory setting. Afterward, it was disassembled, packed into two containers, and loaded onto the German icebreaker research vessel Polarstern and transported via Cape Town in South Africa to Antarctica. 400 m from the German Neumayer III station, the two containers were assembled and connected again to build one unit consisting of the greenhouse, the service section (SS), and a cold porch (CP; Schlacht et al., 2019). The greenhouse is confined half-autonomous and contains its own nutrient delivery system (NDS), special LED lights with adapted wavelengths for the specific plants, and an air management system (Zabel et al., 2015; Imhof et al., 2018). The EDEN ISS greenhouse was closed with the only exception of the entering and leaving of the same operator once per day for reasons, like sowing, harvesting, filling the nutrient tanks, and cleaning work. There was no direct exchange between the greenhouse itself and the environment, since the operator was entering the container via the CP and the SS.

Between February and November 2018, the EDEN ISS container was successfully used to produce fresh vegetables for the 10 overwintering crew members at Neumayer III station. According to their statements, the additional availability of vegetables improved the morale of the crew significantly (Schlacht et al., 2019). After further investigation of this psychological effect, it might be a useful tool to improve the quality of life for crew members on space ships. Antarctica was chosen as a testbed for several reasons. The microbial burden is low in Antarctic ice (Pearce et al., 2009) and thus, it is easier to monitor the microbial loads inside of the greenhouse, because microorganisms are less likely to be introduced from the outside. Moreover, it is a cold and hostile environment and therefore has properties that come closest to the conditions in space and on other planets. The command center for the EDEN ISS container is located in Germany, the supervisor there has to remotely monitor the functionality of the greenhouse, and the operator within the greenhouse has to get along with what he already has on site (Zeidler et al., 2019). Therefore, the framework conditions are similar to a space mission.

Plants in general as well as edible vegetables host vast amounts of microorganisms on their surfaces (Lindow and Brandl, 2003; Lopez-Galvez et al., 2014). While the root microbiota, also called rhizosphere microbiota, has been a subject to research for many decades now, the leaf microbiota is still inadequately investigated. The origin of microorganisms on leaves is not completely understood until today. The leaf and fruit surface of plants, the so-called phyllosphere, is very diverse and organisms can be introduced via air, soil, other plants, animals, and water (Vorholt, 2012). The fact that many plants re-establish their microbial communities each year leads to the assumption that there is a core microbiota in the soil and on the seeds that is responsible for this effect (Knief et al., 2010). Because the leaves are the entry site for many plant pathogens (Schulze-Lefert and Robatzek, 2006), it is of high importance that the microbial burden on the leaf surfaces is under strong control in greenhouses in general and especially in greenhouses used in future space missions.

Even though the EDEN-ISS plants were not germinated gnotobiotically, some of the factors that usually contribute to the microbial diversity of the phyllosphere are minimized in the EDEN ISS system. For instance, the introduction of soil microorganisms is improbable since the plants were cultivated in an aeroponic system. The strong evolutionary pressure from the harsh environment can give rise to specially adapted cells with high heat and desiccation tolerances (Mora et al., 2016). Therefore, not only the natural accumulation of microorganisms in nutrient-rich greenhouses can pose a risk, but also these special circumstances. Due to this, it is of high importance to monitor the general microbial burden in order to evaluate the risks that may arise.

The goal of this study was to provide a survey of the global situation of the microbial community inside the EDEN ISS greenhouse for different time points during the 9 months of operation time to track and record microbial fluxes for assessing the contamination risks. Thereby, a broad overview of the amount, diversity, and distribution of microorganisms on different pieces of the cultivated plants,

the NDS, and different surface areas within the EDEN ISS container was obtained.

MATERIALS AND METHODS

Sampling in Antarctica

Between January and November 2018, samples were taken from different plant parts of different plant species. Additionally, samples from the nutrition solutions for the plants and different surfaces in different areas of the test facility [CP, SS, and future exploration greenhouse (FEG)] were taken consecutively during the time of operation and the sampling events (SEs) are named accordingly (**Figure 1**).

The sampling was performed by the overwintering crew member Paul Zabel from the German Aerospace Center in Bremen. Different surface sampling locations inside the three parts of the greenhouse container were selected: two locations in CP (floor right from entrance, CP1; door to service module, around door handle, CP2), four locations in the SS (floor under working bench, SS1; lid of a tank, SS2; right beside sink, SS3; air duct, SS4), and 10 positions in the FEG module (filter above entrance door, FEG1; wall on the right side, FEG2; growing tray, FEG3; growing tray, FEG4; rack on the left side, FEG5; handle of trolley, FEG6; ceiling in front of emergency exit, FEG7; floor cattle grid, FEG8; floor under cattle grid, FEG9; door to SS around door handle, FEG10). The surface samples were obtained using sterile moistened swabs to sample an area of 25 cm^2 each. Then the swabs were put into sterile 15 mL Falcon tubes containing 2.5 mL sterile phosphate buffered saline (PBS). Additionally, samples without surface contact were taken (negative controls). Therefore, a clean swab was taken out of the package, wagged in the air of the FEG and the SS, respectively, and put into the Falcon tubes containing 2.5 mL PBS. All controls (FEG and SS) did not show any CFU for all time points.

The plants were cultivated with an aeroponic system and the hanging roots were sprinkled regularly with a nutrient solution of the NDS. There were two different NDS tanks with different compositions. The ingredients of the nutrient solutions are listed in **Supplementary Table S1**. In 11 SEs, 50 mL samples of the plant nutrient solution were taken by submerging 50 mL Falcon tubes completely into the tank with clean tongs before closure. Additionally, the fresh water tank was sampled in the last four SEs (**Figure 1**). The water from this tank was used to prepare the nutrition solution for the plants.

For the plant samples, single-use sterile tweezers and sterile scalpels were used to hold and cut the different plant leaves and fruits. Afterward, the samples were put into 50 mL Falcon tubes. The following plants were sampled: basil, cucumber Picowell, lettuce Batavia, lettuce Expertise, lettuce Outredgeous, lettuce Waldman's Green, parsley, pepper Cupid (leaf), pepper 1001-M, rucola, swiss chard, tomato cherry, tomato Harzfeuer (leaf), tomato orange. The first samples were taken on the 12 May 2018, 94 days after the first plants were sown (7 February 2018) (**Figure 1**). Generally, the edible part of the plant was sampled. Thus, the tomato Cherry, tomato Orange, as well the cucumber Picowell samples were fruits except where otherwise specified. All other samples were leaves. For comparison, different produce from a German grocery were handled in the same way as the Antarctic samples. The following plants from a grocery were analyzed: basil, tomato Cherry, chives, cucumber, lamb's lettuce, parsley, rucola, romaine lettuce (dark red), and romaine lettuce (light green).

All Falcon tubes with samples from Antarctica (swabs in buffer, plant pieces, and liquids) were frozen and stored at -40°C without cryoprotectant. On the 8 December 2018, the freezer containing the samples was loaded into an airplane and shipped to DLR Cologne via South Africa and Frankfurt and transported by car to Cologne. The freezer arrived in Cologne on the 14 December 2018 without any interruption of the cold chain as proved by the data from a temperature logger inside the freezer.

Sample Treatment

The plant samples of one SE and the frozen produce samples were thawed for 2 h at room temperature. Ten mL of sterile PBS and four autoclaved glass beads (Ø 4 mm) were added to each 50 mL Falcon tube. The samples were vortexed for 3 min at 2000 r/min. Afterward, 50 μL of the original supernatant and its dilutions (three orders of magnitude) were plated onto selective Reasoner's 2A Agar (R2A) plates containing 50 mg/L cycloheximide and selective Potato Dextrose Agar (PDA) plates containing 50 mg/L chloramphenicol to prevent the growth of fungi and the growth of bacteria, respectively.

In accordance with the standardized bioburden and biodiversity measurements specified for spacecraft assembly facilities and spacecraft for astrobiological missions, an adapted protocol of the ECSS-Q-ST-70-55C[1] (Koskinen et al., 2017) standard protocol was used for the evaluation of the surface samples. In short, the tubes from a single SE, each containing a swab and 2.5 mL PBS, were thawed for 2 h at room temperature. After thawing, the samples were vortexed for 5 s on highest setting, followed by an ultrasonic bath for 2 min; 250 μL of each sample suspension was plated on four selective R2A plates containing 50 mg/L cycloheximide and four selective PDA plates containing 50 mg/L chloramphenicol. The remaining 500 μL from each sample was heat-shocked in a water bath (80°C; 15 min) and afterward chilled on ice until room temperature was reached. The swab tubes were vortexed shortly on highest setting and 250 μL of each heat shocked solution was plated on an R2A plate.

Liquid samples were processed as follows: The samples from one SE were thawed for 2 h at room temperature on an overhead shaker. The samples were vortexed for 10 s and then up to thousand fold diluted. The dilutions were plated onto four selective R2A plates containing 50 mg/L cycloheximide and selective PDA plates containing 50 mg/L chloramphenicol.

All plates were incubated upside down for seven days at 20°C. The CFU were determined after day 1, 2, 3, 6, and 7. All plating procedures were performed at least three times independently.

[1] https://ecss.nl/

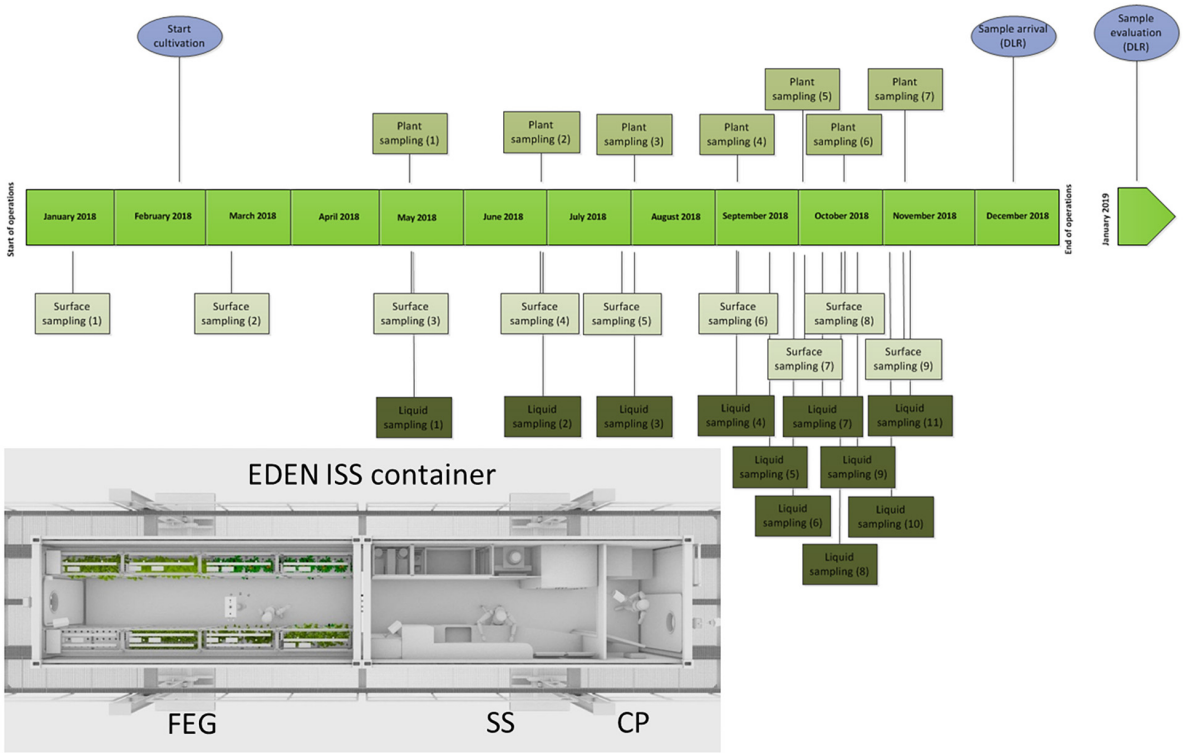

FIGURE 1 | Schedule of the sampling events in the EDEN ISS container from January to December 2018; light blue: special events. Overview of the EDEN ISS container with its three compartments: cold porch (CP), service section (SS), future exploration greenhouse (FEG).

Isolation of Bacterial Colonies and Preparation for Sequencing

After completion of the 7 day incubation period, all plates were examined for distinguishable colonies. They were marked, numbered, and sorted according to their morphology using standard phase-contrast light microscopy with 400x or 1000x magnification. Individual colonies were picked and spread onto fresh R2A plates without cycloheximide. These plates were incubated at 20°C until individual colonies formed. The plates with the isolates were stored at 4°C until preparation for sequencing. For 16S rRNA gene sequencing of the isolated bacteria, colonies were picked and transferred into sterile 96-well plates wells filled with 200 μL sterile R2A and sent to the Belgian Nuclear Research Centre (SCK CEN) for analysis. The fungi were only evaluated quantitatively.

Identification of Bacterial Isolates

DNA was extracted from stationary phase bacterial cultures grown in R2A at 30°C. In a next step, the 16S rRNA gene was amplified, purified, and sequenced (BaseClear, Netherlands; proprietary method). The 16S rRNA gene sequences were analyzed using mothur software (V1.39) (Schloss et al., 2009). First, all forward/reverse sequences were merged and sorted using merge.files and sort.seqs commands, respectively. Reads were trimmed to a maximum length of 1000 bp using trim.seqs command and each pair was assembled into one contig using make.contig command, specifying "sanger" as the format parameter. To confirm the merging, the produced contigs were assessed by aligning both forward and reverse sequences against the SILVA database (release 132 from https://www.mothur.org/wiki/Silva_reference_files, Quast et al., 2013), and comparing their alignment positions to the assembled contig alignment position. Taxonomic classification of the assembled reads was obtained using classify.seqs command against the Ribosomal database project database (v16, from https://www.mothur.org/wiki/RDP_reference_files, Cole et al., 2013). To confirm the taxonomy, blastn was used against the NCBI 16S microbial database (Match/Mismatch and Gap Costs = Match 2, Mismatch 3, Existence 5, Extension 2; Expectation value = 10.0; Word size = 11; Mask lower case = No; Filter low complexity = Yes; Maximum number of hits = 5) (Johnson et al., 2008).

RESULTS

Cultivable Organisms on Plant Samples

On all plant samples, cultivable organisms were found on selective R2A and on selective PDA (**Table 1**). From the 14 different plant species sampled in the EDEN ISS greenhouse, six could be compared directly to their corresponding produce from a German grocery. Some samples were combined, all different

salads were grouped into leafy greens, and all results from different peppers (leaves) and different tomatoes (fruits) were grouped together.

In general, four trends are recognizable within the data. (i) There are large differences between the plant species. For example, the number of organisms on the parsley samples was up to two magnitudes higher than on the basil samples regardless of the sample origin, i.e., the EDEN ISS greenhouse or the grocery. Chives reached the highest microbial load with $1.1 \pm 1.4 \times 10^8$ CFU/g on selective R2A. (ii) There are differences depending on which part of the plant was sampled. On the leaves of the tomato plant, three orders of magnitude more organisms were found as on the fruits. (iii) There is a strong, statistically significant correlation between the number of organisms grown on R2A containing 50 mg/L cycloheximide and the number of organisms grown on PDA containing 50 mg/L chloramphenicol (produce: $p = 145{,}116 \times 10^{-6}$; EDEN: $p = 128{,}381 \times 10^{-12}$; evaluated with student t-test). In many cases, the number of organisms on R2A was up to one order of magnitude higher as the number of cells on PDA. (iv) The bioburden on the produce was generally higher than on the EDEN plants. The most impressive difference was found for the cucumber samples with $1.3 \pm 0.5 \times 10^5$ and $1.8 \pm 1.6 \times 10^1$ CFU/g on the cucumbers of the grocery and the EDEN ISS greenhouse, respectively.

Liquid Samples

In general, it was observed by cultivation and microscopic observation that in both tanks fungi were not present at most sampling time points. During the 9 months of operation, the nutrition solution was sampled 11 times. The tank solutions were exchanged a few times during the sampling period. Between SE1 and SE2 and between SE4 and SE5, the solution in the NDS1 tank was exchanged. Additionally, the solution in the NDS tank 2 was replaced between SE1 and SE2 and between SE3 and SE4. Considering the data from the NDS tank 1, the exchange of the solutions does not seem to have an effect on the amounts of cultivable organisms (**Figure 2**). A decline in total viable count was observed for NDS tank 2, between SE1 and SE2 as well as SE3 and SE4, which might arise from the exchange. In general, the amount of cultivable microorganisms rises two times in the NDS tank 1, with the lowest point on SE 6. From this time on, the microbial burden increased again. In NDS tank 2, the number of cultivable organisms increased almost continuously. Generally, the NDS shows an increase in microbial burden over the time of operation.

The fresh water tank that was used to prepare the nutrition solutions was sampled four times toward the end of the operation. The number of fungi was very low which is in line with the results of the nutrition solution tanks. The number of bacteria fluctuated between zero and 2.3×10^4 CFU/mL.

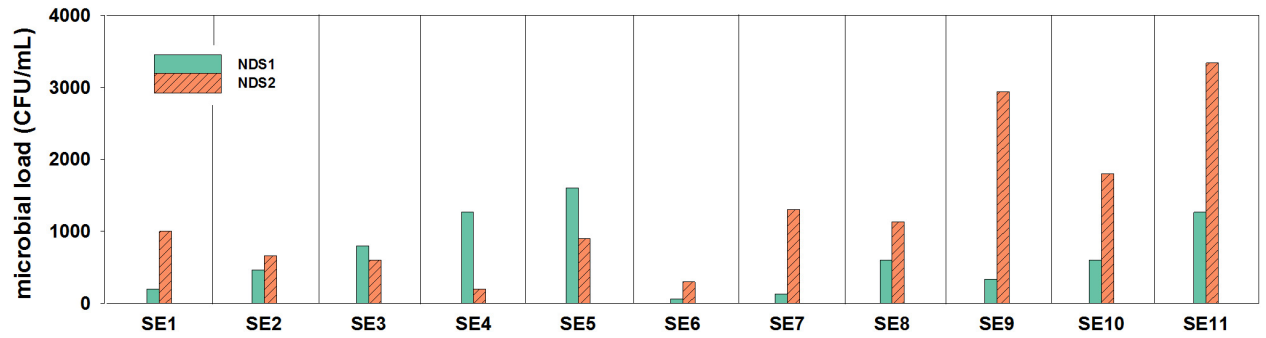

FIGURE 2 | Microbial loads (CFU/mL) inside of the two nutrition tanks (NDS1 and NDS2) used to spray the plant roots, sampling period from May to November 2018; only the results from selective R2A are shown, the selective PDA plates hardly showed any growth.

TABLE 1 | Overview of cultivable organisms on produce and on EDEN plants.

Plant	Produce	EDEN	Produce	EDEN
	Selective R2A (CFU/g)	Selective R2A (CFU/g)	Selective PDA (CFU/g)	Selective PDA (CFU/g)
Basil	$2.4 \times 10^3 \pm 1.6 \times 10^3$	$4.1 \times 10^2 \pm 4.1 \times 10^2$	$8.0 \times 10^2 \pm 8.0 \times 10^2$	$4.0 \times 10^2 \pm 4.2 \times 10^2$
Chives	$1.1 \times 10^8 \pm 0.4 \times 10^8$	n. d.	$1.7 \times 10^7 \pm 2.9 \times 10^7$	n. d.
Cucumber (fruit)	$1.3 \times 10^5 \pm 0.5 \times 10^5$	18 ± 16	$2.1 \times 10^5 \pm 1.2 \times 10^5$	8.2 ± 9.3
Leafy greens	$1.2 \times 10^7 \pm 1.9 \times 10^7$	$2.6 \times 10^3 \pm 3.6 \times 10^3$	$3.3 \pm 5.4 \times 10^6$	$2.3 \times 10^3 \pm 3.3 \times 10^3$
Parsley	$2.4 \times 10^5 \pm 1.0 \times 10^5$	$8.1 \times 10^4 \pm 1.5 \times 10^5$	$2.5 \times 10^4 \pm 8.0 \times 10^3$	$7.5 \times 10^4 \pm 1.4 \times 10^5$
Pepper (leaf)	n. d.	$1.1 \times 10^3 \pm 1.0 \times 10^3$	n. d.	$1.5 \pm 1.5 \times 10^3$
Rucola	$4.7 \times 10^6 \pm 2.4 \times 10^6$	$2.9 \times 10^3 \pm 5.0 \times 10^3$	$1.1 \times 10^6 \pm 0.2 \times 10^6$	$2.6 \times 10^3 \pm 4.7 \times 10^3$
Tomato (fruit)	6 ± 11	21.2 ± 22.6	8 ± 10	23.8 ± 34.4
Tomato (leaf)	n. d.	$1.8 \times 10^3 \pm 2.1 \times 10^3$	n. d.	$2.5 \times 10^3 \pm 1.2 \times 10^3$

n.d.: not determined, these samples were not available.

Cultivable Organisms From the Surface Samples

The three compartments (CP, SS, and FEG) of the EDEN ISS container were sampled and the results showed that the number of cultivable organisms is different in each compartment. The surface contamination in the CP was very low during the entire operation. The SS showed a low microbial burden with exception of position SS3, which is the space right beside the sink.

For CP, the number of bacteria peaked at SE 5. At this SE, the CP1 position had a microbial burden of 113 CFU/cm^2. In the CP2 samples, almost no viable cells were detected over the complete time of operation. The complete data from the CP can be seen in **Supplementary Table S2**.

For SS, no viable bacteria were detected on position SS4 (air duct in the service module) during the whole operation time (**Figure 3**). For the selective R2A plates, the highest number of microorganisms was found in position SS3 with a peak in SE 7. The corresponding selective R2A plates were overgrown already after 48 h of incubation (20°C) (**Figure 3A**). The amount of fungi was much lower in the SS, fungal growth was only shown for the SS3 position toward the end of the operation time (**Figure 3C**).

The highest numbers of organisms within the surface samples were found within FEG samples of the greenhouse itself (**Figure 4**). In general, it seemed that the number of organisms accumulated from CP, over SS, to the FEG area. In samples from some areas inside the FEG compartment, very low numbers of organisms (bacteria and fungi) were found: the wall on the right side (FEG2), rack on the left side (FEG5), and ceiling in front of the emergency exit (FEG7). The number of bacteria fluctuated strongly for the filter above the entrance door (FEG1), the area under the cattle grid (FEG9), and the growing tray (FEG4) (**Figure 4**). The numbers of microorganisms in these three positions reached the experimental contingent count limit of 250 CFU/cm^2. Viable counts on selective PDA were very low except for positions FEG1 and FEG9. Toward the end of the operation time, the amount of microorganisms increased slightly for FEG2, FEG3, and FEG8. FEG1, the filter above the entrance door, contained the highest number of fungi and was consecutively overgrown from SE3 onward. For FEG9 (floor under cattle grid), the amount of organisms was also very high on both media, especially on SE3, SE5, and SE6.

For the selective enumeration of spore-forming and other heat tolerant organisms, samples were heat shocked before the total viable count. Spore-forming bacteria were detected on the different surfaces within the whole EDEN ISS greenhouse (**Figures 3B**, **4B**). With a few exceptions, the number on the selective R2A plates exceeds the number of bacteria on the heat-shock plates. The trend of accumulation of organisms from CP, over SS to FEG was visible within these samples as well.

Identification of the Bacterial Isolates via Sequencing

Along with the bacteria, also eukaryotic organisms were isolated as described above, but these fungal isolates are not further analyzed herein. These included different strains from the *Trichocomaceae* family.

From the different samples, a total of 485 bacterial isolates were purified and identified at least on phylum level. The distribution of the different bacterial phyla is shown in **Figure 5**.

Comparing the purchased plants with the EDEN plants, it is obvious that the distribution of some phyla is the same (**Figures 5A,B** and **Table 2**). In case of the purchased plants as well as the EDEN plants, was Actinobacteria the most abundant phylum followed by Proteobacteria and Firmicutes. One bacterial strain from the pretests was found to be a member of the *Deinococcus* genus. It has to be taken into account that the number of sequenced isolates from the pretest was more than three times higher than for the EDEN ISS plants, because only 30 isolates were found on the latter (n = 108 vs. n = 30; **Supplementary Table S3**). All other organisms isolated from the EDEN plants were affiliated to the fungal kingdom.

In the two nutrition solution tanks, 37% of the 95 sequenced isolates belong to the Firmicutes, 20% to the Actinobacteria, and 18% to the Proteobacteria (**Figure 5C**). One isolate, *Mucilaginibacter carri*, belongs to the Bacteroidetes phylum (**Table 3**).

From the FEG isolates, 68% belong to the Firmicutes (**Figure 5D**), making it the predominant phylum in this part of the greenhouse. The second most abundant phylum was Actinobacteria with 15%. Some bacterial species were found in many SEs (**Table 4**). For example, *Bacillus wiedmannii* was found in five SEs. *Paenibacillus taichungensis* was identified in six different SEs. *Fictibacillus phosphorivorans* was detected in five different SEs. A member of the same genus, *Fictibacillus rigui*, was found in four SEs. Another frequently found organism was *Bacillus mobilis*. In general, many species belonging to the *Paenibacillus* and *Bacillus* genera were found in the FEG. The isolates from the SEs five and nine contained many species from the genus *Microbacteria*. The species *Cohnella rhizosphaerae* was found occasionally.

Summarizing all bacteria identified by 16S rRNA gene sequencing, the Firmicutes phylum constituted the largest part. The *Bacillus* and *Paenibacillus* genera are the dominant ones within Firmicutes. Actinobacteria and Proteobacteria are the second and third most abundant phyla. For the Actinobacteria, *Microbacterium* and *Brevibacterium* are the most abundant genera. The results from the three different sampling sites (CP, SS, and FEG) showed a divers mixture of bacteria and strong fluctuations in the temporal distribution of the microbial burden. The SS and CP parts of the EDEN ISS greenhouse showed very low numbers of microorganisms compared to the rest of the samples.

DISCUSSION

In general, the EDEN ISS project showed that it is feasible to cultivate fresh edible food in a greenhouse in an extreme environment. Over 9.5 months, a total of 268 kg of food were produced on an area of only 12.5 m^2, including 67 kg of cucumbers, 117 kg of lettuce, and 50 kg of tomatoes. This study showed that all tested samples can be considered as harmless and safe. Therefore, the vegetables from the EDEN

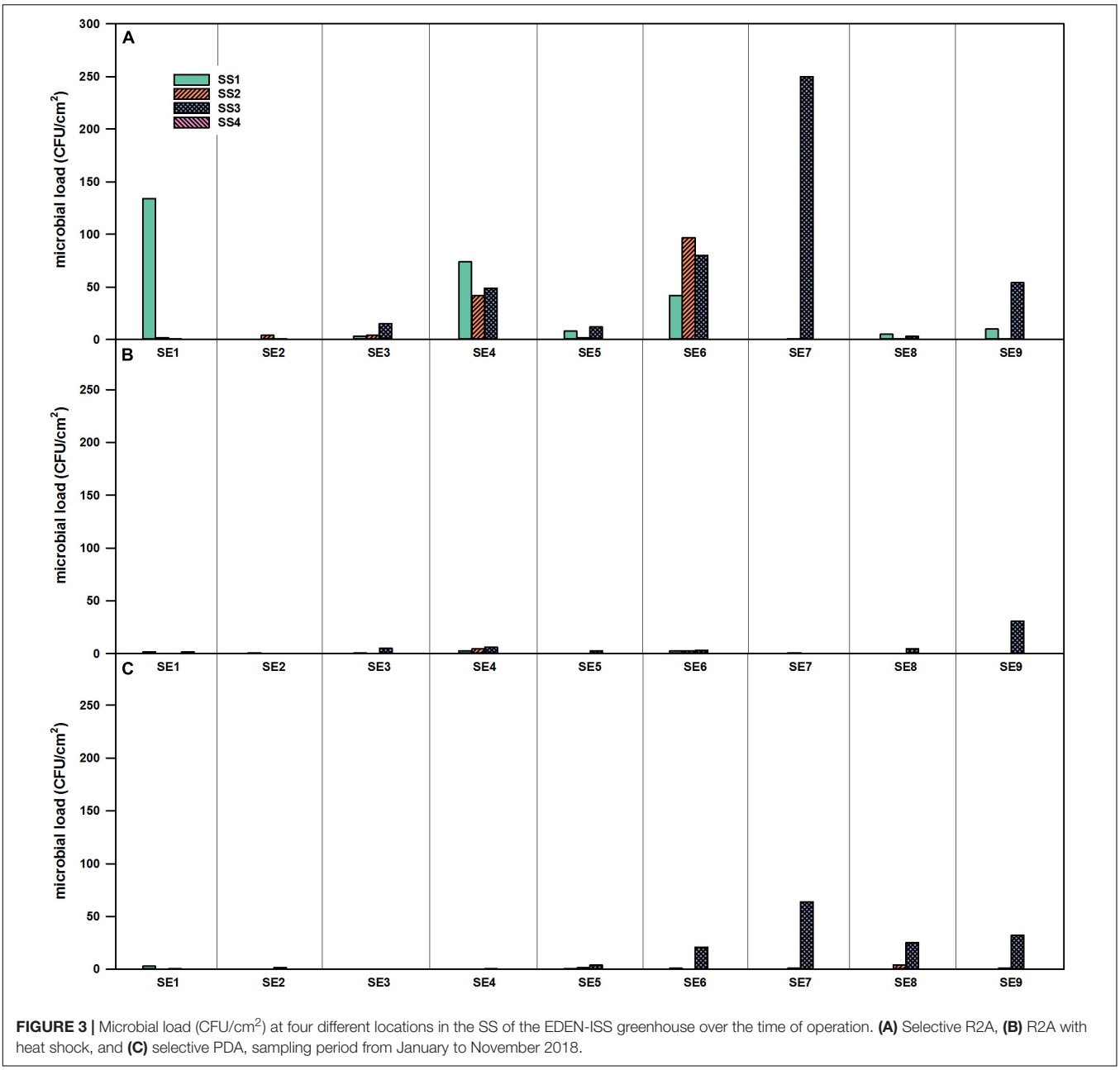

FIGURE 3 | Microbial load (CFU/cm^2) at four different locations in the SS of the EDEN-ISS greenhouse over the time of operation. **(A)** Selective R2A, **(B)** R2A with heat shock, and **(C)** selective PDA, sampling period from January to November 2018.

ISS container are suitable for consumption and have been consumed during the operation phase of the EDEN ISS mission. Although the microbial greenhouse samples differed from the purchased samples, only a very small number of potentially human pathogenic organisms were found. The infective potential of these organisms has not been investigated in the present study. Nevertheless, close control of the microbial load should be carried out in a future application in space, on other planets or moons.

Microbial Load Within the EDEN ISS Container

The phyllosphere microbiota is very diverse and many different factors contribute to it. The amount of microorganisms on the leaf surface fluctuates strongly between plant species and locations around the globe. Previous studies showed that leaf surfaces often host 10^6–10^7 CFU/cm^2 (Lindow and Brandl, 2003) or 10^3–10^9 CFU per gram plant material (Zagory, 1999). For example, it was found that for aromatic plants, the cell counts differ strongly. For rosemary, the cell count is about 4×10^2 and 5×10^5 CFU/g for lavender (Karamanoli et al., 2000). The basil tested in order to obtain a baseline for the EDEN ISS samples showed $2.4 \times 10^3 \pm 1.6 \times 10^3$ CFU/g. Therefore, this value fits the range of aromatic plants. For parsley, the microbial load was found to be in the range of 10^5–10^6 CFU/g (Morris et al., 1998), which corresponds to the value from the pretest ($2.4 \times 10^5 \pm 1.0 \times 10^5$ CFU/g).

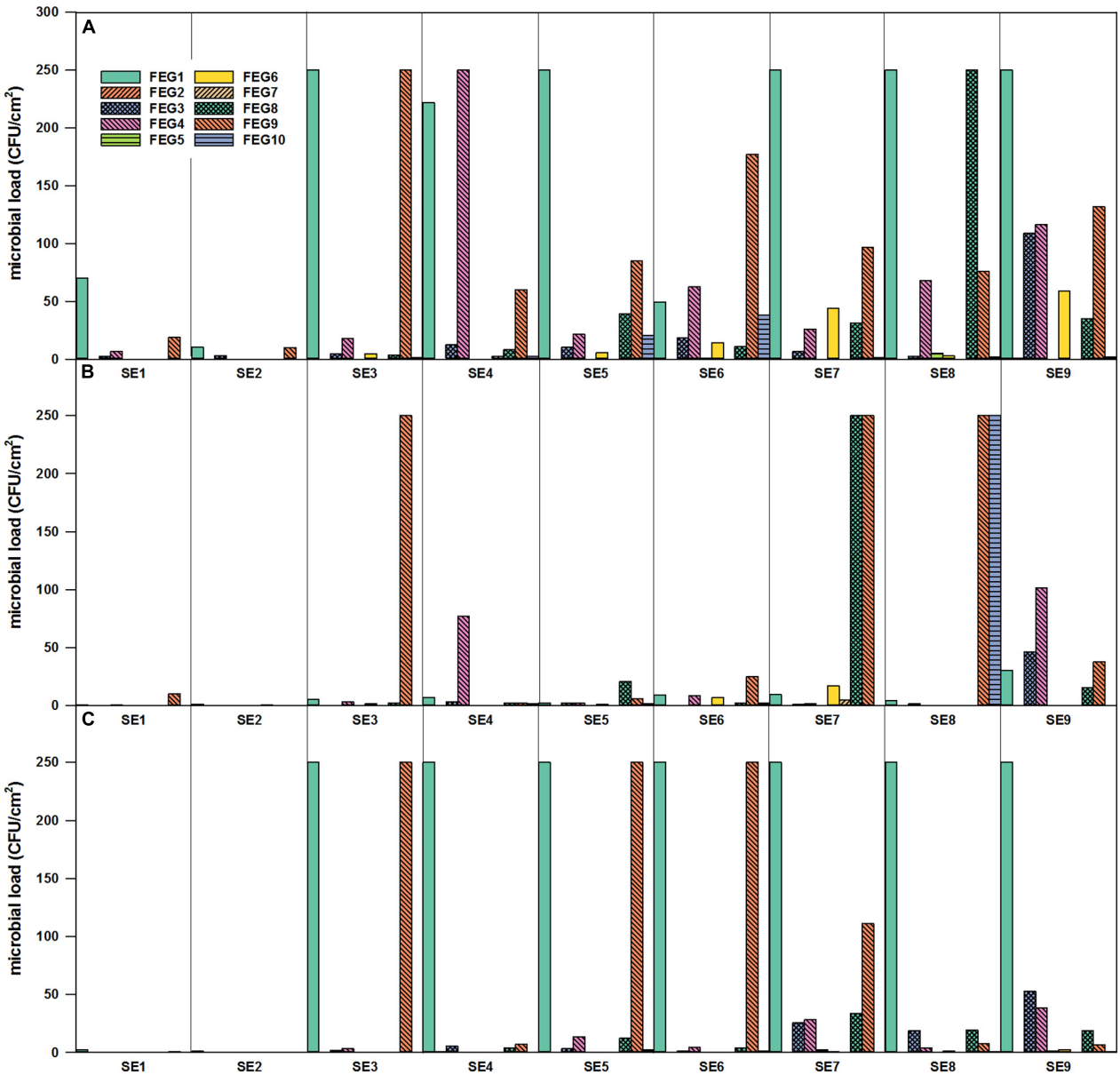

FIGURE 4 | Microbial load (CFU/cm^2) in the FEG compartment over time of operation. FEG1 – FEG10: different sampling positions inside the compartment. **(A)** Selective R2A, **(B)** R2A with heat shock, and **(C)** selective PDA, sampling period from January to November 2018.

Additionally, the bacterial counts for different lettuces were found to range between 4×10^5 and 5×10^6 CFU/g (Hunter et al., 2010), which is in accordance with the cell numbers of the purchased plants in this study (10^3–10^8 CFU/g). Due to the lack of a standardized protocol to remove and cultivate bacteria from the phyllosphere, this comparison should be used with caution. For some plant species that were also grown in the EDEN ISS greenhouse, no phyllosphere studies have been performed so far, therefore no values for comparison are available. Some studies claimed that the bacterial load in the phyllosphere fluctuates strongly (Karamanoli et al., 2005), while others indicated that for one specific plant, the bacterial community stays the same over different samples (Hunter et al., 2010). In general, comparing these results with the data from the EDEN greenhouse (10^2–10^4 CFU/g depending on the investigated plant), it is obvious that the microbiota from the EDEN plants is most likely different from the natural one. It can be stated that the overall microbial burden of the plants is much lower than on commercially available plants from fields and regular greenhouses. It is not completely understood if this is an overall beneficial feature or not. It was shown in previous studies that some bacteria can be beneficial for the plant growth or even necessary for maturation processes (Carlier and Eberl, 2012). The number

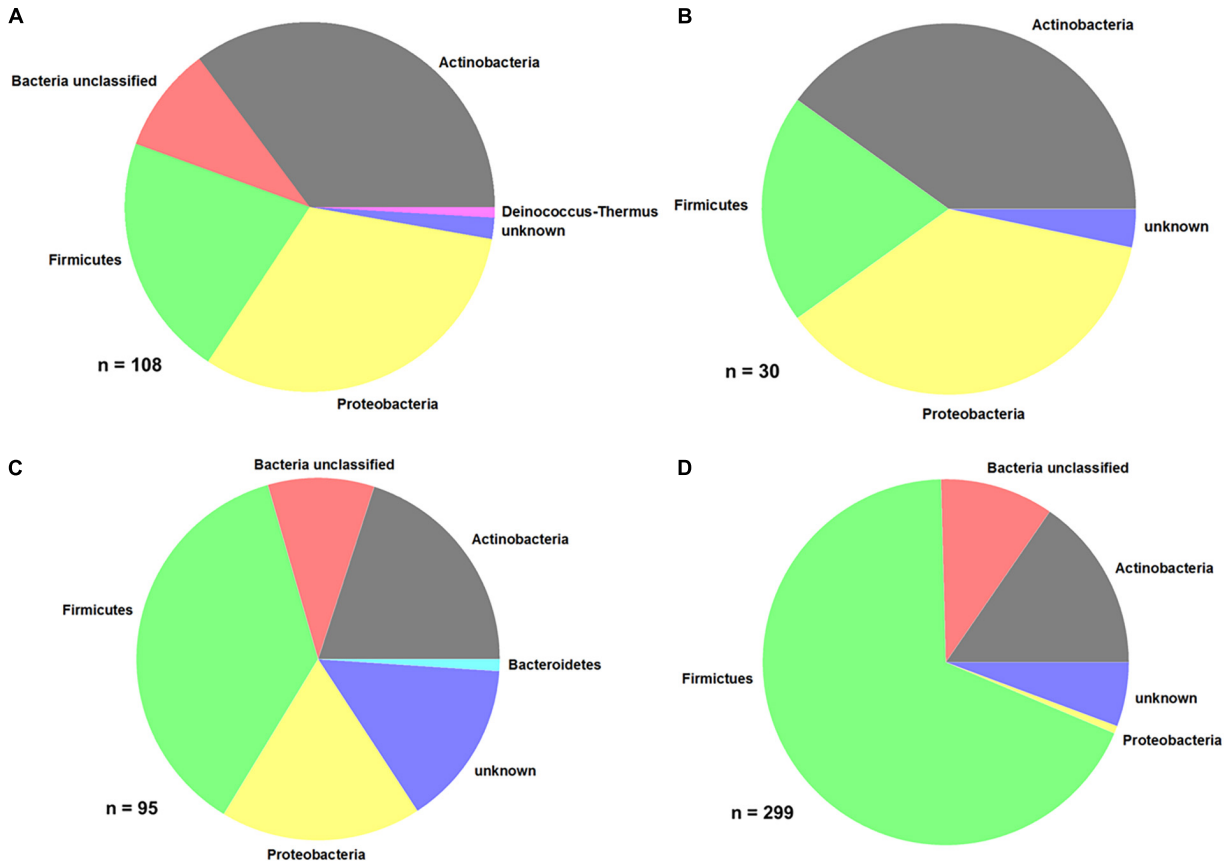

FIGURE 5 | Distribution of bacterial phyla. **(A)** Produce, **(B)** EDEN ISS plants, **(C)** liquid nutrient samples, and **(D)** surface samples (FEG).

of fungi visible on the investigated plates, even on selective R2A plates with the fungicide cycloheximide, exceeded the numbers of bacteria strongly; this was vice versa for the purchased plants. This can be an indication for a distorted balance between bacteria and fungi. Additionally, the quantitative evaluation of fungi can be difficult because the filamentous fungi tend to overgrow the plates with only a few colonies (Waksman, 1922). One explanation for the difference between the EDEN ISS plants and the purchased plants could be the absence of soil during plant cultivation. In the EDEN ISS greenhouse, an aeroponic system was used in which the seeds were sown into rock wool mats and the freely hanging roots were regularly sprayed with a nutrition solution (Nir, 1981; Imhof et al., 2018).

The used nutrition solution was changed several times during the operation. In order to keep the microbial burden low, ozone was added. The ozone generator was active for 30 min per hour. Nevertheless, the number of cultivable cells increased over time. The overall increase of the microbial burden in both tanks probably arose from the growth despite the regular application of ozone. The fact that the NDS tank 2 accumulated higher amounts of bacteria could be explained by the higher amount of nutrients in the NDS tank 2 solution (**Supplementary Table S1**) (Button, 1985). The number of organisms in the NDS tanks is quite high toward the end of the operation ($\sim 10^3$ CFU/mL), but nevertheless, no bacteria with assured pathogenicity were found and therefore a risk for humans is rather low. The microbial load is still not high in comparison to the numbers found in other greenhouse systems. For example, 10^6 CFU/mL were found in the nutrition solution of a hydroponic system (Waechter-Kristensen et al., 1997). A single peak in the microbial load was observed for the fresh water tank, with $\sim 10^4$ CFU/mL at 2 November 2018. It has to be mentioned that this water was only used for the tanks and not as a source of drinking water. Most of the colonies shared a yellow, smooth, and round morphology. It was found that these belong to the species *Sphingomonas echinoides*. This finding aligns with a statement from the greenhouse operator Paul Zabel that the pump from the fresh water supply appeared to be contaminated with a yellow organism.

The surfaces in the mobile test facility were sampled nine times in total, the different surfaces showed widely varying numbers of CFU as well as diverse bacterial species. In the CP, only very few microorganisms were found. To give comparable values, the European Commission laid down that cleaned and disinfected surfaces in establishments for the production and marketing of fresh meat have an acceptable range when total viable counts are below 10 CFU/cm^2 (2001/471/EC). In the United States, surfaces with < 5 CFU/cm^2 are considered as

TABLE 2 | Bacterial genera isolated from the produce and from EDEN ISS plants.

Plant species	Phylum	Class	Order	Family	Genus	Produce	EDEN ISS
Basil	Actinobacteria	Actinobacteria	Actinomycetales	Micrococcaceae	***Arthrobacter***	1	–
		Actinobacteria	Actinomycetales	Micrococcaceae	***Micrococcus***	–	2
		Actinobacteria	Actinomycetales	Brevibacteriaceae	***Brevibacterium***	1	–
		Actinobacteria	Actinomycetales	Microbacteriaceae	***Curtobacterium***	3	–
		Actinobacteria	Actinomycetales	Microbacteriaceae	***Frigoribacterium***	1	–
	Firmicutes	Bacilli	Bacillales	Paenibacillaceae	***Paenibacillus***	–	1
		Bacilli	Bacillales	Bacillaceae	***Bacillus***	2	–
	Proteobacteria	Gammaproteobacteria	Pseudomonadales	Pseudomonadaceae	***Pseudomonas***	1	1
		Gammaproteobacteria	Xanthomonadales	Xanthomonadaceae	***Stenotrophomonas***	–	1
		Alphaproteobacteria	Sphingomonadales	Sphingomonadaceae	***Sphingomonas***	1	–
Cucumber	Actinobacteria	Actinobacteria	Actinomycetales	Microbacteriaceae	***Curtobacterium***	3	
		Actinobacteria	Actinomycetales	Microbacteriaceae	***Microbacterium***	7	–
		Actinobacteria	Actinomycetales	Micrococcaceae	***Kocuria***	–	3
		Actinobacteria	Actinomycetales	Dermacoccaceae	***Dermacoccus***	–	1
		Actinobacteria	Nakamurellales	Nakamurellaceae	***Nakamurella***	–	1
	Proteobacteria	Alphaproteobacteria	Rhizobiales	Methylobacteriaceae	***Methylobacterium***	2	–
		Gammaproteobacteria	Pseudomonadales	Pseudomonadaceae	***Pseudomonas***	4	–
		Alphaproteobacteria	Rhizobiales	Rhizobiaceae	***Rhizobium***	1	–
		Alphaproteobacteria	Sphingomonadales	Sphingomonadaceae	***Sphingobium***	4	–
		Alphaproteobacteria	Sphingomonadales	Sphingomonadaceae	***Sphingomonas***	2	–
		Gammaproteobacteria	Xanthomonadales	Xanthomonadaceae	***Stenotrophomonas***	1	–
		Gammaproteobacteria	Pseudomonadales	Moraxellaceae	***Moraxella***	–	1
		Alphaproteobacteria	Caulobacterales	Caulobacteraceae	***Brevundimonas***	–	1
Parsley	Actinobacteria	Actinobacteria	Actinomycetales	Micrococcaceae	***Arthrobacter***	1	–
		Actinobacteria	Actinomycetales	Microbacteriaceae	***Agrococcus***	1	–
		Actinobacteria	Actinomycetales	Microbacteriaceae	***Curtobacterium***	3	–
		Actinobacteria	Actinomycetales	Microbacteriaceae	***Frigoribacterium***	1	–
		Actinobacteria	Actinomycetales	Microbacteriaceae	***Frondihabitans***	1	–
		Actinobacteria	Actinomycetales	Intrasporangiaceae	***Janibacter***	1	–
		Actinobacteria	Actinomycetales	Micrococcaceae	***Kocuria***	1	–
		Actinobacteria	Actinomycetales	Microbacteriaceae	***Microbacterium***	1	–
		Actinobacteria	Actinomycetales	Micrococcaceae	***Pseudarthrobacter***	1	–
		Actinobacteria	Actinomycetales	Nocardiaceae	***Rhodococcus***	2	–
	Firmicutes	Bacilli	Bacillales	Bacillaceae	***Bacillus***	1	–
		Bacilli	Bacillales	Staphylococcaceae	***Staphylococcus***	1	–
		Bacilli	Bacillales	Paenibacillaceae	***Paenibacillus***	–	1
	Proteobacteria	Alphaproteobacteria	Sphingomonadales	Sphingomonadaceae	***Sphingomonas***	2	–
		Gammaproteobacteria	Xanthomonadales	Xanthomonadaceae	***Stenotrophomonas***	3	–
		Betaproteobacteria	Burkholderiales	Comamonadaceae	***Variovorax***	1	–
Rucola	Actinobacteria	Actinobacteria	Actinomycetales	Dermabacteraceae	***Brachybacterium***	1	–
		Actinobacteria	Actinomycetales	Microbacteriaceae	***Curtobacterium***	1	–
		Actinobacteria	Actinomycetales	Microbacteriaceae	***Frigoribacterium***	4	–
		Actinobacteria	Actinomycetales	Micrococcaceae	***Kocuria***	1	–
		Actinobacteria	Actinomycetales	Microbacteriaceae	***Rathayibacter***	1	–
		Actinobacteria	Actinomycetales	Micrococcaceae	***Micrococcus***	–	2
		Actinobacteria	Actinomycetales	Micrococcaceae	***Pseudarthrobacter***	–	1
	Deinococcus–Thermus	Deinococci	Deinococcales	Deinococcaceae	***Deinococcus***	1	–
	Proteobacteria	Gammaproteobacteria	Pseudomonadales	Pseudomonadaceae	***Pseudomonas***	7	1
		Alphaproteobacteria	Rhizobiales	Rhizobiaceae	***Rhizobium***	1	–
		Alphaproteobacteria	Sphingomonadales	Sphingomonadaceae	***Sphingomonas***	2	–
		Gammaproteobacteria	Xanthomonadales	Xanthomonadaceae	***Stenotrophomonas***	2	1
		Alphaproteobacteria	Rhizobiales	Rhizobiaceae	***Shinella***	–	1

TABLE 3 | Bacterial genera isolated from the NDS tanks.

Phylum	Class	Order	Family	Genus	NDS1	NDS2
Actinobacteria	Actinobacteria	Actinomycetales	Gordoniaceae	***Gordonia***	–	1
	Actinobacteria	Actinomycetales	Microbacteriaceae	***Microbacterium***	5	8
	Actinobacteria	Actinomycetales	Mycobacteriaceae	***Mycolicibacterium***	–	1
	Actinobacteria	Actinomycetales	Nocardiaceae	***Nocardia***	–	1
	Actinobacteria	Actinomycetales	Nocardiaceae	***Rhodococcus***	1	2
Bacteroidetes	Sphingobacteria	Sphingobacteriales	Sphingobacteriaceae	***Mucilaginibacter***	–	1
Firmicutes	Bacilli	Bacillales	Bacillaceae	***Bacillus***	13	5
	Bacilli	Bacillales	Paenibacillaceae	***Cohnella***	3	–
	Bacilli	Bacillales	Paenibacillaceae	***Paenibacillus***	9	4
Proteobacteria	Gammaproteobacteria	Nevskiales	Sinobacteraceae	***Hydrocarboniphaga***	–	2
	Betaproteobacteria	Burkholderiales	Comamonadaceae	***Polaromonas***	1	1
	Gammaproteobacteria	Pseudomonadales	Pseudomonadaceae	***Pseudomonas***	2	–
	Betaproteobacteria	Burkholderiales	Burkholderiaceae	***Ralstonia***	1	
	Gammaproteobacteria	Xanthomonadales	Xanthomonadaceae	***Stenotrophomonas***	1	3
	Gammaproteobacteria	Xanthomonadales	Xanthomonadaceae	***Thermomonas***	1	–

TABLE 4 | Bacterial genera isolated from the FEG compartment.

Actinobacteria genera	Number of isolates	Position (# findings)
Brevibacterium	13	FEG1 (1), FEG3 (2), FEG4 (1), FEG5 (1), FEG6 (3), FEG8 (2), FEG9 (3)
Curtobacterium	1	FEG9 (1)
Dermacoccus	6	FEG1 (1), FEG3 (2), FEG4 (1), FEG9 (1), FEG10 (1)
Kocuria	2	FEG2 (1), FEG6 (1)
Microbacterium	20	FEG2 (1), FEG3 (5), FEG4 (1), FEG5 (1), FEG6 (4), FEG8 (3) FEG9 (3), FEG10 (2)
Micrococcus	10	FEG1 (1), FEG3 (1), FEG4 (2), FEG6 (1), FEG8 (4), FEG9 (1)
Nakamurella	1	FEG6 (1)
Rhodococcus	9	FEG6 (1), FEG3 (1), FEG6 (3), FEG8 (2), FEG9 (1), FEG10 (1)
Firmicutes genera		
Aerococcus	1	FEG9 (1)
Bacillus	56	FEG1 (4), FEG2 (2), FEG3 (14), FEG4 (5), FEG5 (6), FEG6 (6), FEG8 (6) FEG9 (10), FEG10 (3)
Cohnella	10	FEG4 (3), FEG6 (1), FEG8 (3), FEG9 (1), FEG10 (2)
Fictibacillus	14	FEG1 (1), FEG3 (4), FEG6 (3), FEG8 (2), FEG9 (1), FEGC (3)
Lysinibacillus	1	FEG3 (1)
Paenibacillus	64	FEG1 (7), FEG3 (21), FEG4 (7), FEG6 (5), FEG8 (5), FEG9 (8), FEG10 (11)
Staphylococcus	8	FEG1 (4), FEG6 (1), FEG8 (2) FEG9 (1)
Streptococcus	1	FEG6 (1)
Proteobacteria genera		
Pseudomonas	1	FEG8 (1)

safe for food preparation (Dancer, 2004). The CP2 surface never reached this value. The CP is mainly used as an entrance to the greenhouse and the greenhouse operator only stayed in this room for short times. Additionally, the CP is the furthest place from the plants; therefore, it is unlikely that microorganisms from the plants get translocated to the CP. The SS was cleaned irregularly with a disinfectant during the operation time. In the SS compartment, the surface next to the sink (SS3 position) showed the highest number of cultivable organisms. The amounts fluctuated strongly over the operation time. A possible reason is that this area was cleaned irregularly with cleaning agent. In the FEG, some of the positions showed high numbers of CFU/cm^2 (FEG1, FEG4, and FEG9). In general, the numbers of cultivable organisms were low but fluctuated. This fluctuating trend was also observed in other studies concerning closed environments, like the MARS 500 study. MARS 500 was a habitat and test facility for future manned Mars missions, consisting of different modules for test persons to live, work, and sleep. It worked as a closed system for 520 days and the microbial load on its surfaces in this enclosed environment fluctuated strongly between 0 and 2.9×10^5 CFU/cm^2. The highest values were obtained in the habitat module, where the subjects lived (Schwendner et al., 2017). Nevertheless, the microbial burden in the EDEN ISS container never reached levels counted for MARS 500. On the other hand, the Russian module of the ISS was tested for its microbial load as described in Reidt et al. (2014). It was shown that the microbial contamination was between 0 and 88.9 CFU/cm^2 depending on the material sampled. These levels are indeed much lower than those from the MARS 500 habitat and are comparable to the results from the CP as well as the SS of the EDEN ISS Greenhouse, but the FEG part of the greenhouse exceeded these numbers.

Identification of the Organisms From the EDEN ISS Container

Only cultivated isolates from the surface sampling in the FEG compartment were sent for sequencing which revealed a highly diverse mixture of organisms. As expected, mostly non-hazardous, plant and soil associated bacteria were found. The typical soil resident *Brevibacterium frigoritolreans* was

found very often (Jariyal et al., 2015). But also *B. wiedmannii*, a psychrotolerant organism that has cytotoxic traits and occurs in dairy products, was detected (Miller et al., 2016). Another soil resident, *P. taichungensis*, was found in six different SEs. *F. phosphorivorans*, a soil resident with toxic activity against nematodes, was found in five different SE (Zheng et al., 2016). Another frequently found organism was *B. mobilis*, an organism that belongs to the *Bacillus cereus* group (Liu et al., 2017). *Cohnella rhizospharae* was previously isolated from the rhizosphere of sweet corn (Kämpfer et al., 2014) and was found occasionally on the surfaces in the EDEN ISS greenhouse. Some of the species, for example, *Staphylococcus edaphicus*, were previously found some other areas in Antarctica (Pantucek et al., 2018). Therefore, the entry of these microorganisms from the outside seems to be likely. It is important to consider these leaks of microorganisms for space missions in order to find ways to prevent the entry of microorganisms to the surface of other planets (Horneck et al., 2012).

In case of the NDS tanks, the Firmicutes phylum was most abundant. Actinobacteria and Proteobacteria are on the second and third place respectively. In total, four isolates were identified as *Microbacterium schleiferi*, previously isolated from dairy sewage (Yokota et al., 1993). *B. wiedmannii* was found four times as well. It is a psychrotolerant organism with cytotoxic traits (Miller et al., 2016). It was also found in the FEG positions. Similar to the plant isolates, members of the genus *Paenibacillus* are strongly present. The genera *Microbacterium* and *Bacillus* play an important role as well. *Gordonia polyisoprenivorans* was isolated from NDS tank 2. This species is able to degrade rubber (Linos et al., 1999) and might degrade parts of the NDS system over time. Degradation processes on space relevant materials by *Bacillus paralicheniformis* and *Cupriavidus metallidurans* have been shown recently (Mora et al., 2019). Culture-independent methods might reveal other species that are able to degrade materials found in the greenhouse. Therefore, this has to be considered in future experiments.

In total, 108 isolates from plants from a grocery were sent for sequencing. In case of the basil samples, except for *Pseudomonas lactis*, which was so far isolated from bovine raw milk (von Neubeck et al., 2017), all isolates are soil or plant-associated bacteria. For example, *Curtobacterium luteum*, a psychrotrophic soil resident (Kuddus and Ramteke, 2008) was found. From the cucumber samples, 24 isolates could be identified on species level. A very diverse mixture of bacteria was found. A plant pathogen that mainly infests beans, *Curtobacterium flaccumfaciens*, was found (Sammer and Reiher, 2012). *Methylobacterium hispanicum*, which was previously isolated from drinking water (Gallego et al., 2005), *Microbacterium arborescens* that resides usually in sand dunes (Godinho and Bhosle, 2009), as well as *M. schleiferi* that was previously isolated from dairy sewage (Yokota et al., 1993) were detected. Additionally, some typical plant-associated microorganisms like *Sphingobium yanoikuyae* were found. *Rhizobium pusense* that lives in the rhizosphere of chickpea (Panday et al., 2011) was also found. One isolate belonged to the *Sphingomonas aerolata* species, which is psychrotolerant and can be found in many different environments (Busse et al., 2003). The parsley plants also showed very diverse microorganisms. *C. flaccumfaciens* and *Stenotrophomonas maltophilia* were found here as well. Another isolate from these samples is *Arthrobacter humicola*, an endophytic bacterial strain that produces phytotoxic compounds (Chung et al., 2010). Additionally, two soil bacteria (Groth et al., 1996; Miwa et al., 2008), *Agrococcus jenensis* and *Variovorax boronicumulans* were detected. *Janibacter melonis*, a microorganism that was originally isolated from spoiled melons (Yoon et al., 2004), was isolated from parsley. *S. aerolata* and the highly related *Sphingomonas aurantiaca* were isolated from cucumber and rucola. Both *Sphingomonas* strains are psychrotolerant species (Busse et al., 2003). *S. maltophilia* was detected on the rucola samples as well. Rucola hosted, for example, *Brachybacterium nesterenkovii*, that was isolated from milk products (Gvozdyak et al., 1992), *Deinococcus seoulensis* from sediment in Seoul (Lee et al., 2016), *Frigoribacterium faeni*, a psychrophilic organism (Kämpfer et al., 2000), the salt tolerant species *Pseudomonas extremorientalis* (Egamberdieva et al., 2013), and *Rathayibacter festucae* which was isolated from different phyllospheres (Dorofeeva et al., 2002). In summary, the diversity as well as quantity of microorganisms on the produce was high but in the expected range. Most of the isolates were harmless plant- or soil-associated bacteria. Other studies that investigated purchased products assigned many isolates to the Enterobacteriaceae which include representatives of human pathogens such as *Escherichia* and *Salmonella* (Leff and Fierer, 2013), which were not detected in this study.

In total, 30 bacterial isolates from the EDEN ISS plants were sent for sequencing. Even though it might be a coincidence, it was noticeable that only for the cucumber, an isolate appeared multiple times. The species, *Kocuria palustris*, seems to be harmless for plants and humans (Kovács et al., 1999). *S. maltophilia,* previously found in clean rooms (Mora et al., 2016), was the only organism that was isolated from both, the purchased rucola as well as the rucola from the EDEN ISS greenhouse. It is remarkable that all other isolates either only appear in the EDEN ISS samples or in those from the grocery. *K. palustris* was found on the purchased rucola and on the EDEN ISS cucumber. On the EDEN ISS plants, the *Micrococcus* and *Paenibacillus* genera represented a large proportion of the isolates while these genera were not detected on the purchased plants. *Micrococcus antarcticus* was found on the rucola samples in the EDEN ISS greenhouse. This species was previously isolated from Antarctica (Liu et al., 2000). Thus, it is possible that it entered as a spore from the outside of the greenhouse. Even though the species isolated differ widely, there were some similarities on the phylum level. Actinobacteria is the most abundant phylum in both batches, followed by Proteobacteria and Firmicutes. Previous studied showed that Proteobacteria is the most abundant phylum for many plant phyllospheres followed by Actinobacteria (Vorholt, 2012), whereas others found that Firmicutes were the largest group for most plants (Jackson et al., 2015). These studies used culture-independent methods

to determine the distribution of the phyla, i.e., 16S rRNA gene shotgun sequencing. Thus, comparability has to be questioned.

CONCLUSION

Overall, the quantity and quality of the identified microorganisms from the EDEN ISS container, as well from the plants themselves are part of a normal plant microbiome. Moreover, this microbiome can counteract to plant pathogenic outbreaks, and some of these bacteria are known as growth enhancer (Berg et al., 2014; Di Benedetto et al., 2017). From the point of view to get more food out of the greenhouse, it is desirable for these organisms to be present there.

DATA AVAILABILITY STATEMENT

The datasets generated for this study are available on request to the corresponding author.

AUTHOR CONTRIBUTIONS

DS, PZ, and PR contributed to conceptualization. JF, CF, RV, and MM contributed to formal analysis. JF, CF, and KB-V contributed to methodology. DS and PR contributed to project administration. JF and KB-V contributed to writing—original draft. PZ, MM, RV, BE, and PR contributed to writing—review and editing.

FUNDING

The EDEN ISS project (Evaluation and Design of Environmentally-closed Nutrition-sources) was funded by the European Union's Research and Innovation Action program Horizon 2020 (Grant Agreement ID: 636501).

ACKNOWLEDGMENTS

The authors thank Rüdiger Pukall (Leibniz Institute DSMZ-German Collection of Microorganisms and Cell Cultures, Braunschweig, Germany) for assistance to identify eukaryotic/fungal strains and Elke Rabbow and Corinna Panitz (DLR Cologne) for assistance during the swab sample evaluation.

SUPPLEMENTARY MATERIAL

The Supplementary Material for this article can be found online at: https://www.frontiersin.org/articles/10.3389/fmicb.2020.00525/full#supplementary-material

REFERENCES

Berg, G., Grube, M., Schloter, M., and Smalla, K. (2014). Unraveling the plant microbiome: looking back and future perspectives. *Front. Microbiol.* 5:148. doi: 10.3389/fmicb.2014.00148

Busse, H.-J., Denner, E. B., Buczolits, S., Salkinoja-Salonen, M., Bennasar, A., and Kämpfer, P. (2003). *Sphingomonas aurantiaca* sp. nov., *Sphingomonas aerolata* sp. nov. and *Sphingomonas faeni* sp. nov., air-and dustborne and Antarctic, orange-pigmented, psychrotolerant bacteria, and emended description of the genus *Sphingomonas*. *Int. J. Syst. Evol. Microbiol.* 53, 1253–1260.

Button, D. (1985). Kinetics of nutrient-limited transport and microbial growth. *Microbiol. Rev.* 49, 270–297.

Carlier, A. L., and Eberl, L. (2012). The eroded genome of a *Psychotria* leaf symbiont: hypotheses about lifestyle and interactions with its plant host. *Environ. Microbiol.* 14, 2757–2769. doi: 10.1111/j.1462-2920.2012.02763.x

Chung, E.-J., Park, J.-H., Park, T.-S., Ahn, J.-W., and Chung, Y.-R. (2010). Production of a phytotoxic compound, 3-phenylpropionic acid by a bacterial endophyte, *Arthrobacter humicola* yc6002 isolated from the root of *Zoysia japonica*. *Plant Pathol. J.* 26, 245–252.

Cole, J. R., Wang, Q., Fish, J. A., Chai, B., McGarrell, D. M., Sun, Y., et al. (2013). Ribosomal database project: data and tools for high throughput rRNA analysis. *Nucleic Acids Res.* 42, D633–D642. doi: 10.1093/nar/gkt1244

Dancer, S. J. (2004). How do we assess hospital cleaning? A proposal for microbiological standards for surface hygiene in hospitals. *J. Hosp. Infect.* 56, 10–15.

Di Benedetto, N. A., Corbo, M. R., Campaniello, D., Cataldi, M. P., Bevilacqua, A., Sinigaglia, M., et al. (2017). The role of plant growth promoting bacteria in improving nitrogen use efficiency for sustainable crop production: a focus on wheat. *AIMS Microbiol.* 3, 413–434. doi: 10.3934/microbiol.2017.3.413

Dorofeeva, L. V., Evtushenko, L. I., Krausova, V. I., Karpov, A. V., Subbotin, S. A., and Tiedje, J. M. (2002). *Rathayibacter caricis* sp. nov. and *Rathayibacter festucae* sp. nov., isolated from the phyllosphere of *Carex* sp. and the leaf gall induced by the nematode *Anguina graminis* on *Festuca rubra* L., respectively. *Int. J. Syst. Evol. Microbiol.* 52, 1917–1923.

Egamberdieva, D., Jabborova, D., and Mamadalieva, N. (2013). Salt tolerant *Pseudomonas extremorientalis* able to stimulate growth of *Silybum marianum* under salt stress. *Med. Aromat. Plant Sci. Biotechnol.* 7, 7–10.

Gallego, V., García, M. T., and Ventosa, A. (2005). *Methylobacterium hispanicum* sp. nov. and *Methylobacterium aquaticum* sp. nov., isolated from drinking water. *Int. J. Syst. Evol. Microbiol.* 55, 281–287.

Godinho, A. L., and Bhosle, S. (2009). Sand aggregation by exopolysaccharide-producing *Microbacterium arborescens* – AGSB. *Curr. Microbiol.* 58, 616–621. doi: 10.1007/s00284-009-9400-4

Groth, I., Schumann, P., Weiss, N., Martin, K., and Rainey, F. (1996). *Agrococcus jenensis* gen. nov., sp. nov., a new genus of actinomycetes with diaminobutyric acid in the cell wall. *Int. J. Syst. Evol. Microbiol.* 46, 234–239.

Gvozdyak, O., Nogina, T., and Schumann, P. (1992). Taxonomic study of the genus *Brachybacterium*: *Brachybacterium nesterenkovii* sp. nov. *Int. J. Syst. Evol. Microbiol.* 42, 74–78.

Horneck, G., Moeller, R., Cadet, J., Douki, T., Mancinelli, R. L., Nicholson, W. L., et al. (2012). Resistance of bacterial endospores to outer space for planetary protection purposes – experiment protect of the EXPOSE-E mission. *Astrobiology* 12, 445–456. doi: 10.1089/ast.2011.0737

Hunter, P. J., Hand, P., Pink, D., Whipps, J. M., and Bending, G. D. (2010). Both leaf properties and microbe-microbe interactions influence within-species variation in bacterial population diversity and structure in the lettuce (*Lactuca* species) phyllosphere. *Appl. Environ. Microbiol.* 76, 8117–8125. doi: 10.1128/AEM.01321-10

Imhof, B., Schlacht, I., Waclavicek, R., Schubert, D., Zeidler, C., Vrakking, V., et al. (2018). "EDEN-ISS–a simulation testbed to an advanced exploration design concept for a greenhouse for moon and mars," in *Proceedings of the 69th International Astronautical Congress (IAC), Bremen, Germany, 1-5 October 2018.IAC-18 B, 3*, Bremen.

Jackson, C., Stone, B., and Tyler, H. (2015). Emerging perspectives on the natural microbiome of fresh produce vegetables. *Agriculture* 5, 170–187.

Jariyal, M., Gupta, V., Mandal, K., and Jindal, V. (2015). *Brevibacterium frigoritolerans* as a novel organism for the bioremediation of phorate. *B. Environ. Contam. Tox.* 95, 680–686. doi: 10.1007/s00128-015-1617-2

Johnson, M., Zaretskaya, I., Raytselis, Y., Merezhuk, Y., McGinnis, S., and Madden, T. L. (2008). NCBI BLAST: a better web interface. *Nucleic Acids Res.* 36, W5–W9. doi: 10.1093/nar/gkn201

Kämpfer, P., Glaeser, S. P., McInroy, J. A., and Busse, H.-J. (2014). *Cohnella rhizosphaerae* sp. nov., isolated from the rhizosphere environment of *Zea mays*. *Int. J. Syst. Evol. Microbiol.* 64, 1811–1816. doi: 10.1099/ijs.0.060814-0

Kämpfer, P., Rainey, F., Andersson, M., Lassila, E. N., Ulrych, U., Busse, H., et al. (2000). *Frigoribacterium faeni* gen. nov., sp. nov., a novel psychrophilic genus of the family microbacteriaceae. *Int. J. Syst. Evol. Microbiol.* 50, 355–363. doi: 10.1099/00207713-50-1-355

Karamanoli, K., Menkissoglu-Spiroudi, U., Bosabalidis, A. M., Vokou, D., and Constantinidou, H.-I. A. (2005). Bacterial colonization of the phyllosphere of nineteen plant species and antimicrobial activity of their leaf secondary metabolites against leaf associated bacteria. *Chemoecology* 15, 59–67.

Karamanoli, K., Vokou, D., Menkissoglu, U., and Constantinidou, H.-I. (2000). Bacterial colonization of phyllosphere of mediterranean aromatic plants. *J. Chem. Ecol.* 26, 2035–2048.

Knief, C., Ramette, A., Frances, L., Alonso-Blanco, C., and Vorholt, J. A. (2010). Site and plant species are important determinants of the methylobacterium community composition in the plant phyllosphere. *ISME J.* 4, 719–728. doi: 10.1038/ismej.2010.9

Koskinen, K., Rettberg, P., Pukall, R., Auerbach, A., Wink, L., Barczyk, S., et al. (2017). Microbial biodiversity assessment of the European space agency's ExoMars 2016 mission. *Microbiome* 5:143.

Kovács, G., Burghardt, J., Pradella, S., Schumann, P., Stackebrandt, E., and Màrialigeti, K. (1999). *Kocuria palustris* sp. nov. and *Kocuria rhizophila* sp. nov., isolated from the rhizoplane of the narrow-leaved cattail (*typha angustifolia*). *Int. J. Syst. Evol. Microbiol.* 49, 167–173.

Kuddus, M., and Ramteke, P. W. (2008). Purification and properties of cold-active metalloprotease from *Curtobacterium luteum* and effect of culture conditions on production. *Chin. J. Biotechnol.* 24, 2074–2080.

Lee, J.-J., Lee, Y.-H., Park, S.-J., Lim, S., Jeong, S.-W., Lee, S.-Y., et al. (2016). *Deinococcus seoulensis* sp. nov., a bacterium isolated from sediment at Han river in Seoul, Republic of Korea. *J. Microbiol.* 54, 537–542. doi: 10.1007/s12275-016-6253-y

Leff, J. W., and Fierer, N. (2013). Bacterial communities associated with the surfaces of fresh fruits and vegetables. *PLoS One* 8:e59310. doi: 10.1371/journal.pone.0059310

Lindow, S. E., and Brandl, M. T. (2003). Microbiology of the phyllosphere. *Appl. Environ. Microbiol.* 69, 1875–1883.

Linos, A., Steinbüchel, A., Spröer, C., and Kroppenstedt, R. M. (1999). *Gordonia polyisoprenivorans* sp. nov., a rubber-degrading actinomycete isolated from an automobile tyre. *Int. J. Syst. Evol. Microbiol.* 49, 1785–1791.

Liu, H., Xu, Y., Ma, Y., and Zhou, P. (2000). Characterization of *Micrococcus antarcticus* sp. nov., a psychrophilic bacterium from Antarctica. *Int. J. Syst. Evol. Microbiol.* 50, 715–719. doi: 10.1099/00207713-50-2-715

Liu, Y., Du, J., Lai, Q., Zeng, R., Ye, D., Xu, J., et al. (2017). Proposal of nine novel species of the *Bacillus cereus* group. *Int. J. Syst. Evol. Microbiol.* 67, 2499–2508. doi: 10.1099/ijsem.0.001821

Lopez-Galvez, F., Allende, A., Pedrero-Salcedo, F., Alarcon, J. J., and Gil, M. I. (2014). Safety assessment of greenhouse hydroponic tomatoes irrigated with reclaimed and surface water. *Int. J. Food Microbiol.* 191, 97–102. doi: 10.1016/j.ijfoodmicro.2014.09.004

Miller, R. A., Beno, S. M., Kent, D. J., Carroll, L. M., Martin, N. H., Boor, K. J., et al. (2016). *Bacillus wiedmannii* sp. nov., a psychrotolerant and cytotoxic *Bacillus cereus* group species isolated from dairy foods and dairy environments. *Int. J. Syst. Evol. Microbiol.* 66, 4744–4753. doi: 10.1099/ijsem.0.001421

Miwa, H., Ahmed, I., Yoon, J., Yokota, A., and Fujiwara, T. (2008). *Variovorax boronicumulans* sp. nov., a boron-accumulating bacterium isolated from soil. *Int. J. Syst. Evol. Microbiol.* 58, 286–289. doi: 10.1099/ijs.0.65315-0

Mora, M., Perras, A., Alekhova, T. A., Wink, L., Krause, R., Aleksandrova, A., et al. (2016). Resilient microorganisms in dust samples of the international space station – survival of the adaptation specialists. *Microbiome* 4:65. doi: 10.1186/s40168-016-0217-7

Mora, M., Wink, L., Kögler, I., Mahnert, A., Rettberg, P., Schwendner, P., et al. (2019). Space station conditions are selective but do not alter microbial characteristics relevant to human health. *Nat. Commun.* 10:3990.

Morris, C. E., Monier, J.-M., and Jacques, M.-A. (1998). A technique to quantify the population size and composition of the biofilm component in communities of bacteria in the phyllosphere. *Appl. Environ. Microbiol.* 64, 4789–4795.

Nir, I. (1981). "Growing plants in aeroponics growth system," in *Proceedings of the Symposium on Substrates in Horticulture other than Soils In Situ*: Acta Horticulturae, Vol. 126, Leuven, 435–448. doi: 10.1093/aob/mcs275

Panday, D., Schumann, P., and Das, S. K. (2011). *Rhizobium pusense* sp. nov., isolated from the rhizosphere of chickpea (*Cicer arietinum l.*). *Int. J. Syst. Evol. Microbiol.* 61, 2632–2639. doi: 10.1099/ijs.0.028407-0

Pantucek, R., Sedlacek, I., Indrakova, A., Vrbovska, V., Maslanova, I., Kovarovic, V., et al. (2018). *Staphylococcus edaphicus* sp nov., isolated in Antarctica, harbors the mecc gene and genomic islands with a suspected role in adaptation to extreme environments. *Appl. Environ. Microbiol.* 84:e01746-17. doi: 10.1128/AEM.01746-17

Pearce, D. A., Bridge, P. D., Hughes, K. A., Sattler, B., Psenner, R., and Russell, N. J. (2009). Microorganisms in the atmosphere over Antarctica. *FEMS Microbiol. Ecol.* 69, 143–157. doi: 10.1111/j.1574-6941.2009.00706.x

Perchonok, M. H., Cooper, M. R., and Catauro, P. M. (2012). Mission to mars: food production and processing for the final frontier. *Annu. Rev. Food. Sci. Technol.* 3, 311–330. doi: 10.1146/annurev-food-022811-101222

Quast, C., Pruesse, E., Yilmaz, P., Gerken, J., Schweer, T., Yarza, P., et al. (2013). The SILVA ribosomal RNA gene database project: improved data processing and web-based tools. *Nucleic Acids Res.* 41, D590–D596. doi: 10.1093/nar/gks1219

Reidt, U., Helwig, A., Plobner, L., Lugmay, R. V., Treutlein, U., Kharin, S., et al. (2014). Study of initial colonization by environmental microorganisms in the Russian segment of the international space station (ISS). *Gravit. Space Res.* 2, 46–57.

Sammer, U. F., and Reiher, K. (2012). *Curtobacterium flaccumfaciens* pv. *flaccumfaciens* on soybean in Germany – a threat for farming. *J. Phytopathol.* 160, 314–316.

Schlacht, I. L., Kolrep, H., Daniel, S., and Musso, G. (2019). "Impact of plants in isolation: the EDEN ISS human factors investigation in Antarctica," in *Proceedings of the International Conference on Applied Human Factors and Ergonomics, July 24-28 2019*, Washington, DC, 794–806.

Schloss, P. D., Westcott, S. L., Ryabin, T., Hall, J. R., Hartmann, M., Hollister, et al. (2009). Introducing mothur: open-source, platform-independent, community-supported software for describing and comparing microbial communities. *Appl. Environ. Microbiol.* 75, 7537–7541. doi: 10.1128/AEM.01541-09

Schulze-Lefert, P., and Robatzek, S. (2006). Plant pathogens trick guard cells into opening the gates. *Cell* 126, 831–834.

Schwendner, P., Mahnert, A., Koskinen, K., Moissl-Eichinger, C., Barczyk, S., Wirth, R., et al. (2017). Preparing for the crewed Mars journey: microbiota dynamics in the confined Mars500 habitat during simulated mars flight and landing. *Microbiome* 5:129. doi: 10.1186/s40168-017-0345-8

von Neubeck, M., Huptas, C., Glück, C., Krewinkel, M., Stoeckel, M., Stressler, T., et al. (2017). *Pseudomonas lactis* sp. nov. and *Pseudomonas paralactis* sp. nov., isolated from bovine raw milk. *Int. J. Syst. Evol. Microbiol.* 67, 1656–1664. doi: 10.1099/ijsem.0.001836

Vorholt, J. A. (2012). Microbial life in the phyllosphere. *Nature Rev. Microbiol.* 10, 828–840.

Waechter-Kristensen, B., Caspersen, S., Adalsteinsson, S., Sundin, P., and Jensen, P. (1997). "Organic compounds and micro-organisms in closed, hydroponic culture: occurrence and effects on plant growth and mineral nutrition," in *Proceedings of the International Symposium on Growing media and Hydroponics 481, Windsor, Canada, May 19-26 1997*, Windsor, 197–204.

Waksman, S. A. (1922). A method for counting the number of fungi in the soil. *J. Bacteriol.* 7, 339–341.

Yokota, A., Takeuchi, M., Sakane, T., and Weiss, N. (1993). Proposal of six new species in the genus *Aureobacterium* and transfer of *Flavobacterium*

esteraromaticum omelianski to the genus *Aureobacterium* as *Aureobacterium esteraromaticum* comb. nov. *Int. J. Syst. Evol. Microbiol.* 43, 555–564.

Yoon, J.-H., Lee, H. B., Yeo, S.-H., and Choi, J.-E. (2004). *Janibacter melonis* sp. nov., isolated from abnormally spoiled oriental melon in Korea. *Int. J. Syst. Evol. Microbiol.* 54, 1975–1980.

Zabel, P., Bamsey, M., Zeidler, C., Vrakking, V., Johannes, B.-W., Rettberg, P., et al. (2015). "Introducing EDEN-ISS – a European project on advancing plant cultivation technologies and operations," in *Proceedings of the 45th International Conference on Environmental Systems, 12-16 July 2015*, Bellevue, WA.

Zagory, D. (1999). Effects of post-processing handling and packaging on microbial populations. *Postharvest Biol. Technol.* 15, 313–321.

Zeidler, C., Zabel, P., Vrakking, V., Dorn, M., Bamsey, M., Schubert, D., et al. (2019). The plant health monitoring system of the EDEN ISS space greenhouse in Antarctica during the 2018 experiment phase. *Front. Plant Sci.* 10:1457. doi: 10.3389/fpls.2019.01457

Zheng, Z., Zheng, J., Liu, H., Peng, D., and Sun, M. (2016). Complete genome sequence of *Fictibacillus phosphorivorans* g25-29, a strain toxic to nematodes. *J. Biotechnol.* 239, 20–22. doi: 10.1016/j.jbiotec.2016.09.014

Conflict of Interest: The authors declare that the research was conducted in the absence of any commercial or financial relationships that could be construed as a potential conflict of interest.

frontiers in Microbiology

ORIGINAL RESEARCH
published: 03 April 2020
doi: 10.3389/fmicb.2020.00560

Aspergillus niger Spores Are Highly Resistant to Space Radiation

Marta Cortesão[1], Aram de Haas[1], Rebecca Unterbusch[1], Akira Fujimori[2], Tabea Schütze[3], Vera Meyer[3] and Ralf Moeller[1]*

[1] Space Microbiology Research Group, Radiation Biology Department, Institute of Aerospace Medicine, German Aerospace Center, Cologne, Germany, [2] Department of Basic Medical Sciences for Radiation Damages, National Institutes for Quantum and Radiological Science and Technology, Chiba, Japan, [3] Chair of Applied and Molecular Microbiology, Institute of Biotechnology, Technische Universität Berlin, Berlin, Germany

The filamentous fungus *Aspergillus niger* is one of the main contaminants of the International Space Station (ISS). It forms highly pigmented, airborne spores that have thick cell walls and low metabolic activity, enabling them to withstand harsh conditions and colonize spacecraft surfaces. Whether *A. niger* spores are resistant to space radiation, and to what extent, is not yet known. In this study, spore suspensions of a wild-type and three mutant strains (with defects in pigmentation, DNA repair, and polar growth control) were exposed to X-rays, cosmic radiation (helium- and iron-ions) and UV-C (254 nm). To assess the level of resistance and survival limits of fungal spores in a long-term interplanetary mission scenario, we tested radiation doses up to 1000 Gy and 4000 J/m^2. For comparison, a 360-day round-trip to Mars yields a dose of 0.66 ± 0.12 Gy. Overall, wild-type spores of *A. niger* were able to withstand high doses of X-ray (LD_{90} = 360 Gy) and cosmic radiation (helium-ion LD_{90} = 500 Gy; and iron-ion LD_{90} = 100 Gy). Drying the spores before irradiation made them more susceptible toward X-ray radiation. Notably, *A. niger* spores are highly resistant to UV-C radiation (LD_{90} = 1038 J/m^2), which is significantly higher than that of other radiation-resistant microorganisms (e.g., *Deinococcus radiodurans*). In all strains, UV-C treated spores (1000 J/m^2) were shown to have decreased biofilm formation (81% reduction in wild-type spores). This study suggests that *A. niger* spores might not be easily inactivated by exposure to space radiation alone and that current planetary protection guidelines should be revisited, considering the high resistance of fungal spores.

Keywords: *Aspergillus niger*, *A. niger* spores, spore survival, space, radiation, X-ray, UV, international space station

OPEN ACCESS

Edited by:
André Antunes, Macau University of Science and Technology, China

Reviewed by:
Douglas Galante, National Center for Research in Energy and Materials (CNPEM), Brazil
Marta Filipa Simões, Macau University of Science and Technology, China

****Correspondence:***
Marta Cortesão
marta.cortesao@dlr.de

Specialty section:
This article was submitted to Extreme Microbiology, a section of the journal Frontiers in Microbiology

Received: *21 January 2020*
Accepted: *16 March 2020*
Published: *03 April 2020*

Citation:
Cortesão M, de Haas A, Unterbusch R, Fujimori A, Schütze T, Meyer V and Moeller R (2020) Aspergillus niger Spores Are Highly Resistant to Space Radiation. Front. Microbiol. 11:560. doi: 10.3389/fmicb.2020.00560

INTRODUCTION

Radiation is the most challenging factor for life in the space environment (Horneck et al., 2010; Chancellor et al., 2014). On the one hand, the Sun emits UV radiation (non-ionizing), X-rays (ionizing electromagnetic waves) and solar flares (intense bursts of high-energy ionizing radiation) (Sliney, 2007). On the other hand, cosmic events such as supernova explosions or pulsars, emit

galactic cosmic radiation (GCR) (Chancellor et al., 2018). GCR particle spectrum spans from light particles, such as hydrogen-ions (85%) and helium-ions (He, 14%), to high charge Z and energy particles (HZE) like iron-ions (Fe, 0.03%) (Horneck et al., 2010). Radiation shielding on the International Space Station (ISS) is provided by both the Earth's magnetosphere and the walls of the space station. However, not all types of radiation are easily shielded. For instance, HZE particles are still capable of penetrating current space vehicles (Chancellor et al., 2018). Protecting living systems from radiation becomes particularly challenging beyond low Earth orbit (LEO). Due to the absence of Earth's magnetosphere, space missions toward the Moon or Mars will be exposed to substantially higher radiation doses than those currently experienced on the ISS (Cucinotta et al., 2013; Chancellor et al., 2014, 2018; Narici et al., 2017). Studies on how radiation affects cells have identified two main types of damage: direct and indirect. Direct damage targets DNA (e.g., single- or double-strand breaks), proteins, or lipids. Whereas indirect damage is induced by the generation of reactive oxygen species (ROS) – which are produced by the interaction of radiation with cellular water molecules in a process called radiolysis (Cadet et al., 2015; Moeller et al., 2017).

Regardless of the damage, many microorganisms, especially spore formers, are able to withstand high radiation doses (Horneck et al., 2010; Moeller et al., 2010). Spores of the bacterium *Bacillus subtilis* are known to be highly resistant to extreme space conditions and therefore are currently being used as indicators for decontamination protocols and planetary protection policies (Kminek et al., 2019). However, while survival of bacterial spores has been extensively studied in both Earth and spaceflight contexts (Moeller et al., 2014; Setlow, 2014; Khodadad et al., 2017), survival of fungal spores has not. Samples from the ISS indoor microbiome identified *Aspergillus niger* as one of the most common fungal contaminants (Novikova et al., 2006; Checinska et al., 2015). Contrary to *B. subtilis* spores, which are formed as a response to stressful conditions, asexual spores of *A. niger* (i.e., conidia) are produced as a natural part of its life cycle (Krijgsheld et al., 2013). *A. niger* spores are highly pigmented and can be easily dispersed through the air which facilitates habitat colonization. Also, as an opportunistic human pathogen, inhalation of *A. niger* spores can lead to human respiratory infections (Silverman et al., 1967; Latgé, 1999; Esbelin et al., 2013). Thus, the ability of *A. niger* to survive and grow in the spaceflight environment is a potential threat to both astronaut health and spacecraft safety. Nonetheless, *A. niger* is also a well-established cell factory used in modern-day biotechnology to produce various compounds such as proteins, enzymes, and pharmaceuticals (Meyer et al., 2015; Cairns et al., 2018). This makes *A. niger* a potential asset in long-term space missions, where astronauts will have to produce their own compounds of interest such as vitamins or antibiotics (Cortesão et al., 2020).

Despite the relevance of *A. niger* spores in the space context, it is not yet known whether they are able to withstand extreme space radiation conditions. Fungal spore survival generally depends on two main components. One is the spore cell wall, which helps to prevent radiation damage on the DNA. The spore cell wall is composed of polysaccharides (mainly chitin and glucans), and is covered by an outer layer of rodlets (hydrophobins) and pigments (e.g., melanin). These outer layers of the cell wall make spores highly hydrophobic and highly pigmented (Beauvais et al., 2014). Pigments, such as melanin, are known to be involved in different cellular processes, from adhesion to virulence, as well as to protect cells from radiation-induced stress and ROS (Cockell and Knowland, 1999; Eisenman and Casadevall, 2012; Cordero and Casadevall, 2017). Melanized fungi have been reported in Chernobyl sites (Zhdanova et al., 2000; Casadevall et al., 2017), and some were even found displaying increased growth after X-ray irradiation (Dadachova et al., 2007). Previous studies have reported the presence of melanin in *A. niger* spores as an adaptive trait conferring resistance toward UV-A (315–400) (Singaravelan et al., 2008). Moreover, studies on clinical isolates of *Aspergillus fumigatus* reported the involvement of DHN-melanin in UV-C protection. Here, loss of a polyketide synthase from the DHN-melanin pathway (Δ*pksP*) resulted in decreased survival, when exposed to 100 J/m^2. This was not the case for an *A. fumigatus* strain isolated from the ISS, where loss of *pksP* did neither reduce nor increase viability (Blachowicz et al., 2020). However, a recent review emphasizes that pigment biosynthesis in *Aspergillus* species is not yet fully understood (Chang et al., 2020). Pigmentation in *A. niger* is particularly puzzling. The pigment spectrum of *A. niger* spores was shown to have two main absorbance peaks, which together absorb light in the entire VIS-spectrum and thus result in the black color. These are thought to be two distinct components – one green (peak at ∼575 nm), and one brown component (∼425 nm) – and were both shown to be FwnA dependent (Jorgensen et al., 2011). FwnA is an ortholog of pksP, and deletion of the *fwnA* gene (Δ*fwnA*) results in fawn-colored (not white as for *A. fumigatus*) spores. Knowing if and how pigmentation is involved in spore resistance will be crucial to understand the limits of spore survival, which will, in turn, help develop adequate decontamination approaches. Another important component in fungal spore resistance is DNA repair. When damage occurs, several pathways can be activated: nucleotide excision repair (NER), mismatch repair (MMR), homologous recombination (HR), or non-homologous end-joining (NHEJ) recombination (Sinha and Hader, 2002). *A. niger* strains deficient in NHEJ (Δ*kusA*) are widely used to generate mutant strains, but it was also shown that these strains are more sensitive to UV and X-ray irradiation (Meyer et al., 2007).

When considering fungal contamination in indoor habitats, the ability to colonize is not only dependent on spore survival, but also on the ability for spores to adhere to a surface, germinate, and grow. Germination and hyphal growth are established through polarized growth (Kwon et al., 2011, 2013). In *A. niger*, the stabilization of polarity axes during germination is dependent on the Rho GTPase RacA. A *racA* deletion displays a hyperbranching phenotype which results in compact colonies (Kwon et al., 2011). Spore adhesion to surfaces is facilitated by proteins in the cell wall that help fungi to grow on a wide-range of substrates (e.g., from quartz used on

windows to silicone and polycarbonate used in medical/scientific instruments) (Makimura et al., 2001; Mora et al., 2016, 2019). Furthermore, fungal growth is surface-associated, which can induce biocorrosion. In fact, fungal-induced biocorrosion has led to major problems in spacecraft safety such as those in the Mir space station (Klintworth and Reher, 1999; Novikova et al., 2006). Understanding whether polar growth impacts spore revival and subsequent surface-associated growth is important to better control fungal contamination in the spaceflight context.

For these reasons, understanding whether *A. niger* spores resist to space radiation, and to what extent, will be crucial to assess both the risks and opportunities of fungal spore survival during space travel. This study has assessed *A. niger* spore survival to different types of space radiation (X-rays, cosmic radiation, and UV-C). Three mutant strains were included to elucidate the role of pigmentation (Δ*fwnA*) and DNA repair (Δ*kusA*) on spore resistance to radiation. In addition, high radiation doses were tested to assess the limits of resistance of fungal spores and their survival potential during long-term space travel. In addition, a fourth strain deficient in polar growth (Δ*racA*) was tested to assess the impact of UV-C treatment in spore revival and consequent ability for surface colonization.

MATERIALS AND METHODS

Strains and Media

Aspergillus niger wild-type (N402) and three mutant strains with defects in pigmentation (Δ*fnwA)*, DNA repair (Δ*kusA*), and polar growth control (Δ*racA*), were used in this study and are listed in **Table 1**. *A. niger* spores were harvested from 3-day-old cultures incubated on complete medium (CM) at 30°C [55 mM glucose, 11 mM KH_2PO_4, 7 mM KCl, 178 nM H_3BO_3, 2 mM $MgSO_4$, 76 nM $ZnSO_4$, 70 mM $NaNO_3$, 6.2 nM Na_2MoO_4, 18 nM $FeSO_4$, 7.1 nM $CoCl_2$, 6.4 nM $CuSO_4$, 25 nM $MnCl_2$, 174 nM EDTA, 0.5% (w/v) yeast extract and 0.1% (w/v) casamino acids] by flooding the agar plates with saline solution (0.9% NaCl) and harvesting the spores using a cotton stick. Spore suspensions were filtered using Miracloth (Millipore) to remove hyphal fragments and were kept at 4°C. Counting was done using a Neubauer chamber. All experiments were performed with spore suspensions not older than 2 weeks. Viability assays were done using minimal medium (MM) [55 mM glucose, 11 mM KH_2PO_4, 7 mM KCl, 178 nM H_3BO_3, 2 mM $MgSO_4$, 76 nM $ZnSO_4$, 70 mM $NaNO_3$, 6.2 nM Na_2MoO_4, 18 nM $FeSO_4$, 7.1 nM $CoCl_2$, 6.4 nM $CuSO_4$, 25 nM $MnCl_2$, 174 nM EDTA]. For MM or CM agar plates, 15 g agar was added per liter (adapted from Carvalho et al., 2010).

X-Ray Radiation Exposure

Spores of *A. niger* strains were exposed to X-ray radiation in PCR tubes (Brand), each filled with 100 μl of saline solution (0.9% NaCl) at a concentration of 10^7 spores/ml. This concentration was chosen after testing the effect of initial spore concentration (inoculum) on survivability toward X-rays (**Supplementary Figure 1**). Radiation exposure was performed using the RS225 X-ray machine (Gulmay Medical Systems, Camberley, Surrey, United Kingdom) operated without filter at 200 kV and 15 mA which allowed exposure of high doses in a short amount of time. Dose rate, in Gy/min, was determined using the UNIDOS webline with an ionization chamber type TM30013 (PTW, Freiburg, Germany). For each desired dose, the sample exposure time was adjusted given that distance and dose rate were kept constant. X-ray exposure time was calculated as follows:

$$t\ (\text{min}) = \frac{R\ (\text{Gy})}{d\ (\text{Gy/min})}$$

where t = time (in minutes); R = desired radiation dose (in Gy), d (dosimeter value in Gy/min). Samples were exposed to 50, 100, 250, 500, and 1000 Gy. Given that the average dose rate was ∼20 Gy/min, the maximum time a sample was exposed to X-ray radiation was 50 min (corresponding to 1000 Gy). To test irradiation of dried spores, 25 μl of a spore suspension (to a total of 10^7 spores per PCR tube) either in water (H_2O) or in saline solution (0.9% NaCl) was placed in PCR tubes, which were left to air-dry overnight on the bench (22°C) before irradiation. After irradiation, the spores were suspended in 100 μl of water (H_2O) or saline solution (0.9% NaCl). Radiation exposure included at least three biological replicates per strain and was performed two independent times (n = 6). Viability was determined by colony forming units (CFUs) (see section "Viability Assay").

Cosmic Radiation Exposure

Spores were exposed to helium- and iron-ions (two components of cosmic radiation) in PCR tubes (Brand) each filled with 100 μl of saline solution (0.9% NaCl) at a concentration of 10^7 spores/ml. PCR tubes were placed inside Petri dishes stacked together inside plastic bags and placed directly facing the ion beam. Samples were exposed to 10, 100, 250, and 500 Gy. Non-irradiated controls were left at room temperature. Viability was calculated by CFU (see section "Viability Assay"). Radiation exposure included three biological replicates per strain (n = 3). Cosmic radiation exposure was performed at the Heavy Ion Medical Accelerator (HIMAC) facility at the National Institute of Radiological Sciences (NIRS) in Chiba, Japan. The helium-ion beam had an energy of 150 MeV/n and linear energy transfer (LET) of 2.2 keV/μm. The iron-ion beam had an energy of 500 MeV/n and LET of 200 keV/μm. Each tested dose was adjusted by exposure time, since beam energy and LET was kept constant.

UV-C Radiation Exposure

Spores of *A. niger* were exposed to UV radiation in Petri dishes with an initial concentration of 10^6 spores/ml in 15 ml of saline solution (0.9% NaCl). The concentration of 10^6 spores/ml ensures a spore monolayer and prevents survival due to shielding by the spores themselves. The UV lamp (MagneTel, Menomonee Falls, WI, United States) was used a UV-C monochromatic wavelength of 254 nm. During irradiation, magnetic stirrers continuously mixed the spore suspension in order to avoid

TABLE 1 | *Aspergillus niger* strains used in the study.

Name	Strain	Relevant genotype	Description	References
Wild-type	N402		Wild-type strain capable of DNA repair and pigment formation which give black-colored spores	Bos et al., 1988
Color mutant	MA93.1	Δ*fwnA*	Loss of pigment, due to lack of polyketide synthase results in fawn-colored spores	Jorgensen et al., 2011
NHEJ mutant	MA78.6	Δ*kusA*	Inactive in NHEJ pathway and thus impaired in DNA repair	Meyer et al., 2007
Polar growth mutant	MA80.1	Δ*kusA*, Δ*racA*	Inactive in NHEJ pathway and polar growth control	Kwon et al., 2011

mutual shielding of the spores. The radiation dose [J/m^2] was adjusted through exposure time, since the height of the UV lamp was kept constant. For that, UV fluence was determined using the dosimeter (UVP UVX radiometer), and exposure time was adjusted for each sample to reach each desired UV dose (i.e., 150, 250, 500, 1000, 2000, 3000, and 4000 J/m^2). UV-C exposure time was calculated as follows:

$$t\ (\mathrm{s}) = \frac{R\ (\mathrm{J/m^2}) \times 100}{d\ (\mu\mathrm{W/cm^2})}$$

where t = time (in seconds); R = desired radiation dose (in J/m^2), d (dosimeter value for UV fluence, in $\mu W/cm^2$). After each time point, corresponding to a certain dose, 100 μl of sample were taken in triplicate from the spore suspension and transferred into PCR tubes. Viability was calculated by CFU (see section "Viability Assay"). Radiation exposure included at least three biological replicates per strain and was performed two independent times ($n = 6$).

Oxidative Stress Assay

Oxidative stress resistance toward hydrogen peroxide (H_2O_2) was measured using a protocol adapted from Riesenman and Nicholson (2000). Spores of *A. niger* were diluted to a final concentration of 10^8 spores/ml in saline solution (0.9% NaCl), 833 μl of which were placed in a 5 ml tube (Eppendorf). Afterward 167 μl of 30% H_2O_2 were added (Sigma-Aldrich). The spore-H_2O_2 suspension was gently mixed at RT (∼22°C) and incubated for up to 15 min in a final concentration of 5% H_2O_2. 30 μl of the suspension were taken at different time points and diluted 1:10 in saline solution (0.9% NaCl) with bovine catalase (100 μg/ml) to stop the oxidation reaction. Samples were serially diluted and used to determine viability (see section "Viability Assay"). This assay included three biological replicates per tested strain, and was performed two independent times ($n = 6$).

Viability Assay

Viability of *A. niger* spores was determined by their ability to form colonies after exposure to the tested environments. Samples were serially diluted up to 10^{-8} using a 96-well plate, each well with a total volume of 300 μl. To count the CFUs, 20 μl of each dilution was plated out in triplicate on 1/8 of a Petri dish with MM agar, containing Triton X-100 (0.05%) to facilitate counting. The plates were incubated for 2 days at 30°C before the colonies were counted. This allowed calculation of the survival fraction ratio (N/N0, in which N is the number of CFU of the treated samples and N0 that of the controls). To analyze the microscopic morphology, previously irradiated samples were diluted 100-fold before plating 10 μl on a MM agar plate. These were incubated for 1 day at 30°C, after which a Zeiss microscope (Axio Imager.M2) was used to take images of representative areas on the agar plate for further analysis (**Supplementary Figure 2**). Viability assays included three biological replicates per tested strain and were performed at two independent times ($n = 6$).

Crystal Violet Assay

To assess fungal biofilm formation, i.e., surface-associated growth with production of extracellular matrix, a crystal violet assay was performed, adapted from Mowat et al. (2007). In a 96-well plate each well contained 100 μl spore suspension (to a total concentration of 10^5 spores/ml per well), 100 μl MM, and 100 μl of distilled H_2O (dH_2O) (the controls contained an additional 100 μl MM instead of 100 μl spore suspension) and were incubated for 48 h at 30°C. After incubation, the wells were washed three times with dH_2O, and 300 μl of crystal violet (0.5%) were added to each well to stain the surface-associated biomass (crystal violet stains hyphae and extracellular matrix that do not detach after washing). Excess staining was removed by washing with dH_2O. De-staining was carried out by adding 300 μl of 95% ethanol. The absorbance of the ethanol-crystal violet solution was measured at 570 nm. The higher the absorbance value the greater the quantity of biological material. The absorbance was evaluated using the VICTOR Nivo Multimode Microplate Reader (PerkinElmer, Waltham, MA, United States). The assay included eight biological replicates per tested strain and was performed twice ($n = 16$).

Data Analysis

Student's *t*-test was performed to analyze the significance between individual data points where a two-tailed p-value ≤ 0.05, was considered significant. Error bars as standard error. Linear regression on survival fraction data was used to calculate the lethal dose for 90% of the population (LD_{90} values) – which is the same as D_{10} values (10% survivability).

RESULTS

Aspergillus niger Spore Resistance Toward X-Ray Radiation

Spores from the wild-type, color mutant (Δ*fwnA)* and NHEJ mutant (Δ*kusA*) strains were exposed to different X-ray doses

TABLE 2 | Lethal dose (LD_{90}) values for *Aspergillus niger* spores irradiated with X-rays under different space-relevant conditions.

Strain	0.9% NaCl	H_2O	Air-dried (0.9% NaCl)	Air-dried (H_2O)
Wild-type	366 (R^2 = 0.97)	362 (R^2 = 0.96)	187 (R^2 = 0.99)	204 (R^2 = 0.99)
Color mutant (Δ*fwnA*)	353 (R^2 = 0.98)	306 (R^2 = 0.99)	175 (R^2 = 0.99)	185 (R^2 = 0.99)
NHEJ mutant (Δ*kusA*)	57 (R^2 = 0.93)	55 (R^2 = 0.92)	35 (R^2 = 0.99)	45 (R^2 = 0.95)

Data reported as LD_{90} values – dose of radiation treatment leading to a 90% inactivation of the initial CFU (same as D_{10} values). Values in Gray (Gy).

TABLE 3 | Lethal dose (LD_{90}) values for *Aspergillus niger* spores irradiated with different types of ionizing radiation.

Strain	X-rays (Gy)	Helium-ion (Gy)	Iron-ion (Gy)
Wild-type	366 (R^2 = 0. 97)	506 (R^2 = 0.98)	112 (R^2 = 0.99)
Color mutant (Δ*fwnA*)	353 (R^2 = 0.98)	567 (R^2 = 0.96)	112 (R^2 = 0.99)
NHEJ mutant (Δ*kusA*)	57 (R^2 = 0.93)	55 (R^2 = 0.99)	50 (R^2 = 0.99)

Data reported as LD_{90} values – dose of radiation treatment leading to a 90% inactivation of the initial CFU (same as D_{10} values).

(up to 1000 Gy) in saline solution. The lethal dose required to inactivate 90% of the spores was similar for both wild-type (LD_{90} = 366 Gy) and Δ*fwnA* strains (LD_{90} = 353 Gy). After the maximum tested radiation dose of 1000 Gy, the Δ*fwnA* strain demonstrated no significant differences in survival when compared with the wild-type ($5.3 \times 10^3 \pm 1.3 \times 10^3$ CFU/ml, versus $1 \times 10^4 \pm 3.2 \times 10^3$ CFU/ml). In contrast, at 500 Gy, Δ*kusA* was shown to be significantly more sensitive to X-ray radiation ($1.25 \times 10^4 \pm 1.1 \times 10^3$ CFU/ml with a LD_{90} of 57 Gy), when compared to the wild-type ($5 \times 10^6 \pm 8.7 \times 10^5$ CFU/ml) (p = 0.000). No CFU were detected above 500 Gy for Δ*kusA*. Survivability and LD_{90} values of the strains toward X-ray radiation, in all tested conditions, are shown summarized in **Table 2**.

Air-Drying of *A. niger* Spores Reduces Their Resistance Toward X-Ray Radiation

Survivability of air-dried *A. niger* spores was compared with survivability of wet spores (both in water and saline solution). The highest X-ray dose at which there were detectable colonies was 500 Gy for both wild-type and Δ*fwnA* strains, and 250 Gy for Δ*kusA*. Results show that survivability of dried spores was decreased in comparison to wet spores (both in water and saline solution) in all tested strains (**Figure 1**). At 500 Gy, wild-type spores in water ($4.9 \times 10^6 \pm 1.1 \times 10^6$ CFU/ml) survive better than dried spores from water ($4.6 \times 10^4 \pm 7.2 \times 10^3$ CFU/ml) (p = 0.001). The same is seen for spores in saline solution where wet spores ($5 \times 10^6 \pm 8.7 \times 10^5$ CFU/ml) survived better than dried spores from saline solution ($8.2 \times 10^3 \pm 1.2 \times 10^3$ CFU/m) (p = 0.000) (**Table 2**). When comparing water- versus saline-dried spores, wild-type spores dried from saline solution ($8.2 \times 10^3 \pm 1.2 \times 10^3$ CFU/ml) survive significantly less than spores dried from water ($4.6 \times 10^4 \pm 7.2 \times 10^3$ CFU/ml) (p = 0.000). Loss of pigmentation did not affect resistance to desiccation (0 Gy) (p = 0.6); or radiation resistance (at 500 Gy) when spores were air-dried from saline solution (p = 0.4). However, loss of pigmentation decreased spore survival in irradiated spores dried in water: at 500 Gy, Δ*fwnA* spores were significantly more sensitive ($5.2 \times 10^3 \pm 1.2 \times 10^3$ CFU/ml) than wild-type spores ($4.6 \times 10^4 \pm 7.2 \times 10^3$ CFU/ml) (p = 0.002).

Aspergillus niger Spores Resistance Toward Cosmic Radiation

The effect of cosmic radiation on the survival of *A. niger* was tested by irradiating spores with helium- and iron-ions. Spores from the wild-type, color mutant (Δ*fwnA)* and NHEJ mutant (Δ*kusA*) strains were exposed to up to 500 Gy of helium- and iron-ions. At 500 Gy, wild-type spores survived less when irradiated with iron-ions ($4.7 \times 10^2 \pm 6.01 \times 10^1$ CFU/ml) than when irradiated with X-rays ($5 \times 10^6 \pm 8.7 \times 10^5$ CFU/ml) (p = 0.06), or helium-ions ($8.7 \times 10^6 \pm 1.9 \times 10^6$ CFU/ml) (p = 0.01) (**Table 3**). The same trend holds for Δ*fwnA* spores at 500 Gy, where survival toward iron-ions ($4.3 \times 10^2 \pm 1.9 \times 10^2$ CFU/ml) was decreased in comparison to both X-rays ($3.4 \times 10^6 \pm 5.4 \times 10^5$ CFU/ml) (p = 0.004) and helium-ions ($1.2 \times 10^7 \pm 2.0 \times 10^6$ CFU/ml) (p = 0.004) (**Figures 1**, **2** and **Table 3**). This is consistent with the fact that helium-ions are lighter elements in cosmic radiation whereas iron-ions are heavier particles, which cause greater damage to cells (Cucinotta and Durante, 2006). At 250 Gy, survival of Δ*kusA* spores was significantly reduced when irradiated with iron-ions ($1.9 \times 10^3 \pm 9.9 \times 10^1$ CFU/ml) than when irradiated with X-rays ($4.7 \times 10^2 \pm 6.01 \times 10^1$ CFU/ml) (p = 0.02), with no colony formation being observed above 250 Gy of cosmic radiation (**Figure 2**). Exposure to helium- and iron-ions (cosmic radiation) showed that both wild-type and Δ*kusA* spores were able to germinate after exposure to 250 and 500 Gy, respectively (**Supplementary Figure 2**), suggesting that there is a greater level of resistance if germination would be considered instead of colony forming ability. Since Δ*fwnA* spores do not show reduced resistance toward X-ray radiation (and subsequent ROS) in comparison to the wild-type strain, we tested whether pigmentation is involved in protecting the spore from H_2O_2-induced oxidative-stress by incubating the spores up to 15 min in 5% H_2O_2 (**Figure 3**). Both the wild-type and color mutant strains decreased in survival when incubated with H_2O_2. The survival of Δ*fwnA* spores after 15 min was lower than that of the wild-type, with the LD_{90} value for the

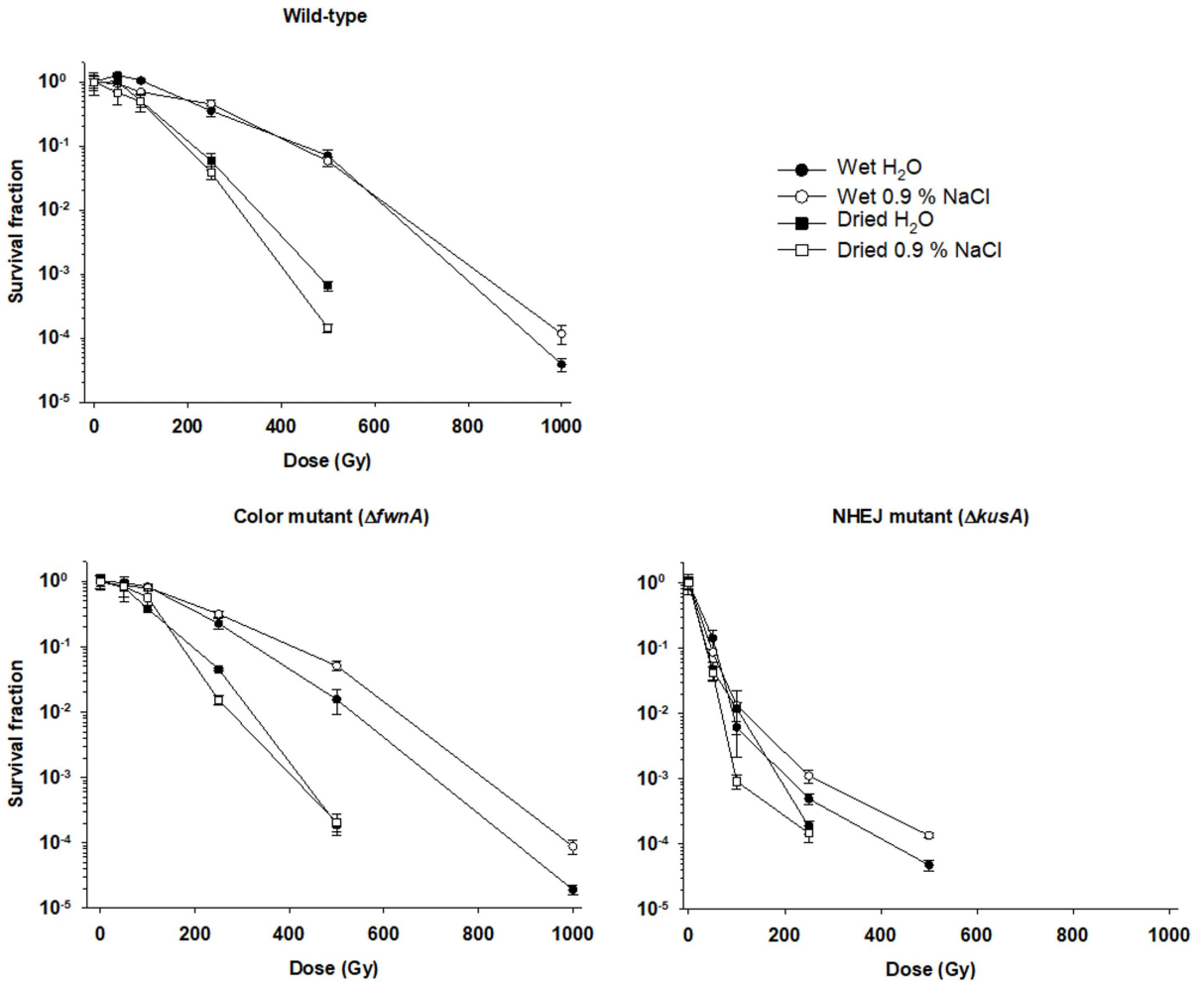

FIGURE 1 | Effect of desiccation in survival to X-ray radiation of spores of different *Aspergillus niger* mutant strains. Spores were irradiated in either liquid suspensions (water or saline solution) or air-dried (from water or from saline solution). Survival fraction was calculated relatively to the non-irradiated controls.

wild-type strain (5 min) being higher than that of the Δ*fwnA* (3.1 min) (**Figure 3**).

Aspergillus niger Spores Are Highly Resistant Toward UV-C Radiation

To investigate the impact of UV radiation on *A. niger* spore survivability, spore suspensions with 10^6 spores/ml (spore monolayer) were exposed to 0–4000 J/m^2 UV-C radiation (254 nm). At the highest tested dose of 4000 J/m^2, both the wild-type ($7.1 \times 10^2 \pm 4.3 \times 10^2$ CFU/ml) and polar growth mutant ($4.2 \times 10^1 \pm 2.5 \times 10^1$ CFU/ml) demonstrated high survival (**Figure 4**). No CFU were detected for Δ*kusA* at 4000 J/m^2. All tested strains were able to cope with 3000 J/m^2 of UV-C exposure. At 3000 J/m^2 wild-type spores ($1.3 \times 10^3 \pm 6.8 \times 10^2$ CFU/ml) and Δ*racA* spores ($2.3 \times 10^2 \pm 1.3 \times 10^2$ CFU/ml) displayed high survivability; whereas Δ*fwnA* spores ($6.3 \times 10^1 \pm 3.7 \times 10^1$ CFU/ml) and Δ*kusA* spores ($1.2 \times 10^2 \pm 0.1 \times 10^1$ CFU/ml) displayed low survivability. The UV-C dose required to eliminate 90% of the wild-type spores (LD_{90}) was 1038 J/m^2. LD_{90} of Δ*racA* spores was 826 J/m^2, of Δ*kusA* spores was 580 J/m^2, and for Δ*fwnA* spores it was 512 J/m^2. The data also shows that deletion of *racA* increases survival toward UV-C (**Figure 4**), in all tested doses.

Defect in Both NHEJ and Polar Growth Decreases *A. niger* Biofilm Formation

When assessing *A. niger* biofilm formation (quantified as amount of surface-adhered biomass detected in the well after washing), a defect in pigmentation (Δ*fwnA*) decreased biofilm formation by 23% ($p = 0.02$); a defect in the NHEJ pathway (Δ*kusA*) decreased biofilm formation by 25% ($p = 0.01$); and a defect in both NHEJ and polar growth (Δ*kusA*, Δ*racA*) showed a decrease of 49% ($p = 0.007$) (**Figure 5B**). When assessing the effect of UV-C radiation in wild-type biofilm formation, we found that biomass decreased as doses increased up to 4000 J/m^2 (**Figure 5A**). Thus, because the UV-C LD_{90} value for wild-type spores was 1000 J/m^2, we tested biofilm formation after treatment with 1000 J/m^2 UV-C for all strains. UV-C treatment led to 81% reduction in biofilm

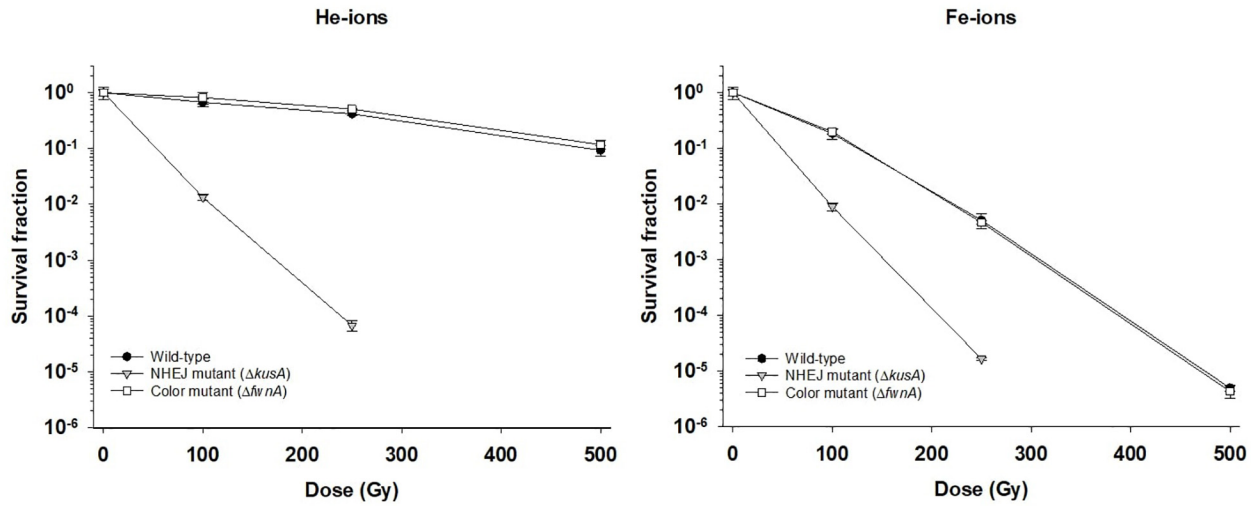

FIGURE 2 | Effect of cosmic radiation (helium-ions – left; and iron-ions – right) on survival of spores of different *Aspergillus niger* strains. Survival fraction was calculated relatively to the non-irradiated controls.

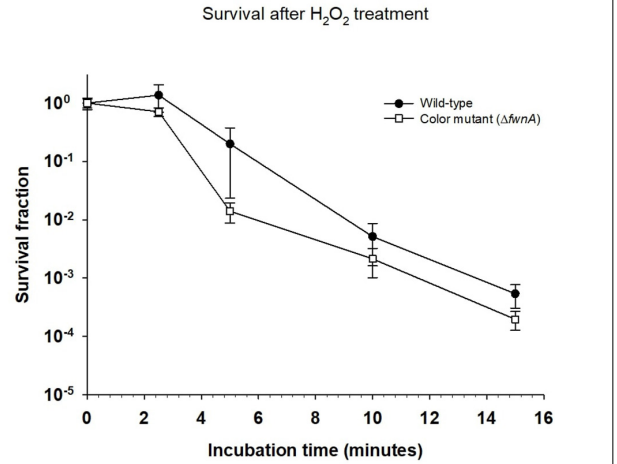

FIGURE 3 | Effect of incubation with H_2O_2 on *Aspergillus niger* spore survival. Survival fraction was calculated relative to the non-treated (0 min) samples.

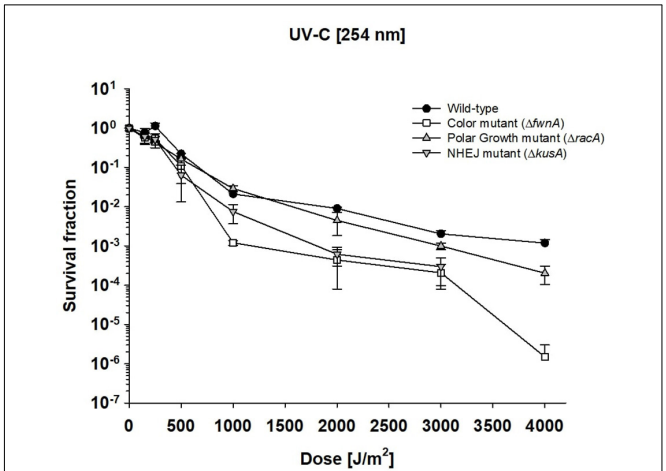

FIGURE 4 | Effect of UV-C radiation in survival of *Aspergillus niger* spores. Survival fraction was calculated relative to the non-irradiated control samples. Error bars as standard error.

formation for wild-type spores (p = 0.04), 97% reduction in Δ*fnwA* spores, (p = 0.001), 82% in Δ*kusA* spores (p = 0.001), and 94% in Δ*racA*Δ*kusA* spores, (p = 0.005) (**Figure 5B**).

DISCUSSION

Air Drying *A. niger* Spores Reduces Their Resistance Toward X-Ray Radiation

Spore survival toward X-rays was tested in both air-dried and liquid conditions (a comparison is provided in **Table 4**). Results show that air-dried spores have lower survival rates than spores irradiated in liquid suspension (either in water, or in saline solution) (**Figure 1**). This result is unexpected, as the presence of water is known to decrease radiation resistance via ROS formation. Nevertheless, *A. niger* spores have previously been shown to have increased radiation sensitivity when vacuum-dried and irradiated in air compared to wet spores irradiated in air (Silverman et al., 1967). However, the same study reported that vacuum-dried spores irradiated in vacuum were found to be more resistant to radiation, which implies that space vacuum desiccation might increase *A. niger* spore resilience (Silverman et al., 1967). Interestingly, a study assessing the impact of water in radiation resistance of yeast reports that small amounts of water substantially increases radiation sensitivity (Hutchinson et al., 1957). Thus, we consider the possibility that drying the spores overnight might have not been enough to retrieve all water from the spore suspension.

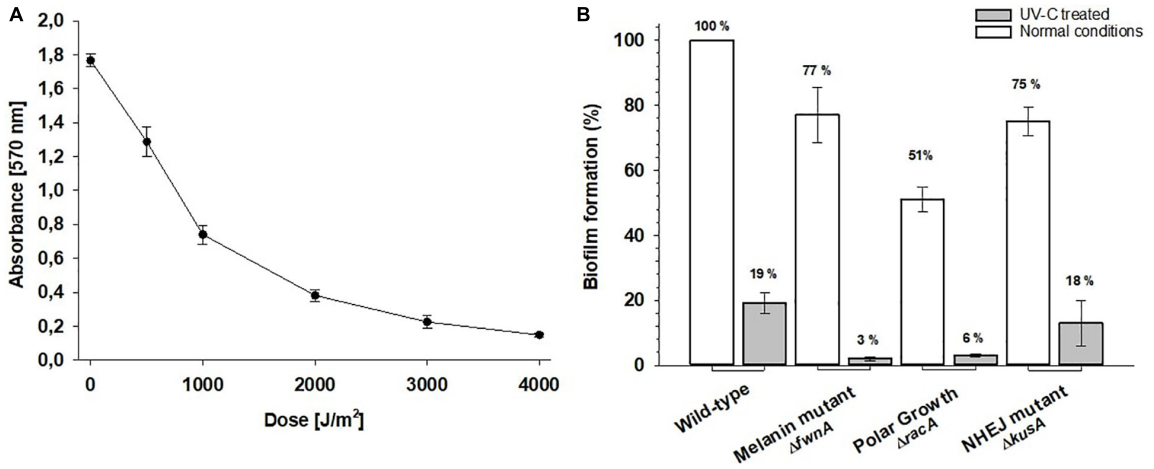

FIGURE 5 | (A) Biofilm formation of *Aspergillus niger* wild-type after 0 to 4000 J/m^2 UV-C (254 nm). Absorbance values are proportional to the amount of detected biomass. **(B)** Effect of UV-C treatment on *A. niger* biofilm formation. The biofilm formation is shown for normal conditions (white bars) and after treatment with 1000 J/m^2 UV-C (gray bars).

TABLE 4 | Lethal dose (LD_{90}) values for *Aspergillus niger* spores in comparison to different organisms in response to UV-C radiation (254 nm) and X-ray radiation. Values for cells/spores in suspension (wet), irradiated in air.

Strain	UV-C (J/m^2)	References	X-rays (Gy)	References
Aspergillus niger (spores)	1038	This study	366	This study
Bacillus subtilis (spores)	100	Newcombe et al., 2005	857	Moeller et al., 2014
Deinococcus radiodurans (cells)	656	Bauermeister et al., 2009	ca. 8000	Moseley and Laser, 1965; Driedger et al., 1970

Data reported as LD_{90} values – dose of radiation treatment leading to a 90% inactivation of the initial CFU (same as D_{10} values).

Additionally, pigmentation did not have an effect on desiccation resistance (at 0 Gy), which is consistent with previous findings concerning the role of pigmentation in fungal survival to low water activity (Segers et al., 2018). When irradiating air-dried spores with 500 Gy, there was no difference between wild-type and color mutant for spores dried in saline. However, the color mutant had increased sensitivity when spores were dried in water. Thus, to fully understand the effect of desiccation (air- or vacuum-induced) on fungal spore resistance to extreme radiation further studies are required.

High-Versus Low-LET Response in *A. niger* Spores

The biological effectiveness of radiation in a given biological sample is dependent on the LET. This means that equal doses of different types of radiation can induce different types of damage, and thus different cellular responses (Moeller et al., 2017). With this, previous studies with animals suggest that indirect damage is the main biological effect of low-LET radiations (such as X-rays or helium-ions), whereas direct damage is the main biological effect of high-LET radiation (such as iron-ions) (Kennedy, 2014). In contrast, the current study suggests that direct damage, in the form of DNA double-strand breaks, is induced by low-LET radiation exposure (X-rays and helium-ions), given that *A. niger* spore survivability was highly dependent on the NHEJ pathway (Δ*kusA*). Additionally, Δ*kusA* spores showed similar survival rates toward both high-LET iron-ion radiation (**Figure 2**) and low-LET X-ray radiation (**Figure 1**). This implies that radiation with iron-ions promotes additional cellular damages besides double-strand breaks, possibly as indirect damage in the form of ROS generation. Multiple experiments have shown similar results in yeasts exposed to ion radiation (Ikpeme et al., 1995; Kiefer et al., 2002). Conversely, a study with the filamentous fungus *Neurospora crassa*, showed that an NHEJ-deficient strain had ∼80% survival after 100 Gy of high-LET carbon-ion irradiation (Ma et al., 2013), whereas the NHEJ-deficient *A. niger* strain tested in the current study demonstrated survival of only ∼17% after 100 Gy of low-LET helium-ion radiation (a lighter element than carbon). Nevertheless, this discrepancy in survival might be attributed to the fact that hyphal compartments of *N. crassa* can contain up to 100 nuclei, which in turn can lower the hit rate of radiation induced DNA damage (Roper et al., 2011).

High Resistance of *A. niger* Spores Toward UV-C

UV-derived decontamination methods are commonly used in modern laboratories and healthcare systems (Yang et al., 2019), with UV-C lamps used to sterilize biosafety cabinets reaching around 300 J/m^2 in 12.5 min (Meechan and Wilson, 2006). Yet, in this study *A. niger* wild-type spores demonstrated high resistance toward UV-C (**Figure 4**, and **Supplementary Figure 3**), where the lethal dose required to eliminate 90% of wild-type spores was 1038 J/m^2. This is significantly higher than the LD_{90} of other microorganisms (**Table 4**), and becomes particularly clear

in comparison with previously characterized radiation-resistant organisms such as *Deinococcus radiodurans* (LD_{90} = 660 J/m^2) or *B. subtilis* spores (LD_{90} = 100 J/m^2). In a study using UV-C to treat drinking water, *A. niger* was found to be completely inactivated after exposure to 1920 J/m^2 UV-C (Sisti et al., 2017), which is in agreement with our study (LD_{90} = 1038 J/m^2).

The NHEJ pathway was shown to be an important DNA repair mechanism for survival of *A. niger* spores after exposure to UV-C and X-ray radiation. Interestingly, previous studies with NHEJ mutants of *N. crassa* and *Cryptococcus neoformans* did not show differences in survival after UV-C irradiation when compared to the wild-type (Ninomiya et al., 2004; Goins et al., 2006). It is possible that point mutations and single-strand breaks caused by UV radiation can be repaired by KusA independent repair mechanisms (Eckardt-Schupp and Klaus, 1999; Goldman et al., 2002). However, the higher nucleus number per hyphal compartment in *N. crassa*, and the capsule formation of *C. neoformans* spores (McFadden and Casadevall, 2001) may contribute to their increased radiation tolerance despite mutations in this repair pathway.

Pigmentation as Key-Protection Against UV-C but Not X-Rays or Cosmic Radiation

Pigments, such as melanin are involved in different cellular processes from adhesion to virulence (Eisenman and Casadevall, 2012), and are known to help cells against radiation-induced stress and ROS (Cockell and Knowland, 1999). Studies concerning the role of pigmentation in radiation resistance of fungal spores have been performed with monochromatic UV-C (254 nm) and pulsed light up to 1770 J/m^2 on inoculated agar with concentrations up to 10^7–10^8 spores/ml (Esbelin et al., 2013). The current study irradiated spore suspensions in liquid, using a concentration of 10^6 spores/ml. This concentration was chosen to guarantee a spore monolayer and prevent self-shielding (**Figure 4**). As expected, pigment-deficient spores (Δ*fwnA*) demonstrated lower survivability after exposure to UV-C radiation. Interestingly, deficiency in pigmentation did not alter survivability after exposure to ionizing radiation (X-rays or cosmic radiation) (**Figures 1**, **2**). This seems to contradict previous studies where melanin was shown to have a protective effect against X-ray irradiation in the fungi *C. neoformans* and *Cryomyces antarcticus* (Pacelli et al., 2017). However, it is to note that the strain tested in the current study lacks a putative polyketide synthase which results in fawn-colored (not white) spores, which might provide sufficient amount of pigmentation to display protective properties.

Both ionizing radiation and hydrogen peroxide are known to affect cell survival through the generation of ROS. To better understand how pigment-deficient spores resist to ionizing radiation, these were incubated in hydrogen peroxide. Results show that Δ*fwnA* spores were more sensitive to hydrogen peroxide than wild-type spores (**Figure 3**). This indicates that pigmentation is involved in protecting the spore from H_2O_2-induced oxidative-stress, but not in X-ray- or cosmic radiation-induced oxidative stress. Previous studies analyzing the effect of H_2O_2 on *A. niger* spores were able to show that ROS scavenging was facilitated by increased catalase expression resistance (Angelova et al., 2005). From the results presented here, contrary to what has been suggested, pigmentation does not influence *A. niger* survival to space-like ionizing radiation.

UV-C Radiation Decreases Biofilm Formation Effectively

To address the contamination risks and possible decontamination procedures concerning *A. niger* growth in the spaceflight environment, wild-type spores were exposed to up to 4000 J/m^2 of UV-C and we assessed the impact of UV-C on surface-associated growth, i.e., biofilm formation (**Figure 5A**). Because wild-type spores were 90% inactivated at a dose of 1000 J/m^2, the ability for biofilm formation was assessed, for all strains, before and after treatment with 1000 J/m^2 UV-C. Here, one additional strain, deficient in polar growth, was included. This strain lacks the Rho GTPase RacA involved in establishing polarized tip extension via regulation of the actin filaments, which is important for proper cell wall formation in *A. niger* hyphae (Kwon et al., 2011, 2013). Results show that Δ*racA* spores ability for biofilm formation was reduced by 49% before UV-C treatment, and 94% after UV-C treatment, when compared with the wild-type (**Figure 5B**). The underlying molecular mechanism for reduced surface-associated growth (before UV-C) might be due reduced adhesion to hydrophobic surfaces, and/or results in less spore aggregation during spore outgrowth – a hypothesis worth studying further. The reduction of surface-associated growth after exposure to radiation suggests that the function of RacA plays a role (direct or indirect) in UV-C resistance of *A. niger*. Moreover, the tested color mutant (Δ*fwnA*) strain also demonstrated decreased ability of surface-associated growth, both before and after UV-C treatment, which suggests the involvement of pigments in spore adhesion.

CONCLUSION

This study shows that spores of *A. niger* are extremely resistant to space radiation. Spores were able to withstand high doses of X-ray (LD_{90} = 360 Gy), cosmic radiation (helium-ion LD_{90} = 500 Gy; and iron-ion LD_{90} = 100 Gy), and UV-C radiation (LD_{90} = 1038 J/m^2). *A. niger* spore resistance to UV-C is particularly interesting, given that it is even higher than that of other radiation-resistant microorganisms (e.g., *D. radiodurans*). Air-drying the spores made them more susceptible to X-ray radiation. Moreover, wild-type spores treated with 1000 J/m^2 UV-C were shown to have decreased biofilm formation ability (81% reduction). It is important to note that the ionizing radiation doses used in this study (up to 1000 Gy) are multiple times higher than doses expected from traveling in interplanetary space. For example, a 360-day round-trip to Mars would yield a dose of 0.66 ± 0.12 Gy (Zeitlin et al., 2013). It is therefore unlikely that

A. niger spores become easily inactivated due to space radiation alone. We thus recommend that current planetary protection guidelines are revisited to address the high resistance of fungal spores in space travel scenarios. In addition, further studies are needed in order to address fungal spore resistance to other space environmental factors such as vacuum, changes in pressure, and extreme temperature fluctuations.

DATA AVAILABILITY STATEMENT

All datasets generated for this study are included in the article/**Supplementary Material**.

AUTHOR CONTRIBUTIONS

MC, AH, and RU performed the experiments, analyzed the data, and wrote the manuscript. VM, TS, RM, and AF contributed to the conception and design of the study, and manuscript preparation.

FUNDING

RM was supported by the DLR grant FuE-Projekt "ISS LIFE" (Programm RF-FuW, Teilprogramm 475). MC was supported by the DLR/DAAD Research Fellowship Doctoral Studies in Germany, 2017 (57370122). AF and RM – MEXT Grant-in-Aid for Scientific Research on Innovative Areas "Living in Space" (Grant Numbers: 15H05935, 15K21745).

ACKNOWLEDGMENTS

We thank Andrea Schröder and the HIMAC operators for their excellent technical assistance during parts of this research.

SUPPLEMENTARY MATERIAL

The Supplementary Material for this article can be found online at: https://www.frontiersin.org/articles/10.3389/fmicb.2020.00560/full#supplementary-material

REFERENCES

Angelova, M. B., Pashova, S. B., Spasova, B. K., Vassilev, S. V., and Slokoska, L. S. (2005). Oxidative stress response of filamentous fungi induced by hydrogen peroxide and paraquat. *Mycol. Res.* 109, 150–158. doi: 10.1017/s0953756204001352

Bauermeister, A., Bentchikou, E., Moeller, R., and Rettberg, P. (2009). Roles of PprA, IrrE, and RecA in the resistance of *Deinococcus radiodurans* to germicidal and environmentally relevant UV radiation. *Arch. Microbiol.* 191, 913–918. doi: 10.1007/s00203-009-0522-7

Beauvais, A., Fontaine, T., Aimanianda, V., and Latge, J. P. (2014). Aspergillus cell wall and biofilm. *Mycopathologia* 178, 371–377. doi: 10.1007/s11046-014-9766-0

Blachowicz, A., Raffa, N., Bok, J. W., Choera, T., Knox, B., Lim, F. Y., et al. (2020). Contributions of spore secondary metabolites to UV-C protection and virulence vary in different *Aspergillus fumigatus* Strains. *mBio* 11:e03415-19. doi: 10.1128/mBio.03415-19

Bos, C. J., Debets, A. J., Swart, K., Huybers, A., Kobus, G., and Slakhorst, S. M. (1988). Genetic analysis and the construction of master strains for assignment of genes to six linkage groups in *Aspergillus niger*. *Curr. Genet.* 14, 437–443. doi: 10.1007/bf00521266

Cadet, J., Grand, A., and Douki, T. (2015). "Solar UV radiation-induced DNA bipyrimidine photoproducts: formation and mechanistic insights," in *Photoinduced Phenomena in Nucleic Acids II: DNA Fragments and Phenomenological Aspects*, eds M. Barbatti, A. C. Borin, and S. Ullrich (Cham: Springer International Publishing), 249–275. doi: 10.1007/128_2014_553

Cairns, T. C., Nai, C., and Meyer, V. (2018). How a fungus shapes biotechnology: 100 years of *Aspergillus niger* research. *Fungal. Biol. Biotechnol.* 5:13. doi: 10.1186/s40694-018-0054-5

Carvalho, N. D., Arentshorst, M., Jin Kwon, M., Meyer, V., and Ram, A. F. (2010). Expanding the ku70 toolbox for filamentous fungi: establishment of complementation vectors and recipient strains for advanced gene analyses. *Appl. Microbiol. Biotechnol.* 87, 1463–1473. doi: 10.1007/s00253-010-2588-1

Casadevall, A., Cordero, R. J. B., Bryan, R., Nosanchuk, J., and Dadachova, E. (2017). Melanin, radiation, and energy transduction in fungi. *Microbiol. Spectr* 5, 1–6.

Chancellor, J. C., Blue, R. S., Cengel, K. A., Auñón-Chancellor, S. M., Rubins, K. H., Katzgraber, H. G., et al. (2018). Limitations in predicting the space radiation health risk for exploration astronauts. *NPJ Micrograv.* 4:8. doi: 10.1038/s41526-018-0043-2

Chancellor, J. C., Scott, G. B. I., and Sutton, J. P. (2014). Space radiation: the number one risk to astronaut health beyond low earth orbit. *Life* 4, 491–510. doi: 10.3390/life4030491

Chang, P.-K., Cary, J. W., and Lebar, M. D. (2020). Biosynthesis of conidial and sclerotial pigments in *Aspergillus* species. *Appl. Microbiol. Biotechnol.* 104, 2277–2286. doi: 10.1007/s00253-020-10347-y

Checinska, A., Probst, A. J., Vaishampayan, P., White, J. R., Kumar, D., Stepanov, V. G., et al. (2015). Microbiomes of the dust particles collected from the international space station and spacecraft assembly facilities. *Microbiome* 3:50. doi: 10.1186/s40168-015-0116-3

Cockell, C. S., and Knowland, J. (1999). Ultraviolet radiation screening compounds. *Biol. Rev. Camb. Philos. Soc.* 74, 311–345. doi: 10.1111/j.1469-185x.1999.tb00189.x

Cordero, R. J., and Casadevall, A. (2017). Functions of fungal melanin beyond virulence. *Fungal Biol. Rev.* 31, 99–112. doi: 10.1016/j.fbr.2016.12.003

Cortesão, M., Schütze, T., Marx, R., Moeller, R., and Meyer, V. (2020). "Fungal biotechnology in space: why and how?," in *Grand Challenges in Fungal Biotechnology*, ed. H. Nevalainen (Cham: Springer International Publishing), 501–535. doi: 10.1007/978-3-030-29541-7_18

Cucinotta, F. A., and Durante, M. (2006). Cancer risk from exposure to galactic cosmic rays: implications for space exploration by human beings. *Lancet. Oncol.* 7, 431–435. doi: 10.1016/s1470-2045(06)70695-7

Cucinotta, F. A., Kim, M.-H. Y., Chappell, L. J., and Huff, J. L. (2013). How safe is safe enough? Radiation risk for a human mission to Mars. *PLoS One* 8:e74988. doi: 10.1371/journal.pone.0074988

Dadachova, E., Bryan, R. A., Huang, X., Moadel, T., Schweitzer, A. D., et al. (2007). Ionizing radiation changes the electronic properties of melanin and enhances the growth of melanized fungi. *PLoS One* 2:e457. doi: 10.1371/journal.pone.0000457

Driedger, A. A., James, A. P., and Grayston, M. J. (1970). Cell survival and X-ray-induced DNA degradation in *Micrococcus radiodurans*. *Radiat. Res.* 44, 835–845.

Eckardt-Schupp, F., and Klaus, C. (1999). Radiation inducible DNA repair processes in eukaryotes. *Biochimie* 81, 161–171. doi: 10.1016/s0300-9084(99)80049-2

Eisenman, H. C., and Casadevall, A. (2012). Synthesis and assembly of fungal melanin. *Appl. Microbiol. Biotechnol.* 93, 931–940. doi: 10.1007/s00253-011-3777-2

Esbelin, J., Mallea, S., Ram, A. F., and Carlin, F. (2013). Role of pigmentation in protecting *Aspergillus niger* conidiospores against pulsed light radiation. *Photochem. Photobiol.* 89, 758–761. doi: 10.1111/php.12037

Goins, C. L., Gerik, K. J., and Lodge, J. K. (2006). Improvements to gene deletion in the fungal pathogen *Cryptococcus neoformans*: absence of Ku proteins increases homologous recombination, and co-transformation of independent DNA molecules allows rapid complementation of deletion phenotypes. *Fungal. Genet. Biol.* 43, 531–544. doi: 10.1016/j.fgb.2006.02.007

Goldman, G. H., Mcguire, S. L., and Harris, S. D. (2002). The DNA damage response in filamentous fungi. *Fungal Genet. Biol.* 35, 183–195. doi: 10.1006/fgbi.2002.1344

Horneck, G., Klaus, D. M., and Mancinelli, R. L. (2010). Space microbiology. *Microbiol. Mol. Biol. Rev.* 74, 121–156. doi: 10.1128/MMBR.00016-09

Hutchinson, F., Preston, A., and Vogel, B. (1957). Radiation sensitivity of enzymes in wet and in dry yeast cells. *Radiat. Res.* 7, 465–472.

Ikpeme, S., Lobrich, M., Akpa, T., Schneider, E., and Kiefer, J. (1995). Heavy ion-induced DNA double-strand breaks with yeast as a model system. *Radiat. Environ. Biophys.* 34, 95–99. doi: 10.1007/bf01275213

Jorgensen, T. R., Park, J., Arentshorst, M., Van Welzen, A. M., Lamers, G., Vankuyk, P. A., et al. (2011). The molecular and genetic basis of conidial pigmentation in *Aspergillus niger*. *Fungal Genet Biol.* 48, 544–553. doi: 10.1016/j.fgb.2011.01.005

Kennedy, A. R. (2014). Biological effects of space radiation and development of effective countermeasures. *Life Sci. Space Res.* 1, 10–43. doi: 10.1016/j.lssr.2014.02.004

Khodadad, C. L., Wong, G. M., James, L. M., Thakrar, P. J., Lane, M. A., Catechis, J. A., et al. (2017). Stratosphere conditions inactivate bacterial endospores from a Mars spacecraft assembly facility. *Astrobiology* 17, 337–350. doi: 10.1089/ast.2016.1549

Kiefer, J., Egenolf, R., and Ikpeme, S. (2002). Heavy ion-induced DNA double-strand breaks in yeast. *Radiat. Res.* 157, 141–148. doi: 10.1667/0033-7587(2002)157[0141:hiidds]2.0.co;2

Klintworth, R., and Reher, H. J. (1999). Biological induced corrosion of materials II: new test methods and experiences from mir station. *Acta Astronaut.* 44, 569–578. doi: 10.1016/s0094-5765(99)00069-7

Kminek, G., Fellous, J., Rettberg, P., Moissl-Eichinger, C., Sephton, M. A., Royle, S. H., et al. (2019). The international planetary protection handbook. *Space Res. Today* 205, e1–e120. doi: 10.1016/j.srt.2019.09.001

Krijgsheld, P., Bleichrodt, R., Van Veluw, G. J., Wang, F., Müller, W. H., Dijksterhuis, J., et al. (2013). Development in *Aspergillus*. *Stud. Mycol.* 74, 1–29. doi: 10.3114/sim0006

Kwon, M. J., Arentshorst, M., Roos, E. D., Van Den Hondel, C. A., Meyer, V., and Ram, A. F. (2011). Functional characterization of Rho GTPases in *Aspergillus niger* uncovers conserved and diverged roles of Rho proteins within filamentous fungi. *Mol. Microbiol.* 79, 1151–1167. doi: 10.1111/j.1365-2958.2010.07524.x

Kwon, M. J., Nitsche, B. M., Arentshorst, M., Jorgensen, T. R., Ram, A. F., and Meyer, V. (2013). The transcriptomic signature of RacA activation and inactivation provides new insights into the morphogenetic network of *Aspergillus niger*. *PLoS One* 8:e68946. doi: 10.1371/journal.pone.0068946

Latgé, J. P. (1999). *Aspergillus fumigatus* and aspergillosis. *Clin. Microbiol. Rev.* 12, 310–350. doi: 10.1128/CMR.12.2.310

Ma, L., Kazama, Y., Inoue, H., Abe, T., Hatakeyama, S., and Tanaka, S. (2013). The type of mutations induced by carbon-ion-beam irradiation of the filamentous fungus *Neurospora crassa*. *Fungal. Biol. Biotechnol.* 117, 227–238. doi: 10.1016/j.funbio.2013.01.002

Makimura, K., Hanazawa, R., Takatorl, K., Tamura, Y., Fujisaki, R., Nishiyama, Y., et al. (2001). Fungal flora on board the Mir-space station, identification by morphological features and ribosomal DNA sequences. *Microbiol. Immunol.* 45, 357–363. doi: 10.1111/j.1348-0421.2001.tb02631.x

McFadden, D. C., and Casadevall, A. (2001). Capsule and melanin synthesis in *Cryptococcus neoformans*. *Med. Mycol.* 39(Suppl. 1), 19–30. doi: 10.1080/744118883

Meechan, P. J., and Wilson, C. (2006). Use of ultraviolet lights in biological safety cabinets: a contrarian view. *Appl. Biosaf.* 11, 222–227. doi: 10.1177/153567600601100412

Meyer, V., Arentshorst, M., El-Ghezal, A., Drews, A. C., Kooistra, R., Van Den Hondel, C. A., et al. (2007). Highly efficient gene targeting in the *Aspergillus niger* kusA mutant. *J. Biotechnol.* 128, 770–775. doi: 10.1016/j.jbiotec.2006.12.021

Meyer, V., Fiedler, M., Nitsche, B., and King, R. (2015). "The cell factory *Aspergillus* enters the big data era: opportunities and challenges for optimising product formation," in *Filaments in Bioprocesses*, eds R. Krull and T. Bley (Cham: Springer), 91–132. doi: 10.1007/10_2014_297

Moeller, R., Raguse, M., Leuko, S., Berger, T., Hellweg, C. E., Fujimori, A., et al. (2017). STARLIFE-An international campaign to study the role of galactic cosmic radiation in astrobiological model systems. *Astrobiology* 17, 101–109. doi: 10.1089/ast.2016.1571

Moeller, R., Raguse, M., Reitz, G., Okayasu, R., Li, Z., Klein, S., et al. (2014). Resistance of *Bacillus subtilis* spore DNA to lethal ionizing radiation damage relies primarily on spore core components and DNA repair, with minor effects of oxygen radical detoxification. *Appl. Environ. Microbiol.* 80, 104–109. doi: 10.1128/AEM.03136-13

Moeller, R., Reitz, G., Berger, T., Okayasu, R., Nicholson, W. L., and Horneck, G. (2010). Astrobiological aspects of the mutagenesis of cosmic radiation on bacterial spores. *Astrobiology* 10, 509–521. doi: 10.1089/ast.2009.0429

Mora, M., Mahnert, A., Koskinen, K., Pausan, M. R., Oberauner-Wappis, L., Krause, R., et al. (2016). Microorganisms in confined habitats: microbial monitoring and control of intensive care units, operating rooms, cleanrooms and the international space station. *Front. Microbiol.* 7:1573. doi: 10.3389/fmicb.2016.01573

Mora, M., Wink, L., Kögler, I., Mahnert, A., Rettberg, P., Schwendner, P., et al. (2019). Space Station conditions are selective but do not alter microbial characteristics relevant to human health. *Nat. Commun.* 10:3990.

Moseley, B. E., and Laser, H. (1965). Repair of X-ray in *Micrococcus radiodurans*. *Proc. R. Soc. Lond. B. Biol. Sci.* 162, 210–222. doi: 10.1098/rspb.1965.0035

Mowat, E., Butcher, J., Lang, S., Williams, C., and Ramage, G. (2007). Development of a simple model for studying the effects of antifungal agents on multicellular communities of *Aspergillus fumigatus*. *J. Med. Microbiol.* 56, 1205–1212. doi: 10.1099/jmm.0.47247-0

Narici, L., Casolino, M., Di Fino, L., Larosa, M., Picozza, P., Rizzo, A., et al. (2017). Performances of Kevlar and Polyethylene as radiation shielding on-board the International Space Station in high latitude radiation environment. *Sci. Rep.* 7, 1644–1644. doi: 10.1038/s41598-017-01707-2

Newcombe, D. A., Schuerger, A. C., Benardini, J. N., Dickinson, D., Tanner, R., and Venkateswaran, K. (2005). Survival of spacecraft-associated microorganisms under simulated martian UV irradiation. *Appl. Environ. Microbiol.* 71, 8147–8156. doi: 10.1128/aem.71.12.8147-8156.2005

Ninomiya, Y., Suzuki, K., Ishii, C., and Inoue, H. (2004). Highly efficient gene replacements in *Neurospora* strains deficient for nonhomologous end-joining. *Proc. Natl. Acad. Sci. U.S.A.* 101:12248. doi: 10.1073/pnas.0402780101

Novikova, N., De Boever, P., Poddubko, S., Deshevaya, E., Polikarpov, N., Rakova, N., et al. (2006). Survey of environmental biocontamination on board the International Space Station. *Res. Microbiol.* 157, 5–12. doi: 10.1016/j.resmic.2005.07.010

Pacelli, C., Bryan, R. A., Onofri, S., Selbmann, L., Shuryak, I., and Dadachova, E. (2017). Melanin is effective in protecting fast and slow growing fungi from various types of ionizing radiation. *Environ. Microbiol.* 19, 1612–1624. doi: 10.1111/1462-2920.13681

Riesenman, P. J., and Nicholson, W. L. (2000). Role of the spore coat layers in *Bacillus subtilis* spore resistance to hydrogen peroxide, artificial UV-C. UV-B, and solar UV radiation. *Appl. Environ. Microbiol.* 66, 620–626. doi: 10.1128/aem.66.2.620-626.2000

Roper, M., Ellison, C., Taylor, J. W., and Glass, N. L. (2011). Nuclear and genome dynamics in multinucleate ascomycete fungi. *Curr. Biol.* 21, R786–R793. doi: 10.1016/j.cub.2011.06.042

Segers, F. J. J., Wosten, H. A. B., and Dijksterhuis, J. (2018). Aspergillus niger mutants affected in conidial pigmentation do not have an increased susceptibility to water stress during growth at low water activity. *Lett. Appl. Microbiol.* 66, 238–243. doi: 10.1111/lam.12846

Setlow, P. (2014). Spore resistance properties. *Microbiol. Spectr.* 2, 1–14.

Silverman, G. J., Davis, N. S., and Beecher, N. (1967). Resistivity of spores to ultraviolet and gamma radiation while exposed to ultrahigh vacuum or at atmospheric pressure. *Appl. Microbiol.* 15, 510–515. doi: 10.1128/aem.15.3.510-515.1967

Singaravelan, N., Grishkan, I., Beharav, A., Wakamatsu, K., Ito, S., and Nevo, E. (2008). Adaptive melanin response of the soil fungus *Aspergillus niger* to UV radiation stress at "evolution canyon", mount carmel, Israel. *PLoS One* 3:e2993. doi: 10.1371/journal.pone.0002993

Sinha, R. P., and Hader, D. P. (2002). A UV-induced DNA damage and repair: a review. *Photochem. Photobiol. Sci*. 1, 225–236. doi: 10.1039/b201230h

Sisti, M., Schiavano, G. F., Santi, M. D., and Brandi, G. (2017). Ultraviolet germicidal irradiation in tap water contaminated by *Aspergillus* spp. *J. Prev. Med. Hyg.* 58, E315–E319. doi: 10.15167/2421-4248/jpmh2017.58.4.777

Sliney, D. H. (2007). Radiometric quantities and units used in photobiology and photochemistry: recommendations of the commission internationale de l'eclairage (international commission on illumination). *Photochem. Photobiol.* 83, 425–432. doi: 10.1562/2006-11-14-ra-1081

Yang, J. H., Wu, U. I., Tai, H. M., and Sheng, W. H. (2019). Effectiveness of an ultraviolet-C disinfection system for reduction of healthcare-associated pathogens. *J. Microbiol. Immunol. Infect.* 52, 487–493. doi: 10.1016/j.jmii.2017.08.017

Zeitlin, C., Hassler, D. M., Cucinotta, F. A., Ehresmann, B., Wimmer-Schweingruber, R. F., Brinza, D. E., et al. (2013). Measurements of energetic particle radiation in transit to mars on the mars science laboratory. *Science* 340, 1080–1084. doi: 10.1126/science.1235989

Zhdanova, N. N., Zakharchenko, V. A., Vember, V. V., and Nakonechnaya, L. T. (2000). Fungi from chernobyl: mycobiota of the inner regions of the containment structures of the damaged nuclear reactor. *Mycol. Res.* 104, 1421–1426. doi: 10.1017/s0953756200002756

Conflict of Interest: The authors declare that the research was conducted in the absence of any commercial or financial relationships that could be construed as a potential conflict of interest.

frontiers in Microbiology

ORIGINAL RESEARCH
published: 07 April 2020
doi: 10.3389/fmicb.2020.00515

Radiation Tolerance of *Pseudanabaena catenata*, a Cyanobacterium Relevant to the First Generation Magnox Storage Pond

Lynn Foster[1], Howbeer Muhamadali[2], Christopher Boothman[1], David Sigee[1], Jon K. Pittman[1], Royston Goodacre[2], Katherine Morris[1] and Jonathan R. Lloyd[1]**

[1] Research Centre for Radwaste Disposal and Williamson Research Centre for Molecular Environmental Science, School of Earth and Environmental Sciences, University of Manchester, Manchester, United Kingdom, [2] Department of Biochemistry, Institute of Integrative Biology, University of Liverpool, Biosciences Building, Liverpool, United Kingdom

OPEN ACCESS

Edited by:
Rakesh Mogul,
California State Polytechnic University, Pomona, United States

Reviewed by:
Aharon Oren,
Hebrew University of Jerusalem, Israel
Tetyana Milojevic,
University of Vienna, Austria

***Correspondence:**
Lynn Foster
lynn.foster@manchester.ac.uk
Jonathan R. Lloyd
jon.lloyd@manchester.ac.uk

Specialty section:
This article was submitted to Extreme Microbiology, a section of the journal Frontiers in Microbiology

Received: 23 July 2019
Accepted: 10 March 2020
Published: 07 April 2020

Citation:
Foster L, Muhamadali H, Boothman C, Sigee D, Pittman JK, Goodacre R, Morris K and Lloyd JR (2020) Radiation Tolerance of Pseudanabaena catenata, a Cyanobacterium Relevant to the First Generation Magnox Storage Pond. Front. Microbiol. 11:515. doi: 10.3389/fmicb.2020.00515

Recently a species of *Pseudanabaena* was identified as the dominant photosynthetic organism during a bloom event in a high pH (pH ∼11.4), radioactive spent nuclear fuel pond (SNFP) at the Sellafield Ltd., United Kingdom facility. The metabolic response of a laboratory culture containing the cyanobacterium *Pseudanabaena catenata,* a relative of the major photosynthetic microorganism found in the SNFP, to X-ray irradiation was studied to identify potential survival strategies used to support colonization of radioactive environments. Growth was monitored and the metabolic fingerprints of the cultures, during irradiation and throughout the post-irradiation recovery period, were determined using Fourier transform infrared (FT-IR) spectroscopy. A dose of 95 Gy delivered over 5 days did not significantly affect growth of *P. catenata*, as determined by turbidity measurements and cell counts. Multivariate statistical analysis of the FT-IR spectral data revealed metabolic variation during the post-irradiation recovery period, with increased polysaccharide and decreased amide spectral intensities. Increases in polysaccharides were confirmed by complementary analytical methods including total carbohydrate assays and calcofluor white staining. This observed increased production of polysaccharides is of significance, since this could have an impact on the fate of the radionuclide inventory in the pond via biosorption of cationic radionuclides, and may also impact on downstream processes through biofilm formation and biofouling.

Keywords: cyanobacteria, FT-IR spectroscopy, metabolic fingerprint, radiation, polysaccharide, spent nuclear fuel pond

INTRODUCTION

Microorganisms are ubiquitous and inhabit a wide range of environments including those with extremes of pH, temperature, pressure, availability of water, salinity, and radiation (Billi and Potts, 2002; Blanco-Rivero et al., 2005; Katz et al., 2007; Pikuta et al., 2007). The presence of microorganisms in extreme radioactive environments has been reported, for example in Spent Nuclear Fuel Ponds (SNFPs) (Diósi et al., 2003; Chicote et al., 2004, 2005; Sarró et al., 2003, 2005, 2007; Rivasseau et al., 2010, 2016; Dekker et al., 2014; Karley et al., 2017; MeGraw et al., 2018)

and in contaminated land surrounding the Chernobyl nuclear reactor (Dadachova et al., 2008). Many microorganisms that are capable of withstanding high doses of radiation are also known to be able to withstand extreme environmental conditions such as desiccation, for example *Deinococcus radiodurans* and the cyanobacterium *Chroococcidiopsis* spp. are able to survive doses of 10 kGy of ionizing radiation and periods of desiccation (Billi et al., 2000; Billi and Potts, 2002; Jolivet et al., 2003).

Studies investigating the presence of microorganisms in SNFPs across several sites, including in Spain, United States, France, India and the United Kingdom, have shown that each site exhibits a unique microbial community profile (Diósi et al., 2003; Chicote et al., 2004, 2005; Sarró et al., 2003, 2005, 2007; Rivasseau et al., 2010, 2016; Dekker et al., 2014; Karley et al., 2017; MeGraw et al., 2018). The majority of sites are dominated by *Proteobacteria*, although photosynthetic microorganisms, including eukaryotic microalgae have also been identified as dominant at some sites (Rivasseau et al., 2010). The presence of microorganisms in SNFPs is challenging since high levels of biomass can result in reduced visibility (increased turbidity) within the water column (hampering pond management), may lead to microbiologically induced corrosion (MIC) and also lead to the formation of organic-rich radioactive wastes. Bruhn et al. (2009) highlighted the potential for the formation of biofilms and MIC in the presence of elevated levels of radiation, which signals the possibility of MIC occurring on waste storage containers and fuel cladding. Indeed, several studies investigating biofilm forming organisms in ponds at the Confrentes site (Valencia, Spain) have shown the occurrence of MIC on steel coupons (Sarró et al., 2003, 2005, 2007; Chicote et al., 2004, 2005). The potential for MIC on waste storage containers and fuel cladding could have implications for the longevity of spent fuel storage in pond environments. Microorganisms have also been shown to accumulate fission products as shown with the free-living eukaryotic microalga *Coccomyxa actinabiotis*, isolated from a SNFP in research reactor in France, which has been shown to accumulate large quantities of ^{137}Cs (Rivasseau et al., 2013).

The early Magnox gas cooled reactors form a significant part of the UK's legacy nuclear fleet. The fuel rods used in these reactors were clad in a magnesium non-oxide (Magnox) alloy (Jensen and Nønbel, 1999; Gregson et al., 2011a,b; Jackson et al., 2014). Spent fuel rods containing this cladding have been stored in open air legacy storage ponds, including the First Generation Magnox Storage Pond (FGMSP) situated on the Sellafield site (Cumbria, United Kingdom), since the late 1950s (Jackson et al., 2014). Within the FGMSP, fuel storage times have been longer than anticipated and the spent fuel has been subject to extensive corrosion due to the Magnox cladding and the uranium metallic fuel having limited chemical stability in water. This extended storage has led to the formation of a high hazard radioactive environment with corroded spent nuclear fuel, pond effluent (NDA, 2016; Foster et al., 2020) and sludge (NDA, 2016). In order to provide thermal cooling and minimize further corrosion of the fuel rods and the growth of microorganisms, the pond is continuously purged with alkaline dosed demineralized water (pH ∼11.4) (Gregson et al., 2011a,b; Jackson et al., 2014). However, there is clear visible evidence for the presence of microorganisms in the pond, including events reported as "algal blooms", which are most prominent when the purge cycling is not active (Gregson et al., 2011a,b; Konovalovaite, 2019; Foster et al., 2020).

The microbial community of this open-air legacy SNFP has recently been investigated over a three year period, including during a microbial bloom period in August 2016 (Foster et al., 2020). Over the course of the investigation, highly pigmented organisms with photosynthetic or hydrogen-metabolizing capabilities were identified. Background water samples indicated that *Proteobacteria* were the dominant microorganisms in the pond, whilst a single cyanobacterial species, *Pseudanabaena catenata*, was dominant during the bloom event (Foster et al., 2020). *Pseudanabaena* spp. are filamentous cyanobacteria, displaying a simple morphology, and lack the ability to form branches or differentiate (Acinas et al., 2009; Zhu et al., 2015). Reports of *Pseudanabaena* spp. in the scientific literature are limited, with little known about their physiology or molecular and metabolic characteristics, and although they are associated with bloom events in a range of environments, they are often overlooked (Acinas et al., 2009; Webster-Brown et al., 2015; Zhu et al., 2015; Bukowska et al., 2017; Khan et al., 2018).

The occurrence of cyanobacterial blooms in the FGMSP disrupts waste retrieval operations and downstream processes. Although the microbial community structure of the legacy SNFP has been determined, there have been no studies so far to characterize how the microorganisms are able to tolerate and colonize this highly radioactive, alkaline environment. The purpose of this study is to determine the adaptive response of a *P. catenata* culture to ionizing radiation, to help understand the potential impacts of microbial colonization on pond biogeochemistry and ultimately to inform control strategies employed onsite. It was not possible to isolate the *Pseudanabaena* species that resides in the FGMSP due to radiological safety limitations, and therefore a close-relative of the major photosynthetic microorganism was acquired from a culture collection to use in the following study. To determine the physiological and metabolic response of a *P. catenata*-containing culture to irradiation, Fourier transform infrared (FT-IR) spectroscopy and classical microbiological techniques were utilized. FT-IR spectroscopy is a metabolic fingerprinting technique that can be used to determine the phenotype in a given microbial sample, while shifts in these fingerprints can be correlated with metabolic consequences when the environment of the microbe is changed (Muhamadali et al., 2015a). Here, we demonstrate that a culture containing *P. catenata* as the sole cyanobacterial species is capable of surviving significant doses of X-ray irradiation over a period of 5 days. When grown photoautotrophically, the culture did not display any physiological differences to untreated cultures during the irradiation treatment, however, increases in polysaccharides and a reduction in chlorophyll-a (Chl-a) became more pronounced during the post-irradiation period. This study provides insights into the radiation resistance mechanisms employed by photosynthetic microorganisms related to those colonizing the FGMSP. Understanding the behavior of the

microorganisms in response to radiation (and other stress responses) will underpin radiation adaptation mechanisms in extremophiles, and inform more effective control strategies to minimize microbial growth and bloom formation.

MATERIALS AND METHODS

Culturing and X-Ray Irradiation of *P. catenata*

It was not possible to culture organisms directly from water taken from the SNFP due to radiological safety limitations. A culture of the closest known relative to the *Pseudanabaena* species detected in the pond, *P. catenata* was obtained from the NIVA Culture Collection of Algae (NIVA-CYA 152), Norway. The *P. catenata* was inoculated in unbuffered BG11 media (Culture Collection of Algae and Protozoa) and incubated at 25 ± 1°C, and shaken at 100 rpm in a light incubator with a photon flux density of 150 μmol m^{-2} s^{-1}, and a 16:8 h light–dark cycle (supplied by cool fluorescent daylight lamps). Biological triplicates were prepared by inoculating 20 mL BG11 medium with *P. catenata* to a starting optical density 0.2 (OD_{600nm}). The cultures were exposed to daily doses of ionizing radiation using a Faxitron CP-160 Cabinet X-radiator (160 kV; 6 mA; tungsten target). The FGMSP has a reported dose of 5.65 Gy h^{-1} associated with the sludge, and 0.15 mGy h^{-1} associated with the pond water (Jackson et al., 2014). A dose of 1 Gy min^{-1} for 19 min per day was administered to the cultures over five consecutive days to give a total dose of 95 Gy. A further triplicate set of "no dose" controls were placed inside the irradiator, shielded by an appropriate thickness of lead, to mimic the environmental conditions within the Faxitron cabinet (e.g., any heating due to radiation). All cultures were incubated following the treatment as previously described.

DNA Extraction and 16S rRNA Gene Sequencing of the *P. catenata* Culture

It was not possible to source an axenic culture of *P. catenata* from any culture collection for this study, therefore a non-axenic *P. catenata* culture was used for this work. The culture was characterized using 16S rRNA gene sequencing to monitor the relative abundance of all the prokaryotic microorganisms, and quantify any differences in the cultures at the end of the experiment. Samples (1 mL) of irradiated and control cultures at day 16 were passed through a sterile 0.2 μm filter using a vacuum filtration technique. DNA was then extracted using the MoBio PowerWater DNA isolation kit (MoBio Laboratories, Inc., Carlsbad, CA, United States). The 16S rRNA gene was sequenced from PCR amplicons on the Illumina MiSeq platform (Illumina, San Diego, CA, United States) targeting the V4 hyper variable region (forward primer, 515F, 5′-GTGYCAGCMGCCGCGGTAA-3′; reverse primer, 806R, 5′-GGACTACHVGGGTWTCTAAT-3′) for 2 × 250-bp paired-end sequencing (Illumina) (Caporaso et al., 2011, 2012). The Roche FastStart High Fidelity PCR System (Roche Diagnostics Ltd., Burgess Hill, United Kingdom) was used to perform the PCR amplifications (50 μL reactions) under the following conditions; initial denaturation at 95°C for 2 min, followed by 36 cycles of 95°C for 30 s, 55°C for 30 s, 72°C for 1 min, and a final extension step of 5 min at 72°C. The SequalPrep Normalization Kit (Fisher Scientific, Loughborough, United Kingdom) was used to purify and normalize the PCR products to ∼20 ng each. The PCR amplicons from all samples were pooled in equimolar ratios. The run was performed using a 4 pM sample library spiked with 4 pM PhiX to a final concentration of 10% following the method of Schloss and Kozich (Kozich et al., 2013).

A sequencing pipeline was used to divide the raw sequences into samples by barcodes (up to one mismatch was permitted). Cutadapt (Martin, 2011), FastQC[1], and Sickle (Joshi and Fass, 2011) were used to perform quality control and trimming, whilst SPADes (Nurk et al., 2013) was used to carry out MiSeq error corrections. Forward and reverse reads were incorporated into full-length sequences with Pandaseq (Masella et al., 2012). ChimeraSlayer (Haas et al., 2011) was utilized to remove chimeras, and OTUs were generated UPARSE (Edgar, 2013) generated OTUs, that were classified by Usearch (Edgar, 2010) at the 97% similarity level, and singletons were removed. Rarefaction analysis was conducted using the original detected OTUs in Qiime (Caporaso et al., 2010). The RDP classifier, version 2.2 (Wang et al., 2007) was used to perform the taxonomic assignment.

Growth, Chlorophyll-a (Chl-a) Concentration and pH Measurements

To quantify the total biomass in cultures by turbidity, absorbance values at 600 nm (OD_{600nm}) were recorded for 1 mL aliquots of the *P. catenata* cultures using a Jenway 6700 UV/Vis spectrophotometer (Bibby Scientific Limited, Staffordshire).

The concentration of Chl-a was determined as follows: 1 mL samples were centrifuged at 14,000 × *g* for 10 min to pellet the cells. The supernatant was then discarded and the cells re-suspended in 1 mL of 70% ethanol and incubated at room temperature for 2 h. The samples were then centrifuged at 14,000 × *g* for 10 min, the supernatant was then removed and analyzed using the Jenway 6700 UV/Vis spectrophotometer (Bibby Scientific Limited, Staffordshire). The absorbance was measured at 665 nm (Chl-a) and at 750 nm to correct for turbidity (Bellinger and Sigee, 2010). The concentration of Chl-a was then calculated using the formula of Jespersen and Christoffersen (Jespersen and Christoffersen, 1987).

The pH of the cultures was measured using a FiveEasyPlus pH meter (Mettler Toledo Ltd., Leicestershire, United Kingdom).

Light Microscopy

All light microscopy was carried out using a Zeiss Axio Imager A1 (Carl Zeiss Microimaging 234 GmbH, Germany) light microscope fitted with an Axiocam 506 mono camera using Zen2 imaging software.

Cell Counts of *P. catenata*

Direct counts of *P. catenata* were carried out routinely throughout the experiment using a Sedgewick Rafter counting chamber. Ten images were taken of random sites across the

samples. ImageJ was used to determine the length of filaments and individual cells. An average cell count was determined by dividing the total filament length by the average cell length. Samples were diluted with sterile BG11 medium to an appropriate concentration as required for analysis.

Calcofluor White Staining of β-Polysaccharides

Cells were washed twice and re-suspended in sterile normal saline (9 g L^{-1} NaCl), 5 μL of each sample was placed on a glass slide and 5 μL of calcofluor white stain (Sigma-Aldrich, Dorest, United Kingdom) was added and a cover slide placed over the sample. The samples were left to incubate for 10 min in the dark prior to being analyzed.

The auto-fluorescence of the culture was observed using filter set 00 (530–585 nm excitation and 615–4095 nm emission). Calcofluor white stain fluorescence was observed using filter set 49 (335–383 nm excitation and 420–470 nm emission).

Carbohydrate Quantification

A total carbohydrate assay kit (Sigma-Aldrich, Dorset, United Kingdom) was used to determine carbohydrate concentrations. Prior to using the kit, the cells were prepared by washing twice with sterile normal saline solution (9 g L^{-1} NaCl), the cell pellets were flash frozen in liquid nitrogen and stored at -80°C until they were analyzed. All samples were normalized to an optical density of OD_{600} 15 (as per FT-IR preparation). Following this, a 200 μL aliquot was then centrifuged and re-suspended in the assay buffer, incubated for 10 min at room temperature. The samples were centrifuged at 14,000 × *g* for 5 min and 15 μL aliquots from the samples were used for the assay reaction and made up to 30 μL with Roche PCR grade water. The sample preparation was then carried out as detailed in the kit technical bulletin.

Metabolic Profile of the Cultures by FT-IR Spectroscopy

Normalized samples were spotted as 20 μL aliquots onto a Bruker 96-well FT-IR silicon plate (Bruker Ltd., Coventry, United Kingdom) in triplicates, and heated to dryness (20–30 min) in an oven at 55°C (Muhamadali et al., 2015b). All FT-IR spectra were recorded in the mid-infrared range (4000–600 cm^{-1}) with 4 cm^{-1} resolution and 64 spectral co-adds in absorbance mode using a HXT™ module on a Bruker Equinox 55 infrared spectrometer (Muhamadali et al., 2015c).

Multivariate Statistical Analysis

The collected FT-IR spectra were analyzed using MATLAB version 9 (The MathWorks Inc., Natick, MA). All spectra were scaled using the extended multiplicative signal correction (EMSC) method (Martens et al., 2003), followed by replacement of the CO_2 bands (2400 to 2275 cm^{-1}) with a linear trend. The pre-processed FT-IR spectral data were analyzed by the unsupervised method of principal component analysis (PCA) to reduce the dimensionality of the data and PC scores plots generated to determine any between group variations, and PC loadings plots visualized to determine which molecular vibrations were important (Wold et al., 1986).

RESULTS

The Effect of X-Ray Irradiation on the Growth and Chlorophyll Concentration of the *P. catenata* Culture

In order to determine the effect of ionizing radiation on the growth and photosynthetic pigment characteristics of the *P. catenata* culture, the optical density at 600 nm (OD_{600nm}), cell counts and Chl-a concentration were monitored during and after the cultures were subjected to a total of 95 Gy (1 Gy min^{-1}) of X-ray irradiation over a five day period (**Figure 1**). The optical density of *P. catenata* cultures was measured at 600 nm over a period of 16 days (**Figure 1A**). There was a steady increase in the optical density recorded over time for both the irradiated cultures and the unirradiated controls. The control cultures started at an average OD_{600nm} of 0.16 and reached an OD_{600nm} of 2.92 at day 16 whilst the irradiated culture started at a slightly lower average OD_{600nm} of 0.13 and reached 2.79 by day 16. The overall growth profile, between irradiated and unirradiated samples, showed very similar trends indicating that the amount of biomass developed in the cultures was not significantly different. Optical density measurements were also taken at 680 nm and 750 nm, and showed the same trends as the measurements taken at 600 nm (data not shown). Since the cultures contained other prokaryotic microorganisms in addition to *P. catenata*, direct cell counts (**Figure 1C**) were carried out using a light microscope to ensure the trends seen in the turbidity measurements reflected the proliferation of the cyanobacterium, with its characteristic chain morphology. Observation of both irradiated and control cultures showed that *P. catenata* dominated the field of view, supporting the sequencing data which shows it was the most abundant organism in the culture. Additionally, the 16S rRNA gene sequencing showed the close relationship of the cultured *Pseudanabaena* species to one identified in the pond (**Supplementary Figure 1**) and that there were no changes in the community following the irradiation treatment (**Supplementary Figure 2**). Both the irradiated and control cultures started with around 8 × 10^6 cells mL^{-1} and showed an increase in cell numbers over time. By day 16 the average cell counts for the irradiated cultures were 31% higher than those for the control at 2.8 × 10^8 cells mL^{-1} and 2.2 × 10^8 cells mL^{-1}, respectively. Both the turbidity measurements and the cell counts show the same overall trends in growth, with no significant difference between the two sets of cultures observed. The concentration of Chl-a differed between the irradiated and unirradiated samples (**Figure 1B**). The initial Chl-a concentrations were 0.4 mg L^{-1} and 0.5 mg L^{-1} for the control and irradiated cultures, respectively. Both cultures showed similar increases in the Chl-a concentration at day 4 and whilst the irradiation treatment was still being administered. The control cultures then showed a continued increase in the Chl-a concentrations, with 7.8 μg L^{-1} measured on day 16. By contrast, the Chl-a levels in the irradiated cultures were consistently lower after day 4, at day 16 a concentration of 2.6 mg L^{-1} was recorded, which is ∼66% less than the control value. Normalization of the Chl-a concentration to cell number showed that by day 4,

the concentration of Chl-a per cell increased in both treatments and reached the maximum of 1.1×10^{-4} μg L^{-1} $cell^{-1}$ and 1.0×10^{-4} μg L^{-1} $cell^{-1}$ for the control and irradiated cultures, respectively (**Supplementary Figure 3**). Both sets of cultures showed a decline in the average Chl-a concentration per cell from day 8, which plateaued toward the end of the experiment, and the irradiated culture consistently showed significantly reduced concentrations of Chl-a per cell compared to the control. At day 16 the values were 9.4×10^{-6} μg L^{-1} $cell^{-1}$ and 3.7×10^{-5} μg L^{-1} $cell^{-1}$, for the irradiated and control cultures, respectively. The pH of the unbuffered cultures was monitored over the course of the sampling period, both cultures started off at a pH of 7.3 which increased to pH > 10 by day 4. The pH of the irradiated culture started to decline after day 4 reaching pH 9.2 at day 16 (**Figure 1D**). The pH of the control sample increased to 10.8 at day 8 and then gradually fell to 9.8 at day 16. The pH of the irradiated culture was significantly lower than seen in the control culture.

Metabolic Response of the *P. catenata* Culture to X-Ray Irradiation Determined by FT-IR Spectroscopy

FT-IR spectroscopy was utilized to obtain a metabolic fingerprint of the cultures, and to explore any physiological changes associated with irradiation. A principal component analysis (PCA) scores plot of the data (**Figure 2**) displayed clear separation of the two treatments according to PC1, which accounted for 88.6% of the total explained variance (TEV). At day 4 both sets of samples clustered together, indicating that although one set of cells was receiving the X-ray irradiation treatment there was no significant difference between the cultures; in contrast, by day 8 there was clear separation of the samples according to the PC1 axis. The samples collected on day 4 were separated from all other samples according to the PC2 axis (TEV = 5.8%), which emphases the fact that after day 4, significant metabolic changes were occurring. The control samples from day 8 to 16 form a tight cluster (in top left part of the PCA scores plot) which was distinct from the cluster at day 4. Interestingly the irradiated samples showed continued separation over time according to PC1 (from left to right) with each time point clustering closely.

According to the PC1 loadings plot (**Figure 3**) the main vibrational regions that contribute toward the separation of the samples included: 1655 cm^{-1} (amide I, C = O of proteins and peptides) (Maquelin et al., 2002); 1545 cm^{-1} (amide II, combination of in-plane N-H bending (60%) and C-N stretching (40%) of proteins, secondary structure of protein) (Lu et al., 2011); 1153 cm^{-1} (stretching vibrations of hydrogen bonded C-O groups; carbohydrates) (Pop et al., 2013; Simonova and Karamancheva, 2013); 1080 cm^{-1} (carbonyl groups in cell wall,

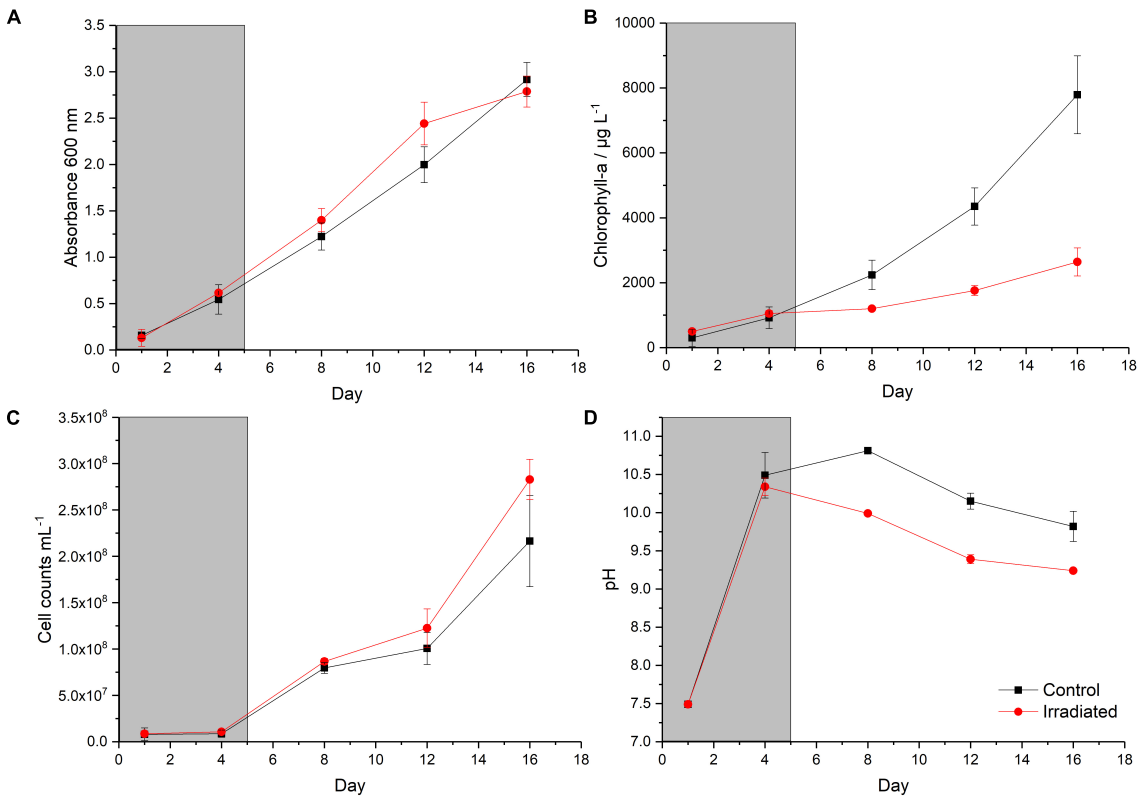

FIGURE 1 | Growth of the *P. catenata* culture with and without radiation treatment: **(A)** absorbance at 600 nm; **(B)** chlorophyll-a concentration (μg L^{-1}); **(C)** mean cell counts of *P. catenata*; **(D)** pH. The gray panel indicated the period in which the irradiation treatment was being administered. Red lines are irradiated samples; black lines are control samples. Error bars are the standard deviation of three replicates.

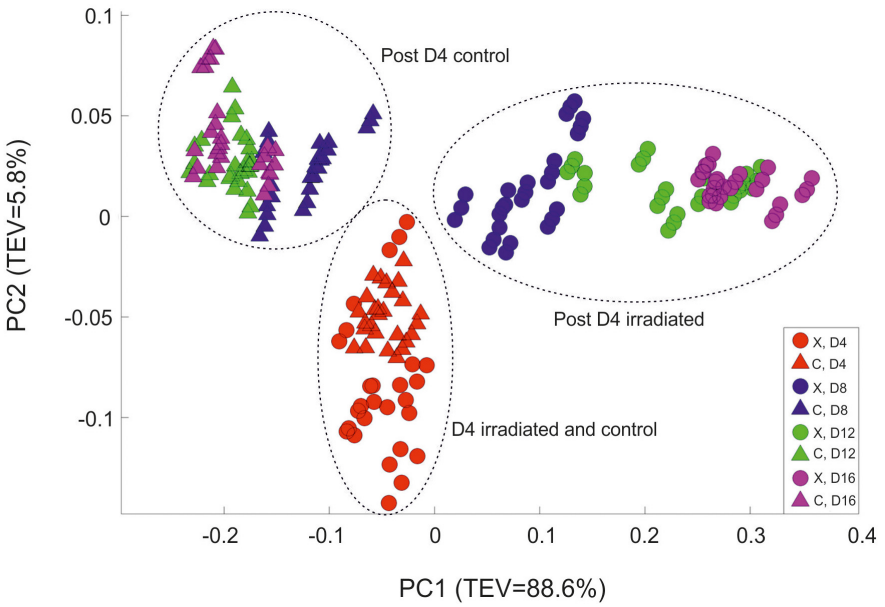

FIGURE 2 | Principal component analysis scores plot of all the FT-IR spectroscopy data. Circles represent the irradiated (X) samples; triangles are control (C) samples. Color code: Red- day 4; Blue- day 8; Green- day 12; and Purple day 16. TEV = Total Explained Variance.

glycopeptides); P = O stretching, P-O-C (P-O-P) of phospholipids and esters) (Filip et al., 2008); 1024 cm^{-1} (C-O bending and stretching typical of glycogen) (Lewis et al., 2010). The FT-IR spectra confirmed the PCA findings, with clear variance in the baseline corrected spectra apparent, which became more pronounced in the irradiated samples taken at the later time points (**Supplementary Figure 4**). Over the course of the experiment the irradiated samples showed increased spectral intensities from 1200 to 900 cm^{-1}, which is indicative of an increase in total polysaccharides (Naumann, 2000; Ellis et al., 2012). Conversely, reduced spectral intensities were apparent in the amide I and II regions at 1655 cm^{-1} and 1545 cm^{-1} which indicates that there was a reduction in the total peptide content as the irradiated cultures age (Naumann, 2000; Ellis et al., 2012). The total carbohydrate band heights at 1160, 1086, 1050, and 1036 cm^{-1} were quantified and normalized by expressing them as a "ratio value" to the lipid band at 1740 cm^{-1}, as there was no significant differences observed in this lipid band region. At day 4, the ratio value at 1160 cm^{-1} (**Figure 4**) for the irradiated sample was 1.35 (SD 0.11) compared to 1.43 (SD 0.08) in the equivalent control sample, showing that there was no significant difference in the polysaccharide levels during the irradiation treatment. The ratio value of the control samples did not vary much over the course of the sampling period, starting at 1.89 at day 4 with a slight reduction to 1.87 at day 16. The irradiated samples showed continued increases in the ratio value reaching 2.49 at day 16, a 1.85 fold increase compared to day 4. At day 16 there was a 1.97 fold increase in the polysaccharide signature of the irradiated samples compared the control. The carbohydrate bands at 1086, 1050, and 1036 cm^{-1} all showed the same trend in ratio values. The largest fold change between the day 16 samples was observed at the 1036 cm^{-1} band, which had a 2.69 fold increase in the irradiated samples.

Total Carbohydrate Concentrations

To investigate the FT-IR spectroscopy findings further, the total carbohydrate concentrations in the day 4 and day 16 samples (OD_{600nm} normalized to 15) were determined (**Figure 5**). At day 4, the concentrations were 0.13 and 0.10 $\mu g\ mL^{-1}$ for the control and irradiated samples, respectively. By day 16 the control sample had shown a slight reduction in carbohydrate levels to 0.09 $\mu g\ mL^{-1}$, which is in agreement with the ratio plots taken from the FT-IR spectroscopy data. The irradiated samples showed an increase to 0.26 $\mu g\ mL^{-1}$ at day 16 (2.69 fold increase), which is also in agreement with the FT-IR ratio plots. A comparison of the carbohydrate concentrations at day 16 showed a 2.96 fold increase in the concentration of the irradiated samples compared to the control.

Fluorescent Light Microscopy Determination of Cell Morphology and Polysaccharide Staining

Calcofluor white stain was used to label β-linked polysaccharides associated with cells in the culture, to determine if the changes seen in the FT-IR spectra and carbohydrate analyses were due to upregulation of polysaccharides associated with cells of *P. catenata*. The auto-fluorescence of *P. catenata* was also noted throughout the experiment, which gave a qualitative assessment of the levels of photosynthetic pigments in the cells/filaments. There was little difference in both the auto-fluorescence and the binding of the calcofluor white stain to the *P. catenata* filaments in either the control or the irradiated cultures whilst they were

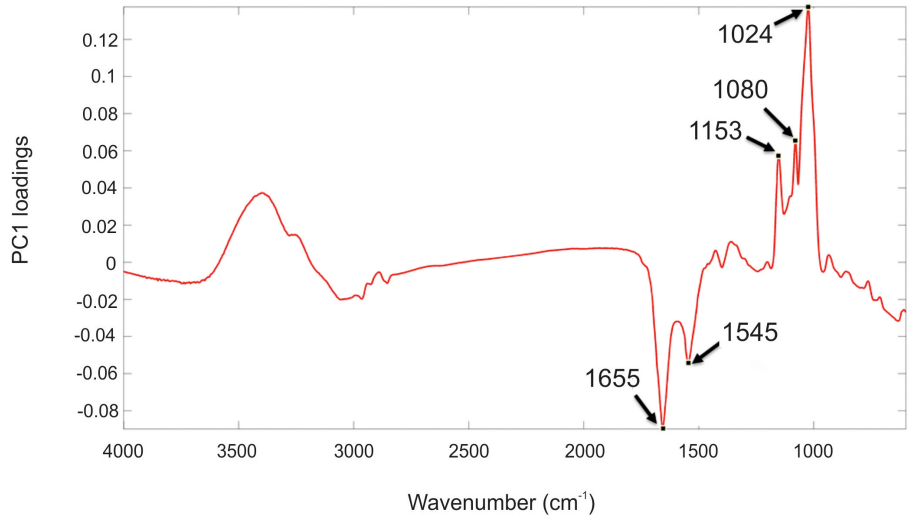

FIGURE 3 | PC1 loading plot including the wavenumbers contributing to the shifts seen across PC1. Spectral features highlighted refer to the following: 1655 cm^{-1} (amide I); 1545 cm^{-1} (amide II); 900–1200 cm^{-1} (carbohydrates).

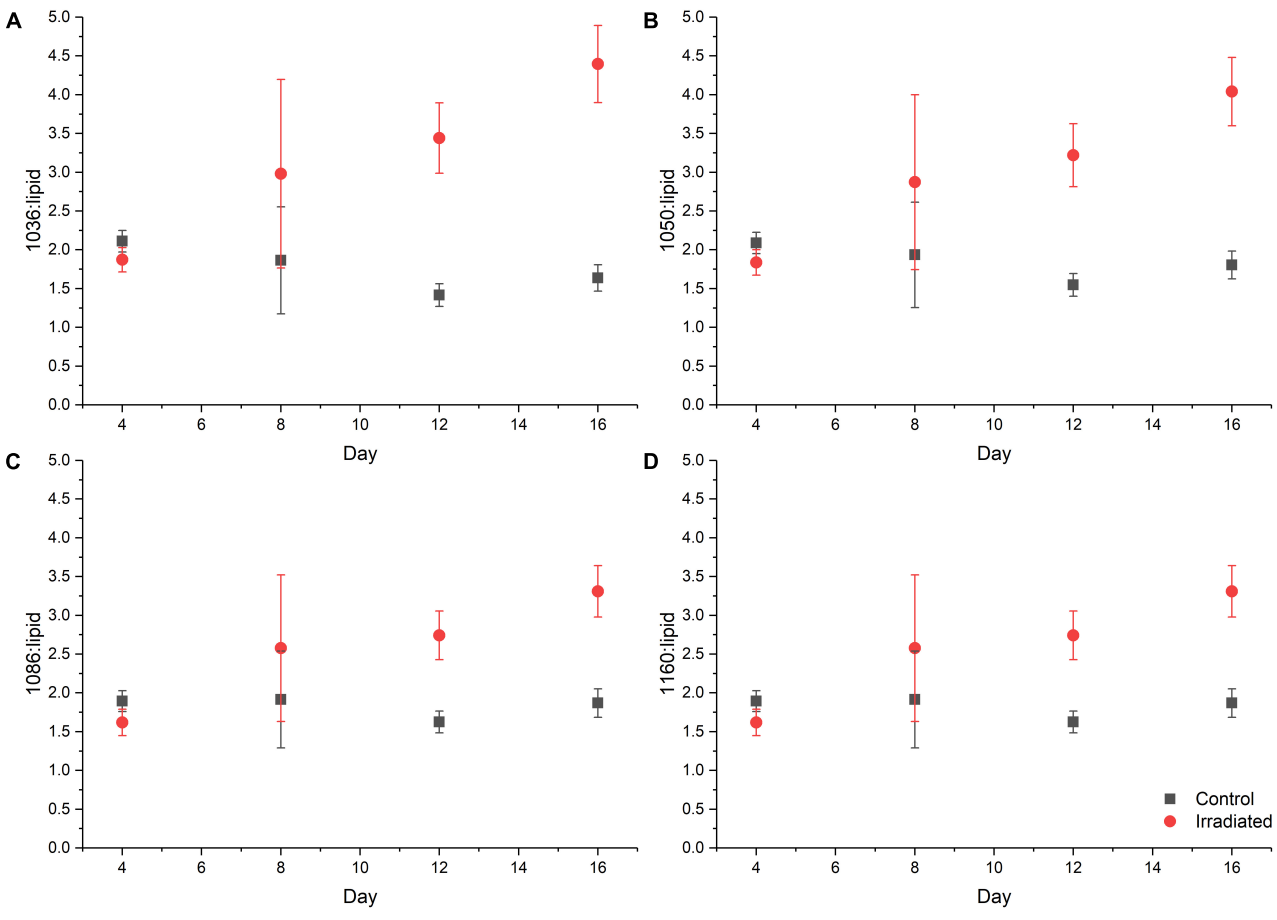

FIGURE 4 | Ratio plot of carbohydrate absorbance peaks: **(A)** 1036 cm^{-1}; **(B)** 1050 cm^{-1}; **(C)** 1086 cm^{-1}; and **(D)** 1160 cm^{-1} normalized to the lipid peak at 1740 cm^{-1} taken from FT-IR data, symbols are the means from FT-IR spectra and error bars denote one standard deviation from the mean value.

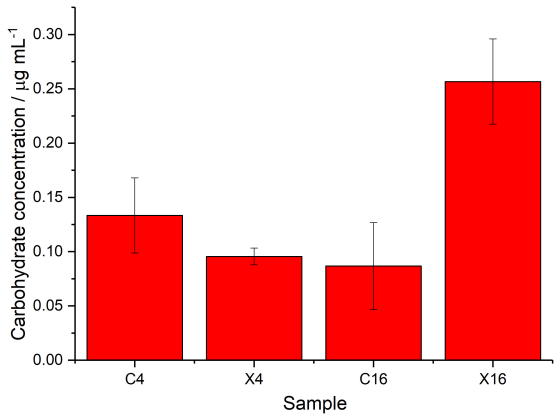

FIGURE 5 | Total cell carbohydrate concentrations measured using Sigma-Aldrich kit, samples include controls (C), and irradiated (X) at day 4 and 16, bars are the mean values from 3 measurements and error bars denote standard deviations.

still receiving the treatment at day 4 (**Supplementary Figures 5A,C**). However, by day 16 the auto-fluorescence seen across all of the *P. catenata* filaments in both treatments was more variable, with some cells lacking fluorescence altogether (**Figures 6A,C**). Interestingly, the cells that had been exposed to the irradiation treatment showed a greater degree of variability in the auto-fluorescence levels, with a higher proportion of the irradiated cells showing reduced fluorescence compared to the non-treated filaments. At day 4 the level of fluorescence with the calcofluor polysaccharide stain was comparable between the treated and non-treated cultures (**Supplementary Figures 5B,D**). The non-irradiated controls showed the same level of fluorescence with the calcofluor white stain at day 4 and day 16, suggesting similar levels of β-polysaccharides with time. The irradiated samples, however, showed increased levels of fluorescence of the calcofluor white stain at day 16 compared to the control cultures, providing evidence that irradiated *P. catenata* had higher levels of β-polysaccharides associated with the cell walls or extracellular mucilage (**Figures 6B,D**). Unwashed samples were also inspected using the calcofluor white stain, and the non-irradiated cells showed low levels of binding and fluorescence (**Figure 6E**). The stain was concentrated at the poles of the unwashed non-irradiated cells where they were connected within the filament. The unwashed irradiated cells showed the same elevated levels of fluorescence with the calcofluor stain as the washed samples. The calcofluor stain was also bound to extracellular material apparently associated with the unwashed irradiated *P. catenata* filaments, localized at the points where the cells in the filaments were connected (**Figure 6F**). This suggests that the cells were releasing β-polysaccharide containing materials into the supernatant which were removed upon washing.

DISCUSSION

The FGMSP located on the Sellafield site is colonized by microorganisms with diverse metabolic capabilities, including the potential to drive primary colonization by photosynthesis. During a microbial bloom in August 2016, a cyanobacterium belonging to the genus *Pseudanabaena* dominated the pond community (Foster et al., 2020). Here, we investigated the effect of X-ray irradiation on the growth and metabolism of a non-axenic culture of *P. catenata*. 16S rRNA gene sequencing revealed the presence of five OTUs within the *P. catenata* culture, which were consistent with genera identified in the FGMSP, making this culture an excellent representative of the pond community for model studies. The levels of radiation associated with the legacy SNFP are significant; Jackson et al. (2014) reported doses of 5.65 Gy h^{-1} associated with sludge and 0.15 mGy h^{-1} with the pond water. The dose will also be dynamic as the ponds are consistently purged with water and in pond handling activities change the radiation flux that the microorganisms are likely to be in contact with. This study assesses the effect of radiation on a *P. catenata* culture, which is related to the major photosynthetic microorganism found in a high pH and significantly radioactive legacy SNFP; here delivered at representative doses, over consecutive days.

Collectively the results of our experiments show that while the irradiation treatment was being administered to the culture there were no visible phenotypic differences observed compared to the control cultures. This suggests that the entire irradiated culture, including all microorganisms present, was able to fully tolerate the radiation dose administered. Differences between the two treatments only became apparent during the post-irradiation recovery period, and became more pronounced over time. The estimation of total biomass by the $OD_{600\,nm}$ and cell counts were the only measurements that remained comparable between the two treatments. Although the cell counts of *P. catenata* increased over time, the recorded Chl-a concentrations did not increase in line with cell numbers. Inspection of the auto-fluorescence at day 16, when the differences were greatest, showed varied levels of fluorescence across filaments. This suggests that within a filament of *P. catenata*, cells were showing different levels of photosynthetic capacity. The differences between the Chl-a concentrations, the cell numbers, and optical density readings suggest that irradiated *P. catenata* filaments had fewer photosynthetically active cells than in the control cultures. A study by Sigee et al. (2007) highlighted that estimations of total abundance of cyanobacterial populations might be misleading as some organisms are at different stages of growth and may be in a senescent state. Thus, the increase in cell numbers predicted by the optical density measurements alone may not match the number of viable and actively dividing cells.

Previous studies investigating the effect of ionizing radiation on axenic cultures of cyanobacteria have reported similar drops in chlorophyll concentrations, but after much higher doses from a ^{60}Co-gamma radiation source. El-Fatah Abomohra et al. (2016) reported up to a 25% reduction in the chlorophyll concentrations of *Arthrospira platensis* 15 days after exposure to 2.5 kGy of radiation. This coincided with a reduction in total biomass production by 34%. At lower doses of 1 and 1.5 kGy, no recorded drop in biomass was reported, however, chlorophyll concentrations were reduced by 8 and 12%, respectively. The effects of irradiation treatments on chlorophyll production is

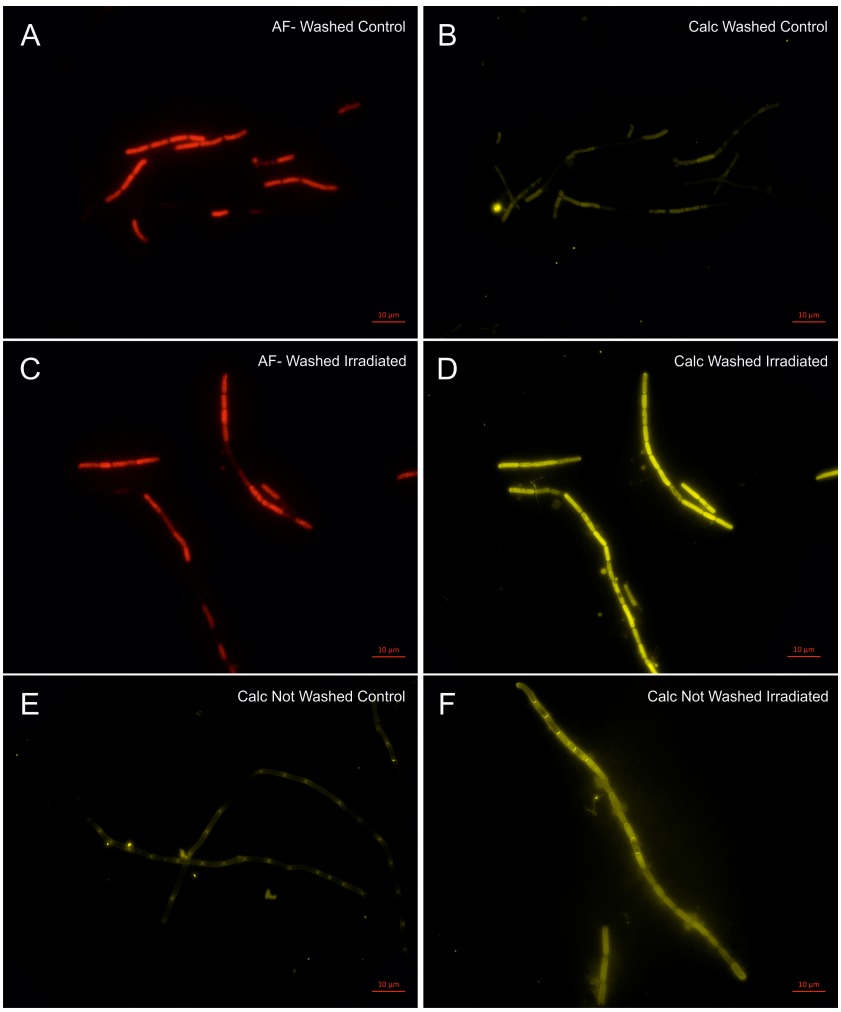

FIGURE 6 | Light microscopy of *P. catenata* filaments at day 16: **A–D** were washed twice with normal saline [0.9 g L^{-1} NaCl] **(A)** auto-fluorescence of control culture; **(B)** calcofluor white stained control culture; **(C)** auto-fluorescence of irradiated culture; **(D)** calcofluor white stained irradiated culture; **(E)** calcofluor white stained unwashed control culture; and **(F)** calcofluor white stained unwashed irradiated culture. Scale bar denotes 10 μm.

varied, however, as Badri et al. (2015) reported no significant impacts on chlorophyll when exposing *Arthrospira* cultures to similar doses used by El-Fatah Abomohra et al. (2016). The authors reported a reduction in the antenna pigments allophycocynanin and phycocynanin in addition to an increasing lag phase in growth as the dose of radiation increased. *Anabaena* cultures exposed to gamma irradiation showed bleaching of their pigments immediately after exposure to 6 kGy, with a 42.5% reduction in chlorophyll-a concentration. However, all cultures were able to recover following irradiation, although longer lag phases were observed at higher doses (Singh et al., 2013). Several studies have reported that low doses of ionizing radiation can stimulate the growth of cyanobacteria, for example Wang et al. (1998) demonstrated this with an *Arthrospira* spp. at 500 Gy, whilst several studies report the enhanced growth of a *Synechococcus* spp. at dose rates of 20 mGy y^{-1} (Conter et al., 1984, 1986). The stimulatory effect of lower chronic doses of ionizing radiation could offer a plausible explanation for the continued increase in cell numbers we observed despite the drop in chlorophyll concentration and auto-fluorescence in *P. catenata*. These studies show that the effect of radiation can be varied and that photosynthetic pigments are affected but the dose at which this is observed differs between species. The reduction in the concentration of Chl-a, alongside other processes to downregulate photosynthetic activity, could be an adaptive response to environmental stress in order to prevent photodamage and the accumulation of reactive oxygen species, that can otherwise form through uncontrolled photosynthetic electron flow (Latifi et al., 2009). Regardless, the doses applied in the current work (total of 95 Gy) were selected to be broadly representative of likely doses within the FGMSP and thus tailored to provide relevant insights. Further experimental work utilizing transcriptomic or proteomic techniques could help determine the ability of this cyanobacterium to continue to proliferate despite the reduction in Chl-a, this is, however, out of the scope of the current study.

The collected FT-IR spectral data, ratio plots of vibrational features, total cell carbohydrate concentrations and calcofluor white staining all show an overall increase in carbohydrate production over time in the irradiated cultures. From the FT-IR spectra it is not possible to determine which organisms are responsible for the differences observed, as the interrogation beam has a diameter of ∼1 mm and so measures the whole microbial community. The wavenumbers observed in the PCA loadings plots, contributing to the shifts seen in the PCA scores plots, indicate that there are potentially changes associated with intracellular and extracellular polysaccharides. The wavenumber 1024 cm^{-1} is indicative of glycogen which is a common storage molecule in cyanobacteria and some bacteria. Nutrient stress has been shown to result in increased storage of glycogen in *Synechococcus* species, however, this coincides with a reduction of growth (Klotz et al., 2016), which is not observed in the current study. Calcofluor white stain is commonly used to identify the presence of chitin, a β-polysaccharide found in fungal cell walls, but it is also used to stain a variety of β-polysaccharides (Anderson et al., 2010; Dunker et al., 2017). In our study, the calcofluor white stain was associated with the outer surface of the *P. catenata* cells, suggesting that there is an increase in β-polysaccharides associated with extracellular polymeric substances (Singh et al., 2013). It should be noted that doses of 0.5 – 1.5 kGy gamma irradiation have been shown to result in the increased production of carbohydrates in *Arthrospira* spp. in other studies (El-Fatah Abomohra et al., 2016). It is thought that the polymeric substances provide an array of functions including increasing cell buoyancy, binding metals, accumulating nutrients, aggregation of cells to one another, the formation of biofilms on surfaces and a barrier to protect against environmental stress (Nobles et al., 2001; Xu et al., 2013; Gao et al., 2015). It is not known whether the microorganisms in the legacy SNFP produce such polymeric substances; however, the similarities between the community profile in the pond and the culture used in this study suggest that this is feasible and warrants further investigation. The increased production of polysaccharides/polymeric substances by organisms in the pond could provide a mechanism to protect microorganisms from the damaging effects of reactive oxygen species, which are formed as a result of the radiolysis of water (Kottemann et al., 2005; Gao et al., 2015).

The presence of polysaccharides or polymeric substances associated with the microorganisms would also have implications for the fate of radionuclides in the pond and downstream processes. Cationic metals are able to adsorb to negatively charged functional groups on the surfaces of the microorganisms and polysaccharide containing mucilage of some cyanobacteria at neutral to alkaline pH (Gadd, 1990, 2009; Javanbakht et al., 2014; Decho and Gutierrez, 2017). Extracellular polymeric substances also have the ability to trap organic and inorganic colloids and nanoparticles, which are thought to be present in the pond (Maher et al., 2016; Decho and Gutierrez, 2017; Neil et al., 2018). The same experimental set-up described in this study was used recently to investigate the interaction of ^{90}Sr with the cell free medium from irradiated and control cultures (Ashworth et al., 2018). All of the ^{90}Sr remained in solution when it was added to the cell free medium from the control cultures, whilst the irradiated samples resulted in the removal of approximately 10% of ^{90}Sr from solution. Analyses of the supernatants showed higher total carbon levels in the control cultures (324 mg L^{-1}) compared to the medium from the irradiated cultures (162 mg L^{-1}). The lower levels of TOC in the irradiated medium observed was surprising, particularly as the calcofluor staining presented in this study indicates the presence of extracellular material in unwashed samples which are not present following centrifugation and washing. The reduced TOC in the medium from the irradiated cultures suggests that irradiated medium either has modified functional groups which better facilitate interactions with ^{90}Sr or that the irradiation treatment has resulted in the secretion of additional metabolites not present in the control samples. As noted by Ashworth et al. (2018) the level of interaction although being low is worth exploring further, as is the interaction of strontium in the presence of the microorganisms in the culture.

This study provides an insight into broad scale changes in the metabolism of a microbial community dominated by *P. catenata* in response to doses of irradiation. The metabolic responses revealed by FT-IR spectroscopy are representative of a culture-wide response, and it is therefore difficult to attribute to an individual organism. However, *P. catenata* specific responses were observed with the decline in photosynthetic pigments, whilst the calcofluor staining showed some of the changes observed in the polysaccharide levels are most likely attributed to this organism. Furthermore, the data presented here show that FT-IR spectroscopy would be a very powerful tool to investigate broad scale changes in the metabolic state of the pond community *in situ*. The utilization of additional metabolomics techniques, such as GC-MS on cell extracts and spent medium would provide further more detailed information about the different metabolic pathways, and metabolite levels that support such irradiation tolerance. In addition, other molecular techniques such as metatranscriptomics and metaproteomics, would provide information about changes in gene expression and thus provide insights into the reduced amide spectral intensities seen in the FT-IR spectroscopy data.

The FGMSP on the Sellafield site is currently being decommissioned, which involves amongst other things the removal of waste stored in the pond. In order to safely and efficiently carry out routine pond operations, visibility within the pond must be maintained. The presence of microorganisms in the pond has the potential to reduce visibility and cause delays in the on-site operations, particularly during microbial bloom events. Whilst the microbial community has recently been determined (Foster et al., 2020), little was known about the survival mechanisms the organisms used to colonize the pond. The results presented in this study provide new insights into the adaptive response of a *P. catenata* dominated culture to FGMSP relevant doses of irradiation. As noted above, the identification of increased cell polysaccharide levels is of importance since elevated polysaccharide levels could affect the behavior and fate of key radionuclides present in the pond (Gadd, 1990). High levels of polysaccharide containing material could also play a role in supporting the growth of the heterotrophic microbial community whilst

providing the microorganisms a protective barrier against the environment (Song et al., 2016). Analysis of microbial communities inhabiting SNFPs so far, indicate that the communities are specific to individual ponds. Recently the dominant algal species causing microbial blooms in a near neutral pH SNFP on the Sellafield Ltd., site, was shown to synthesize large quantities of the carotenoid astaxanthin, which is known to have antioxidant properties (MeGraw et al., 2018). The research carried out in this current study and in McGraw et al. (MeGraw et al., 2018) indicate that the adaptive response of the microbial communities is unique to the specific microorganism and the SNFP that they have colonized. A greater understanding of the microbial responses to the radiation and other stresses they encounter in the legacy pond will help to optimize control strategies used on site to control the microbial load in the pond and prevent blooms occurring during the planned decommissioning of the FGMSP over the next 20 + years. This study also provides further information about the response of microorganisms to doses of ionizing radiation that have not previously been studied, but which are relevant to critical engineered environments, including a wider range of nuclear facilities worldwide. In this context, understanding how microorganisms able to tolerate high radiation doses interact with key radionuclides, could also be key to developing innovative biotechnological approaches for treating pond waters and nuclear effluents, and is therefore an area of intense interest worldwide.

DATA AVAILABILITY STATEMENT

The raw data obtained in this research were deposited to NCBI SRA (Sequence Read Archive; http://www.ncbi.nlm.nih.gov/sra/) under the project accession number: PRJNA607014.

AUTHOR CONTRIBUTIONS

LF was the principal author, carried out the experimental work and data analysis. HM collected and analyzed the FT-IR data. CB carried out the DNA sequencing and reviewed the manuscript. DS, JP, RG, and KM developed the concept and reviewed the manuscript. JL developed the concept and extensively reviewed the manuscript.

FUNDING

LF was supported by an EPSRC PhD CASE Studentship (Grant number EP/G037426/1) with Sellafield Ltd. The authors declare that this study received funding from Sellafield Ltd. The funder had no role in the study design and analysis, decision to publish, or preparation of the manuscript.

ACKNOWLEDGMENTS

We would also like to thank Kaye Williams and Ayse Latif for allowing us the use of the Faxitron CP-160 Cabinet X-radiator.

SUPPLEMENTARY MATERIAL

The Supplementary Material for this article can be found online at: https://www.frontiersin.org/articles/10.3389/fmicb.2020.00515/full#supplementary-material

REFERENCES

Acinas, S. G., Haverkamp, T. H., Huisman, J., and Stal, L. J. (2009). Phenotypic and genetic diversification of *Pseudanabaena* spp. (*cyanobacteria*). *ISME J.* 378, 31–46. doi: 10.1038/ismej.2008.78

Anderson, C. T., Carroll, A., Akhmetova, L., and Somerville, C. (2010). Real-Time imaging of cellulose reorientation during cell wall expansion in *Arabidopsis* roots. *Plant Physiol.* 152, 787–796. doi: 10.1104/pp.109.150128

Ashworth, H., Abrahamsen, L., Bryan, N., Foster, L., Lloyd, J. R., Kellet, S., et al. (2018). Effect of humic acid and bacterial exudates on sorption-desorption interactions of ^{90}Sr with brucite. *Environ. Sci. Process. Impacts* 20, 956–964. doi: 10.1039/c8em00073e

Badri, H., Monsieurs, P., Coninx, I., Wattiez, R., and Leys, N. (2015). Molecular investigation of the radiation resistance of edible cyanobacterium *Arthrospira* sp. PCC 8005. *Microbiologyopen* 4, 187–207. doi: 10.1002/mbo3.229

Bellinger, E. G., and Sigee, D. C. (2010). *Freshwater Algae: Identification and use as Bioindicators*, 6th Edn. Hoboken, NJ: John Wiley & SONS, Ltd.

Billi, D., Friedmann, E. I., Hofer, K. G., Caiola, M. G., and Ocampo-Friedmann, R. (2000). Ionizing-radiation resistance in the desiccation-tolerant cyanobacterium *Chroococcidiopsis*. *Appl. Environ. Microbiol.* 66, 1489–1492. doi: 10.1128/aem.66.4.1489-1492.2000

Billi, D., and Potts, M. (2002). Life and death of dried prokaryotes. *Res. Microbiol.* 153, 7–12. doi: 10.1016/S0923-2508(01)01279-1277

Blanco-Rivero, A., Leganés, F., Fernández-Valiente, E., Calle, P., and Fernández-Piñas, F. (2005). mrpA, a gene with roles in resistance to Na^+ and adaptation to alkaline pH in the cyanobacterium *Anabaena* sp. PCC7120. *Microbiology* 151, 1671–1682. doi: 10.1099/mic.0.27848-27840

Bruhn, D. F., Frank, S. M., Roberto, F. F., Pinhero, P. J., and Johnson, S. G. (2009). Microbial biofilm growth on irradiated, spent nuclear fuel cladding. *J. Nucl. Mater.* 384, 140–145. doi: 10.1016/j.jnucmat.2008.11.008

Bukowska, A., Kaliñski, T., Koper, M., Kostrzewska-Szlakowska, I., Kwiatowski, J., Mazur-Marzec, H., et al. (2017). Predicting blooms of toxic cyanobacteria in eutrophic lakes with diverse cyanobacterial communities. *Sci. Rep.* 7, 1–12. doi: 10.1038/s41598-017-08701-8708

Caporaso, J. G., Kuczynski, J., Stombaugh, J., Bittinger, K., Bushman, F. D., Costello, E. K., et al. (2010). correspondence QIIME allows analysis of high-throughput community sequencing data Intensity normalization improves color calling in SOLiD sequencing. *Nat. Publ. Gr.* 7, 335–336. doi: 10.1038/nmeth0510-335

Caporaso, J. G., Lauber, C. L., Walters, W. A., Berg-Lyons, D., Huntley, J., Fierer, N., et al. (2012). Ultra-high-throughput microbial community analysis on the Illumina HiSeq and MiSeq platforms. *ISME J.* 6, 1621–1624. doi: 10.1038/ismej.2012.8

Caporaso, J. G., Lauber, C. L., Walters, W. A., Berg-Lyons, D., Lozupone, C. A., Turnbaugh, P. J., et al. (2011). Global patterns of 16S rRNA diversity at a depth of millions of sequences per sample. *Proc. Natl. Acad. Sci. U.S.A.* 108, 4516–4522. doi: 10.1073/pnas.1000080107

Chicote, E., García, A. M., Moreno, D. A., Sarró, M. I., Lorenzo, P. I, and Montero, F. (2005). Isolation and identification of bacteria from spent nuclear fuel pools. *J. Ind. Microbiol. Biotechnol.* 32, 155–162. doi: 10.1007/s10295-005-0216-213

Chicote, E., Moreno, D. A., García, A. M., Sarró, M. I., Lorenzo, P. I., and Montero, F. (2004). Biofouling on the walls of a spent nuclear fuel pool with radioactive ultrapure water. *Biofouling* 20, 35–42. doi: 10.1080/0892701041000166 2670

Conter, A., Dupouy, D., and Planel, H. (1984). Light modulation of radiosensitivity of *Synechococcus lividus* to very low doses of ionizing radiation. *Environ. Exp. Bot.* 24, 229–237. doi: 10.1016/0098-8472(84)90003-0

Conter, A., Dupouy, D., and Planel, H. (1986). Effects of dose rate on response of *Synechococcus lividus* to very low doses of chronic γ radiation : influence of enzymatic equipment of starting cells. *Radiat. Res.* 105, 379–386.

Dadachova, E., Bryan, R. A., Howell, R. C., Schweitzer, A. D., Aisen, P., Nosanchuk, J. D., et al. (2008). The radioprotective properties of fungal melanin are a function of its chemical composition, stable radical presence and spatial arrangement. *Pigment Cell Melanoma Res.* 21, 192–199. doi: 10.1111/j.1755-148X.2007.00430.x

Decho, A. W., and Gutierrez, T. (2017). Microbial extracellular polymeric substances (EPSs) in ocean systems. *Front. Microbiol.* 8:922. doi: 10.3389/fmicb.2017.00922

Dekker, L., Osborne, T. H., and Santini, J. M. (2014). Isolation and identification of cobalt- and caesium-resistant bacteria from a nuclear fuel storage pond. *FEMS Microbiol. Lett.* 359, 81–84. doi: 10.1111/1574-6968.12562

Diósi, G., Telegdi, J., Farkas, G., Gazsó, L. G., and Bokori, E. (2003). Corrosion influenced by biofilms during wet nuclear waste storage. *Int. Biodeterior. Biodegrad* 51, 151–156. doi: 10.1016/S0964-8305(02)00138-135

Dunker, S., Althammer, J., Pohnert, G., and Wilhelm, C. (2017). A fateful meeting of two phytoplankton species—chemical vs. cell-cell-interactions in co-cultures of the green algae *Oocystis marsonii* and the cyanobacterium *Microcystis aeruginosa*. *Microb. Ecol.* 74, 22–32. doi: 10.1007/s00248-016-0927-921

Edgar, R. C. (2010). Search and clustering orders of magnitude faster than BLAST. *Bioinformatics* 26, 2460–2461. doi: 10.1093/bioinformatics/btq461

Edgar, R. C. (2013). UPARSE: highly accurate OTU sequences from microbial amplicon reads. *Nat. Methods* 10, 996–998. doi: 10.1038/nmeth.2604

El-Fatah Abomohra, A., El-Shouny, W., Sharaf, M., and Abo-Eleneen, M. (2016). Effect of gamma radiation on growth and metabolic activities of *Arthrospira platensis*. *Brazilian Arch. Biol. Technol.* 59, 1–12. doi: 10.1590/1678-4324-2016150476

Ellis, D. I., Brewster, V. L., Dunn, W. B., Allwood, J. W., Golovanov, A. P., and Goodacre, R. (2012). Fingerprinting food: current technologies for the detection of food adulteration and contamination. *Chem. Soc. Rev.* 41:5706. doi: 10.1039/c2cs35138b

Filip, Z., Hermann, S., and Demnerová, K. (2008). FT-IR spectroscopic characteristics of differently cultivated *Escherichia coli*. *Czech J. Food Sci.* 26, 458–463. doi: 10.1016/j.micres.2004.05.002

Foster, L., Boothman, C., Ruiz-Lopez, S., Boshoff, G., Jenkinson, P., Sigee, D., et al. (2020). Microbial bloom formation in a high pH spent nuclear fuel pond. *Sci. Total Environ.* 720:137515. doi: 10.1016/j.scitotenv.2020.137515

Gadd, G. M. (1990). Heavy metal accumulation by bacteria and other microorganisms. *Experientia* 46, 834–840. doi: 10.1007/BF01935534

Gadd, G. M. (2009). Biosorption: critical review of scientific rationale, environmental importance and significance for pollution treatment. *J. Chem. Technol. Biotechnol.* 84, 13–28. doi: 10.1002/jctb.1999

Gao, L., Pan, X., Zhang, D., Mu, S., Lee, D. J., and Halik, U. (2015). Extracellular polymeric substances buffer against the biocidal effect of H2O2 on the bloom-forming cyanobacterium *Microcystis aeruginosa*. *Water Res.* 69, 51–58. doi: 10.1016/j.watres.2014.10.060

Gregson, C. R., Goddard, D. T., Sarsfield, M. J., and Taylor, R. J. (2011a). Combined electron microscopy and vibrational spectroscopy study of corroded Magnox sludge from a legacy spent nuclear fuel storage pond. *J. Nucl. Mater.* 412, 145–156. doi: 10.1016/j.jnucmat.2011.02.046

Gregson, C. R., Hastings, J. J., Sims, H. E., Steele, H. M., and Taylor, R. J. (2011b). Characterisation of plutonium species in alkaline liquors sampled from a UK legacy nuclear fuel storage pond. *Anal. Methods* 3:1957. doi: 10.1039/c1ay05313b

Haas, B. J., Gevers, D., Earl, A. M., Feldgarden, M., Ward, D. V., Giannoukos, G., et al. (2011). Chimeric 16S rRNA sequence formation and detection in Sanger and 454-Pyrosequenced PCR amplicons. *Genome Res.* 21, 494–504. doi: 10.1101/gr.112730.110.Freely

Jackson, S. F., Monk, S. D., and Riaz, Z. (2014). An investigation towards real time dose rate monitoring, and fuel rod detection in a First Generation Magnox Storage Pond (FGMSP). *Appl. Radiat. Isot.* 94, 254–259. doi: 10.1016/j.apradiso.2014.08.019

Javanbakht, V., Alavi, S. A., and Zilouei, H. (2014). Mechanisms of heavy metal removal using microorganisms as biosorbent. *Water Sci. Technol.* 69, 1775–1787. doi: 10.2166/wst.2013.718

Jensen, S. E., and Nønbel, E. (1999). *Description of the Magnox Type of Gas Cooled Reactor (MAGNOX)*. Available online at: https://inis.iaea.org/collection/NCLCollectionStore/_Public/30/052/30052480.pdf.

Jespersen, A.-M., and Christoffersen, K. (1987). Measurements of chlorophyll-a from phytoplankton using ethanol as extraction solvent. *Arch. Hydrobiol.* 109, 445–454.

Jolivet, E., Matsunaga, F., Ishino, Y., Forterre, P., Prieur, D., and Myllykallio, H. (2003). Physiological responses of the hyperthermophilic archaeon "*Pyrococcus abyssi*" to DNA damage caused by ionizing radiation. *J. Bacteriol.* 185, 3958–3961. doi: 10.1128/JB.185.13.3958

Joshi, N. A., and Fass, F. N. (2011). *Sickle: A Sliding-Window, Adaptive, Quality-Based Trimming Tool for FastQ Files (version 1.33)*. Available online at: https://github.com/najoshi/sickle.

Karley, D., Shukla, S. K., and Rao, T. S. (2017). Isolation and characterization of culturable bacteria present in the spent nuclear fuel pool water. *Environ. Sci. Pollut. Res.* 25, 20518–20526. doi: 10.1007/s11356-017-0376-375

Katz, A., Waridel, P., Shevchenko, A., and Pick, U. (2007). Salt-induced changes in the plasma membrane proteome of the halotolerant alga *Dunaliella salina* as revealed by blue native gel electrophoresis and nano-LC-MS/MS analysis. *Mol. Cell. Proteomics* 6, 1459–1472. doi: 10.1074/mcp.M700002-MCP200

Khan, Z., Maznah, W., Omar, W., Merican, F., Sidik, M., and Convey, P. (2018). Characterisation of *Pseudanabaena amphigranulata* (Synechococcales) isolated from a man-made pond, Malaysia: a polyphasic approach. *J. Appl. Phycol.* 30, 3187–3196. doi: 10.1007/s10811-018-1392-7

Klotz, A., Georg, J., Bučinská, L., Watanabe, S., Reimann, V., Januszewski, W., et al. (2016). Awakening of a dormant cyanobacterium from nitrogen chlorosis reveals a genetically determined program. *Curr. Biol.* 26, 2862–2872. doi: 10.1016/j.cub.2016.08.054

Konovalovaite, J. (2019). *Control of Algae in Fuel Storage Ponds*. Manchester: Univeristy of Manchester. PhD thesis.

Kottemann, M., Kish, A., Iloanusi, C., Bjork, S., and DiRuggiero, J. (2005). Physiological responses of the halophilic archaeon *Halobacterium* sp. *strain NRC*1 to desiccation and gamma irradiation. *Extremophiles* 9, 219–227. doi: 10.1007/s00792-005-0437-434

Kozich, J. J., Westcott, S. L., Baxter, N. T., Highlander, S. K., and Schloss, P. D. (2013). Development of a dual-index sequencing strategy and curation pipeline for analyzing amplicon sequence data on the MiSeq Illumina sequencing platform. *Appl. Environ. Microbiol.* 79, 5112–5120. doi: 10.1128/AEM.01043-1013

Latifi, A., Ruiz, M., and Zhang, C. C. (2009). Oxidative stress in cyanobacteria. *FEMS Microbiol. Rev.* 33, 258–278. doi: 10.1111/j.1574-6976.2008.00134.x

Lewis, P. D., Lewis, K. E., Ghosal, R., Bayliss, S., Lloyd, A. J., Wills, J., et al. (2010). Evaluation of FTIR spectroscopy as a diagnostic tool for lung cancer using sputum. *BMC Cancer* 10:640. doi: 10.1186/1471-2407-10-640

Lu, X., Liu, Q., Wu, D., Al-Qadiri, H. M., Al-Alami, N. I., Kang, D. H., et al. (2011). Using of infrared spectroscopy to study the survival and injury of *Escherichia coli* O157:H7, *Campylobacter jejuni* and *Pseudomonas aeruginosa* under cold stress in low nutrient media. *Food Microbiol.* 28, 537–546. doi: 10.1016/j.fm.2010.11.002

Maher, Z., Ivanov, P., O'Brien, L., Sims, H., Taylor, R. J., Heath, S. L., et al. (2016). Americium and plutonium association with magnesium hydroxide colloids in alkaline nuclear industry process environments. *J. Nucl. Mater.* 468, 84–96. doi: 10.1016/j.jnucmat.2015.11.010

Maquelin, K., Kirschner, C., Choo-Smith, L. P., Van Den Braak, N., Endtz, H. P., Naumann, D., et al. (2002). Identification of medically relevant microorganisms by vibrational spectroscopy. *J. Microbiol. Methods* 51, 255–271. doi: 10.1016/S0167-7012(02)00127-126

Martens, H., Nielsen, J. P., and Engelsen, S. B. (2003). Light scattering and light absorbance separated by extended multiplicative signal correction. Application

to near-infrared transmission analysis of powder mixtures. *Anal. Chem.* 75, 394–404. doi: 10.1021/ac020194w

Martin, M. (2011). Cutadapt removes adapter sequences from high-throughput sequencing reads. *EMBnet.J.* 17:10. doi: 10.14806/ej.17.1.200

Masella, A. P., Bartram, A. K., Truszkowski, J. M., Brown, D. G., and Neufeld, J. D. (2012). PANDAseq: PAired-eND assembler for Illumina sequences. *BMC Bioinformatics* 13:31. doi: 10.1186/1471-2105-13-31

MeGraw, V. E., Brown, A. R., Boothman, C., Goodacre, R., Morris, K., Sigee, D., et al. (2018). A novel adaptation mechanism underpinning algal colonization of a nuclear fuel storage pond. *MBio* 9: 02395-17. doi: 10.1128/mBio.02395-2317

Muhamadali, H., Weaver, D., Subaihi, A., AlMasoud, N., Trivedi, D. K., Ellis, D. I., et al. (2015a). Chicken, beams, and *Campylobacter*: rapid differentiation of foodborne bacteria via vibrational spectroscopy and MALDI-mass spectrometry. *Analyst* 141, 111–122. doi: 10.1039/c5an01945a

Muhamadali, H., Xu, Y., Ellis, D. I., Allwood, J. W., Rattray, N. J. W., Correa, E., et al. (2015b). Metabolic profiling of *Geobacter sulfurreducens* during industrial bioprocess scale-up. *Appl. Environ. Microbiol.* 81, 3288–3298. doi: 10.1128/AEM.00294-215

Muhamadali, H., Xu, Y., Ellis, D. I., Trivedi, D. K., Rattray, N. J. W., Bernaerts, K., et al. (2015c). Metabolomics investigation of recombinant mTNFα production in *Streptomyces lividans*. *Microb. Cell Fact.* 14, 1–12. doi: 10.1186/s12934-015-0350-351

Naumann, D. (2000). "Infrared spectroscopy in microbiology,"in *Encyclopedia of Analytical Chemistry*, ed. R. A. Meyers (Hoboken, NJ: Wiley), 102–131.

NDA (2016). *Nuclear Decommissioning Authority: Business Plan 2017 to 2020. Gov.uk*. Available online at: https://www.gov.uk/government/consultations/nuclear-decommissioning-authority-business-plan-2017-to-2020 (Accessed May 4, 2018).

Neil, T. S., Morris, K., Pearce, C. I., Sherriff, N. K., Burke, M. G., Chater, P. A., et al. (2018). Stability, composition and core-shell particle structure of uranium(IV)-silicate colloids. *Environ. Sci. Technol.* 52:16. doi: 10.1021/acs.est.8b01756

Nobles, D. R., Romanovicz, D. K., and Brown, R. M. Jr. (2001). Cellulose in cyanobacteria. Origin of vascular plant cellulose synthase? *Plant Physiol.* 127, 529–542. doi: 10.1104/pp.010557

Nurk, S., Bankevich, A., Antipov, D., Gurevich, A., Korobeynikov, A., Lapidus, A., et al. (2013). "Assembling genomes and mini-metagenomes from highly chimeric reads," in *Conference: Proceedings of the 17th international conference on research in computational molecular biology, RECOMB 2013*, Bejing, 158–170. doi: 10.1007/978-3-642-37195-0_13

Pikuta, E. V., Hoover, R. B., and Tang, J. (2007). Microbial extremophiles at the limits of life. *Crit. Rev. Microbiol.* 33, 183–209. doi: 10.1080/10408410701451948

Pop, C., Apostu, S., Rotar, A. M., Semeniuc, C. A., Sindic, M., and Mabon, N. (2013). FTIR spectroscopic characterization of a new biofilm obtained from kefiran. *J. Agroaliment. Process. Technol.* 19, 157–159.

Rivasseau, C., Farhi, E., Atteia, A., Couté, A., Gromova, M., de Gouvion Saint Cyr, D., et al. (2013). An extremely radioresistant green eukaryote for radionuclide bio-decontamination in the nuclear industry. *Energy Environ. Sci.* 6, 1230–1239. doi: 10.1039/C2ee23129h

Rivasseau, C., Farhi, E., Compagnon, E., de Gouvion Saint Cyr, D., van Lis, R., Falconet, D., et al. (2016). *Coccomyxa actinabiotis* sp. nov. (Trebouxiophyceae, Chlorophyta), a new green microalga living in the spent fuel cooling pool of a nuclear reactor. J. Phycol. 52, 689–703. doi: 10.1111/jpy.12442

Rivasseau, C., Farhi, E., Gromova, M., Ollivier, J., and Bligny, R. (2010). Resistance to irradiation of micro-algae growing in the storage pools of a nuclear reactor investigated by NMR and neutron spectroscopies. *Spectroscopy* 24, 381–385. doi: 10.3233/SPE-2010-2459

Sarró, M. I., García, A. M., and Moreno, D. A. (2005). Biofilm formation in spent nuclear fuel pools and bioremediation of radioactive water. *Int. Microbiol* 8, 223–230.

Sarró, M. I., García, A. M., Moreno, D. A., and Montero, F. (2007). Development and characterization of biofilms on stainless steel and titanium in spent nuclear fuel pools. *J. Ind. Microbiol. Biotechnol.* 34, 433–441. doi: 10.1007/s10295-007-0215-217

Sarró, M. I., Moreno, D. A., Chicote, E., Lorenzo, P. I., García, A. M., and Montero, F. (2003). Biofouling on austenitic stainless steels in spent nuclear fuel pools. *Mater. Corros. Und Korrosion* 54, 535–540. doi: 10.1002/maco.200390117

Sigee, D. C., Selwyn, A., Gallois, P., and Dean, A. P. (2007). Patterns of cell death in freshwater colonial cyanobacteria during the late summer bloom. *Phycologia* 46, 284–292. doi: 10.2216/06-69.1

Simonova, D., and Karamancheva, I. (2013). Application of Fourier transform infrared spectroscopy for tumor diagnosis. *Biotechnol. Biotechnol. Equip.* 27, 4200–4207. doi: 10.5504/BBEQ.2013.0106

Singh, H., Anurag, K., and Apte, S. K. (2013). High radiation and desiccation tolerance of nitrogen-fixing cultures of the cyanobacterium *Anabaena* sp. *strain PCC* 7120 emanates from genome/proteome repair capabilities. *Photosynth. Res.* 118, 71–81. doi: 10.1007/s11120-013-9936-9939

Song, W., Zhao, C., Zhang, D., Mu, S., and Pan, X. (2016). Different resistance to UV-B radiation of extracellular polymeric substances of two cyanobacteria from contrasting habitats. *Front. Microbiol.* 7:1208. doi: 10.3389/fmicb.2016.01208

Wang, Q., Garrity, G. M., Tiedje, J. M., and Cole, J. R. (2007). Naïve Bayesian classifier for rapid assignment of rRNA sequences into the new bacterial taxonomy. *Appl. Environ. Microbiol.* 73, 5261–5267. doi: 10.1128/AEM.00062-67

Wang, Z., Xu, B., Zhao, X., Jiang, J., and Chen, S. (1998). The effect of gamma-irradiation on different strains and morphological filaments of *Spirulina*. *Acta Agric. Univ. Zhejiangensis* 24, 121–125.

Webster-Brown, J. G., Hawes, I., Jungblut, A. D., Wood, S. A., and Christenson, H. K. (2015). The effects of entombment on water chemistry and bacterial assemblages in closed cryoconite holes on Antarctic glaciers. *FEMS Microbiol. Ecol.* 91, 1–14. doi: 10.1093/femsec/fiv144

Wold, S., Ebensen, K., and Geladi, P. (1986). Principal component analysis. *Chemom. Intell. Lab. Syst.* 2, 37–52.

Xu, H., Yu, G., and Jiang, H. (2013). Investigation on extracellular polymeric substances from mucilaginous cyanobacterial blooms in eutrophic freshwater lakes. *Chemosphere* 93, 75–81. doi: 10.1016/j.chemosphere.2013.04.077

Zhu, M., Yu, G., Song, G., Chang, J., Wan, C., and Li, R. (2015). Molecular specificity and detection for *Pseudanabaena* (cyanobacteria) species based on rbcLX sequences. *Biochem. Syst. Ecol.* 60, 110–115. doi: 10.1016/j.bse.2015.04.009

Conflict of Interest: The authors declare that the research was conducted in the absence of any commercial or financial relationships that could be construed as a potential conflict of interest.

frontiers in Microbiology

ORIGINAL RESEARCH
published: 21 May 2020
doi: 10.3389/fmicb.2020.00931

Metabolomic Analysis of *Aspergillus niger* Isolated From the International Space Station Reveals Enhanced Production Levels of the Antioxidant Pyranonigrin A

Jillian Romsdahl[1], Adriana Blachowicz[1,2], Yi-Ming Chiang[1], Kasthuri Venkateswaran[2] and Clay C. C. Wang[1,3]**

[1] Department of Pharmacology and Pharmaceutical Sciences, School of Pharmacy, University of Southern California, Los Angeles, CA, United States, [2] Biotechnology and Planetary Protection Group, Jet Propulsion Laboratory, California Institute of Technology, Pasadena, CA, United States, [3] Department of Chemistry, Dornsife College of Letters, Arts, and Sciences, University of Southern California, Los Angeles, CA, United States

OPEN ACCESS

Edited by:
Rakesh Mogul,
California State Polytechnic University, Pomona, United States

Reviewed by:
Gang Liu,
Institute of Microbiology (CAS), China
Ekaterina Shelest,
German Centre for Integrative Biodiversity Research (iDiv), Germany

***Correspondence:**
Kasthuri Venkateswaran
kjvenkat@jpl.nasa.gov
Clay C. C. Wang
clayw@usc.edu

Specialty section:
This article was submitted to Extreme Microbiology, a section of the journal Frontiers in Microbiology

Received: 23 January 2020
Accepted: 20 April 2020
Published: 21 May 2020

Citation:
Romsdahl J, Blachowicz A, Chiang Y-M, Venkateswaran K and Wang CCC (2020) Metabolomic Analysis of Aspergillus niger Isolated From the International Space Station Reveals Enhanced Production Levels of the Antioxidant Pyranonigrin A. Front. Microbiol. 11:931. doi: 10.3389/fmicb.2020.00931

Secondary metabolite (SM) production in *Aspergillus niger* JSC-093350089, isolated from the International Space Station (ISS), is reported, along with a comparison to the experimentally established strain ATCC 1015. The analysis revealed enhanced production levels of naphtho-γ-pyrones and therapeutically relevant SMs, including bicoumanigrin A, aurasperones A and B, and the antioxidant pyranonigrin A. Genetic variants that may be responsible for increased SM production levels in JSC-093350089 were identified. These findings include INDELs within the predicted promoter region of *flbA*, which encodes a developmental regulator that modulates pyranonigrin A production via regulation of Fum21. The pyranonigrin A biosynthetic gene cluster was confirmed in *A. niger*, which revealed the involvement of a previously undescribed gene, *pyrE*, in its biosynthesis. UVC sensitivity assays enabled characterization of pyranonigrin A as a UV resistance agent in the ISS isolate.

Keywords: secondary metabolites, *Aspergillus niger*, International Space Station, pyranonigrin A, antioxidant

INTRODUCTION

Filamentous fungi are ubiquitous in spacecraft environments due to anthropogenic contamination and an inability to completely sterilize the craft and cargo (Pierson, 2001; Novikova et al., 2006; Van Houdt et al., 2012). Microbial infections are a major health risk for astronauts, and are exacerbated by the combined stresses of microgravity, sleep disruption, alterations in food intake, confined living space, and high levels of radiation that can compromise the immune system (Pierson, 2001; Sonnenfeld et al., 2003). Additionally, several studies have indicated that spacecraft environments increase microbial virulence and antimicrobial resistance (Tixador et al., 1985; Wilson et al., 2007, 2008). As we make strides toward human interplanetary exploration, investigations into the characteristics of filamentous fungi that reside in spacecraft environments are critical for crew health. Additionally, such studies present diverse industrial and therapeutic opportunities, as fungi produce a plethora of bioactive secondary metabolites (SMs) in response to

external stressors. These small molecules often kill or inhibit growth of other organisms, enabling fungi to successfully compete within the complex ecosystem they reside in. While some SMs are toxic to humans, others have diverse industrial and therapeutic applications, including antibiotic, anticancer, antioxidant, immunosuppressant, and cholesterol-lowering activities (Newman and Cragg, 2012). The remarkable structural and functional diversity of fungal SMs arise from the combinatorial and modular nature of their biosynthesis, in which the SM core backbone is biosynthesized by a core synthase enzyme, such as a polyketide synthase (PKS), a nonribosomal peptide synthetase (NRPS), or a hybrid PKS-NRPS, and further diversified by a number of tailoring enzymes that are clustered together within the genome (Fischbach and Walsh, 2006).

In order to understand the characteristics of microbes residing in the International Space Station (ISS), National Aeronautics and Space Administration (NASA) has implemented a robust microbial monitoring system (Pierson et al., 2013). The filamentous fungus *Aspergillus niger* has been reported to be a predominant ISS isolate (Checinska et al., 2015), and is frequently detected in other built environments (Haleem Khan and Mohan Karuppayil, 2012; Varga et al., 2014). *A. niger* is a melanized fungal species commonly used in the biotech industry as a production host for citric acid and enzymes (Schuster et al., 2002). Melanized fungi are commonly isolated from highly irradiated environments (Singaravelan et al., 2008; Selbmann et al., 2015), and it has been reported that the electronic properties of melanin change following exposure to ionizing radiation (Dadachova et al., 2007). Additionally, several studies have reported the association of melanin production with fungal virulence (Kwon-Chung et al., 1982; Wang et al., 1995; Nosanchuk et al., 1998). Together, these findings demonstrate the need for studies that assess the characteristics of melanized fungi inhabiting spacecraft environments.

Naphtho-γ-pyrones are the predominant class of SMs produced by *A. niger*, and they possess a diverse array of reported biological properties, including anti-HIV, anti-hyperuricemia, anti-tubercular, antimicrobial, antitumor, and antioxidant activities (Choque et al., 2015). Advances in genome sequencing of *A. niger* have revealed its capacity to produce many other SMs in addition to the naphtho-γ-pyrones, as its genome harbors 46 PKSs, 35 NRPSs, and 9 NRPS-PKS hybrid genes (Romsdahl and Wang, 2019). Many of these SM biosynthesis genes are silent or expressed at very low levels in standard laboratory conditions, which has resulted in a lack of studies on SMs that may have useful industrial and therapeutic properties. Given that fungi produce SMs in response to environmental stress, investigations into SM production of *A. niger* strains isolated from space environments may reveal enhanced production levels of bioactive molecules and provide insight into the mechanisms underlying such adaptations.

Here, we report the SM production of JSC-093350089, a previously described strain of *A. niger* isolated from surfaces of the International Space Station (ISS) (Romsdahl et al., 2018). Our analysis revealed that the ISS isolate produces high levels of the antioxidant pyranonigrin A (Miyake et al., 2007), along with other bioactive SMs, such as kotanin, pestalamide B, and naphtho-γ-pyrones, when compared to the experimentally established strain ATCC 1015. To investigate differences between the strains that may explain the increased production of some SMs in JSC-093350089, we conducted a comparative genetic analysis of biosynthesis clusters and regulators of differentially produced SMs. Finally, the UV resistance potential of pyranonigrin A was assessed.

MATERIALS AND METHODS

Secondary Metabolite Extraction and Analysis

JSC-093350089 and ATCC 1015 were cultivated at 28°C on GMM agar plates, starting with 1×10^7 spores per Petri dish (D = 10 cm). After 5 days, agar was chopped into small pieces and extracted with 25 ml methanol (MeOH), followed by 25 ml 1:1 MeOH-dichloromethane, each with 1 h of sonication and filtration. The extract was evaporated *in vacuo* and re-dissolved in 2 ml of 20% dimethyl sulfoxide in MeOH and a portion (10 μl) was examined by high performance liquid chromatography-photodiode array detection-mass spectroscopy (HPLC-DAD-MS) analysis. HPLC-MS was carried out using a ThermoFinnigan LCQ Advantage ion trap mass spectrometer with a reverse-phase C18 column (3 μm; 2.1 by 100 mm; Alltech Prevail) at a flow rate of 125 μl/min. The solvent gradient for HPLC-DAD-MS was 95% MeCN/H_2O (solvent B) in 5% MeCN/H_2O (solvent A) both containing 0.05% formic acid, as follows: 0% solvent B from 0 to 5 min, 0 to 100% solvent B from 5 min to 35 min, 100 to 0% solvent B from 40 to 45 min, and re-equilibration with solvent B from 45 to 50 min.

Strains and Molecular Manipulations

The *A. niger* wild-type and mutant strains used in this study are listed in **Supplementary Table S1**, primers used in this study are listed in **Supplementary Table S2**, and diagnostic PCR results are shown in **Supplementary Figure S1**. Deletion cassettes were generated using the double joint PCR technique (**Supplementary Figure S2**; Yu et al., 2004). DNA insertions into the *A. niger* genome were performed using protoplasts and standard PEG transformation. To develop an efficient gene targeting system in JSC-093350089, the *kusA* gene was first deleted by replacing it with the hygromycin resistance marker (*hph*). The two amplified flanking sequences and the hygromycin phosphortransferase gene (*hph)* marker cassette amplified from pCB1003 (Fungal Genetics Stock Center) were fused together into one construct by fusion PCR using nested primers, and the mutation was selected for by growth on media containing 100 μg/ml hygromycin. Diagnostic PCR was performed on the deletant strain using external primers (P1 and P6) from the first round of PCR. The difference in size between the gene replaced by the selection marker and the native gene allowed us to determine whether the transformants carried the correct gene replacement.

Next, an auxotrophic mutant in the *kusA*- background was generated by deleting the *pyrG* gene. Two ∼1500 base pair fragments upstream and downstream of *pyrG* were amplified and fused together (**Supplementary Figure S3**). The mutation was

selected for by growth on media supplemented with 1.5 mg/ml of 5-fluoroorotic acid (5-FOA), as only cells lacking the *pyrG* gene can survive when 5-FOA is present. The correct transformants were identified by performing diagnostic PCR on the deletant strain using external primers (P1 and P6) from the first round of PCR. All other deletant strains were generated by replacing each target gene with the *A. fumigatus pyrG* gene (*AfpyrG*). Double deletion mutants were generated by recycling the *AfpyrG* gene in CW12006. This involved amplifying two ∼1500 base pair fragments upstream and downstream from the *alba*::*AfpyrG* region of JSC-093350089 *albA*Δ genome, which were then fused together. The mutation was selected for by growth on media supplemented with 1.5 mg/ml of 5-FOA. Correct transformants were identified using diagnostic PCR with external and internal primers (P1 and *AfpyrG* rev; *AfpyrG* Fw and P6).

To reintegrate the *kusA* gene into the genome of CW12005, the A*fpyrG* gene used to initially delete *pyrA* was deleted according to the strategy described in **Supplementary Figure S3**, which generated CW12014. The *kusA* gene was amplified from JSC-093350089 gDNA to include ∼1500 base pair fragment upstream and ∼500 bp fragment downstream from *kusA*. This fragment was then fused to the *AfpyrG* gene and the original 3′ region amplified for initial *kusA* deletion (**Supplementary Figure S4**). The *kusA* was reintegrated into the genome of CW12014 to generate CW12015. Correct transformants were identified using diagnostic PCR with external primers (P1 and P6).

Genetic Variant Analysis

Paired-end Illumina sequence reads, obtained from a previous study (Romsdahl et al., 2018), were trimmed using Trimmomatic v 0.36 (Bolger et al., 2014) and quality was checked using FastQC v 0.11.7 (Andrews, 2010). The *A. niger* ATCC 1015 genome and annotation files were downloaded from the FungiDB web portal (Stajich et al., 2012). Trimmed reads were mapped to the ATCC 1015 reference genome using the Burrows-Wheeler Aligner (BWA) software package v 0.7.17 (Li and Durbin, 2009). Mapped read files were further processed using SAMtools v 1.9 (Li et al., 2009) and PCR artifacts were removed using Picard tools MarkDuplicates[1]. Single nucleotide polymorphisms (SNPs) and insertions/deletions (INDELs) were identified using GATK v 3.8.7 (McKenna et al., 2010). Sequence reads containing putative INDELs were realigned using GATK's IndelRealigner and variants within each sample were called using GATK's Haplotype Caller. GATK's VariantFiltration was used to filter the resulting Variant Call Format (VCF) file using stringent cutoffs for quality and coverage {SNPs: QD < 2.0, MQ < 40.0, QUAL < 100, FS > 60.0, MQRankSum < -12.5, SOR > 4.0, ReadPosRankSum < -8.0; INDELs: QD < 2.0, FS > 200.0, MQRankSum < -12.5, SOR > 4, InbreedingCoeff < -0.8, ReadPosRankSum < -20.0}, so that only high-quality variants remained. PromPredict was used to predict if any upstream intergenic variants within 1000 bps of the coding sequence (CDS) occurred within the promoter region (Rangannan and Bansal, 2010; Yella et al., 2018).

[1]https://broadinstitute.github.io/picard/

UVC Resistance Analysis

UVC radiation resistance was assessed using JSC-093350089 WT and CW12015. Both strains were cultivated at 28°C on GMM agar plates by seeding 1×10^7 spores per Petri dish (D = 10 cm). Spores were collected after 5 days of growth and counted. An equal amount of spores were resuspended in 5 ml of GMM agar and poured onto Petri dishes consisting of 20 ml GMM agar. Mycelia-containing plates were exposed to varying doses of UVC radiation in triplicate using a CL-1000 Ultraviolet Crosslinker (UVP, Inc.).

RESULTS

Secondary Metabolite Analysis of JSC-093350089

SM profiles of JSC-093350089 and ATCC 1015 were examined after growth on GMM agar medium using high-performance liquid chromatography coupled with diode-array detection and electrospray ionization tandem mass spectrometry (HPLC-DAD-MS). SMs were identified based on mass, UV-Vis absorption, and retention time (**Supplementary Figure S5**), which were in good agreement with literature (Chiang et al., 2011). The identity of pyranonigrin A was further verified by purchasing the pure compound from Enzo Life Sciences (**Supplementary Figure S6**). The data revealed that each strain produced a distinct SM profile, with the production yield of most SMs significantly altered (**Figure 1A**). Production yield analysis was carried out for each SM (**Figure 1B** and **Supplementary Figure S7**). Compared to ATCC 1015, a significant decrease in the production of nigragillin, an insecticide (Isogai et al., 1975), was observed (P = 0.0001). The most significant difference was observed with the antioxidant pyranonigrin A (Miyake et al., 2007), highlighted in purple in **Figure 1A**, which exhibited a 6000% increase in production in JSC-093350089 (P = 0.04), as it was produced at basal levels in ATCC 1015. Nigerazine B displayed no statistical difference in production levels (P = 0.06). In the ISS strain, pestalamide B production was approximately 2 times that of ATCC 1015 (P = 0.03), and bicoumanigrin, which was reported to have cytotoxic activity against human cancer cell lines (Hiort et al., 2004), exhibited a production yield 2.5 times that of ATCC 1015 (P = 0.01). Kotanin production in the ISS strain was approximately 10 times that of ATCC 1015 (P = 0.03).

The majority of SMs produced were identified as naphtho-γ-pyrones, including aurasperone A, B, and C, fonsecinone A, B, and C, a fonsecinone C derivative, and asperpyrone B and C. These SMs, highlighted in green in **Figure 1A**, are biosynthesized by the PKS AlbA (Chiang et al., 2011). The molecular formula of the final SM, labeled as peak 6 in **Figure 1A**, was predicted using high-resolution mass spectrometry, and a thorough literature search revealed that no known *A. niger* SM matched this formula. This SM was later determined to also be biosynthesized by the *albA* pathway when *A. niger* devoid of AlbA failed to produce the unknown compound. The combined production yields of *albA* pathway SMs were approximately 2.5 times higher in the ISS stain compared to ATCC 1015 (P = 0.03).

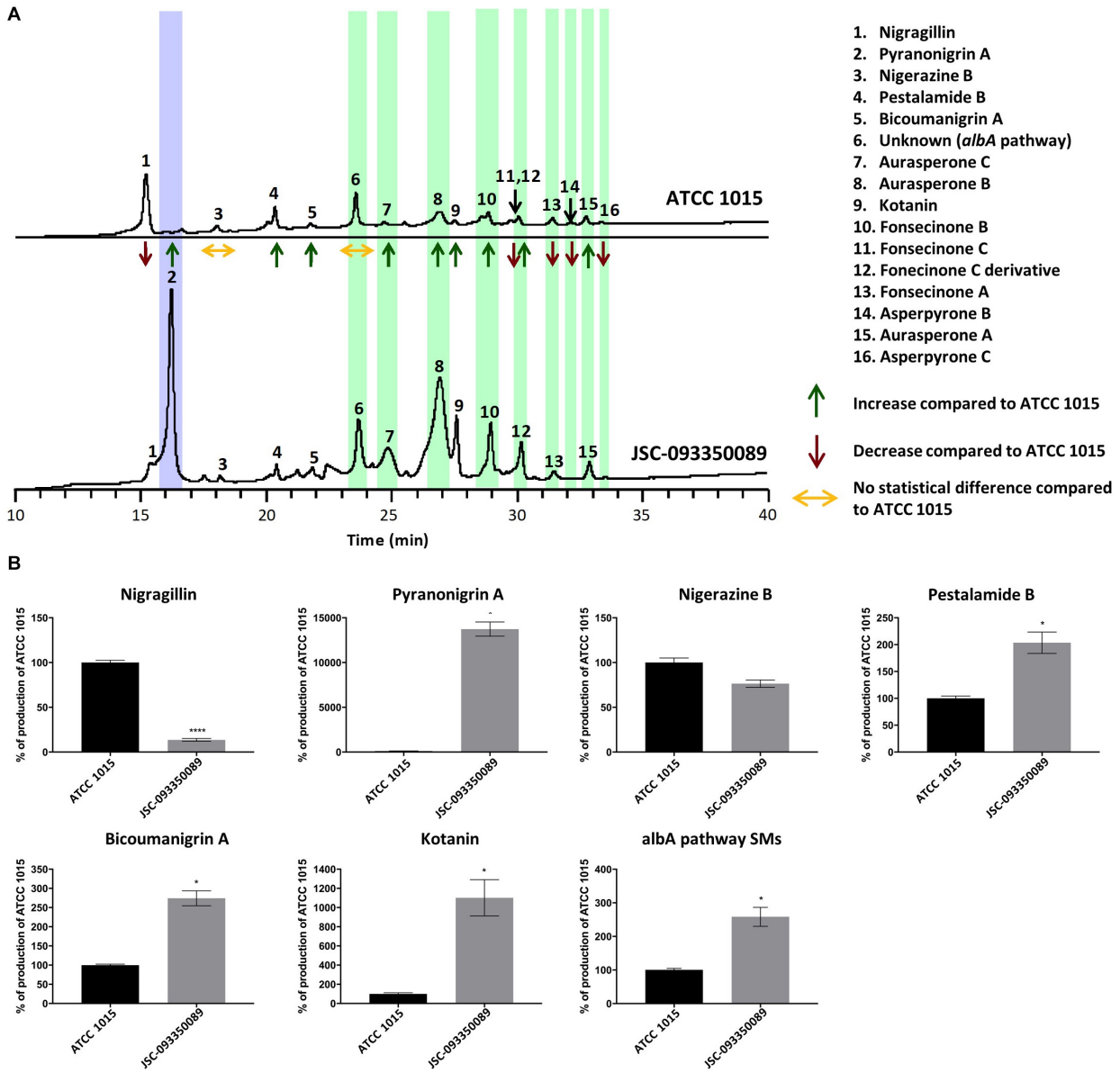

FIGURE 1 | (A) Secondary metabolite production in JSC-093350089 relative to ATCC 1015 following growth on GMM for 5 days, as detected by DAD total scan. Each individual metabolite's production yield is reported as increased, decreased, or no change, compared to that of ATCC 1015. Pyranonigrin A is highlighted in purple and *albA* pathway SMs are highlighted in green. **(B)** Quantification of secondary metabolites showing percent change for each metabolite in JSC-093350089 when compared to ATCC 1015. Significance was determined using Welch's *t*-test. $^{*}P \leq 0.05$; $^{****}P \leq 0.0001$.

Analysis of the Potential Gene Clusters Responsible for Production of Pyranonigrin A *in silico*

To facilitate a more detailed analysis of the underlying genetics that may have led to enhanced production of pyranonigrin A in JSC-093350089, we set out to identify the biosynthetic gene cluster in *A. niger*. First, we searched for the core backbone synthase gene involved in pyranonigrin A biosynthesis. The biosynthetic pathway of pyranonigrin E, a SM very similar to pyranonigrin A, was recently proposed and *pynA* (An11g00250) was identified as the PKS-NRPS hybrid involved in its biosynthesis (Awakawa et al., 2013). We hypothesized that pyranonigrin A is either biosynthesized by the same cluster responsible for pyranonigrin E production, or by a different cluster harboring a PKS-NRPS hybrid gene similar to *pynA*. The genome of ATCC 1015 possesses 8 PKS-NRPS hybrid genes other than *pynA*. BLAST analysis was performed using the Joint Genome Institute (JGI) MycoCosm database (Grigoriev et al., 2014) on the 8 remaining PKS-NRPS hybrids to determine which genes possessed high sequence homology to *pynA*. The results revealed that An18g00520 (*pyrA*) possessed high sequence

similarity to *pynA*, with 53.4% sequence identity and 89.8% subject coverage (**Supplementary Table S3**).

Development of an Efficient Gene Targeting System in JSC-093350089 and Identification of the PKS-NRPS Hybrid Responsible for Pyranonigrin A Biosynthesis

To determine which of the two putative PKS-NRPS hybrids is involved in the biosynthesis of pyranonigrin A, a genetic system was developed in JSC-093350089. The *kusA* gene was first deleted to decrease the rate of nonhomologous integration of transforming DNA fragments, thereby improving gene targeting efficiency (Meyer et al., 2007). Next, the *pyrG* gene was deleted in the *kusA*- background to generate CW12003, an auxotrophic mutant that requires uracil and uridine supplementation (Arentshorst et al., 2015). CW12003 was then used to generate mutant strains CW12004 and CW12005, which had the *pynA* gene and An18g00520 genes deleted, respectively. JSC-093350089 and the two mutant strains were then cultured on GMM, and SMs were extracted following 5 days of growth and subjected to HPLC-DAD-MS analysis. Observation of SM traces as detected by UV-Vis total scan and mass spectroscopy in positive ion mode $[M+H]^+$ $m/z = 224$ revealed pyranonigrin A production in *pynA*- (CW12004) and the complete elimination of pyranonigrin A in An18g00520- (CW12005) (**Supplementary Figure S8**), indicating that An18g00520 is responsible for the production of pyranonigrin A. This finding was recently confirmed in *Penicillium thymicola* and reported while our work was being completed (Tang et al., 2018).

Identification of Pyranonigrin A Biosynthesis Gene Cluster

Next, we aimed to identify additional genes involved in pyranonigrin A biosynthesis. To accomplish this, we identified genes surrounding *pyrA* (**Figure 2A** and **Table 1**), as the genes involved in fungal SM biosynthesis are usually clustered in the genome (Keller et al., 2005). Interestingly, when we compared the genes surrounding *pyrA* in *A. niger* to their homologs *in P. thymicola* using the JGI MycoCosm database (Grigoriev et al., 2014), we noticed that the distribution of genes surrounding *pyrA* differed between the *P. thymicola* and *A. niger* genomes (**Supplementary Figure S9**; Tang et al., 2018). For example, *pyrD*, a hydrolase predicted to be involved in pyranonigrin A biosynthesis in *P. thymicola*, is adjacent to *pyrC* in the *P. thymicola* genome and has only two genes separating it from *pyrA*. However, its homolog within the *A. niger* genome, An18g00470, is adjacent to An18g00480 and has four genes separating it from *pyrA*. Similarly, although An18g00510 is adjacent to *pyrA* in the *A. niger* genome, its *P. thymicola* homolog has three genes separating it from *pyrA* in the *P. thymicola* genome, and was predicted to not be involved in pyranonigrin A biosynthesis (Tang et al., 2018). To investigate these observations and identify genes encoding pyranonigrin A biosynthetic tailoring enzymes, we generated a gene deletion library to identify the genes involved in pyranonigrin A biosynthesis.

A. niger produces large quantities of naphtho-γ-pyrone SMs (Chiang et al., 2011), which we suspected may hinder our ability to detect any intermediate compounds in JSC-093350089 tailoring enzyme deletant strains. To circumvent this, we first generated CW12006, a JSC-093350089 mutant strain deficient in AlbA, and therefore also deficient in naphtho-γ-pyrone production. The *AfpyrG* gene was then recycled (**Supplementary Figure S3**) to enable the generation of additional deletion mutations in CW12007. Next, we used CW12007 to individually delete 5 genes surrounding *pyrA* and generate a pyranonigrin A biosynthetic gene cluster mutant library with *albA*- genetic background. The deletant strains were cultured in pyranonigrin A-producing conditions and their SM production was analyzed using HPLC-DAD-MS (**Figure 2B**). Deletion strains CW12009, CW12010, and CW12011, which had An18g00490, An18g00500, and An18g00510 deleted, respectively, resulted in the complete elimination of pyranonigrin A, which confirmed their involvement in its biosynthesis. Deletion strains CW12008 and CW12013, which had An18g00480 and An18g00530 deleted, respectively, resulted in unchanged SM profiles, which indicated that these two genes are not involved in pyranonigrin A biosynthesis. These results suggest that the pyranonigrin A biosynthetic gene cluster includes *pyrA*, *pyrB*, *pyrC*, and An18g00510, which we designated as *pyrE* (**Figure 2A** and **Table 1**).

These findings are in contrast to the recent study conducted in *P. thymicola*, which did not include *pyrE* in the proposed pyranonigrin A biosynthetic gene cluster (Tang et al., 2018). In this study, heterologous expression of the suspected *pyr* cluster and adjacent genes, which included *pyrE,* led to production of pyranonigrin A. However, *pyrE* (*orf2*) was excluded from the proposed pathway because it was found to not be expressed with the rest of the cluster in pyranonigrin A-producing conditions. Our data indicates that *pyrE* is involved in pyranonigrin A biosynthesis, which as an oxidoreductase may be responsible for the final dehydrogenation or hydroxylation step, which were previously proposed to both be carried out by *pyrB*. This does not exclude the potential involvement of *pyrD* in pyranonigrin A biosynthesis, which was found by Tang et al. (2018) to be co-regulated with *pyrA-pyrC* and was suggested to be involved in tetramic acid formation.

Genetic Variant Analysis of Clusters Producing SMs That Exhibit Increased Production Levels in JSC-093350089

Having identified the genes responsible for pyranonigrin A production in *A. niger*, we next conducted a genome-level analysis to investigate potential reasons for the enhanced pyranonigrin A production levels in JSC-093350089 relative to ATCC 1015. For this analysis, we also investigated genes involved in the production of kotanin, pestalamide B, and *albA* pathway SMs (aurasperones, fonsecinones, asperpyrones), all of which also featured increased production levels in JSC-093350089 (**Figure 1**). The biosynthetic gene cluster for kotanin

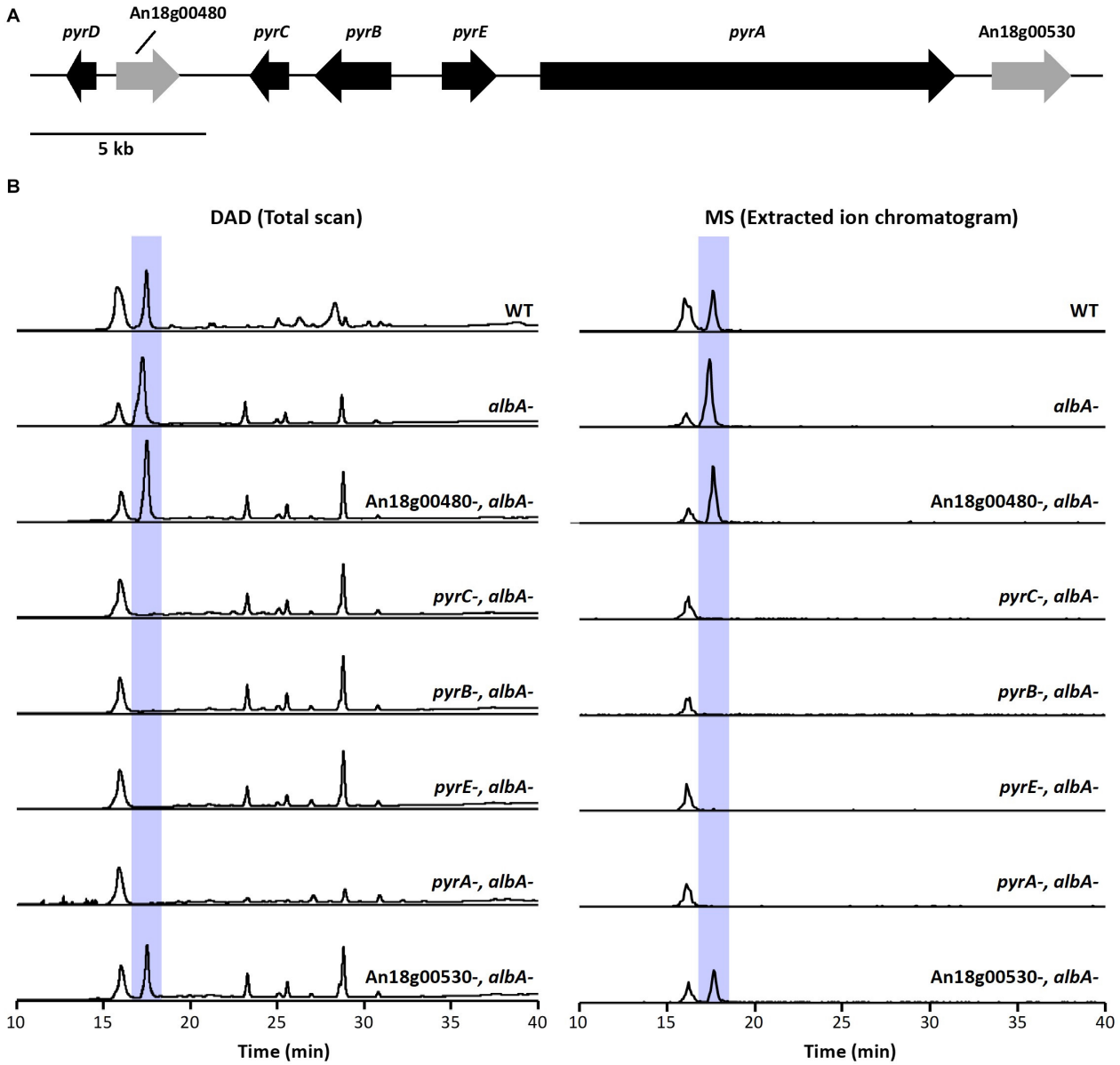

FIGURE 2 | (A) Schematic representation of *pyr* cluster. Arrows indicate direction of transcription and the relative size of each open reading frame (ORF). **(B)** DAD total scan and MS extracted ion chromatogram at *m/z* 224 of extracts from the *pyr* mutant library generated in JSC-093350089 with the *albA*- genetic background. Highlighted peaks indicate pyranonigrin A production.

TABLE 1 | Putative function of genes within the pyranonigrin A biosynthetic gene cluster and their homologs in *Penicillium thymicola*.

Pyranonigrin A biosynthesis gene	Gene name	*P. thymicola* homolog JGI protein ID	Identity (%)	Putative function
pyrD	An18g00470	180933	148/256 (58%)	Hydrolase
	An18g00480	104760	386/554 (70%)	Cyclohexamide resistance protein
pyrC	An18g00490	104735	190/269 (71%)	FAD binding monooxygenase
pyrB	An18g00500	104701	296/453 (65%)	Cytochrome P450
pyrE	An18g00510	168730	326/454 (72%)	FAD binding oxidoreductase
pyrA	An18g00520	168734	2371/3881 (61%)	PKS-NRPS hybrid
	An18g00530			Hypothetical protein

has been identified in *A. niger*, and includes genes encoding non-reducing-PKS (NR-PKS) *ktnS*, O-methytransferase *ktnB*, cytochrome P450 *ktnC*, and flavine-binding monooxygenase *ktnD* (Gil Girol et al., 2012). The biosynthetic gene cluster for pestalamide A was recently elucidated following deletion of the histone acetyltransferase *gcnE*, which led to production of pestalamide A as well as other SMs (Wang et al., 2018). Pestalamide A is a 4*H*-pyran-4-one derivative of pestalamide B, and therefore pestalamide B is likely formed from the same cluster as pestalamide A. This cluster harbors genes encoding NR-PKS *epaA*, ferulate:CoA ligase *epaB*, acyl-CoA transferase *epaC*, oxidoreductase orf1, 3-hydroxybenzoate 4-hydoxylase orf2, and salicylate hydroxylase orf3. Naphtho-γ-pyrones, including the aurasperones, fonsecinones, asperpyrones, are biosynthesized by *albA*, which encodes a PKS that is also crucial for melanin production (Chiang et al., 2011). Tailoring enzymes involved in the biosynthesis of these naphtho-γ-pyrones are not clustered with *albA* and have not been identified.

With this information at hand, we set out to identify SNPs and INDELs occurring in SM cluster regions in JSC-093350089 when compared to ATCC 1015. To accomplish this, JSC-093350089 paired-end reads, obtained from a previous study (Romsdahl et al., 2018), were aligned to the ATCC 1015 reference genome, which resulted in the identification of 5264 SNPs (**Supplementary Table S4**) and 47446 INDELs (**Supplementary Table S5**). Variants occurring within the *pyr*, *ktn*, and *epa* clusters and near the *albA* gene are displayed in **Table 2**. Within the *pyr* cluster, no variants were observed within the coding sequence (CDS) or in the upstream intergenic promoter region. One INDEL was identified downstream of the *pyrA* gene. Two INDEL variations were also observed in *pyrC* introns, and the region downstream of the *pyrC* gene was highly variable compared to ATCC 1015, harboring 19 INDELs.

Within the kotanin biosynthetic gene cluster, several mutations were observed which may have influenced regulation and/or activity of *ktnD*, whose specific role in kotanin biosynthesis remains uncharacterized (Gil Girol et al., 2012). One synonymous and two missense SNPs were observed within *ktnD*, and 3 deletions were observed in the *ktnD* upstream intergenic region 339, 458, and 555 bps away from the 5′ untranslated region (UTR). Notably, the second of these deletions, which featured a loss of 13 bps, was predicted to be within the promoter region (genomic coordinates 23456–23311) using PromPredict, which predicts promoter regions based on DNA duplex stability and has been verified across a broad range of eukaryotic genomes (Rangannan and Bansal, 2010; Yella et al., 2018). Other variations occurring within the *ktn* cluster included 3 SNPs within the intron region of *ktnA*.

Many variants were observed within the pestalamide biosynthetic gene cluster, including two missense SNPs within *epaA*, whose gene product was proposed to perform the initial reaction in pestalamide biosynthesis (Wang et al., 2018). INDELs were observed within the 3′ UTR of *epaB*, and in both the 5′ and 3′ UTR of orf1. Additionally, intergenic INDELs were observed upstream of *epaC*, orf1, and orf3, and downstream of *epaA*, e*paC*, and orf2. One synonymous SNP was observed within PKS-encoding *albA*, along with a 2 bp insertion in the downstream intergenic region.

Genetic Variant Analysis of SM Cluster Regulators

Next, we turned our attention to variations occurring in genes known to regulate the SMs that exhibited differential production in JSC-093350089, as variations in these genes may explain increased SM production levels. The transcription factor Fum21 has been reported to play a role in both pyranonigrin A and fumonisin production, with Fum21 deficiency resulting in a 25% reduction in pyranonigrin A production and complete elimination of fumonisin production (Aerts et al., 2018). Fum21 is regulated by FlbA, which is a regulator of G-protein signaling and plays a major role in sporulation (Krijgsheld et al., 2013). While the only variant associated with *fum21* was a downstream intergenic INDEL, several genetic variants within the *flbA* promoter (genomic coordinates 815849-815999) were observed, including a 16 bp insertion, a 7 bp deletion, and a 6 bp deletion (**Table 3**). Our investigation also revealed one splice region insertion and two intergenic INDELs downstream of *flbA*.

We then searched for variations within and/or nearby *gcnE*, which encodes a histone acetyltransferase responsible for the repression of several SMs in FGSC A1279, a SM-silent strain of *A. niger*, including the pestalamides and *albA* pathway naphtho-γ-pyrones (Wang et al., 2018). Our analysis revealed an upstream intergenic SNP 26 bps away from the CDS start codon, as well as a deletion in the intron region and an insertion in the downstream intergenic region (**Table 3**). Finally, we turned our attention to *azaR*, which is harbored within the pestalamide biosynthetic gene cluster and encodes a pathway-specific transcription factor (Zabala et al., 2012). We identified an insertion 222 bps away from the CDS start codon, along with a synonymous SNP and 2 downstream intergenic INDELs (**Table 3**).

Assessment of the UV Resistance Potential of Pyranonigrin A

We hypothesized that the enhanced production levels of pyranonigrin A in the ISS isolate played a role in protecting the strain from the high levels of radiation present in the spacecraft. This hypothesis was evaluated by comparing the UV sensitivity of pyranonigrin A-producing JSC-093350089 to pyranonigrin A-deficient JSC-093350089. It has been reported that *kusA* deletion significantly enhances the sensitivity of *A. niger* to UV exposure (Meyer et al., 2007). Therefore, to investigate whether pyranonigrin A confers UV resistance to *A. niger*, the *kusA* gene was first reintegrated into the *pyrA*- deletion strain (CW12005) to generate CW12015. Next, the JSC-093350089 WT and *pyrA*- strains were exposed to varying doses of UVC radiation ranging from 5–25 mJ/cm^2 in triplicate. The results indicated that pyranonigrin A deficiency significantly reduces the viability of UV-exposed strains at doses greater than 15 mJ/cm^2

TABLE 2 | Genetic variants occurring in selected SM biosynthetic cluster regions in JSC-093350089 relative to ATCC 1015.

Gene name	ATCC 1015 gene (ASPNIDRAFT2_)	CBS 513.88 gene	JSC-093350089 variant	Mutation type	SM(s) produced
pyrD	1160356	An15g00470			Pyranonigrin A
pyrC	1154752	An18g00490	• Chr20.1_A99382AACC • Chr20.1_TCCA99386T • Chr20.1_TG99395T • Chr20.1_CA99512C • Chr20.1_C99516CT • Chr20.1_G99534GA • Chr20.1_TGC99735T • Chr20.1_A99738AAT • Chr20.1_T99840TA • Chr20.1_T99874TA • Chr20.1_AT99901A • Chr20.1_A99950AGC • Chr20.1_TAA99951T • Chr20.1_T99991TG • Chr20.1_AG100072A • Chr20.1_T100104TATC • Chr20.1_T100138TTAG • Chr20.1_AG100245A • Chr20.1_TATAG100617T • Chr20.1_G101007GA • Chr20.1_AAGG101585A	• Intergenic INDEL (downstream) • Intergenic INDEL (downstream) • Intergenic INDEL (downstream) • Intergenic INDEL (downstream) • Intergenic INDEL (downstream) • Intergenic INDEL (downstream) • Intergenic INDEL (downstream) • Intergenic INDEL (downstream) • Intergenic INDEL (downstream) • Intergenic INDEL (downstream) • Intergenic INDEL (downstream) • Intergenic INDEL (downstream) • Intergenic INDEL (downstream) • Intergenic INDEL (downstream) • Intergenic INDEL (downstream) • Intergenic INDEL (downstream) • Intergenic INDEL (downstream) • Intergenic INDEL (downstream) • Intergenic INDEL (downstream) • Intron INDEL • Intron INDEL	
pyrB	1188024	An18g00500			
pyrE	1139558	An18g00510			
*pyrA**	1128344	An18g00520	Chr20.1_TGA121427T	Intergenic INDEL (downstream)	
ktnA	1222896	An04g09510	• Chr18.1_A6084T • Chr18.1_T6157C • Chr18.1_A6299G	• Intron SNP • Intron SNP • Intron SNP	Kotanin
ktnB	1126846	An04g09520			
*ktnS**	1126849	An04g09530			
ktnC	1094747	An04g09540			
ktnD	1167408	An04g09540	• Chr18.1_C21654G • Chr18.1_G21655T • Chr18.1_T21665C • Chr18.1_GA23281G • Chr18.1_TGGACTTCATTGAC23400T • Chr18.1_AG23497A	• Synonymous SNP • Missense SNP • Missense SNP • Intergenic INDEL (upstream) • Promoter region INDEL • Intergenic INDEL (upstream)	
epaC	1114645	An09g01800	• Chr1.1_CT423438C • Chr1.1_T423443TA • Chr1.1_GC425206G	• Intergenic INDEL (downstream) • Intergenic INDEL (downstream) • Intergenic INDEL (upstream)	Pestalamides
epaB	1155683	An09g01820	Chr1.1_T426759TAA	3′ UTR INDEL	
orf3	1114655	An09g01840	Chr1.1_A430682AC	Intergenic INDEL (upstream)	
orf2	1080155	An09g01850	Chr1.1_AC432567A	Intergenic INDEL (downstream)	
*epaA**	1080089	An09g01860	• Chr1.1_T436165G • Chr1.1_T439007G • Chr1.1_TC443237T • Chr1.1_GT443250G • Chr1.1_C443255CT	• Missense SNP • Missense SNP • Intergenic INDEL (downstream) • Intergenic INDEL (downstream) • Intergenic INDEL (downstream)	
orf1 (*azaJ*)	1114656	An09g01880	• Chr1.1_TTTA446289T • Chr1.1_C447318G • Chr1.1_CAA447488C • Chr1.1_A447492AAG • Chr1.1_T447561TG	• 3′ UTR INDEL • Synonymous SNP • 5′ UTR INDEL • 5′UTR INDEL • Intergenic INDEL (upstream)	
*albA**	1099425	An09g05730	• Chr1.1_T1340832TTA • Chr1.1_C1346092T	• Intergenic INDEL (downstream) • Synonymous SNP	Aurasperones, fonsecinones, asperpyrones, and melanin

**Indicates core SM synthase gene (e.g., PKS, PKS-NRPS).*

TABLE 3 | Genetic variants occurring in selected SM regulators in JSC-093350089 relative to ATCC 1015.

Gene name	ATCC 1015 gene (ASPNIDRAFT2_)	CBS 513.88 gene	JSC-093350089 variant	Mutation type	SMs regulated
fum21	225717	An01g06900	Chr4.1_TAACTCTACATCGTAG ACTATAATCTC1760977T	Intergenic INDEL (downstream)	Pyranonigrin A and fumonisins
gcnE	1149812	An01g08160	• Chr4.1_A2074326AT • Chr4.1_TC2075538T • Chr4.1_A2075689C	• Intergenic INDEL (downstream) • Intron INDEL • Intergenic SNP (upstream)	Pestalamides and aurasperones
flbA	1158125	An02g03160	• Chr10.1_CTTTTTT815881C • Chr10.1_TTTTTTTC815912T • Chr10.1_A815964ATTTTTT TTTTACCCAT • Chr10.1_C816876CT • Chr10.1_C818639CT • Chr10.1_TA819635T	• Promoter region INDEL • Promoter region INDEL • Promoter region INDEL • Splice region INDEL • Intergenic INDEL (downstream) • Intergenic INDEL (downstream)	Pyranonigrin A and fumonisins via Fum21
azaR	1079852	An09g01870	• Chr1.1_ATAC443324A • Chr1.1_T443371TATC • Chr1.1_T444140G • Chr1.1_T445465TC	• Intergenic INDEL (downstream) • Intergenic INDEL (downstream) • Synonymous SNP • Intergenic INDEL (upstream)	Pestalamides

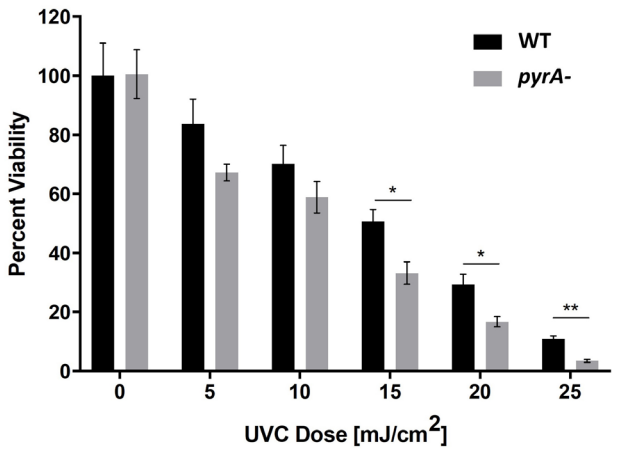

FIGURE 3 | Percent survival following exposure to varying doses of UVC radiation for JSC-093350089 WT and JSC-093350089 *pyrA-* (CW12005). $^{*}P \leq 0.05$; $^{**}P \leq 0.01$.

(**Figure 3**). The effect became more pronounced as the radiation dose increased, with an approximate viability reduction of 34% observed at 15 mJ/cm^2 ($P = 0.005$), 43% observed at 20 mJ/cm^2 ($P = 0.005$), and 68% observed at 25 mJ/cm^2 ($P = 0.0002$).

DISCUSSION

Although the persistence of *A. niger* in spacecraft (Pierson et al., 2013; Checinska et al., 2015) has been well-documented, few studies have investigated how spacecraft conditions alter its SM production. Metabolomic characterization combined with genetic analysis of *A. niger* strains that have inhabited spacecraft can provide valuable information about SM-based adaptation mechanisms of fungi capable of surviving in such environments. Additionally, despite a substantial effort to map fungal SMs to their biosynthesis genes, most clusters remain unlinked to their final product, which, in many cases, is due to the low production levels of many metabolites. There is therefore significant potential in analyzing SM production in fungal species isolated from various extreme environments, as such conditions may naturally optimize production yields of useful SMs, thereby reducing the cost of laborious laboratory-based optimization.

Metabolomic analysis of the *A. niger* laboratory strain and ISS isolate revealed significant differences in SM production levels. This finding is not surprising given the unique stresses associated with spaceflight and the fact that SM production is an evolutionary-derived trait to confer selective advantage in distinct ecological niches (Brakhage, 2013). While a recent study found that growth in ISS conditions is capable of altering SM production in *Aspergillus nidulans* (Romsdahl et al., 2019), the metabolomic changes encountered in JSC-093350089, which are conserved on Earth, are likely the result of a substantial changes at the genomic or epigenomic level, which may have been selected for by pressures associated with ISS conditions, such as microgravity, enhanced radiation, and low nutrient availability. Interestingly, the spaceflight environment appeared to select for a strain that produces enhanced levels of therapeutically relevant SMs, including the antioxidant pyranonigrin A (Miyake et al., 2007), the human cancer cytotoxic agent bicoumanigrin A (Hiort et al., 2004), the antimicrobial aurasperone A (Shaaban et al., 2012), and the antifungal and antioxidant aurasperone B (Choque et al., 2015).

Perhaps the most significant observation was enhanced production of pyranonigrin A in JSC-093350089 relative to ATCC 1015, which only produces the SM at basal levels. On the ISS, radiation capable of penetrating the spacecraft generates reactive oxygen species (ROS) within biological systems (Gabani and Singh, 2013). Oxidative stress occurs when ROS overwhelm an organism's antioxidant defense mechanisms, resulting in the generation of oxidative damage among DNA, proteins, lipids, and other vital cell components (Lehnert and Iyer, 2002; Gabani and Singh, 2013). Antioxidants have enormous therapeutic potential,

as they neutralize the harmful effects of ROS, which can cause or exacerbate a range of human diseases, including cancer, diabetes, cardiovascular, and neurodegenerative diseases (Firuzi et al., 2011). Examination of metabolic reserves of fungi isolated from enhanced radiation environments therefore provides a means of identifying fungal strains that produce optimized levels of specific therapeutics, as illustrated by this study. Further, investigation into the underlying genetics that may be responsible for increased production of bioactive compounds provides a useful starting point for future production yield optimization efforts.

We suspected that the conserved increase in some SM production levels may be due to variations within genomic regions that commonly possess regulatory elements, such as the promoter, the 5′ UTR, or the 3′ UTR. This was investigated by performing a comparative genetic analysis of SM clusters and regulators. This initially required identification of the pyranonigrin A biosynthetic gene cluster in *A. niger*, which has a different genetic architecture than the cluster identified in *P. thymicola* (**Supplementary Figure S9**; Tang et al., 2018). While confirming the involvement of these genes in *A. niger*, we identified an additional cluster gene, *pyrE*, that was previously reported to not be involved in pyranonigrin A biosynthesis.

Unexpectedly, we did not identify any variants within the *pyr* cluster that could clearly explain the significant increase in pyranonigrin A production in the ISS strain. We therefore extended our study to include genes encoding products known to regulate pyranonigrin A. Thus far, this is limited to the transcription factor Fum21, which is regulated by FlbA, a regulator of G-protein signaling that plays a critical role in sporulation and whose deficiency results in thin cell walls and cell lysis (Krijgsheld et al., 2013; Aerts et al., 2018). It has been reported that Fum21 deficiency leads to downregulation of genes from 4 different SM clusters, accompanied by a 25% reduction in pyranonigrin A production and complete elimination of fumonisin production (Aerts et al., 2018). Although we did not identify any critical mutation within/near *fum21*, our investigation revealed 3 INDELs that account for the modification of 29 bps within the promoter region of *flbA*. It is highly probable that these mutations could lead to altered regulation of FlbA, which may help explain the dramatic increase in pyranonigrin A production in the ISS strain. Further experiments should be conducted to confirm this possibility, and to explore the potential impact of the observed promoter-region mutations on other biological processes within *A. niger*, such as sporulation and cell wall structure, as such studies may provide insight into why these variations may be favorable in ISS conditions. On the other hand, increased pyranonigrin A production levels may also be the result of differences at the epigenetic level, which would be an interesting avenue to explore but was outside the scope of this investigation.

Second only to pyranonigrin A, kotanin exhibited a 10-fold increase in production levels in JSC-093350089. Within its biosynthetic gene cluster, mutations were observed within *ktnD* that could have altered both its regulation and activity, including a 13 bp deletion within the promoter region and 2 missense mutations. It is unclear whether altered regulation of *ktnD* could explain the increase in kotanin production levels, as the specific role of KtnD, a monooxygenase, in the biosynthesis of kotanin has not been determined, and KtnS was proposed to be the rate-limiting step in the pathway (Gil Girol et al., 2012).

Within the pestalamide biosynthetic cluster, several mutations were observed which may explain its twofold increase in production in the ISS strain. Two missense mutations were observed within the gene encoding EpaA, the NR-PKS proposed to perform the initial reaction in pestalamide biosynthesis. Notably, INDELs were observed within the 5′ UTR and 3′ UTR of orf1. UTRs often contain regulatory elements that play key roles in appropriate expression of a gene, and therefore the observed variation may be responsible for altered regulatory patterns of orf1, which encodes for an oxidoreductase. The gene product of orf1, also known as AzaJ, is also involved in the biosynthesis of the azanigerones, which are produced by the same cluster as the pestalamides (Zabala et al., 2012). In azanigerone biosynthesis, AzaJ is proposed to catalyze the oxidation of an aldehyde to a carboxylic acid, partially facilitating the transformation of azanigerone C to azanigerone A. In pestalamide biosynthesis, AzaJ was proposed to be involved in the generation of the intermediate carbonarone A from the polyketide precursor, which involves oxidation and transamination (Wang et al., 2018). Further studies need to be performed to determine if this step in the pathway is rate-limiting, and if altered expression of *azaJ* could be responsible for the increase in pestalamide production levels. Another potentially significant mutation that we observed was an insertion in the 3′ UTR of *epaB*, which encodes an acyl:CoA ligase that may catalyze the formation of 2-methylsuccinyl-CoA, as it plays a similar role in the azanigerone pathway. 2-methylsuccinyl-CoA is then used as a substrate by EpaC followed by cyclization to form pestalamide. Further experiments should be performed to confirm whether the observed 3′ UTR variant alters expression levels of *epaB*, which then leads to altered pestalamide production levels.

Next, we investigated genetic variants associated with genes encoding known regulators of pestalamide, including the pathway-specific transcription factor AzaR and the epigenetic regulator GcnE (Zabala et al., 2012; Wang et al., 2018). However, this analysis did not reveal any substantial findings; while both genes possess upstream intergenic variants in JSC-093350089, they were predicted to outside the promoter region.

It is reasonable to presume that enhanced production of molecules that confer oxidative stress resistance is a key adaptive characteristic of fungi inhabiting high-radiation environments, as this has been observed among other species (Baqai et al., 2009; Robinson et al., 2011). This may explain the enhanced production levels of pyranonigrin A in the ISS isolate, and is supported by the UV resistance study, which suggests that pyranonigrin A plays a role in conferring radiation resistance in *A. niger*. Additionally, we observed a cumulative increase in the production of naphtho-γ-pyrones, which are produced by AlbA, the same PKS responsible for 1,8-dihydroxynaphthalene-melanin (DHN-melanin) biosynthesis. This stays in agreement with the observed enrichment of AlbA in the proteome of JSC-093350089 relative to ATCC 1015 (Romsdahl et al., 2018). Such observations suggest that the ISS isolate produces enhanced levels of DHN-melanin, and is consistent with previous reports

that fungi inhabiting high-radiation environments produce enhanced levels of melanin (Singaravelan et al., 2008). In microbial systems, melanin functions as a UV-protectant, an antioxidant, a thermoregulator, and as a toxin-sequestering agent (Cordero and Casadevall, 2017). It is therefore reasonable to presume that increased melanin production may be an adaptive feature that is selected for by spaceflight environments. We were unable to identify any mutations associated with *albA* that may explain its upregulation and the associated increase in naphtho-γ-pyrone production. Additionally, we could not investigate variants occurring in naphtho-γ-pyrone tailoring enzymes, as those genes are not clustered with *albA* and have not yet been characterized. Further, as discussed before with regard to the pestalamides, while production levels of naphtho-γ-pyrones were reported to increase following deletion of the epigenetic regulator *gcnE*, we did not identify any mutations associated with *gcnE* that may explain increased production levels of naphtho-γ-pyrones.

In summary, this investigation revealed the distinct metabolomic fingerprint of a melanized fungal species capable of withstanding ISS conditions, which featured enhanced production of a molecule with antioxidant and UV-protective properties. Genetic analysis revealed variants that may be responsible for the observed increase in SM production levels. These findings illustrate the therapeutic and economic potential associated with investigating metabolite production in microbes isolated from extreme environments and provide a framework for future efforts to genetically optimize production yields of the bioactive SMs described in this study.

DATA AVAILABILITY STATEMENT

All datasets generated for this study are included in the article/**Supplementary Material**.

AUTHOR CONTRIBUTIONS

JR drafted the manuscript, contributed to sample processing, and was responsible for data analysis and interpretation. AB contributed to sample processing and data interpretation. Y-MC contributed to secondary metabolic analysis and interpretation. KV and CW designed the study, interpreted the data, and drafted the manuscript. All authors read and approved the final manuscript.

FUNDING

This research was supported by the JPL Advanced Concept Development fund awarded to KV that funded a student fellowship for AB. Research at USC was supported by grant from NASA. This research was funded in part by NASA's Space Biology grant number NNX15AB49G awarded to CW.

ACKNOWLEDGMENTS

We thank Duane Pierson and Victoria Castro, Johnson Space Center, for kindly providing the ISS strain used in this study. Part of the research described in this publication was carried out at the Jet Propulsion Laboratory (JPL), California Institute of Technology, under a contract with NASA. © 2020 California Institute of Technology. Government sponsorship acknowledged.

SUPPLEMENTARY MATERIAL

The Supplementary Material for this article can be found online at: https://www.frontiersin.org/articles/10.3389/fmicb.2020.00931/full#supplementary-material

REFERENCES

Aerts, D., Hauer, E. E., Ohm, R. A., Arentshorst, M., Teertstra, W. R., Phippen, C., et al. (2018). The FlbA-regulated predicted transcription factor Fum21 of *Aspergillus niger* is involved in fumonisin production. *Antonie Van Leeuwenhoek* 111, 311–322. doi: 10.1007/s10482-017-0952-1

Andrews, S. (2010). FastQC: a quality control tool for high throughput sequence data.

Arentshorst, M., Lagendijk, E. L., and Ram, A. F. (2015). A new vector for efficient gene targeting to the pyrG locus in *Aspergillus niger*. *Fungal Biol. Biotechnol.* 2:2. doi: 10.1186/s40694-015-0012-4

Awakawa, T., Yang, X.-L., Wakimoto, T., and Abe, I. (2013). Pyranonigrin E: a PKS-NRPS hybrid metabolite from *Aspergillus niger* identified by genome mining. *Chembiochem* 14, 2095–2099. doi: 10.1002/cbic.201300430

Baqai, F. P., Gridley, D. S., Slater, J. M., Luo-Owen, X., Stodieck, L. S., Ferguson, V., et al. (2009). Effects of spaceflight on innate immune function and antioxidant gene expression. *J. Appl. Physiol.* 106, 1935–1942. doi: 10.1152/japplphysiol.91361.2008

Bolger, A. M., Lohse, M., and Usadel, B. (2014). Trimmomatic: a flexible trimmer for illumina sequence data. *Bioinformatics* 30, 2114–2120. doi: 10.1093/bioinformatics/btu170

Brakhage, A. A. (2013). Regulation of fungal secondary metabolism. *Nat. Rev. Microbiol.* 11, 21–32. doi: 10.1038/nrmicro2916

Checinska, A., Probst, A. J., Vaishampayan, P., White, J. R., Kumar, D., Stepanov, V. G., et al. (2015). Microbiomes of the dust particles collected from the International Space Station and Spacecraft Assembly Facilities. *Microbiome* 3:50. doi: 10.1186/s40168-015-0116-3

Chiang, Y.-M., Meyer, K. M., Praseuth, M., Baker, S. E., Bruno, K. S., and Wang, C. C. C. (2011). Characterization of a polyketide synthase in Aspergillus niger whose product is a precursor for both dihydroxynaphthalene (DHN) melanin and naphtho-γ-pyrone. *Fungal Genet. Biol.* 48, 430–437. doi: 10.1016/j.fgb.2010.12.001

Choque, E., El Rayess, Y., Raynal, J., and Mathieu, F. (2015). Fungal naphtho-γ-pyrones—secondary metabolites of industrial interest. *Appl. Microbiol. Biotechnol.* 99, 1081–1096. doi: 10.1007/s00253-014-6295-1

Cordero, R. J. B., and Casadevall, A. (2017). Functions of fungal melanin beyond virulence. *Fungal Biol. Rev.* 31, 99–112. doi: 10.1016/j.fbr.2016.12.003

Dadachova, E., Bryan, R. A., Huang, X., Moadel, T., Schweitzer, A. D., Aisen, P., et al. (2007). Ionizing radiation changes the electronic properties of melanin and enhances the growth of melanized fungi. *PLoS One* 2:e457. doi: 10.1371/journal.pone.0000457

Firuzi, O., Miri, R., Tavakkoli, M., and Saso, L. (2011). Antioxidant therapy: current status and future prospects. *Curr. Med. Chem.* 18, 3871–3888. doi: 10.2174/092986711803414368

Fischbach, M. A., and Walsh, C. T. (2006). Assembly-line enzymology for polyketide and nonribosomal peptide antibiotics: logic, machinery,

and mechanisms. *Chem. Rev.* 106, 3468–3496. doi: 10.1021/cr050 3097

Gabani, P., and Singh, O. V. (2013). Radiation-resistant extremophiles and their potential in biotechnology and therapeutics. *Appl. Microbiol. Biotechnol.* 97, 993–1004. doi: 10.1007/s00253-012-4642-7

Gil Girol, C., Fisch, K. M., Heinekamp, T., Günther, S., Hüttel, W., Piel, J., et al. (2012). Regio- and stereoselective oxidative phenol coupling in *Aspergillus niger*. *Angew. Chem. Int. Ed.* 51, 9788–9791. doi: 10.1002/anie.201203603

Grigoriev, I. V., Nikitin, R., Haridas, S., Kuo, A., Ohm, R., Otillar, R., et al. (2014). MycoCosm portal: gearing up for 1000 fungal genomes. *Nucleic Acids Res.* 42, D699–D704. doi: 10.1093/nar/gkt1183

Haleem Khan, A. A., and Mohan Karuppayil, S. (2012). Fungal pollution of indoor environments and its management. *Saudi J. Biol. Sci.* 19, 405–426. doi: 10.1016/j.sjbs.2012.06.002

Hiort, J., Maksimenka, K., Reichert, M., PerovićOttstadt, S., Lin, W. H., Wray, V., et al. (2004). New natural products from the sponge-derived fungus *Aspergillus niger*. *J. Nat. Prod.* 67, 1532–1543. doi: 10.1021/np030551d

Isogai, A., Horii, T., Suzuki, A., Murakoshi, S., Ikeda, K., Sato, S., et al. (1975). Isolation and identification of nigragillin as a insecticidal metabolite produced by a *Aspergillus niger*. *Agric. Biol. Chem.* 39, 739–740. doi: 10.1271/bbb1961.39.739

Keller, N. P., Turner, G., and Bennett, J. W. (2005). Fungal secondary metabolism — from biochemistry to genomics. *Nat. Rev. Microbiol.* 3, 937–947. doi: 10.1038/nrmicro1286

Krijgsheld, P., Nitsche, B. M., Post, H., Levin, A. M., Müller, W. H., Heck, A. J. R., et al. (2013). Deletion of *flbA* results in increased secretome complexity and reduced secretion heterogeneity in colonies of *Aspergillus niger*. *J. Proteome Res.* 12, 1808–1819. doi: 10.1021/pr301154w

Kwon-Chung, K. J., Polacheck, I., and Popkin, T. J. (1982). Melanin-lacking mutants of Cryptococcus neoformans and their virulence for mice. *J. Bacteriol.* 150, 1414–1421.

Lehnert, B., and Iyer, R. (2002). Exposure to low-level chemicals and ionizing radiation: reactive oxygen species and cellular pathways. *Hum. Exp. Toxicol.* 21, 65–69. doi: 10.1191/0960327102ht212oa

Li, H., and Durbin, R. (2009). Fast and accurate short read alignment with Burrows-Wheeler transform. *Bioinformatics* 25, 1754–1760. doi: 10.1093/bioinformatics/btp324

Li, H., Handsaker, B., Wysoker, A., Fennell, T., Ruan, J., Homer, N., et al. (2009). The sequence alignment/map format and SAMtools. *Bioinformatics* 25, 2078–2079. doi: 10.1093/bioinformatics/btp352

McKenna, A., Hanna, M., Banks, E., Sivachenko, A., Cibulskis, K., Kernytsky, A., et al. (2010). The genome analysis toolkit: a map reduce framework for analyzing next-generation DNA sequencing data. *Genome Res.* 20, 1297–1303. doi: 10.1101/gr.107524.110

Meyer, V., Arentshorst, M., El-Ghezal, A., Drews, A.-C., Kooistra, R., van den Hondel, C. A. M. J. J., et al. (2007). Highly efficient gene targeting in the *Aspergillus niger* kusA mutant. *J. Biotechnol.* 128, 770–775. doi: 10.1016/j.jbiotec.2006.12.021

Miyake, Y., Ito, C., Itoigawa, M., and Osawa, T. (2007). Isolation of the antioxidant Pyranonigrin-A from rice mold starters used in the manufacturing process of fermented foods. *Biosci. Biotechnol. Biochem.* 71, 2515–2521. doi: 10.1271/bbb.70310

Newman, D. J., and Cragg, G. M. (2012). Natural products as sources of new drugs over the 30 years from 1981 to 2010. *J. Nat. Prod.* 75, 311–335. doi: 10.1021/np200906s

Nosanchuk, J. D., Rosas, A. L., and Casadevall, A. (1998). The antibody response to fungal melanin in mice. *J. Immunol. Baltim.* 160, 6026–6031.

Novikova, N., De Boever, P., Poddubko, S., Deshevaya, E., Polikarpov, N., Rakova, N., et al. (2006). Survey of environmental biocontamination on board the International Space Station. *Res. Microbiol.* 157, 5–12. doi: 10.1016/j.resmic.2005.07.010

Pierson, D. L. (2001). Microbial contamination of spacecraft. *Gravitational Space Biol. Bull.* 14, 1–6.

Pierson, D. L., Botkin, D. J., Bruce, R. J., Castro, V. A., Smith, M. J., Oubre, C. M., et al. (2013). *Microbial Monitoring of the International Space Station*. Available online at: https://ntrs.nasa.gov/search.jsp?R=20130013534 (accessed July 6, 2017).

Rangannan, V., and Bansal, M. (2010). High-quality annotation of promoter regions for 913 bacterial genomes. *Bioinformatics* 26, 3043–3050. doi: 10.1093/bioinformatics/btq577

Robinson, C. K., Webb, K., Kaur, A., Jaruga, P., Dizdaroglu, M., Baliga, N. S., et al. (2011). A major role for nonenzymatic antioxidant processes in the radioresistance of *Halobacterium salinarum*. *J. Bacteriol.* 193, 1653–1662. doi: 10.1128/JB.01310-10

Romsdahl, J., Blachowicz, A., Chiang, A. J., Chiang, Y.-M., Masonjones, S., Yaegashi, J., et al. (2019). International Space Station conditions alter genomics, proteomics, and metabolomics in *Aspergillus nidulans*. *Appl. Microbiol. Biotechnol.* 103, 1363–1377. doi: 10.1007/s00253-018-9525-0

Romsdahl, J., Blachowicz, A., Chiang, A. J., Singh, N., Stajich, J. E., Kalkum, M., et al. (2018). Characterization of *Aspergillus niger* isolated from the International Space Station. *mSystems* 3:e00112-18. doi: 10.1128/mSystems.00112-18

Romsdahl, J., and Wang, C. C. C. (2019). Recent advances in the genome mining of *Aspergillus* secondary metabolites (covering 2012– 2018). *Medchemcommun* 10, 840–866.

Schuster, E., Dunn-Coleman, N., Frisvad, J. C., and Van Dijck, P. W. M. (2002). On the safety of *Aspergillus niger*–a review. *Appl. Microbiol. Biotechnol.* 59, 426–435. doi: 10.1007/s00253-002-1032-6

Selbmann, L., Zucconi, L., Isola, D., and Onofri, S. (2015). Rock black fungi: excellence in the extremes, from the Antarctic to space. *Curr. Genet.* 61, 335–345. doi: 10.1007/s00294-014-0457-7

Shaaban, M., Shaaban, K. A., and Abdel-Aziz, M. S. (2012). Seven naphtho-γ-pyrones from the marine-derived fungus *Alternaria alternata*: structure elucidation and biological properties. *Org. Med. Chem. Lett.* 2:6. doi: 10.1186/2191-2858-2-6

Singaravelan, N., Grishkan, I., Beharav, A., Wakamatsu, K., Ito, S., and Nevo, E. (2008). Adaptive melanin response of the soil fungus *Aspergillus niger* to UV radiation stress at "evolution canyon", Mount Carmel, Israel. *PLoS One* 3:e2993. doi: 10.1371/journal.pone.0002993

Sonnenfeld, G., Butel, J. S., and Shearer, W. T. (2003). Effects of the space flight environment on the immune system. *Rev. Environ. Health* 18, 1–18. doi: 10.1515/REVEH.2003.18.1.1

Stajich, J. E., Harris, T., Brunk, B. P., Brestelli, J., Fischer, S., Harb, O. S., et al. (2012). FungiDB: an integrated functional genomics database for fungi. *Nucleic Acids Res.* 40, D675–D681. doi: 10.1093/nar/gkr918

Tang, M.-C., Zou, Y., Yee, D., and Tang, Y. (2018). Identification of the pyranonigrin A biosynthetic gene cluster by genome mining in *Penicillium thymicola* IBT 5891. *AIChE J.* 64, 4182–4186. doi: 10.1002/aic.16324

Tixador, R., Richoilley, G., Gasset, G., Templier, J., Bes, J., Moatti, N., et al. (1985). Study of minimal inhibitory concentration of antibiotics on bacteria cultivated in vitro in space (Cytos 2 experiment). *Aviat. Space Environ. Med.* 56, 748–751.

Van Houdt, R., Mijnendonckx, K., and Leys, N. (2012). Microbial contamination monitoring and control during human space missions. *Planet. Space Sci.* 60, 115–120. doi: 10.1016/j.pss.2011.09.001

Varga, J., Kocsubé, S., Szigeti, G., Baranyi, N., Vágvölgyi, C., Jakšić Despot, D., et al. (2014). Occurrence of black *Aspergilli* in indoor environments of six countries. *Arch. Ind. Hyg. Toxicol.* 65, 219–223. doi: 10.2478/10004-1254-65-2014-2450

Wang, B., Li, X., Yu, D., Chen, X., Tabudravu, J., Deng, H., et al. (2018). Deletion of the epigenetic regulator GcnE in *Aspergillus niger* FGSC A1279 activates the production of multiple polyketide metabolites. *Microbiol. Res.* 217, 101–107. doi: 10.1016/j.micres.2018.10.004

Wang, Y., Aisen, P., and Casadevall, A. (1995). *Cryptococcus neoformans* melanin and virulence: mechanism of action. *Infect. Immun.* 63, 3131–3136.

Wilson, J. W., Ott, C. M., Quick, L., Davis, R., Zu Bentrup, K. H., Crabbé, A., et al. (2008). Media ion composition controls regulatory and virulence response of *Salmonella* in spaceflight. *PLoS One* 3:e3923. doi: 10.1371/journal.pone.0003923

Wilson, J. W., Ott, C. M., Zu Bentrup, K. H., Ramamurthy, R., Quick, L., Porwollik, S., et al. (2007). Space flight alters bacterial gene expression and virulence and reveals a role for global regulator Hfq. *Proc. Natl. Acad. Sci. U.S.A.* 104, 16299–16304. doi: 10.1073/pnas.0707155104

Yella, V. R., Kumar, A., and Bansal, M. (2018). Identification of putative promoters in 48 eukaryotic genomes on the basis of DNA free energy. *Sci. Rep.* 8:4520. doi: 10.1038/s41598-018-22129-8

Yu, J.-H., Hamari, Z., Han, K.-H., Seo, J.-A., Reyes-Domínguez, Y., and Scazzocchio, C. (2004). Double-joint PCR: a PCR-based molecular tool for gene manipulations in filamentous fungi. *Fungal Genet. Biol.* 41, 973–981. doi: 10.1016/j.fgb.2004.08.001

Zabala, A. O., Xu, W., Chooi, Y.-H., and Tang, Y. (2012). Characterization of a silent azaphilone gene cluster from *Aspergillus niger* ATCC 1015 reveals a hydroxylation-mediated pyran-ring formation. *Chem. Biol.* 19, 1049–1059. doi: 10.1016/j.chembiol.2012.07.004

Conflict of Interest: The authors declare that the research was conducted in the absence of any commercial or financial relationships that could be construed as a potential conflict of interest.

frontiers in Microbiology

ORIGINAL RESEARCH
published: 29 July 2020
doi: 10.3389/fmicb.2020.01626

Novel Antimicrobial Cellulose Fleece Inhibits Growth of Human-Derived Biofilm-Forming Staphylococci During the SIRIUS19 Simulated Space Mission

*Daniela Wischer[1], Dominik Schneider[2], Anja Poehlein[2], Friederike Herrmann[1], Harun Oruc[1], Junias Meinhardt[1], Olaf Wagner[3], Rameez Ahmed[3], Sergey Kharin[4], Natalia Novikova[4], Rainer Haag[3], Rolf Daniel[2] and Elisabeth Grohmann[1]**

[1] Faculty of Life Sciences and Technology, Department of Microbiology, Beuth University of Applied Sciences, Berlin, Germany, [2] Department of Genomic and Applied Microbiology, Göttingen Genomics Laboratory, Institute of Microbiology and Genetics, Georg-August-University Göttingen, Göttingen, Germany, [3] Institute of Chemistry and Biochemistry, Freie Universität Berlin, Berlin, Germany, [4] Institute of Biomedical Problems (IBMP), Moscow, Russia

OPEN ACCESS

Edited by:
Rakesh Mogul,
California State Polytechnic University, Pomona, United States

Reviewed by:
Marinella Silva Laport,
Federal University of Rio de Janeiro, Brazil
Rachel Mackelprang,
California State University, Northridge, United States

***Correspondence:**
Elisabeth Grohmann
Elisabeth.grohmann@beuth-hochschule.de;
elisabeth.grohmann@googlemail.com

Specialty section:
This article was submitted to Extreme Microbiology, a section of the journal Frontiers in Microbiology

Received: 24 February 2020
Accepted: 22 June 2020
Published: 29 July 2020

Citation:
Wischer D, Schneider D, Poehlein A, Herrmann F, Oruc H, Meinhardt J, Wagner O, Ahmed R, Kharin S, Novikova N, Haag R, Daniel R and Grohmann E (2020) Novel Antimicrobial Cellulose Fleece Inhibits Growth of Human-Derived Biofilm-Forming Staphylococci During the SIRIUS19 Simulated Space Mission. Front. Microbiol. 11:1626. doi: 10.3389/fmicb.2020.01626

Two novel antimicrobial surface coatings were assessed for their lasting antibacterial effect under simulated space conditions during the SIRIUS-19 study. Because long-term space travel can affect the human immune system, astronauts are particularly susceptible to infectious disease. Moreover, the space flight environment can alter the composition of microbial communities within the spacecraft and increase bacterial virulence and resistance to antibiotics. In addition to protecting the crew from infection by human pathogens, prevention and elimination of bacterial contamination is important to avoid corrosion and damage of the technical equipment. The antimicrobial coating AGXX® consists of micro-galvanic cells composed of silver and ruthenium which damage bacterial cells through the release of reactive oxygen species. Over the last years, several studies on the antimicrobial effect of AGXX® have demonstrated an effective inhibition of growth and even complete elimination of many pathogenic bacteria – including multiresistant microorganisms – as well as their biofilms. The second antimicrobial coating, GOX, consists of chemically modified graphene oxide. Through a positive surface charge and its flexible scaffold, GOX can multivalently bind and immobilize bacteria via electrostatic attraction. Here, AGXX® and GOX were applied to non-metallic carriers not previously tested. The antimicrobial coated materials, as well as uncoated control samples, were exposed in the SIRIUS artificial space module and analyzed at different time points during the 4-months isolation study. Survival and growth of airborne heterotrophic, aerobic bacteria on the surfaces were assessed by cultivation-based methods, employing growth conditions suitable for potential human pathogens. Human-associated, biofilm-forming *Staphylococcus* spp. (*S. hominis*, *S. haemolyticus*,

and *S. epidermidis*) strongly dominated at all time points, most were resistant against erythromycin, kanamycin, and ampicillin. AGXX® coatings completely inhibited growth of these opportunistic pathogens on all tested surface materials. Particularly, AGXX®-cellulose fleece achieved a clear reduction in bacterial load able to recover post contact. GOX-cellulose fleece effectively immobilized bacteria. Sequence analysis of 16S rRNA gene amplicons revealed that the isolated *Staphylococcus* spp. did not dominate the overall bacterial community, accounting for only 0.1–0.4% of all sequences. Instead, molecular data revealed *Lactobacillus*, *Comamonas*, *Pseudomonas*, *Sporosarcina*, and *Bacillus* as the dominant genera across all samples and time points.

Keywords: antimicrobial material, SIRIUS, isolated environment, space microbiology, antibiotic resistance, human-commensal bacteria

INTRODUCTION

Space stations are confined, closed habitats with conditions that pose unique challenges to the human body and can impact the health and performance of astronauts. These stressors include environmental factors such as microgravity and radiation, as well as social stresses including isolation and sleep deprivation. Among other health effects, space flight can significantly alter immune response, and cause reactivation of latent viruses (Stowe et al., 2001; Pierson et al., 2005; Sonnenfeld, 2005; Taylor, 2015; Crucian et al., 2018; Wu et al., 2018).

Importantly, space flight conditions affect not only humans but also the microorganisms within spacecrafts, including the astronauts' microbiome (Jiang et al., 2019; Voorhies et al., 2019). Bacteria exposed to space flight conditions have been shown to respond with changes in cell morphology and cell wall thickness (Novikova et al., 2006; Zea et al., 2017), an increase in secondary metabolite and extracellular polysaccharide production (Mauclaire and Egli, 2010), increased growth rate, biofilm formation, enhanced virulence, and increased resistance to antibiotics (Rosenzweig et al., 2010; Kim et al., 2013; Taylor, 2015; Aunins et al., 2018; Fajardo-Cavazos et al., 2018; Urbaniak et al., 2018; Bai et al., 2019; Liu et al., 2019; Mora et al., 2019; Zhang et al., 2019).

Without access to medical experts, any bacterial infections arising during space missions require treatment with broad-spectrum antibiotics which further facilitates the development of antibiotic resistance (Barratt and Pool, 2008). Therefore, preventing bacterial infections of crew members during space missions is paramount. In addition to health concerns, bacterial colonization of surfaces within the spacecraft can also lead to corrosion and damage of technical equipment (Klintworth et al., 1999; Alekhova et al., 2005).

Bacterial resistance to antibiotics is becoming a serious global threat, necessitating research into effective antimicrobial alternatives. Due to its high bactericidal effect, especially silver (both in ionic and nanoparticulate form) is frequently used in wound dressings, medical devices, water treatment, textile fibers, food packaging, and anti-fouling paints (Vonberg et al., 2008; Greulich et al., 2012; Sim et al., 2018; Vila Domínguez et al., 2020). However, the extensive use of silver nanoparticles has raised concerns over the health risks and environment impacts of these products (Chopra, 2007; Greulich et al., 2012; Ostaszewska et al., 2018; Liao et al., 2019). Additionally, resistance to silver compounds in *Salmonella* spp., *Escherichia coli*, and *Pseudomonas aeruginosa* is an increasing problem (Gupta et al., 1999; Silver, 2003; Panáček et al., 2018). With this rising resistance against both conventional antibiotics and antimicrobial metals, there is an urgent need for alternative ways to fight bacterial infection.

AGXX® is an antimicrobial surface coating that combines the two noble metals silver (Ag) and ruthenium (Ru) into micro-galvanic cells conditioned with ascorbic acid. The coating can be applied to a wide range of carrier materials, including steel, glass, ceramics, and organic polymers (Guridi et al., 2015; Clauss-Lendzian et al., 2018; Loi et al., 2018; Vaishampayan et al., 2018). The antimicrobial properties of AGXX® mainly result from the release of reactive oxygen species (ROS) such as H_2O_2 and OH which are formed through a series of redox reactions (Guridi et al., 2015; Clauss-Lendzian et al., 2018; Loi et al., 2018). AGXX® is active against a wide range of microorganisms, including both Gram-positive and Gram-negative bacteria, filamentous fungi, yeasts, and some viruses (Guridi et al., 2015; Landau et al., 2017; Sobisch et al., 2019). The antibacterial effect of AGXX® is also successful against multiresistant pathogens: AGXX® killed multiresistant clinical strains of *E. faecalis*, *E. faecium*, *S. epidermidis* as well as methicillin-resistant *Staphylococcus aureus* (MRSA) and strongly reduced growth of *Legionella erythra* and the highly pathogenic Shiga toxin-producing *E. coli* O104:H4 strain (Guridi et al., 2015; Mayer et al., 2016; Clauss-Lendzian et al., 2018; Vaishampayan et al., 2018). Studies using next generation RNA sequencing revealed that exposure to AGXX® induces a broad general stress response in *E. faecalis* with up-regulation of heat shock genes and a strong oxidative stress response (Clauss-Lendzian et al., 2018). Similar studies of MRSA strains exposed to AGXX® revealed a thiol-specific oxidative stress response (Loi et al., 2018) and repression of genes for biofilm formation, virulence factors, and quorum sensing systems (Vaishampayan et al., 2018). To date, bacterial resistance against AGXX® has not been observed, making AGXX® a promising broad-spectrum antimicrobial. In a recent study carried out on the International Space Station (ISS), AGXX® was shown to strongly reduce bacterial growth on surfaces prone to

contamination, particularly by biofilm-forming Staphylococci (Sobisch et al., 2019).

Building on results by Sobisch et al. (2019) we investigated the long-term antimicrobial effect of AGXX® during SIRIUS19, a 4-months simulated space mission taking place inside the NEK facility (referred to as SIRIUS module in the text), an on-ground artificial space habitat at the Institute for Medical and Biomedical Problems at the Russian Academy of Sciences (IBMP-RAS) in Moscow, Russia. In addition to AGXX®, we investigated the effect of a second, recently developed antimicrobial coating based on graphene oxide (GO). The surface charge of the GO sheets was switched to positive by functionalization with polymers carrying positive charged groups. The resulting positively charged flexible micrometer-sized sheets are named GOX. A physical property that almost all bacteria share is their overall negative surface charge (Dickson and Koohmaraie, 1989; Silhavy et al., 2010). Positively charged surfaces can therefore promote adhesion and immobilization of bacterial cells (Gottenbos, 2001). GOX can be applied to a wide range of substrates and has been reported to exhibit antibacterial activity toward both Gram-positive and Gram-negative bacteria (*E. coli* and *S. aureus*) (Ahmed et al., 2020).

We investigated the inhibiting effect of AGXX® and GOX on surface colonization by airborne, potentially pathogenic, bacteria during the SIRIUS19 isolation study. Since these organisms are most commonly derived from the astronauts' themselves, we exposed the antimicrobial materials in an area experiencing high human traffic and physical activity by the crew members. Applications of the two antimicrobial coatings to three different, non-metallic carrier materials were tested. Bacterial communities surviving on the materials were analyzed after 1, 2, and 4 months through a combination of culture-based analyses (selecting for aerobic, heterotrophic bacteria) and 16S rRNA gene amplicon sequencing. Medically relevant bacterial isolates were characterized with regards to their antibiotic resistance profiles and biofilm formation.

MATERIALS AND METHODS

Preparation and Exposure of Antimicrobial Materials

Four different antimicrobial materials were tested: (i) fibrous web fleece (made of polyester fibers) with AGXX®, (ii) cellulose fleece with AGXX®, (iii) cellulose fleece with GOX, and (iv) polypropylene plate coated with AGXX®. Uncoated samples of each carrier material were used as controls. AGXX®-coated materials were provided by Largentec GmbH, Berlin, Germany. GOX-coated materials were supplied by the Institute of Chemistry and Biochemistry, Freie Universität Berlin, Germany. A total of 16 cm^2 of the sample materials were sterilized by autoclaving at 121°C for 20 min (fibrous web fleece, cellulose fleece) or soaking in 70% isopropyl alcohol for 30 min and drying at 60°C (polypropylene plastic) and mounted onto specially designed aluminum frames (target books, **Figure 1**) in duplicates. Two samples per material were mounted: one for cultivation experiments and one for molecular analysis. Three sets of target books, one for each time point ($t1$ = 1 month, $t2$ = 2 months, and $t3$ = 4 months, thus representing a cumulative bacterial load) were fixed on the walls of the crew's exercise room (high human traffic and high humidity) inside the SIRIUS facility at the IMBP, Moscow, Russia. In parallel, a reference experiment with the same materials and time points was set up inside a non-isolated control environment with high human traffic (microbiology laboratory at Beuth University of Applied Sciences, Berlin, Germany). At the end of each time point, samples were placed into sterile zip lock bags, transported to Berlin at 4°C and processed immediately after arrival to the laboratory.

Isolation of Bacteria and Phylogenetic Affiliation

Conditions for bacterial isolation were chosen suitable for aerobic, heterotrophic potential human pathogens, most commonly deriving from the crew's microbiome. R2A agar was used in order to accommodate also slower-growing bacteria and maximize diversity of isolates. To analyze the growth-inhibiting effect of the antimicrobial materials and to recover bacteria that survived on the surfaces following 1, 2, or 4 months exposure, the sample materials were imprinted onto R2A agar plates, allowing for transfer of cells adhering to the material. Three plates were prepared per sample, the material was pressed onto the agar with the exposed side facing down and removed after a few seconds. An additional plate was prepared for each sample where the material was not removed but remained in direct contact with the agar throughout incubation. All plates were incubated at 37°C for 24–48 h. Morphologically distinct colonies were cultivated at 37°C until pure isolates were obtained. Isolates showing weak growth on R2A were cultured on LB agar (*Staphylococci*) or glucose yeast malt extract (GYM) agar (*Actinomycetes*). Phylogenetic affiliation of isolates was carried out by matrix-assisted laser desorption ionization time-of-flight mass spectrometry (MALDI-TOF MS, Bruker Daltonics MALDI Biotyper system, Bremen, Germany) following extraction of proteins with ethanol and formic acid according to the manufacturer's instructions (Bruker MALDI Biotyper 3.1 User Manual Revision 1, D2.2). Mass spectra were compared with the MALDI-BDAL Database (Version 3.1, 7,311 entries). According to the manufacturer, the following identification scores were used: 2.0–2.299 = secure genus identification, probable species identification; and 2.3–3.0 = highly probable species identification. Scores $\geq$ 2.0 were considered as acceptable species-level identification (Schulthess et al., 2013). Each isolate was run at least three times. If identification with MALDI-TOF MS failed, isolates were phylogenetically affiliated by 16S rRNA gene sequencing (Eurofins Genomics Germany GmbH). Colony PCR was conducted as described in the section "Bacterial Colony PCR Assays." Phylogenetic affiliation of the 16S rRNA gene sequences was performed with the BLAST sequence analysis tool (Altschul et al., 1990). 16S rRNA gene sequences were compared against the nt database for initial classification and subsequently aligned against validated type strains of relevant species as specified in the List of Prokaryotic names with Standing in

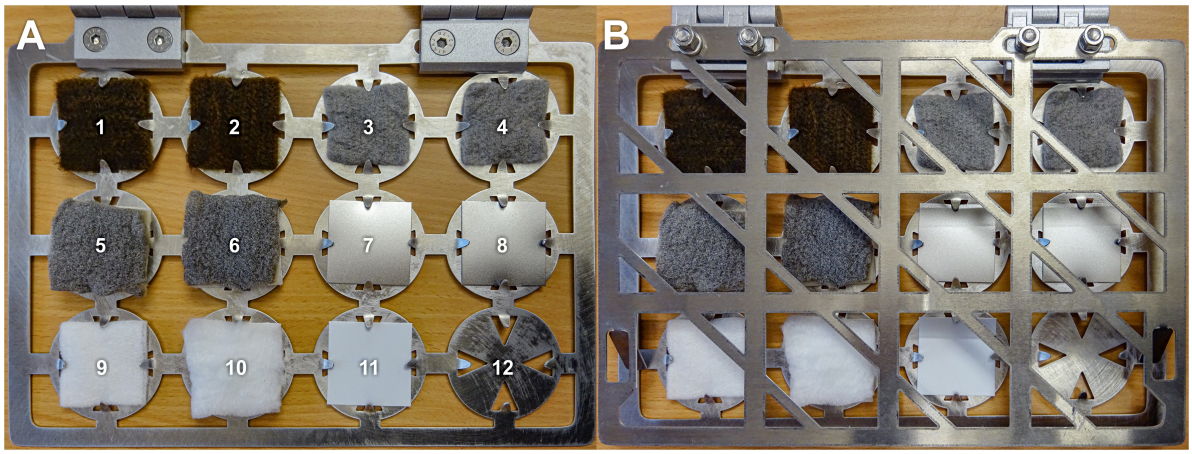

FIGURE 1 | Target book containing antimicrobial coated and uncoated sample materials (size of samples: 4 × 4 cm). **(A)** open; **(B)** closed. 1 and 2, cellulose fleece with AGXX®; 3 and 4, cellulose fleece with GOX; 5 and 6, fibrous web fleece with AGXX®; 7 and 8: polypropylene with AGXX®; 9, uncoated cellulose fleece; 10, uncoated fibrous web fleece; 11, uncoated polypropylene; and 12, empty.

Nomenclature (LPSN) online resource[1] (Parte, 2018). The isolates are denominated according to following scheme: (i) the carrier material and (ii) the antimicrobial coating they were isolated from, (iii) the study site, (iv) the exposure time (1, 2, or 3 for time points t1, t2, or t3), and (v) the order of isolation.

Biofilm Screening Assay

Biofilm formation test was carried out according to Vaishampayan et al. (2018). Briefly, bacterial isolates grown overnight in LB medium at 37°C with shaking (150 rpm) were diluted to an initial OD_{600} of 0.05 and re-grown to exponential phase (OD_{600} ∼1.5). Cultures were transferred to translucent 96-well microtitration plates (Carl Roth® GmbH & Co. KG) in replicates of eight and incubated at 37°C for 24 h. After careful removal of planktonic cultures, the wells were washed twice with 12 mM phosphate buffered saline (pH 7.4) and dried at 55°C for 1 h. Biofilms were stained with 200 µL 0.4% crystal violet solution and briefly rinsed with demineralized water. Biofilm formation was measured at 570 nm (OD_{570}) in a SpectraMax® 384 Plus Microplate Reader (Molecular Devices). *Staphylococcus aureus* 04-02981, a strong biofilm former, was used as a positive control, LB medium was used as negative control. Means of five values each and three biological replicates were used. The following criteria were used for the interpretation of the results, ODc = negative control; OD ≤ ODc = non-adherent, ODc ≤ OD ≤ (2 × ODc) = weakly adherent, (2 × ODc) < OD ≤ (4 × ODc) = moderately adherent, (4 × ODc) < OD = strongly adherent (Nyenje et al., 2013).

Antibiotic Disk Diffusion Method

Antibiotic resistance of the isolates was analyzed with the disk diffusion method (disks from Oxoid™) on Mueller Hinton agar according to guidelines of the European Committee on Antimicrobial Susceptibility Testing[2] (EUCAST, version 10.0). Sixteen medically relevant antibiotics were selected: ampicillin, oxacillin, ciprofloxacin, ofloxacin, norfloxacin, nalidixic acid, imipenem, meropenem, gentamicin, kanamycin, tetracycline, tigecycline, clindamycin, erythromycin, vancomycin, and nitrofurantoin. Of those, isolates were only screened against the ones recommended for the genus by EUCAST (**Supplementary Table 2**). Since no criteria for sensitivity testing were available for *Roseomonas* or *Paracoccus*, EUCAST criteria for *Pseudomonas* spp. were used. Each test was performed in triplicates. Multidrug-resistant (MDR) strains were defined as non-susceptible to at least one antimicrobial agent in three or more antimicrobial categories as proposed by Magiorakos et al. (2012).

DNA Extraction

Metagenomic DNA was extracted from coated and uncoated cellulose fleece samples using the NucleoSpin® Soil DNA extraction kit (Macherey-Nagel). For removal of cells from the material, the cellulose squares were cut into small pieces, suspended in phosphate buffered saline (pH 7.4), thoroughly vortexed for 5 min and incubated in an ultrasound bath (Sonorex RK 106S, Bandelin) for 20 min. Cellulose fibers were removed by passing the suspension through sterile syringes. The filtrate was pelleted by centrifugation at 18,500 × *g* for 30 min in a Thermo Scientific™ Heraeus™ Multifuge™ X3 (Thermo Scientific™). Cell pellets were resuspended with lysis buffer SL2 from the extraction kit, transferred to NucleoSpin® Soil bead tubes and processed according to the manual.

Bacterial Colony PCR Assays

Details of all primer sets can be found in **Supplementary Table 1**. For 16S rRNA gene colony PCR assays the primer set 27_fwd/536_rev was used. A single bacterial colony was suspended in 200 µL sterile, nuclease-free water and incubated at

[1]https://lpsn.dsmz.de/

[2]http://www.eucast.org

95°C for 5 min. A total of 1 μL was used as template for a 10 μL PCR reaction. PCR reactions contained 0.25 U Taq-Polymerase (VWR), 1 μL 10× PCR reaction buffer S (VWR), 0.2 μM of each primer, 250 μM of each deoxynucleoside triphosphate (dNTP), 0.6 μg/μL bovine serum albumin (BSA), and 1 μL template DNA. All DNA amplifications were carried out in a S10000^{TM} Thermal Cycler (BIO-RAD). Thermal cycling conditions for colony PCR were as follows: initial denaturation for 1 min at 95°C, 30 cycles at 95°C for 30 s, 30 s at 55°C, and 10 s at 72°C, and a final extension at 72°C for 5 min.

Amplicon Sequence Analysis

PCR Assays

For amplicon sequencing, bacterial 16S rRNA genes were amplified using primer set S-D-Bact-0341-b-S-17-N/S-D-Bact-0785-a-A-21-N (Herlemann et al., 2011; Klindworth et al., 2013; **Supplementary Table 1**) and the Phusion® High Fidelity PCR kit (New England Biolabs). A total of 50 μL PCR reactions were carried out in triplicates. Each reaction contained 1 U Phusion® high-fidelity DNA-polymerase, 10 μL 5× Phusion GC buffer, 0.2 mM $MgCl_2$, 0.2 μM of each primer, 200 μM of each dNTP, 0.6 μg/μL BSA, 5% dimethylsulfoxide (DMSO), and 1–3 ng template DNA. Thermal cycling scheme for bacterial amplicons was as follows: initial denaturation for 1 min at 98°C, 30 cycles at 98°C for 45 s, 45 s at 57°C, and 30 s at 72°C, and a final extension at 72°C for 5 min. The resulting PCR products were analyzed and quantified by agarose gel electrophoresis, purified using the NucleoMag® 96 PCR clean-up kit (Macherey-Nagel) and pooled for amplicon sequencing.

Library Preparation and Sequencing

PCR products were used to attach indices and Illumina sequencing adapters using the Nextera XT Index kit (Illumina, San Diego). Index PCR was performed using 5 μL of template PCR product, 2.5 μL of each index primer, 12.5 μL of 2× KAPA HiFi HotStart ReadyMix and 2.5 μL PCR grade water. Thermal cycling scheme was as follows: 95°C for 3 min, eight cycles of 30 s at 95°C, 30 s at 55°C, and 30 s at 72°C and a final extension at 72°C for 5 min. Quantification of the products was performed using the Quant-iT dsDNA HS assay kit and a Qubit fluorometer (Invitrogen GmbH, Karlsruhe, Germany) following the manufacturer's instructions. MagSi-NGS^{PREP} Plus Magnetic beads (Steinbrenner Laborsysteme GmbH, Wiesenbach, Germany) were used for purification of the indexed products as recommended by the manufacturer and normalization of all libraries to the same concentration was performed using the Janus Automated Workstation from Perkin Elmer (Perkin Elmer, Waltham, MA, United States). Sequencing was conducted using Illumina MiSeq platform using dual indexing and MiSeq reagent kit v3 (600 cycles) as recommended by the manufacturer.

Sequence Processing and Analyses

Demultiplexing and clipping of adapter sequences from the raw amplicon sequences were performed with the CASAVA software (Illumina). The program fastp (v0.20.0) (Chen et al., 2018) was used for quality-filtering and included removal of sequences with a minimum phred score of 20, a minimum length of 50 base pairs, soft clipping of low quality base pairs with a sliding window size of four bases and phred score of 20, read correction by overlap and adapter removal of the Illumina Nextera primers. Quality-filtered paired-end reads were merged with the paired-end read merger (PEAR, v.0.9.11) (Zhang et al., 2014) with default settings. Additionally, forward and reverse primer sequences were removed with cutadapt (v2.5) (Martin, 2011) with default settings. Sequences were then ordered by length (sequences $\leq$ 300 bp were removed) and dereplicated by vsearch (version 2.14.1; Rognes et al., 2016). Denoising was performed with the UNOISE3 module of vsearch and a set minimum size of eight reads. Chimeric sequences were excluded with the UCHIME3 module of vsearch. This included *de novo* chimera removal followed by reference-based chimera removal against the SILVA SSU 138 NR database (Bolyen et al., 2019; Quast et al., 2013), resulting in the final set of amplicon sequence variants (ASVs). Quality-filtered and primer-clipped sequences were mapped to ASVs by vsearch with a set identity of 0.97. Taxonomy assignments were performed with BLAST+ (blastn megablast, version 2.9.0) (Camacho et al., 2009) against the SILVA SSU 138 NR database with a minimum identity threshold of 90%. Additionally, we used identity and query coverage to mark uncertain blast hits. As recommended by the SILVA ribosomal RNA database project, we removed the taxonomic assignment for blast hits which did not meet the equation "(percent identity + query coverage)/2 $\leq$ 93" to obtain reliable taxonomic assignments. A phylogenetic tree was generated by aligning all sequences of the filtered dataset with MAFFT v7.407 (Katoh and Standley, 2013) at a maximum of 100 iterations. The tree was calculated using FastTree 2.1.7 (OpenMP) (Price et al., 2010) saved in newick format and midpoint rooted using FigTree (version 1.4.4) (Rambaut, 2018). Alpha-diversity indices and species richness were calculated with the ampvis2 package (version 2.5.9) (Andersen et al., 2018) and Faith's phylogenetic diversity with picante (version 1.8.1) (Kembel et al., 2010) at same surveying effort (3,010 rarefied sequences per sample). Abundance bar charts, heatmap, and boxplots were created from ASVs with the ggplot2, ampvis2 package in RStudio® v3.6.3 (R Core Team, 2017) with RStudio v1.1.456 (Wickham, 2016).

Nucleotide Sequence Accession Numbers

Nucleotide gene sequences obtained from bacterial isolates in this study (see section "Isolation of Bacteria and Phylogenetic Affiliation") were deposited in the GenBank® nucleotide sequence database[3] under the accession numbers MT254759 – MT254802. 16S rRNA gene amplicon sequences were submitted to the NCBI Sequence Read Archive[4] (SRA) under the NCBI BioProject accession number PRJNA610782. The raw sequencing reads are available from the NCBI SRA under accession numbers SRR11250184 – SRR11250201. A detailed list of all accession codes is given in **Supplementary Tables 3** and **4**.

[3]https://www.ncbi.nlm.nih.gov/genbank/

[4]https://www.ncbi.nlm.nih.gov/sra

RESULTS AND DISCUSSION

Bacterial Colonization of Different Materials and Inhibition of Growth by AGXX® and GOX

The survival of cultivable, potentially pathogenic bacteria on the antimicrobial coated and uncoated sample materials was assessed after 1 (t1), 2 (t2), and 4 (t3) months exposure on board of the SIRIUS module and in the non-isolated control environment. The focus of this study was the occurrence of aerobic, heterotrophic bacteria.

Bacterial growth was inhibited in the presence of the antimicrobial coating AGXX®. R2A agar plates directly incubated with AGXX® showed no bacterial growth regardless of exposure time (**Figure 2A**). Extensive bacterial growth occurred on uncoated control samples (**Figure 2C**). This supports evidence from earlier studies (Guridi et al., 2015; Landau et al., 2017; Loi et al., 2018; Vaishampayan et al., 2018; Sobisch et al., 2019) and demonstrates that the antimicrobial, growth-inhibiting properties of AGXX® remain effective when applied to the new carrier materials.

To determine whether the new AGXX®-coated materials have a lasting, antibacterial effect, an additional cultivation approach was performed by imprinting the different materials from each time point onto R2A agar plates, allowing for transfer of adhering cells onto the agar. Without direct contact to the inhibiting material, bacterial colonies were recovered from all samples at all time points. This revealed that at least some bacteria can survive and resume growth upon removal of the contact catalyst AGXX®. The number of colony-forming units (CFUs) on agar plates following incubation revealed no notable reduction in viable cells by AGXX® applied to polypropylene plastic or fibrous web polyester fleece. Counts of CFUs were not performed due to the often swarming, rapid growth of some bacterial isolates.

In contrast, a notable reduction of bacterial growth was observed for AGXX® coating applied to cellulose fleece: out of six samples, four showed 50–70% growth reduction on AGXX®-cellulose agar imprints compared to uncoated cellulose control imprints (**Supplementary Table 5**). For this reason, only cellulose fleece was selected for further analysis (isolation and characterization of surviving bacteria and 16S rRNA gene amplicon analysis, see below). However, for two of the samples, the CFU for AGXX® cellulose fleece was higher than for uncoated control fleece. These outliers may be explained by the low overall bacterial load (6–74 colonies per plate), suggesting cautious interpretation of low biomass data. Additionally, an important factor is the difference in cell recovery efficiency for the different materials and coatings. For example, spiking experiments with *B. subtilis* spores applied to the materials revealed that fewer cells are recovered from uncoated cellulose fleece (10–12% of applied cells) compared to the corresponding AGXX®-coated material (16–20%) (Ergün, 2019).

The novel, GO-based antimicrobial GOX, which was applied to cellulose fleece, "trapped" bacterial cells on its surface. We observed very localized bacterial growth, visible as microcolonies growing along the GOX-coated fibers that were in direct contact with the agar surface (**Figure 2B**). In contrast, uncoated cellulose fleece allowed extensive bacterial growth both underneath the sample material and on the surrounding agar (**Figure 2C**). The bacteria-immobilizing effect of GOX-cellulose fleece remained the same over the course of the 4 months incubation for both study sites.

Bacterial Isolates Obtained From SIRIUS Module and Non-isolated Control Environment

To analyze which bacteria had survived on the antimicrobial materials, especially in terms of pathogenicity, bacterial colonies obtained from R2A agar plates imprinted with AGXX®-cellulose fleece, GOX-cellulose fleece and uncoated cellulose fleece after 1, 2, and 4 months exposure (see section "Bacterial Colonization of Different Materials and Inhibition of Growth by AGXX® and GOX") were purified and identified. Isolates belonging to Biosafety Level 2 (BSL-2) were characterized with regards to their antibiotic resistance profiles and ability to form biofilms.

The cultivated bacterial communities differed markedly between the SIRIUS module and the control environment. Both study sites share their high level of human traffic, but while the SIRIUS module is completely isolated, the control environment (microbiology laboratory) remains in steady contact with the outside environment through staff members coming and going. Notably, all isolates from both environments belonged to either the *Firmicutes*, *Actinobacteria* or *Proteobacteria*.

Staphylococcus spp. and *Bacillus* spp. Dominate Cultivated Bacterial Community in SIRIUS Module

Eighty bacterial isolates were recovered from coated and uncoated cellulose fleece materials across the three time-intervals and identified by MALDI-TOF biotyping and 16S rRNA gene sequencing. Most of the isolated species belong to the genera *Staphylococcus* (n = 43) and *Bacillus* (n = 10) (**Table 1A**). In addition, the following species were isolated: *Brevibacillus agri* (n = 2), *Paenibacillus vini* (n = 1), all of which belonging to the *Firmicutes*, *Corynebacterium mucifaciens* (n = 1), *Kocuria palustris* (n = 1), *Micrococcus luteus* (n = 8), *Rothia terrae* (n = 1), belonging to the *Actinobacteria*, *Moraxella osloensis* (n = 1) and *Roseomonas mucosa* (n = 1), the only two *Proteobacteria* (**Table 1A**). Noticeably, *M. luteus* was only isolated from uncoated cellulose fleece at the final time point and was not recovered from AGXX®- or GOX-cellulose.

Out of 80 bacterial isolates, 55 belong to BSL-2 and are potential human pathogens (**Table 1A**). Almost all isolated BSL-2 organisms belong to the genus *Staphylococcus* (51 out of 55), namely *S. hominis* (n = 31), *S. haemolyticus* (n = 11), *S. epidermidis* (n = 8), and *S. caprae* (n = 1). The remaining BSL-2 organisms are *Aerococcus viridans*, *Corynebacterium mucifaciens*, *Roseomonas mucosa*, and *Moraxella osloensis* with one isolate each. While most of the *S. epidermidis* isolates were recovered from AGXX®-cellulose fleece (n = 6), most of the

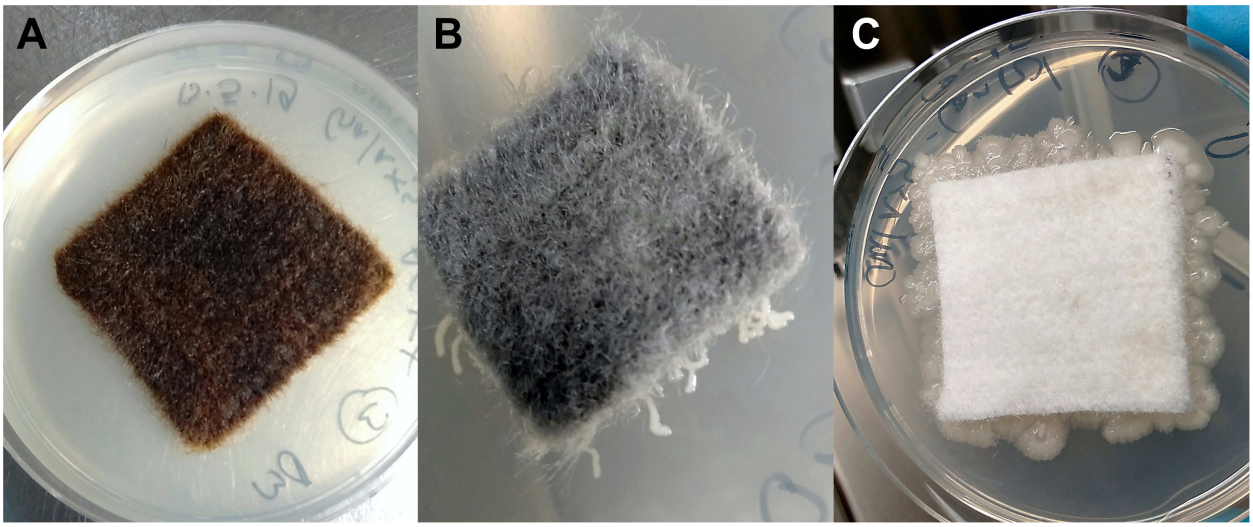

FIGURE 2 | Cellulose fleece with and without antimicrobial coating after 48 h incubation at 37°C on R2A agar (following 2 months exposure): AGXX®-cellulose fleece **(A)**, GOX-cellulose fleece **(B)**, and uncoated cellulose fleece **(C)**.

TABLE 1A | Bacteria recovered from antimicrobial and uncoated surfaces in SIRIUS.

Phylum	Genus	Species	Biosafety level	Cellulose-AGXX	Cellulose-GOX	Cellulose control	Total counts
Firmicutes	***Aerococcus***	***viridans***	**2**	1	0	0	**1**
	Bacillus	*licheniformis*	1	1	1	1	**3**
	Bacillus	*simplex*	1	2	0	0	**2**
	Bacillus	*subtilis*	1	0	2	1	**3**
	Bacillus	sp.[1]	1	1	0	0	**1**
	Bacillus	sp.[2]	1	0	0	1	**1**
	Brevibacillus	*agri*	1	0	2	0	**2**
	Paenibacillus	*vini*	1	0	0	1	**1**
	Staphylococcus	*capitis*	1	1	0	0	**1**
	Staphylococcus	***caprae***	**2**	0	0	1	**1**
	Staphylococcus	***epidermidis***	**2**	6	2	0	**8**
	Staphylococcus	***haemolyticus***	**2**	3	8	0	**11**
	Staphylococcus	***hominis***	**2**	8	14	9	**31**
	Staphylococcus	*warneri*	1	0	0	1	**1**
Proteobacteria	***Moraxella***	***osloensis***	**2**	0	0	1	**1**
	Roseomonas	***mucosa***	**2**	1	0	0	**1**
Actinobacteria	***Corynebacterium***	***mucifaciens***	**2**	0	1	0	**1**
	Kocuria	*palustris*	1	0	1	0	**1**
	Micrococcus	*luteus*	1	5	3	0	**8**
	Rothia	*terrae*	1	0	0	1	**1**
				29	34	17	**80**

Phylogenetic affiliation as assessed by MALDI-TOF-MS and 16S rRNA gene sequence analysis. The following isolates shared the same level of sequence identity with more than one species: [1]B. pumilus (99.6%)/B. safensis (99.6%), [2]B. velezensis (99.6%)/B. siamensis (99.6%). BSL-2 organisms are printed in bold.

S. haemolyticus isolates originated from GOX-cellulose fleece (n = 9). Remarkably, no *S. epidermidis* or *S. haemolyticus* isolates were recovered from uncoated control samples. Meanwhile, *S. hominis*, the most abundant *Staphylococcus* species, was recovered from all three materials: (AGXX®-cellulose, n = 8; GOX-cellulose, n = 14; and uncoated cellulose fleece, n = 9). There was no noticeable tendency regarding the distribution of BSL-2 organisms in terms of antimicrobial coating or time points.

Diverse Bacterial Community Isolated From Control Environment

While the bacterial community isolated from SIRIUS-derived samples was strongly dominated by *Staphylococcus* spp. and *Bacillus* spp., the 103 isolates from the control environment were affiliated to 17 different genera within the *Firmicutes*, *Proteobacteria*, and *Actinobacteria* (**Table 1B**). *Micrococcus luteus* (n = 27) and *Roseomonas mucosa* (n = 12) were the most

TABLE 1B | Bacteria recovered from antimicrobial and uncoated surfaces in the control environment.

Phylum	Genus	Species	Biosafety level	Cellulose-AGXX	Cellulose-GOX	Cellulose-control	Total Counts
Firmicutes	***Aerococcus***	***viridans***	**2**	0	0	1	**1**
	Bacillus	*firmus*	1	0	1	0	**1**
	Bacillus	*licheniformis*	1	1	1	2	**4**
	Bacillus	*megaterium*	1	0	1	1	**2**
	Bacillus	*pumilus*	1	0	0	1	**1**
	Bacillus	sp.[1]	1	1	1	0	**2**
	Bacillus	sp.[2]	1	0	0	2	**2**
	Paenibacillus	*lactis*	1	0	0	4	**4**
	Staphylococcus	*capitis*	1	0	4	0	**4**
	Staphylococcus	***epidermidis***	**2**	0	0	1	**1**
	Staphylococcus	***haemolyticus***	**2**	0	3	0	**3**
	Staphylococcus	***hominis***	**2**	3	0	0	**3**
Proteobacteria	*Massilia*	*timonae*	1	1	0	0	**1**
	Moraxella	***osloensis***	**2**	1	2	1	**4**
	Pantoea	***eucrina***	**2**	1	0	1	**2**
	Paracoccus	*contaminans*	1	1	0	1	**2**
	Paracoccus	***yeei***	**2**	2	2	1	**5**
	Pseudomonas	*stutzeri*	1	0	0	1	**1**
	Roseomonas	***mucosa***	**2**	6	1	5	**12**
	Sphingomonas	*desiccabilis*	1	0	1	0	**1**
Actinobacteria	*Dermacoccus*	*nishinomiyaensis*	1	3	0	0	**3**
	Gordonia	*rubripertincta*	1	1	1	0	**2**
	Kocuria	*rhizophila*	1	1	1	2	**4**
	Kocuria	*marina*	1	1	0	0	**1**
	Micrococcus	*luteus*	1	12	5	10	**27**
	Pseudoarthrobacter	*oxydans*	1	0	1	0	**1**
	Streptomyces	*thingirensis*	1	2	0	2	**4**
	Streptomyces	*canus*	1	0	0	1	**1**
	Streptomyces	sp.[3]	1	2	1	1	**4**
				38	26	39	**103**

The following isolates shared the same level of sequence identity (≥99%) with more than one bacterial species: [1]B. stratosphericus/B. altitudinis/B. aerophilus.[2]B. velezensis/B. siamensis. [3]S. aureorectus/S. calvus/S. asterosporus. BSL-2 organisms are printed in bold.

abundant species. Additionally, six *Bacillus* species (n = 12) were recovered while *Staphylococcus* species were much less abundant (n = 11) than on the SIRIUS module. The percentage of BSL-2 organisms (potential human pathogens) was significantly lower than on SIRIUS with 31 out of 103 isolates (30%). Most of the potential pathogens were *Proteobacteria*: *R. mucosa* (n = 12), *Paracoccus yeei* (n = 5), *Moraxella osloensis* (n = 4), and *Pantoea eucrina* (n = 2). Apart from one *Aerococcus viridans* isolate, all remaining BSL-2 organisms belonged to *Staphylococcus*: *S. haemolyticus* (n = 3), *S. hominis* (n = 3), and *S. epidermidis* (n = 1).

Prevalence of Human Commensal Bacteria in Confined Habitats

Dominance of human-derived bacteria is expected in confined, human-made habitats with no access to the natural environment. All *Staphylococcus* species isolated on the SIRIUS module (*S. hominis*, *S. haemolyticus*, *S. epidermidis*, *S. capitis*, *S. caprae*, and *S. warneri*) are commonly associated with the human skin and mucosal flora. Since many of these bacteria can act as opportunistic human pathogens, the prevalence of BSL-2 organisms within SIRIUS (69% of isolates) was accordingly higher than in the control environment (30% of isolates). Indeed, over 92% of BSL-2 organisms isolated from SIRIUS samples belonged to the *Staphylococci*. The high abundance of *Staphylococcus* and *Bacillus* isolates inside SIRIUS is in accordance with observations by Schwendner et al. (2017), who carried out an extensive survey of the microbial community during the Mars500 project, the first simulated space mission taking place inside the SIRIUS module over 17 months. They found that *Staphylococcus* spp. strongly dominated the airborne cultivable community. By comparison, the microbial community on surfaces showed a greater diversity and was dominated by both *Bacillus* spp. and *Staphylococcus* spp. alongside less abundant genera from the *Proteobacteria* and *Actinobacteria*.

Prevalence of *Staphylococcus* and *Bacillus* species has also been reported by numerous cultivation-based surveys of the microbial community on the ISS (Novikova et al., 2006; Checinska et al., 2015; Sobisch et al., 2019). No serious harmful pathogens such

as MRSA were detected in any of our samples. Furthermore, in contrast to the ISS surveys, we detected no enterococci, enterobacteria or corynebacteria.

Antibiotic Resistance and Biofilm Formation of Isolates

Potential human pathogens were characterized in terms of biofilm formation and antibiotic resistance. Disk diffusion assays revealed resistance to at least one antibiotic in all 25 tested BSL-2 organisms isolated from SIRIUS samples. Most were multiresistant (resistant to antimicrobial agents from three or more categories **Table 2A**). Resistance against erythromycin, kanamycin, and ampicillin was common amongst *Staphylococcus* isolates. Of all *Staphylococcus* isolates, 78% were resistant to erythromycin, 70% to kanamycin, and 48% to ampicillin (**Table 2A**). Antibiotic resistance profiles showed considerable variation between isolates, including strains of the same species derived from the same material and time point. The isolate with the highest level of antibiotic resistance (*S. haemolyticus* GAM2-7, isolated from AGXX® – cellulose fleece) was resistant to eight out of the 12 antibiotics tested: ampicillin, ciprofloxacin, clindamycin, erythromycin, kanamycin, oxacillin, tetracycline, and tigecycline. The abundance of resistances among isolates did not change over time (1 to 4 months).

Staphylococcal resistance against erythromycin and ampicillin was also abundant amongst isolates retrieved from AGXX® samples exposed on the ISS (Sobisch et al., 2019), while resistance against kanamycin (detected in 70% of *Staphylococcus* spp. from SIRIUS) was rare in coagulase negative Staphylococci from the ISS (Schiwon et al., 2013; Sobisch et al., 2019). Notably, BSL-2 isolates from the non-isolated control environment showed significantly fewer resistances, with many isolates being sensitive to all tested antibiotics (**Table 2B**). Out of 23 isolates, nine showed no resistance against any of the antibiotics tested. Moreover, the frequency of erythromycin and kanamycin resistance among *Staphylococcus* spp. was considerably lower (**Table 2B**). This may be explained by several facts: (i) isolates from the non-confined environment comprised many environmental organisms in contrast to human inhabitants, (ii) the microbiome of individuals differs considerably according to their exposure to antibiotics, and (iii) under confined conditions, bacteria in the SIRIUS module lack competition with microorganisms from the natural environment.

In addition to testing for antibiotic resistance, potential human pathogens were screened for their ability to form biofilms. Only those isolates that showed sufficiently fast growth under the conditions specified in the protocol by Vaishampayan et al. (2018) were tested (**Tables 2A,B**). All tested BSL-2 isolates from the fleece materials exposed on SIRIUS and the control environment were capable of biofilm formation. Out of 23 SIRIUS isolates (all *Staphylococcus* spp.), seven showed strong, 11 moderate, and five weak biofilm formation. Out of 11 tested isolates from the control environment (*Paracoccus yeei*, *Staphylococcus* spp.), two showed strong, seven moderate, and two weak biofilm formation. In both environments, strong and weak biofilm formers were isolated from all three materials and time points with no visible correlation between biofilm formation and level of antibiotic resistance.

The ability to form biofilms could provide competitive advantages over other airborne bacteria. In contrast to Sobisch et al. (2019) correlation between antimicrobial coating and frequency or degree of antibiotic resistance was not detected.

TABLE 2A | Antibiotic resistant and biofilm forming BSL-2 isolates from SIRIUS.

Number	Name	Species	Biofilm formation	Antibiotic resistance
1	GAM1-25	*A. viridans*	[A]	NIT
2	GCM1-14	*M. osloensis*	[A]	ERY, MEM, NAL
3	GXM3-1b	*S. caprae*	+++	ERY
4	GAM1-42	*S. epidermidis*	++	ERY, KAN, TET[B]
5	GAM1-43	*S. epidermidis*	+++	ERY, KAN
6	GXM2-7	*S. epidermidis*	++	AMP, ERY, KAN, OXA, OFX, TET
7	GCM1-15	*S. haemolyticus*	++	ERY, KAN, TET
8	GAM2-7	*S. haemolyticus*	++	AMP, CIP, CLI[B], ERY[B], KAN, OXA, TET, TGC
9	GAM3-3a	*S. haemolyticus*	++	KAN, NIT, NOR, OFX, OXA
10	GAM3-5a	*S. haemolyticus*	++	ERY, KAN, OXA
11	GXM2-4a	*S. haemolyticus*	++	CLI, ERY, OXA, OFX, TGC
12	GXM3-8b	*S. haemolyticus*	++	AMP, ERY, KAN, OXA, TET
13	GCM1-57	*S. hominis*	+++	AMP[B], ERY
14	GCM1-53	*S. hominis*	++	AMP, ERY
15	GCM1-59	*S. hominis*	+++	AMP, ERY
16	GCM3-1a	*S. hominis*	+	AMP, CIP, ERY, KAN, TET
17	GAM1-24	*S. hominis*	+	ERY, KAN, OXA, TET[B]
18	GAM2-5	*S. hominis*	+++	ERY, KAN, TET
19	GAM3-2	*S. hominis*	++	ERY
20	GXM1-1c	*S. hominis*	+++	KAN, OFX
21	GXM1-8	*S. hominis*	+	GEN, KAN, OFX
22	GXM2-2	*S. hominis*	+	AMP
23	GXM3-1a	*S. hominis*	+	AMP, CLI*, ERY, KAN, NIT
24	GXM3-2	*S. hominis*	++	AMP, KAN
25	GCM1-63	*S. warneri*	+++	AMP, ERY, KAN, OFX, OXA

+++, strong biofilm formation; ++, moderate biofilm formation; +, weak biofilm formation; –, no biofilm formation; AMP, ampicillin, 2 μg; CIP, ciprofloxacin, 5 μg; CLI, clindamycin, 2 μg; ERY, erythromycin, 15 μg; GEN, gentamicin, 10 μg; KAN, kanamycin, 30 μg; MEM, meropenem, 10 μg; OXA, oxacillin, 1 μg, OFX, ofloxacine, 5 μg; NAL, nalidixic acid, 30 μg; TGC, tigecycline, 15 μg; TET, tetracycline 30 μg; NOR, norfloxacin, 10 μg; NIT, nitrofurantoin, 100 μg. [A]Biofilm formation for these isolates was not analyzed as growth rates in standard media were too low to follow the standard protocol. [B]Inhibition zone diameters for these antibiotics were on the border between resistant and susceptible. Concentrations are μg per disk. Strain denominations: GCM1, Galaxy, Control, Moscow, t1; GAM1, Galaxy, AGXX, Moscow, t1; GXM1, Galaxy, GOX, Moscow, t1; GCM2, Galaxy, Control, Moscow, t2; GAM2, Galaxy, AGXX, Moscow, t2; GXM2, Galaxy, GOX, Moscow, t2; GCM3, Galaxy, Control, Moscow, t3; GAM3, Galaxy, AGXX, Moscow, t3; GXM3; Galaxy, GOX, Moscow, t3.

TABLE 2B | Antibiotic resistance and biofilm formation of BSL-2 isolates from control environment.

Number	Name	Species	Biofilm formation	Antibiotic resistance
1	GCB1-10	*A. viridans*	[A]	NIT, MEM, NOR
2	GAB1-9	*M. osloensis*	[A]	/
3	GXB2-1a	*M. osloensis*	[A]	ERY, NAL
4	GCB1-14	*M. osloensis*	[A]	ERY, MEM, NAL, TET
5	GXB2-2	*P. yeei*	++	/
6	GXB3-2c	*P. yeei*	+++	CIP, GEN
7	GCB3-1b	*P. yeei*	++	/
8	GCB3-1d	*P. yeei*	++	/
9	GCB2-6	*R. mucosa*	[A]	MEM
11	GAB2-6	*R. mucosa*	[A]	MEM
12	GAB2-7	*R. mucosa*	[A]	/
14	GAB3-2b	*R. mucosa*	[A]	/
15	GCB1-9b	*R. mucosa*	[A]	/
16	GCB3-2a3	*R. mucosa*	[A]	/
17	GXB1-8	*S. capitis*[B]	++	AMP, OXA, OFX
18	GCB1-13	*S. epidermidis*	++	AMP, ERY
19	GXB1-10	*S. haemolyticus*	++	GEN, KAN
20	GXB1-6	*S. haemolyticus*	++	AMP, OXA
21	GAB3-1h	*S. hominis*	+	AMP
22	GAB2-2	*S. hominis*	+++	AMP, ERY
23	GAB2-3	*S. hominis*	+	/

+++, strong biofilm formation; ++, moderate biofilm formation; +, weak biofilm formation; –, no biofilm formation; AMP, ampicillin, 2 μg; CIP, ciprofloxacin, 5 μg; CLI, clindamycin, 2 μg; ERY, erythromycin, 15 μg; GEN, gentamicin, 10 μg; KAN, kanamycin, 30 μg; MEM, meropenem, 10 μg; OXA, oxacillin, 1 μg, OFX, ofloxacine, 5 μg; NAL, nalidixic acid, 30 μg; TGC, tigecycline, 15 μg; TET, tetracycline 30 μg; NOR, norfloxacin, 10 μg; NIT, nitrofurantoin, 100 μg. /, no resistance detected. Concentrations are μg per disk. [A]Biofilm formation for these isolates was not analyzed as growth rates on standard media were too low to follow the standard protocol. [B]S. capitis is a BSL-1 organism; 16S rRNA gene sequence analysis for this isolate was inconclusive with the same level of sequence identity to S. capitis and S. caprae (BSL-2). Therefore, the isolate was included. Additional MALDI-TOF MS analysis, however, identified the isolate as S. capitis. Strain denominations: GCB1, Galaxy, Control, Berlin, t1; GAB1, Galaxy, AGXX, Berlin, t1; GXB1, Galaxy, GOX, Berlin, t1; GCB2, Galaxy, Control, Berlin, t2; GAB2, Galaxy, AGXX, Berlin, t2; GXB2, Galaxy, GOX, Berlin, t2; GCB3, Galaxy, Control, Berlin, t3; GAB3, Galaxy, AGXX, Berlin, t3; GXB3; Galaxy, GOX, Berlin, t3.

This effect may be more pronounced after longer exposure times. However, the isolate with the highest number of antibiotic resistances (resistance against 8 of 12 antibiotics tested) was a strain of *S. haemolyticus* retrieved from AGXX®-coated fleece.

Bacterial Community Composition – Similar Taxa Occur in Both Environments

The growth conditions applied in this study were chosen to select for common human pathogens, and targeted aerobic, heterotrophic bacteria. To supplement cultivation-based results and identify potential pathogens not detected by isolation, the bacterial communities present on the three materials after 1, 2, and 4 months exposure were examined by analysis of 16S rRNA gene amplicons from DNA extracted from fleece samples.

While culture-based communities differed considerably between SIRIUS and the control environment, amplicon sequence data suggest that the bacterial community composition of the two environments is highly similar (**Figures 3**, **4**). The dominant phyla in both sites were *Firmicutes* (34–47% of the total bacterial community), *Proteobacteria* (22–39%), and *Actinobacteria* (10–14%). Together, *Firmicutes*, *Proteobacteria*, and *Actinobacteria* constituted over 90% of the communities in all the samples. Additional dominant phyla not recovered by cultivation studies were *Bacteroidetes* (6–9%) and *Chloroflexi* (5–7%).

The majority of *Firmicutes* belonged to the class *Bacilli* (19–29% of total bacterial population), followed by *Clostridia* (7–9%) and *Limnochordia* (4–6%). While more than half of all SIRIUS isolates belonged to *Staphylococcus* spp. (**Tables 1A,B**), *Staphylococcales* only constituted 0.1–0.6% of total sequences. Instead, *Bacillales* (9–12%) and *Lactobacillales* (6–13%) were the dominant orders within the *Bacilli* based on amplicon sequence data (**Figure 3**). Within the *Actinobacteria*, *Micrococcales* (2–2.5% of total sequences), *Corynebacteriales* (2–2.5%), and *Bifidobacteriales* (2–2.5%) were the dominant orders (**Figure 3**). Proteobacterial sequences mostly belonged to the *Pseudomonadales* (6–19%), *Burkholderiales* (7–9%), and *Rhizobiales* (5–6%) (**Figure 3**). At genus level, the dominant taxa were *Lactobacillus* (6–13% of total reads), *Pseudomonas* (4–5%), *Comamonas* (2–6%), *Bacillus* (2–3%), *Sporosarcina* (2–3%), *Bifidobacterium* (2–2.5%), *Solibacillus* (1.5–2.5%), *Devosia* (1.5–2%), and *Acinetobacter* (0.5–2%) (**Figure 4**). *Moraxella* and *Roseomonas* (the only *Proteobacteria* isolated from SIRIUS) made up less than 0.05% of amplicon sequences. There was no correlation between the distribution of the different taxa and exposure time or antimicrobial coating (**Figure 4**).

The relative abundance of the dominant bacterial taxa was highly similar between the two sites (**Figures 3**, **4**), but analysis of the alpha-diversity revealed that the overall bacterial diversity was lower in SIRIUS than in the non-confined control environment (**Figure 5**).

In summary, the same taxa appear to dominate both the SIRIUS module and the control environment, even though the alpha-diversity was lower in SIRIUS. The community composition was not affected by the antimicrobial materials during the time course of the study. Opportunistic, human commensal pathogens identified by isolation do not appear to dominate the bacterial communities within SIRIUS.

Comparison of the SIRIUS Microbiome to Microbial Communities in Similar Confined Habitats

Prevalence of *Firmicutes*, *Proteobacteria*, and *Actinobacteria* has been reported almost uniformly by both cultivation-dependent and molecular surveys of the ISS microbiome (Novikova et al., 2006; Checinska et al., 2015; Singh et al., 2018; Sobisch et al., 2019; Voorhies et al., 2019). The bacterial community inside the NEK facility during the MARS500 project revealed the same phyla using DNA microarrays and next generation sequencing (Schwendner et al., 2017). However, when comparing our results to those of Schwendner et al. (2017) at class and genus level, there are pronounced differences in the bacterial communities from

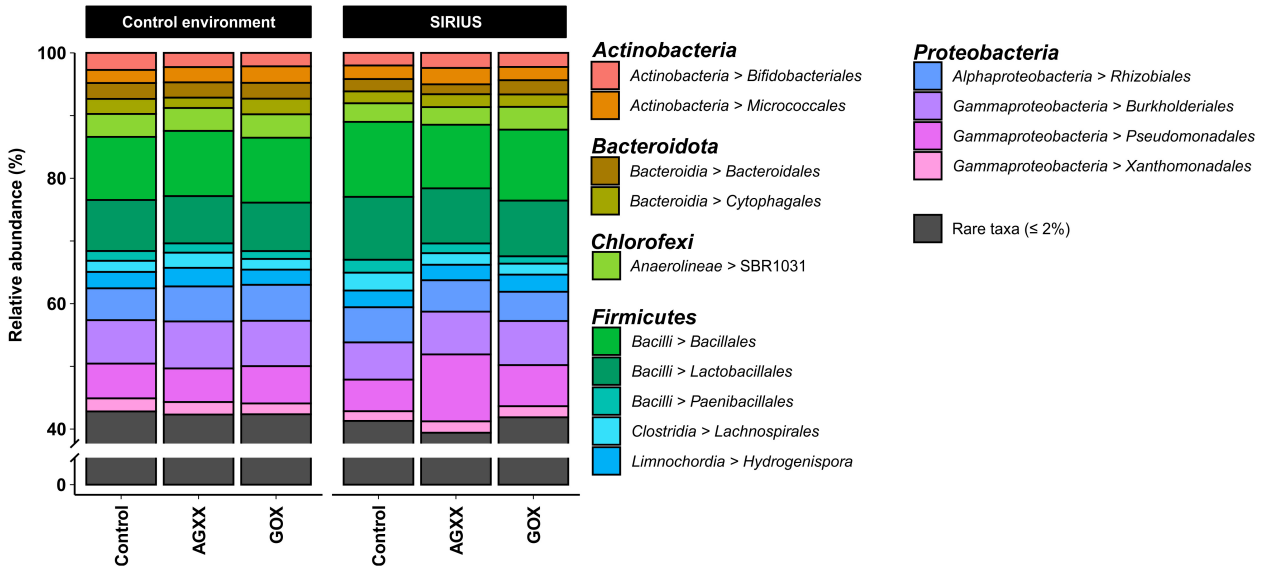

FIGURE 3 | Relative abundance of bacterial orders from antimicrobial and uncoated cellulose fleece exposed in SIRIUS and in non-isolated control environment detected by amplicon sequencing. Reads from time points t1, t2, and t3 were condensed for each sample in this illustration.

SIRIUS19 and MARS500 samples. Strikingly, there is a much higher percentage of potential, opportunistic pathogens in the bacterial communities reported by Schwendner et al. (2017).

Proteobacteria rather than *Firmicutes* were most abundant in the study by Schwendner et al., with *Ralstonia*, *Acinetobacter*, *Pseudomonas*, *Burkholderia*, and *Moraxella* being the major genera. Our proteobacterial sequences on the other hand mostly belonged to *Comamonas* and *Pseudomonas* (**Figure 4**, **Supplementary Figure 1**). *Acinetobacter* was less abundant; *Ralstonia*, *Burkholderia*, and *Moraxella* constituted less than 0.05% of sequences, even though *Moraxella* was identified by isolation. While over 60% of *Firmicutes* sequences from SIRIUS belonged to the *Bacilli* (19–27% of total reads) and only 20% to *Clostridia* (6–10% of total reads), two thirds of the *Firmicutes* in the study by Schwendner et al. (2017) were represented by *Clostridia* (over 22% of total reads). In contrast to our findings, *Staphylococcus* was one of the dominant genera within the *Firmicutes* (6% compared to 0.1–0.4% of SIRIUS sequences) alongside *Streptococcus* (4.8% compared to 0.2%). In contrast, *Firmicutes* sequences from SIRIUS samples were dominated by *Lactobacillus* (6–13% of total reads), *Bacillus* (2–3%), *Sporosarcina* (2–3%), and *Solibacillus* (1.5–2.5%). The composition of the microbial community within the NEK facility differs strongly from one study to the next which is potentially linked to a changing crew with individual microbiomes.

Bacterial Community Composition on SIRIUS Remains Stable Throughout 4-Months Study

The microbial community composition on our sample materials exposed inside SIRIUS did not change over time in terms of the dominant taxa (**Figures 3**, **4**). Sobisch et al. (2019) reported an increase in microbial diversity on AGXX® samples exposed on the ISS after 12 and 19 months, with appearance of additional genera like *Enterococcus* and *Pseudomonas* at later timepoints. Voorhies et al. (2019) observed a decrease in *Proteobacteria* over time with a simultaneous increase in *Firmicutes*, *Bacteroidetes*, and *Actinobacteria* in ISS crew members' skin microbiomes during a long-term space mission. This suggests that competition between these groups is affected by spaceflight. In a microbial succession study in an inflated lunar/Mars analog habitat, Mayer et al. (2016) observed a similar shift from predominantly *Proteobacteria* and *Firmicutes* (especially *Bacillaceae*) to other members of *Firmicutes* (*Clostridiales*) and *Actinobacteria* (especially *Corynebacteriaceae*) following human occupation. By comparison, Schwendner et al. (2017) found strong fluctuations in the microbial community within SIRIUS during the Mars500 project without any directional trend. They attributed this to the unequal distribution of bacteria in air. Our molecular data meanwhile revealed no directional shift of the detected taxa over time.

Outlook

As part of the next SIRIUS isolation experiment (scheduled to start in autumn 2020 over a period of 8 months), we plan to carry out further studies on the long-term antimicrobial effect of AGXX® and GOX. The longer time frame will give an enhanced insight into the effect of the two antimicrobials on survival and composition of the bacterial community on surfaces inside the artificial space station. Improving the methodology to recover microbial cells from the sample materials will allow for thorough assessment of bacterial survival rates and the identity of viable bacteria, as

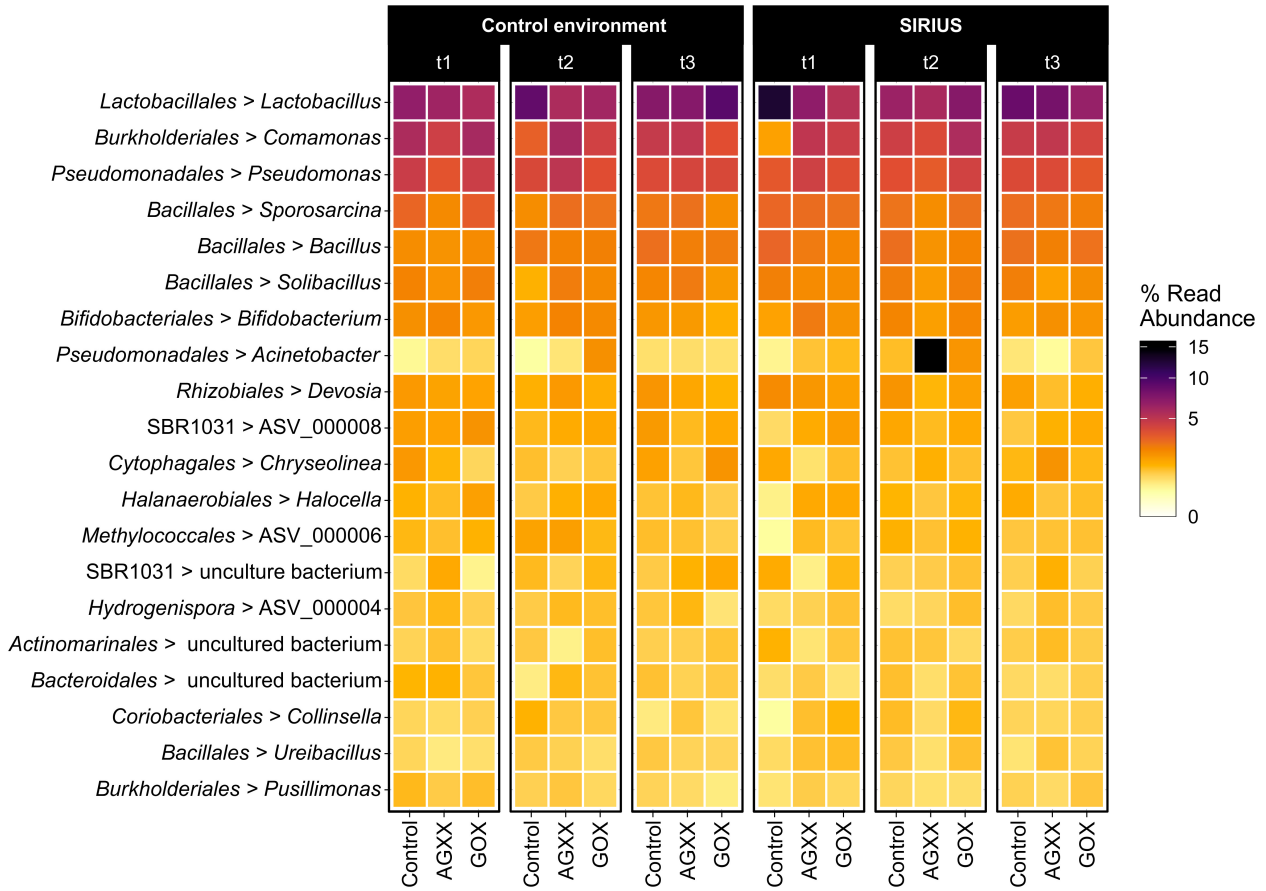

FIGURE 4 | Heatmap showing the top 20 dominant bacterial genera from antimicrobial and uncoated fleece samples exposed in SIRIUS and the non-confined control environment at different timepoints detected by amplicon sequencing. Abbreviations: t1, time point 1, 1 month; t2, time point 2, 2 months; t3, time point 3, 4 months.

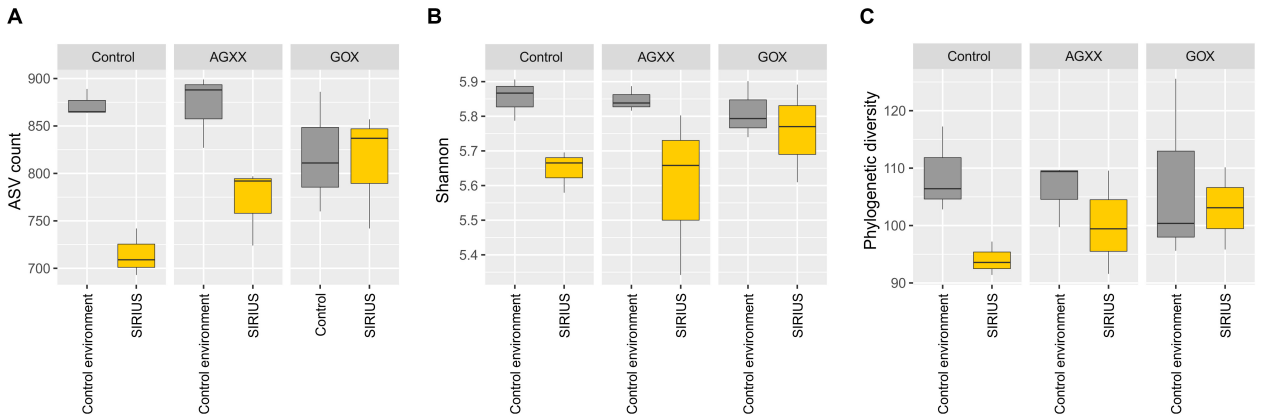

FIGURE 5 | Boxplots of alpha-diversity indices of all samples summarized by time. **(A)** Observed ASVs, **(B)** Shannon index, **(C)** Faiths phylogenetic diversity index. Comparisons were performed at same sequencing effort (rarefied selection of 3,010 reads per sample) and phylogenetic diversity (Faith's PD) was calculated on a midpoint-rooted phylogenetic tree of all ASVs.

well as provide increased DNA yields. This will enable us to assess not only the microbial composition based on 16S rRNA gene amplicons, but rather study the whole metagenome including virulence and resistance factors in order to reveal the survival strategies of microorganisms surviving on the antimicrobial materials.

DATA AVAILABILITY STATEMENT

The sequence data that support the findings of this study are openly available in GenBank® and the NCBI Sequence Read Archive under accession codes detailed in **Supplementary Tables 3** and **4**.

AUTHOR CONTRIBUTIONS

EG and DW designed the project and supervised all the experiments. DW, DS, AP, FH, HO, JM, and SK performed the experiments and analyzed the data. RA designed and prepared the GOX materials. DW, AP, DS, SK, and EG wrote the manuscript and designed the figures and tables. NN provided us access to the facilities at the IMBP in Moscow, Russia. RD, NN, RH, and OW contributed with insightful discussions on the experimental design. All authors interpreted the results, read, and revised the manuscript. All authors contributed to the article and approved the submitted version.

FUNDING

Funding by DLR, German Aerospace Centre (grant 50WB1831) is highly acknowledged.

ACKNOWLEDGMENTS

We thank U. Landau and C. Meyer from Largentec GmbH, Berlin, for providing us with the antimicrobial materials and for helpful discussions on the design of the experiments. We thank Melanie Heinemann and Sarah Teresa Schüssler for technical assistance.

SUPPLEMENTARY MATERIAL

The Supplementary Material for this article can be found online at: https://www.frontiersin.org/articles/10.3389/fmicb.2020.01626/full#supplementary-material

REFERENCES

Ahmed, R., Vaishampayan, A., Cuellar-Camacho, J. L., Wight, D. J., Donskyi, I., Unger, W., et al. (2020). Multivalent bacteria binding by flexible polycationic microsheets matching their surface charge density. *Adv. Mater. Interfaces* 1902066. doi: 10.1002/admi.201902066

Alekhova, T., Aleksandrova, A., Novozhilova, T., Lysak, L., Zagustina, N., and Bezborodov, A. (2005). Monitoring of microbial degraders in manned space stations. *Appl. Biochem. Microbiol.* 41, 382–389. doi: 10.1007/s10438-005-0065-x

Altschul, S. F., Gish, W., Miller, W., Myers, E. W., and Lipman, D. J. (1990). Basic local alignment search tool. *J. Mol. Biol.* 215, 403–410. doi: 10.1016/S0022-2836(05)80360-2

Andersen, K. S., Kirkegaard, R. H., Karst, S. M., and Albertsen, M. (2018). ampvis2: an R package to analyse and visualise 16S rRNA amplicon data. *BioRxiv* [preprint]. doi: 10.1101/299537

Aunins, T. R., Erickson, K. E., Prasad, N., Levy, S. E., Jones, A., Shrestha, S., et al. (2018). Spaceflight modifies *Escherichia coli* gene expression in response to antibiotic exposure and reveals role of oxidative stress response. *Front. Microbiol.* 9:310. doi: 10.3389/fmicb.2018.00310

Bai, P., Zhang, B., Zhao, X., Li, D., Yu, Y., Zhang, X., et al. (2019). Decreased metabolism and increased tolerance to extreme environments in Staphylococcus warneri during long-term spaceflight. *MicrobiologyOpen* 8:e917. doi: 10.1002/mbo3.917

Barratt, M. R., and Pool, S. L. (eds). (2008). *Principles of Clinical Medicine for Space Flight*. Berlin: Springer Science & Business Media. doi: 10.1007/978-0-387-68164-1

Bolyen, E., Rideout, J. R., Dillon, M. R., Bokulich, N. A., Abnet, C. C., Al-Ghalith, G. A., et al. (2019). Reproducible, interactive, scalable and extensible microbiome data science using QIIME 2. *Nat. Biotechnol.* 37, 852–857.

Camacho, C., Coulouris, G., Avagyan, V., Ma, N., Papadopoulos, J., Bealer, K., et al. (2009). BLAST+: architecture and applications. *BMC Bioinformatics* 10:421. doi: 10.1186/1471-2105-10-421

Checinska, A., Probst, A. J., Vaishampayan, P., White, J. R., Kumar, D., Stepanov, V. G., et al. (2015). Microbiomes of the dust particles collected from the International space station and spacecraft assembly facilities. *Microbiome* 3:50. doi: 10.1186/s40168-015-0116-3

Chen, S., Zhou, Y., Chen, Y., and Gu, J. (2018). fastp: an ultra-fast all-in-one FASTQ preprocessor. *Bioinformatics* 34, i884–i890. doi: 10.1093/bioinformatics/bty560

Chopra, I. (2007). The increasing use of silver-based products as antimicrobial agents: a useful development or a cause for concern? *J. Antimicrob. Chemother.* 59, 587–590. doi: 10.1093/jac/dkm006

Clauss-Lendzian, E., Vaishampayan, A., de Jong, A., Landau, U., Meyer, C., Kok, J., et al. (2018). Stress response of a clinical Enterococcus faecalis isolate subjected to a novel antimicrobial surface coating. *Microbiol. Res.* 207, 53–64. doi: 10.1016/j.micres.2017.11.006

Crucian, B. E., Choukèr, A., Simpson, R. J., Mehta, S., Marshall, G., Smith, S. M., et al. (2018). Immune system dysregulation during spaceflight: potential countermeasures for deep space exploration missions. *Front. Immunol.* 9:1437. doi: 10.3389/fimmu.2018.01437

Dickson, J., and Koohmaraie, M. (1989). Cell surface charge characteristics and their relationship to bacterial attachment to meat surfaces. *Appl. Environ. Microbiol.* 55, 832–836. doi: 10.1128/aem.55.4.832-836.1989

Ergün, D. (2019). *Study of the Influence of Antimicrobial Substances on Germination of Bacillus subtilis Spores*. master's thesis, Beuth University of Applied Sciences, Berlin.

Fajardo-Cavazos, P., Leehan, J. D., and Nicholson, W. L. (2018). Alterations in the spectrum of spontaneous rifampicin-resistance mutations in the *Bacillus subtilis* rpoB gene after cultivation in the human spaceflight environment. *Front. Microbiol.* 9:192. doi: 10.3389/fmicb.2018.00192

Gottenbos, B. (2001). Antimicrobial effects of positively charged surfaces on adhering Gram-positive and Gram-negative bacteria. *J. Antimicrob. Chemother.* 48, 7–13. doi: 10.1093/jac/48.1.7

Greulich, C., Braun, D., Peetsch, A., Diendorf, J., Siebers, B., Epple, M., et al. (2012). The toxic effect of silver ions and silver nanoparticles towards bacteria and human cells occurs in the same concentration range. *RSC Adv.* 2:6981. doi: 10.1039/c2ra20684f

Gupta, A., Matsui, K., Lo, J.-F., and Silver, S. (1999). Molecular basis for resistance to silver cations in *Salmonella*. *Nat. Med.* 5, 183–188. doi: 10.1038/5545

Guridi, A., Diederich, A.-K., Aguila-Arcos, S., Garcia-Moreno, M., Blasi, R., Broszat, M., et al. (2015). New antimicrobial contact catalyst killing antibiotic resistant clinical and waterborne pathogens. *Mater. Sci. Eng. C* 50, 1–11. doi: 10.1016/j.msec.2015.01.080

Herlemann, D. P., Labrenz, M., Jürgens, K., Bertilsson, S., Waniek, J. J., and Andersson, A. F. (2011). Transitions in bacterial communities along the 2000 km salinity gradient of the Baltic Sea. *ISME J.* 5, 1571–1579. doi: 10.1038/ismej.2011.41

Jiang, P., Green, S. J., Chlipala, G. E., Turek, F. W., and Vitaterna, M. H. (2019). Reproducible changes in the gut microbiome suggest a shift in microbial and

host metabolism during spaceflight. *Microbiome* 7:113. doi: 10.1186/s40168-019-0724-4

Katoh, K., and Standley, D. M. (2013). MAFFT multiple sequence alignment software version 7: improvements in performance and usability. *Mol. Biol. Evol.* 30, 772–780. doi: 10.1093/molbev/mst010

Kembel, S. W., Cowan, P. D., Helmus, M. R., Cornwell, W. K., Morlon, H., Ackerly, D. D., et al. (2010). Picante: R tools for integrating phylogenies and ecology. *Bioinformatics* 26, 1463–1464. doi: 10.1093/bioinformatics/btq166

Kim, W., Tengra, F. K., Young, Z., Shong, J., Marchand, N., Chan, H. K., et al. (2013). Spaceflight promotes biofilm formation by *Pseudomonas aeruginosa*. *PLoS One* 8:e62437. doi: 10.1371/journal.pone.0062437

Klindworth, A., Pruesse, E., Schweer, T., Peplies, J., Quast, C., Horn, M., et al. (2013). Evaluation of general 16S ribosomal RNA gene PCR primers for classical and next-generation sequencing-based diversity studies. *Nucleic Acids Res.* 41:e1. doi: 10.1093/nar/gks808

Klintworth, R., Reher, H. J., Viktorov, A. N., and Bohle, D. (1999). Biological induced corrosion of materials II: new test methods and experiences from Mir station. *Acta Astronautica* 44, 569–578. doi: 10.1016/s0094-5765(99)00069-7

Landau, U., Meyer, C., and Grohmann, E. (2017). AGXX – beitrag der oberflächentechnik zur vermeidung von Biofilmen (Teil 2). *Galvanotechnik* 108, 1110–1121.

Liao, C., Li, Y., and Tjong, S. (2019). Bactericidal and cytotoxic properties of silver nanoparticles. *IJMS* 20:449. doi: 10.3390/ijms20020449

Liu, Z., Luo, G., Du, R., Sun, W., Li, J., Lan, H., et al. (2019). Effects of spaceflight on the composition and function of the human gut microbiota. *Gut Microb.* 11, 807–819. doi: 10.1080/19490976.2019.1710091

Loi, V. V., Busche, T., Preuß, T., Kalinowski, J., Bernhardt, J., and Antelmann, H. (2018). The AGXX® antimicrobial coating causes a thiol-specific oxidative stress response and protein S-bacillithiolation in *Staphylococcus aureus*. *Front. Microbiol.* 9:3037. doi: 10.3389/fmicb.2018.03037

Magiorakos, A.-P., Srinivasan, A., Carey, R. B., Carmeli, Y., Falagas, M. E., Giske, C. G., et al. (2012). Multidrug-resistant, extensively drug-resistant and pandrug-resistant bacteria: an international expert proposal for interim standard definitions for acquired resistance. *Clin. Microbiol. Infect.* 18, 268–281. doi: 10.1111/j.1469-0691.2011.03570.x

Martin, M. (2011). Cutadapt removes adapter sequences from high-throughput sequencing reads. *EMBnet J.* 17:10. doi: 10.14806/ej.17.1.200

Mauclaire, L., and Egli, M. (2010). Effect of simulated microgravity on growth and production of exopolymeric substances of *Micrococcus luteus* space and earth isolates. *FEMS Immunol. Med. Microbiol.* 59, 350–356. doi: 10.1111/j.1574-695X.2010.00683.x

Mayer, T., Blachowicz, A., Probst, A. J., Vaishampayan, P., Checinska, A., Swarmer, T., et al. (2016). Microbial succession in an inflated lunar/Mars analog habitat during a 30-day human occupation. *Microbiome* 4:22. doi: 10.1186/s40168-016-0167-0

Mora, M., Wink, L., Kögler, I., Mahnert, A., Rettberg, P., Schwendner, P., et al. (2019). Space Station conditions are selective but do not alter microbial characteristics relevant to human health. *Nat. Commun.* 10:3990. doi: 10.1038/s41467-019-11682-z

Novikova, N., De Boever, P., Poddubko, S., Deshevaya, E., Polikarpov, N., Rakova, N., et al. (2006). Survey of environmental biocontamination on board the International Space Station. *Res. Microbiol.* 157, 5–12. doi: 10.1016/j.resmic.2005.07.010

Nyenje, M. E., Green, E., and Ndip, R. N. (2013). Evaluation of the effect of different growth media and temperature on the suitability of biofilm formation by *Enterobacter cloacae* strains isolated from food samples in South Africa. *Molecules* 18, 9582–9593. doi: 10.3390/molecules18089582

Ostaszewska, T., Śliwiński, J., Kamaszewski, M., Sysa, P., and Chojnacki, M. (2018). Cytotoxicity of silver and copper nanoparticles on rainbow trout (*Oncorhynchus mykiss*) hepatocytes. *Environ. Sci. Pollut. Res.* 25, 908–915. doi: 10.1007/s11356-017-0494-0

Panáček, A., Kvítek, L., Smékalová, M., Večeřová, R., Kolář, M., Röderová, M., et al. (2018). Bacterial resistance to silver nanoparticles and how to overcome it. *Nat. Nanotech.* 13, 65–71. doi: 10.1038/s41565-017-0013-y

Parte, A. C. (2018). LPSN — list of prokaryotic names with standing in nomenclature (bacterio.net), 20 years on. *Int. J. Syst. Evol. Microbiol.* 68, 1825–1829. doi: 10.1099/ijsem.0.002786

Pierson, D. L., Stowe, R. P., Phillips, T. M., Lugg, D. J., and Mehta, S. K. (2005). Epstein–Barr virus shedding by astronauts during space flight. *Brain Behav. Immun.* 19, 235–242. doi: 10.1016/j.bbi.2004.08.001

Price, M. N., Dehal, P. S., and Arkin, A. P. (2010). FastTree 2 – approximately maximum-likelihood trees for large alignments. *PLoS One* 5:e9490. doi: 10.1371/journal.pone.0009490

Quast, C., Pruesse, E., Yilmaz, P., Gerken, J., Schweer, T., Yarza, P., et al. (2013). The SILVA ribosomal RNA gene database project: improved data processing and web-based tools. *Nucl. Acids Res.* 41, D590–D596. doi: 10.1093/nar/gks1219

R Core Team (2017). *A Language and Environment For Statistical Computing*. Vienna: R Foundation for Statistical Computing.

Rambaut, A. (2018). *FigTree - Tree Figure Drawing Tool*. Edinburgh: University of Edinburgh.

Rognes, T., Flouri, T., Nichols, B., Quince, C., and Mahé, F. (2016). VSEARCH: a versatile open source tool for metagenomics. *PeerJ* 4:e2584. doi: 10.7717/peerj.2584

Rosenzweig, J. A., Abogunde, O., Thomas, K., Lawal, A., Nguyen, Y. U., Sodipe, A., et al. (2010). Spaceflight and modeled microgravity effects on microbial growth and virulence. *Appl. Microbiol. Biotechnol.* 85, 885–891. doi: 10.1007/s00253-009-2237-8

Schiwon, K., Arends, K., Rogowski, K. M., Fürch, S., Prescha, K., Sakinc, T., et al. (2013). Comparison of antibiotic resistance, biofilm formation and conjugative transfer of *Staphylococcus* and *Enterococcus* isolates from international space station and antarctic research station concordia. *Microb. Ecol.* 65, 638–651. doi: 10.1007/s00248-013-0193-4

Schulthess, B., Brodner, K., Bloemberg, G. V., Zbinden, R., Bottger, E. C., and Hombach, M. (2013). Identification of gram-positive cocci by use of matrix-assisted laser desorption ionization-time of flight mass spectrometry: comparison of different preparation methods and implementation of a practical algorithm for routine diagnostics. *J. Clin. Microbiol.* 51, 1834–1840. doi: 10.1128/JCM.02654-12

Schwendner, P., Mahnert, A., Koskinen, K., Moissl-Eichinger, C., Barczyk, S., Wirth, R., et al. (2017). Preparing for the crewed Mars journey: microbiota dynamics in the confined Mars500 habitat during simulated Mars flight and landing. *Microbiome* 5:129. doi: 10.1186/s40168-017-0345-8

Silhavy, T. J., Kahne, D., and Walker, S. (2010). The bacterial cell envelope. *Cold Spring Harb. Perspect. Biol.* 2:a000414. doi: 10.1101/cshperspect.a000414

Silver, S. (2003). Bacterial silver resistance: molecular biology and uses and misuses of silver compounds. *FEMS Microbiol. Rev.* 27, 341–353. doi: 10.1016/S0168-6445(03)00047-0

Sim, W., Barnard, R., Blaskovich, M. A. T., and Ziora, Z. (2018). Antimicrobial silver in medicinal and consumer applications: a patent review of the past decade (2007–2017). *Antibiotics* 7:93. doi: 10.3390/antibiotics7040093

Singh, N. K., Wood, J. M., Karouia, F., and Venkateswaran, K. (2018). Succession and persistence of microbial communities and antimicrobial resistance genes associated with International Space Station environmental surfaces. *Microbiome* 6:204. doi: 10.1186/s40168-018-0585-2

Sobisch, L.-Y., Rogowski, K. M., Fuchs, J., Schmieder, W., Vaishampayan, A., Oles, P., et al. (2019). Biofilm forming antibiotic resistant gram-positive pathogens isolated from surfaces on the International Space Station. *Front. Microbiol.* 10:543. doi: 10.3389/fmicb.2019.00543

Sonnenfeld, G. (2005). The immune system in space, including earth-based benefits of space-based research. *Curr. Pharm. Biotechnol.* 6, 343–349. doi: 10.2174/1389201054553699

Stowe, R. P., Mehta, S. K., Ferrando, A. A., Feeback, D. L., and Pierson, D. L. (2001). Immune responses and latent herpesvirus reactivation in spaceflight. *Aviat Space Environ. Med.* 72, 884–891.

Taylor, P. (2015). Impact of space flight on bacterial virulence and antibiotic susceptibility. *Infect Drug Resist.* 8, 249–262. doi: 10.2147/IDR.S67275

Urbaniak, C., Sielaff, A. C., Frey, K. G., Allen, J. E., Singh, N., Jaing, C., et al. (2018). Detection of antimicrobial resistance genes associated with the International Space Station environmental surfaces. *Sci. Rep.* 8:814. doi: 10.1038/s41598-017-18506-4

Vaishampayan, A., de Jong, A., Wight, D. J., Kok, J., and Grohmann, E. (2018). A novel antimicrobial coating represses biofilm and virulence-related genes in methicillin-resistant *Staphylococcus aureus*. *Front. Microbiol.* 9:221. doi: 10.3389/fmicb.2018.00221

Vila Domínguez, A., Ayerbe Algaba, R., Miró Canturri, A., Rodríguez Villodres, Á., and Smani, Y. (2020). Antibacterial activity of colloidal silver against gram-negative and gram-positive bacteria. *Antibiotics (Basel)*. 9:36. doi: 10.3390/antibiotics9010036

Vonberg, R. P., Sohr, D., Bruderek, J., and Gastmeier, P. (2008). Impact of a silver layer on the membrane of tap water filters on the microbiological quality of filtered water. *BMC Infect. Dis.* 8:133. doi: 10.1186/1471-2334-8-133

Voorhies, A. A., Mark Ott, C., Mehta, S., Pierson, D. L., Crucian, B. E., Feiveson, A., et al. (2019). Study of the impact of long-duration space missions at the International Space Station on the astronaut microbiome. *Sci. Rep.* 9:9911. doi: 10.1038/s41598-019-46303-8

Wickham, H. (2016). *ggplot2: Elegant Graphics for Data Analysis*. New York: Springer-Verlag.

Wu, B., Wang, Y., Wu, X., Liu, D., Xu, D., and Wang, F. (2018). On-orbit sleep problems of astronauts and countermeasures. *Military Med. Res.* 5:17. doi: 10.1186/s40779-018-0165-6

Zea, L., Larsen, M., Estante, F., Qvortrup, K., Moeller, R., Dias de Oliveira, S., et al. (2017). Phenotypic changes exhibited by *E. coli* cultured in space. *Front. Microbiol.* 8:1598. doi: 10.3389/fmicb.2017.01598

Zhang, B., Bai, P., Zhao, X., Yu, Y., Zhang, X., Li, D., et al. (2019). Increased growth rate and amikacin resistance of *Salmonella* enteritidis after one-month spaceflight on China's Shenzhou-11 spacecraft. *Microbiol. Open* 8:e00833. doi: 10.1002/mbo3.833

Zhang, J., Kobert, K., Flouri, T., and Stamatakis, A. (2014). PEAR: a fast and accurate Illumina Paired-End reAd mergeR. *Bioinformatics* 30, 614–620. doi: 10.1093/bioinformatics/btt59

Conflict of Interest: The authors declare that the research was conducted in the absence of any commercial or financial relationships that could be construed as a potential conflict of interest.

frontiers in Microbiology

ORIGINAL RESEARCH
published: 31 July 2020
doi: 10.3389/fmicb.2020.01792

Iron Ladies – How Desiccated Asexual Rotifer *Adineta vaga* Deal With X-Rays and Heavy Ions?

Boris Hespeels[1,2], Sébastien Penninckx[3†], Valérie Cornet[2†], Lucie Bruneau[1], Cécile Bopp[3], Véronique Baumlé[1,2], Baptiste Redivo[2], Anne-Catherine Heuskin[3], Ralf Moeller[4,5], Akira Fujimori[6], Stephane Lucas[3] and Karine Van Doninck[1,2]*

[1] Research Unit in Environmental and Evolutionary Biology (URBE), Laboratory of Evolutionary Genetics and Ecology (LEGE), NAmur Research Institute for Life Sciences (NARILIS), University of Namur, Namur, Belgium, [2] Research Unit in Environmental and Evolutionary Biology (URBE), Institute of Life, Earth & Environment (ILEE), University of Namur, Namur, Belgium, [3] Laboratory of Analysis by Nuclear Reaction (LARN), NAmur Research Institute for Life Sciences (NARILIS), University of Namur, Namur, Belgium, [4] Space Microbiology Research Group, Radiation Biology Department, Institute of Aerospace Medicine, German Aerospace Center (DLR), Cologne, Germany, [5] Department of Natural Sciences, University of Applied Sciences Bonn-Rhein-Sieg (BRSU), Rheinbach, Germany, [6] Department of Basic Medical Sciences for Radiation Damages, National Institute of Radiological Sciences (NIRS), Chiba, Japan

OPEN ACCESS

Edited by:
Rakesh Mogul, California State Polytechnic University, Pomona, United States

Reviewed by:
Tim Barraclough, University of Oxford, United Kingdom
Fernando Rodriguez, Marine Biological Laboratory (MBL), United States
Dinakar Challabathula, Central University of Tamil Nadu, India

***Correspondence:**
Boris Hespeels
boris.hespeels@unamur.be

† These authors have contributed equally to this work

Specialty section:
This article was submitted to Extreme Microbiology, a section of the journal Frontiers in Microbiology

Received: *25 February 2020*
Accepted: *09 July 2020*
Published: *31 July 2020*

Citation:
Hespeels B, Penninckx S, Cornet V, Bruneau L, Bopp C, Baumlé V, Redivo B, Heuskin A-C, Moeller R, Fujimori A, Lucas S and Van Doninck K (2020) Iron Ladies – How Desiccated Asexual Rotifer Adineta vaga Deal With X-Rays and Heavy Ions? Front. Microbiol. 11:1792. doi: 10.3389/fmicb.2020.01792

Space exposure experiments from the last 15 years have unexpectedly shown that several terrestrial organisms, including some multi-cellular species, are able to survive in open space without protection. The robustness of bdelloid rotifers suggests that these tiny creatures can possibly be added to the still restricted list of animals that can deal with the exposure to harsh condition of space. Bdelloids are one of the smallest animals on Earth. Living all over the world, mostly in semi-terrestrial environments, they appear to be extremely stress tolerant. Their desiccation tolerance at any stage of their life cycle is known to confer tolerance to a variety of stresses including high doses of radiation and freezing. In addition, they constitute a major scandal in evolutionary biology due to the putative absence of sexual reproduction for at least 60 million years. *Adineta vaga*, with its unique characteristics and a draft genome available, was selected by ESA (European Space Agency) as a model system to study extreme resistance of organisms exposed to space environment. In this manuscript, we documented the resistance of desiccated *A. vaga* individuals exposed to increasing doses of X-ray, protons and Fe ions. Consequences of exposure to different sources of radiation were investigated in regard to the cellular type including somatic (survival assay) and germinal cells (fertility assay). Then, the capacity of *A. vaga* individuals to repair DNA DSB induced by different source of radiation was investigated. Bdelloid rotifers represent a promising model in order to investigate damage induced by high or low LET radiation. The possibility of exposure both on hydrated or desiccated specimens may help to decipher contribution of direct and indirect radiation damage on biological processes. Results achieved through this study consolidate our knowledge about the radioresistance of *A. vaga* and improve our capacity to compare extreme resistance against radiation among living organisms including metazoan.

Keywords: bdelloid rotifer, LET, DNA damage, extremophile, astrobiology, panspermia

INTRODUCTION

The exposition of cells to ionizing radiations (IR) generates a succession of physical, chemical and biological processes that differ in time, spatial and energy-scale leading to a cellular response complicated to predict (Joiner and van der Kogel, 2018). The ionization density in particle tracks is usually characterized by a physical parameter called Linear Energy Transfer (LET) describing the average energy (in keV) given up by a charged particle traversing a distance of 1 μm. High-Z charged particles (such as Fe ions) are high LET particles that will produce dense ionizations along their path while photons (like X-rays) which produce sparse ionizations are considered as low LET IR (Joiner and van der Kogel, 2018; Hagiwara et al., 2019). Although a same dose of radiation leads to the same amount of ionizations, the differences in their spatial distribution is translated into different types of damages at biological level. It was demonstrated that sparse ionizations originating from low LET radiations mainly induce DNA base oxidation and single strand breaks (Lehnert, 2007). Contrastingly, complex DNA damages including clustered double strand breaks (DSBs) are preferentially created following high-LET exposition resulting in a poor survival of irradiated organisms (Semenenko and Stewart, 2004). Moreover, an increasing amount of studies highlighted that the complexity of damages induced by high LET particles was associated to lower repair kinetic leading to an increase in chromosomal aberrations and cancer incidence (Loucas and Cornforth, 2013; Penninckx et al., 2019). Although the health risks from exposure to terrestrial radiations (electrons and photons) are well known, the ones associated to heavy ions particles (HZE) remain poorly understood since they are only naturally present in space. Therefore, the lack of data regarding whole-body response following HZE exposure and solutions to counteract their deleterious effects were identified as major showstoppers for future long-duration space missions (White and Averner, 2001; Cucinotta and Durante, 2006). Within the animals, bdelloid rotifers are known to survive high doses of high and low LET ionizing radiation (Gladyshev and Meselson, 2008; Hespeels et al., 2014; Jönsson and Wojcik, 2017), making them a new, suitable model system for space research.

Bdelloid rotifers are among the smallest animals on Earth, with most species being less than 1 mm in size and containing ∼1,000 cells. Despite their small size, these eutelic (i.e., a fixed number of cells at maturity) metazoans have a complete nervous, muscular, digestive and excretory system (Ricci and Melone, 2000). One remarkable feature of bdelloid rotifers, being even more unusual among animals, is the absence of males, vestigial male structures or hermaphrodites in any of the populations studied within the 460 described morphospecies (Segers, 2007). Bdelloid rotifers are females apparently cloning themselves since millions of years. While the exact nature of their parthenogenetic reproductive mode remains unknown, bdelloid rotifers are considered an "evolutionary scandal" because they persist without sexual reproduction (Maynard Smith, 1986).

Living all over the world, mostly in semi-terrestrial environments, they appear to be extremely stress tolerant. Around 90% of bdelloid species were described to live in semi-terrestrial habitats and in particular limno-terrestrial environments such as mosses and lichens (Melone and Fontaneto, 2005). Their desiccation tolerance at any stage of their life cycle allows bdelloid rotifers to thrive in semi-terrestrial environments but also confers tolerance to a variety of stresses including freezing, deep vacuum, UV and high doses of ionizing radiation (Ricci et al., 2005; Gladyshev and Meselson, 2008; Fischer et al., 2013; Hespeels et al., 2014; Jönsson and Wojcik, 2017; Ricci, 2017).

Nevertheless, an overview of the radiation tolerance among bdelloids is lacking and only few radiation studies have been published. No lethal dose is currently available in the literature. In 2008, Gladyshev and Meselson demonstrated that two bdelloid rotifer species maintained hydrated, *Adineta vaga* and *Philodina roseola*, are extraordinary resistant to ionizing radiation (IR), surviving up to 1,200 Gy of gamma radiation with fecundity and fertility showing a dose response (Gladyshev and Meselson, 2008). These doses were contrasting the Lethal Dose 50 (i.e., dose required to kill 50% of the irradiated population) of mammalian cells ranging from 2 to 6 Gy after X-ray exposure (Kohn and Kallman, 1957; Mole, 1984). In 2014, Hespeels et al. demonstrated that the rehydration process of desiccated *A. vaga* individuals was not affected by doses up to 800 Gy of protons 1,7 MeV. In 2017, Jönsson and Wojcik highlighted that desiccated bdelloid *Mniobia russeola* is able to tolerate exposure to iron ions up to at least 2,000 Gy with no apparent impact in term of survival and egg production (Jönsson and Wojcik, 2017).

By analogy with the desiccation- and radiation resistant bacterium *D. radiodurans* (Mattimore and Battista, 1996), it has been postulated that the extraordinary radiation resistance of bdelloid rotifers reflects an adaptation to survive desiccation and a high capacity to deal with numerous DNA DSBs (Gladyshev and Meselson, 2008; Gladyshev and Arkhipova, 2010). Indeed, high radiation doses are known to induce numerous cellular damages, through the formation of reactive oxygen species (ROS) and inducing DNA DSBs (Riley, 1994). We previously demonstrated that *A. vaga* accumulate DNA double strand breaks (DSBs) with time spent in dehydrated state. Upon rehydration, rehydrated animals were able to reassemble large fragments of DNA supporting the presence of active DNA repair mechanisms. Even when the genome was entirely shattered into small DNA fragments by exposure to 800 Gy of protons 1.7 MeV radiations, *A. vaga* individuals were able to efficiently recover from desiccation and to repair the DNA DSBs (Hespeels et al., 2014). Krisko et al. (2012) demonstrated that *A. vaga* is far more resistant to IR-induced protein carbonylation than is the much more radiosensitive nematode *Caenorhabditis elegans*. Therefore, like bacteria *Deinococcus radiodurans*, bdelloid rotifers appear to survive such extreme conditions because of efficient antioxidants and DNA repair mechanisms (Flot et al., 2013; Latta et al., 2019). However, the exact biological processes of these resistance mechanisms remain largely unknown.

Space exposure experiments from the last 15 years have unexpectedly shown that several terrestrial organisms, including some multi-cellular species, are able to survive in open space without protection. In the absence of protective effects from the atmosphere and the magnetic field, organisms are exposed

to a mixture of radiations and accelerated particles. More specifically, biological samples in space are expected to be exposed to galactic cosmic rays (GCR) and to radiation bursts generated by solar eruption (Simpson, 1983; Wilson, 1991). GCR, originating from extra solar events like supernova, are composed of 83% protons, 12% alpha particles and 1.5% high atomic number and energy particle (HZE) including Fe (Ferrari and Szuszkiewicz, 2009). Despite reduced occurrence in terms of particle number, Fe ions driven by their huge LET are the primary component of GCR in term of energy deposited on the target (Leuko and Rettberg, 2017; Moeller et al., 2017). In addition, the collision of GCR with matter may result in the generation of low LET gamma and X-ray radiation (Dartnell, 2011; Leuko and Rettberg, 2017). The robustness of bdelloid rotifers toward IR suggests that these tiny creatures can possibly be added to the still restricted list of animals used for astrobiology experiments, including exposure to simulated deep space environment. Bdelloid rotifers can indeed contribute significantly to our understanding of living in extreme environments. The bdelloid species *A. vaga*, whose genome was sequenced (Flot et al., 2013), got recently selected for an astrobiology experiment aimed at identifying and quantifying biological damage suffered by bdelloids when exposed to space environment. Through this project, bdelloid rotifers will be exposed to a combination of full-spectrum electromagnetic radiation from the Sun, cosmic particle radiations, vacuum, wide temperature fluctuations and microgravity. In the preparation of this experiment, the present manuscript aims to determine the limits and consequences of bdelloid rotifer extreme resistance to radiation.

In this study, the resistance of *A. vaga* versus multiple sources of radiation was investigated. The biological response of these animals to high doses of low and high LET was evaluated, respectively, using X-ray, protons 4 MeV and Fe 0.5 GeV particles. The high resistance of *A. vaga* individuals to radiation prone them as a good model to study the prevalence of direct and indirect damages coming from high doses of ionizing radiation (>100 Gy). Here, hydrated and desiccated *A. vaga* individuals were exposed to increasing dose of X-ray, and only desiccated *A. vaga* to proton and Fe ions. For each radiation dose, we evaluated the survival and the capacity of irradiated animals to produce viable offspring. These data were confronted with the amount of DNA damage, evaluated by pulsed field gel electrophoresis (PFGE), and with the capacity of irradiated animals to repair, at least in somatic cells, DNA breaks induced by X-ray, proton and Fe radiation. Results achieved through this study consolidate our knowledge about the radioresistance of bdelloid rotifer *A. vaga* and improve our capacity to compare extreme resistance against low and high LET radiation among living organisms including metazoan.

MATERIALS AND METHODS

Bdelloid Rotifer Cultures

Experiments were performed using isogenic *A. vaga* clones issued from a single individual from the laboratory of Matthew Meselson at Harvard University (Flot et al., 2013). The cultures were maintained hydrated in Petri dishes supplemented with natural spring water (Spa), in thermostatic chambers at 21°C, and fed with sterilized lettuce juice (*Lactuca sativa*). Bacterial proliferation and dirt accumulation were avoided by changing the water minimum twice a month.

X-Ray Exposure

Desiccated and hydrated *A. vaga* individuals were irradiated using an X-ray irradiator PXi X-RAD 225 XL, with a dose rate of ∼7.8 Gy/min (19 mA, 225 kV, no filter) available at LARN (UNamur-Belgium). Irradiation time was calculated from this dose rate to obtain the different doses. All samples, including control samples, were put on a refrigerated water bag to mitigate heating from X-ray. For each dose, a minimum of three replicates were recorded from at least two independent exposure campaigns (except for 5,000 and 7,500 Gy where 3 replicates per dose were obtained during one exposure campaign). The exposure of hydrated animals was limited to 1,500 Gy. For hydrated samples, a total of 2,000 to 5,000 living and healthy animals stored in 2 mL of Spa water supplemented by 100 μL of sterile lettuce juice were exposed to X-ray in refrigerated multi-well plates. As animals were metabolically active during irradiation and because maximum dose rate was limited, it was decided to expose hydrated *A. vaga* individuals to a maximum dose of 1,500 Gy. For desiccated *A. vaga* samples individuals were dried for 1 day (see desiccation protocol below) before irradiation to X-rays doses ranging from 100 to 7,500 Gy.

4 MeV Proton Exposure

Only desiccated *A. vaga* were irradiated with a homogenous broad proton beam defocused over 1 cm^2 area, produced by a 2 MV Tandem accelerator (High Voltage Engineering Europa). A thorough description of the experimental set-up and the irradiation procedure is given in Wéra et al. (2011). Briefly, 4 MeV pristine proton beam was extracted in air through a 1 μm silicon nitride window. The linear energy transfer (LET) at the sample location was computed using SRIM software (Ziegler et al., 2010), using two stacked layers representing the setup: 1 μm Si_3N_4 exit window and a small 3 mm air gap between the exit window and the sample dish. The energy of transmitted particles was averaged and the LET was obtained for this average proton energy. The irradiation chambers were placed vertically on a sample holder fixed at the end of the beamline. Rotifer samples were thus positioned perpendicularly to the incoming beam. Homogeneity was achieved by defocusing the beam and checked using a passivated implanted planar silicon detector moved along x and y directions. Dose rate was assessed every millimeter in a 1 cm^2 surface with errors less than 5% in the cell sample region. Dataset generated for this study was acquired through 6 campaigns of irradiation. Between campaigns, the dose rate ranged from 42 to 134 Gy min^{-1}. The particle flux was accordingly adjusted using the classic broad beam formula (Turner, 2007) as shown below (Eq. 1):

$$\dot{D} = \frac{1.6\ 10^{-9}\ LET\ \emptyset}{\rho} \quad (1)$$

Here the density ρ is taken as 1 g cm^{-3} and Φ is the proton beam flux in part cm^{-2} s^{-1}. For each dose, a minimum of 3 replicates were recorded from at least 2 independent campaigns.

The desiccated *A. vaga* individuals were exposed to 4 MeV proton, with a LET of 10 keV/μm, ranging from 100 to 10,000 Gy.

Fe 500 MeV/n Exposure

Only desiccated *A. vaga* individuals were also irradiated with iron ions (Fe 500 MeV/n, with a LET of 200 keV/μm and a dose rate of 10 Gy/min). Desiccated *A. vaga* individuals were stored in 0.2 mL PCR tubes and sent to the Heavy Ion Medical Accelerator in Chiba (HIMAC) facility at the National Institute of Radiological Sciences (NIRS) in Chiba (Japan). Two campaigns of irradiations were performed in January 2018 and June 2018, respectively. During the first campaign, samples were exposed to 250, 500, 1,000, and 2,000 Gy. In the second campaign, desiccated *A. vaga* rotifers were exposed to 1,000, 2,000, and 3,000 Gy Fe ions. For each campaign a set of 4 replicates per dose was prepared. In parallel, two sets of controls were prepared for each exposure campaign. One set consisted of desiccated *A. vaga* individuals that were sent to HIMAC facility and back to Belgium without irradiation (Control transport). The second set consisted of desiccated *A. vaga* individuals stored dry at controlled temperature (15°C) in LEGE laboratory (UNamur) for the whole duration of the exposure experiment (from sample preparation, exposure to HIMAC, and travel back to Belgium). For each campaign, it was impossible to rehydrate the whole dataset of desiccated samples on the same day due to the workload and analysis required post rehydration. As a consequence, samples were rehydrated randomly after their return to Belgium. Therefore, samples from first campaign were desiccated for a minimum and a maximum duration of 30 to 37 days, respectively. For the second campaign, the total desiccation ranged between 39 and 48 days.

Desiccation and Survival Rate

For desiccation experiments, we used the protocol previously described in Hespeels et al. (2014). Briefly, healthy cultures were shortly washed in filtered Spa water. Individuals were collected using quick vortex and transferred to a 50 mL Falcon tube for centrifugation. The pellet of concentrated *A. vaga* individuals was resuspended in 1.25 mL of Spa water and placed in the center of Petri dishes containing 30 mL of 3% LMP agarose (Invitrogen). Plates with approximately 15,000–45,000 *A. vaga* individuals are placed in a climatic chamber (WEKK 0028) for desiccation following the optimized desiccation protocol: (1) linear decrease of relative humidity from 70 to 55% for 17 h (temperature: 23°C), (2) linear decrease of relative humidity from 55 to 41% for 1 h (temperature: 23°C), and (3) maintenance of 41% RH and 23°C during the whole exposure period. After desiccation, dried bdelloid individuals were rehydrated using 15 mL Spa® water and stored at 21°C for 48 h. Bdelloids were considered alive when they had fully recovered motility or when the mastax moved in contracted individuals. All living and dead animals were collected separately. Then, the survival rate was estimated manually by counting living and dead individuals under the binocular. When the number of individuals was higher than ∼750, the number of individuals was extrapolated by counting 6 times the number of living/dead animals observed in 2 μL taken from a homogenously mixed culture in a final volume of 2–5 mL. Data are available in **Supplementary Data S1**. In the absence of intermediary exposure doses between 5,000 and 7,500 Gy, it was not possible to compute an accurate LD50 for each radiation type.

Fertility Assays

The reproductive capacity was defined as the ability for each *A. vaga* individual to lay eggs and to develop clonal populations after being desiccated and potentially irradiated. We tested the fertility of 1 day desiccated and irradiated individuals by randomly selecting and isolating a minimum of 60 successfully rehydrated individuals per condition; each isolated female was deposited in a well of a 12-well petri plate. Each well was filled with 2 mL of Spa water and 50 μL of sterilized lettuce juice. After 30 days, wells were observed under a binocular stereoscope checking for: (1) the presence of a population (minimum 2 adults and 1 egg per well), (2) the presence of only eggs that did not hatch (+eventually the single adult from the start defined as a sterile individual), and (3) the presence of only dead individual (s). When the number of survivors after irradiation was below 60 individuals, the number of isolated individuals lacking to arrive at this total was automatically associated with the category dead individual (s). This correction avoids the overweighting of certain values following the drastic reduction of survivors at dose equal or higher than 5,000 Gy (X-ray and proton only). Data are available in **Supplementary Data S1**. Based on these data, it was possible to evaluate the minimal dose required to sterilize 50% of the irradiated population. A similar approach to the evaluation of a standard LD_{50} was applied here to define the Sterilizing Dose 50 (SD_{50}). All curve fittings were performed with the OriginLab® software (MA, United States). A dose-response equation was used to fit fertility data according to the following equation (Eq. 2):

$$Sterilization = A_1 + \frac{A_2 - A_1}{1 + 10^{(logx0 - x)p}} \quad (2)$$

Where A_1 is the bottom asymptote (i.e., *representing the fertility of sterilized animals),* A_2 is the top asymptote (i.e., *representing the fertility of control animals)*, logx0 correspond to SD_{50} and p is the hill slope.

Statistical Analysis

Data were expressed as means ± standard deviations (SD). Statistical analyses were performed using Rstudio software version 3.6.3 (RStudio Team, 2015) with packages car version 3.0–7 (Fox and Weisberg, 2019) and multcomp version 1.4–13 (Hothorn et al., 2008). Effects of radiation dose were analyzed using a Global Linear Model (using a Gaussian family). *Post hoc* comparisons at a 5% significant

level were performed with General Linear Hypotheses (Tukey's test) and multiple comparisons for GLM. This approach allowed not restricting the statistical analysis to the comparison of each condition *versus* the control condition (i.e., non-irradiated samples). Multiple comparisons between each dose ensure to discriminate significant differences between all conditions. Group characterized letters indicate the significant differences between groups: a significant difference (P-value < 0.05) between two conditions is observed when these conditions do not share any letter.

Genomic DNA Integrity

The genomic integrity, i.e., the accumulation of DNA DSBs induced by desiccation or radiation, and the DNA repair kinetics were screened using Pulsed Field Gel Electrophoresis (PFGE) according to a protocol adapted from Hespeels et al. (2014). The genomic integrity was checked on hydrated and desiccated samples after their exposure to increasing dose of radiation. In order to screen the potential DNA repair process occurring post irradiation (and post rehydration for desiccated samples), the genomic integrity was evaluated after 2, 30, 8, 24, 48, and 168 h of rehydration by PFGE.

For each time point, *A. vaga* individuals were isolated in 1,300 μL of EDTA 50 mM pH 8 and Tris HCl 10 mM pH 8 and stored at −80°C until their analysis. Plugs were prepared by mixing a volume of 31 μL of EDTA 50 mM pH 8 and Tris HCl 10 mM pH 8 containing approx. 1,000 individuals and 19 μL of melted CleanCut agarose 2% (Bio-Rad, Hercules, CA, United States). After 15 min of polymerization at 4°C, plugs were individually transferred into 500 μL of digestion buffer 100 mM EDTA 50 mM Tris pH 8, supplemented with 1 mg/mL proteinase K (Thermo Fisher Scientific, Waltham, MA, United States) and 3.3% N-Lauroylsarcosine sodium solution. Plugs were stored 1 h at 4°C and incubated 18 h at 56°C. Then, plugs were rinsed three times with 0.5x Tris Borate EDTA (TBE) and kept for 3 h in 0.5x TBE at 4°C. Finally, plugs were stored at 4°C in 500 μL 0.5 M EDTA pH 8 after a last rinse with 0.5x TBE before use. Plugs were loaded in a 0.8% agarose gel (Lonza, Rockland, ME, United States) along *Saccharomyces cerevisiae* chromosomes as ladder (Bio-Rad, Hercules, CA, United States). Samples were run on PFGE using appropriate running program on BIORAD CHEF Mapper XA according to the following parameters: migration time = 22 h, temperature = 14°C, Volts/cm = 5.5, switch angle = 120°, switch times = 60 to 185 s with a linear ramp (resolution ranging from 225 to 1600 kb). To better separate DNA fragments within the shorter range (15–291 kbp) by PFGE, a similar protocol was followed except for a few changes: switch times = 1 to 25 s with a linear ramp for 24 h run time; temperature = 15°C; Volts/cm = 6; 1% agarose gel. Gels were stained with SYBR Gold (Invitrogen, Carlsbad, CA, United States) and analyzed by a BioRad Chemidoc XRS camera. Images were processed using ImageLab 3.0 and ImageJ. Photometric scans of gel lanes were obtained using the plot profile tool (ImageJ) calculated on straight lines of identical length.

RESULTS

Evaluation of the Survival Rate of *A. vaga* Individuals Exposed to X-Ray, PROTONS and Fe Sources

Desiccated *A. vaga* individuals were exposed to increasing doses of ionizing radiation. The maximal doses achieved were about 3,000 Gy for Fe radiation, 7,500 Gy for X-ray and up to 10,000 Gy for protons 4 MeV. The survival rate of desiccated, irradiated individuals was investigated 2 days post rehydration.

For the proton exposure assay, unirradiated rotifers presented a survival rate of 94.8% (SD ± 3.5%). After exposure to protons 4 MeV, no significant differences were reported for samples exposed from 0 to 1,000 Gy (**Figure 1A**. group a). A significant decrease, in comparison with unirradiated samples, was reported after exposure to 2,500 Gy and more (**Figure 1A**. group b and c). Then, the survival rate of desiccated *A. vaga* individuals decreased to 19,1% (SD ± 34.1%) at 5,000 Gy, with a large variation observed between replicates. Finally, the clonal population of desiccated *A. vaga* individuals were dead when exposed to 7,500 Gy proton or more.

In comparison, X-ray exposed desiccated *A. vaga* do not show any significant decrease of survival rate until 2,500 Gy (**Figure 1B**. group a). Unirradiated samples were characterized by a survival rate of 95,6% (SD ± 2.5%). The survival rate at 5,000 Gy was 82,7% (SD ± 11.4%) and most animals (>99%) died after exposure to a dose of 7,500 Gy X-ray (see **Figure 1B**. group b and c, respectively).

Both for proton and X-ray exposure, few animals remained (<0.1%) active 2 days post rehydration at maximum doses (see **Supplementary Data S1**).

In the case of Fe irradiated dried samples, the survival of controls was affected by the transport to and from the irradiation site in Chiba (Japan). *A. vaga* individuals that were stored dry in our laboratory at 15°C for 1 month displayed a survival rate of 75.8% (SD ± 15.6) while unirradiated samples exposed to transportation were characterized by a survival rate of 50.1% (SD ± 13.3). No decrease of the survival rate was reported in *A. vaga* individuals exposed to Fe radiation up to 2,000 Gy (**Figure 1C** group b) in comparison with unirradiated, transported sample (**Figure 1C** "0T"). A significant decrease in survival rate of 30.8% was reported, in comparison with control samples, after an irradiation of 3,000 Gy to Fe (**Figure 1C** group c). The dose required to kill all the *A. vaga* individuals using Fe radiation was not achieved during this study.

The impact of irradiation on hydrated, active *A. vaga* animals was assessed up to 1,500 Gy using X-ray. No significant decrease of viability was reported in exposed animals up to the maximal dose of 1,500 Gy (**Figure 2A** group b). The significant difference in term of survival between hydrated and desiccated *A. vaga* individuals was attributed to the desiccation process that introduced more heterogeneity and mortality in the dataset of

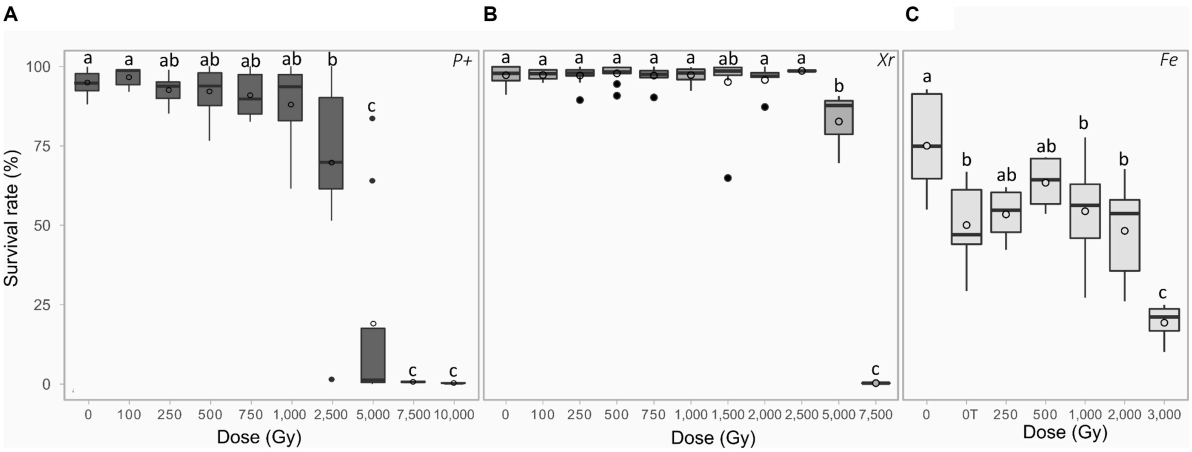

FIGURE 1 | Survival rate of desiccated *A. vaga* individuals exposed to increasing doses of **(A)** protons (p+) **(B)** X-ray (Xr) **(C)** Fe. Survival rate of desiccated, irradiated *A. vaga* individuals was evaluated 48 h post rehydration. For Fe exposure, the dose of 0 Gy corresponded to laboratory control and "0T" corresponded to unirradiated, transported samples. X-ray and proton exposed samples were desiccated for a period of 24 h. Fe samples, irradiated in Japan, were stored approx. 1 month in desiccated state. A minimum of 3 replicates per dose was achieved. Data were visualized as boxplot (○ = average; – = median). Letters indicate the significant differences between groups (*P*-value < 0.05).

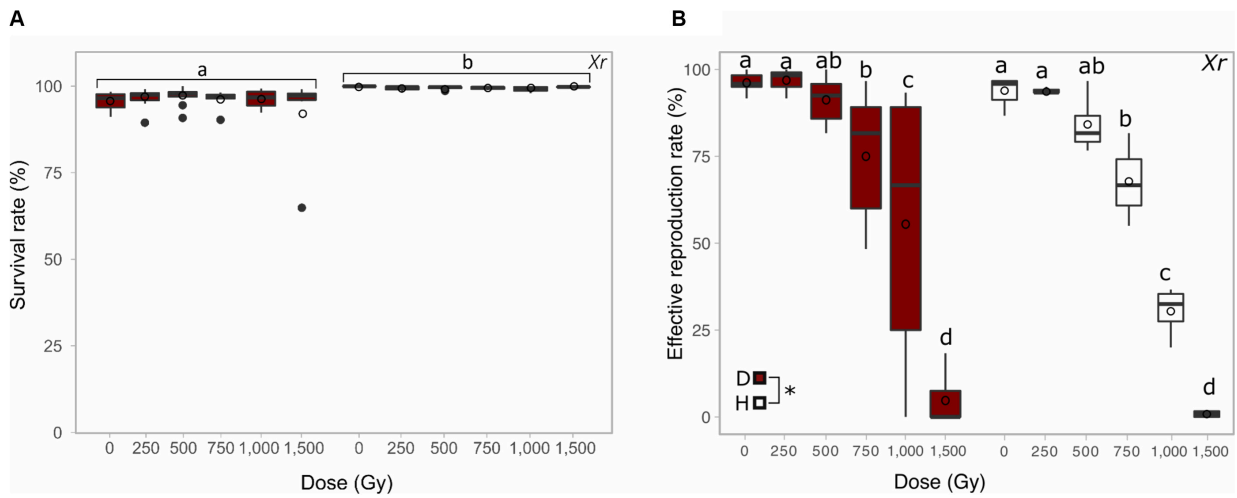

FIGURE 2 | Comparison between the survival rate **(A)** and the reproductive capacity **(B)** of desiccated (red) and hydrated (white) *A. vaga* individuals exposed to X-ray. Survival rate was evaluated 2 days post rehydration or post radiation and evaluated on minimum 3 replicates. The reproductive capacity was evaluated with a minimum of 3 replicates per dose (see section "Materials and Methods"). For each replicate, reproduction was evaluated by direct observation under binocular 30 days after rehydration/radiation. Effective reproduction was validated when at least 2 adults and 1 egg per well were observed. Statistical analysis included comparison between and within each group of desiccated and hydrated individuals. Statistical analysis of survival data highlights the significant effect of hydrated/desiccated status. The reproductive capacity was characterized by independent effect of doses and hydrated/desiccated status. Data were visualized as boxplot (○ = average; – = median). Letters or "*" indicate the significant differences between groups (*P*-value < 0.05).

desiccated animals (**Figure 2A** group a). No sign of abnormal behavior was reported 2 days post irradiation.

Comparing the Reproductive Capacity of *A. vaga* Individuals Exposed to X-Ray, Proton and Fe Sources

The reproductive capacity of irradiated *A. vaga* was evaluated by checking their capacity to lay eggs and to restart a new population of clonal *A. vaga* within a month post rehydration and isolation.

For proton radiation, no significant decrease of fertility was reported up to 250 Gy (**Figure 3A** group a). However, the fertility started to decrease significantly at 500 Gy where a big variability between replicates was observed (**Figure 3A** group b). Above 500 Gy, most *A. vaga* individuals were sterilized by proton 4 MeV radiation (**Figure 3A** group c).

For X-ray radiation on desiccated samples, no significant decrease of fertility was reported at doses ranging from 0 to 750 Gy. However, a significant drop was reported at 1,000 Gy where a higher variability between replicates was observed. Then,

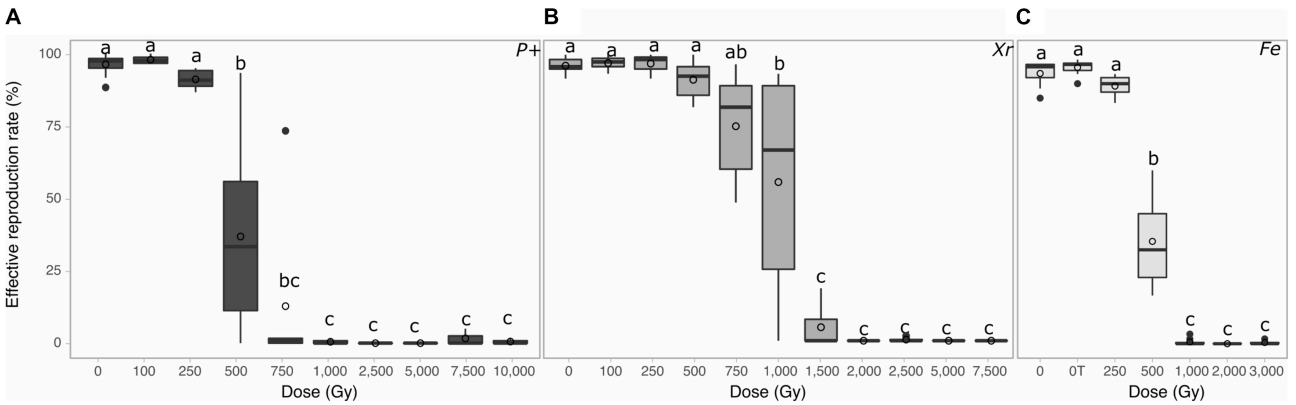

FIGURE 3 | Reproductive capacity of desiccated *A. vaga* individuals exposed to **(A)** protons (P +) **(B)** X-ray (Xr) **(C)** Fe. The reproductive capacity was calculated with a minimum of 3 replicates per dose. For each replicate, 60 individuals were randomly isolated and individually placed in multi-well plates. Reproduction was evaluated by direct observation under binocular 30 days after rehydration/radiation. Effective reproduction was validated when at least 2 adults and 1 egg per well were observed. Data were visualized as boxplot (○ = average; – = median). Letters indicate the significant differences between groups (*P*-value < 0.05).

a significant decrease of fertility was reported from 1,500 Gy, and most *A. vaga* individuals were sterilized at X-ray doses of 2,000 Gy and higher when desiccated (**Figure 3B** group c).

For Fe exposure, no significant difference in reproductive capacity between lab and transport control was reported. Moreover, no decrease of the fertility capacity was reported up to 250 Gy of Fe radiation (**Figure 3C** group a). A significant decrease of fertility was reported at 500 Gy (**Figure 3C** group b) and a complete sterilization of samples was reported at 1,000 Gy and higher (**Figure 3C** group c).

Based on collected data, it was possible to evaluate the minimal dose required to sterilize 50% of the irradiated *A. vaga* population. The median dose to sterilize a population [Sterilizing Dose 50 (SD_{50})] were 1,035 ± 20 Gy, 453 ± 23 Gy and 460 ± 1 Gy for X-ray, proton and iron radiation, respectively (see **Supplementary Figure S1**).

The failure of irradiated *A. vaga* individuals to restart a new population was not automatically linked with the non-ability of animals to produce eggs. Up to 2,500 Gy we noticed an increase of animals laying eggs that were unable to perform a complete embryonic development independently of radiation type (see **Supplementary Figure S2**). Multiple cellular divisions were reported in these sterile eggs that failed to reach a complete embryonic development (binocular observation of DAPI stained eggs, B. Hespeels and M. Terwagne, personal communication). Higher doses were characterized by an increased proportion of animals unable to lay eggs or dying within a month (see **Supplementary Figure S2**).

The effect of the hydration state (desiccated or hydrated) on irradiated animals was investigated through X-ray using doses ranging from 0 to 1,500 Gy. A higher impact of radiation on hydrated samples versus desiccated samples was highlighted by the comparison of both SD_{50}. Those were evaluated to 1,125 ± 88 Gy and 889 ± 12 Gy for samples exposed desiccated or hydrated, respectively (see **Supplementary Figure S1b**). Statistical analysis (see section "Materials and Methods") reveal the absence of interaction between factors dose and hydrated/desiccated status of samples when looking at the effective reproduction rate data. As suggested by SD_{50} a significant difference between hydrated and desiccated samples was reported: independently of the dose, the reproduction rate was significantly higher in desiccated samples than hydrated specimens. However, no significant difference was reported when data collected from hydrated and desiccated samples were compared for each tested dose (**Figure 2B**). At 1,000 Gy the fertility rate of desiccated samples was characterized by a high variability (55.5 ± 40.9%) in comparison with hydrated samples (30.4 ± 7.5%). 1% (SD ± 1%) of the exposed hydrated *A. vaga* were able to restart a population after exposure to 1,500 Gy X-ray in contrast to desiccated samples where 5% (SD ± 8%) of animals were still able to produce offspring after radiation. These differences were not statistically significant (**Figure 2B**). Nevertheless, a significant increase of animals unable to lay eggs or with premature deaths were reported in hydrated samples exposed to doses equal or higher to 1,000 Gy in comparison with desiccated, irradiated samples (**Supplementary Figure S3b** group c and d).

Loss of Genomic Integrity in Desiccated and Irradiated *A. vaga* Individuals Exposed to Increasing Dose of Radiation

To investigate how different types of radiation can affect the genomic integrity of *A. vaga* genome, the loss of genomic integrity induced by the accumulation of DNA DSBs was assessed using PFGE on 1,000 *A. vaga* individuals. As observed previously for *A. vaga* species (Hespeels et al., 2014), the genomic integrity of hydrated or 1 day desiccated bdelloid individuals was characterized by large DNA fragments remaining in the gel plug with a very weak signal around 2200 kbp (**Figures 4A–C** lanes 2 and 3; **Figure 4B** lane 2). At a dose of 100 Gy, loss of genomic integrity was observed through the visualization of a smear ranging between 225

to 2,200 kbp. Size of DNA fragments was negatively linked with the increase of the radiation exposure. After a dose of 1,000 Gy and higher, the genomes of *A. vaga* individuals were fragmented in DNA pieces mostly ranging between 225 and 1000 kbp (**Figures 4A–D**). Interestingly, for a similar dose, it was not possible to observe any significant variation in term of DNA fragmentation between X-ray, Proton and Iron radiation (see photometric scans **Figure 4E**). Moreover, when comparing hydrated and desiccated individuals exposed to similar dose of X-ray, no difference was reported (**Figures 4A,B,E**).

For samples exposed to Fe radiation, desiccated and unirradiated control presented a slight smear of DNA fragments ranging from small to high molecular weight. These controls were exposed to 1 month of dry storage and transported from Belgium to Chiba irradiation location and vice versa. These data are congruent with previous results suggesting that DNA DSB are accumulating with time in dried *A. vaga* even in absence of irradiation. As a consequence, the number of DNA DSBs may be overestimated in the dataset of samples exposed to increasing dose of Fe radiation.

Second, the genomic integrity of desiccated *A. vaga* individuals exposed to X-ray and proton was investigated with a resolution window of DNA fragments ranging between 15 to 242 kbp (**Figure 4F**). No smear was observed in hydrated and 1-day desiccated *A. vaga* individuals. However, both samples were characterized by a band of size >945 kbp. In contrast to previous results, different patterns between 1-day desiccated, irradiated *A. vaga* individuals exposed to 800 Gy of X-ray and proton were reported. The X-ray sample was characterized by intense signal for DNA fragments >600 kbp followed by a smear of decreasing intensity for DNA fragments <600 kbp. The sample exposed to proton radiation presented a reduced signal intensity for >600 kbp fragments and a smear of higher intensity than X-ray < 600 kbp. Similar patterns, highlighting progressive loss of genomic integrity, were reported when comparing 1-day desiccated samples irradiated at 500 and 1,000 Gy (see **Supplementary Figure S4**).

Partial Restoration of Genomic Integrity After Exposure to Radiation

The potential repair of DNA fragmentation induced by 800 Gy of X-ray and proton radiation in the somatic cells of (re-)hydrated animals were assessed through a kinetic from 0 to 1-week post exposure (**Figures 5A–C**). Following the rehydration or irradiation arrest (for hydrated animals), the genomic integrity was characterized by a smear of small DNA fragments (<2,200 kb, average size of 450 kbp) progressively vanishing within 24 h. The large (≥2,200 kb) DNA segments gradually re-appeared in the gel, revealing the presence of an active DNA DSB repair mechanism among *A. vaga* following massive genome breakage. Independently of the radiation type and the hydration state, DNA repair took place but the genomic profile of the control samples was not restored after 48 or 168 h post irradiation: in all tested exposure types, a smear of fragments ranging from 225 to 2,200 kbp was still observed.

DISCUSSION

This research highlights that lethal doses for desiccated *A. vaga* individuals range between 5,000 to 7,500 Gy using low and high LET radiation (for X-ray and Proton, respectively, see **Figure 1**). At dose of 5,000 Gy, the survival rate was higher for animals exposed to X-ray (82.7% SD ± 11.4) than to proton radiation (19.1% SD ± 34.1). This is in congruence with the idea that high LET radiation has a higher relative biological effectiveness than low LET radiation (Goodhead, 1999). A similar trend was reported for *A. vaga* samples exposed to high energy Fe particles despite the lack of exposure to doses higher than 3,000 Gy (see **Figure 1**). Noticeably, doses associated with drop of survival or fertility rates, in both X-ray and proton radiation exposure, were characterized by a higher level of heterogeneity between replicates. We hypothesize that this variability is linked to the uncertainty of the delivered dose. Although this is low (of the order of 1 to 2% of the delivered dose depending on the irradiation system used), it can become non-negligible in view of the total doses delivered in this study. Moreover, the dose received by animals is a Gaussian centered around the average reported dose (Poisson statistic). This is a characteristic specific to the use of broad beam radiation system and is a well-known source of variability in radiobiology. Finally, other uncontrolled biological factors, such as the average age of the exposed population between each assay, may contribute to the variability observed.

The radio-resistance of *A. vaga* individuals was differentially interpreted, in term of magnitude, when focusing on the survival rate or on their capacity to produce viable offspring. In our study, for X-ray for example, a factor of approximately 3 was reported between doses required to sterilize a population or to kill all exposed animals (compare **Figures 1**, **3**: dose required to sterilize 100% *A. vaga* population is between 1,500 and 2,000 Gy X-ray while it is between 5,000 and 7,500 Gy to kill the entire population). At minimal doses required to sterilize *A. vaga* individuals, no decrease of survival rate is observed in comparison with controls (see **Figures 1**, **3**). Animals were sterilized by doses of 750, 2,000 and 1,000 Gy for Protons, X-ray and Fe radiation, respectively (**Figure 3**). The median sterilizing doses (SD_{50}) for the *A. vaga* clone were 1,035 ± 20 Gy, 453 ± 23 Gy and 461 ± 1 Gy for X-ray, protons and iron, respectively (see **Supplementary Figure S1**). Due to the lack of intermediary dose for Fe particles between 500 and 1,000 Gy, no significant difference was reported between Protons and Fe. Nevertheless, data confirmed a clear difference between low and high LET radiation at the reproductive level. A 2.3 factor was reported when comparing SD_{50} of X-ray versus protons and Fe particles. Indeed, it would have taken twice as much dose deposited in the case of X-rays to sterilize individuals in comparison with protons and iron particles. The precise causes of these differences remain to be investigated but may be informative to the documentation of damage type induced by low and high LET radiation on a radioresistant metazoan.

The observed shift between survival rate and sterilization dose was previously also reported for other metazoan species like tardigrades. *Milnesium tardigradum* survived high doses of

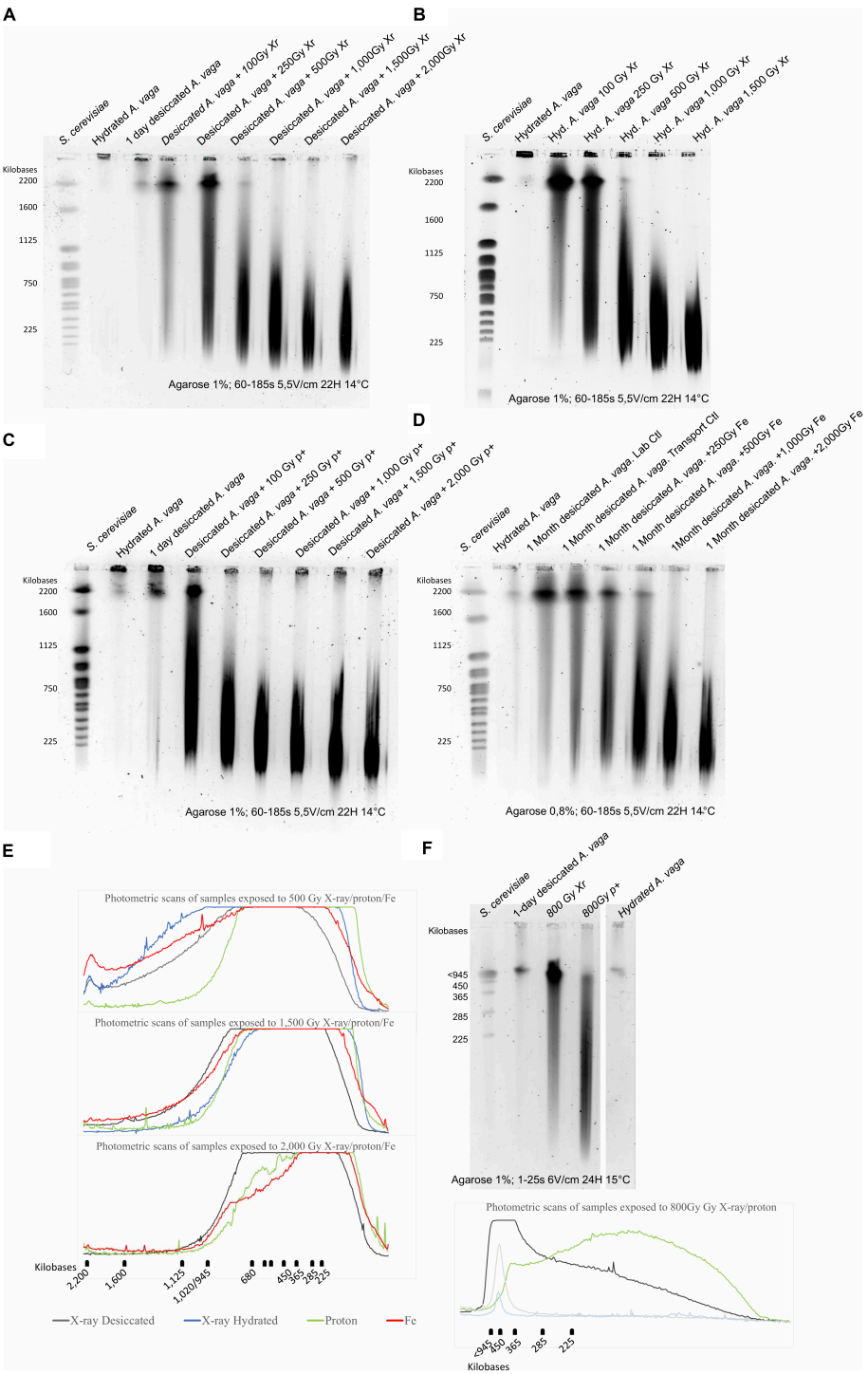

FIGURE 4 | Loss of genomic integrity in *A. vaga* individuals exposed to increasing doses of X-ray **(A,B)**, Protons 4 MeV **(C)** and Fe 1 GeV **(D)**; Comparative analysis of photometric scans from samples exposed to 500; 1,500 and 2,000 Gy **(E)**; Comparative analysis of 1-day desiccated *A. vaga* individuals exposed to 800 Gy of X-ray and protons 4 MeV using short fragments run parameters (15–291 kbp) **(F)**. For X-ray exposure, rotifers were irradiated after 1 day of desiccation **(A)** or irradiated in hydrated state **(B)**. Rotifers were desiccated 1 day before exposure to Protons 4 MeV **(C)**. However, samples exposed to Fe were desiccated 1 month **(D)**. The first lane on the pulsed-field gel electrophoresis corresponds to the karyotype of Saccharomyces cerevisiae. Second lanes correspond to the control (1,000 hydrated *A.vaga* individuals). Third lanes of **(A,C)** correspond to DNA fragmentation induced by 1-day desiccation on 1,000 individuals. Other lanes correspond to 1,000 desiccated **(A,C,D)** or hydrated individuals **(B)** after exposition to 100, 250, 500, 1,000, 1,500 and 2,000 Gy (in exception of **(B)** where maximum dose was 1.500 Gy). For the comparative analysis focusing on short DNA fragments dose of 800 Gy of respectively X-ray and protons was used (Lane 3 and 4). Hydrated control was in lane 5. 1-day desiccated *A. vaga* individuals was at lane 2. The run parameters are documented under each gel. Photometric scans were generated using ImageJ (see "Materials and Methods" section). Top flat lines from photometric scans correspond to saturated levels.

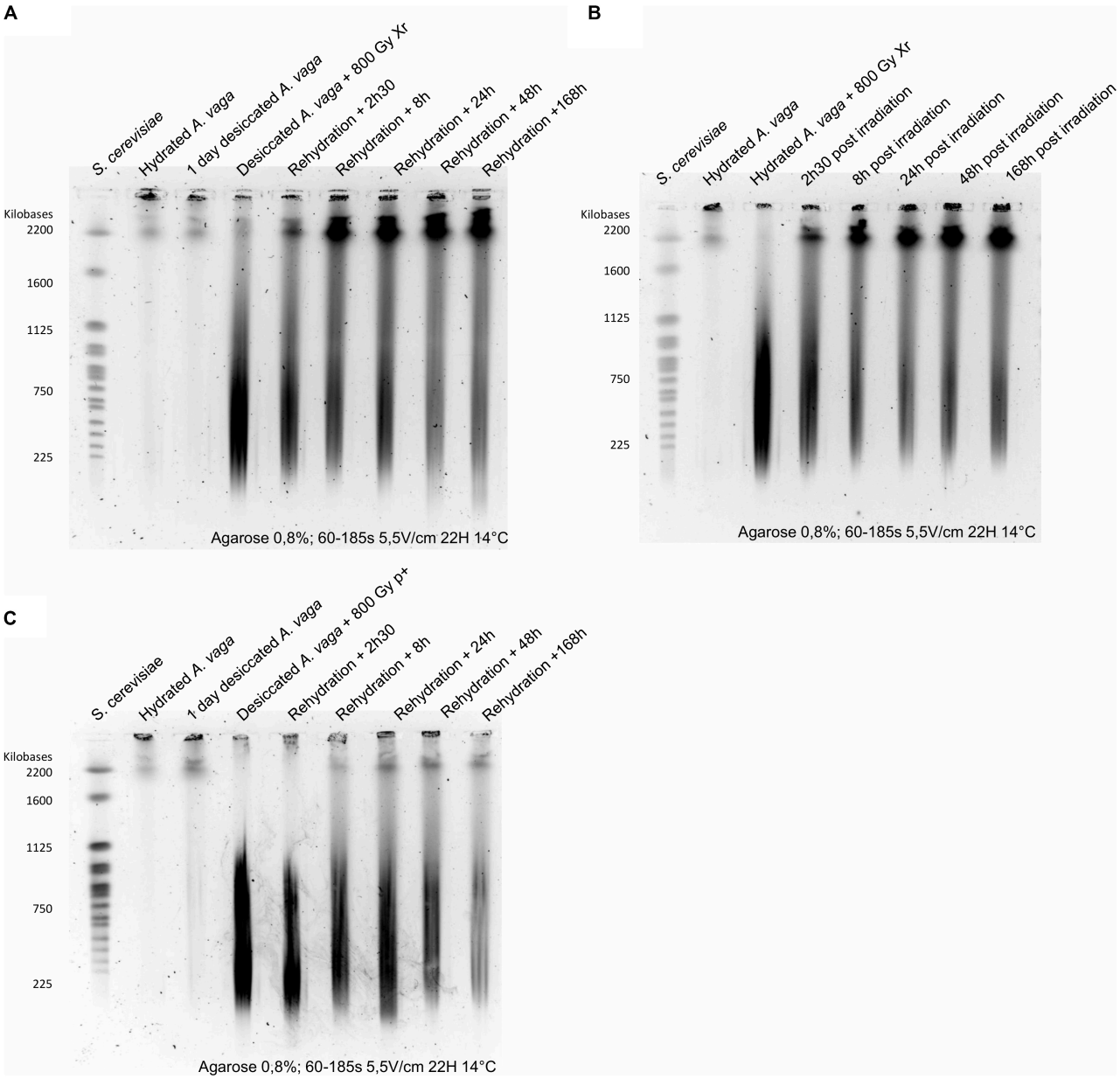

FIGURE 5 | Repair kinetic of *A. vaga* individuals on hydrated or desiccated samples with exposure to 800 Gy of X-ray [**(A)** 1-day desiccated samples **(B)** hydrated animals] and protons [**(C)** 1-day desiccated samples]. The first lane on the pulsed-field gel electrophoresis correspond to the karyotype of *Saccharomyces cerevisiae*. Second lanes correspond to the control (1,000 hydrated individuals). Third and fourth lanes correspond, respectively, to hydrated or desiccated bdelloids not submitted and submitted to 800 Gy radiation. Other lanes correspond to 1,000 desiccated individuals after 2, 30, 8, 24, 48, and 168 h of rehydration/post exposure. The run parameters are documented under each gel.

gamma radiation in both hydrated ($LD_{50/48\ h}$ 5,000 ± 1,900 Gy) and anhydrobiotic ($LD_{50/48\ h}$ 4,400 ± 500 Gy) states, but an irradiation dose >1,000 Gy makes them sterile (Horikawa et al., 2006). Similarly, the tardigrade *Hypsibius dujardini* exposed to gamma radiation presented a $LD_{50/48\ h}$ for survival estimated at ∼ 4,200 Gy, and doses higher than 100 Gy reduced drastically production and hatchability of laid eggs (Beltran-Pardo et al., 2015). These observations reported for tardigrades and bdelloids, both eutelic, may be attributed to the nature of the cells evaluated through survival or fecundity rate assays. The survival rate in those metazoans is related to non-dividing somatic cells, while fertility data is linked to germinal cells that will ensure cellular multiplication during embryonic development and as consequence are more sensitive to damages induced by radiation (Pagani et al., 1993; Beltran-Pardo et al., 2015). Nevertheless, when compared to other metazoans, the tested bdelloid rotifer and tardigrade species show a very high resistance to ionizing radiation (for examples see Krisko et al., 2012).

For future comparative analysis between radiation sensitive and radioresistant organisms, it may be more relevant to focus on fertility rate. Moreover, in term of evolution, there is no advantage to survive to extreme dose of radiation if no offspring is produced. As expected, the exposure to high doses of ionizing radiation was visualized through PFGE as an increased level of DNA fragmentation in function of the dose (**Figure 4**). An attempt was made here to discriminate DNA fragmentation induced by low and high LET, as well as the contribution of indirect damages by exposing hydrated *A. vaga* individuals to X-ray. No significant difference was reported between radiation source for comparable dose when focusing on fragment sizes ranging between 225 and 1,600 kbp. Similarly, it was not possible to detect significant differences in DNA fragmentation between samples exposed in hydrated or desiccated state (**Figure 4**). Nevertheless, absence of differences may be due to the lack of resolution inherent to PFGE focusing on high molecular weight DNA fragments. The resolution range of 225 kbp to 1,600 kbp is hypothesized to miss clustered damages induced by high LET radiation that may result in short DNA fragments. A comparative analysis was performed in order to check the genomic integrity pattern of fragments ranging from 15 to 240 kbp. Using this resolution window, it was possible to observe different DNA migration patterns between X-ray and proton irradiated *A. vaga* individuals (see **Figure 4F**). The increased smear of short size DNA fragments reported after proton exposure, in comparison to X-ray irradiated samples, may be attributed to the clustered damages generated by proton exposure resulting in the higher relative biological effectiveness of proton radiation vs X-rays. However, these data need to be validated by a systematic approach testing the impact of different particles, with increasing LET and other resolution range. Indeed, fine quantification of short DNA fragments induced by radiation is still challenging (Höglund et al., 2000; Alloni et al., 2013; Barbieri et al., 2019).

The loss of genomic integrity induced by low or high doses of radiation do not prevent the recovery process of *A. vaga*, neither in hydrated nor in desiccated state (**Figure 4**). Despite the dramatic loss of genomic integrity, *A. vaga* individuals were able to repair, at least partially, DNA damage induced by 800 Gy of X-ray or proton radiation in the somatic cells of (re-)hydrated animals (**Figure 5**). Indeed the 1,000 *A. vaga* individuals of the PFGE analysis contain only few germline cells per individual (<30) that are probably not recorded here, and only the signal of DNA repair in somatic cells is observed (>900). DNA repair kinetics suggest that most DNA damage induced by radiation are repaired within 24 h independently of the radiation source or on the reproductive capacity (see **Figures 2**, **3**, **5**). At first glance, these results suggest that the DNA repair kinetic taking place in somatic cells of irradiated *A. vaga* individuals appeared to be insensitive to the complexity of damage induced by low vs. high LET radiation exposures. The exact mechanism of DNA repair and the potential divergence in mechanism taking place in somatic or germline cells remain mostly unknown. Moreover, consequences of such massive DNA fragmentation, expected to occur also in germline cells, remain to be investigated at genomic scale on offspring originated from irradiated individuals. The genome of rotifer *A. vaga* was previously reported to carry an enriched complement of DNA repair genes compared to other invertebrates models (Flot et al., 2013; Hecox-Lea and Mark Welch, 2018). Genes of both homology-directed and non-homologous end joining (NHEJ) repair pathways are present in numerous copies, some of which likely acquired by horizontal transfers (Hecox-Lea and Mark Welch, 2018). Functional genetics are, however, required to determine the exact nature of their DNA repair process.

It is well known that ionizing radiation damages on biological samples can be generated by two paths of action. The first one, called "direct damage" literally means either the incident radiation itself or secondary particles ionize the target and generate breaks in the molecules. The second one, called "indirect action" refers to the generation of effectors such as reactive oxygen species (ROS), most frequently generated through water radiolysis, due to the incident radiation that, in turn, will generate the damages to cell compounds (Dartnell, 2011). In this line of thought, the contribution of direct and indirect damages remains to be investigated at high doses of radiation. The capacity of bdelloid rotifers to be exposed to ionizing radiation in hydrated and desiccated state constitutes an opportunity to evaluate biological effectiveness played by direct and indirect damages. Here, the impact of X-ray on desiccated and hydrated *A. vaga* was investigated. Within a radiation range of 0 to 1,500 Gy, no significant effects on the survival rate of irradiated *A. vaga* were reported 48 h post-exposition and eventual rehydration (see **Figure 2A**). Nevertheless, SD_{50} of hydrated individuals appeared to be lower than the one calculated for desiccated individuals. These data may suggest an increased level of damages due to the presence of liquid water (see **Figure 2B**). However, no significant difference was found when compared fertility rate of both conditions. In contrast, a higher proportion of dead animals, unable to produce eggs was reported 30 days post exposure among *A. vaga* individuals exposed in hydrated state starting 1,000 Gy (see **Supplementary Figure S3b**, group "d"). This latest result may be interpreted as a harmful impact of X-ray on hydrated animals that appeared to die prematurely in comparison with desiccated and irradiated samples. Indeed, the survival rate was only recorded 2 days post irradiation or rehydration and provides, as consequence, an evaluation of it at a short term. Investigation at different time points should be implemented to confirm the premature dead reported in hydrated samples. Inversely, these data may contribute to support the fact that somatic cells of desiccated bdelloid individuals are less affected by radiation in comparison with hydrated ones. According to the literature, 60 to 70% of damages induced *in vitro* cells by X-ray exposure originate from indirect damages (Komatsu, 2019). However, the comparison of SD_{50} from animals exposed hydrated (SD_{50} = 889 ± 12 Gy) or desiccated (1,125 ± 88 Gy) suggested a contribution of only 21% of indirect damages on *A. vaga* fecundity rate (see **Supplementary Figure S1b**). The radioresistance of *A. vaga* was previously attributed to the presence of an unusually effective system of anti-oxidant protection, protecting also the DNA repair proteins required to

repair the fragmented genome (Krisko et al., 2012). The reduced contribution of indirect damage observed here in hydrated, exposed samples may be linked to the efficiency of the antioxidant protection system present in *A. vaga*. Complementary studies must be addressed to document the biological response of living organisms to low and high LET radiation as well as the contribution of direct and indirect damage using desiccated and hydrated individuals.

CONCLUSION

In conclusion, the robustness of bdelloid rotifers against multiple stresses coupled with their desiccation tolerance at any stage of their life cycle prone them to the short list of animals that can be used as model systems to study how life can be adapted and could evolve in extra-terrestrial environments (Jönsson et al., 2008; Vukich et al., 2012; Rabbow et al., 2015). As a reference, this study focused on the bdelloid species *A. vaga*. It remains unknown if *A. vaga*, isolated 40 years ago from the wild and continuously maintained hydrated in laboratory condition, may reflect the overall limit of bdelloid radioresistance. Moreover, it is not excluded that this species presents a lower radioresistant phenotype in comparison with species living in extreme environments and Mars analog sites like Antarctic or Atacama Desert (Robeson et al., 2009; Iakovenko et al., 2015). Further studies are ongoing to decipher the impact of the environment of bdelloid species to their desiccation/radiation tolerance. Finally, the exposure of biological organisms in laboratory remains a simple view of the complex radiation flux found in space environment (Moeller et al., 2017) and experiments ongoing on ISS may reveal more insights into the resistance to cosmic radiation and space environment. Nevertheless, the combination of different type of low and high LET radiations, exposure to UV radiation, variation of temperature may significantly affect the biological effectiveness of unprotected samples ongoing lithopanspermia or "living" on martian-like atmosphere.

DATA AVAILABILITY STATEMENT

All datasets generated for this study are included in the article/**Supplementary Material**.

AUTHOR CONTRIBUTIONS

BH, LB, CB, and VB maintained the rotifer cultures. BH and LB performed all the experiments with help of CB and VB. Exposures to radiation were performed by BH, VB, CB, and LB under the supervision of A-CH, SL, RM, and AF. The results were analyzed by BH, VC, BR, and SP. The manuscript was written by BH. The manuscript was revised by KV, A-CH, SL, VC, RM, AF, and SP. The project was designed and supervised by BH and KV. The acquisition of funding was done by BH and KV. All authors contributed to the article and approved the submitted version.

FUNDING

The authors were supported by the European Space Agency (ESA) and the Belgian Federal Science Policy Office (BELSPO) in the framework of the PRODEX Programme. Fe radiation was part of STARLIFE astrobiology inter-comparison experiments at HIMAC (led by RM). STARLIFE was supported by the MEXT Grant-in-Aid for Scientific Research on Innovative Areas "Living in Space" (Grant Numbers: 15H05935 and 15K21745). RM was supported by the DLR grant FuE-Projekt "ISS LIFE" (Programm RF-FuW, TP 475). SP was funded by the Walloon Region (PROTHERWAL, grant n° 7289).

ACKNOWLEDGMENTS

R. Coos, R. Tonneau, and T. Tabarrant are strongly acknowledged for their assistance at any time during X-rays and proton exposure sessions. The authors also thank the European Space Agency (ESA) and the Belgian Federal Science Policy Office (BELSPO) for their support in the framework of the PRODEX Program.

SUPPLEMENTARY MATERIAL

The Supplementary Material for this article can be found online at: https://www.frontiersin.org/articles/10.3389/fmicb.2020.01792/full#supplementary-material

FIGURE S1 | Evaluation of Sterilizing Dose 50 (SD_{50}, Gy) for *A. vaga* individuals exposed to X-ray **(a,b)**, protons **(c)** and Fe **(d)**, overview **(e)**. Each dose was tested in min 3 replicates. For each replicate, 60 individuals were randomly isolated and individually placed in multiwell plates. Reproduction was evaluated by direct observation under binocular 30 days after irradiation and rehydration. All curve fittings were performed with the OriginLab® software (MA, United States) (see section "Materials and Methods"). Two SD_{50} for desiccated *A. vaga* species irradiated with X-ray were calculated. First SD_{50} included all data from 0 to 7,500 Gy X-ray. The second SD_{50} was calculated by limiting the dose range from 0 to 1,500 Gy X-ray. This last value was used for comparison with SD_{50} of hydrated specimens exposed to X-ray similarly calculated with dose from 0 to 1,500 Gy.

FIGURE S2 | Production of sterile eggs or premature dead in desiccated *A. vaga* individuals exposed to **(a)** protons (P +) **(b)** X-ray (Xr) c. Fe. For each replicate, 60 individuals were randomly isolated and individually placed in multi-well plates. Reproduction was evaluated by direct observation under binocular 30 days after irradiation and rehydration. Samples were characterized as "Sterile egg production" when one *A. vaga* individual and minimum one sterile egg was reported. If animals died within a month or were not able to lay eggs, it was annotated as "Dead or no egg production." When the number of survivors was below 60 individuals, the number of isolated individuals lacking to arrive at this total was automatically associated with the category "Dead or no egg production." This correction avoids the overweighting of certain values following the drastic reduction of survivors at dose equal or higher than 5,000 Gy (X-ray and proton only). Data were visualized as boxplot (○ = average; – = median). Letters indicate the significant differences between groups (P-value < 0.05; see section "Materials and Methods").

FIGURE S3 | Production of sterile eggs **(a)** or premature dead **(b)** in *A. vaga* individuals exposed to X-ray in desiccated (Red) or hydrated (white) state. Each dose was tested in min 3 replicates. For each replicate, 60 individuals were randomly isolated and individually placed in multiwell plates. Reproduction was evaluated by direct observation under binocular 30 days after irradiation and

rehydration. Sample were characterized as "Sterile eggs production" when one *A. vaga* individuals and min one sterile eggs was reported. If animals died within a month or was not able to lay egg, it was annotated as "Dead or no eggs production." Statistical analysis of the sterile eggs production highlighted only an effect of dose. Related to premature dead data, an interaction effect between dose factor and hydrated/desiccated status was highlighted. Data were visualized as boxplot (○ = average; – = median). Letters indicate the significant differences between groups (P-value < 0.05; see section "Materials and Methods").

FIGURE S4 | Genomic integrity of 1-day desiccated *A. vaga* individuals exposed to 500 and 1,000 Gy with X-rays and 4 MeV Protons, respectively, using short fragments run parameters (15–291 kbp). Lanes 1 and 5 on the pulsed-field gel electrophoresis corresponds to the karyotype of *Saccharomyces cerevisiae*. Lanes 2 and 6 correspond to the control (1,000 hydrated *A. vaga* individuals). Lanes 3 and 7 correspond to 1-day desiccated *A. vaga* individuals exposed, respectively, to 500 and 1,000 Gy of X-ray radiation. Lanes 4 and 8 correspond to 1-day desiccated *A. vaga* individuals exposed, respectively, to 500 and 1,000 Gy of protons 4 MeV radiation. The run parameters are documented under the gel. Samples used for **Supplementary Figure 4**, were irradiated and prepared independently from samples used for **Figure 4**.

DATA S1 | Survival and fertility data.

REFERENCES

Alloni, D., Campa, A., Friedland, W., Mariotti, L., and Ottolenghi, A. (2013). Integration of Monte Carlo Simulations with PFGE Experimental Data Yields Constant RBE of 2.3 for DNA Double-Strand Break Induction by Nitrogen Ions between 125 and 225 keV/μm LET. *Radiat. Res.* 179, 690–697. doi: 10.1667/r3043.1

Barbieri, S., Babini, G., Morini, J., Friedland, W., Buonanno, M., Grilj, V., et al. (2019). Predicting DNA damage foci and their experimental readout with 2D microscopy: a unified approach applied to photon and neutron exposures. *Sci. Rep.* 9:14019. doi: 10.1038/s41598-019-50408-5

Beltran-Pardo, E., Jonsson, K. I., Harms-Ringdahl, M., Haghdoost, S., and Wojcik, A. (2015). Tolerance to gamma radiation in the tardigrade *Hypsibius dujardini* from embryo to adult correlate inversely with cellular proliferation. *PLoS One* 10:e0133658. doi: 10.1371/journal.pone.0133658

Cucinotta, F. A., and Durante, M. (2006). Cancer risk from exposure to galactic cosmic rays: implications for space exploration by human beings. *Lancet Oncol.* 7, 431–435. doi: 10.1016/S1470-2045(06)70695-7

Dartnell, L. R. (2011). Ionizing radiation and life. *Astrobiology* 11, 551–582. doi: 10.1089/ast.2010.0528

Ferrari, F., and Szuszkiewicz, E. (2009). Cosmic rays: a review for astrobiologists. *Astrobiology* 9, 413–436. doi: 10.1089/ast.2007.0205

Fischer, C., Ahlrichs, W. H., Buma, A. G. J., van de Poll, W. H., and Bininda-Emonds, O. R. P. (2013). How does the "ancient" asexual *Philodina roseola* (Rotifera: Bdelloidea) handle potential UVB-induced mutations? *J. Exp. Biol.* 216(Pt 16), 3090–3095. doi: 10.1242/jeb.087064

Flot, J.-F., Hespeels, B., Li, X., Noel, B., Arkhipova, I., Danchin, E. G. J., et al. (2013). Genomic evidence for ameiotic evolution in the bdelloid rotifer *Adineta vaga*. *Nature* 500, 453–457. doi: 10.1038/nature12326

Fox, J., and Weisberg, S. (2019). *An {R} Companion to Applied Regression* (Third). Available online at: https://socialsciences.mcmaster.ca/jfox/Books/Companion/ (accessed June 1, 2020).

Gladyshev, E., and Meselson, M. (2008). Extreme resistance of bdelloid rotifers to ionizing radiation. *Proc. Natl. Acad. Sci. U.S.A.* 105, 5139–5144. doi: 10.1073/pnas.0800966105

Gladyshev, E. A., and Arkhipova, I. R. (2010). Genome structure of bdelloid rotifers: Shaped by asexuality or desiccation? *J. Heredity* 101(Suppl. 1), 85–93. doi: 10.1093/jhered/esq008

Goodhead, D. T. (1999). Mechanislns for the Biological Effectiveness of High-LET Radiations. *J. Radiat. Res.* 40(Suppl.), 1–13. doi: 10.1269/jrr.40.s1

Hagiwara, Y., Oike, T., Niimi, A., Yamauchi, M., Sato, H., Limsirichaikul, S., et al. (2019). Clustered DNA double-strand break formation and the repair pathway following heavy-ion irradiation. *J. Radiat. Res.* 60, 69–79. doi: 10.1093/jrr/rry096

Hecox-Lea, B. J., and Mark Welch, D. B. (2018). Evolutionary diversity and novelty of DNA repair genes in asexual Bdelloid rotifers. *BMC Evol. Biol.* 18:177. doi: 10.1186/s12862-018-1288-9

Hespeels, B., Knapen, M., Hanot-Mambres, D., Heuskin, A.-C., Pineux, F., Lucas, S., et al. (2014). Gateway to genetic exchange? DNA double-strand breaks in the bdelloid rotifer *Adineta vaga* submitted to desiccation. *J. Evol. Biol.* 27, 1334–1345. doi: 10.1111/jeb.12326

Höglund, E., Blomquist, E., Carlsson, J., and Stenerlöw, B. (2000). DNA damage induced by radiation of different linear energy transfer: Initial fragmentation. *Int. J. Radiat. Biol.* 76, 539–547. doi: 10.1080/095530000138556

Horikawa, D. D., Sakashita, T., Katagiri, C., Watanabe, M., Kikawada, T., Nakahara, Y., et al. (2006). Radiation tolerance in the tardigrade *Milnesium tardigradum*. *Int. J. Radiat. Biol.* 82, 843–848. doi: 10.1080/09553000600972956

Hothorn, T., Bretz, F., and Westfall, P. (2008). Simultaneous inference in general parametric models. *Biom. J.* 50, 346–363. doi: 10.1002/bimj.200810425

Iakovenko, N. S., Smykla, J., Convey, P., Kasparova, E., Kozeretska, I. A., Trokhymets, V., et al. (2015). Antarctic bdelloid rotifers: diversity, endemism and evolution. *Hydrobiologia* 761, 5–43. doi: 10.1007/s10750-015-2463-2

Joiner, M. C., and van der Kogel, A. J. (2018). *Basic Clinical Radiobiology*. Available online at: https://books.google.be/books?id=pnxqDwAAQBAJ (accessed May 27, 2020).

Jönsson, K. I., Rabbow, E., Schill, R. O., Harms-Ringdahl, M., and Rettberg, P. (2008). Tardigrades survive exposure to space in low Earth orbit. *Curr. Biol.* 18, 729–731. doi: 10.1016/j.cub.2008.06.048

Jönsson, K. I., and Wojcik, A. (2017). Tolerance to X-rays and heavy ions (Fe, He) in the tardigrade *Richtersius coronifer* and the bdelloid rotifer *Mniobia russeola*. *Astrobiology* 17, 163–167. doi: 10.1089/ast.2015.1462

Kohn, H. I., and Kallman, R. F. (1957). The influence of strain on acute X-Ray lethality in the mouse: II. Recovery rate studies. *Radiat. Res.* 6, 329–338. doi: 10.2307/3570613

Komatsu, K. (2019). *Contemporary Radiobiology*. Available online at: https://books.google.be/books?id=CRu7DwAAQBAJ (accessed May 27, 2020).

Krisko, A., Leroy, M., Radman, M., and Meselson, M. (2012). Extreme anti-oxidant protection against ionizing radiation in bdelloid rotifers. *Proc. Natl. Acad. Sci. U.S.A.* 109, 2354–2357. doi: 10.1073/pnas.1119762109

Latta, L. C., Tucker, K. N., and Haney, R. A. (2019). The relationship between oxidative stress, reproduction, and survival in a bdelloid rotifer. *BMC Ecol.* 19:7. doi: 10.1186/s12898-019-0223-2

Lehnert, S. (2007). *Biomolecular Action of Ionizing Radiation*. Boca Raton, FL: CRC Press.

Leuko, S., and Rettberg, P. (2017). The effects of HZE particles, γ and X-ray radiation on the survival and genetic integrity of *Halobacterium salinarum* NRC-1, *Halococcus hamelinensis*, and *Halococcus morrhuae*. *Astrobiology* 17, 110–117. doi: 10.1089/ast.2015.1458

Loucas, B. D., and Cornforth, M. N. (2013). The LET dependence of unrepaired chromosome damage in human cells: A break too far? *Radiat. Res.* 179, 393–405. doi: 10.1667/RR3159.2

Mattimore, V., and Battista, J. R. (1996). Radioresistance of *Deinococcus radiodurans*: functions necessary to survive ionizing radiation are also necessary to survive prolonged desiccation. *J. Bacteriol.* 178, 633–637. doi: 10.1128/jb.178.3.633-637.1996

Maynard Smith, J. (1986). Contemplating life without sex. *Nature* 324, 300–301. doi: 10.1038/324300a0

Melone, G., and Fontaneto, D. (2005). Trophi structure in bdelloid rotifers. *Hydrobiologia* 546, 197–202. doi: 10.1007/s10750-005-4197-z

Moeller, R., Raguse, M., Leuko, S., Berger, T., Hellweg, C. E., Fujimori, A., et al. (2017). STARLIFE -An international campaign to study the role of galactic cosmic radiation in astrobiological model systems. *Astrobiology* 17, 101–109. doi: 10.1089/ast.2016.1571

Mole, R. H. (1984). The LD50 for uniform low LET irradiation of man. *Br. J. Radiol.* 57, 355–369. doi: 10.1259/0007-1285-57-677-355

Pagani, M., Ricci, C., and Redi, C. A. (1993). Oogenesis in *Macrotrachela quadricornifera* (Rotifera, Bdelloidea). *Hydrobiologia* 255-256, 225–230. doi: 10.1007/BF00025843

Penninckx, S., Cekanaviciute, E., Degorre, C., Guiet, E., Viger, L., Lucasb, S., et al. (2019). Dose, LET and strain dependence of radiation-induced 53BP1 foci in 15 mouse strains *ex vivo* introducing novel DNA damage metrics. *Radiat. Res.* 192, 1–12. doi: 10.1667/RR15338.1

Rabbow, E., Rettberg, P., Barczyk, S., Bohmeier, M., Parpart, A., Panitz, C., et al. (2015). The astrobiological mission EXPOSE-R on board of the international space station. *Int. J. Astrobiol.* 14, 3–16. doi: 10.1017/S1473550414000202

Ricci, C. (2017). Bdelloid rotifers: 'sleeping beauties' and 'evolutionary scandals', but not only. *Hydrobiologia* 796, 277–285. doi: 10.1007/s10750-016-2919-z

Ricci, C., Caprioli, M., Boschetti, C., and Santo, N. (2005). *Macrotrachela quadricornifera* featured in a space experiment. *Hydrobiologia* 534, 239–244. doi: 10.1007/s10750-004-1509-7

Ricci, C., and Melone, G. (2000). Key to the identification of the genera of bdelloid rotifers. *Hydrobiologia* 418, 73–80. doi: 10.1023/A:1003840216827

Riley, P. A. (1994). Free radicals in biology: oxidative stress and the effects of ionizing radiation. *Int. J. Radiat. Biol.* 65, 27–33. doi: 10.1080/09553009414550041

Robeson, M. S., Costello, E. K., Freeman, K. R., Whiting, J., Adams, B., Martin, A. P., et al. (2009). Environmental DNA sequencing primers for eutardigrades and bdelloid rotifers. *BMC Ecol.* 9:25. doi: 10.1186/1472-6785-9-25

RStudio Team (2015). *RStudio: Integrated Development Environment for R*. Available online at: http://www.rstudio.com/ (accessed June 1, 2020).

Segers, H. (2007). Annotated checklist of the rotifers (Phylum Rotifera), with notes on nomenclature, taxonomy and distribution. *Zootaxa* 1564, 1–104. doi: 10.11646/zootaxa.1564.1.1

Semenenko, V. A., and Stewart, R. D. (2004). A fast monte carlo algorithm to simulate the spectrum of DNA damages formed by ionizing radiation. *Radiat. Res.* 161, 451–457. doi: 10.1667/RR3140

Simpson, J. A. (1983). "Introduction to the galactic cosmic radiation," in *Composition and Origin of Cosmic Rays*, ed. M. M. Shapiro (Dordrecht: Reidel Publishing), 1–24. doi: 10.1007/978-94-009-7166-0_1

Turner, J. (2007). *Atoms, Radiaiton, and Radiation Protection*, Third Edn. Hoboken, NJ: Wiley-VCH Verlag GmbH. doi: 10.1002/9783527616978

Vukich, M., Ganga, P. L., Cavalieri, D., Rizzetto, L., Rivero, D., Pollastri, S., et al. (2012). BIOKIS: a model payload for multidisciplinary experiments in microgravity. *Microgravity Sci. Technol.* 24, 397–409. doi: 10.1007/s12217-012-9309-6

Wéra, A.-C., Riquier, H., Heuskin, A.-C., Michiels, C., and Lucas, S. (2011). In vitro irradiation station for broad beam radiobiological experiments. *Nucl. Inst. Methods Phys. Res. Sect. B* 269, 3120–3124. doi: 10.1016/j.nimb.2011.04.104

White, R. J., and Averner, M. (2001). Humans in space. *Nature* 409, 1115–1118. doi: 10.1038/35059243

Wilson, J. W. (1991). *Transport Methods and Interactions for Space Radiations*, Vol. 1257. Washington, DC: National Aeronautics and Space Administration, Office of Management, Scientific and Technical Information Program.

Ziegler, J. F., Ziegler, M. D., and Biersack, J. P. (2010). SRIM - The stopping and range of ions in matter (2010). *Nucl. Inst. Methods Phys. Res. Sect. B* 268, 1818–1823. doi: 10.1016/j.nimb.2010.02.091

Conflict of Interest: The authors declare that the research was conducted in the absence of any commercial or financial relationships that could be construed as a potential conflict of interest.

frontiers in Microbiology

ORIGINAL RESEARCH
published: 18 August 2020
doi: 10.3389/fmicb.2020.01957

Description of Chloramphenicol Resistant *Kineococcus rubinsiae* sp. nov. Isolated From a Spacecraft Assembly Facility

*Snehit Mhatre[1†], Nitin K. Singh[1†], Jason M. Wood[1†], Ceth W. Parker[1], Rüdiger Pukall[2], Susanne Verbarg[2], Brian J. Tindall[2], Meina Neumann-Schaal[2] and Kasthuri Venkateswaran[1]**

[1] Biotechnology and Planetary Protection Group, Jet Propulsion Laboratory, California Institute of Technology, Pasadena, CA, United States, [2] Leibniz-Institute DSMZ-German Collection of Microorganisms and Cell Cultures, Braunschweig, Germany

A Gram-positive, coccoid, motile, aerobic bacterium, designated strain B12^T was isolated from a Jet Propulsion Laboratory spacecraft assembly cleanroom, Pasadena, CA, United States. Strain B12^T was resistant to chloramphenicol (100 μg/mL), and is a relatively slow grower (3–5 days optimal). Strain B12^T was found to grow optimally at 28 to 32°C, pH 7 to 8, and 0.5% NaCl. Fatty acid methyl ester analysis showed that the major fatty acid of the strain B12^T was anteiso $C_{15:0}$ (66.3%), which is also produced by other *Kineococcus* species. However, arachidonic acid ($C_{20:4}$ ω6,9,12,16c) was present in strain B12^T and *Kineococcus glutinatus* YIM 75677^T but absent in all other *Kineococcus* species. 16S rRNA analysis revealed that strain B12^T was 97.9% similar to *Kineococcus radiotolerans* and falls within the *Kineococcus* clade. Low 16S rRNA gene sequence similarities (<94%) with other genera in the family *Kineosporiaceae*, including *Angustibacter* (93%), *Kineosporia* (94% to 95%), *Pseudokineococcus* (93%), *Quadrisphaera* (93%), and *Thalassiella* (94%) demonstrated that the strain B12^T does not belong to these genera. Phylogenetic analysis of the *gyrB* gene show that all known *Kineococcus* species exhibited <86% sequence similarity with B12^T. Multi-locus sequence and whole genome sequence analyses confirmed that B12^T clades with other *Kineococcus* species. Average nucleotide identity of strain B12^T were 75–78% with other *Kineococcus* species, while values ranged from 72–75% with species from other genera within family *Kineosporiaceae*. Average amino-acid identities were 66–72% with other *Kineococcus* species, while they ranged from 50–58% with species from other genera. The dDDH comparison of strain B12^T genome with members of genera *Kineococcus* showed 20–22% similarity, again demonstrating that B12^T is distantly related to other members of the genus. Furthermore, analysis of whole proteome deduced from WGS places strain B12^T in order *Kineosporiales*, confirming that strain B12^T is a novel member of family *Kineosporiaceae*. Based on these analyses and other genome characteristics, strain B12^T is assigned to a novel species within the genus *Kineococcus*, and the name *Kineococcus rubinsiae* sp. nov., is proposed. The type strain is B12^T (=FJII-L1-CM-PAB2^T; NRRL B-65556^T, DSM 110506^T).

Keywords: antibiotic resistant bacteria, genome, cleanroom, spacecraft assembly facility, *Kineococcus rubinsiae*

OPEN ACCESS

Edited by:
Rakesh Mogul, California State Polytechnic University, Pomona, United States

Reviewed by:
Ramprasad E. V. V., University of Hyderabad, India
Cristina Sánchez-Porro, Seville University, Spain

***Correspondence:**
Kasthuri Venkateswaran
kjvenkat@jpl.nasa.gov

† These authors have contributed equally to this work

Specialty section:
This article was submitted to Extreme Microbiology, a section of the journal Frontiers in Microbiology

Received: *01 October 2019*
Accepted: *24 July 2020*
Published: *18 August 2020*

Citation:
Mhatre S, Singh NK, Wood JM, Parker CW, Pukall R, Verbarg S, Tindall BJ, Neumann-Schaal M and Venkateswaran K (2020) Description of Chloramphenicol Resistant Kineococcus rubinsiae sp. nov. Isolated From a Spacecraft Assembly Facility. Front. Microbiol. 11:1957. doi: 10.3389/fmicb.2020.01957

INTRODUCTION

Traditionally, biochemical characteristics (Phillips et al., 2002), chemotaxonomic analyses (Lee et al., 2016), and DNA-DNA hybridization analyses (Satomi et al., 2006) were used to describe novel microbial species, including members belonging to the *Actinobacteria* phylum. Furthermore, fatty acid methyl ester (FAME) (Diogo et al., 1999) and matrix-assisted laser desorption/ionization time of flight (MALDI-TOF) mass spectrometry analyses (Seuylemezian et al., 2018) have been shown to be a useful alternative or adjunct to phenotypic methodologies for the identification of many bacteria. Most of these traditional bacterial identification methods were not feasible for environmental bacteria since traditional databases were dependent on fast growing, clinically important microorganisms. The slow growing *Actinobacteria* tend to secrete biochemical compounds and enzymes differentially in various cultivation media and also depend on specific growth conditions, hence phenotype-based characterization will not resolve to their species.

Identifying bacterial species, despite its eminent practical significance for identification, diagnosis, quarantine, and diversity surveys, remains a very difficult issue to advance. To overcome issues related to potentially unknown cultivation conditions for an organism, genomic sequences have recently been used to unambiguously identify microbial taxa (Singh et al., 2019). Several strategies, including amplicon sequencing of phylogenetic marker genes (16S rRNA, *gyrB*, etc.), multi-locus sequencing analysis (MLSA), and whole genome sequencing (WGS) were implemented to differentiate hard to identify microbial species (Venkateswaran et al., 2017; Singh et al., 2019). Furthermore, minimal standards for the use of genome data for the taxonomy of prokaryotes were proposed (Konstantinidis et al., 2017; Chun et al., 2018). Phylogenetically indistinguishable members detected using 16S rRNA gene sequence analysis in the *Bacillus cereus* group (La Duc et al., 2004) were differentiated using MLSA analysis (Helgason et al., 2000). Genomics now offers novel insights into intra-species/genus diversity and the potential for emergence of a more soundly based system (Chun et al., 2018). Konstantinidis et al. (2006) analyzed several bacterial strains and revealed what is actually encompassed in a species according to the current standards, in terms of WGS and gene-content diversity. Konstantinidis et al. (2006) and Varghese et al. (2015) reported that the genome-wide average nucleotide identity (ANI) metric, which is widely acknowledged as a robust measure of genomic relatedness, should be combined with the digital DNA-DNA hybridization (dDDH) values between two genomes to accurately define microbial taxa. The average amino-acid identity (AAI) metric has also been proposed as a standard for high-quality descriptions of microbial taxa (Konstantinidis et al., 2017). The ANI, AAI, and dDDH values were used to address the novelty of a strain isolated during this study for bacterial species classification and as the primary guide for new taxonomic genus/species assignment, supplemented by the traditional polyphasic approach.

At the time of writing, the order *Kineosporiales* of phylum *Actinobacteria* is comprised of six genera: *Angustibacter* (Ko and Lee, 2017), *Kineococcus* (Phillips et al., 2002), *Kineosporia* (Kudo et al., 1998), *Pseudokineococcus* (Jurado et al., 2011), *Quadrisphaera* (Maszenan et al., 2005), and *Thalassiella* (Lee et al., 2016). *Actinobacteria* represent a very primitive lineage of prokaryotes known to be ubiquitous, slow growing, and is comprised of aerobes and anaerobes, are motile or non-motile, spore formers and non-spore formers, and have a high GC content in genomic DNA (Gao and Gupta, 2005). *Actinobacteria* also play an important role in several biological processes, including bioremediation (Chen et al., 2015), bio-weathering (Cockell et al., 2013), biogeochemical cycles, and promoting plant growth (Palaniyandi et al., 2013). Additionally, they produce a vast array of industrially important bioactive compounds like antibiotics, enzyme inhibitors, anti-inflammatory compounds, and anti-tumor compounds (Jiang et al., 2017). Actinobacteria are known to occur in many extreme environments mainly characterized by extremes of pH, temperature, salinity, radiation, or low levels of nutrients and carbon sources (Zenova et al., 2011). Owing to their diverse metabolism and physiology, *Actinobacteria* can survive hostile and unfavorable conditions (Mohammadipanah and Wink, 2016).

In this communication, an aerobic, coccoid-shaped, and Gram-positive bacterium that was isolated from the National Aeronautics and Space Administration (NASA) Jet Propulsion Laboratory (JPL) spacecraft assembly facility (SAF) cleanroom surface is described. Bacterial classification of the novel species is presented to describe *Kineococcus rubinsiae* sp. nov. that belongs to the family *Kineosporiaceae* of phylum *Actinobacteria*. The whole-genome sequence (WGS) and annotation of *K. rubinsiae* sp. nov., are documented in classifying it as a new member of the family *Kineosporiaceae*.

MATERIALS AND METHODS

Sample Collection and Isolation of Bacteria

Samples were collected from the JPL-SAF, Pasadena, California from 10 locations of 1 m^2 area using sterile polyester wipes (23 cm × 23 cm; ITW Texwipe, Mahwah, NJ, United States) premoisented with phosphate buffer saline (PBS). Subsequently, each wipe was individually transferred to 200 mL PBS and vortexed at maximum speed for 5 s. The resulting suspension was then concentrated to appropriate volume (∼30-fold) with a concentration pipette CP-150 (Innova Prep, Drexel, MO, United States) using a 0.20 μm hollow fiber polysulfone tip (Kwan et al., 2011). The concentrated samples were then split in two 3 mL aliquots where one aliquot was treated with 100 μg/mL of chloramphenicol (Sigma, St. Louis, MO, United States) and the other aliquot was untreated. The sample amended with chloramphenicol was incubated at 25°C for 24 h and subsequently subjected to downstream processing utilizing both traditional microbiology and molecular biological techniques. At the time the experiments were conducted, the aim was the isolation of novel fungal species thriving in the JPL SAF, and hence a 100 μL suspension of the samples that were treated with and without

chloramphenicol was spread onto antibiotic supplemented (chloramphenicol 100 μg/mL) media like potato dextrose agar (PDA) and Dichloran Rose Bengal Chloramphenicol Agar (DRBC) and incubated at 25°C for 5 days. Among several fungal colonies purified, some bacterial colonies also surfaced onto the PDA and DRBC media, and were selected for further characterization. Since the isolation was carried out on antibiotic treated samples, bacteria exhibiting resistance to chloramphenicol were interesting. The bacterial strains resistant to chloramphenicol that exhibited higher 16S rRNA gene similarities (>99%) with already described species were not further studied in this project. However, one of the several bacterial colonies (strain B12^T) showed 97.9% 16S rRNA gene sequence similarity with its closest neighbor (see below for details). Strain B12^T was further assayed for its polyphasic taxonomic and WGS characterization. Distinct colonies of strain B12^T were isolated and transferred to fresh PDA medium and subsequently archived in semi-solid R2A media and stored at room temperature as well as in glycerol stock for further characterization.

Morphological and Phenotypic Characterizations of Strain B12^T

The cells of strain B12^T were fixed for scanning electron microscopy (SEM) by first suspending two separate colonies of the strain B12^T in 0.1 M phosphate buffered saline (PBS, pH 7.2; Sigma-Aldrich) in separate 1.5 mL microcentrifuge tubes. In order to obtain B12^T cells with decreased amounts of extracellular polysaccharides (EPS), the first tube was vigorously pipetted and then vortexed for 30 s, followed by filtration of the suspension through a 0.2 μm polycarbonate filter membrane on a vacuum manifold. The original tube was washed two more times with 0.1 M PBS, and then passed through the same filter. The filter membrane was then removed and placed into a fresh 1.5 mL microcentrifuge tube. The unbroken-up colony of B12^T (with preserved EPS) had excess PBS aliquoted off. The following steps were performed for both samples identically. Suitable aliquots (750 μL) of 2.5% glutaraldehyde in 0.1 M PBS was added to each tube and then incubated in the refrigerator at 4°C for 1 h. Without disturbing the colony or the filter membrane, the majority of the solution was aliquoted from the microcentrifuge tube and replaced with 1 mL of 0.1 M PBS, and returned to the refrigerator for a 10 min. incubation. This wash step was repeated for a total of three times. Next the samples underwent an ethanol (EtOH) dehydration series. The solution was aliquoted out of the microcentrifuge tubes and replaced with an increasing concentration of EtOH diluted in 0.1 M PBS. After each new EtOH solution was added, the tube was incubated in the refrigerator for 10 min. The EtOH concentrations were 50, 70, 80, 90, 95, and 100%. The 100% EtOH was aliquoted out and replaced with fresh 100% EtOH a total of three times, and stored in the refrigerator. The samples then underwent critical point drying in a Tousimis Automegasamdri 915B critical point dryer (Rockville, MD, United States). Samples were then adhered to carbon tape (Ted Pella Inc., Redding, CA, United States) and sputter coated with AuPd using an Anatech Hummer (Sparks, NV, United States) sputter coater. SEM was performed on a FEI Quanta 200F (Themo Fisher, Waltham, MA, United States).

Phenotypic characterization of the strain B12^T was performed by following standardized protocols (Jones, 1981). For phenotypic tests, strain B12^T was grown in sterile peptone-tryptone-yeast extract-glucose (PTYG; 5 g each per liter) medium incubated at 32°C with pH 7 and 0.5% NaCl, unless otherwise stated. Morphology, size, and pigmentation were observed on PTYG medium after 72 h of incubation. A commercially available kit (BD Difco) was used to determine the Gram-staining status of the strain. Motility was determined by inoculating a loopful of culture into a PTYG broth and incubating it for a period of 72 h. Subsequently, a loopful of broth was tested for motility using a previously established technique (Skerman, 1960). Growth in various temperature conditions (5–45°C) was tested by increasing incubation temperature in increments of 5°C and grown in PTYG broth. Similarly, the pH tolerance (4–10) was tested by adjusting the pH of the PTYG broth with biological buffers (Xu et al., 2005). The NaCl tolerance (0–5%) tests were carried out in 1% sterile peptone broth containing appropriate amounts of NaCl. The carbon substrate utilization profile was carried out as per the BioLog protocol for actinobacteria using GEN III MicroPlate test assay with a Biolog system. The test panel comprises 71 carbon sources with 23 chemical sensitivity assays and thus provides a "Phenotypic Fingerprint" of the tested microorganism. Since B12^T cells grown either in tryptic soy broth or Luria broth and washed in buffer before placing in BioLog plates did not exhibit any carbon substrate utilization profile, cells were grown in PTYG medium but such modified growth medium also did not show carbon utilization in BioLog plates. This is unusual for the bacterium not to utilize any of the carbon substrate provided in BioLog. The BioLog system

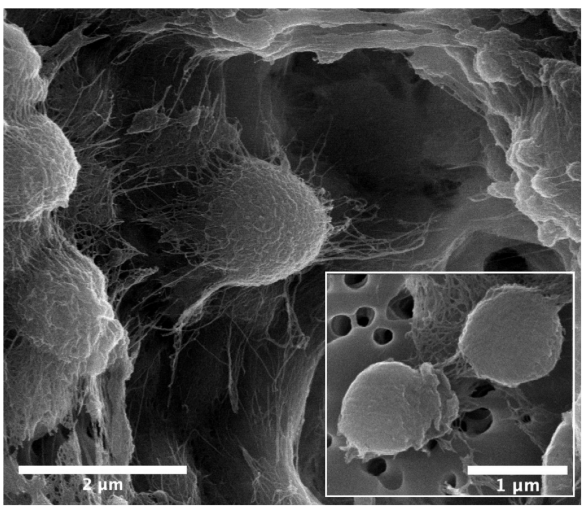

FIGURE 1 | SEM micrographs of *Kineococcus rubinsiae* B12^T. The compact clustering might be due to the production of extracellular polysaccharide (EPS) seen in abundance (thread-like structures). Upon vigorous agitation the EPS are removed and individual coccoid cells are visualized (inset).

TABLE 1 | Differential characteristics of strain B12^T and type strains of genus *Kineococcus*.

Characteristic	*Strain B12^T	*K. terrestris* YIM 121936^T	*K. aureolus* YIM 121940^T	*K. gypseus* YIM 121300^T	*K. aurantiacus* JCM 10180^T	*K. glutinatus* YIM 75677^T	*K. endophytica* KCTC 19886^T	*K. rhizosphaerae* KCTC 19366^T	*K. radiotolerans* DSM 14245^T
Growth at/in:									
5°C	+	+	−	−	−	−	+	+	+
45°C	−	+	+	−	−	+	+	−	−
pH 10.0	−	+	−	+	−	−	−	−	−
pH 5.0	+	+	−	−	−	−	+	−	+
6% NaCl	−	+	+	−	−	−	+	+	−
8% NaCl	−	+	−	−	−	−	+	−	−
Oxidase	+	+	+	−	−	+	+	+	−
DNA G + C content (mol%)	74.2	74.7	75.2	75.1	72.1	74.8	73.4	73.8	74.3
Polar lipids	DPG, PG, PI, PLs	DPG, PG, PGL, PI, PIM, PLs	DPG, PG PGL, PI, PIM, PLs	DPG, PG, PI, PIM, PL	DPG, PG, 2PL	DPG, PG, PI, PIM, PL	DPG, PG, PI, PIM, PL, GL, 3L	DPG, PG, PI, PLs	DPG, PG, PI, PLs
Characteristic sugars	Gal, Glu, Man	Ara, Gal, Glu, Man, Rib	Ara, Gal, Glu, Man, Rib	Ara, Gal, Glu, Man, Rib	Ara, Gal	Glu, Gal, Man, Rib	Ara, Gal	Ara, Gal, Xyl	Ara, Gal

*B12^T strain phenotypic characteristics were carried out during this study, whereas characteristics of other strains were reproduced from another study (Xu et al., 2017). Differential biochemical characteristics of the new species were not presented because strain B12^T would not grow using minimal media. To grow this slow growing strain, either yeast extract or glucose concentration of 0.1% is required. However, B12^T strain phenotypic characteristics can be deduced from the genome annotation and pathway analysis (see **Supplementary Table S1**).*

determines respiratory activity and the tetrazolium dye used to assay the respiratory activity might be potentially toxic to certain organisms. More research is needed for identifying appropriate growth promoting substances before defining the carbon substrate utilization profile of strain B12^T.

Chemotaxonomic Characterizations of Strain B12^T

Cellular fatty acids were analyzed by collecting biomass of a freshly grown culture at optimum growth conditions stated above. The cellular fatty acids were extracted, methylated, and analyzed by gas chromatography, as per the Sherlock Microbial Identification System (MIDI version 4.0) described previously (Muller et al., 1998; Pandey et al., 2002). A combined analysis by gas chromatography coupled to a mass spectrometer was used to confirm the identity of the fatty acids based on retention time and mass spectral data. The position of the double bond was confirmed by a derivatization to the corresponding dimethyl disulfide adduct (Moss and Lambert-Fair, 1989). Whole cell sugars and the peptidoglycan structure were determined according to Schumann (2011). The analyses of respiratory quinones and polar lipids were performed with 200 mg freeze-dried cells, which were previously incubated in glucose yeast extract malt extract medium (GYM) medium at 28°C and harvested in the stationary phase. The extraction of quinones was carried out using the two-stage method (Tindall, 1990a).

Polar lipids were separated by two-dimensional silica gel thin layer chromatography (Macherey-Nagel, 2007). The first direction was developed in chloroform:methanol:water (65:25:4, v/v/v), and the second in chloroform:methanol:acetic acid:water (80:12:15:4, v/v/v/v). Total lipid material was detected using molybdatophosphoric acid and specific functional groups by using spray reagents specific for the groups (Tindall, 1990b).

Phylogenetics of Strain B12^T

A loopful of purified B12^T culture was subjected to DNA extraction with the Quick DNA Fungal/Bacterial Miniprep kit (Zymo Research, Irvine, CA, United States), as per the manufacturer's protocol. The extracted DNA was eluted in 50 μL of molecular grade water and stored at −20°C until further analysis. The 16S rRNA gene (Suzuki et al., 2001; Checinska et al., 2015) was amplified using a universal primer set (Yamamoto and Harayama, 1995) as per previously established protocols. The amplified products were treated with Antarctic phosphatase and exonuclease (New England Biolabs, Ipswich, MA, United States) to remove 5′- and 3′-phosphates from unused dNTPs before sequencing. The resulting sequences were assembled using SeqMan Pro from the DNAStar Lasergene package (DNASTAR Inc., Madison, WI, United States). Bacterial sequences were compared with the EzTaxon-e and EzBioCloud databases (Kim et al., 2012; Yoon et al., 2017) and identified based on the closest percentage similarity to previously identified microbial type strains. An alignment of the B12^T 16S rRNA Sanger sequence and those collected from 50 members of class *Actinobacteria* found in public database was created using Clustal Omega (v. 1.2.1). A maximum-likelihood phylogeny

TABLE 2 | Cellular fatty acid composition of strain B12^T and the reference strains.

Fatty acid	Strain B12^T	*K. terrestris*	*K. aureolus*	*K. gypseus*	*K. aurantiacus*	*K. glutinatus*	*K. endophyticus*	*K. rhizosphaerae*	*K. radiotolerans*
$C_{12:0}$	0.7			1.1					
$C_{14:0}$ iso	0.8	2.2	2.2		1.9		3.4	1.3	16.5
$C_{14:0}$	1.9		1.6	1.5	1.5	2.4	1.6	2.0	
$C_{14:0}$ 2-OH							1.9	1.6	
$C_{15:1}$ anteiso A	2.3	3.8	2.2	6.9					5.9
Iso-$C_{15:0}$						5.4	1.8		
$C_{15:0}$ anteiso	63.0	70.8	74.7	58.4	72.8	60.6	76.8	73.8	70.2
$C_{16:0}$ N alcohol	0.4	1.6	1.2	3.2		1.3	1.1	2.0	1.0
$C_{16:0}$ Iso									1.1
$C_{16:0}$	3.7	2.6	3.7	6.6	4.1	5.3	1.8	3.9	0.8
$C_{16:0}$ 3OH	3.0								
$C_{17:0}$ 2OH	2.7	3.7	4.4	3.7	5.1	1.3	2.2	3.3	
$C_{17:0}$ 3OH		3.8	2.1	1.8	1.4	1.7			1.3
$C_{17:1}$ ω7c									0.7
$C_{18:1}$ ω9c	0.8								
$C_{18:0}$	2.8	1.7		7.0	4.4	4.2	1.7	4.1	
$C_{18:0}$ 3OH						1.3			
$C_{18:3}$ ω6c(6,9,12)		1.1							
$C_{19:0}$	0.7								
$C_{19:0}$ 10-methyl		1.2		1.0					
$C_{20:4}$ ω6,9,12,15c	16.2					3.3			
$C_{20:2}$ ω6,9c	1.2								
Summed feature 1					1.1				
Summed feature 4		2.7	2.5	5.3	2.1	5.3	2.4	2.5	
Summed feature 7		1.6	1.0	2.1	1.1	1.4	1.0	1.6	

Values are percentages of total fatty acids. The FAME profiles of the species other than B12^T strain were taken from Phillips et al. (2002), Li et al. (2015), and Xu et al. (2017).

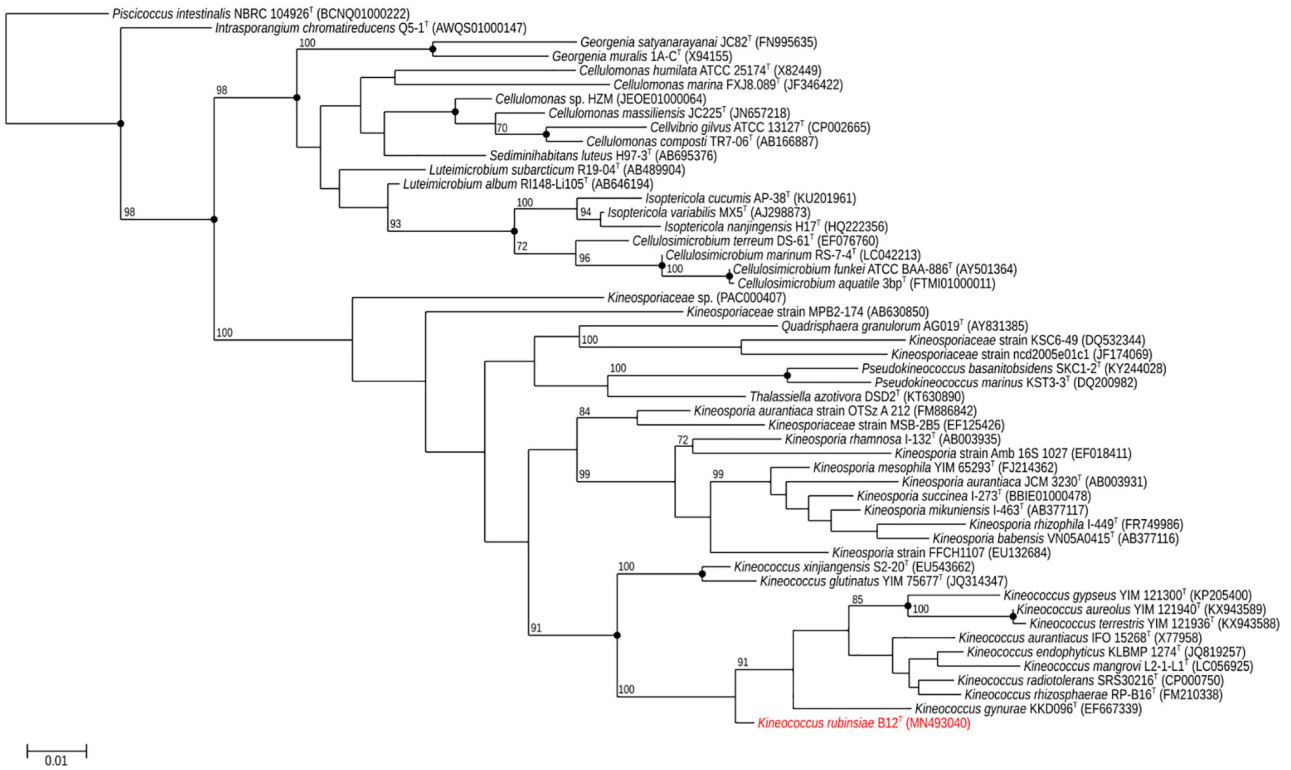

FIGURE 2 | Maximum-likelihood 16S rRNA phylogeny for *Kineococcus rubinsiae* B12^T and other members of class *Actinobacteria* reconstructed from 16S rRNA sequences found in public databases. The 16S rRNA sequence from *Piscicoccus intestinalis* NBRC 104926^T was used for the out-group. Bootstrapping values are included on internal nodes in the phylogeny, and represent the number of trials (out of 100) that included that particular branching pattern. Strain numbers followed by GenBank accession numbers are included for each sequence in the phylogeny. Black dots on internal nodes represent branch agreement between this maximum-likelihood phylogeny, a neighbor-joining phylogeny, and a maximum-parsimony phylogeny generated from the same sequence alignment.

based on this 16S rRNA gene alignment was generated using FastTree (v. 2.1.10), and bootstrap values were calculated using PHYLIP Seqboot (v. 3.696) and a script provided by the authors of FastTree, CompareToBootstrap.pl. Neighbor-joining and maximum-parsimony phylogenies based on the same 16S rRNA gene alignment were generated using PHYLIP (v. 3.696) and nodes with the same branching pattern in all three algorithms are highlighted in the phylogenetic tree (**Figure 2**).

Whole Genome Sequencing of Strain B12^T

The sequencing and analysis of the WGS were carried out as previously described (Singh et al., 2017) with minor modifications. In brief, sequencing libraries from isolated B12^T strain DNA was prepared using the Nextera DNA Library Preparation Kit from Illumina as per the manufacturer's instructions. Paired-end sequencing (100 bp) was performed on an Illumina HiSeq 2500 instrument. The data was filtered for high-quality vector, and adapter free reads using cutoff read length of 80 bp and quality score of 20 for genome assembly by using the NGS QC Toolkit v2.3 (Patel and Jain, 2012). The high-quality vector filtered reads were then assembled using the SPAdes genome assembler (Nurk et al., 2013) with default parameters. Subsequently, the assembled genome was annotated using Rapid Annotations using Subsystems Technology (RAST) (Aziz et al., 2008), and their quality was assessed using the Quast package (Gurevich et al., 2013). Furthermore, pairwise ANI was calculated using the established algorithm (Nurk et al., 2013) with EzTaxon-e (Kim et al., 2012). Pairwise AAI comparisons were calculated using an established method (Konstantinidis and Tiedje, 2005). Additionally, dDDH analysis was performed using the Genome-to-Genome Distance Calculator 2.0 (GGDC 2.0) (Meier-Kolthoff et al., 2013). A whole-genome alignment was generated using the CLC (v. 20.0.2) whole genome alignment plugin, and a phylogenetic tree was generated from the alignment using FastTree (v. 2.1.10).

Multi-Locus Sequence Analysis of Strain B12^T

Multi-locus sequence analysis (MLSA) based phylogenetic affiliation was performed as reported elsewhere to interpret the phylogenetic affiliation of the *Kineosporiaceae* members considered in this study (Gao and Gupta, 2005). Representative genomes of *Angustibacter, Kineococcus*, *Kineosporia, Pseudo kineococcus, Quadrisphaera*, and *Thalassiella* were used to determine the correct phylogenetic position of strain B12^T.

TABLE 3 | Differential characteristics of strain B12^T and related taxa.

Characteristic	Strain B12^T	*Kineococcus*	*Pseudokineococcus*	*Quadrisphaera*	*Kineosporia*	*Angustibacter*
Cell morphology	Cocci in pairs, tetrads and clusters	Cocci in tetrad arrangements	Cocci singly, in pairs or in clusters	Cocci in tetrad arrangements	Single spores borne at tips of substrate hyphae and spore clusters on a sporophore	Irregular rods and cocci
Motility	Motile	Motile	Motile	Non-motile	Motile	Non-motile
Cell-wall diamino acid(s)	*meso-Dap, A1 gamma, A31*	*meso*-A_2pm	*meso*-A_2pm	*meso*-A_2pm	*meso*- and LL-A_2pm	*meso*-A_2pm
Fatty acid type	S, I, A	S, I, A	S, I, A	S, I, A, U	S, U, M	S, I, A, U, M
Predominant menaquinone	MK-9(H_2)	MK-9(H_2)	MK-9(H_2)	MK-8(H_2)	MK-9(H4)	MK-9(H_4)
Polar lipids	DPG, PG, PI, PLs	DPG, PG, GL	PG, PI	DPG, PG, PI	PC, DPG, PI, PIM	DPG, PG, PI, PIM
Characteristic sugars	Gal, Glu, Man	Gal, Ara	Gal, Ara	ND	Gal, Glu, Man, Rib	Gal, Glu, Rib
DNA G + C content (mol%)	74.2	73–77	76.6	75	69–71	71

Data from Lee (2006) and Tamura et al. (2010) and this study; A_2pm, diaminopimelic acid; A, anteiso-methyl-branched; I, iso-methyl-branched; M, 9- 10-methyl-branched; S, straight-chain saturated; U, monounsaturated; DPG, diphosphatidylglycerol; GL, unknown glycolipid; PC, phosphatidylcholine; PG, phosphatidylglycerol; PI, phosphatidylinositol; PIM, phosphatidylinositol mannosides; PL, unknown phospholipids; PGL, unknown phosphoglycolipid; Ara, arabinose; Gal, galactose; Glu, glucose; Man, mannose; Rha, rhamnose; Rib, ribose; ND, no data.

Nakamurella multipartita DSM 44233^T was included in the phylogeny to serve as the out-group. Members of genus *Kineosporia* and *Thalassiella* were not selected for MLSA due to the absence of full-length genes in the publicly available database. Full-length DNA sequences for housekeeping genes *frr*, *gyrB*, *nusA*, *rplS*, *rpsB*, and *tsf* were retrieved from eight genomes (including strain B12^T), and an MLSA phylogenetic tree was generated. Gene sequences were individually aligned using Clustal Omega (v. 1.2.1), and concatenated together using a custom Perl script in the order listed. An approximate maximum-likelihood phylogenetic tree was generated from concatenated sequences using FastTree (v. 2.1.10), and bootstrap values were added to the tree using PHYLIP Seqboot (v. 3.696) and the CompareToBootstrap.pl script provided by the authors of FastTree.

RESULTS AND DISCUSSION

Phenotypic Characteristics

Cells of strain B12^T were non-spore forming, Gram-positive, motile, and strictly aerobic. Orange pigmented, round with rough edges and cluster forming colonies (0.6–1.0 mm diameter) were isolated after 72 h of incubation. The optimum growth conditions for the cells of strain B12^T were 32°C, 7 to 8 pH, and 0.5% NaCl concentration. Since strain B12^T is a slow grower, at least 3–5 days of incubation time was required to see the first visible growth when incubated at the optimum cultural conditions in PTYG medium. Since strain B12^T was isolated from chloramphenicol supplemented medium, the purified strain was re-streaked again in PTYG agar medium supplemented with 100 μg chloramphenicol, confirming that strain B12^T was resistant to chloramphenicol. The SEM images revealed that the cells of strain B12^T are coccoid in shape with 1.0 μm diameter (**Figure 1**). In general, cells of strain B12^T form in clusters due to extracellular polymeric substance (**Figure 1**), but individual motile cells were also observed.

Comparison of phenotypic characteristics of strain B12^T with other members of genus *Kineococcus* are provided in **Table 1**. Briefly, B12^T most closely matches characteristics of its closest neighbor, *K. radiotolerans*, except B12^T strain was oxidase positive. Since B12^T strain was not able to grow in a minimal media with less than 0.1% glucose or 0.1% yeast extract, phenotypic screening for carbon sources was not successful; instead, genome based phenotypic characterization was performed (**Supplementary Table S1**). All *Kineococcus* species, including the B12^T strain, could be differentiated from *K. radiotolerans* by the utilization of d-fructose and l-alanine as sole carbon and nitrogen sources, respectively. The absence of sucrose utilization by *K. endophytica* and *K. rhizosphaerae* might differentiate them from other members of the *Kineococcus* genera, including the B12^T strain. Likewise, d-xylitol assimilation and milk peptonization were observed in *K. glutinatus*, but not in other *Kineococcus* species. L-tryptophan was utilized by most *Kineococcus* species, including strain B12^T, except by *K. glutinatus* and *K. gypseus*. Gelatin was hydrolyzed by only *K. aureolus* and *K. rhizosphaerae*. *K. aurantiacus* and

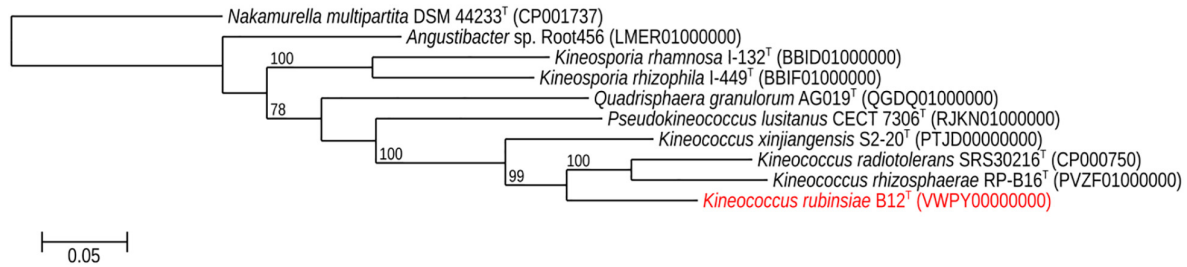

FIGURE 3 | Maximum-likelihood *gyrB* phylogeny for *Kineococcus rubinsiae* B12^T and other members of family *Kineosporiaceae* reconstructed from full-length *gyrB* sequences found in public databases. The *gyrB* sequence from *Nakamurella multipartita* DSM 4423^T was used for the out-group. Bootstrapping values are included on internal nodes in the phylogeny, and represent the number of trials (out of 100) that included that branching pattern. Strain numbers followed by GenBank accession numbers are included for each sequence in the phylogeny.

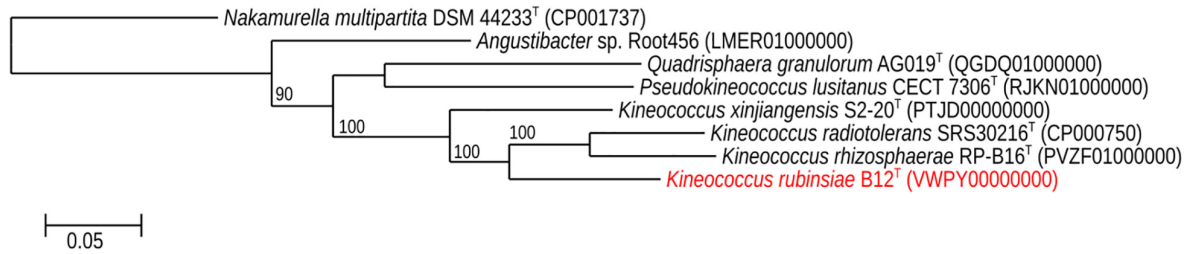

FIGURE 4 | Maximum-likelihood phylogeny for *Kineococcus rubinsiae* B12^T and other members of family Kineosporiaceae reconstructed from concatenated, full-length nucleotides sequences of genes *frr*, *gyrB*, *nusA*, *rplS*, *rpsB*, and *tsf*. The concatenated sequence from *Nakamurella multipartita* DSM 4423^T was used for the out-group. Bootstrapping values are included on internal nodes in the phylogeny, and represent the number of trials (out of 100) that included that branching pattern. Strain numbers followed by GenBank accession numbers are included for each sequence in the phylogeny.

K. radiotolerans were the only members of the genus, including B12^T, to lack the capability for nitrate reduction. In addition, strain B12^T had different characteristic cell wall sugars (Gal, Glu, and Man instead of Ara, and Gal) when compared to other members of the *Kineococcus* genus.

Chemotaxonomic Characteristics of Strain B12^T

FAME profiles of strain B12^T and related *Kineococcus* genera are shown in **Table 2**. The majority of the fatty acids produced by strain B12^T consisted of anteiso 15:0 (66.3%), similar to other members of *Kineococcus* genera (58–77%). Minor amounts of other fatty acids were detected including anteiso-$C_{15:1}$ ω10c (4.6%), iso-$C_{14:0}$ (1.0%), iso-$C_{15:0}$ (1.1%), and $C_{14:0}$ (1.6%). The peak assigned to $C_{14:0}$ 2OH by the MIDI system was identified as anteiso-$C_{15:0}$ dimethyl acetal (DMA) (2.9%) by GC-MS. Further two peaks that were assigned as $C_{20:4}$ (16.4%) and $C_{17:0}$ 2OH (2.2%) by the MIDI system, could not be confirmed to represent fatty acid methyl esters by GC-MS and have to be assigned as non-identified hydrophobic compounds. The presence of DMA derivatives in the sample appeared at first sight to be surprising as they are usually only detected in anaerobic bacteria but they show a clear diagnostic fragment at m/z 75 [(M-OCH_3)$^+$] and a typical [M–31]$^+$ fragment in the GC-MS analysis (Maulik et al., 1993; Alves et al., 2013). The presence of significant amounts of branched chain dimethylacetals has been detected in the aerobic taxa *Subtercola boreus* and *Subtercola frigoramans* (Männistö et al., 2000) that was also confirmed by GC-MS. The misidentification of dimethylacetals may be attributed to the fact that the identification of DMA derivatives by the MIDI system is only possible with the use of the ANAEROBE six reference database. This is in contrast to the misidentification of hydroxylated fatty acids as dimethylacetals in members of the *Selenomonadales* (Moore et al., 1994; Helander and Haikara, 1995; Strompl et al., 2000). It is possible that DMA derivatives may be present in other members of genera *Kineococcus* but have been misidentified as hydroxy fatty acids by the MIDI system. The presence of dimethylacetals in the hydrolyzed cellular fatty acid fraction is also indicative of plasmalogens in the polar lipids.

The differential characteristics of various genera of the family *Kineosporiaceae* based on chemotaxonomic profiles are shown in **Table 3**. Most of these chemotaxonomic characteristics are similar to the other members of genus *Kineococcus*. The major menaquinone of strain B12^T is MK-9(H2), with minor amounts MK-9 and MK-8(H2) detected (**Supplementary Figure S1**). Mycolic acids were not detected. The polar lipid analysis of strain B12^T showed the presence of diphosphatidylglycerol, phosphatidylglycerol, phosphatidylinositol, a monoacylated dimannosylphosphatdylinositol, several unidentified phospholipids, an unidentified glycolipid, and an unidentified lipid (**Supplementary Figure S2**). The polar lipids may contain plasmalogens. However, the novel strain B12^T showed major differences in its cell-wall diamino acid composition with the

TABLE 4 | Genome assembly characteristics and quality check.

Attribute	Value
# contigs	119
# contigs (≥0 bp)	119
# contigs (≥1000 bp)	119
# contigs (≥5000 bp)	106
# contigs (≥10000 bp)	90
# contigs (≥25000 bp)	61
# contigs (≥50000 bp)	32
Largest contig	392,027
Total length	4,880,137
Total length (≥0 bp)	4,880,137
Total length (≥1000 bp)	4,880,137
Total length (≥5000 bp)	4,823,868
Total length (≥10000 bp)	4,710,190
Total length (≥25000 bp)	4,229,606
Total length (≥50000 bp)	3,215,408
N50	66,629
N75	35,634
L50	19
L75	43
GC (%)	74.16
# N's	0
# N's per 100 kbp	0
Coverage	100×
Coding sequences	4872
Finishing quality	High-quality draft
Library used	Illumina paired-end
Assembler	Spades v3.2

members of genus *Kineococcus*. The cell wall of strain B12^T contain meso-diaminopimelic acid, A1 gamma, and A31, whereas *Kineococcus* species were reported to contain only meso-diaminopimelic acid (Lee, 2006; Tamura et al., 2010). Furthermore, whole cell wall sugars detected for strain B12^T are galactose, glucose, and mannose, while other *Kineococcus* species possess galactose, and arabinose. Except a few, there were no major cell-wall and polar-lipid characteristic differences between the *Kineococcus* and related genera as shown in **Table 3**.

Phylogenomic Characteristics of Strain B12^T

The16S rRNA gene sequences of ∼1,000 strains archived from the SAF were queried against the 16S rRNA gene retrieved from the WGS of strain B12^T. Phylogenetic analysis of the 16S rRNA gene (1,508 bp) indicated that it formed a distinct cluster with members of the genus *Kineococcus* within the radiation tolerant members of the family *Kineosporiaceae*. The 16S rRNA sequence of strain B12^T exhibited high sequence similarity with *K. radiotolerans* ATCC BAA 149 (97.9%). Low 16S rRNA gene sequence similarities (93.2–97.9%) with 28 members of the family *Kineosporiaceae* (**Figure 2**), including *Angustibacter* (93%), *Kineococcus* (96% to 97%), *Kineosporia* (94% to 95%), *Pseudokineococcus* (93%), *Quadrisphaera* (93%), and *Thalassiella* (94%), showed that strain B12^T belong to the members of this family. Similarly, when 1-kb *gyrB* sequences were retrieved from WGS of the strain B12^T and compared with available *gyrB* sequences (**Figure 3**) of other members of the family *Kineosporiaceae, K. radiotolerans* ATCC BAA 149 was the closest relative, but the low similarity percentage (85.6%) confirmed that strain B12^T is phylogenetically distinct from *K. radiotolerans*.

The MLSA phylogenetic tree with full-length DNA sequences for housekeeping genes *frr*, *gyrB*, *nusA*, *rplS*, *rpsB*, and *tsf* was generated and shown in **Figure 4**. Genomes belonging to *Angustibacter, Kineococcus*, *Pseudokineococcus*, and *Quadrisphaera* formed a family level clade but showed

TABLE 5 | ANI, AAI, and dDDH comparison between strain B12^T and phylogenetic neighbors from *Kineococcus*, *Angustibacter, Kineosporia, Nakamurella, Pseudokineococcus*, and *Quadrisphaera* genera.

Reference genomes compared with B12^T*	GenBank accession	ANI value (%)	AAI value (%)**	dDDH
Angustibacter sp. Root456	GCA_001426435.1	72.87	57	19.7
Kineococcus radiotolerans ATCC BAA 149^T	GCF_000017305.1	77.87	72	21.7
Kineococcus rhizosphaerae DSM 19711^T	GCA_003002055.1	76.89	71	21.4
Kineococcus xinjiangensis DSM 22857^T	GCA_002934625.1	75.03	66	20.3
Kineosporia aurantiaca JCM 3230^T	GCA_001315325.1	73.74		22.1
Kineosporia mikuniensis JCM 9961^T	GCA_001315725.1	75.05		24.4
Kineosporia rhamnosa JCM 9954^T	GCA_001315665.1	72.87		21.0
Kineosporia rhizophila JCM 9960^T	GCA_001315705.1	73.01		20.4
Kineosporia sp. A 224	GCA_002198655.1	73.27	54	19.7
Kineosporia sp. R H 3	GCA_002198675.1	73.21	54	19.5
Kineosporia succinea JCM 9957^T	GCA_001315685.1	75.05		21.4
Nakamurella multipartita DSM 44233^T	GCA_000024365.1	70.23	50	18.3
Pseudokineococcus lusitanus CECT 7306^T	GCA_003751265.1	72.73	58	19.0
Quadrisphaera granulorum DSM 44889^T	GCA_003149145.1	72.39	57	18.9
Quadrisphaera sp. DD2A	GCA_008041935.1	72.73	58	18.7
Quadrisphaera sp. DSM 44207	GCA_900101335.1	73.42	50	19.4

**Available genomes of nearest neighbors, based on 16S rRNA and gyrB gene similarities, were compared. **AAI comparisons not run for phylogenetic neighbors missing amino acid sequences in public databases.*

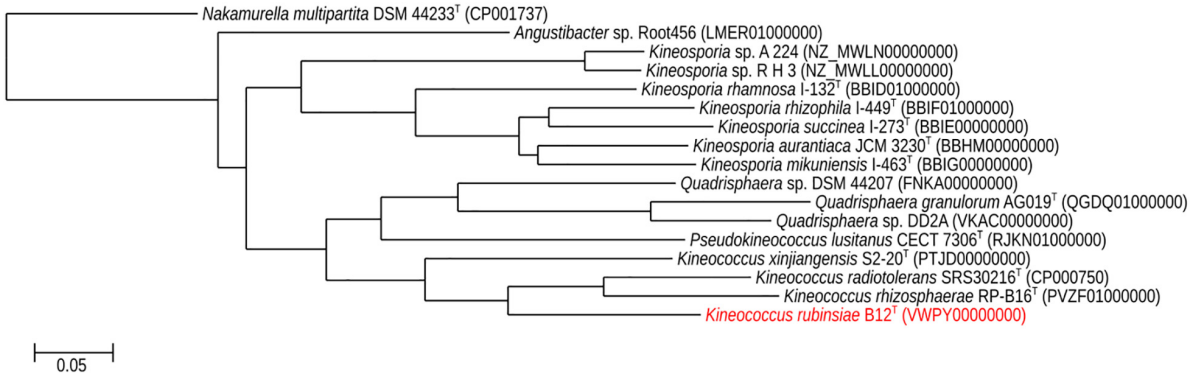

FIGURE 5 | Maximum-likelihood phylogeny for *Kineococcus rubinsiae* B12^T and other members of family Kineosporiaceae reconstructed from full-length genome sequences. The genome of *Nakamurella multipartita* DSM 4423^T was used for the out-group. Strain numbers followed by GenBank accession numbers are included for each sequence in the phylogeny.

inter-genus distinction among themselves. Similar to the *gyrB* phylogeny, the MLSA tree clearly showed strain B12^T far separated from the type strain of *K. radiotolerans*, but within the *Kineococcus* clade.

Genome Sequence Characteristics of Strain B12^T

The Illumina HiSeq 2500 platform yielded 5,435,202 paired-end reads from the sequencing of strain B12^T. Subsequent trimming and quality filtering of the paired-end sequences resulted in a total of 5,352,711 reads. The final assembled draft genome consists of 119 contigs comprising 4,880,137 bp with an N50 contig length of 66,629 bp. The largest contig assembled accounted for 392,027 bp. The final draft genome has a mean coverage of 100×, and G + C mol% of 74.16%, similar to other members of the *Kineococcus* genera. **Table 4** provides a complete summary of genome assembly statistics.

The ANI, AAI, and dDDH values of the strain B12^T were compared with the members of the *Kineococcus* genus (**Table 5**). The closest genomic neighbor to strain B12^T was *Kineococcus radiotolerans* GCF_000017305.1, which was evident from the ANI, AAI, and dDNA-DNA hybridization values (**Table 5**). The ANI values showed 72–78% similarity, and AAI values showed 66–72% with other members of the *Kineococcus* genera, demonstrating that B12^T is a novel species within this genus (<95% for ANI and AAI). The dDDH comparison of strain B12^T genome with *Kineococcus* genera showed only 20–22% similarity, demonstrating that B12^T is a novel species (<70%) that is distantly related to other members of genera *Kineococcus*.

A phylogenetic tree (**Figure 5**) was generated from a whole-genome alignment of 17 genomes, employing FastTree (v. 2.1.10) and PHYLIP Seqboot (v. 3.696). Even though MLSA clearly placed strain B12^T within the *Kineococcus* genus, whole genome phylogenetic analysis was carried out to validate these results using all available WGS of *Kineosporiaceae* reference genomes (n = 17) from GenBank. The whole-genome analyses confirmed and gave a strong validation to the MLST/*gyrB* data, confirming that strain B12^T is a novel member of a genus *Kineococcus*.

TABLE 6 | Number and proportion of genes associated with various functions in strain B12^T.

Functional description	Predicted genes*	Percentage (%)
Cofactors. vitamins. prosthetic groups. pigments	141	8.45
Cell Wall and capsule	24	1.44
Virulence. disease and defense	50	3.00
Potassium metabolism	7	0.42
Miscellaneous	49	2.94
Membrane transport	64	3.83
Iron acquisition and metabolism	4	0.24
RNA Metabolism	33	1.98
Nucleosides and nucleotides	95	5.69
Protein metabolism	207	12.40
Motility and chemotaxis	36	2.16
Regulation and cell signaling	22	1.32
Secondary metabolism	8	0.48
DNA metabolism	100	5.99
Fatty acids. lipids., and isoprenoids	79	4.73
Nitrogen metabolism	13	0.78
Dormancy and sporulation	2	0.12
Respiration	59	3.54
Stress response	48	2.88
Metabolism of aromatic compounds	26	1.56
Amino acids and derivatives	299	17.91
Sulfur metabolism	20	1.20
Phosphorus metabolism	37	2.22
Carbohydrates	246	14.74

**Total protein coding genes as per annotated genome.*

Functional Gene Properties of Strain B12^T

The strain B12^T genome was analyzed to understand its genetic makeup and its metabolic potential. RAST annotation detected

4,872 coding sequences in the B12^T WGS. A major fraction of the annotated genes was comprised of amino acids and derivatives (299), carbohydrate metabolism (246), protein metabolism (207), genes associated with cofactors, vitamins, prosthetic groups, pigments metabolism (141), and DNA (100) and RNA (33) metabolism (**Table 6**). Genes responsible for motility and chemotaxis (36), metabolism of aromatic compounds (26), and stress response (48) were also observed.

A close look at the annotated draft genome (**Supplementary Dataset 1**) predicts that strain B12^T may be highly resistant to osmotic, oxidative, and periplasmic stress, a prime requirement for survival in a SAF-like ultra-low biomass environment regularly cleaned with industrial reagents (La Duc et al., 2012). Strain B12^T also harbors the degradation pathway for geraniol, dichlorodiphenyltrichloroethane, chlorocyclohexane, chlorobenzene, benzoate, bisphenol, fluorobenzoate, and furfural, which may provide a pathway for survival from industrial-strength cleaning reagents. *Actinobacteria* have been known to produce antibiotics, and the WGS of the strain B12^T also revealed genetic pathways related to the production of these antibiotics. Pathway analysis predict the production of novobiocin, puromycin, tetracycline, penicillin, and cephalosporin from the draft genome. The production of antibiotics would be helpful in reducing competition for B12^T, and may provide an advantage in the ultralow biomass SAF environment. This makes the organism B12^T a potential candidate for industrial use.

Proposal for a New Species

Strain B12^T shares a maximum 97.9% 16S rRNA similarity with *K. radiotolerans,* its closest phylogenetic neighbor within the *Kineosporiaceae* family. These values fall below the 98.7% threshold as demonstrated to delineate bacterial species (Stackebrandt and Ebers, 2006). The phenotypic, phylogenetic, morphological, and genomic characteristics provide evidence to differentiate strain B12^T from the members of family *Kineosporiaceae*. Similarly, the ANI, AAI, and dDDH values were lower than the threshold, further corroborating the findings to classify strain B12^T as a new species within the family *Kineosporiaceae*. Based on polytaxonomic and WGS analyses, a novel species, *K. rubinsiae* sp. nov., is proposed, with strain B12^T (=FJII-L1-CM-PAB2^T = DSM 110506^T) being the type strain of the species *K. rubinsiae*.

Description of *Kineococcus rubinsiae* sp. nov.

Kineococcus rubinsiae sp. nov. (ru.bin.si.ae. N.L. fem. n. *rubinsiae* named in honor of a NASA astronaut (Kate Rubins) who is a molecular microbiologist and the first person to perform DNA sequencing in space).

Cells are Gram-positive cocci that are 0.6–1.0 mm in diameter and occur in tetrads or clusters due to extracellular polysaccharide secretion. Colonies are circular, convex with a diameter of approximately 0.6–1.0 mm, and orange in color after 72 h of incubation on PDA or PTYG medium at 28 to 32°C. A slow growing aerobic bacterium with an optimum temperature of 32°C and incubation period of 3–5 days. Bacteria can exhibit motility after 72 h of growth in a liquid medium. Cells exhibit growth in a cluster formation. The pH tolerance is between 6.0 and 9.0, and shows positive growth at 0–5% NaCl. Cells will not utilize any of the carbon substrates in the BioLog system. Cells are resistant to chloramphenicol and multiply in the PDA supplemented with 100 μg/mL. The predominant fatty acid is anteiso-$C_{15:0}$. Whole cell sugars were galactose, glucose and mannose with minor amounts of arabinose and ribose. The major menaquinone is MK-9(H2) (**Supplementary Figure S1**). Polar lipids comprise diphosphatidylglycerol, phosphatidylglycerol, phosphatidyl inositol, an unidentified phospholipid, an unidentified glycolipid and an unidentified phosphoglycolipid (**Supplementary Figure S2**). The DNA G + C content of the type strain is 74.16 mol%.

The type strain, B12^T (=FJII-L1-CM-PAB2^T; NRRL B-65556^T = DSM 110506^T), was isolated from the East side of the JPL-SAF cleanroom where crew enter the room. WGS (VWPY00000000) and 16S rRNA Sanger sequence (MN493040) are available in NCBI GenBank.

Nucleotide Sequence Deposition

The draft genome sequence of type strain B12^T was deposited in NCBI GenBank. The version described in this paper is the first version, and the accession number for the *K. rubinsiae* strain B12^T is VWPY00000000. The Sanger sequence of the 16S rRNA gene is deposited in GenBank under accession number MN493040.

DATA AVAILABILITY STATEMENT

The datasets generated for this study can be found in the NCBI-VWPY00000000.

AUTHOR CONTRIBUTIONS

KV, SM, and NS conceived and designed the experiments. SM, NS, JW, and CP performed the experiments. NS analyzed the genomic data analysis inclusive of *de novo* assemblies and verification, scaffold quality assessment, and annotation and generated all the whole genome and protein level alignment for positional description of organism in the tree of life. JW independently verified the genome assembly, generated alignments for all gene trees in the manuscript, and manually curated the tree images. SM isolated the type strain, carried out the phenotypic assays, FAME, and biochemical characterization. CP conducted SEM related tests and imaged the microscopic characteristics of the strain. KV compiled the contribution of write-ups from all authors associated with phenotype (SM), genotype and table generation (NS), MLSA and figure generation (JW), as well as SEM images (CP). BT, SV, RP, and MN-S conducted the chemotaxonomic analysis. All authors read and approved the final manuscript.

FUNDING

This research was funded by a NASA Research Announcement Research Opportunities in Space and Earth Sciences (NRA ROSES 15-PPR15-0001) grant.

ACKNOWLEDGMENTS

The research described in this publication was carried out in part at the Jet Propulsion Laboratory, California Institute of Technology, under a contract with the National Aeronautics and Space Administration. Cynthia Ly and Moogega Stricker from Biotechnology and Planetary Protection Group are acknowledged for helping to collect samples from JPL-SAF. We thank Ronald Ruiz from JPL for his expertise with sputter coating samples for SEM analysis. We gratefully acknowledge the critical support and infrastructure provided for this work by The Kavli Nanoscience Institute at Caltech. Anja Frühling, Gesa Martens, Anika Wasner, and Gabriele Pötter are acknowledged for helping to perform chemotaxonomic analyses.

SUPPLEMENTARY MATERIAL

The Supplementary Material for this article can be found online at: https://www.frontiersin.org/articles/10.3389/fmicb.2020.01957/full#supplementary-material

FIGURE S1 | Quinone determination of *Kineococcus rubinsiae* B12^T.

FIGURE S2 | Lipid profiles of *Kineococcus rubinsiae* B12^T.

REFERENCES

Alves, S. P., Santos-Silva, J., Cabrita, A. R. J., Fonseca, A. J. M., and Bessa, R. J. B. (2013). Detailed dimethylacetal and fatty acid composition of rumen content from lambs fed lucerne or concentrate supplemented with soybean oil. *PLoS One* 8:e58386. doi: 10.1371/journal.pone.0058386

Aziz, R. K., Bartels, D., Best, A. A., Dejongh, M., Disz, T., Edwards, R. A., et al. (2008). The RAST server: rapid annotations using subsystems technology. *BMC Genomics* 9:75. doi: 10.1186/1471-2164-9-75

Checinska, A., Probst, A. J., Vaishampayan, P., White, J. R., Kumar, D., Stepanov, V. G., et al. (2015). Microbiomes of the dust particles collected from the international space station and spacecraft assembly facilities. *Microbiome* 3:50.

Chen, M., Xu, P., Zeng, G., Yang, C., Huang, D., and Zhang, J. (2015). Bioremediation of soils contaminated with polycyclic aromatic hydrocarbons, petroleum, pesticides, chlorophenols and heavy metals by composting: applications, microbes and future research needs. *Biotechnol. Adv.* 33, 745–755. doi: 10.1016/j.biotechadv.2015.05.003

Chun, J., Oren, A., Ventosa, A., Christensen, H., Arahal, D. R., Da Costa, M. S., et al. (2018). Proposed minimal standards for the use of genome data for the taxonomy of prokaryotes. *Int. J. Syst. Evol. Microbiol.* 68, 461–466. doi: 10.1099/ijsem.0.002516

Cockell, C. S., Kelly, L. C., and Marteinsson, V. (2013). Actinobacteria—an ancient phylum active in volcanic rock weathering. *Geomicrobiol. J.* 30, 706–720. doi: 10.1080/01490451.2012.758196

Diogo, A., Verissimo, A., Nobre, M. F., and Da Costa, M. S. (1999). Usefulness of fatty acid composition for differentiation of *Legionella* species. *J. Clin. Microbiol.* 37, 2248–2254. doi: 10.1128/jcm.37.7.2248-2254.1999

Gao, B., and Gupta, R. S. (2005). Conserved indels in protein sequences that are characteristic of the phylum *Actinobacteria*. *Int. J. Syst. Evol. Microbiol.* 55, 2401–2412. doi: 10.1099/ijs.0.63785-0

Gurevich, A., Saveliev, V., Vyahhi, N., and Tesler, G. (2013). QUAST: quality assessment tool for genome assemblies. *Bioinformatics* 29, 1072–1075. doi: 10.1093/bioinformatics/btt086

Helander, I. M., and Haikara, A. (1995). Cellular fatty acyl and alkenyl residues in *Megasphaera* and *Pectinatus* species: contrasting profiles and detection of beer spoilage. *Microbiology* 141, 1131–1137. doi: 10.1099/13500872-141-5-1131

Helgason, E., Økstad, O. A., Caugant, D. A., Johansen, H. A., Fouet, A., Mock, M., et al. (2000). *Bacillus anthracis*, *Bacillus cereus*, and *Bacillus thuringiensis*—one species on the basis of genetic evidence. *Appl. Environ. Microbiol.* 66, 2627–2630. doi: 10.1128/aem.66.6.2627-2630.2000

Jiang, X., Ellabaan, M. M. H., Charusanti, P., Munck, C., Blin, K., Tong, Y., et al. (2017). Dissemination of antibiotic resistance genes from antibiotic producers to pathogens. *Nat. Commun.* 8:15784.

Jones, D. M. (1981). Manual of methods for general bacteriology. *J. Clin. Pathol.* 34, 1069–1069. doi: 10.1136/jcp.34.9.1069-c

Jurado, V., Laiz, L., Ortiz-Martinez, A., Groth, I., and Saiz-Jimenez, C. (2011). *Pseudokineococcus lusitanus* gen. nov., sp. nov., and reclassification of *Kineococcus marinus* lee 2006 as *Pseudokineococcus marinus* comb. nov. *Int. J. Syst. Evol. Microbiol.* 61, 2515–2519. doi: 10.1099/ijs.0.026195-0

Kim, O. S., Cho, Y. J., Lee, K., Yoon, S. H., Kim, M., Na, H., et al. (2012). Introducing EzTaxon-e: a prokaryotic 16S rRNA gene sequence database with phylotypes that represent uncultured species. *Int. J. Syst. Evol. Microbiol.* 62, 716–721. doi: 10.1099/ijs.0.038075-0

Ko, D. H., and Lee, S. D. (2017). *Angustibacter speluncae* sp. nov., isolated from a lava cave stalactite. *Int. J. Syst. Evol. Microbiol.* 67, 3283–3288. doi: 10.1099/ijsem.0.002108

Konstantinidis, K. T., Ramette, A., and Tiedje, J. M. (2006). The bacterial species definition in the genomic era. *Philos. Trans. R. Soc. Lond. B Biol. Sci.* 361, 1929–1940. doi: 10.1098/rstb.2006.1920

Konstantinidis, K. T., Rosselló-Móra, R., and Amann, R. (2017). Uncultivated microbes in need of their own taxonomy. *ISME J.* 11, 2399–2406. doi: 10.1038/ismej.2017.113

Konstantinidis, K. T., and Tiedje, J. M. (2005). Towards a Genome-Based Taxonomy for Prokaryotes. *J. Bacteriol.* 187, 6258–6264. doi: 10.1128/jb.187.18.6258-6264.2005

Kudo, T., Matsushima, K., Itoh, T., Sasaki, J., and Suzuki, K. (1998). Description of four new species of the genus *Kineosporia*: *Kineosporia succinea* sp. nov., *Kineosporia rhizophila* sp. nov., *Kineosporia mikuniensis* sp. nov. and *Kineosporia rhamnosa* sp. nov., isolated from plant samples, and amended description of the genus *Kineosporia*. *Int. J. Syst. Bacteriol.* 48(Pt 4), 1245–1255. doi: 10.1099/00207713-48-4-1245

Kwan, K., Cooper, M., La Duc, M. T., Vaishampayan, P., Stam, C., Benardini, J. N., et al. (2011). Evaluation of procedures for the collection, processing, and analysis of biomolecules from low-biomass surfaces. *Appl. Environ. Microbiol.* 77, 2943–2953. doi: 10.1128/aem.02978-10

La Duc, M. T., Satomi, M., Agata, N., and Venkateswaran, K. (2004). gyrB as a phylogenetic discriminator for members of the *Bacillus anthracis-cereus-thuringiensis* group. *J. Microbiol. Methods* 56, 383–394. doi: 10.1016/j.mimet.2003.11.004

La Duc, M. T., Vaishampayan, P., Nilsson, H. R., Torok, T., and Venkateswaran, K. (2012). Pyrosequencing-derived bacterial, archaeal, and fungal diversity of spacecraft hardware destined for Mars. *Appl. Environ. Microbiol.* 78, 5912–5922. doi: 10.1128/aem.01435-12

Lee, D., Jang, J. H., Cha, S., and Seo, T. (2016). *Thalassiella azotovora* gen. nov., sp. nov., a new member of the Family kineosporiaceae isolated from sea water in South Korea. Current Microbiology 73, 676–683. doi: 10.1007/s00284-016-1112-y

Lee, S. D. (2006). Kineococcus marinus sp. nov., isolated from marine sediment of the coast of Jeju, Korea. *Int. J. Syst. Evol. Microbiol.* 56, 1279–1283. doi: 10.1099/ijs.0.64128-0

Li, Q., Li, G., Chen, X., Xu, F., Li, Y., Xu, L., et al. (2015). *Kineococcus gypseus* sp. nov., isolated from saline sediment. *Int. J. Syst. Evol. Microbiol.* 65, 3703–3708. doi: 10.1099/ijsem.0.000478

Macherey-Nagel (2007). *Thin Layer Chromatography of Ether Lipids. Art. No. 818 135*. Washington D.C: American Society for Microbiology.

Männistö, M. K., Schumann, P., Rainey, F. A., Kämpfer, P., Tsitko, I., Tiirola, M. A., et al. (2000). *Subtercola boreus* gen. nov., sp. nov. and *Subtercola frigoramans* sp. nov., two new psychrophilic actinobacteria isolated from boreal groundwater. *Int. J. Syst. Evol. Microbiol.* 50, 1731–1739. doi: 10.1099/00207713-50-5-1731

Maszenan, A. M., Tay, J.-H., Schumann, P., Jiang, H.-L., and Tay, S. T.-L. (2005). *Quadrisphaera granulorum* gen. nov., sp. nov., a Gram-positive polyphosphate-accumulating coccus in tetrads or aggregates isolated from aerobic granules. *Int. J. Syst. Evol. Microbiol.* 55, 1771–1777. doi: 10.1099/ijs.0.63583-0

Maulik, N., Bagchi, D., Jones, R., Cordis, G., and Das, D. K. (1993). Identification and characterization of plasmalogen fatty acids in swine heart. *J. Pharm. Biomed. Anal.* 11, 1151–1156. doi: 10.1016/0731-7085(93)80097-k

Meier-Kolthoff, J. P., Auch, A. F., Klenk, H. P., and Goker, M. (2013). Genome sequence-based species delimitation with confidence intervals and improved distance functions. *BMC Bioinformatics* 14:60. doi: 10.1186/1471-2105-14-60

Mohammadipanah, F., and Wink, J. (2016). *Actinobacteria* from arid and desert habitats: diversity and biological activity. *Front. Microbiol.* 6:1541. doi: 10.3389/fmicb.2015.01541

Moore, L. V., Bourne, D. M., and Moore, W. E. (1994). Comparative distribution and taxonomic value of cellular fatty acids in thirty-three genera of anaerobic gram-negative bacilli. *Int. J. Syst. Bacteriol.* 44, 338–347. doi: 10.1099/00207713-44-2-338

Moss, C. W., and Lambert-Fair, M. A. (1989). Location of double bonds in monounsaturated fatty acids of *Campylobacter cryaerophila* with dimethyl disulfide derivatives and combined gas chromatography-mass spectrometry. *J. Clin. Microbiol.* 27, 1467–1470. doi: 10.1128/jcm.27.7.1467-1470.1989

Muller, K., Schmid, E. N., and Kroppenstedt, R. M. (1998). Improved identification of mycobacteria by using the microbial identification system in combination with additional trimethylsulfonium hydroxide pyrolysis. *J. Clin. Microbiol.* 36, 2477–2480. doi: 10.1128/jcm.36.9.2477-2480.1998

Nurk, S., Bankevich, A., Antipov, D., Gurevich, A., Korobeynikov, A., Lapidus, A., et al. (2013). "Assembling genomes and mini-metagenomes from highly chimeric reads," in *Research in Computational Molecular Biology*, eds M. Deng, R. Jiang, F. Sun, and X. Zhang (Berlin: Springer), 158–170. doi: 10.1007/978-3-642-37195-0_13

Palaniyandi, S. A., Yang, S. H., Zhang, L., and Suh, J. W. (2013). Effects of actinobacteria on plant disease suppression and growth promotion. *Appl. Microbiol. Biotechnol.* 97, 9621–9636. doi: 10.1007/s00253-013-5206-1

Pandey, K. K., Mayilraj, S., and Chakrabarti, T. (2002). *Pseudomonas indica* sp. nov., a novel butane-utilizing species. *Int. J. Syst. Evol. Microbiol.* 52, 1559–1567. doi: 10.1099/ijs.0.01943-0

Patel, R. K., and Jain, M. (2012). NGS QC toolkit: a toolkit for quality control of next generation sequencing data. *PLoS One* 7:e30619. doi: 10.1371/journal.pone.0030619

Phillips, R. W., Wiegel, J., Berry, C. J., Fliermans, C., Peacock, A. D., White, D. C., et al. (2002). *Kineococcus radiotolerans* sp. nov., a radiation-resistant, gram-positive bacterium. *Int. J. Syst. Evol. Microbiol.* 52, 933–938. doi: 10.1099/ijs.0.02029-0

Satomi, M., La Duc, M. T., and Venkateswaran, K. (2006). *Bacillus safensis* sp. nov., isolated from spacecraft and assembly-facility surfaces. *Int. J. Syst. Evol. Microbiol.* 56, 1735–1740. doi: 10.1099/ijs.0.64189-0

Schumann, P. (2011). "Peptidoglycan structure," in *Methods in Microbiology*, eds R. Fred and O. Aharon (Cambridge, MA: Academic Press), 101–129.

Seuylemezian, A., Aronson, H. S., Tan, J., Lin, M., Schubert, W., and Vaishampayan, P. (2018). Development of a Custom MALDI-TOF MS database for species-level identification of bacterial isolates collected from spacecraft and associated surfaces. *Front. Microbiol.* 9:780. doi: 10.3389/fmicb.2018.00780

Singh, N. K., Carlson, C., Sani, R. K., and Venkateswaran, K. (2017). Draft genome sequences of thermophiles isolated from yates shaft, a deep-subsurface environment. *Genome Announc.* 5:e00405-17.

Singh, N. K., Wood, J. M., Mhatre, S. S., and Venkateswaran, K. (2019). Metagenome to phenome approach enables isolation and genomics characterization of *Kalamiella piersonii* gen. nov., sp. nov. from the International Space Station. *Appl. Microbiol. Biotechnol.* 103, 4483–4497. doi: 10.1007/s00253-019-09813-z

Skerman, V. B. D. (1960). A guide to the identification of the genera of bacteria. *Acad. Med.* 35:92.

Stackebrandt, E., and Ebers, J. (2006). Taxonomic parameters revisited: tarnished gold standards. *Microbiol. Today* 8, 6–9.

Strompl, C., Tindall, B. J., Lunsdorf, H., Wong, T. Y., Moore, E. R., and Hippe, H. (2000). Reclassification of *Clostridium quercicolum* as *Dendrosporobacter quercicolus* gen. nov., comb. nov. *Int. J. Syst. Evol. Microbiol.* 50(Pt 1), 101–106. doi: 10.1099/00207713-50-1-101

Suzuki, M. T., Beja, O., Taylor, L. T., and Delong, E. F. (2001). Phylogenetic analysis of ribosomal RNA operons from uncultivated coastal marine bacterioplankton. *Environ. Microbiol.* 3, 323–331. doi: 10.1046/j.1462-2920.2001.00198.x

Tamura, T., Ishida, Y., Otoguro, M., Yamamura, H., Hayakawa, M., and Suzuki, K. (2010). *Angustibacter luteus* gen. nov., sp. nov., isolated from subarctic forest soil. *Int. J. Syst. Evol. Microbiol.* 60, 2441–2445. doi: 10.1099/ijs.0.019448-0

Tindall, B. J. (1990a). A comparative study of the lipid composition of *Halobacterium saccharovorum* from various sources. *Syst. Appl. Microbiol.* 13, 128–130. doi: 10.1016/s0723-2020(11)80158-x

Tindall, B. J. (1990b). Lipid composition of *Halobacterium lacusprofundi*. *FEMS Microbiol. Lett.* 66, 199–202. doi: 10.1111/j.1574-6968.1990.tb03996.x

Varghese, N. J., Mukherjee, S., Ivanova, N., Konstantinidis, K. T., Mavrommatis, K., Kyrpides, N. C., et al. (2015). Microbial species delineation using whole genome sequences. *Nucleic Acids Res.* 43, 6761–6771. doi: 10.1093/nar/gkv657

Venkateswaran, K., Singh, N. K., Checinska Sielaff, A., Pope, R. K., Bergman, N. H., Van Tongeren, S. P., et al. (2017). Non-toxin-producing *Bacillus cereus* strains belonging to the *B. anthracis* clade isolated from the International space station. *mSystems* 2:e00021-17.

Xu, F.-J., Li, Q.-Y., Li, G.-D., Chen, X., Jiang, Y., and Jiang, C.-L. (2017). *Kineococcus terrestris* sp. nov. and Kineococcus aureolus sp. nov., isolated from saline sediment. *Int. J. Syst. Evol. Microbiol.* 67, 4801–4807. doi: 10.1099/ijsem.0.002380

Xu, P., Li, W. J., Tang, S. K., Zhang, Y. Q., Chen, G. Z., Chen, H. H., et al. (2005). *Naxibacter alkalitolerans* gen. nov., sp. nov., a novel member of the family 'Oxalobacteraceae' isolated from China. *Int. J. Syst. Evol. Microbiol.* 55, 1149–1153. doi: 10.1099/ijs.0.63407-0

Yamamoto, S., and Harayama, S. (1995). PCR amplification and direct sequencing of gyrB genes with universal primers and their application to the detection and taxonomic analysis of *Pseudomonas* putida strains. *Appl. Environ. Microbiol.* 61, 1104–1109. doi: 10.1128/aem.61.3.1104-1109.1995

Yoon, S. H., Ha, S. M., Kwon, S., Lim, J., Kim, Y., Seo, H., et al. (2017). Introducing EzBioCloud: a taxonomically united database of 16S rRNA gene sequences and whole-genome assemblies. *Int. J. Syst. Evol. Microbiol.* 67, 1613–1617. doi: 10.1099/ijsem.0.001755

Zenova, G. M., Manucharova, N. A., and Zvyagintsev, D. G. (2011). Extremophilic and extremotolerant actinomycetes in different soil types. *Eurasian Soil Sci.* 44, 417–436. doi: 10.1134/s1064229311040132

Conflict of Interest: The authors declare that the research was conducted in the absence of any commercial or financial relationships that could be construed as a potential conflict of interest.

frontiers in Microbiology

ORIGINAL RESEARCH
published: 21 August 2020
doi: 10.3389/fmicb.2020.01975

Constant Light Exposure Alters Gut Microbiota and Promotes the Progression of Steatohepatitis in High Fat Diet Rats

*Lin Wei[1], Fangzhi Yue[1], Lin Xing[1], Shanyu Wu[1], Ying Shi[1], Jinchen Li[2], Xingwei Xiang[1], Sin Man Lam[3], Guanghou Shui[3], Ryan Russell[4] and Dongmei Zhang[1]**

[1] Department of Endocrinology, Xiangya Hospital, Central South University, Changsha, China, [2] Department of Geriatrics, National Clinical Research Center for Geriatric Disorders, Xiangya Hospital, Central South University, Changsha, China, [3] State Key Laboratory of Molecular Developmental Biology, Institute of Genetics and Developmental Biology, Chinese Academy of Sciences, Beijing, China, [4] Cardiomatabolic Exercise Lab Director, Department of Health and Human Performance, College of Health Professions, University of Texas Rio Grande Valley, Brownsville, TX, United States

Background: Non-alcoholic fatty liver disease (NAFLD) poses a significant health concern worldwide. With the progression of urbanization, light pollution may be a previously unrecognized risk factor for NAFLD/NASH development. However, the role of light pollution on NAFLD is insufficiently understood, and the underlying mechanism remains unclear. Interestingly, recent studies indicate the gut microbiota affects NAFLD/NASH development. Therefore, the present study explored effects of constant light exposure on NAFLD and its related microbiotic mechanisms.

Materials and Methods: Twenty-eight SD male rats were divided into four groups (n = 7 each): rats fed a normal chow diet, and exposed to standard light-dark cycle (ND-LD); rats fed a normal chow diet, and exposed to constant light (ND-LL); rats fed a high fat diet, and exposed to standard light-dark cycle (HFD-LD); and rats on a high fat diet, and exposed to constant light (HFD-LL). Body weight, hepatic pathophysiology, gut microbiota, and short/medium chain fatty acids in colon contents, serum lipopolysaccharide (LPS), and liver LPS-binding protein (LBP) mRNA expression were documented post intervention and compared among groups.

Result: In normal chow fed groups, rats exposed to constant light displayed glucose abnormalities and dyslipidemia. In HFD-fed rats, constant light exposure exacerbated glucose abnormalities, insulin resistance, inflammation, and liver steatohepatitis. Constant light exposure altered composition of gut microbiota in both normal chow and HFD fed rats. Compared with HFD-LD group, HFD-LL rats displayed less *Butyricicoccus, Clostridium,* and *Turicibacter*, butyrate levels in colon contents, decreased colon expression of occludin-1 and zonula occluden−1 (ZO-1), and increased serum LPS and liver LBP mRNA expression.

Conclusion: Constant light exposure impacts gut microbiota and its metabolic products, impairs gut barrier function and gut-liver axis, promotes NAFLD/NASH progression in HFD rats.

Keywords: non-alcoholic fatty liver disease, light pollution, gut microbiota, short chain fatty acids, gut-liver axis

OPEN ACCESS

Edited by:
Ralf Moeller,
Helmholtz Association of German Research Centers (HZ), Germany

Reviewed by:
Ren-You Gan,
Institute of Urban Agriculture (CAAS), China
Tarique Hussain,
Nuclear Institute for Agriculture and Biology, Pakistan

****Correspondence:***
Dongmei Zhang
drdmzhang@csu.edu.cn

Specialty section:
This article was submitted to Microbial Physiology and Metabolism, a section of the journal Frontiers in Microbiology

Received: *28 December 2019*
Accepted: *27 July 2020*
Published: *21 August 2020*

Citation:
Wei L, Yue F, Xing L, Wu S, Shi Y, Li J, Xiang X, Lam SM, Shui G, Russell R and Zhang D (2020) Constant Light Exposure Alters Gut Microbiota and Promotes the Progression of Steatohepatitis in High Fat Diet Rats. Front. Microbiol. 11:1975. doi: 10.3389/fmicb.2020.01975

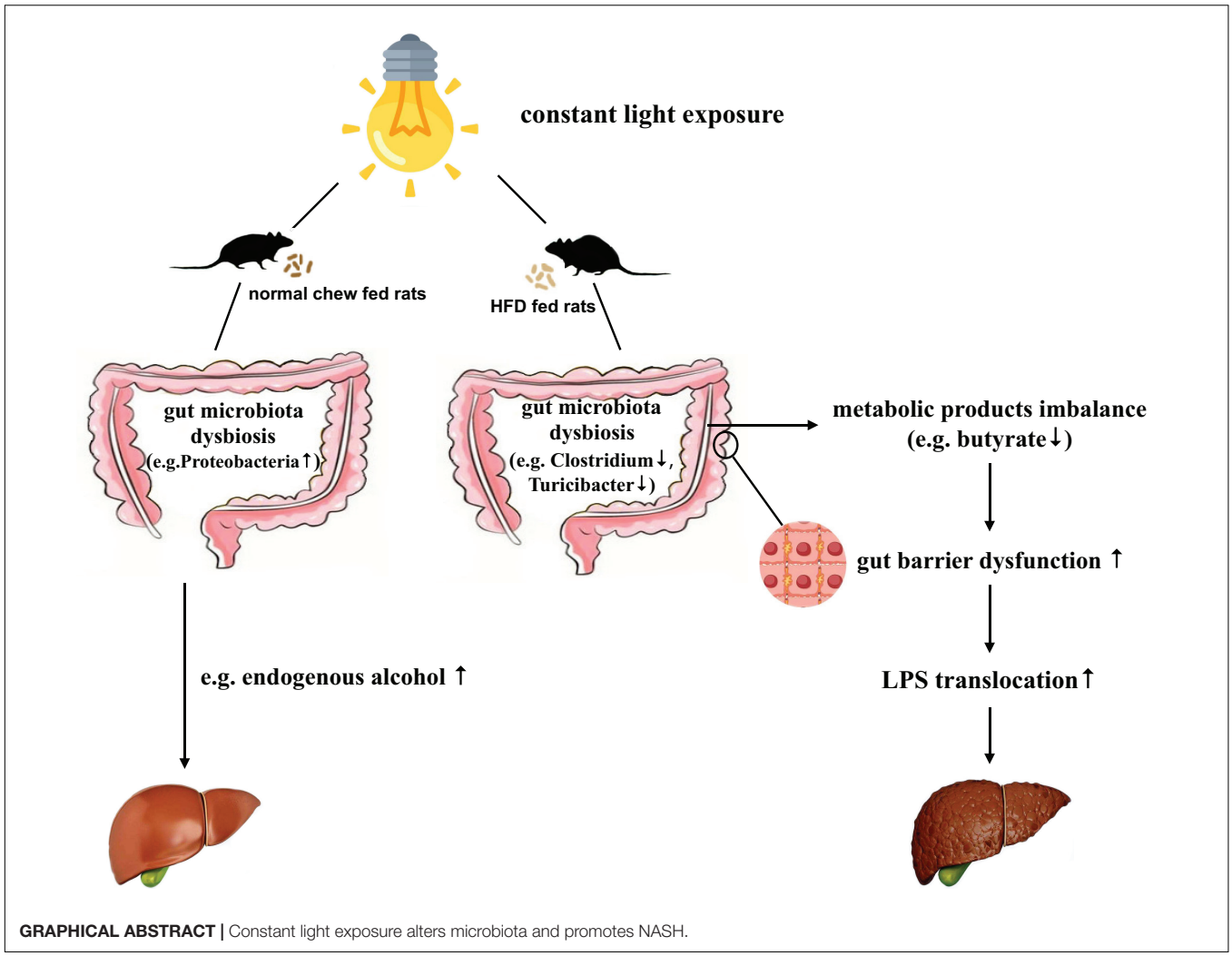

GRAPHICAL ABSTRACT | Constant light exposure alters microbiota and promotes NASH.

HIGHLIGHTS

- Constant light exposure promotes NAFLD/NASH progression in HFD rats.
- Constant light exposure alters composition of gut microbiota.
- Constant light exposure impairs gut barrier function and gut-liver axis in HFD rats.

Abbreviations: ALT, alanine aminotransferase; AST, aspartate aminotransferase; AUC, area under the curve; GEE, generalized estimated equation; HDL-C, high-density lipoprotein cholesterol; HFD, high fat diet; IHC, immunohistochemistry; IL-6, interleukin-6; IPGTT, intraperitoneal glucose tolerance test; ITT, insulin tolerance test; KEGG, Kyoto Encyclopedia of Genes and Genomes; LBP, LPS-binding protein; LDA, linear discriminant analysis; LDL-C, low-density lipoprotein cholesterol; LEfSe, LDA effect size; LPS, lipopolysaccharide; MCFAs, medium chain fatty acids; NAFLD, non-alcoholic fatty liver disease; NAS, NAFLD activity score; NASH, non-alcoholic steatohepatitis; ND, normal chow diet; OTUs, operational taxonomic units; PCA, principal component analysis; PICRUSt, phylogenetic investigation of communities by reconstruction of unobserved states; RT-PCR, reverse transcription polymerase chain reaction; SCFAs, short chain fatty acids; SCN, suprachiasmatic nuclei; TC, total cholesterol; TG, triglyceride; TNF-α, tumor necrosis factor-alpha; ZO-1, zonula occluden−1.

INTRODUCTION

Non-alcoholic fatty liver disease (NAFLD) is defined as the presence of hepatic steatosis in at least 5% of hepatocytes which is not attributed to alcohol consumption or other secondary causes of steatosis (Cairns and Peters, 1983). Although steatosis has long been considered as a benign liver disease, it may progress into a more aggressive form of non-alcoholic steatohepatitis (NASH), which in turn may lead to cirrhosis and, sometimes, to hepatocellular carcinoma (Xanthakos et al., 2006). NAFLD is becoming the most common chronic liver disease worldwide, affecting about 20–30% of the general population (Sheka et al., 2020).

Although fatty liver and steatohepatitis most commonly stem from overnutrition and lack of exercise, additional mediators, such as environmental factors, have recently been postulated (Eslam et al., 2018). One novel environmental risk factor for NAFLD is light pollution. Light pollution, defined as the alteration of natural light levels due to the introduction of artificial light at night, is a major side-effect of urbanization (Falchi et al., 2016). Artificial light

allows people to extend daytime activities into the night and engage in countercyclical nighttime shift work. As such, it may adversely affect health via circadian rhythm disruption (Lunn et al., 2017).

Circadian rhythms refer to physiological processes that occur with a repeating period of approximately 24 h, and ensure that internal physiology is synchronized with the external environment (Gachon et al., 2004). In mammals, suprachiasmatic nuclei (SCN) acts as the master circadian clock. SCN communicates time-of-day information by synaptic and diffusible signals to clocks in various brain regions and peripheral organs (i.e., peripheral clock). Light information is transmitted by way of the retino-hypothalamic tract connecting the eye to the SCN and is the most potent synchronizing factor and the main zeitgeber that synchronizes the clock with the external environment (Panda et al., 2002). Thus, the SCN serves to synchronize the timing of rhythmic activities throughout the body to the light/dark cycle, and responds to light more rapidly than peripheral tissues (Welsh et al., 2010). Taken together, the endogenous biological clocks can be disrupted by nighttime light exposure (light pollution).

It is reasonable to suspect light pollution affects physiological function due to the importance of the circadian system in regulating homeostatic functions. Data show that circadian disruptions from light pollution cause significant disruptions in physiological function. Epidemiological evidence from shift workers exposed to high levels of light at night suggest that prolonged exposure to light at night increases the risk for cancer, mood disorders, and metabolic dysfunction (Kubo et al., 2011; Xiao et al., 2019). Additionally, the increase in exposure to light at night parallels the global increase in the prevalence of obesity and metabolic disorders (Koo et al., 2016), well-known risk factors for NAFLD. However, the effects of environmental light pollution on the development of NAFLD remains unclear.

The gut microbiota is recognized as an "external" organ playing an important role in host physiology and metabolism (Lozupone et al., 2012; Raman et al., 2013). Both animal and observational studies in NAFLD patients suggest links between gut microbiota changes and NAFLD (Chiu et al., 2017; Tripathi et al., 2018; Zhou et al., 2018). The changes of gut microbiota may disrupt the gut tight junctions, leading to increased gut permeability and LPS translocation. Increased LPS translocation induces "metabolic endotoxemia," which triggers inflammatory reactions, insulin resistance, and promotes the development of NAFLD (Leung et al., 2016; Aron-Wisnewsky et al., 2020).

It has been reported that circadian disruption by constant light exposure changes gut microbiome taxa and their functional gene composition (Wu et al., 2018). However, data on the effects of light pollution on gut microbiome in NAFLD subjects is limited. High fat diet (HFD) feeding is an extensively used model of NAFLD in rodents. Accumulating evidence shows that HFD reduces microbial diversity and alters gut microbiota composition (Cani et al., 2008; Zhang et al., 2012). In the present animal study, we observed the effects of constant light exposure on NAFLD and explored changes of gut microbiota in the colon content in HFD-fed rats model of NAFLD.

MATERIALS AND METHODS

Animal Experiment

Twenty-eight male Sprague-Dawley (SD) rats (6 weeks old) were purchased from Hunan Slac-Jingda Laboratory Animal Co. (Changsha, China). All rats were housed under specific pathogen-free conditions in a temperature-controlled room with free access to water and food. All rats were fed with normal chow diet (ND, fat 12%, carbohydrate 66%, protein 22%, 3.50 kcal/g) and under 12:12 h light/dark cycle for 1 week to adapt to the environment. The rats were then randomly divided into 4 experimental groups and placed in two separate rooms ($n = 7$ each): (1) ND-LD group: rats on a normal diet (ND), and exposed to standard light/dark (LD) cycle; (2) ND-LL group: rats on a ND, and exposed to constant light (LL); (3) HFD-LD group: rats fed on a HFD (fat 37%, protein 17.5%, carbohydrate 45.5%, 4.50 kcal/g), and exposed to standard LD cycle; and (4) HFD-LL group: rats on HFD, and exposed to constant light (LL). The LD rats were placed in a room with a standard 12 h light/dark (LD) cycle: lights on between 8 a.m. and 8 p.m., with the light intensity in the cage set at 200 lux. The LL rats were placed in a constant-light room where they were exposed to 200 lux of continuous light at cage level. The light sources were natural white fluorescent light tubes with a wavelength range of 400∼560 nm.

Food intake and body weight were recorded weekly for all animals throughout the experiment for 16 weeks. Animal protocols were approved by the Animal Use and Care Committee of Central South University and were conducted according to the regulations set by Central South University (No.2018sydw184).

Intraperitoneal Glucose Tolerance Test (IPGTT) and Insulin Tolerance Test (ITT)

An IPGTT was performed in the 14th week of experiment after an overnight fast. The rats were given an intraperitoneal injection of 50% D-glucose (2.0 g/kg) after fasting. Blood samples were measured from the tip of the tail at 0, 15, 30, 60, and 120 min after glucose injection using a portable glucose monitor (ACCU-CHEK; Roche Diagnostics, Mannheim, Germany).

ITT was carried out 5 days after IPGTT. Insulin (0.75 IU/kg, Novolin R, Novo Nordisk, Denmark) was injected intraperitoneally after an overnight fast, and blood glucose measurement procedure was the same as IPGTT.

Body Composition Assessment

Dual Energy X-ray Absorptiometry (DXA, GE Lunar Corp., United States) was utilized to assess body fat mass using small animal software (GE Medical Systems Lunar, Madison, WI, United States).

Sample Collection

After 16 weeks of intervention, rats were sacrificed in 2 consecutive days from 8 a.m. to 12 p.m. after fasting for 12 h. They were sacrificed while under anesthesia (inhaled) with 1.5–3.0% isoflurane (RWD Life Since Co., China). The abdominal cavity was then rapidly opened, and blood samples were collected from

the superior vena cava and centrifuged at 2000 × g for 20 min to isolate serum (stored at −20°C).

Liver tissues were collected and weighed. Liver tissues were then either fixed with 4% paraformaldehyde solution or frozen in liquid nitrogen and stored at −80°C until analysis.

Colon content samples were collected under a sterile fume to prevent miscellaneous bacterium contamination and then frozen in liquid nitrogen and stored at −80°C until they were analyzed for gut microbiota or short/medium chain fatty acids measurements.

Proximal colon segments were collected and then fixed with 4% paraformaldehyde solution for immunohistochemical analysis.

Relative Visceral Fat Weight

Epididymal fat were quickly excised and weighed. The epididymal fat relative body weight was represented for relative visceral fat weight.

Serum Biochemical Analysis

Serum levels of triglycerides (TG), total cholesterol (TC), low-density lipoprotein cholesterol (LDL-C), high-density lipoprotein cholesterol (HDL-C), alanine aminotransferase (ALT), and aspartate aminotransferase (AST) were measured using commercial reagents (Serotec Co., Sapporo, Japan) according to the manufacturer's recommendations.

Liver Pathology

Paraffin-embedded liver sections (5 μm) were stained by hematoxylin and eosin (H&E). The NAFLD activity score (NAS) was assessed by an experienced physiologist using indices of inflammation, steatosis, and hepatocyte ballooning as previously published (Kleiner et al., 2005).

Gut Microbiota Analysis

Microbial DNA was extracted by FastDNA^{TM} Spin Kit for Soil (MP bio, United States) and quantified using NanoDrop 2000. The V3–V4 region of the 16S rRNA gene was intensified by PCR (94°C for 2 min, followed by 25 cycles at 94°C for 30 s, 55°C for 30 s, and 72°C for 1 min and a final extension at 72°C for 10 min) using primers 5′- CCTACGGGNGGCWGCAG -3′ for 341F and 5′-GACTACHVGGGTATCTAATCC -3′ for 805R. The Agencourt AMPure XP PCR Purification Beads (Bechman Coulter, United States) was used to purify the amplicons. The solution was checked for integrity using Agilent 2100 Bioanalyzer (Agilent Technologies, United States) and quantified using Invitrogen Qubit3.0 spectrophotometer (Thermo Fisher Scientific, United States). The Miseq Reagnent Kit V3 was used for normalization and sequencing on an Illumina MiSeq (Illumina, United States).

Adapter sequences and low-quality ends were removed using Trimmomatic v0.33. Fastq files were demultiplexed and quality-filtered with FLASH2. The operational taxonomic units (OTUs) which reached a 97% sequence identity were subjected to alpha-diversity analyses to evaluate samples biodiversity using mothur software (version 1.30.1). The R package (R 3.6.0) was used for the visualization of bacterial community classification and distribution. Linear discriminant analysis (LDA) effect size (LEfSe) was performed to identify taxonomic biomarkers that characterize the differences between groups with the logarithmic LDA score threshold set at 2.5. A generalized estimated equation (GEE) analysis was performed using R package to investigate whether changes of microbiota were associated with NAS. Functional capacity for each sequence was analyzed with phylogenetic investigation of communities by reconstruction of unobserved states (PICRUSt). The Kyoto Encyclopedia of Genes and Genomes (KEGG) analysis was used to identify credible biological functions.

Short and Medium Chain Fatty Acids Measurement

Short chain fatty acids (SCFAs) and medium chain fatty acids (MCFAs) in colon contents were measured using HPLC-MS/MS method as previously described (Li et al., 2019). Briefly, samples were extracted with solvent mixtures containing acetonitrile and double distilled water and analyzed on a Thermo Fisher DGLC-3000 coupled to Sciex QTRAP 6500 Plus system. Octanoic acid-1-$^{13}C_1$ was used as an internal standard.

Serum IL-6 and TNF-α

Serum IL-6 and TNF-α were measured using respective commercial rat-specific enzyme-linked immunosorbent assay (ELISA) kit (Cusabio, Wuhan, China).

Immunohistochemical Analysis

Paraffin-embedded colon tissues (4 μm) were stained with occludin (1:200; Abcam, Hong Kong) or zonula occluden−1 (ZO-1, 1:100; Affinity Bioscience, United States) primary antibodies and incubated in a humidified chamber overnight at 4°C. The sections were then incubated with biotinylated goat anti−rabbit secondary antibodies (Boster Biological Technology, Wuhan, China) at room temperature for 20 min. Finally, color was developed in diaminobenzidine (DAB; ZSGB Biotechnology, Beijing, China) substrate solution. The average optical density (AOD) value of immunohistochemical intensity was analyzed by the Image J software (version 1.53a; National Institutes of Health, United States).

Serum Lipopolysaccharide (LPS) and Liver LPS-Binding Protein (LBP) Quantitative Real Time-PCR Analysis

LPS, a component of the outer membrane of gram-negative bacteria, is an indicator of intestinal leakiness (Summa et al., 2013). The concentration of serum LPS was measured with commercially available limulus amebocyte lysate chromogenic kit (Dynamiker Biotechnology, Tianjin, China) according to the manufacturer's protocol.

LBP is a type 1 acute phase protein that is constitutively produced by the liver and rapidly upregulated during acute phase responses. LBP binds LPS to facilitate immune responses in conjunction with cell-surface pattern recognition receptors and is used as an indicator of LPS exposure (Summa

et al., 2013). Liver expression of LBP mRNA was assessed by quantitative real time -PCR. Primers sequence of LBP were as follows: F: 5′-TTACCGCCTGACTCCAACAT-3′, R: 5′-CAAGCCGGAAGACAGATTCG-3′). Quantification of LBP gene expression was performed using a ΔΔCt method with glyceraldehyde 3- phosphate dehydrogenase (GADPH) as an internal control.

Statistical Analysis

All data were analyzed using SPSS 23.0 (IBM, Armok, United States.). A one-way analysis of variance (ANOVA) followed by Tukey's *post hoc* test was used to identify statistical differences between groups. Data were shown as mean ± standard error of the mean. Statistical significance was defined as $p < 0.05$.

RESULTS

Constant Light Exposure Aggravated Obesity and Visceral Adiposity in HFD Rats

There were no significant differences in food intakes, body weights, body fat mass, and relative visceral fat weights between ND-LD and ND-LL group (**Figure 1**). In HFD rats, body weights in HFD-LL group were significantly higher than those in HFD-LD group from the 11th week of HFD feeding, and no difference in caloric intake was noted between HFD-LD and HFD-LL groups (**Figures 1A–D**). Compared with the HFD-LD group, body weight and visceral fat weights in the HFD-LL group were significantly higher after 16 weeks (**Figures 1E,F**).

Effects of Constant Light Exposure on Glucose Homeostasis and Serum Lipid Profiles

In normal chow fed rats, serum TC in the ND-LL group was significantly higher than that of the ND-LD group (**Table 1**). During the IPGTT, blood glucose levels at 30and 60 min in the ND-LL group were higher than those noted in the ND-LD group. The area under the curve (AUC) of the IPGTT in the ND-LL group was higher than that in the ND-LD group (**Figures 2A,B**). ITT suggested an increased tendency of AUC_{ITT} in the ND-LL group vs. the ND-LD group ($p = 0.0844$) (**Figures 2C,D**).

In HFD rats, serum TC and LDL-C in the HFD-LL group was significantly higher than those in the HFD-LD group (**Table 1**). During IPGTT, the HFD-LL group displayed increased levels of blood glucose starting at 15 min post-glucose injection vs. the HFD-LD group (**Figure 2A**). ITT demonstrated greater insulin resistance in the HFD-LL group vs. the HFD-LD group (**Figure 2D**).

Constant Light Exposure Promotes the Progress of NAFLD in HFD Rats

Compared with the ND-LD group, the ND-LL group had increased serum IL-6 concentration and AST/ALT ratio (**Table 1**). Liver histopathological examination showed more inflammatory cell infiltration in the ND-LL group as well (**Figures 3A,B**).

In HFD rats, hepatic steatosis and inflammatory infiltrates were significantly elevated in the HFD-LL group (**Figure 3A**). Also, the HFD-LL group had higher NAS and inflammation scores than the HFD-LD group ($p < 0.05$, **Figure 3B**). Serum TNF-α, IL-6, and AST/ALT ratio were also higher in the HFD-LL group (**Table 1**).

Constant Light Exposure Altered Intestinal Microbial Communities

There were no significant differences in alpha diversity and beta diversity between the ND-LD and ND-LL groups (**Figures 4A,B**). LEfSe analysis showed the relative higher abundance of *Protobacteria*, *Firmicutes, Spirochaetes* phylum, *Spirochaetes* class, *Spirochaetales* order, *Spirochaetaceae,* and *Odoribacteraceae* families, and *Treponema* genus in the ND-LL group compared to the ND-LD group (**Figure 4F**).

Compared with the ND-LD group, HFD-LD rats had decreased alpha diversity, increased abundance of *Firmicutes*, *Proteobacteria,* and *Verrucomicrobia* and decreased abundance of *Bacteroides* (**Figures 4C–E**).

The alpha diversity did not reveal significant differences between the HFD-LL and HFD-LD groups. The PCA represented structural change by the second principal component (PC2) with no statistic differences in PC1 (**Figures 4A,B**). The LEfSe analysis demonstrated constant light exposure restrained the growth of genus *Butyricicoccus*, *Clostridium*, *Turicibacter,* and class *Bacilli* in HFD fed rats. Compared with the HFD-LD group, the amounts of *Christensenella* and *Dehalobacterium* were higher in the HFD-LL group (**Figure 4G**). Consistent with the notion that constant light exposure causes increased severity of NASH, GEE analysis demonstrated that NAS was inversely correlated with genus *Turicibacter* ($p < 0.01$) and genus *Clostridium* ($p < 0.05$) (**Figures 4H,I**).

Pathways related to type 2 diabetes mellitus were elevated in the ND-LL group vs. those of the ND-LD group. Compared with the HFD-LD group, LPS biosynthesis phagosome, LPS biosynthesis proteins, Vitamin B6 metabolism, and antimicrobial drug resistance were significantly upregulated in the HFD-LL group (**Figure 4J**).

Effects of Constant Light Exposure on SCFAs/MCFAs Levels of Colon Content

There were no significant differences in SCFAs and MCFAs levels of colon contents between ND-LD and ND-LL groups. Compared with ND-LD group, an increase in acetate acid, propionate acid, and a decrease in butyrate acid, valerate acid, and MCFAs in colon contents were detected in the HFD-LD group. Among HFD groups, reduced butyrate acid was observed in the HFD-LL rats (**Figures 5A–D**).

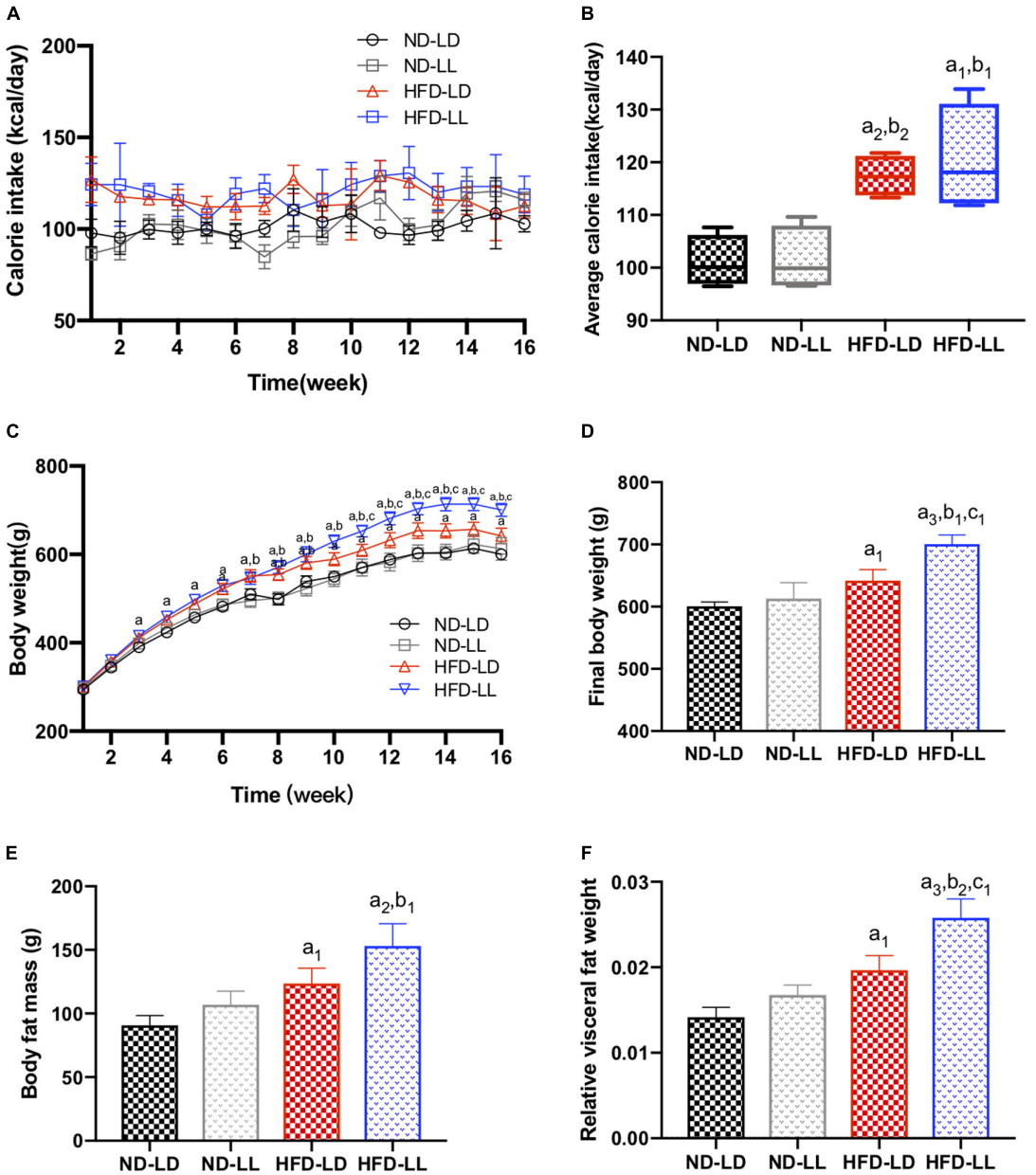

FIGURE 1 | Constant light exposure aggravated obesity and visceral adiposity in HFD rats. **(A)** Calorie intakes, **(B)** average calorie intakes, **(C)** body weights, **(D)** final body weights, **(E)** body fat mass, and **(F)** relative visceral fat weight. Data were expressed as Mean ± SEM, $n = 7$ per group, $^{a1}p < 0.05$, $^{a2}p < 0.01$, $^{a3}p < 0.001$, vs. ND-LD group; $^{b1}p < 0.05$, $^{b2}p < 0.01$, vs. ND-LL group; $^{c1}p < 0.05$, vs. HFD-LD group.

Constant Light Exposure Caused Gut Barrier Dysfunction

Gut barrier dysfunction plays an important role in the progression of NASH (Xue et al., 2017). Imbalances of gut microbiota and decreased SCFAs (e.g., butyrate acid) are associated with gut barrier dysfunction (Hamer et al., 2008; Lee et al., 2019). Compared to the control (ND-LD) group, HFD groups had lower expression of occludin and ZO-1 in proximal colon, and significantly higher circulating LPS levels and liver LBP mRNA expression. In HFD rats, constant light exposure caused a further increase in serum LPS and liver LBP mRNA expression, with further decrement of occludin and ZO-1 expression (all $p < 0.05$) (**Figures 6A–D**).

DISCUSSION

With the widespread prevalence of electric lights, particularly at night, light pollution is rising by approximately 6% per year worldwide (Holker et al., 2010). Light pollution is expected to rise dramatically in the next several decades through more

TABLE 1 | Comparison of serum lipids, AST/ALT and serum IL-6, TNF-α among groups at the end of the experiment.

Group	ND-LD	ND-LL	HFD-LD	HFD-LL
n	7	7	7	7
TG (mmol/L)	0.74 ± 0.10	0.80 ± 0.27	0.86 ± 0.07	0.82 ± 0.17
TC (mmol/L)	1.41 ± 0.06	1.71 ± 0.08^{a}	1.71 ± 0.09^{a}	2.05 ± 0.12^{a,b,c}
HDL-C (mmol/L)	0.87 ± 0.07	0.86 ± 0.05	0.65 ± 0.03^{a,b}	0.63 ± 0.04^{a,b}
LDL-C (mmol/L)	0.48 ± 0.05	0.54 ± 0.03	0.74 ± 0.05^{a,b}	0.93 ± 0.07^{a,b,c}
AST(U/L)	92.56 ± 6.95	106.63 ± 10.08	129.89 ± 21.61	209.74 ± 33.07^{a,b}
ALT(U/L)	36.24 ± 3.09	33.31 ± 2.95	41.11 ± 9.03	45.59 ± 8.33
AST/ALT	2.56 ± 0.16	3.24 ± 0.19^{a}	3.47 ± 0.30^{a}	4.79 ± 0.22^{a,b,c}
IL-6 (pg/mL)	26.82 ± 1.65	40.26 ± 2.75^{a}	46.26 ± 2.21^{a,b}	70.01 ± 2.10^{a,b,c}
TNF-α (pg/mL)	8.38 ± 0.51	8.86 ± 0.15	11.84 ± 0.61^{a,b}	14.92 ± 0.59^{a,b,c}

Results were expressed as Mean ± SEM. $^{a}p < 0.05$, compared with ND-LD group. $^{b}p < 0.01$, compared with ND-LL group. $^{c}p < 0.01$, compared with HFD-LD group. TG, triglyceride; TC, total cholesterol; HDL-C, high-density lipoprotein cholesterol; LDL-C, low-density lipoprotein cholesterol; AST, aspartate aminotransferase; ALT, alanine aminotransferase; IL-6, interleukin-6; TNF-α, tumor necrosis factor-alpha.

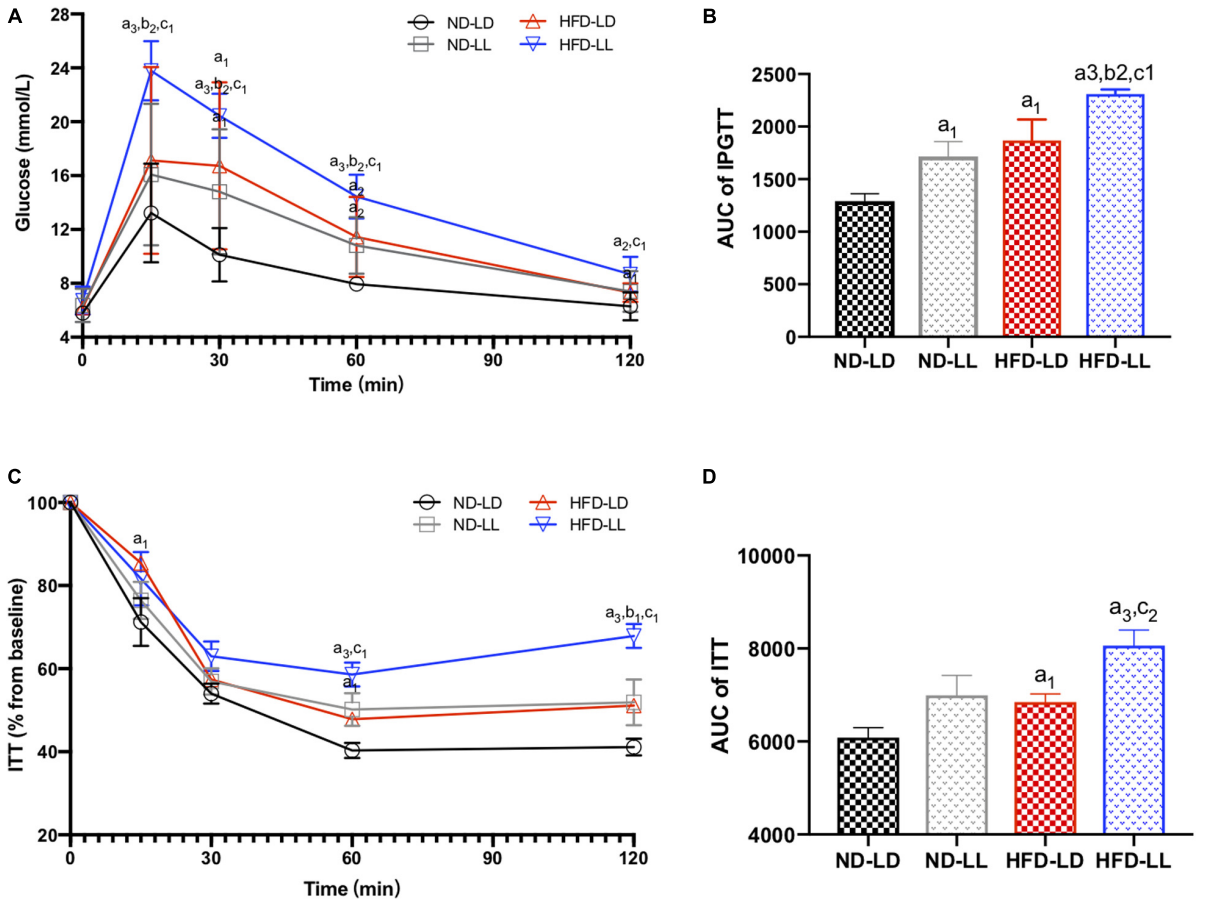

FIGURE 2 | Effects of constant light exposure on glucose homeostasis. **(A)** IPGTT, **(B)** AUC of IPGTT, **(C)** ITT (% basal), and **(D)** AUC of ITT. Data were expressed as Mean ± SEM, $n = 7$ per group, $^{a1}p < 0.05$, $^{a2}p < 0.01$, $^{a3}p < 0.001$, vs. ND-LD group; $^{b1}p < 0.05$, $^{b2}p < 0.01$, vs. ND-LL group; $^{c1}p < 0.05$,$^{c2}p < 0.01$ vs. HFD-LD group.

urban development, such as street lighting, vehicles lighting, and security lighting. However, consequences of light pollution remain largely unknown. In this report, we demonstrated that constant light exposure predisposed HFD rats, a widely used animal model of obesity and NAFLD, to increased obesity and NAFLD/NASH progression. This suggests that light pollution is a novel risk factor for NAFLD/NASH progression. In normal chow fed rats, ND-LL rats showed increased levels of TC and blood glucose, and higher levels of IL-6, also suggesting deleterious effects of constant light exposure on metabolism.

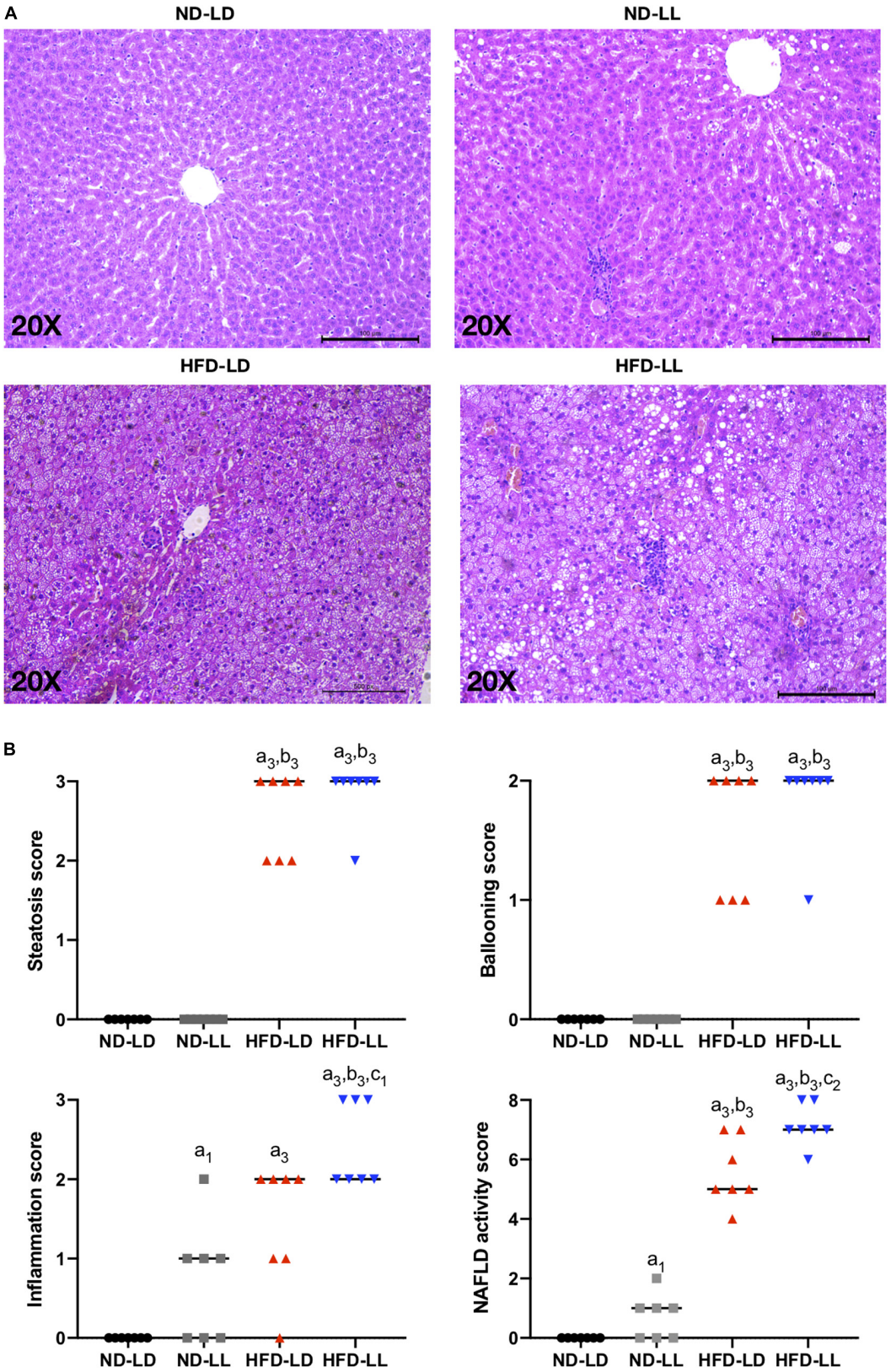

FIGURE 3 | Constant light exposure aggravated the progression of NAFLD/NASH. **(A)** Representative pictures of H&E staining (200 × magnifications) in liver tissue. **(B)** NAFLD activity score. Data were expressed as Median, $^{a1}p < 0.05$, $^{a3}p < 0.001$, vs. ND-LD group; $^{b3}p < 0.001$, vs. ND-LL group; $^{c1}p < 0.05$, $^{c2}p < 0.01$, vs. HFD-LD group.

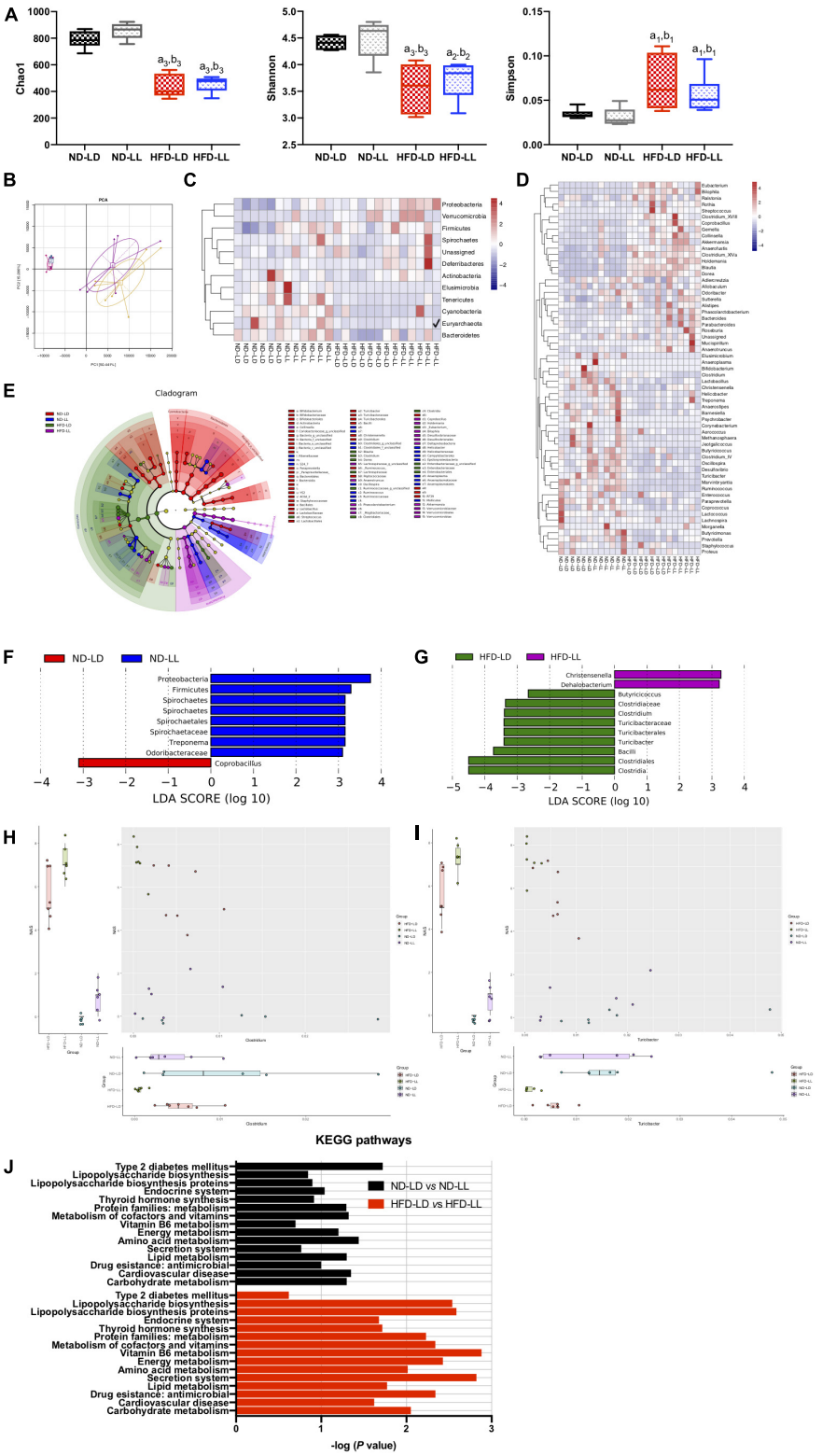

FIGURE 4 | Constant light exposure altered colon microbiota. **(A)** Alpha diversity of colon microbiota estimated by Chao 1, Shannon and Simpson indexes, **(B)** principle component analysis (PCA), **(C,D)** heatmap of colon microbiota at phylum **(C)** and genus **(D)** level, **(E)** cladogram, **(F,G)** scores of taxonomic biomarkers identified by linear discriminant analysis (LDA) using LEfSe in normal chow-fed rats **(F)** and HFD-fed rats **(G)**, LDA value > 2.5 were showed in the figure, **(H,I)** correlation between NAS and abundance of *Clostridium* **(H)**, *Turicibacter* **(I)** revealed by generalized estimated equation (GEE) analysis, **(J)** KEGG pathways changed by constant light exposure. $^{a1}p < 0.05$, $^{a2}p < 0.01$, $^{a3}p < 0.001$, vs. ND-LD group; $^{b1}p < 0.05$, $^{b2}p < 0.01$, $^{b3}p < 0.001$, vs. ND-LL group.

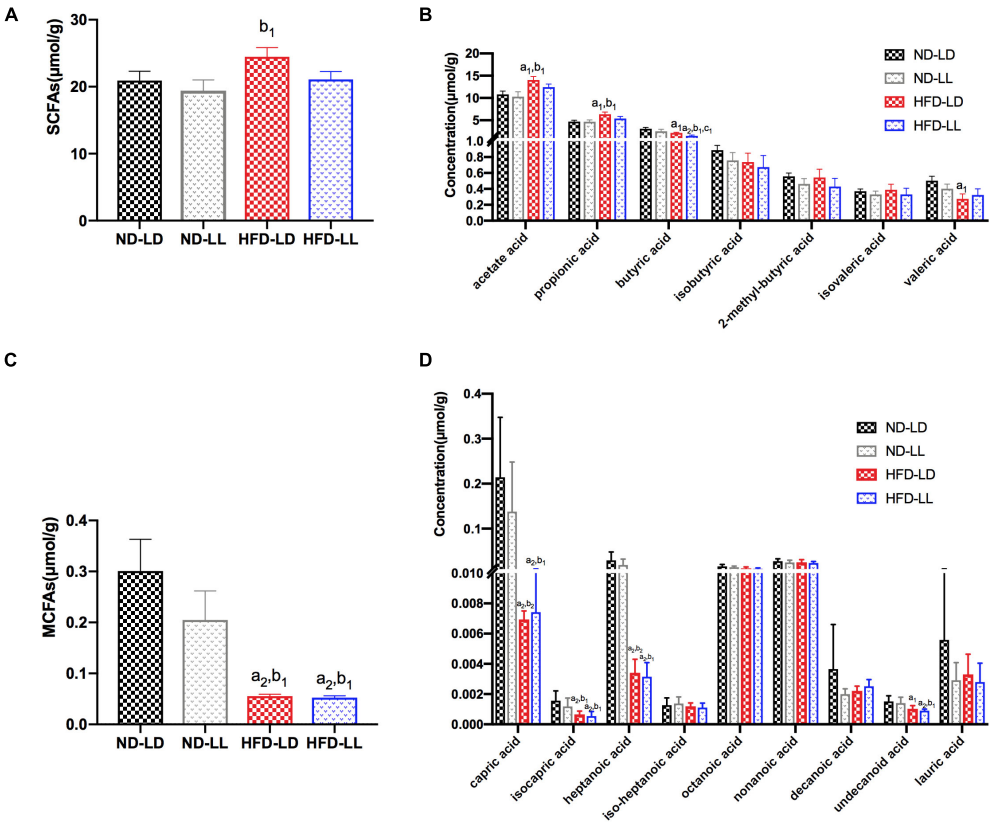

FIGURE 5 | Effects of constant light exposure on short chain fatty acids (SCFAs) and medium chain fatty acids (MCFAs) of colon contents. **(A)** Total amount of SCFAs, **(B)** SCFAs species, **(C)** total amount of MCFAs, **(D)** MCFAs species. Data were expressed as Mean ± SEM, $^{a1}p < 0.05$, $^{a2}p < 0.01$, vs. ND-LD group; $^{b1}p < 0.05$, vs. ND-LL group; $^{c1}p < 0.05$, vs. HFD-LD group.

Gut dysbiosis is associated with the development of NAFLD (Tripathi et al., 2018). Studies suggest that the development of NAFLD is associated with marked changes of fecal microbiota composition (Aron-Wisnewsky et al., 2013; Wang et al., 2018). In addition, results of both animal and human studies suggest that targeting intestinal microbiota may have protective effects on the development of NAFLD (Tripathi et al., 2018). However, changes in gut microbiota were not entirely consistent among studies (Kolodziejczyk et al., 2019). For example, among NAFLD individuals, an increase in *Proteobacteria* and *Bacteroidetes* has been reported (Boursier et al., 2016; Shen et al., 2017), while a reduction in *Proteobacteria* and *Bacteroidetes* was also observed (Shin et al., 2017; Koopman et al., 2019). Different ethnicities and living environments may help explain these discrepancies. Our experiment showed an increase of *Firmicutes*, *Proteobacteria*, *Verrucomicrobia,* and a decrease of *Bacteroides* in the HFD-LD vs. ND-LD group.

Evidences indicate that circadian clock has a profound impact on gut microbiota (Liang et al., 2015; Voigt et al., 2016). Circadian disruption by constant darkness or *Clock*$^{\Delta\ 19}$ mutation changes the composition and diurnal oscillation of gut microbiome in normal chow fed mice (Voigt et al., 2014, 2016; Wu et al., 2018). In normal chow fed rats, we found that constant light exposure increased *Proteobacteria* and *Firmicutes*. It has been reported that *Proteobacteria* ferment to produce alcohol, and higher concentrations of endogenous alcohols are thought to contribute to liver injury and inflammation (Leung et al., 2016). Thus, the increased abundance of *Proteobacteria* may explain the increased AST/ALT and liver inflammatory cells infiltration in the ND-LL group.

Very few experiments have been performed to study the effects of constant light exposure on gut microbiome in HFD-fed animals. The present study was the first to note increased *Christensenella* and *Dehalobacterium,* and a decrease in genus *Butyricicoccus*, *Clostridium*, *Turicibacter,* and class *Bacilli* in HFD rats exposed to constant light. *Clostridium* has been associated with improved lipid regulation, reduced risk of hyperlipidemia, intestinal permeability, inhibition of harmful pathogens, and normalization of lipid metabolism (Ling et al., 2016). In NAFLD patients, a negative correlation between severity of NASH and abundance of *Clostridium* has been reported (Pataky et al., 2016; Zhou et al., 2019). The present animal study also demonstrated a negative correlation between NAS and abundance of genus *Clostridium*.

Another interesting discovery of our study was that constant light exposure caused decreased butyrate acid levels in colon content of HFD rats. The impact of gut microbiota on NAFLD is considered to be mediated by its metabolic

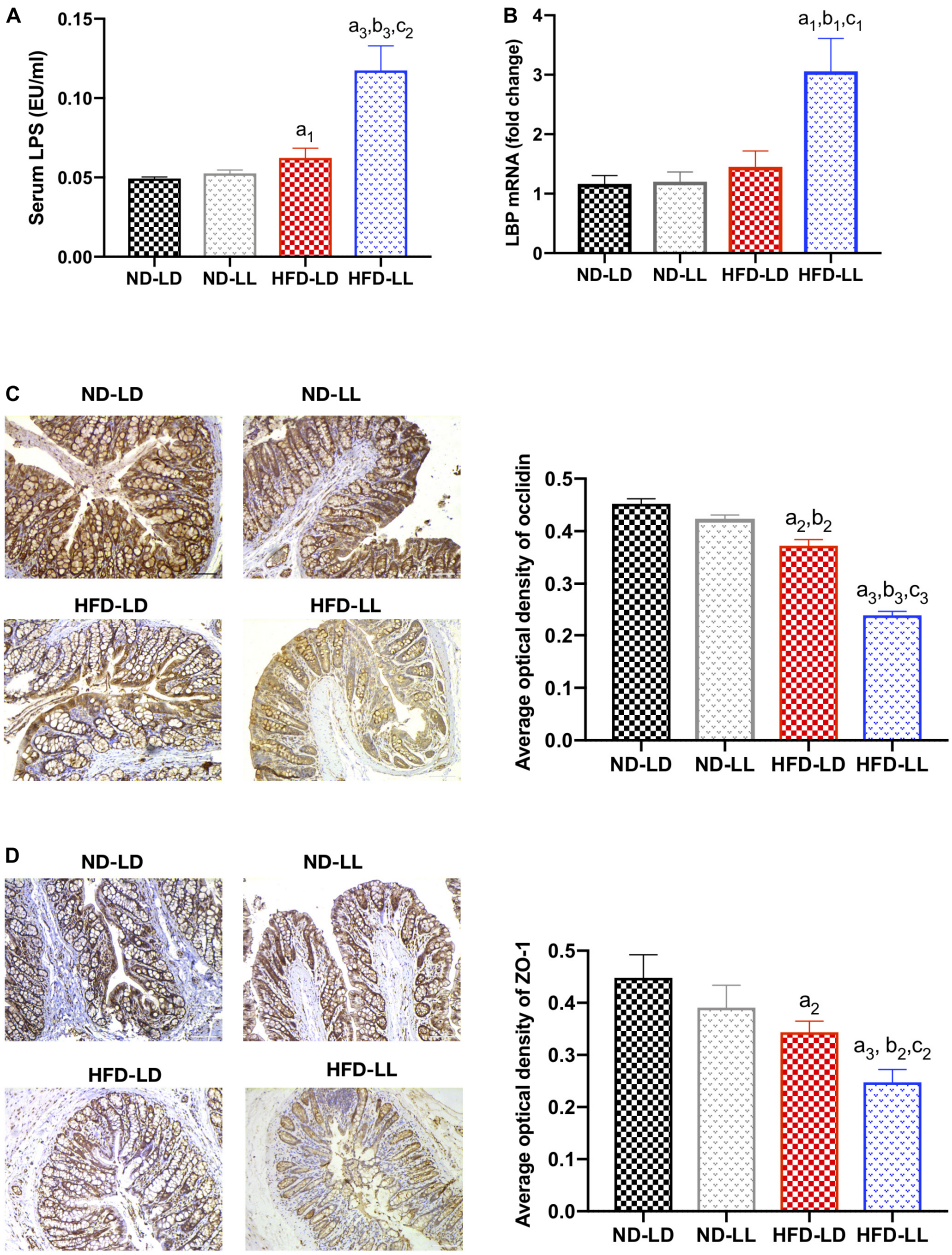

FIGURE 6 | Constant light exposure impaired gut barrier function and gut-liver axis in HFD rats. **(A)** Serum LPS concentration, **(B)** hepatic LBP mRNA expression by RT-PCR, **(C)** expression of occludin in colon by IHC (200×), **(D)** expression of ZO-1 in colon by IHC (200×). Data were expressed as Mean ± SEM, $^{a1}p < 0.05$, $^{a2}p < 0.01$, $^{a3}p < 0.001$, vs. ND-LD group; $^{b1}p < 0.05$, $^{b2}p < 0.01$, $^{b3}p < 0.001$, vs. ND-LL group; $^{c1}p < 0.05$,$^{c2}p < 0.01$, $^{c3}p < 0.001$ vs. HFD-LD group.

products, such as SCFAs. Among SCFAs, butyrate has been reported to upregulate the expression of tight junction proteins, and consequently can enhance the gut barrier function (Lu et al., 2016). Butyrate supplementation to animals has been demonstrated to reduce hepatic fat accumulation and hepatic inflammation (Canfora et al., 2019). The decreased butyrate level in the HFD-LL group is consistent with the reduction in *Clostridium* genus, as the *Clostridium* genus has butyrate-producing effects (Vital et al., 2014; Ganesan et al., 2018). Targeting gut microbiota therapy has protective effects on the development of NAFLD (Tripathi et al., 2018). Light pollution is sometimes inevitable, e.g., shift workers, medical staff, et cetera. It may be possible that supplementation of some bacteria (e.g., *Clostridium* genus) or butyrate acid can be used as an intervention therapy for early-stage NASH caused by light pollution.

NAFLD is associated with increased gut permeability and impaired gut-liver axis (Jiang et al., 2015; Szabo, 2015). Gut hyperpermeability permits the translocation of proinflammatory bacterial products (most prominently, LPS) from the lumen of

the gut into systemic circulation and promotes the progression of NASH (Okubo et al., 2016). We found that HFD-LL rats had decreased colon expression of tight junction proteins ZO-1 and occludin, and increased serum LPS level and liver LBP mRNA expression vs. the HFD-LD group, suggesting increased gut barrier dysfunction and impaired gut-liver axis exists in HFD rats exposed to constant light.

Taken together, the results presented herein demonstrate that constant light exposure alters gut microbiota and its metabolic products, impairs gut barrier function and gut-liver axis, and promotes the progression of NAFLD/NASH in HFD rats.

LIMITATIONS

This study was the first to explore the impact of constant light exposure on NAFLD. However, there are some limitations to note. First, the light intensity was only set at 200 lux. Different results may occur when light intensity changes. Second, the illumination wavelength in our study was 400∼560 nm. It has been reported that circadian responses have different spectral sensitivity, peaking at wavelengths between 450 and 490 nm (Dominoni et al., 2016). This suggests that illumination with different wavelengths may have varying effects. Our experiment used a circadian clock-disrupting light source, though specifying which wavelength has the most impact cannot be determined. Last, we carried out the experiment only in male SD rats, though gender is thought to be an important factor in metabolic syndrome and its outcomes. There are gender differences in prevalence, risk factors, and mechanisms of NAFLD. It is still unknown the effects of constant light exposure on female subjects. Moreover, the number of animals was small.

CONCLUSION

Constant light exposure changes gut microbiota and its metabolic products, impairs gut barrier function and gut-liver axis, and promotes the progression of NAFLD/NASH in HFD rats.

DATA AVAILABILITY STATEMENT

The datasets generated for this study can be found in the NCBI Sequence Read Archive under BioProject PRJNA597851 (https://www.ncbi.nlm.nih.gov/bioproject/PRJNA597851).

ETHICS STATEMENT

The experiments were conducted according to the Animal Use and Care Committee of Central South University and were conducted according to the regulations set by Central South University (No. 2018sydw184).

AUTHOR CONTRIBUTIONS

LW and DZ conceived and designed the study. LW, FY, LX, SW, YS, and XX performed the experiments. LW, FY, JL, LX, SW, and YS analyzed the data. SM and GS analyzed the concentration of microbiota metabolites. LW and FY drafted the manuscript. DZ and RR revised the manuscript. All authors have read, commented on, and approved the manuscript for publication.

FUNDING

This work was supported by the National Science and Foundation of China (No. 81670788) and Bethune-Merck Diabetes Research Fund (No. G2018030).

ACKNOWLEDGMENTS

We thank Dr. Zhijun Zhou, The Director of Department of Zoology, Xiangya Medical College, Central South University, for the support and assistance in this study.

REFERENCES

Aron-Wisnewsky, J., Gaborit, B., Dutour, A., and Clement, K. (2013). Gut microbiota and non-alcoholic fatty liver disease: new insights. *Clin. Microbiol. Infect.* 19, 338–348. doi: 10.1111/1469-0691.12140

Aron-Wisnewsky, J., Vigliotti, C., Witjes, J., Le, P., Holleboom, A. G., Verheij, J., et al. (2020). Gut microbiota and human NAFLD: disentangling microbial signatures from metabolic disorders. *Nat. Rev. Gastroenterol. Hepatol.* 17, 279–297. doi: 10.1038/s41575-020-0269-9

Boursier, J., Mueller, O., Barret, M., Machado, M., Fizanne, L., Araujo-Perez, F., et al. (2016). The severity of nonalcoholic fatty liver disease is associated with gut dysbiosis and shift in the metabolic function of the gut microbiota. *Hepatology* 63, 764–775. doi: 10.1002/hep.28356

Cairns, S. R., and Peters, T. J. (1983). Biochemical analysis of hepatic lipid in alcoholic and diabetic and control subjects. *Clin. Sci. (Lond)* 65, 645–652. doi: 10.1042/cs0650645

Canfora, E. E., Meex, R. C. R., Venema, K., and Blaak, E. E. (2019). Gut microbial metabolites in obesity. NAFLD and T2DM. *Nat. Rev. Endocrinol.* 15, 261–273. doi: 10.1038/s41574-019-0156-z

Cani, P. D., Bibiloni, R., Knauf, C., Waget, A., Neyrinck, A. M., Delzenne, N. M., et al. (2008). Changes in gut microbiota control metabolic endotoxemia-induced inflammation in high-fat diet-induced obesity and diabetes in mice. *Diabetes* 57, 1470–1481. doi: 10.2337/db07-1403

Chiu, C. C., Ching, Y. H., Li, Y. P., Liu, J. Y., Huang, Y. T., Huang, Y. W., et al. (2017). Nonalcoholic fatty liver disease is exacerbated in high-fat diet-fed gnotobiotic mice by colonization with the gut microbiota from patients with nonalcoholic steatohepatitis. *Nutrients* 9:1220. doi: 10.3390/nu9111220

Dominoni, D. M., Borniger, J. C., and Nelson, R. J. (2016). Light at night, clocks and health: from humans to wild organisms. *Biol. Lett.* 12, 20160015. doi: 10.1098/rsbl.2016.0015

Eslam, M., Valenti, L., and Romeo, S. (2018). Genetics and epigenetics of NAFLD and NASH: clinical impact. *J. Hepatol.* 68, 268–279. doi: 10.1016/j.jhep.2017.09.003

Falchi, F., Cinzano, P., Duriscoe, D., Kyba, C. C., Elvidge, C. D., Baugh, K., et al. (2016). The new world atlas of artificial night sky brightness. *Sci. Adv.* 2:e1600377. doi: 10.1126/sciadv.1600377

Gachon, F., Nagoshi, E., Brown, S. A., Ripperger, J., and Schibler, U. (2004). The mammalian circadian timing system: from gene expression to physiology. *Chromosoma* 113, 103–112. doi: 10.1007/s00412-004-0296-2

Ganesan, K., Chung, S. K., Vanamala, J., and Xu, B. (2018). Causal relationship between diet-induced gut microbiota changes and diabetes: a novel strategy to transplant faecalibacterium prausnitzii in preventing diabetes. *Int. J. Mol. Sci.* 19:3720. doi: 10.3390/ijms19123720

Hamer, H. M., Jonkers, D., Venema, K., Vanhoutvin, S., Troost, F. J., and Brummer, R. J. (2008). Review article: the role of butyrate on colonic function. *Aliment Pharmacol. Ther.* 27, 104–119. doi: 10.1111/j.1365-2036.2007.03562.x

Holker, F., Moss, T., Griefahn, B., Kloas, W., Voigt, C. C., Henckel, D., et al. (2010). The dark side of light: a transdisciplinary research agenda for light pollution policy. *Ecol. Soc.* 15:13.

Jiang, W., Wu, N., Wang, X., Chi, Y., Zhang, Y., Qiu, X., et al. (2015). Dysbiosis gut microbiota associated with inflammation and impaired mucosal immune function in intestine of humans with non-alcoholic fatty liver disease. *Sci. Rep.* 5:8096. doi: 10.1038/srep08096

Kleiner, D. E., Brunt, E. M., Van Natta, M., Behling, C., Contos, M. J., Cummings, O. W., et al. (2005). Design and validation of a histological scoring system for nonalcoholic fatty liver disease. *Hepatology* 41, 1313–1321. doi: 10.1002/hep.20701

Kolodziejczyk, A. A., Zheng, D., Shibolet, O., and Elinav, E. (2019). The role of the microbiome in NAFLD and NASH. *EMBO Mol. Med.* 11:e9302. doi: 10.15252/emmm.201809302

Koo, Y. S., Song, J. Y., Joo, E. Y., Lee, H. J., Lee, E., Lee, S. K., et al. (2016). Outdoor artificial light at night, obesity, and sleep health: cross-sectional analysis in the KoGES study. *Chronobiol. Int.* 33, 301–314. doi: 10.3109/07420528.2016.1143480

Koopman, N., Molinaro, A., Nieuwdorp, M., and Holleboom, A. G. (2019). Review article: can bugs be drugs? the potential of probiotics and prebiotics as treatment for non-alcoholic fatty liver disease. *Aliment Pharmacol. Ther.* 50, 628–639. doi: 10.1111/apt.15416

Kubo, T., Oyama, I., Nakamura, T., Shirane, K., Otsuka, H., Kunimoto, M., et al. (2011). Retrospective cohort study of the risk of obesity among shift workers: findings from the industry-based shift workers'. health study, Japan. *Occup. Environ. Med.* 68, 327–331. doi: 10.1136/oem.2009.054445

Lee, S., Kirkland, R., Grunewald, Z. I., Sun, Q., Wicker, L., and De La Serre, C. B. (2019). Beneficial effects of non-encapsulated or encapsulated probiotic supplementation on microbiota composition, intestinal barrier functions, inflammatory profiles, and glucose tolerance in high fat fed rats. *Nutrients* 11:1975. doi: 10.3390/nu11091975

Leung, C., Rivera, L., Furness, J. B., and Angus, P. W. (2016). The role of the gut microbiota in NAFLD. *Nat. Rev. Gastroenterol. Hepatol.* 13, 412–425. doi: 10.1038/nrgastro.2016.85

Li, B., Li, L., Li, M., Lam, S. M., Wang, G., Wu, Y., et al. (2019). Microbiota depletion impairs thermogenesis of brown adipose tissue and browning of white adipose tissue. *Cell Rep.* 26, 2720–2737.e5. doi: 10.1016/j.celrep.2019.02.015

Liang, X., Bushman, F. D., and Fitzgerald, G. A. (2015). Rhythmicity of the intestinal microbiota is regulated by gender and the host circadian clock. *Proc. Natl. Acad. Sci. U.S.A.* 112, 10479–10484. doi: 10.1073/pnas.1501305112

Ling, Z., Jin, C., Xie, T., Cheng, Y., Li, L., and Wu, N. (2016). Alterations in the fecal microbiota of patients with hiv-1 infection: an observational study in a chinese population. *Sci. Rep.* 6:30673. doi: 10.1038/srep30673

Lozupone, C. A., Stombaugh, J. I., Gordon, J. I., Jansson, J. K., and Knight, R. (2012). Diversity, stability and resilience of the human gut microbiota. *Nature* 489, 220–230. doi: 10.1038/nature11550

Lu, Y. Y., Fan, C. N., Li, P., Lu, Y. F., Chang, X. L., and Qi, K. M. (2016). Short chain fatty acids prevent high-fat-diet-induced obesity in mice by regulating g protein-coupled receptors and gut microbiota. *Sci. Rep.* 6:37589.

Lunn, R. M., Blask, D. E., Coogan, A. N., Figueiro, M., Gorman, M. R., Hall, J. E., et al. (2017). Health consequences of electric lighting practices in the modern world: a report on the National Toxicology Program's workshop on shift work at night, artificial light at night, and circadian disruption. *Sci. Total Environ.* 607, 1073–1084. doi: 10.1016/j.scitotenv.2017.07.056

Okubo, H., Kushiyama, A., Sakoda, H., Nakatsu, Y., Iizuka, M., Taki, N., et al. (2016). Involvement of resistin-like molecule beta in the development of methionine-choline deficient diet-induced non-alcoholic steatohepatitis in mice. *Sci. Rep.* 6:20157. doi: 10.1038/srep20157

Panda, S., Antoch, M. P., Miller, B. H., Su, A. I., Schook, A. B., Straume, M., et al. (2002). Coordinated transcription of key pathways in the mouse by the circadian clock. *Cell* 109, 307–320. doi: 10.1016/s0092-8674(02)00722-5

Pataky, Z., Genton, L., Spahr, L., Lazarevic, V., Terraz, S., Gaia, N., et al. (2016). Impact of hypocaloric hyperproteic diet on gut microbiota in overweight or obese patients with nonalcoholic fatty liver disease: a pilot study. *Dig. Dis. Sci.* 61, 2721–2731. doi: 10.1007/s10620-016-4179-1

Raman, M., Ahmed, I., Gillevet, P. M., Probert, C. S., Ratcliffe, N. M., Smith, S., et al. (2013). Fecal microbiome and volatile organic compound metabolome in obese humans with nonalcoholic fatty liver disease. *Clin. Gastroenterol. Hepatol.* 11, 868–875.e1-3. doi: 10.1016/j.cgh.2013.02.015

Sheka, A. C., Adeyi, O., Thompson, J., Hameed, B., Crawford, P. A., and Ikramuddin, S. (2020). Nonalcoholic steatohepatitis: a review. *JAMA* 323, 1175–1183. doi: 10.1001/jama.2020.2298

Shen, F., Zheng, R. D., Sun, X. Q., Ding, W. J., Wang, X. Y., and Fan, J. G. (2017). Gut microbiota dysbiosis in patients with non-alcoholic fatty liver disease. *Hepatobiliary Pancreat. Dis. Int.* 16, 375–381. doi: 10.1016/S1499-3872(17)60019-5

Shin, N. R., Bose, S., Wang, J. H., Ansari, A., Lim, S. K., Chin, Y. W., et al. (2017). Flos lonicera combined with metformin ameliorates hepatosteatosis and glucose intolerance in association with gut microbiota modulation. *Front. Microbiol.* 8:2271. doi: 10.ARTN 227110.3389/fmicb.2017.02271

Summa, K. C., Voigt, R. M., Forsyth, C. B., Shaikh, M., Cavanaugh, K., Tang, Y., et al. (2013). Disruption of the circadian clock in mice increases intestinal permeability and promotes alcohol-induced hepatic pathology and inflammation. *PLoS One* 8:e67102. doi: 10.1371/journal.pone.0067102

Szabo, G. (2015). Gut-liver axis in alcoholic liver disease. *Gastroenterology* 148, 30–36. doi: 10.1053/j.gastro.2014.10.042

Tripathi, A., Debelius, J., Brenner, D. A., Karin, M., Loomba, R., Schnabl, B., et al. (2018). The gut-liver axis and the intersection with the microbiome. *Nat. Rev. Gastroenterol. Hepatol.* 15, 397–411. doi: 10.1038/s41575-018-0011-z

Vital, M., Howe, A. C., and Tiedje, J. M. (2014). Revealing the bacterial butyrate synthesis pathways by analyzing (meta)genomic data. *mBio* 5:e00889. doi: 10.1128/mBio.00889-14

Voigt, R. M., Forsyth, C. B., Green, S. J., Mutlu, E., Engen, P., Vitaterna, M. H., et al. (2014). Circadian disorganization alters intestinal microbiota. *PLoS One* 9:e97500. doi: 10.1371/journal.pone.0097500

Voigt, R. M., Summa, K. C., Forsyth, C. B., Green, S. J., Engen, P., Naqib, A., et al. (2016). The circadian clock mutation promotes intestinal dysbiosis. *Alcohol. Clin. Exp. Res.* 40, 335–347. doi: 10.1111/acer.12943

Wang, W., Zhao, J., Gui, W., Sun, D., Dai, H., Xiao, L., et al. (2018). Tauroursodeoxycholic acid inhibits intestinal inflammation and barrier disruption in mice with non-alcoholic fatty liver disease. *Br. J. Pharmacol.* 175, 469–484. doi: 10.1111/bph.14095

Welsh, D. K., Takahashi, J. S., and Kay, S. A. (2010). Suprachiasmatic nucleus: cell autonomy and network properties. *Annu. Rev. Physiol.* 72, 551–577. doi: 10.1146/annurev-physiol-021909-135919

Wu, G., Tang, W., He, Y., Hu, J., Gong, S., He, Z., et al. (2018). Light exposure influences the diurnal oscillation of gut microbiota in mice. *Biochem. Biophys. Res. Commun.* 501, 16–23. doi: 10.1016/j.bbrc.2018.04.095

Xanthakos, S., Miles, L., Bucuvalas, J., Daniels, S., Garcia, V., and Inge, T. (2006). Histologic spectrum of nonalcoholic fatty liver disease in morbidly obese adolescents. *Clin. Gastroenterol. Hepatol.* 4, 226–232. doi: 10.1016/s1542-3565(05)00978-x

Xiao, Q., Gee, G., Jones, R. R., Jia, P., James, P., and Hale, L. (2019). Cross-sectional association between outdoor artificial light at night and sleep duration in middle-to-older aged adults: the NIH-AARP diet and health study. *Environ. Res.* 180:108823. doi: 10.1016/j.envres.2019.108823

Xue, L., He, J., Gao, N., Lu, X., Li, M., Wu, X., et al. (2017). Probiotics may delay the progression of nonalcoholic fatty liver disease by restoring the gut microbiota structure and improving intestinal endotoxemia. *Sci. Rep.* 7:45176. doi: 10.1038/srep45176

Zhang, C., Zhang, M., Pang, X., Zhao, Y., Wang, L., and Zhao, L. (2012). Structural resilience of the gut microbiota in adult mice under high-fat dietary perturbations. *ISME J.* 6, 1848–1857. doi: 10.1038/ismej.2012.27

Zhou, W., Guo, R., Guo, W., Hong, J., Li, L., Ni, L., et al. (2019). Monascus yellow, red and orange pigments from red yeast rice ameliorate lipid metabolic disorders and gut microbiota dysbiosis in Wistar rats fed on a high-fat diet. *Food Funct.* 10, 1073–1084. doi: 10.1039/c8fo02192a

Zhou, Y., Zheng, T., Chen, H., Li, Y., Huang, H., Chen, W., et al. (2018). Microbial intervention as a novel target in treatment of non-alcoholic fatty liver disease progression. *Cell Physiol. Biochem.* 51, 2123–2135. doi: 10.1159/000495830

Conflict of Interest: The authors declare that the research was conducted in the absence of any commercial or financial relationships that could be construed as a potential conflict of interest.

frontiers in Microbiology

ORIGINAL RESEARCH
published: 21 August 2020
doi: 10.3389/fmicb.2020.01909

Validating an Automated Nucleic Acid Extraction Device for *Omics in Space* Using Whole Cell Microbial Reference Standards

*Camilla Urbaniak[1†], Season Wong[2†], Scott Tighe[3†], Arunkumar Arumugam[2], Bo Liu[2], Ceth W. Parker[1], Jason M. Wood[1], Nitin K. Singh[1], Dana J. Skorupa[4], Brent M. Peyton[4], Ryan Jenson[5], Fathi Karouia[6], Julie Dragon[3] and Kasthuri Venkateswaran[1]**

[1] NASA Jet Propulsion Laboratory, California Institute of Technology, Pasadena, CA, United States, [2] Al Biosciences, College Station, TX, United States, [3] University of Vermont, Burlington, VT, United States, [4] Montana State University, Bozeman, MT, United States, [5] IRPI LCC, Portland, OR, United States, [6] NASA Ames Research Center, Moffett Field, CA, United States

OPEN ACCESS

Edited by:
Rakesh Mogul, California State Polytechnic University, Pomona, United States

Reviewed by:
Nigel Cook, Jorvik Food & Environmental Virology Ltd., United Kingdom
Tatiana A. Vishnivetskaya, The University of Tennessee, Knoxville, United States

****Correspondence:***
Kasthuri Venkateswaran
kjvenkat@jpl.nasa.gov

† These authors have contributed equally to this work

Specialty section:
This article was submitted to Extreme Microbiology, a section of the journal Frontiers in Microbiology

Received: *29 May 2020*
Accepted: *21 July 2020*
Published: *21 August 2020*

Citation:
Urbaniak C, Wong S, Tighe S, Arumugam A, Liu B, Parker CW, Wood JM, Singh NK, Skorupa DJ, Peyton BM, Jenson R, Karouia F, Dragon J and Venkateswaran K (2020) Validating an Automated Nucleic Acid Extraction Device for Omics in Space Using Whole Cell Microbial Reference Standards. Front. Microbiol. 11:1909. doi: 10.3389/fmicb.2020.01909

NASA has made great strides in the past five years to develop a suite of instruments for the International Space Station in order to perform molecular biology in space. However, a key piece of equipment that has been lacking is an instrument that can extract nucleic acids from an array of complex human and environmental samples. The *Omics in Space* team has developed the μTitan (simulated micro(μ) gravity **t**ested **i**ns**t**rument for **a**utomated **n**ucleic acid) system capable of automated, streamlined, nucleic acid extraction that is adapted for use under microgravity. The μTitan system was validated using a whole cell microbial reference (WCMR) standard comprised of a suspension of nine bacterial strains, titrated to concentrations that would challenge the performance of the instrument, as well as to determine the detection limits for isolating DNA. Quantitative assessment of system performance was measured by comparing instrument input challenge dose vs recovery by Qubit spectrofluorometry, qPCR, Bioanalyzer, and Next Generation Sequencing. Overall, results indicate that the μTitan system performs equal to or greater than a similar commercially available, earth-based, automated nucleic acid extraction device. The μTitan system was also tested in Yellowstone National Park (YNP) with the WCMR, to mimic a remote setting, with limited resources. The performance of the device at YNP was comparable to that in a laboratory setting. Such a portable, field-deployable, nucleic extraction system will be valuable for environmental microbiology, as well as in health care diagnostics.

Keywords: International Space Station (ISS), microbial monitoring, automated DNA extraction, microgravity (μg), extreme environments

INTRODUCTION

All terrestrial organisms exposed to the environmental conditions of space are subjected to reduced gravity, high-energy charged particles, high UV levels, low pressure, and large changes in temperature. When living in such an environment, humans can become immunocompromised (Mehta et al., 2017), microbial behavior can be changed (Kim et al., 2013), and host-microbial

interactions can be altered (Foster et al., 2014). To diagnose patients or to perform microbial monitoring on Earth, samples are immediately sent to a laboratory for testing and results can be obtained in a day or two. However, samples collected from the International Space Station (ISS) will take from 2 to 4 months to return back to Earth before analyses can be performed (Pierson et al., 2012), and it would not be practical for future long-term space missions to send samples back to Earth for analysis. To make exploring and living in space feasible, instruments that automate laboratory analysis will need to be developed. Since most molecular diagnostic methods for assessing and monitoring health are based on nucleic acids (Dwivedi et al., 2017), focused efforts to design portable nucleic acid-based molecular diagnostic assays (Chan et al., 2016a,c; Priye et al., 2016), compatible with microgravity, are a high priority.

In 2016, Dr. Kathleen Rubins, a NASA astronaut, became the first person to sequence DNA on the ISS, using the Oxford Nanopore MinION sequencer (Castro-Wallace et al., 2017). While this was a great milestone for space molecular biology, the DNA that was sequenced had already been extracted and the metagenome libraries prepared on Earth before sending to space for sequencing (Castro-Wallace et al., 2017). In another flight project, bacterial DNA, which also had been isolated on Earth, was sent to the ISS and successfully amplified with the miniPCR^{TM} (Boguraev et al., 2017). More recently, methods have been developed to allow for DNA and RNA extraction to occur on the ISS before *in situ* downstream analyses. For example, with the Genes in Space-3 project, cultured bacterial cells that had been isolated from around the ISS were lysed in a thermocycler and the DNA amplified before being sequenced on the MinION (NASA, 2017). With the WetLab-2 research platform, RNA was successfully isolated from *Escherichia coli* cultures by lysing the cells with bead beating and then capturing the released RNA with the RNAexpress^{TM} column, after which the isolated RNA was analyzed with qPCR (Parra et al., 2017). The current methods are a tremendous advancement for space genomics because they allow for a complete sample-to-analysis process aboard the ISS, but they also have drawbacks. These techniques are manual and take up crew time, are not high throughput, and are better suited for pure cultures rather than complex, mixed microbial communities, as they are not efficient for low biomass samples and the nucleic acids are not pure due to the leftover cell debris. To address these limitations, the "Omics in Space" team developed μTitan (simulated micro(μ) gravity **t**ested **i**ns**t**rument for **a**utomated **n**ucleic acid extraction), an automated sample processing system, that is microgravity compatible, and can process multiple complex samples simultaneously in an easy to use streamlined manner. Although there are automated sample processing devices commercially available for use on the ground to process multiple samples simultaneously (e.g., Maxwell^{TM} 16; Promega, Madison, MI), these instruments are not microgravity compatible nor are they lightweight and compact.

The objectives of this study were two-fold; (i) to develop an automated nucleic acid extraction device that would be microgravity compatible and thus could be used on the ISS, and (ii) to validate system performance of this device (i.e., μTitan) using a whole cell microbial reference (WCMR) standard and to compare this performance against the commercially available, widely used, automated nucleic extraction system, Maxwell^{TM}. The sensitivity and selectivity of the μTitan system and how it compared to the Maxwell^{TM} system was assessed by Qubit (for DNA yield), qPCR (for 16S rRNA gene copy numbers) and the Bioanalyzer (for extracted DNA length). In addition, shotgun metagenomics sequencing was performed on two platforms, Illumina MiSeq and Oxford Nanopore MinION in order to assess the ability to produce reliable sequencing data, in terms of diversity and relative proportions of the bacteria present in the WCMR.

MATERIALS AND METHODS

Preparing the Whole Cell Microbial Reference Standard

The whole cell microbial reference (WCMR) standard used to validate the μTitan system consists of nine bacteria, five of which are Gram positive and four of which are Gram negative. The strains used, their amounts, and other metadata are listed in **Table 1**. The WCMR was produced as part of the Association of Biomolecular Resource Facilities (ABRF) metagenomics research group (Tighe et al., 2017). Briefly, individual bacteria were cultured on either tryptic soy agar or marine 2216 agar until early log phase growth was achieved, followed by harvesting and resuspension in 1x phosphate buffered saline (PBS) without calcium or magnesium. The cell suspension was washed twice with 1x PBS followed by vortexing, to ensure that cells were in a unicellular suspension and not aggregated (confirmed by microscopy) before the fixation step with ethanol. Fixation was performed by adding 100% ethanol in a drop wise fashion while vortexing until the final concentration was between 90–95%. Cells were allowed to settle overnight, and the supernatant was discarded to remove any free-floating DNA. The final sample was resuspended in fresh 90% ethanol and stored at 4°C.

Enumeration of each individual ethanol fixed bacterial suspension was performed by diluting 1 μl of the suspension in 48 μl of 1X PBS and 1 μl of 0.1% sodium dodecyl sulfate. Staining was performed by adding 1 μl of Sytox staining reagent, 1 μl of SYBR green (2.5X), 1 μl of enhancer, and 7 μl of buffer (all reagents from Logos BioSystems, Seoul, S. Korea) to this dilution and incubating in the dark at room temperature for 5 min. Enumeration was performed by adding 4 μl of the stained cell preparation to a INCYTO counting slide (INCYTO C-Chip Hemocytometers, DHC-S025) and counted at 400x magnification using 485 nm/525 nm epifluorescent microscopy according to the manufacturer's protocol. Combining the individual bacterial preparation into one pool was based on a staggered design. Cell concentrations ranged from 10^4 to 10^6 cells/μl, depending on the organism (**Table 1**), resulting in a mixed microbial community containing 7.3×10^6 total cells/μl.

Before using the WCMR to validate the μTitan system, a controlled laboratory extraction of DNA was performed using a modified Qiagen procedure by first washing the cells in 1× PBS followed by enzymatic digestion of the cell walls with 20 μl of Metapolyzyme (MPZ) [stock concentration = 10μg/μl]

TABLE 1 | Metadata of the nine bacteria present in the whole cell microbial reference standard used for validation.

Organism	ATCC Number	Gram stain	Genome size (Mb)	Reference	Volume Combined	Cells/μl	SD
Staphylococcus epidermidis PCI 1200	12228	+	3.5	GCF_000007645.1_ASM764v1	200 μl	1.2×10^6	1.8×10^5
Pseudomonas fluorescens F113	13525	–	8.7	GCF_000237065.1_ASM23706v1	150 μl	7.9×10^5	1.1×10^5
Escherichia coli K-12 substr. MG1655	700926	–	5.6	GCF_000005845.2_ASM584v2	250 μl	9.9×10^5	1.4×10^5
Chromobacter violaceum NCTC 9757	12472	–	2.7	GCF_000007705.1_ASM770v1	100 μl	2.3×10^6	3.2×10^5
Micrococcus luteus NCTC 2665	4698	+	3.2	GCF_000023205.1_ASM2320v1	50 μl	5.6×10^5	9.5×10^4
Pseudoalteromonas haloplanktis TAC125	35231	–	4.0	GCF_000238355.1_Phal_1.0	300 μl	8.9×10^4	5.3×10^3
Bacillus subitilis subsp. subtilis str. 168	23857	+	5.8	GCF_000009045.1_ASM904v1	250 μl	8.3×10^5	1.7×10^5
Halobacillus halophilus DSM 2266	3567	+	5.6	GCF_000284515.1_ASM28451v1	250 μl	4.0×10^5	5.7×10^4
Entercoccus faecalis OG1RF	47077	+	3.6	GCF_000007785.1_ASM778v1	200 μl	8.9×10^4	3.8×10^4

(Millipore Sigma, St. Louis, MO, United States) at 35°C for 4 h, after which DNA extraction was completed using a QIAamp DNA Micro Kit (Qiagen 56304, Germantown, MD) with a pretreatment bead beating step (Matrix A beads MP biomedical 116910050CF) to increase lysis efficiency. Measurements from a Qubit spectrofluorometer indicated that 3.16 ng of DNA was obtained per 10^6 cells.

Overview of μTitan

The μTitan system is based on a fused deposition modeling 3D printer in which the motion and temperature controls have been repurposed for automated NA extraction, with the capability to perform both heated incubation and NA amplification (**Figures 1A,B**). The system is portable and robust and was able to perform extractions while being transported in the back of a sports utility vehicle (SUV) at highway speed (**Figure 1C**). The extraction efficiency of *Chlamydia trachomatis* DNA from urine samples using an early prototype was demonstrated to be comparable to the spin column method from Qiagen (Chan et al., 2016a). Extractions of RNA from the Zika virus in urine and saliva samples also proved to be successful (Chan et al., 2016b).

Mechanics of μTitan Designed for Use on the ISS

The current version of μTitan is 34×34×36 cm when encased with a cover. It weighs about 8 kg including the power adaptor. A laptop is currently used to operate the device, but the protocol program can be saved on a secure digital (SD) card if needed. A comparison between the Maxwell™ and the μTitan specifications are presented in **Table 2**.

Individually enclosed environments for sample extraction are typically used to prevent cross-contamination. This is essential in the ISS environment to avoid the unintentional release of extraction reagents and potentially harmful microbes. Currently, μTitan uses aluminum-foil-sealed, pre-filled reagent strips placed inside a strip holder that can be closed after sample input (**Figure 1D**). Using this approach, magnetic coupling can be used to perform extraction with multiple mounted cartridges. The operation of the coupling mechanism is similar to that of a magnetic fish tank cleaner, where the motion of NA extraction can be controlled inside the cartridge without direct contact from outside. **Figure 2A** shows the basic set-up where an 8-well reagent strip is placed inside an enclosure to become a cartridge. The mechanical movements inside each individual cartridge are enabled by a unique magnetic coupling approach (**Figures 2B,C**). These figures show how nucleic acid extraction is performed by the stepper motors that are programmed to automatically control the movement of the external magnets, which in turn drive the movement of the components inside the cartridge. The "driver magnets" outside of the cartridge precisely control the movement of "follower magnets" within the cartridge to process nucleic extraction and elution. The two sets of magnetic particles (MPs) are held together by the magnetic field that penetrates through the cartridge's plastic wall. Synchronized motions of the magnetic tip-combs enable reproducible and controllable action inside each cartridge, including MP mixing. **Figure 2D** shows the process of effective mixing and washing of MPs. These external "driver magnets" allow for precise positioning of the "MP manipulating tip" located inside the cartridge. The bottom pair of magnets below the wells leads to release and capture of the MPs by this tip, allowing the MPs to move throughout the wash buffer, allowing for effective mixing and washing of these MPs. Under normal gravity, the magnet inside the tip falls back down when the bottom repelling magnet is removed (**Figure 3A**), but this is not the case in reduced gravity as the magnet inside the tip will just remain "floating" inside (**Figure 3B**). For the microgravity adapted machine, a set of opposing field magnets was installed to pull the extraction tip magnet down (**Figure 2D**). These innovative steps allow the elimination of pipetting in space under microgravity, which is difficult, laborious, and often results in mishandling.

DNA Extraction Using μTitan and Maxwell™

Pre-processing

One milliliter of the WCMR was pre-processed by incubating with 48 μl of 10 μg/μl MPZ for 15 min at 35°C, followed by 15 s of bead beating with Matrix Lysing E bead beating tubes (Mp Biomedicals) using a battery-powered oscillating power tool (Ryobi JobPLUS ONE 18V multi tool with P246 console & P570 Head attachment). The sample tube was placed and fixed tightly on the flat end of the blade using blue painters' tape. In YNP, the WCMR was first subjected to bead beating (as above), then incubated with 25 μl MPZ for 1 h at 37°C, followed by another

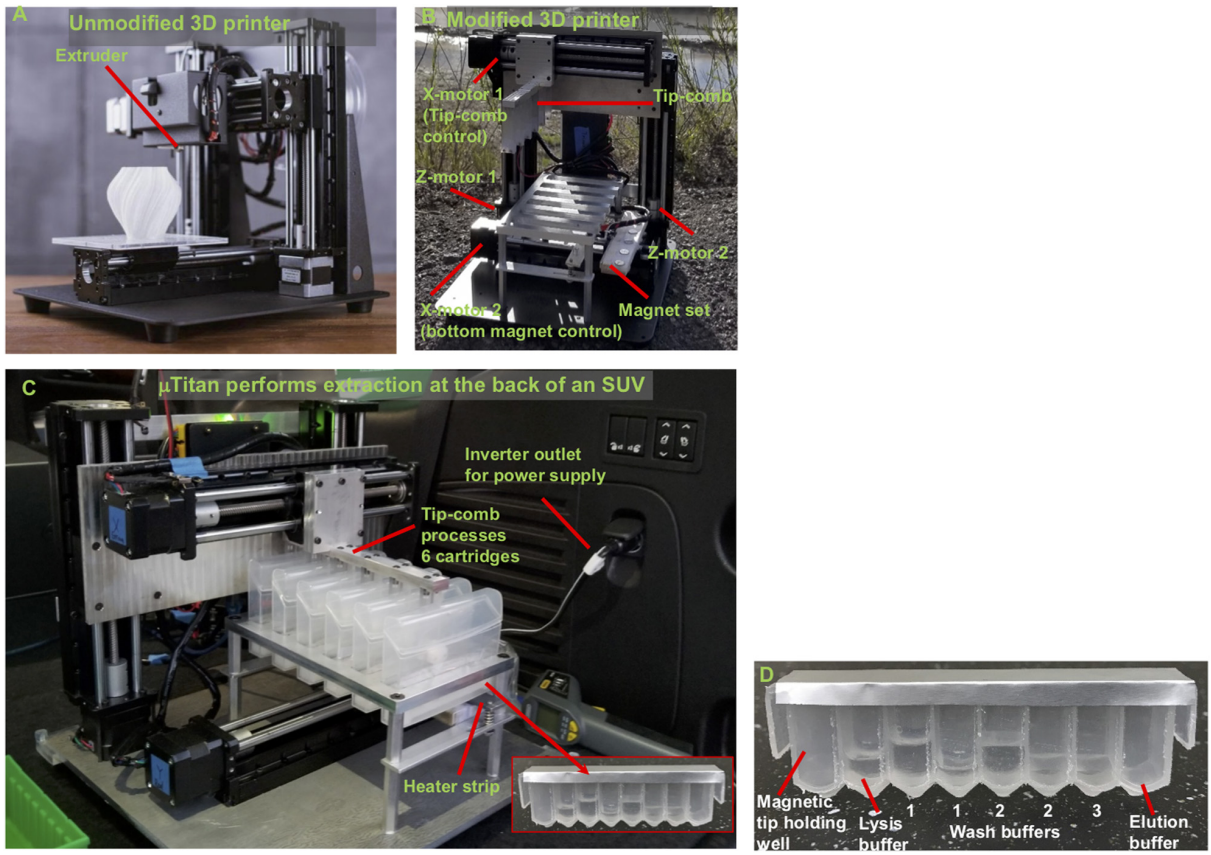

FIGURE 1 | Concept of converting a low-cost 3D printer to perform rapid and automated NA isolation. **(A)** A typical FMD type 3D printer. **(B)** A 3D printer turned extraction device. The extruder of a 3D printer was removed to allow the adaptors to be mounted. The magnetic particle processing tip-comb (tip-comb) was attached on the mount. Its vertical and lateral movements are controlled by two Z-motors and one upper X-motor controls. Another X-motor control below the extraction cartridges enable resuspension of magnetic particles for NA binding and washing (see description later). The tip-comb has 6 fingers with each finger has magnets to use magnetic coupling to externally control the extraction tips inside an extraction cartridge to perform extraction. There is no direct contact between the magnets, the samples, and MPs. Six samples can be processed simultaneously under the same protocol program. The heated strip under the elution wells uses the 3D printer's extruder heater and thermistor to provide precise temperature control for heated NA elution. **(C)** μTitan placed inside the cargo area of an SUV. **(D)** A reagent strip that has been pre-filled with the appropriate extraction reagents.

round of bead beating. Next, 100 μl of the pre-processed sample was added to either the Maxwell™ or μTitan system. The high biomass samples (Tx_Max_High, Tx_μT_High, YNP_μT_High) correspond to an approximate input of 10^7 cells, while the low biomass samples (Tx_Max_Low, Tx_μT_Low) correspond to an approximate input of 10^4 cells. The "medium" biomass samples (YNP_μT_Med) corresponds to an approximate input of 10^6 cells.

TABLE 2 | Specifications of the μTitan and Maxwell™ systems evaluated in this study.

	Maxwell™	μTitan
# samples run simultaneously	16	6
Dimensions (W × D × H)	33 × 44 × 33 cm	34 × 34 × 36 cm
Weight	18.9 kg	8.0 kg
Typical protocol duration	37–40 min	10–20 min
Enclosed cartridge	No	Yes
Heated elution	Yes	Yes
Programmable protocols	Yes	Yes
Power requirements	100–240VAC, 50–60Hz, 2.1A	Power adaptor: 100–240VAC,50–60Hz, 1.8A Output to 12V and 10A

μTitan Extraction

A commercially available magnetic particle–based NA isolation kit (NucliSENS Magnetic Particle Extraction Kit, bioMerieux, Durham, NC) was purchased, and the reagents from this kit were used to pre-fill the μTitan cartridges. These reagents included lysis buffer, magnetic particle solution, wash buffer #1, wash buffer #2, wash buffer #3, and elution buffer. The μTitan extraction protocol (e.g., volume, time of incubation, and number of repeated washing steps) is as follows: 100 μL of the pre-processed sample was added to the second well of a μTitan cartridge containing 400 μL of lysis buffer and incubated for 10 min. Eight microliters of NucliSENS magnetic particles, for

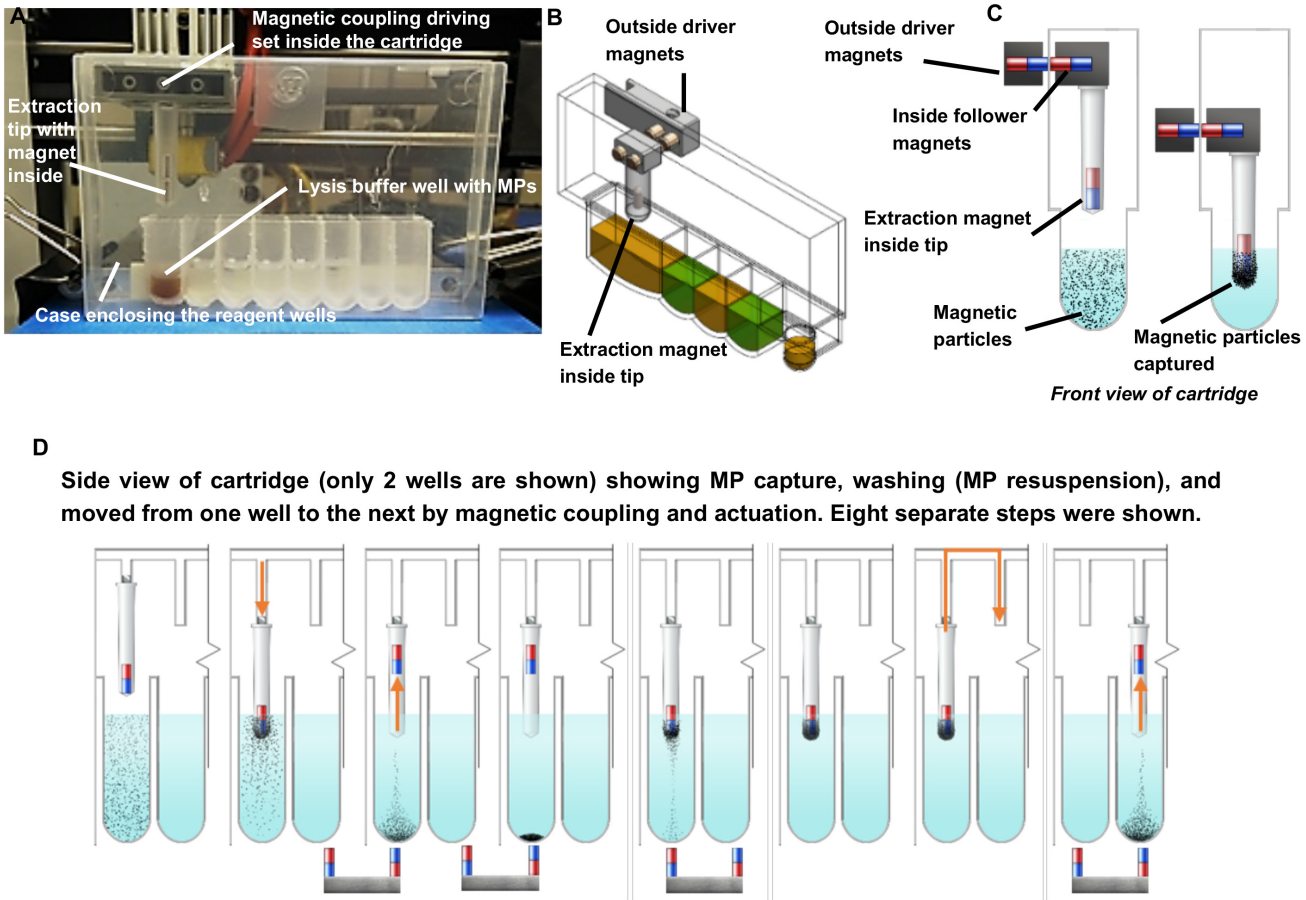

FIGURE 2 | Extraction cartridge, magnetic coupling, and schematic of sample extraction. **(A–C)** External magnetic control and movement of sample by magnetic particles outside of extraction cartridge. **(D)** Detailed overview of magnetic handling, washing, and elution of NAs within the μTitan cartridge. The magnetic tip can move freely on the wall of the cartridge as actuated by the driver and follower magnets. The placement and the polarity of the magnets inside the extraction tip and those underneath the wells enable mixing and washing.

capturing NAs, were then added to the lysed sample solution in the second well. The magnetic particles were intermittently mixed for 10 min, allowing for NA to bind to the MPs. The cartridge was then secured on the μTitan system. An extraction tip mounted on the follower magnet set was placed on the first well of the cartridge. Wells # 3–7 contained wash buffer # 1 (600 μL and 250 μL), wash buffer # 2 (600 μL and 250 μL), and wash buffer # 3 (250 μL). Well # 8 contained an elution buffer (60 μL). Each pre-processed sample was run in triplicate. To ensure the quality of the work and to check for contamination, molecular-grade water was used for extraction during each run of the machine, instead of sample, and is considered the machine control ("Tx_μT_CTL" or "YNP_μT_CTL").

The μTitan system was operated using a laptop computer (connected with a USB cable), loaded with an open-source software called Repetier-Host (Hot-World GmbH & Co., Willich, Germany) that uses G-code based programming commonly used for 3D printing and CNC milling. The G-code written by AI Biosciences for μTitan, was based on that written for a standard 3D printer, which provides instructions on the movement, temperature, and amount of material to be deposited. Since this is pre-programmed, a user just needs to click on the "print" button icon to start the automated extraction process.

Once the program started, the extraction tip comb (driver) magnet picked up the extraction tip magnet inside the cartridge box using a magnetic coupling mechanism and moved it to the subsequent wells of the cartridge. The NA bound magnetic particles attached to the base of the extraction tip were then washed sequentially in wash buffer # 1 and # 2, twice for 2 min each, and wash buffer # 3 for 30 s. Next, the magnetic particles were air-dried for 4 min. When the air-drying process began, the heater strip at the bottom of the elution well of the cartridge was heated to bring the elution buffer temperature to ∼70°C by a cartridge heater commonly used as the extruder of a 3D printer. This extruder heater's function was also controlled by the program, and the temperature was precisely monitored with a thermistor. The NAs captured on the magnetic particles were eluted for 5 min in 60 μL of elution buffer. After elution, the magnetic particles were captured again by the extraction tip and moved back to well # 1, leaving only the eluate in the elution

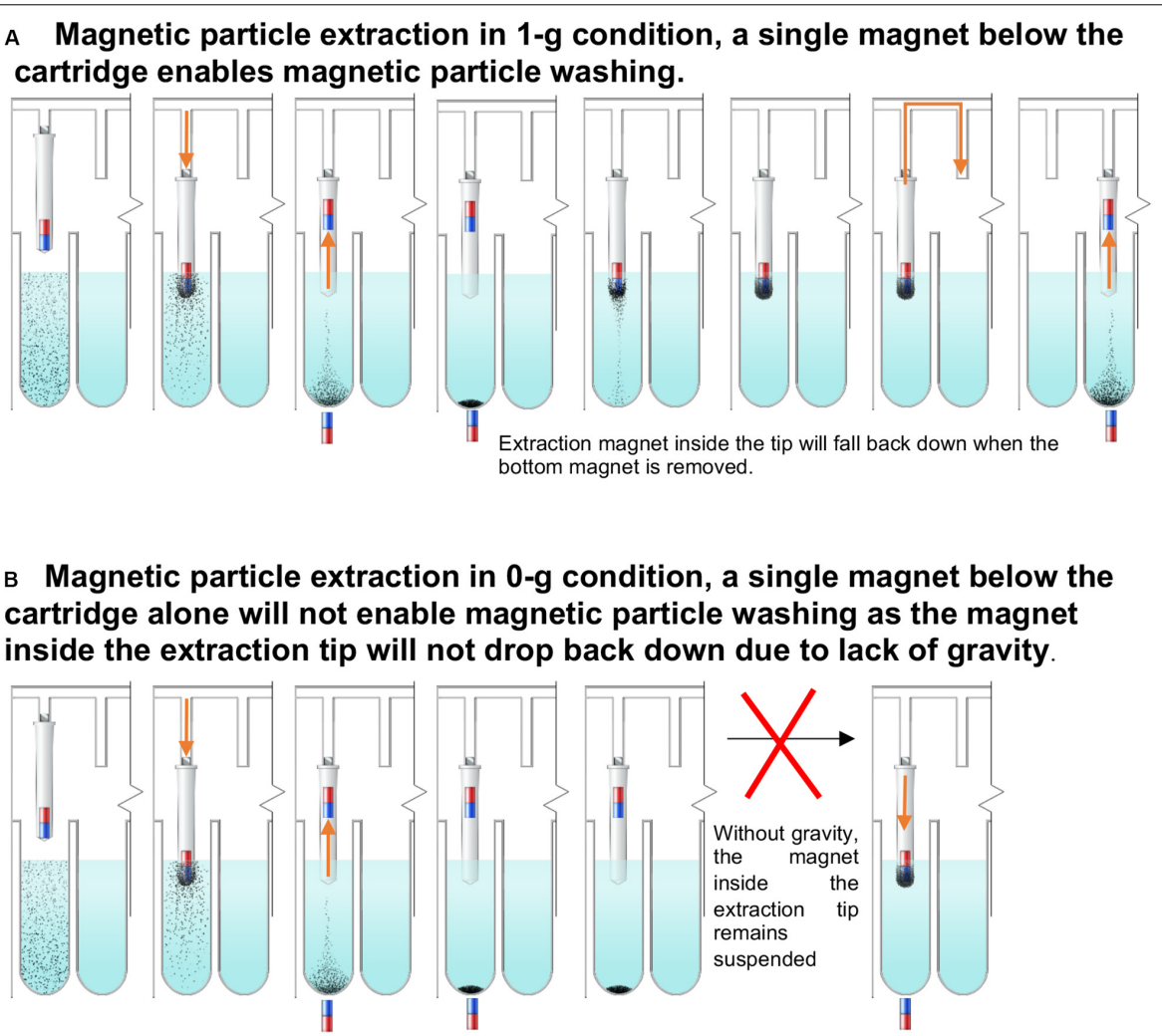

FIGURE 3 | The μTitan cartridge at 1g vs reduced gravity. **(A)** Magnetic particle extraction in 1-g condition. Magnet inside of the extraction tip will fall back down to the bottom of the tip after the magnet with opposite polarity is removed. **(B)** In reduced gravity, the repelled extraction tip will remain afloat even after the bottom magnet is removed. Therefore, the paired-magnets mentioned in Figure SW3D were used.

well (well # 8). The eluate was collected and stored in a 500 μL tube for future analysis. The μTitan system has the capability of processing 6 samples in parallel.

Maxwell™ Processing

Parallel extractions of the pre-processed samples were carried out on the Maxwell™ automated extraction system (Promega Corporation, Madison, WI, United States) using a DNA kit (AS1520) and the "Maxwell™ RSC blood DNA" run program. Briefly, 100 μL of the preprocessed samples were added to the cartridge and placed on the cartridge holder tray, and the DNA was eluted in 60 μL of elution buffer. Each pre-processed sample was run in triplicate. To ensure the quality of the work and to check for contamination, molecular-grade water was used for extraction during each run of the machine, instead of sample, and is considered the machine control ("Tx_Max_CTL"). The purified DNA from both machines was stored at −20°C until further analysis.

Qubit Quantification and Quantitative PCR (qPCR)

Samples were quantified using two methods: the Q32854 Qubit™ dsDNA HS Assay (ThermoFisher, Waltham, MA, United States) and qPCR using a standard curve SYBR green method using two control DNA standards. Qubit assay was performed using a 2 μl aliquot of DNA mixed with 198 μl of the dsDNA HS reagent and read on a Qubit 4 spectrofluorometer.

qPCR was performed on replicate 1 μl samples of 1:10 dilution of test DNA using the PerfeCTa SYBR Green SuperMix (95054 Quanta Bio, Beverly, MA, United States) using primers recommended by the Earth Microbiome Project -515 Forward GTGYCAGCMGCCGCGGTAA (Parada et al., 2016) and 806 Reverse GGACTACNVGGGTWTCTAAT (Walters et al., 2016).

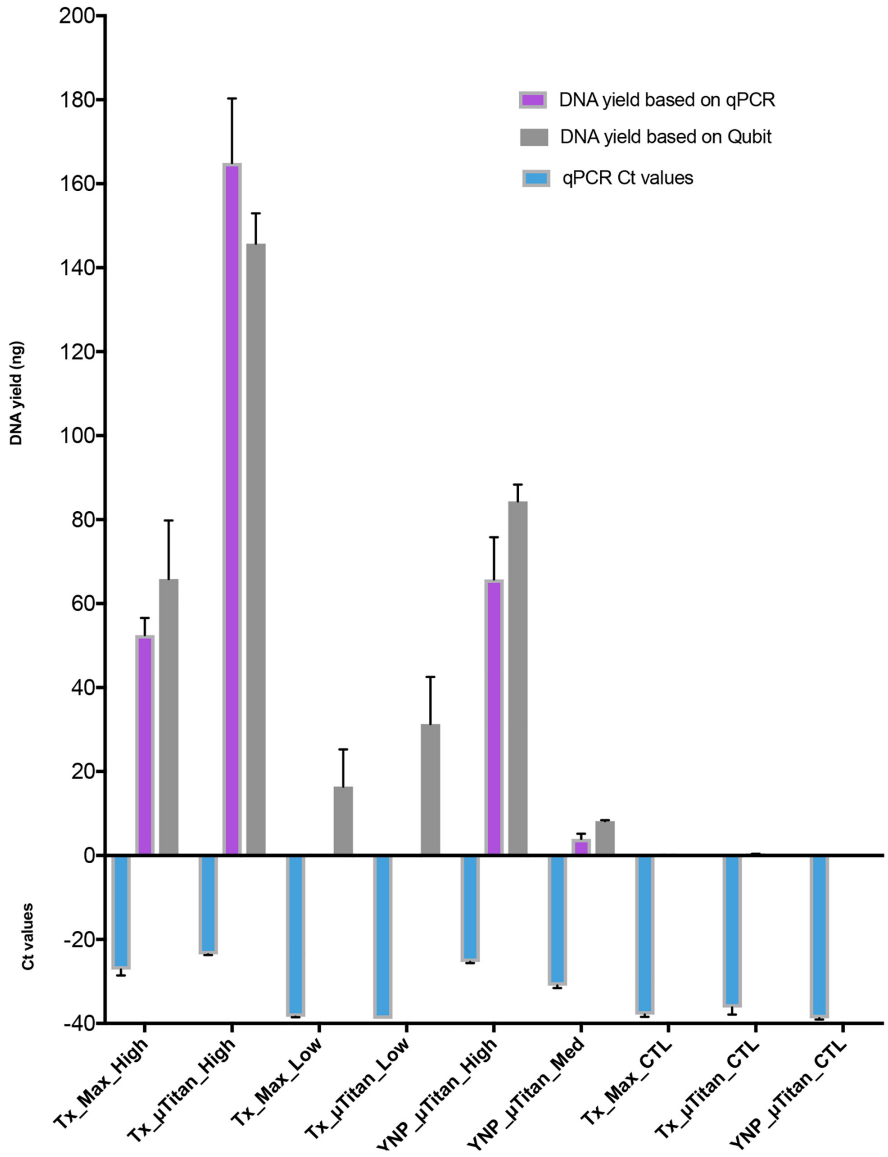

FIGURE 4 | DNA quantification of the extracted WCMR. DNA extraction of the WCMR was performed by both Maxwell™ and μTitan systems in the lab of AI Biosciences (Texas; "Tx") or in the field by μTitan (Yellowstone National Park; "YNP"). The qPCR Ct values are shown by the blue bars. Known amounts of WCMR DNA, extracted by Qiagen, was used to generate a standard curve during qPCR, by which DNA yield in ng could be calculated (purple bars). NB: The lower the Ct value, the higher the amount of DNA in that sample. The DNA yield was also measured by Qubit (gray bars). Different amounts of biomass; high, medium, or low were extracted with both Maxwell™ and μTitan systems. High biomass samples represent inputs of approximately 10^7 cells, low approximately 10^4, and medium approximately 10^6. As can be observed, the μTitan system generated higher DNA yield than the Maxwell™ system for both high and low biomass samples. Also, the μTitan system in the field produced comparable results to that obtained in the lab (YNP_μT_High vs Tx_μT_High).

Standard curves were generated from two separate microbial reference control DNA, including (1) purified genomic DNA (gDNA) from the WCMR that had been extracted with Qiagen and (2) The ABRF/ATCC® MSA-3001 gDNA (ATCC, Manassas, VA). Both standard curves were generated from 2, 0.2, 0.02, 0.002, and 0.0002 ng/μl of DNA. qPCR thermocycling was performed in 25 μl reactions on an ABI 7900HT (Applied Biosystems, Foster City, CA, United States) using the following three-step program: Denatured at 95°C -3 min, 40 cycles of PCR (95°C -15 s| 54°C-60 s| 72°C -60 s), followed by a standard dissociation curve (95°C-15s| 60°C-15s| 95°C-15s). Primers were included at a final concentration of 0.1 μM and low ROX as an internal reference.

DNA Molecular Weight Analysis (Fragment Length) Using Bioanalyzer

DNA fragment size analysis (molecular weight) of the extracted DNA was evaluated using the Agilent Bioanalyzer 2100 with the High Sensitivity DNA chip (5067-4627) and the Advanced Analytical Technologies Fragment Analyzer 5200 with the HS

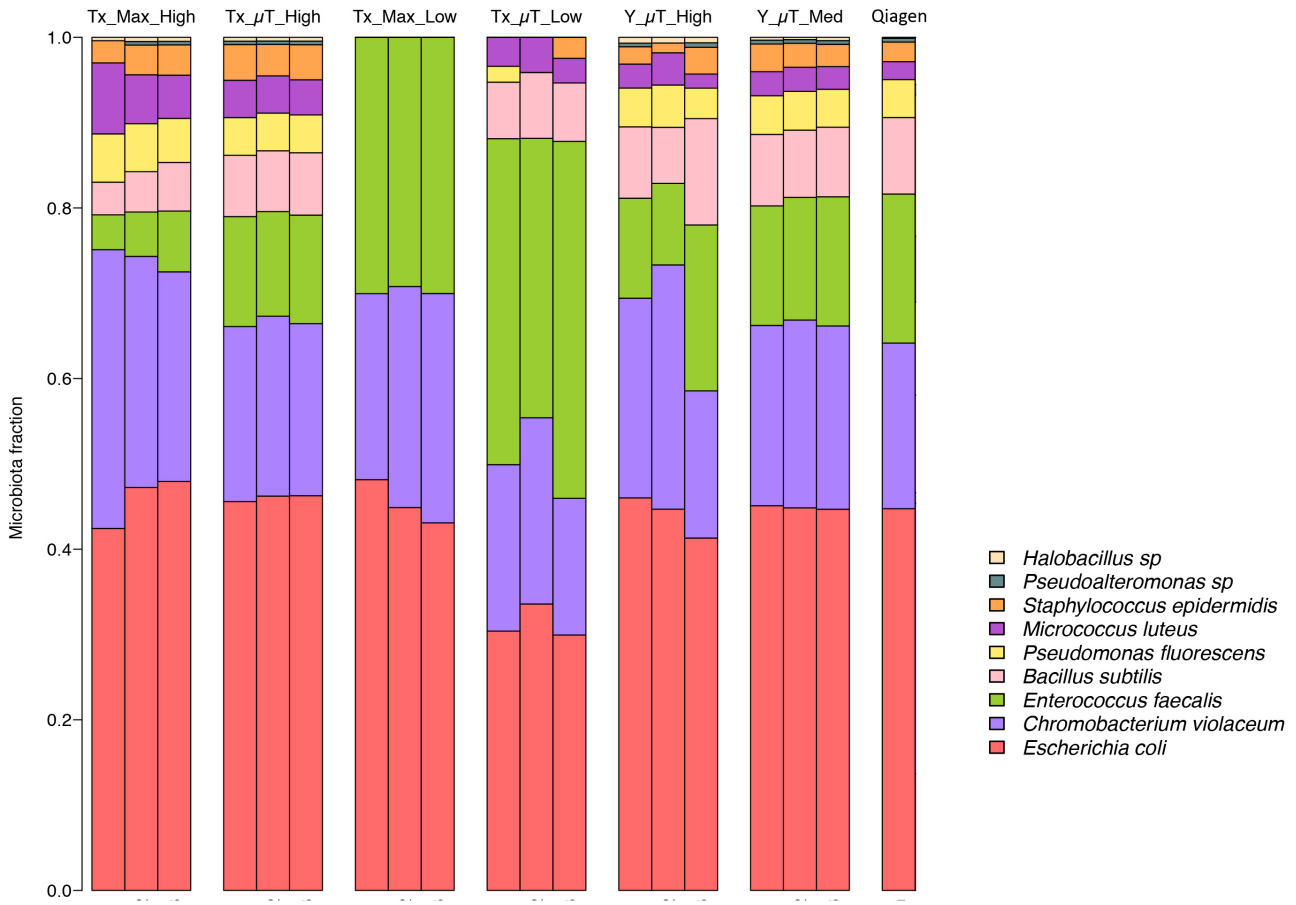

FIGURE 5 | Relative abundances of the nine bacteria present in the WCMR. The WCMR DNA that was extracted by the Maxwell™ and μTitan systems was sequenced on the Illumina HiSeq platform, and the relative abundances of the nine bacteria present in the WCMR shown in this bar graph. Each bar represents a sample, and each colored box represents the proportion of a particular organism in that sample. For comparison, the WCMR was also manually extracted with Qiagen, sequenced, and plotted. The high and medium biomass samples were able to detect all nine organisms, in the same relative abundances, which was also comparable to that observed with Qiagen extraction. The low biomass samples did not detect all bacteria in the WCMR standard, but the μTitan system detected more than the Maxwell™. A complete list of the bacteria detected and their counts are summarized in **Table 3**.

Large Fragment 50kb Kit (DNF-493-0500) according to the manufacturer's instructions.

Illumina Sequencing

Library Preparation

Whole genome shotgun sequencing libraries were synthesized using Nextera XT reagents (Illumina Corp, San Diego, CA, United States) from either 3 ng of total DNA for samples > 0.5 ng/μl or 6 μl input for samples below 0.4 ng/μl. Final libraries were assessed for quality using the Qubit™ dsDNA HS Assay and Agilent Bioanalyzer 2100 assessment using the DNA high sensitivity chip (5067-4626 Agilent Corp., Santa Clara, CA, United States). All samples, including positive and negative controls, were pooled by combining the high input (>0.5 ng/μl), using 2.5 ng of library, with the low input, using 0.25 μl, to prevent over representation of low input samples. Pooled hybridization cocktails were clustered and sequenced using a rapid run SR flow cell (GD-402-4002) for 150 bases on the Illumina HiSeq 1500.

Metagenome Sequence Data Processing

Adapter sequences and low-quality reads (Phred score < 20 across the entire length of the read) were removed with Trimmomatic and reads that were shorter than 80 bp after quality control trimming were discarded. Post-processing resulted in 53,549,976 high-quality reads. DIAMOND (Buchfink et al., 2015) and the weighted lowest common ancestor (LCA) algorithm of MEGAN6 (Huson et al., 2007) (Settings of minScore = 50, maxExpected = 0.01, topPercent = 10, and minSupportPercent = 0.01) was used to cluster high-quality filtered reads to taxonomic and functional levels. BLAST hits of ≥ 20 amino acids and ≥ 90% similarity were collected and used for taxonomic and functional assignment using the NCBI taxonomy database which contains over 6.6×10^5 reference sequences (Sayers et al., 2009), and NCBI-NR protein sequence database which consists of entries from GenPept, SwissProt, PIR, PDB, and RefSeq, were used with MEGAN6 (Huson et al., 2007) to perform the taxonomic and functional binning of the metagenomic reads.

Oxford Nanopore Sequencing

Oxford Nanopore libraries were synthesized for all samples from input ranges of BDL (below detection limit of the Qubit) up to 5 ng for higher input samples using the Rapid PCR barcoding kit (RPB004 Oxford Nanopore Technologies, Oxford, United Kingdom) with the following modifications: high input samples were amplified using the standard method of 14 PCR cycles, while samples that were below the detection limit of Qubit were amplified using 22 PCR cycles. Barcoded libraries were pooled equally at 1 fmol each for the high samples, while the BDL samples were pooled at the maximum volume allowable for library input. Sequencing was performed using the MK1B MinIon with 9.4 flow cell yielding > 1 million reads of 2 Gbases with average read lengths of 2–8 kb. All quality control statistics were within specification as outlined by Oxford Nanopore.

Microbial reference controls were also sequenced on the Oxford Nanopore sequencer, including the purified gDNA from the Qiagen Benchmark sample. Rapid PCR barcoded libraries were synthesized from input concentration identical to the qPCR standard curve at 6, 0.6, 0.06, 0.006 ng. This titration was performed to determine the detection limits, linearity, and efficiency for ultra-low input samples.

Oxford Nanopore data was analyzed using the WIMP (What's In My Pot) module of the EPI2ME software (Oxford Nanopore Technologies, Oxford, United Kingdom), and raw read count data was exported as CSV data for manual parsing and enumeration using Microsoft Excel.

Nanopore detection and sequencing of the low biomass samples revealed negligible concentrations above background. This is not surprising since the input concentrations were below the recommended input for the Rapid PCR barcoding kit. For these reasons, Nanopore data generated from low biomass samples were not included.

Data Analysis

The Illumina sequencing data was analyzed in R version 3.3.1 using the Hmisc, ggplot, compositions and cluster packages. For the PCA plot, the data was first center log ratio (clr) transformed and the Euclidian distances plotted. K-means clustering was used to determine the number of distinct groups and the samples that belonged to these groups.

DNA yield and qPCR graphs were generated in Prism version 7.0. Statistical analyses were executed using one-way analysis of variance (ANOVA) and then using the Benjamini- Hochberg false discovery rate (FDR) multiple test correction. Statistical significance was set at $P < 0.05$.

RESULTS

Testing and Validation of the μTitan System

A whole cell microbial reference standard, that contained intact microbial cells (**Table 1**) was extracted using both μTitan and Maxwell™ instruments in a laboratory setting. High biomass (10^7 cells) and low biomass (10^4) cellular concentrations were

TABLE 3 | Illumina sequencing read counts of the bacterial species present in the whole cell microbial reference standard detected from the μTitan and Maxwell™ systems in both a laboratory and field setting.

Microbial taxa	# sequences retrieved with high biomass samples in a lab (Texas)						# sequences retrieved with low biomass samples in a lab (Texas)						# sequences retrieved with high and medium biomass samples processed with μTitan in the field (YNP)					
	Maxwell™ (Tx_Max_High)			μTitan (Tx_μT_High)			Maxwell™ (Tx_Max_Low)			μTitan (Tx_μT_low)			YNP_μT_High			YNP_μT_Medium		
	rep 1	rep2	rep3	rep1	rep2	rep3	rep1	rep2	rep3	rep1	rep2	rep3	rep1	rep2	rep3	rep1	rep2	rep3
Escherichia coli	2,88,592	3,17,753	3,26,481	2,81,112	2,79,525	2,73,380	1,027	421	561	1,955	1,310	2,171	3,18,603	3,34,962	3,61,581	2,42,269	2,50,667	2,70,935
Chromobacterium violaceum	2,22,242	1,82,297	1,67,347	1,26,575	1,27,509	1,19,165	465	243	350	1,255	852	1,162	1,49,285	1,64,426	1,73,854	1,23,261	1,60,574	1,13,173
Enterococcus faecalis	27,762	34,981	48,527	79,526	74,161	75,180	641	274	391	2,458	1,278	3,034	99,057	1,07,369	1,22,557	61,701	53,609	1,27,570
Bacillus subtilis	26,060	31,835	38,835	44,318	43,126	43,181	–	–	–	426	301	496	59,178	58,916	66,009	44,056	36,867	81,776
Pseudomonas fluorescens	38,503	37,911	35,184	27,282	26,703	26,217	–	–	–	120	–	–	32,041	33,889	35,996	23,954	27,818	23,405
Micrococcus luteus	56,593	38,511	34,463	26,957	26,382	24,319	–	–	–	218	161	210	19,898	21,191	21,476	14,784	21,192	10,843
Staphylococcus epidermidis	17,675	23,449	24,162	25,813	22,314	24,302	–	–	–	–	–	178	22,921	20,992	21,141	10,689	6,422	20,576
Pseudoalteromonas sp.	–	2,793	2,873	2,474	2,399	2,500	–	–	–	–	–	–	3,227	3,213	3,503	2,234	–	3,492
Halobacillus sp.	2706	3298	3182	2775	2621	2618	–	–	–	–	–	–	3590	3754	4177	2341	1966	3132

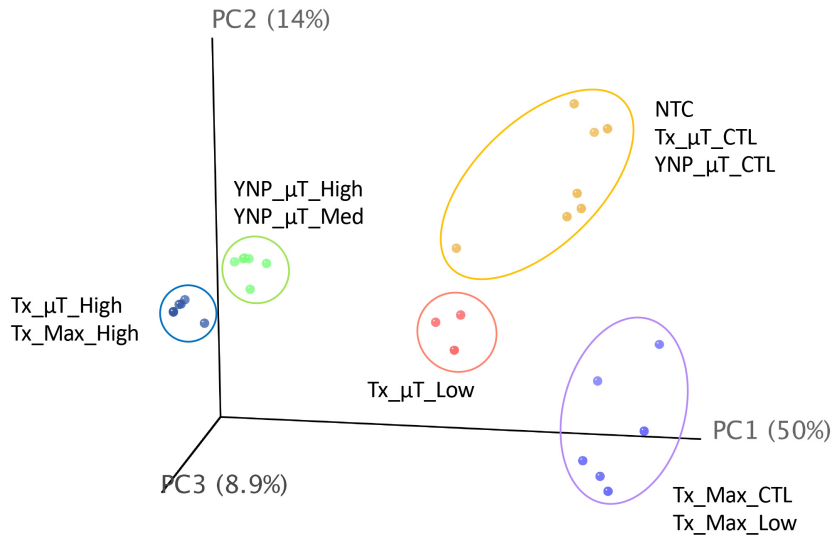

FIGURE 6 | Principal coordinate analysis of shotgun metagenomic sequencing data generated from the Illumina platform. Results for each sample were plotted on a 3-D, 3-axis plane, representing 73% of the variation observed amongst all samples. Each point represents a sample, and the closer a sample is to another, the more similar their microbiome composition (diversity and abundance). There were 5 distinct groups in this dataset, represented by the colored ellipses, which were determined by unsupervised k-means clustering.

used in the validation tests. WCMR standard was extracted using both the μTitan and Maxwell™ instruments in a laboratory setting. The composition of the WCMR (**Table 1**) contains fully intact microbial cells of Gram +/−, high and low GC, and a range of morphologies. Two cellular concentrations were used in the extraction tests of the two instruments representing high biomass (10^7 cells) and low biomass (10^4 cells) inputs and subject to pretreatment with a cell wall digesting enzyme mix (Metapolyenzyme) and mechanical bead beating. After pretreatment, replicate 100 μl aliquots were used as inputs to both instruments. Following extraction, the yield of recovered DNA was determined using a Qubit spectrofluorometer and qPCR (**Figure 4**). These results indicate that the μTitan system produced higher DNA yields, with both the high biomass ("Tx_x_High") and low biomass ("Tx_x_Low") samples; however, only the high cellular concentrations were statistically different.

Shotgun metagenomic sequencing was performed on all samples using the Illumina HiSeq 2500 platform to determine whether the isolated DNA could be used to prepare successful sequencing libraries and obtain high-quality sequencing results. **Table 3** shows the WCMR members detected in each sample from both extraction instruments and their respective counts. The bar graph in **Figure 5** shows the proportion of these nine bacteria in each sample and also includes the proportion of bacteria detected when a manual Qiagen QIAquick extraction (Qiagen Benchmarking Control) was performed in the lab with high efficiency pre-processing steps added. Both **Table 3** and **Figure 5** show that DNA from all nine bacteria could be isolated from the high biomass samples extracted with either the μTitan ("Tx_μT_High") or the Maxwell™ instrument ("Tx_Max_High"). For the low biomass samples, the μTitan system had increased performance over the Maxwell™ and from the DNA extracted, six out of nine bacteria were identified ("Tx_μT_Low"), while from the Maxwell™ extracted DNA, only three out of nine bacteria were identified ("Tx_Max_Low"). The proportions of identified bacteria in the high biomass samples were similar between the two instruments as well as for the Qiagen Benchmarking Control (**Figure 5**).

The μTitan system was further evaluated in a Phase II study at Yellowstone National Park (YNP) to test its performance in a remote setting with limited resources. The Maxwell™ system was not included in this field study due to its size, weight, power, and calibration requirements. In this phase of testing, two concentrations of the WCMR were used; a high biomass sample ("YNP_μT_High") similar to that used in the laboratory test ("Tx_μT_High") and a medium biomass sample composed of a 10-fold dilution of the high biomass sample ("YNP_μT_Med", 10^6 cells).

The resulting DNA yield for the high biomass sample, as measured by qPCR was comparable to the yield obtained in the laboratory tests ("Tx"), indicating the μTitan system is able to produce consistent results even when used in a remote setting (**Figure 4**). Results of the Illumina-based shotgun metagenomic sequencing were also consistent with the laboratory tests in that all nine bacteria in the WCMR were detected in both the high and medium biomass samples (**Table 3**), in the same proportions as that observed in the "Tx_μT_High" and Qiagen benchmark sample (**Figure 5**).

As is expected from any shotgun metagenomics sequencing run, there will be some measure of contaminant reads that come from extraction and sequencing processes (the "kitome"), and this dataset was no exception. The heatmap in **Supplementary Figure S1** shows the bacterial contaminants (i.e., any species that

TABLE 4 | Enumeration and detection of genera belonging to the whole cell microbial reference control using Oxford Nanopore Sequencing.

Microbial taxa	Number of reads for high biomass samples (Texas lab trials)						Number of reads for samples extracted using the μTitan in the remote field location (YNP)						Benchmark control: DNA extracted with Qiagen			
	Maxwell™ (Tx_Max_High)			μTitan (Tx_μ T_High)			YNP_μ T_High			YNP_μ T_Medium			Benchmark DNA Control DNA (ng Input)			
	rep 1	rep2	rep3	rep1	rep2	rep3	rep1	rep2	rep3	rep1	rep2	rep3	6.0	0.6	0.06	0.006
Escherichia	17454	16576	17,445	12,727	13,265	13,598	15442	14494	15710	18035	10155	18087	17420	10799	658	20
Chromobacterium	1998	1280	1,651	941	1510	1051	1085	1090	1447	1223	2501	1216	1618	1810	121	0
Enterococcus	918	1015	1,002	2766	3024	3063	2726	3339	2762	1370	2808	1378	2132	2991	142	11
Bacillus	4659	4883	5,148	5715	6989	5757	8440	8465	8138	8828	8942	8201	8823	8841	434	21
Pseudomonas	7428	4730	6,051	3068	4336	3470	3728	3545	4818	6861	6829	7543	7259	6770	585	35
Micrococcus	84	73	96	28	62	28	17	18	29	18	123	26	46	50	1	0
Staphylococcus	6555	10459	8,060	9891	9280	13032	5114	6098	5050	3289	5344	3727	2553	2843	173	11
Pseudoalteromonas	5850	6471	6,006	6401	6918	6694	9501	9123	8029	5880	7770	5304	6479	7745	350	19
Halobacillus	105	116	113	125	104	111	125	101	89	99	68	109	78	119	2	0

Data normalized to 50,000 reads for sample.

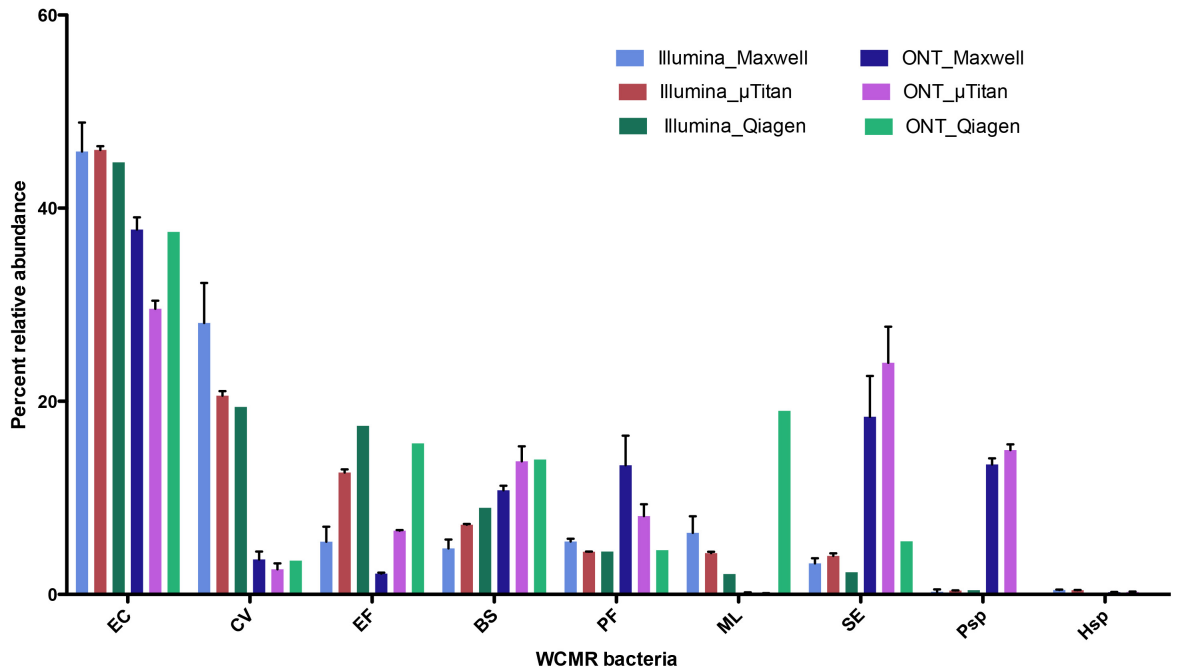

FIGURE 7 | Comparison of Illumina Nextera XT data to Oxford Nanopore Rapid PCR barcoding data. Percent abundance of the WCMR bacteria detected by either Illumina short read versus Oxford Nanopore long reads, from DNA isolated from either the Maxwell™ or μTitan system were compared with boxplots. The height of the box represents the average of triplicate DNA extractions from just the high biomass samples. The error bars represent the standard deviation. Generally, for high biomass samples, the μTitan system performs as well as the Maxwell™, and in this case, Illumina short reads worked better for certain genera (*Chromobacterium*, *Enterococcus*, and *Micrococcus*), while the Nanopore long reads worked better for others (*Pseudomonas*, *Pseudoaltomonas*, *Bacillus*, and *Staphylococcus*).

did not belong to one of the nine bacteria in the WCMR along with their counts) in all samples.

A PCA plot (**Figure 6**) comparing the diversity and relative abundances of the species present in the samples and controls (both WCMR bacteria and contaminants) showed that the high and medium biomass samples had similar microbiomes, regardless of whether they were extracted with the μTitan system (green points) or with the Maxwell™ instrument (blue points), and were distinct from the kitomes and machine controls. With the low biomass samples, the μTitan samples (Tx_μT_Low, pink points) were distinct from their respective controls, but this was not the case with the Maxwell™ samples (Tx_Max_Low, purple points), which were indistinguishable from their respective controls. Additionally, the PCA plot

TABLE 5 | Fragment length and molecular weight results for instrument extracted samples and reference DNAs using the Agilent Bioanalyzer 2100.

DNA Orgin	Replicate	Range (MW)		Mean	Average		
		Low	High		Low	High	Mean
Tx_Max_H	1	527	19642	5484			
	2	580	15785	5817	581	17324	5604
	3	636	16544	5511			
Tx_μT_H	1	510	20213	6337			
	2	543	27570	6463	534	24126	6405
	3	550	24595	6415			
YNP_μT_H	1	200	23683	6683			
	2	527	29271	6977	498	25187	6845
	3	766	22608	6876			
YNP_μT_Medium	1	1035	22040	9412			
	2	1142	19653	9058	1060	23274	9341
	3	1003	28131	9554			
Qiagen extracted WCMR	1	191	41703	8025			
	2	312	34104	7924	234	34924	7912
	3	200	28965	7788			

indicates that replicate extractions with the μTitan system were consistent and produced comparable results (replicates group together on the plot). More importantly, the plot shows that the field-operated μTitan system (YNP_μT_High) and lab-operated system (Tx_μT_High) produced similar results.

In addition to the Illumina HiSeq data, shotgun sequencing was also performed on the high and medium biomass samples using Oxford Nanopore Technologies' MinIon MK1B. The importance of including Nanopore data in this study was to provide an alternative sequencing technique that would avoid any Illumina Nextera short-read sequencing biases due to GC content, to enable detection using long reads with an alternative library synthesis that may influence taxonomic classification due to genome complexity and long genomic repeats (e.g., *Pseudoaltermonas*), and to determine how DNA extracted from μTitan would sequence on the MinION MK1B as this is the sequencing platform that is currently being used on the ISS and in the field. Although read depth, read length, and Q-Score are different between Nanopore and Illumina sequencing technologies, the organisms belonging to the WCMR were just as easily detected and classified with the MinION using DNA isolated from both the Maxwell^{TM} and μTitan systems, in both the laboratory and field settings. Tabulation of organisms in each sample belonging to the WCMR was represented at the Genus level on raw data normalized to 50,000 reads to allow for direct comparison between samples (**Table 4**). These results indicate that, when compared to the Maxwell^{TM} instrument, the μTitan system generated a marginally greater number of reads of *Staphylococcus* and *Bacillus*, and an even greater number of *Enterococcus*, all of which are Gram-positive bacteria. On the other hand, more reads were observed by the Maxwell^{TM} instrument for the Gram-negative bacteria, *Escherichia* and *Pseudomonas*. These trends observed with the Nanopore data are consistent with that observed with the Illumina data.

The proportions of the WCMR were compared between Illumina and Nanopore data for the purpose of detecting any bias inherent to the sequencing method (**Figure 7**). These data indicates that Illumina short-read sequencing using Nextera XT libraries has increased ratios of detection for *Chromobacterium*, *Enterococcus*, and *Micrococcus*, while the Oxford Nanopore rapid PCR data has an increase detection ratio for *Pseudomonas*, *Pseudoalteromonas*, *Bacillus*, and *Staphylococcus*.

The extracted DNA from the high and medium biomass samples were also analyzed using an Agilent Bioanalyzer 2100 to determine the DNA fragment length. For both the Maxwell^{TM} and μTitan instruments, the fragment length amongst the replicates were very consistent, with the μTitan system producing slightly larger DNA fragments (average length: 6,625 bp) compared to the Maxwell^{TM} system (average length: 5,604 bp). These results were confirmed with a subsequent analysis using a high-sensitivity assay with the Advanced Analytical Fragment Analyzer 5200 (data not shown), which was closer to the fragment length obtained by using a Qiagen Benchmark control manual extraction (average length: 7,912 bp) (**Table 5**; **Supplementary Figure S2**).

Microgravity Compatibility Testing of the μTitan System

While the μTitan cartridges used in these experiments were not designed for microgravity compatibility, the newest set of cartridges have been designed to exploit surface tension properties to prevent the unwanted release of fluids (Weislogel et al., 2009, 2011). These cartridges accommodate fluids and a magnetic probe and allow the fluids to preferentially remain at the base of the cartridge well, discouraging wetting of the upper portion of the well, thus preventing liquids from floating free when used in microgravity (Weislogel et al., 2009, 2011). The microgravity fluid physics behind this design comes from

the same team who engineered the "space cup" in 2015, which allowed astronauts on the ISS to drink hot espresso from an open coffee cup for the first time (NASA, 2015). Several 2.1s drop tower tests have been performed on the μTitan system (used in the current study) and the newly designed cartridges, and during these low-gravity tests, the fluids remained at the bottom of the cartridge wells, as designed (**Supplementary Figure S3**), indicating its compatibility with use on the ISS.

DISCUSSION

This manuscript describes the development and validation of the μTitan system, a high-performance, automated, and programmable nucleic acid extraction platform designed for use in both microgravity and Earth-based assays. The system employs the use of magnetic beads, a probe, and specialized chemistry for the isolation of high-quality nucleic acids for downstream analyses such as qPCR and NGS. This has all been made possible by the low cost and high precision of consumer-level 3D printers (Coakley and Hurt, 2016).

The results of the present study have shown that the μTitan system can isolate high molecular weight DNA that can be used for qPCR and high-quality NGS libraries for both Illumina and Oxford Nanopore platforms regardless of the assay. The instrument run time could extract high-quality DNA from the WCMR in 20 min (μTitan) compared to 40 min (Maxwell^{TM}) with the comparative method used in this study. Additionally, the system produced higher DNA yields (Qubit and qPCR) and slightly higher molecule weight DNA fragments (Agilent Bioanalyzer) than the Maxwell^{TM} system. Both the Illumina and Nanopore sequencing platforms showed that the μTitan system is able to isolate DNA from Gram-positive organisms better than the Maxwell^{TM} system. The μTitan system also detected more WCMR bacterial species in the low biomass input and was also less influenced by processing and sequencing contaminants than the Maxwell^{TM} system. The potential for cross contamination when multiple samples are run simultaneously was also examined. Using both high biomass and low biomass samples as input and running them alongside negative control samples (i.e., water as the input), no evidence of carryover from sample to negative control was observed when tested with Qubit and qPCR (data not shown).

While great strides have been made by NASA in the past five years to allow for molecular biology to be performed on the ISS, with WetLab-2 (Parra et al., 2017), miniPCR^{TM} (Boguraev et al., 2017), Razor-EX (Cherie et al., 2013), and MinION (Castro-Wallace et al., 2017), there exists a need for an automated, multiple sample processing system for the ISS for downstream omics analyses. The development of the μTitan system, which can extract nucleic acids (and in the future, protein) from a variety of environmental (manuscript under preparation) and human (Chan et al., 2016a,c) samples now allows for the ability to provide end-to-end processing of biological samples from raw material to purified nucleic acids, all while in orbit. The advantage of the μTitan system over previous ISS studies that have used mechanical bead beating or thermal lysing to extract nucleic acids is that the μTitan system works for various sample types (i.e., environmental or human) of complex microbial communities, for both high biomass and low biomass input, and not only for high concentration of pure bacterial cultures, which the previous methods were tested on. The μTitan system is also automated and requires less crew time than previous protocols. The dedicated clean-up and washing steps allow for cell debris to be removed, leading to higher purity nucleic acids, allowing for better sensitivity for low biomass samples and overall better detection of the diversity within a sample. Most current automated systems on the market, as well a manual extraction kits suggest the inclusion of an optional bead beating step if the user so desires. In addition to bead beating our team also included the use of metapolyenzyme (MPZ), as it has been shown for even greater lysis efficiency than just bead beating alone. The reagents within the μTitan system would be able to extract DNA without bead beating and MPZ treatment but for low biomass samples, when one needs to extract as much DNA as possible, these additional lysis steps are important. An additional pre-processing module is being developed where enzymatic digestion and bead-beating will be performed which will be compatible for the μTitan system and will be in an enclosed system to prevent aerosols on the ISS. The μTitan system is useful for most the microorganisms but for hardy microorganisms such as spore-formers and actinobacteria, a pre-processing step is needed and thus has been included in the design, if needed.

NASA performs routine microbial monitoring on the ISS, but the culture-based methods that are currently used do not provide a comprehensive assessment of what microbes are actually present. For this reason, NASA is actively working toward increasing their monitoring capabilities by testing different *in situ* protocols for DNA extraction that can be used for downstream qPCR on the ISS (Cherie et al., 2013). The advantage of the μTitan system over the other methods currently being tested is that, unlike a minimum of 10^5 cells per μL that is needed to positively detect microorganisms, a μTitan output concentration of 200 cells/μl is able to be successfully analyzed by NGS and qPCR because of the chemical processes involved in the extraction workflow that increase DNA yield and purity. Furthermore, high-quality DNA from six samples can be obtained in 45 min, with only 15 min of crew time, allowing for high-throughput sample processing aboard the ISS as opposed to manual, laborious, and time-consuming pre-existing methods.

The ability to perform high-throughput sample processing onboard the ISS followed by NGS makes it possible for astronauts to know what microbes and their properties are in the environment, at any given time. This is significant when you consider that omics analyses on ISS samples (performed on Earth) have detected novel organisms and/or those with unique properties (Checinska Sielaff et al., 2017; Romsdahl et al., 2018, 2019; Singh et al., 2019; Urbaniak et al., 2019). Furthermore, many terrestrial species that have been sent from Earth to grow on the ISS have become more virulent and antibiotic resistant, and have formed more biofilms (Yamaguchi et al., 2014), all of which are properties that can affect the health of astronauts and the stability of the spacecraft. The μTitan system will also be instrumental for crew monitoring. Having the μTitan system on the ISS to process samples and generate data

provides the capability to immediately detect and measure several biomolecules related to the physiological and immunological effects of living in space. For example, viral presence during spaceflight is a useful *in vivo* biomarker of immunodeficiency in astronauts (Mehta et al., 2004; Pierson et al., 2005) and was recently demonstrated to positively correlate with immune alterations in astronauts after spaceflight (Mehta et al., 2013). The ability to quantify viral load in astronauts in space, in real time, will provide an efficient means to monitor immune function and to allow for proper countermeasures to be implemented, such as vaccination strategies, prophylactic antibiotics, or stress reduction therapies (Kiecolt-Glaser et al., 2010; Kiecolt-Glaser et al., 2014).

CONCLUSION

The μTitan instrument is a compact, portable, robust, energy-efficient device that allows for streamlined and consistent nucleic acid extractions that requires minimal human labor. It provides the ability to perform complex sample processing on the ISS to gain real-time information from environmental and human samples. While this study has validated the instrument for DNA isolation, it has been validated previously for successful extraction of RNA (Chan et al., 2016b) and thus can be used to process samples for microbiome, metagenome, transcriptome, and virome analyses on the ISS and possibility on other deep space missions. The characteristics that make it advantageous for space travel also make it suitable for remote settings here on Earth. Whether the μTitan system is used on the ISS or on Earth, it provides high-quality nucleic acid material for functional genomics, microbial monitoring, and detection of biological signatures related to human health and engineering systems.

DATA AVAILABILITY STATEMENT

The datasets presented in this study can be found in online repositories. The names of the repository/repositories and accession number(s) can be found in the article/**Supplementary Material**.

AUTHOR CONTRIBUTIONS

KV designed the concept and objectives of the study with all authors of the manuscript. CU wrote the manuscript, helped design the study, critically analyzed the data, generated all the figures and performed statistical analyses, wrote the R scripts to analyze the NGS data, and processed the WCMR at YNP. SW invented μTitan and performed all initial studies prior to this validation study, and processed the WCMR in Texas and in YNP. ST helped develop the WCMR; performed quality control on the WCMR before using it for validation studies; and performed NGS, qPCR, Qubit, and bioanalyzer analyses. AA performed initial validation of μTitan and processed the WCMR in Texas and YNP. BL, CP, and JW participated and performed experiments in Texas and YNP. JW and NS processed the raw Nanopore sequencing data and raw Illumina data and helped design the study. JW, BP, and DS obtained safety protocol for using scientific expeditions at YNP with appropriate science permit provided by the YNP and cleared by JPL, Permit #YELL-2019-SCI-5480. BP and DS participated in sample collections and processing in the YNP and also processing in the MSU lab. RJ carried out the microgravity compatibility study, and FK carried out crew procedure development of the μTitan system. All authors critically reviewed the manuscript.

FUNDING

This research was supported by the TRISH through Cooperative Agreement NNX16AO69A awarded to KV. W. M. Keck Foundation supported for DS and BP. The NASA postdoctoral fellowship supported part of CU time. Preliminary work of this research was supported by a NASA SBIR Contract (NNX17CP21P) awarded to SW. The funders had no role in the study design, data collection, and interpretation; the writing of the manuscript; or the decision to submit the work for publication.

ACKNOWLEDGMENTS

Part of the research described in this publication was carried out at the Jet Propulsion Laboratory, California Institute of Technology, under a contract with NASA. Researchers associated with Biotechnology and Planetary Protection Group at JPL are acknowledged for their facility support.

SUPPLEMENTARY MATERIAL

The Supplementary Material for this article can be found online at: https://www.frontiersin.org/articles/10.3389/fmicb.2020.01909/full#supplementary-material

FIGURE S1 | Summary of sequences detected by shotgun metagenomic sequencing not represented in the WCMR standard. Heatmap of counts of non-WCMR-represented species in the 18 samples and 10 controls. These non-represented species indicate contaminants from sample processing, including extraction reagents, library synthesis, or data analysis artifacts. Each sample represents the average of sample extraction triplicates.

FIGURE S2 | Fragment size and molecular weight determination of extracted DNA. Agilent Bioanalyzer 2100 data for samples analyzed with the DNA HS chips for Maxwell™ system extracted samples (laboratory setting in Texas) and μTitan system samples (laboratory setting in Texas and field setting in YNP).

FIGURE S3 | Drop tower test. A 2.1 s drop tower test was performed on the μTitan system and shows the fluid reorientation following a step transition from 1-g to low-g. The case on the left shows a top-down view of fluid reorientation after entering low-g. The case on the right shows a well with a probe partially submerged. A minor change in fluid orientation occurs after entering low-g, but the fluid stays in the preferred position, as desired. Note: Arrows indicate the direction of g prior to entering low-g.

TABLE S1 | Table of read counts generated from Illumina HiSeq sequencing. The first nine organisms are the ones present in the WCMR.

REFERENCES

Boguraev, A.-S., Christensen, H. C., Bonneau, A. R., Pezza, J. A., Nichols, N. M., Giraldez, A. J., et al. (2017). Successful amplification of DNA aboard the international space station. *NPJ Microgravity* 3:26.

Buchfink, B., Xie, C., and Huson, D. H. (2015). Fast and sensitive protein alignment using DIAMOND. *Nat. Meth.* 12, 59–60. doi: 10.1038/nmeth.3176

Castro-Wallace, S. L., Chiu, C. Y., John, K. K., Stahl, S. E., Rubins, K. H., McIntyre, A. B. R., et al. (2017). Nanopore DNA sequencing and genome assembly on the international space station. *Sci. Rep.* 7:18022.

Chan, K., Coen, M., Hardick, J., Gaydos, C. A., Wong, K. Y., Smith, C., et al. (2016a). Low-cost 3D printers enable high-quality and automated sample preparation and molecular detection. *PloS One* 11:e0158502. doi: 10.1371/journal.pone.0158502

Chan, K., Weaver, S. C., Wong, P.-Y., Lie, S., Wang, E., Guerbois, M., et al. (2016b). Rapid, affordable, and portable medium-throughput molecular device for zika virus. *Sci. Rep.* 6:38223.

Chan, K., Wong, P. Y., Yu, P., Hardick, J., Wong, K. Y., Wilson, S. A., et al. (2016c). A rapid and low-cost PCR thermal cycler for infectious disease diagnostics. *PloS One* 11:e0149150. doi: 10.1371/journal.pone.0149150

Checinska Sielaff, A., Kumar, R. M., Pal, D., Mayilraj, S., and Venkateswaran, K. (2017). *Solibacillus kalamii* sp. nov., isolated from a high-efficiency particulate arrestance filter system used in the international space station. *Inte. J. Syst. Evol. Microbiol.* 67, 896–901. doi: 10.1099/ijsem.0.001706

Cherie, M. O., Michele, N. B., Victoria, A. C., Kasthuri, J. V., Parag, A. V., Kathy, U. J., et al. (2013). "Microbial monitoring of common opportunistic pathogens by comparing multiple real-time PCR platforms for potential space applications," in *Proceedings of the 43rd International Conference on Environmental Systems*, (Reston: American Institute of Aeronautics and Astronautics).

Coakley, M., and Hurt, D. E. (2016). 3D Printing in the laboratory: maximize time and funds with customized and open-source labware. *J. Lab. Autom.* 21, 489–495. doi: 10.1177/2211068216649578

Dwivedi, S., Purohit, P., Misra, R., Pareek, P., Goel, A., Khattri, S., et al. (2017). Diseases and molecular diagnostics: a step closer to precision medicine. *Indian J. Clin. Biochem.* 32, 374–398. doi: 10.1007/s12291-017-0688-8

Foster, J. S., Wheeler, R. M., and Pamphile, R. (2014). Host-microbe interactions in microgravity: assessment and implications. *Life* 4, 250–266. doi: 10.3390/life4020250

Huson, D. H., Auch, A. F., Qi, J., and Schuster, S. C. (2007). MEGAN analysis of metagenomic data. *Genome Res.* 17, 377–386. doi: 10.1101/gr.5969107

Kiecolt-Glaser, J. K., Bennett, J. M., Andridge, R., Peng, J., Shapiro, C. L., Malarkey, W. B., et al. (2014). Yoga's impact on inflammation, mood, and fatigue in breast cancer survivors: a randomized controlled trial. *J. Clin. Oncol.* 32, 1040–1049. doi: 10.1200/jco.2013.51.8860

Kiecolt-Glaser, J. K., Christian, L., Preston, H., Houts, C. R., Malarkey, W. B., Emery, C. F., et al. (2010). Stress, inflammation, and yoga practice. *Psychosom. Med.* 72, 113–121. doi: 10.1097/psy.0b013e3181cb9377

Kim, W., Tengra, F. K., Young, Z., Shong, J., Marchand, N., Chan, H. K., et al. (2013). Spaceflight promotes biofilm formation by *Pseudomonas aeruginosa*. *PloS One* 8:e62437. doi: 10.1371/journal.pone.0062437

Mehta, S. K., Cohrs, R. J., Forghani, B., Zerbe, G., Gilden, D. H., and Pierson, D. L. (2004). Stress-induced subclinical reactivation of varicella zoster virus in astronauts. *J. Med. Virol.* 72, 174–179. doi: 10.1002/jmv.10555

Mehta, S. K., Crucian, B. E., Stowe, R. P., Simpson, R. J., Ott, C. M., Sams, C. F., et al. (2013). Reactivation of latent viruses is associated with increased plasma cytokines in astronauts. *Cytokine* 61, 205–209. doi: 10.1016/j.cyto.2012.09.019

Mehta, S. K., Laudenslager, M. L., Stowe, R. P., Crucian, B. E., Feiveson, A. H., Sams, C. F., et al. (2017). Latent virus reactivation in astronauts on the international space station. *NPJ Microgravity* 3:11.

NASA, (2015). *Space Station Espresso Cups: Strong Coffee Yields Stronger Science*. Available at: https://blogs.nasa.gov/ISS_Science_Blog/2015/05/01/space-station-espresso-cups-strong-coffee-yields-stronger-science/ (accessed November 13, 2019).

NASA, (2017). *Genes in Space-3 Successfully Identifies Unknown Microbes in Space*. Available at: https://www.nasa.gov/feature/genes-in-space-3-successfully-identifies-unknown-microbes-in-space/

Parada, A. E., Needham, D. M., and Fuhrman, J. A. (2016). Every base matters: assessing small subunit rRNA primers for marine microbiomes with mock communities, time series and global field samples. *Environ. Microbiol.* 18, 1403–1414. doi: 10.1111/1462-2920.13023

Parra, M., Jung, J., Boone, T. D., Tran, L., Blaber, E. A., Brown, M., et al. (2017). Microgravity validation of a novel system for RNA isolation and multiplex quantitative real time PCR analysis of gene expression on the international space station. *PLoS One* 12:e0183480. doi: 10.1371/journal.pone.0183480

Pierson, D. L., Botkin, D. J., Bruce, R., Castro, V., Smith, M., Oubre, C., et al. (2012). "Microbial monitoring of the international space station," in *Environmental Monitoring: A Comprehensive Handbook*, Vol. 6, ed. J. Moldenhauer, (River Grove, IL: DHI Publishingm LLC), 1–27.

Pierson, D. L., Stowe, R. P., Phillips, T. M., Lugg, D. J., and Mehta, S. K. (2005). Epstein-barr virus shedding by astronauts during space flight. *Brain Behav. Immun.* 19, 235–242. doi: 10.1016/j.bbi.2004.08.001

Priye, A., Wong, S., Bi, Y., Carpio, M., Chang, J., Coen, M., et al. (2016). Lab-on-a-drone: toward pinpoint deployment of smartphone-enabled nucleic acid-based diagnostics for mobile health care. *Anal. Chem.* 88, 4651–4660. doi: 10.1021/acs.analchem.5b04153

Romsdahl, J., Blachowicz, A., Chiang, A. J., Chiang, Y. M., Masonjones, S., Yaegashi, J., et al. (2019). International space Station conditions alter genomics, proteomics, and metabolomics in *Aspergillus nidulans*. *Appl. Microbiol. Biotechno.* 103, 1363–1377. doi: 10.1007/s00253-018-9525-0

Romsdahl, J., Blachowicz, A., Chiang, A. J., Singh, N., Stajich, J. E., Kalkum, M., et al. (2018). Characterization of aspergillus niger isolated from the international space station. *mSystems* 3, e00112–18. doi: 10.1128/mSystems.00112-18

Sayers, E. W., Barrett, T., Benson, D. A., Bryant, S. H., Canese, K., Chetvernin, V., et al. (2009). Database resources of the national center for biotechnology information. *Nucleic Acids Res.* 37, D5–D15.

Singh, N. K., Wood, J. M., Mhatre, S. S., and Venkateswaran, K. (2019). Metagenome to phenome approach enables isolation and genomics characterization of *Kalamiella piersonii* gen. nov., sp. nov. from the international space station. *Appl. Microbiol. Biotechnol.* 103, 4483–4497. doi: 10.1007/s00253-019-09813-z

Tighe, S., Afshinnekoo, E., Rock, T. M., McGrath, K., Alexander, N., McIntyre, A., et al. (2017). Genomic methods and microbiological technologies for profiling novel and extreme environments for the extreme microbiome project (XMP). *J. Biomol. Tech.* 28, 31–39. doi: 10.7171/jbt.17-2801-004

Urbaniak, C., van Dam, P., Zaborin, A., Zaborina, O., Gilbert, J. A., Torok, T., et al. (2019). Genomic characterization and virulence potential of two *Fusarium oxysporum* isolates cultured from the international space station. *mSystems* 4, e00345–18. doi: 10.1128/mSystems.00345-18

Walters, W., Hyde, E. R., Berg-Lyons, D., Ackermann, G., Humphrey, G., Parada, A., et al. (2016). Improved bacterial 16S rRNA gene (V4 and V4-5) and fungal internal transcribed spacer marker gene primers for microbial community surveys. *mSystems* 1:e00009-15.

Weislogel, M., Chen, Y., Collicott, S., Bunnell, C., Green, R., and Bohman, D. (2009). "More Handheld Fluid Interface Experiments for the International Space Station (CFE-2)?," in *Proceedings of the 47th AIAA Aerospace Sciences*

Meeting including The New Horizons Forum and Aerospace Exposition (Reston: AIAA)

Weislogel, M. M., Baker, J. A., and Jenson, R. M. (2011). Quasi-steady capillarity-driven flows in slender containers with interior edges. *J. Fluid Mech.* 685, 271–305. doi: 10.1017/jfm.2011.314

Yamaguchi, N., Roberts, M., Castro, S., Oubre, C., Makimura, K., Leys, N., et al. (2014). Microbial monitoring of crewed habitats in space-current status and future perspectives. *Microbes Environ.* 29, 250–260. doi: 10.1264/jsme2.me14031

Conflict of Interest: AA and BL were employed by AI Biosciences, Inc. SW is the co-founder of AI Biosciences, Inc. RJ was employed by IRPI LLC.

The remaining authors declare that the research was conducted in the absence of any commercial or financial relationships that could be construed as a potential conflict of interest.

frontiers in Microbiology

ORIGINAL RESEARCH
published: 14 October 2020
doi: 10.3389/fmicb.2020.579156

No Effect of Microgravity and Simulated Mars Gravity on Final Bacterial Cell Concentrations on the International Space Station: Applications to Space Bioproduction

Rosa Santomartino[1], Annemiek C. Waajen[1], Wessel de Wit[1], Natasha Nicholson[1], Luca Parmitano[2], Claire-Marie Loudon[1], Ralf Moeller[3], Petra Rettberg[3], Felix M. Fuchs[3†], Rob Van Houdt[4], Kai Finster[5], Ilse Coninx[4], Jutta Krause[2], Andrea Koehler[2], Nicol Caplin[2], Lobke Zuijderduijn[2], Valfredo Zolesi[6], Michele Balsamo[6], Alessandro Mariani[6], Stefano S. Pellari[6], Fabrizio Carubia[6], Giacomo Luciani[6], Natalie Leys[4], Jeannine Doswald-Winkler[7], Magdalena Herová[7], Jennifer Wadsworth[8], R. Craig Everroad[8], Bernd Rattenbacher[7], René Demets[2] and Charles S. Cockell[1]**

[1] UK Centre for Astrobiology, School of Physics and Astronomy, University of Edinburgh, Edinburgh, United Kingdom, [2] European Space Research and Technology Centre (ESTEC), Noordwijk, Netherlands, [3] Radiation Biology Department, German Aerospace Center (DLR), Institute of Aerospace Medicine, Cologne (Köln), Germany, [4] Microbiology Unit, Belgian Nuclear Research Centre, SCK CEN, Mol, Belgium, [5] Department of Biology – Microbiology, Aarhus University, Aarhus C, Denmark, [6] Kayser Italia S.r.l., Livorno, Italy, [7] BIOTESC, Hochschule Luzern Technik und Architektur, Hergiswil, Switzerland, [8] Exobiology Branch, NASA Ames Research Center, Moffet Field, CA, United States

Microorganisms perform countless tasks on Earth and they are expected to be essential for human space exploration. Despite the interest in the responses of bacteria to space conditions, the findings on the effects of microgravity have been contradictory, while the effects of Martian gravity are nearly unknown. We performed the ESA BioRock experiment on the International Space Station to study microbe-mineral interactions in microgravity, simulated Mars gravity and simulated Earth gravity, as well as in ground gravity controls, with three bacterial species: *Sphingomonas desiccabilis*, *Bacillus subtilis*, and *Cupriavidus metallidurans*. To our knowledge, this was the first experiment to study simulated Martian gravity on bacteria using a space platform. Here, we tested the hypothesis that different gravity regimens can influence the final cell concentrations achieved after a multi-week period in space. Despite the different sedimentation rates predicted, we found no significant differences in final cell counts and optical densities between the three gravity regimens on the ISS. This suggests that possible gravity-related effects on bacterial growth were overcome by the end of the experiment. The results indicate that microbial-supported bioproduction and life support systems can be effectively performed in space (e.g., Mars), as on Earth.

Keywords: microgravity (μ*g*), spaceflight, Mars gravity, BioRock, International Space Station (ISS), space microbiology, space bioproduction, bacterial cell concentration

OPEN ACCESS

Edited by:
Richard Allen White III, RAW Molecular Systems LLC, United States

Reviewed by:
John Z. Kiss, University of North Carolina at Greensboro, United States
Khaled Y. Kamal, Texas A&M University, United States

****Correspondence:***
Charles S. Cockell
c.s.cockell@ed.ac.uk
Rosa Santomartino
rosa.santomartino@ed.ac.uk

†Present address:
Felix M. Fuchs, Institute of Electrical Engineering and Plasma Technology, Faculty of Electrical Engineering and Information Sciences, Ruhr University Bochum, Bochum, Germany

Specialty section:
This article was submitted to Extreme Microbiology, a section of the journal Frontiers in Microbiology

Received: *01 July 2020*
Accepted: *09 September 2020*
Published: *14 October 2020*

INTRODUCTION

Microorganisms such as bacteria are the foundation of Earth's biosphere, including the human body, and will necessarily follow humans on their journey during space exploration. Since they play many important roles in biological processes on Earth, they are also expected to be essential in space. They have been shown to pervasively inhabit space stations such as the former Mir (Novikova, 2004) and the International Space Station (ISS) (Ichijo et al., 2016; Mora et al., 2019; Sielaff et al., 2019), with both negative effects and positive uses. Potential roles of microorganisms in space will include manufacturing (Menezes et al., 2015a,b), as building blocks of ecosystems (Gòdia et al., 2002), and in biomining on celestial bodies (Schippers et al., 2013; Reed et al., 2016; Jerez, 2017). Space-based research on microorganisms has been performed for the bioproduction of antibiotics (Klaus et al., 2001; Benoit et al., 2006), other secondary metabolites (Huang et al., 2018) and vaccines (Ruttley et al., 2009) for terrestrial consumption. In addition to being useful, they also present challenges, e.g., through the formation of corrosive biofilms (Gu et al., 1998) and altered virulence in space (Wilson et al., 2007; Rosenzweig and Chopra, 2012).

The term microgravity (μg) is commonly used to describe a gravitational accelerations smaller than $10^{-2} \times g$ and close to $10^{-6} \times g$ (Horneck et al., 2010; Zea et al., 2017; Huang et al., 2018), and it is experienced for instance by objects orbiting around a celestial body in space, such as satellites in Low Earth Orbit (LEO). The effects of microgravity on eukaryotic multicellular organisms has been extensively reported for plants (Gòdia et al., 2002; Matía et al., 2010; Kiss et al., 2012; Paul et al., 2013; Zabel et al., 2016), animals (Wassersug et al., 2005; Bart et al., 2019; Maupin et al., 2019; Tahimic et al., 2019) and humans (Cavanagh et al., 2005; Van Ombergen et al., 2017; Axpe et al., 2020). Results on eukaryotic microorganisms such as *Euglena* and *Paramecium* spp. demonstrated the ability to respond to gravity (Hader, 1996; Hader et al., 1996; Hemmersbach et al., 2001). The effects of microgravity on bacterial growth, in contrast, have been controversial and inconclusively discussed (Leys et al., 2004; Taylor, 2015), despite the enormous interest in their physiological responses to space conditions. Even less studied are the effects of partial gravity conditions, such as lunar ($0.16 \times g$) or Martian ($0.38 \times g$) gravity, on bacterial growth (Hemmersbach et al., 1996; Santosh et al., 2011; McCutcheon et al., 2016).

The majority of the data on bacterial growth in microgravity are the results of separate projects with necessarily diverse experimental designs and a limited number of replicate samples, and overall they addressed various endpoints for distinct scientific questions (Pollard, 1965; Bouloc and D'Ari, 1991; Gasset et al., 1994; Kacena et al., 1997, 1999b; Kacena and Todd, 1997; Klaus et al., 1997; Baker et al., 2004; Nickerson et al., 2004; Horneck et al., 2010; Mulders et al., 2011; Kim et al., 2013a; Zea et al., 2016, 2017; Huang et al., 2018; Milojevic and Weckwerth, 2020; Nicholson and Ricco, 2020). Consequently, it is difficult to draw generalizable conclusions on the effects of gravity on bacterial cell growth.

Some studies concluded that cells with a diameter of less than 10 μm cannot sense gravity directly (Pollard, 1965; Horneck et al., 2010; Zea et al., 2017), and the response observed in a low-gravity experiment was ascribed to indirect effects on the local liquid microenvironment surrounding the cell (Klaus et al., 1997; Zea et al., 2016). *Escherichia coli* ATCC 4157 cells showed an increased final cell concentration in microgravity compared to the ground, which was attributed to factors such as upregulation of starvation-related and carbon source-uptake genes (Zea et al., 2016). Nevertheless, other studies using different *E. coli* strains did not confirm this observation after space flight (Bouloc and D'Ari, 1991; Gasset et al., 1994), while an experiment in simulated microgravity showed medium-dependent changes (Baker et al., 2004). Growth of *Bacillus subtilis* in microgravity produced inconclusive results as well (Kacena et al., 1997, 1999b; Kacena and Todd, 1997; Nicholson and Ricco, 2020). Similar discrepancies were reported for other bacterial species (Kim et al., 2013a) and for eukaryotic microorganisms (Mulders et al., 2011). A summary of the data on microbial growth in microgravity can be found in Huang et al. (2018).

In response to a flight opportunity offered by the European Space Agency (ESA), we conducted the BioRock experiment (Loudon et al., 2018) onboard the ISS with the general aim to advance the knowledge on bacterial responses to microgravity (μg), simulated Mars (Mars g) and Earth (Flight 1-g) gravities, with a view to microbe-mineral interaction and its potential roles in extraterrestrial life support systems, e.g., *in situ* Resource Utilization (ISRU), biomining and soil formation from planetary regolith (Cockell, 2010; Olsson-Francis et al., 2010; Zaets et al., 2011; Menezes et al., 2015a) (**Figure 1**).

We selected three bacterial strains with demonstrated evidence for their ability to interact with rock surfaces or soil, bioleach, grow on surfaces and resist desiccation: *Sphingomonas desiccabilis* CP1D, *Bacillus subtilis* NCIB 3610 and *Cupriavidus metallidurans* CH34. As BioRock had the rare opportunity to study multiple microorganisms in the same set of experimental conditions, one part of this experiment was to test the hypothesis that the gravity condition influences the final cell concentration of the bacterial cultures after a 3-week period. This timeframe was chosen as a point in stationary phase that gives enough time to create microbe-mineral interactions, but not yet in death phase to lead to cell degradation (Loudon et al., 2018). Despite the diverse gravity-dependent phenomena involved, we reported no effect of gravity on the final cell concentrations of the three different bacterial species. We discuss the importance of these results for the future of human space exploration (Horneck et al., 2010), as the duration and ambition for spaceflight missions expands, as well as for terrestrial applications.

MATERIALS AND METHODS

Bacterial Strains, Medium and Fixative

For this experiment, we selected three bacterial species with demonstrated evidence for their ability to grow on and interact with rock surfaces or soil, bioleach elements and resist

FIGURE 1 | Astronaut Luca Parmitano working on BioRock. **(A)** Luca Parmitano installs the hardware into the KUBIK incubator located in the Columbus module onboard the ISS. Image credit: ESA. **(B)** The official BioRock logo (created by Hadrien Jouet and Mauro Manzo).

dessication (Loudon et al., 2018): (i) *Sphingomonas desiccabilis* CP1D (DSM 16792, University of Edinburgh), a Gram-negative, non-motile and non-spore-forming α-proteobacterium (phylum Proteobacteria) (Reddy and Garcia-Pichel, 2007). *S. desiccabilis* was first isolated in the Colorado plateau from soil crusts (Stevens et al., 2019). It was selected for its high resistance to desiccation and for its natural presence in desert crust environments (Reddy and Garcia-Pichel, 2007; Stevens et al., 2019). (ii) *Bacillus subtilis* NCIB 3610 (DSM 10) [German Aerospace Center (DLR) Cologne, Germany] (Nye et al., 2017), a Gram-positive, motile and spore-forming bacillus (phylum Firmicutes). *B. subtilis* is a very well characterized model organism and has been widely used in space experiments (Kacena et al., 1999b; Fajardo-Cavazos et al., 2018; Morrison et al., 2019; Nicholson and Ricco, 2020). It can survive in harsh environments and grow on rock substrates (Song et al., 2007). Moreover, it was found as a common contaminant on the ISS (Nickerson et al., 2004); (iii) *Cupriavidus metallidurans* CH34 (SCK CEN, Belgium), a Gram-negative, non-spore-forming, motile β-proteobacterium (phylum Proteobacteria) (Janssen et al., 2010). Strains of this species have been isolated from rocks and metal-contaminated environments (Janssen et al., 2010; Olsson-Francis et al., 2010; Bryce et al., 2016; Vandecraen et al., 2016), and it has been previously isolated from ISS and used in space experiments (Leys et al., 2009; Monsieurs et al., 2014; Byloos et al., 2017). The main bacterial characteristics of the three strains are summarized (**Supplementary Table 1**).

All organisms were grown in an identical medium which was approved for spaceflight as a compromise to allow the growth of the three species (Loudon et al., 2018). Five milliliters of a 50% v/v solution of R2A growth medium (from now on referred to as 50% R2A) were used for each sample (Reasoner and Geldreich, 1985), containing (g L^{-1}): yeast extract, 0.25; peptone, 0.25; casamino acids, 0.25; glucose, 0.25; soluble starch, 0.25; Na-pyruvate, 0.15; K_2HPO_4, 0.15; $MgSO_4{\cdot}7H_2O$, 0.025, adjusted to a final pH of 7.2.

The fixative chosen to stop cell growth at the end of the experiment was NOTOXhisto (Scientific Device Laboratory), a formalin-free ethanol-based solution previously tested for its ability to stop cell growth of the selected bacteria, for its biocompatibility with the hardware and the safety requirements on the ISS (Loudon et al., 2018). One milliliter of fixative was used for each sample, with a final volume ratio of 1:5 fixative-medium.

Pre-Flight Sample Preparation

Single strain cultures of each bacterial species were desiccated on a sterile basalt slide cut from a rock specimen, taken near Gufunes, Reykjavik in Iceland (64°08'22.18"N, 21°47'21.27"W). Rock sterilization was performed by dry-heat sterilization in a hot air oven for 4–5 h at 250°C. Negative controls were sterile basalt slides without cell inoculation.

Each bacterial population was treated differently for sample preparation. This affected the initial cell numbers on the basalt slides, which was different for each bacterial strain, but it was necessary to ensure optimal storage conditions for each organism during pre-activation.

For *S. desiccabilis*, an overnight culture of the strain was grown in R2A broth at 20–22°C. When the culture reached stationary phase (OD_{600} = 0.88 ± 0.09, corresponding to approximately 1×10^9 CFU mL^{-1}), each basalt slide was soaked in 1 mL of the bacterial culture and samples were air-dried at room temperature in a laminar flow hood under sterile conditions. The protocol for *B. subtilis* spore production and sample preparation has been previously described (Fuchs et al., 2017). Ten microliters of a thoroughly mixed ∼1×10^8 spores mL^{-1} solution were used as inoculum for each basalt slide (resulting in ca. 1×10^6 spores per slide) and air-dried at room temperature in a laminar flow hood under sterile conditions. *C. metallidurans* samples were prepared by using a freeze-drying protocol (Belgian Co-ordinated Collection of Micro-organisms, BCCM). Cells were cultured on solid Tryptone Soya Agar (Oxoid CM0131, BCCM), harvested and suspended in a lyoprotectant [sterile horse serum supplemented with 7.5% w/v trehalose (final concentration) and broth medium n°2 (final concentration: 625 mg L^{-1}; Oxoid CM0131, BCCM)]. Basalt

slides were submerged in 30 mL of a bacterial suspension and gently shaken overnight. Basalt slides were then inserted on a pre-cooled shelf at −50°C, followed by a freezing phase for 90 min at a shelf temperature of −50°C. Primary drying was performed at −18°C and chamber pressure of 400 mTorr, secondary drying was performed at 20°C and a chamber pressure below 10 mTorr. After the procedure, each basalt slide contained approximately 1×10^9 CFU mL^{-1} of *C. metallidurans*.

Samples were stored at room temperature until integration in the Experimental Units (EUs). Samples in each gravity condition, including the negative control, were present in triplicate.

Setup of the Flight Experiment

A diagram of the experimental setup is presented in **Figure 2**. After preparation of the hardware, samples, medium and fixative were integrated under aseptic conditions into the designated flight Experiment Unit (EU) before the launch. Each EU was composed by two BioMining Reactors (BMRs). A BMR represents a culture chamber of 15 × 14 × 23.2 mm that can contain 6 mL of liquid volume after hardware activation and medium injection, delimited by the basalt slide (after sample integration) on one side, and a semipermeable membrane on the remaining five sides. The semi-permeable silicon membrane allowed gas diffusion. Each BMR is connected to a 5 mL medium reservoir and a 1 mL fixative reservoir, which were activated at the appropriate time (**Supplementary Figure 1**). The EUs were also equipped with temperature loggers (installed in four EUs, Signatrol SL52T sensors, Signatrol, United Kingdom) and accelerometers (in all EUs on ISS), that allowed the measurement of the acceleration profiles over the experiment (**Supplementary Table 2**). For a complete description of the EU, refer to Loudon et al. (2018). A total of 36 samples in 18 EUs for the flight experiment and 12 samples in 6 EUs for the ground control were prepared. After integration, the 18 flight EUs were stored at room temperature and sent to the ISS on board of a Space X Falcon-9 rocket (CSR-18 mission) on July 25th, 2019, from the NASA Kennedy Space Centre, Merritt Island, FL, United States. On arrival to the ISS on July 27th, the samples were stored at 2–8°C in an onboard refrigerator until being installed into the two KUBIK (ESA) incubators aboard the station, previously set to 20°C. Once in KUBIKs, the EUs were let to adjust to the incubation temperature for one hour. Then, the automatic timeline of the EUs was activated and medium (5 mL) was injected in consecutive manner to each culture chamber (18 BMRs per KUBIK) within 1.5 h. The medium injection could not be done at once for all BMRs due to KUBIKs power limitations. All samples were then removed from KUBIK 5, first image acquisition was performed, and the EUs were re-installed into the KUBIK 5 (EUs were out of KUBIK for circa 40 min) and this latter was reactivated. The same procedure was then performed for KUBIK 6 (EUs were out of KUBIK for circa 20 min). All crew activities were performed by Luca Parmitano. The KUBIK 5 centrifuge was set to 1.2 × *g* to simulate Earth gravity (Flight 1-*g*), KUBIK 6 was set to 0.5 × *g* to simulate Mars gravity (Mars *g*). These settings were chosen to obtain a final gravity acceleration of 1 × *g* and 0.4 × *g*, respectively, as the geometry of the BMR locates the sample

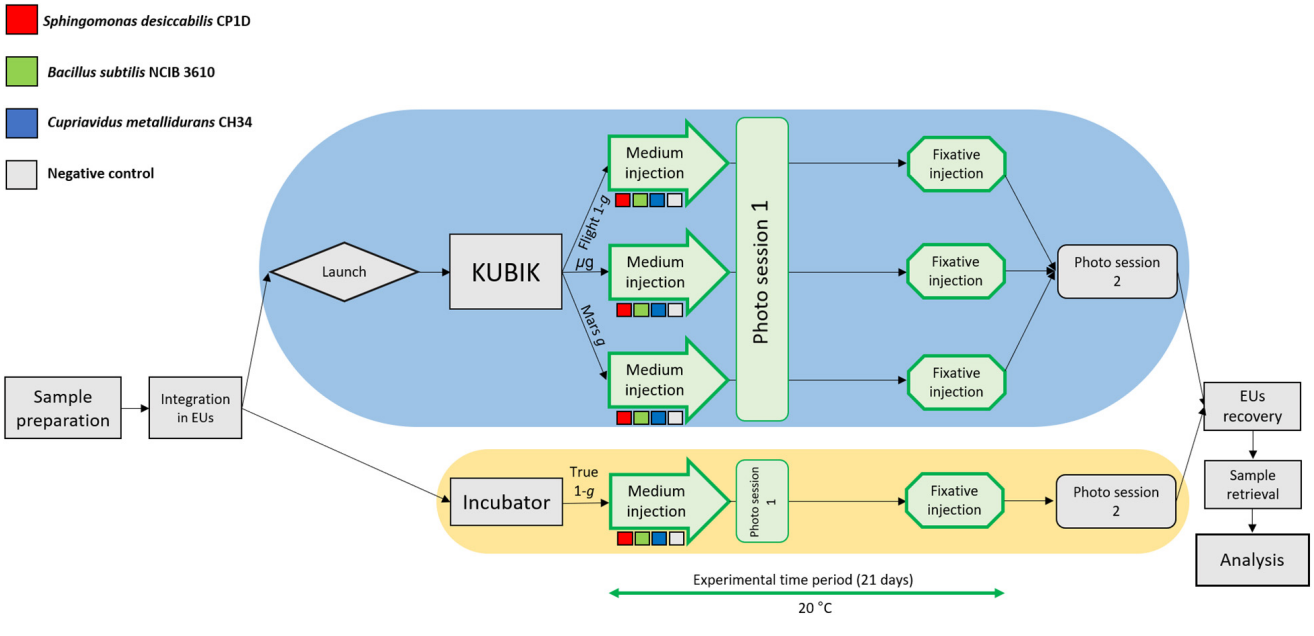

FIGURE 2 | Flow diagram of the BioRock experiment. Three bacterial species were prepared for the experiment: *S. desiccabilis* (red squares), *B. subtilis* (green squares), and *C. metallidurans* (blue squares). Negative controls (gray squares) represented sterile basalt slides. After integration in the experimental units (EUs), the EUs were either launched to the ISS (blue oval), where they were installed in KUBIK incubators and subjected to microgravity (μ*g*), simulated Mars gravity (Mars *g*) or simulated Earth gravity (Flight-1*g*), or kept for incubation on Earth for the ground gravity control (True-1*g*, yellow oval). Steps in green were part of the experimental time period (21 days). Storage passages were omitted for brevity. Each experimental set was represented in triplicate.

at a shorter radius than the reference radius, meaning that the acceleration experienced by the sample is lower than the set-point. Notably, a strict Martian gravity of 0.38 × *g* was not settable on the KUBIK, as the setting allows gravity increments of 0.1 × *g*. Samples grew for 21 days at 20.16°C (temperature loggers). At the end of the experiment, 1 mL of fixative was injected consecutively in the culture chambers within 1.5 h (on August the 20th, 2019). A second photo session was performed and hardware were then cold stored at 2.1–7.1°C (logged data). On orbit, the EUs were stored in the MELFI hardware, and by packaging in a "Double Coldbag" provided by NASA for download, with SpaceX CRS-18 (same vehicle as for upload). Samples were retrieved at NASA Ames Research Centre, Mountain View, CA, United States together with the ground controls.

Prior to the space experiment, the ground control units were shipped in cold stowage (logged data 3.58–4.54°C) to NASA Ames Research Centre. The procedure started two days after the start of the space experiment and the ground experiment was subject to analog procedures and conditions to those occurring to the flight hardware. The six EUs were incubated at 20°C in a laboratory incubator (Percival E30BHO incubator) and attached to a power system to activate the hardware. The temperature loggers recorded a constant temperature of 20.62°C. Medium was injected in a similar manner as in KUBIK onboard the ISS using the KISS (KUBIK Interface Simulation) power system, the first photo session was performed (duration circa 20 min), and the experiment was conducted for a period of 21 days. After fixative injection, photo session 2 was performed (duration circa 20 min) and EUs were stored at 3.06°C (logged data) until sample retrieval. We refer to these samples as True 1-*g*.

Samples were recovered, separating the culture liquids, the basalt slides and the membranes. The liquid cultures analyzed in this work were stored at 2–8°C until analysis. Medium injection was successful in all flight and ground samples. Fixative injection was successful for all the flight BMRs, but four ground BMRs (containing *B. subtilis*, *C. metallidurans*, *C. metallidurans*, and a negative control, respectively) suffered from fixative injection failure. In these cases, 1 mL of NOTOXhisto was added to the liquid samples immediately after sample recovering and before storage. All samples were shipped back to the University of Edinburgh in cold stowage by Altech Space (Torino, Italy) and analyzed.

Images Acquisition (Photo Session) Setup

The photographs onboard the ISS were taken in microgravity with a Nikon D5 camera with a 105 mm lens with the following settings: F/10, ISO-1000. EUs were setup in a dedicated custom-made sample holder, which was fixed on the Maintenance Work Area (MWA; **Supplementary Figure 2**). The camera was fixed on the opposite side of the MWA. A work light was set up next to the camera to minimize reflection on the transparent window of the EU. The photo session for the ground control (True 1-*g*) was performed with a POT-LX1 camera with the following settings: F/1.8, ISO-80. In this case, no sample holder or particular working area was necessary.

Determination of Final Cell Numbers

Cell population after sample retrieval was assessed on the liquid samples by two methods: direct cell counting and optical density.

Direct cell counting was used to determine the cell concentration for each sample by fluorescence microscopy. The cell suspension was diluted in R2A medium and stained with SYBR Gold (Invitrogen by Thermo Fisher Scientific, 1:10,000 diluted). Samples were vortexed for 30 s and incubated in the dark for 30 min. After vortexing the samples again for 30 s, samples were filtered on black polycarbonate Nuclepore Track-Etched Membranes with 0.2 μm pore size (Whatman) and visualized by fluorescence microscope (Leica DM 4000 B, Leica Microsystems). Cell numbers were counted for 50 fields of view at 100× magnification. When cell concentration was too low to ensure an appropriate number of cells per field of view, cell suspensions were concentrated, or 100 fields of view were counted.

For optical density analysis, an absorbance microplate reader (BMG Labtech) set to a wavelength of 600 nm was used.

Statistical comparisons were performed using a one-way ANOVA analysis, followed by a *post hoc* Tukey test to determine whether significant differences existed between different experimental groups (R version 3.6.3). Significance was set at p-values of ≤ 0.05.

Spore Enumeration

Spore enumeration was determined from the liquid samples of *B. subtilis* after spaceflight. A colony formation unit (CFU) assay was used. Total cell count and spore counts (after heating for 15 min at 80°C; 50 μL sample volume per test in triplicates) were determined from appropriate dilutions in sterile buffered phosphate saline (0.7% w/v $Na_2HPO_4 \times 2H_2O$, 0.3% w/v KH_2PO_4, 0.4% w/v NaCl pH 7.5) as colony-forming ability after incubation overnight at 37°C on nutrient broth agar plates (Difco, Detroit, MI, United States). The data shown are expressed as means ± standard deviations. The results were compared statistically using Student's t test (SigmaPlot13, Systat Software). Values were analyzed in multigroup pairwise combinations, and differences with p values ≤ 0.05 were considered statistically significant.

Ground Experiment: Cell Growth in the Presence of the Basalt Rock

Fresh pre-cultures of the three different organisms were grown overnight until reaching stationary phase. Then, optical density (λ = 600 nm) was measured, and an appropriate amount of each culture was diluted in 50% R2A in order to reach a starting OD_{600} of 0.050–0.071. Five milliliters of each bacterial starting solution were then inoculated into a 6-well plate, with and without the presence of a basalt slide, all in triplicates. A 6-well plate for each time-point and for each organism was prepared, plus the same number of samples with fresh 50% R2A for the negative controls. All the samples were kept at 20°C, and OD_{600} was measured at each time point (day 0, 1, 4, 7, 14, and 21). Contrary to the

space experiment, vegetative cells were used in this experiment for all the three organisms, included *B. subtilis*, without previous desiccation on the basalt slide.

Calculations of Cell Sedimentation Rates and Diffusion Under Microgravity, Mars and Earth Gravity

An estimation of the velocity of sedimentation of a single cell (v_{cell}) under the artificial Mars and Earth gravity regimens was calculated using the Navier-Stokes Eq. (1) (Todd, 1989):

$$\upsilon_{cell} = \frac{2 \times (\rho - \rho_0) \times a^2 \times g}{9 \times \eta} \quad (1)$$

where ρ_o is the fluid density (g cm^{-3}), ρ is the density of the particle (in this case the cell, g cm^{-3}), a is the effective Stokes radius of the cell (m), g is the gravitational acceleration (m s^{-2}), and η is the fluid viscosity (kg h^{-1} m^{-1}).

The distance a given cell will sediment (d_{sed}) within the culture chamber in a given time t (s) is given by:

$$d_{sed} = \upsilon_{cell} \times t \quad (2)$$

We also calculated the distance that a cell would cover by Brownian motion over a given time (x), which can be calculated using the Eq. (3):

$$< x >^2 = 2 \times D \times t \quad (3)$$

Where $<x>^2$ is the root-mean-square diffusion distance traveled (cm^2), D is the diffusion coefficient (cm^2 s^{-1}) and t is the time (s).

The diffusion coefficient D was calculated using the Eq. (4) (Klaus et al., 1997):

$$D = \frac{(k_B \times T)}{(6 \times \pi \times \eta \times a)} \quad (4)$$

Where k_B is the Boltzmann constant (1.38×10^{-23} J mol^{-1}) and T is the temperature, which is 295.13 K in our experiments. The diffusion coefficient using Eq. (4) was 4.02×10^{-13} m^2 s^{-1}.

For these calculations, we took an effective Stokes radius of 6.0×10^{-7} m (using a cell diameter of 1.2 μm), a cell density of 1.08 g cm^{-3}, and a fluid density similar to water of 1.01 g cm^{-3}. The medium viscosity was assumed to be similar to water (1.002 mPa s at 20°C).

The KUBIK centrifuges delivered $1 \times g$ (Flight $1 \times g$) and $0.4 \times g$ (Mars g) at the top surface of the basalt slides, with 1.3-fold increase of acceleration at the membrane surface, leading to gravity accelerations of $1.3 \times g$ and $0.5 \times g$ at the membrane surface, respectively. Because sedimentation at a given gravity would imply sedimentation at higher gravity accelerations, we used the lowest experimental values (9.81 and 3.67 m s^{-2} for Earth and Mars, respectively) for these calculations. For the two microgravity regimens, we used 9.81×10^{-2} m s^{-2} and 9.81×10^{-6} m s^{-2} for 1×10^{-2} g and 1×10^{-6} g, respectively.

RESULTS

Final Cell Concentration and Optical Density

The samples launched to the ISS were exposed to three different gravity regimens (microgravity, μg; simulated Martian gravity, Mars g; simulated terrestrial gravity, Flight 1-g), while the reference experiment was conducted on Earth at $1 \times g$ (ground control samples, True $1 \times g$) (**Figure 2**). The cultures were grown for 21 days in the presence of a basalt slide. For *S. desiccabilis* (**Figures 3A,B**), ANOVA on final cell counts showed no difference between the gravity regimens ($0.4–2.7 \times 10^9$ cell mL^{-1}, $F(3, 8) = 1.052$, p-value = 0.421; **Figure 3A**). ANOVA on optical density measurements confirmed the lack of difference between the three gravity conditions tested in space (μg, Mars g and Flight $1 \times g$; **Figure 3B**). However, the optical density of True-1g samples was significantly lower compared to samples subject to μg and Mars g [$F(3,8) = 7.148$, p-value = 0.0119, *post hoc* Tukey test p-values between μg and True-1g = 0.016, and between Mars g and True-1g = 0.018; **Figure 3B**]. This is in contrast to the lack of significant difference observed for final cell counts. Significant differences in optical density were observed neither between μg and Flight-1g, nor between Mars g and Flight-1g (both p values > 0.05; **Figure 3B**). Cultures grown at simulated (Flight-1g) and real (True-1g) Earth gravity showed no significant difference (p-value = 0.06; **Figure 3B**) in optical density. This suggested that the difference in optical densities between the μg or Mars g conditions and the True-1g could not be explained by gravity alone and may have been subject to additional influencing factors.

Bacillus subtilis (**Figures 3C,D**) showed no significant difference in final cell counts [ANOVA: $F(3,8) = 3.806$, p-value = 0.058] and optical densities [ANOVA: $F(3,8) = 0.776$, p-value = 0.54]. No difference was observed between space and ground-based samples ($2.4–8.9 \times 10^7$ cell mL^{-1}, *post hoc* Tukey test p values > 0.05; **Figure 3C**) with the exception of a lower final cell counting of cultures grown under simulated Flight-1g compared with True-1g (*post hoc* Tukey test p-value = 0.04). We note that, in contrast to the other bacterial strains tested in this space experiment, *B. subtilis* cultures were initiated as spores, which had to germinate and form highly motile vegetative cells before they could multiply (Setlow et al., 2017). Furthermore, the use of 50% R2A as a necessary compromise for the three microorganisms could have led to lower cell concentrations compared to media with higher organic concentrations.

Similar to *B. subtilis*, the final cell counts of *C. metallidurans* cultures (**Figures 3E,F**) were not significantly influenced by gravity conditions, as indicated by the results from both analytic methods [ANOVA on cell count data: $F(3,8) = 1.409$, p-value = 0.309; ANOVA on optical density data: $F(3,8) = 0.595$, p-value = 0.636]. This is probably due to a large variability, which resulted in lack of statistically significant differences even when the average values for cell concentration differed in order of magnitude ($\sim 10^8$ cell mL^{-1} for cells in Mars g, $\sim 10^9$ cell mL^{-1} for μg, Flight-1g and True-1g). The cause of this variability is unknown. It could have been produced by a different initial cell

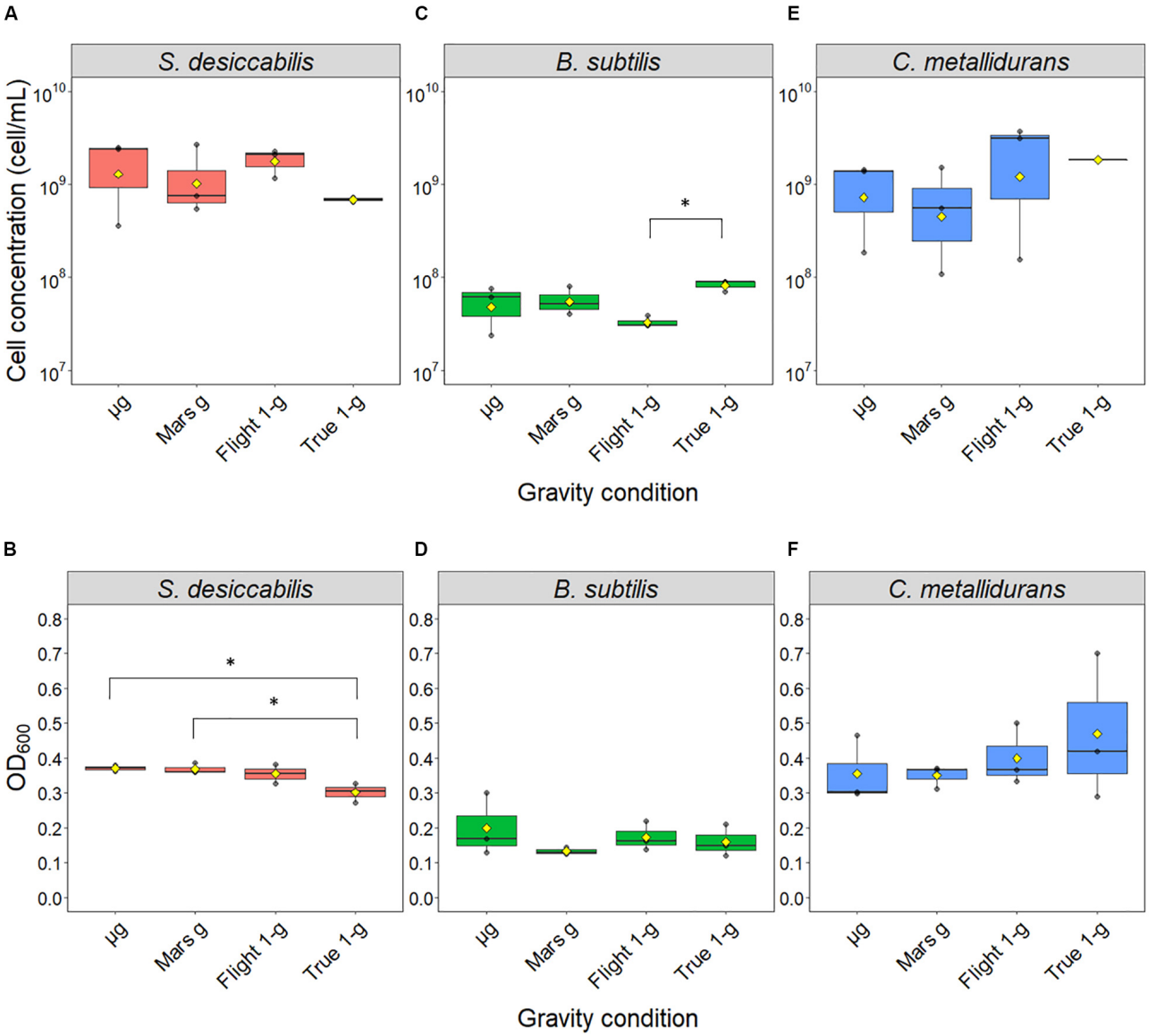

FIGURE 3 | Final cell concentrations obtained after spaceflight. Boxplots of the direct cell counts (upper panel) and optical densities at a wavelength of 600 nm (lower panel) distributions are shown for *S. desiccabilis* **(A, B)**, *B. subtilis* **(C, D)**, and *C. metallidurans* **(E, F)**, respectively. Each dot represents a single measurement ($n = 3$). Yellow diamonds represent mean values. The horizontal bar indicates the median and boxes represents the 25th to 75th percentile. Asterisks (*) indicate statistically significant differences (overall $\alpha = 0.05$, Tukey honestly significant difference correction).

number or a difference in growth phase stage (stationary phase, decline/death phase) elicited by nutrient and oxygen availability.

Spore Enumeration for *B. subtilis* Samples

Bacillus subtilis was the only spore-forming bacterium used in the BioRock experiment. The spore numbers from *B. subtilis* liquid samples were counted.

The initial number of spores inoculated on each basalt slide was 1×10^6 spores/slide. The results (**Table 1**) showed effective germination of the initial spores, growth as vegetative cells and sporulation again in space, thus going through at least one complete life cycle. Spore formation during spaceflight was not affected by the gravity regime (p value > 0.05).

Influence of the Basalt Slide on Cell Growth

As the primary objective of the BioRock experiment was to test the interaction of the microorganisms with minerals in different gravity regimens, the cultures were grown in the presence of a basalt slide. To determine whether the presence of the basalt slide influenced the final cell concentration, a ground experiment was performed. The three bacterial strains used in the BioRock experiment were grown in 50% R2A broth in

TABLE 1 | Enumeration of *B. subtilis* spores in liquid samples. CFU assay data are shown as averages ± standard deviation (n = 9). Each sample was tested in triplicate. The ratio between the number of spores and the total cell counts is shown and expressed as a percentage.

g regime	Total cells count (CFU mL^{-1})	Spore count (CFU mL^{-1})	Spores/total cells (%)
μ*g*	$2.4 \pm 0.5 \times 10^7$	$2.5 \pm 0.2 \times 10^6$	10.5 ± 1.2
Mars *g*	$2.0 \pm 0.2 \times 10^7$	$1.8 \pm 0.5 \times 10^6$	8.5 ± 1.5
Flight 1-*g*	$2.5 \pm 0.3 \times 10^7$	$1.7 \pm 0.4 \times 10^6$	6.9 ± 1.8
True 1-*g*	$2.5 \pm 0.8 \times 10^7$	$2.0 \pm 0.6 \times 10^6$	8.0 ± 2.1

the presence or absence of a basalt slide. Cell-free 50% R2A medium, supplemented with or without basalt, was used as negative control.

The negative control (**Figure 4A**) was used to demonstrate that changes in optical density were not caused by the presence of the basalt slide. The final optical density of *S. desiccabilis* (**Figure 4B**) and *C. metallidurans* (**Figure 4D**) was not influenced by the presence of the basalt slide *per se*, although some fluctuations were observed throughout the experimental period. Interestingly, optical density of *B. subtilis* cultures depended on the presence of the basalt slide for sustained growth (**Figure 4C**). While a higher value was measured after one day of growth in the absence of the rock, the overall optical density was strongly reduced after 14 days, in comparison to the cultures that were grown in the presence of a basalt slide. The CFU assay performed on *B. subtilis* cultures after the 21st day revealed a cell concentration of $1.97 \pm 0.51 \times 10^9$ CFU mL^{-1} (mean ± SE) for the samples grown in the presence of the basalt slide, and $2.03 \pm 0.22 \times 10^8$ CFU mL^{-1} when the slide was absent. Hence, the lower optical density measured for the cultures in the absence of a basalt slide could be partially explained by entrance in a quiescent state and spore formation. We note differences in final

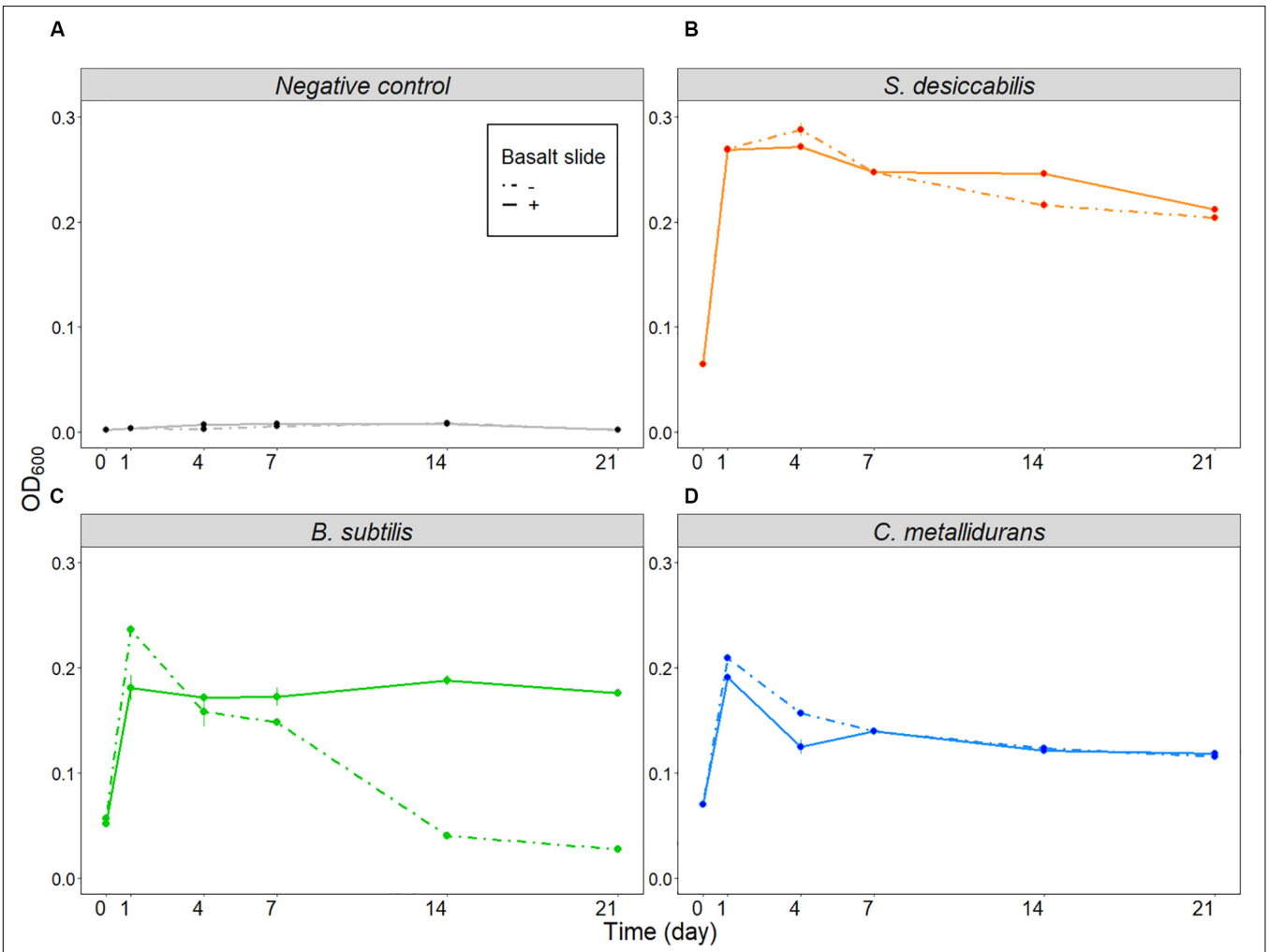

FIGURE 4 | Influence of basalt slide on cell growth (ground experiment). Average optical densities for the three organisms, plus the negative control, over 21 days in the presence or absence of the basalt slide. **(A)** Shows the results for the negative controls, **(B)** for *S. desiccabilis*, **(C)** for *B. subtilis*, and **(D)** for *C. metallidurans*. Dotted lines represent data from cell cultures grown in the absence of the basalt slide, continuous lines represent growth in the presence of the basalt slide. Mean values from three independent experiments are plotted at each time-point (n = 3). Error bars represent standard errors.

cell concentrations of *B. subtilis* in these experiments compared to the True 1-*g* samples. This might be accounted for by technical differences, such as the growth in 6-well plate and the use of a fresh overnight culture of vegetative cells to start the experiment, with no period of prior desiccation. Taken together, our data demonstrated that the presence of the basalt rock in the culture did not hinder bacterial growth, on the contrary it demonstrated the potential to enhance cell growth and survival.

Cell Sedimentation and Diffusion Under Microgravity, Mars and Earth Gravity

Sedimentation of cells has relevant effects on a liquid culture (Benoit and Klaus, 2005); however, it does not occur in microgravity (Klaus et al., 1997). To estimate whether we would expect cell sedimentation under Martian and terrestrial gravity regimens over the timeframe of our experiment, we calculated the velocity of sedimentation of a single cell (v_{cell}). Calculations with two different microgravity regimens were added to demonstrate the negligibility of sedimentation in this gravity condition for the timeframe of our experiment. For the microgravity calculation, we used both the upper limit ($1 \times 10^{-2} \times g$) and one commonly used value when defining microgravity ($1 \times 10^{-6} \times g$). Cell sedimentation velocity (v_{cell}) values for Earth and Mars gravity were 5.48×10^{-8} and 2.05×10^{-8} m s^{-1} (**Table 2**, column III), or 4.74 and 1.77 mm day^{-1}, respectively (**Table 2**, column IV). Considering an estimated maximum length of the culture chamber of 2.3 cm (the distance from the surface of the basalt rock to the outer membrane, **Figure 5**), it would have taken a cell 4.86 and 12.98 days, in Earth and Mars gravity respectively, to settle on the outer membrane (**Table 2**, column VI). A bacterial cell would have taken at least 486 days to settle in the culture chamber in microgravity (**Table 2**, column VI).

By contrast, the diffusion rate is independent of gravity (Klaus et al., 1997). The calculations showed that the distance traveled by a cell-size object due to random Brownian movement would have been only 0.25 mm in one day, and 1.14 mm in 21 days. Therefore, during the time it would have taken for a cell to sediment from one end of the culture chamber to the other (2.3 cm, **Table 2**, column VI) in Earth and Mars gravity conditions, a cell would have randomly traveled only 0.55 and 0.90 mm respectively (**Table 2**, column VII).

It must be noted that these calculations are necessarily estimates, e.g., assuming the cells are spherical shaped. However, due to the dependency of cell shape upon their growth stage, nutritional availability and space conditions (Zea et al., 2017), calculations resulting from modeling the organisms' shape would have been equally approximated. Motility was not considered here. Nevertheless, these calculations allowed us to estimate the occurrence of cell sedimentation in the timeframe of the experiment.

Cell Aggregation Revealed by Post-Fixation Photo Session

Two series of photos (photo sessions) of the Experimental Units (EUs) were taken onboard the ISS and at NASA Ames Research Center (ground reference) during the experiment (see section "Materials and Methods" and **Figure 2**). The first photo session (photo session 1; **Supplementary Figure 3**) verified the successful activation of the experiment by an effective medium injection and consequent re-hydration of the samples (see section "Materials and Methods" for details). The post-fixation photo session (photo session 2, **Figure 6**) was performed after the experiment was completed, immediately following bacterial growth for 21 days and fixative injection. Despite providing qualitative rather than quantitative data, this approach allowed for the visualization of some features of the cell cultures that were no longer observable when the samples were retrieved on Earth after download. Aggregates were present in *S. desiccabilis* and *C. metallidurans* cultures in simulated Earth *g*. For *S. desiccabilis*, a smaller aggregate was observed in Mars *g* (**Figure 6**, yellow arrows) consistent with expectations from the theoretical calculations, but no aggregates were observed in *C. metallidurans* under Martian gravity condition. However, in the True-1*g* chambers, aggregates were absent or only produced in small amounts (i.e., *S. desiccabilis* and *C. metallidurans*). No aggregates were formed in any *B. subtilis* cultures.

In addition, it was possible to observe the presence of small gas inclusions (bubbles) in all samples exposed to microgravity (**Figure 6**, blue arrows). The bubbles in μ*g* appeared larger and more numerous in the cell cultures compared to the cell-free negative controls. In Mars *g*, few very small bubbles were present in the cell cultures, and none were observed in the negative controls. This suggested that their origin was biological. Bubbles were absent in $1 \times g$ (Flight-1*g* and True-1*g*). The largest bubble visible in each container was caused by a void volume present in the hardware's ducts.

TABLE 2 | Values for the calculated sedimentation rates. Cell sedimentation velocity (v_{cell}) was calculated for Earth *g*, Mars *g* and microgravity (columns I–II). For this latter we used two different values ($1 \times 10^{-2} \times g$ and $1 \times 10^{-}6 \times g$). Different units are shown to underline the estimated cell sedimentation rate in the culture chamber over the BioRock experiment (columns III–VI). The distance a cell would travel by random Brownian movements during the time necessary to settle in the culture chamber (column VI) is reported in column VII.

I	II	III	IV	V	VI	VII
Gravity condition	**Gravity regime (× *g*)**	**v_{cell} (m s^{-1})**	**v_{cell} (mm day^{-1})**	**Distance in 21 days (cm)**	**Time to travel 2.3 cm (day)**	**Distance by Brownian diffusion with *t* from VI (mm)**
Earth *g*	1	5.48×10^{-8}	4.74	9.95	4.86	0.55
Mars *g*	0.4	2.05×10^{-8}	1.77	3.72	12.98	0.90
μ*g* (upper value)	1×10^{-2}	5.48×10^{-10}	4.74×10^{-2}	9.95×10^{-2}	4.86×10^{2}	5.49
μ*g* (typical value)	1×10^{-6}	5.48×10^{-14}	4.74×10^{-6}	9.95×10^{-6}	4.86×10^{6}	5.49×10^{2}

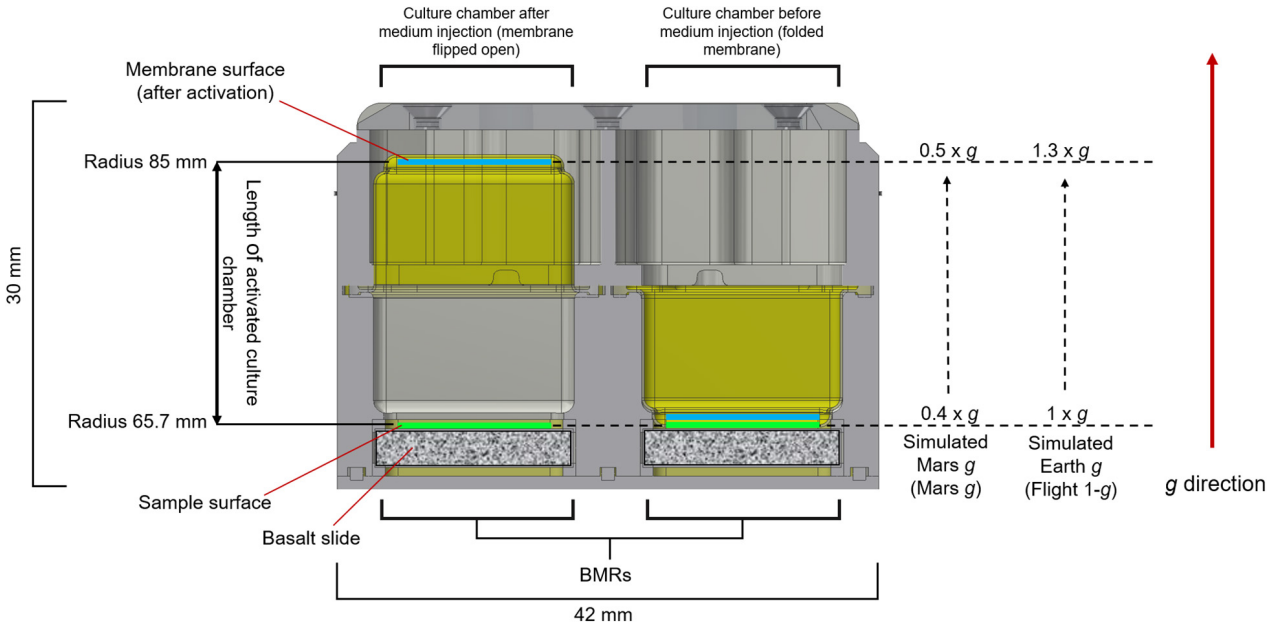

FIGURE 5 | Gravity levels provided by the KUBIK inside the BMR chamber. The image shows a cross-section of the Experimental Unit (EU) before (right BMR) and after (left BMR) activation by medium injection. The membranes are colored in yellow. 1 × *g* and 0.4 × *g* were delivered at the top surface of the basalt slides (sample surface). When the membrane flips (left BMR), following medium injection in the chamber, the radius of the culture chambers ranges from 65.7 mm to approx. 85 mm. In the KUBIK incubators, the direction of the gravity vector imposed on the EU goes from the basalt slide toward the membrane surface. This causes a 1.3-fold increase of gravity across the culture chamber, leading to a gravity acceleration on the membrane surface of 1.3 × *g* (Flight 1-*g*) and 0.5 × *g* (Mars *g*).

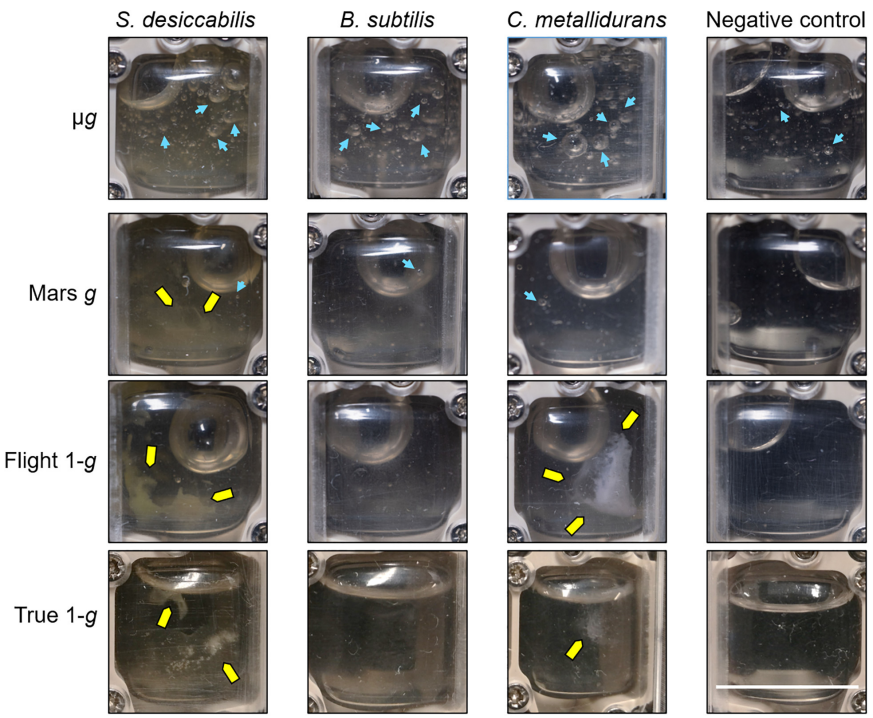

FIGURE 6 | Images from the second (post-fixation) photo session onboard the ISS. Representative photos of the individual culture chambers after three weeks of growth and fixative injection. Each image shows the culture chamber of a single BioMining Reactor (BMR). Pictures of the samples in microgravity (μ*g*), Mars gravity (Mars *g*) and terrestrial gravity (Flight-1*g*) were taken during the spaceflight (in microgravity), while pictures of the ground controls (True-1*g*) were taken at NASA Ames Research Center (at 1 × *g*). Yellow arrows indicate aggregates. Blue arrows indicate some of the small gas inclusions (bubbles) discussed in the main text. The scale bar has been measured on the shorter side of the BMR and corresponds to ∼14 mm.

DISCUSSION

In contrast to other organisms, the effects of reduced gravity regimens, such as microgravity or Martian gravity, on bacterial growth rates and final concentration are controversial. Some of the discrepancies could have been caused by the use of different experimental conditions, due to the variety of scientific questions addressed and the scarcity of spaceflight opportunities, as recently reviewed in Huang et al. (2018). The ESA BioRock experiment examined the microbe-mineral interactions of three bacteria with diverse characteristics (**Supplementary Table 1**), under identical growth conditions, in the same experimental apparatus and during the same spaceflight. The analysis of the liquid cultures after the spaceflight allowed us to measure the final cell concentration and optical density for the three bacterial cultures, and to test the hypothesis that the four examined gravity regimens would influence final cell concentrations.

We did not observe any significant differences in the final cell concentrations, within any of the three organisms, between the three gravity conditions in space (μ*g*, Mars *g* and Flight-1*g*) after 21 days (when all cultures had reached late stationary phase). This was an unexpected result. Due to the different physical and biological conditions, we expected to see significant differences between microgravity and gravities in which sedimentation occurred, i.e., 0.4 × *g* and 1 × *g* (**Table 2**). We suggest three potential explanations for the lack of significant differences observed.

One explanation could be that the cells were not affected by the physical conditions experienced and went through similar growth curves in all conditions, hence arriving at identical final concentrations in the late stationary phase. Arguing against it, lack of cell sedimentation occurring in microgravity is thought to have an important influence on cell growth (Benoit and Klaus, 2005), although difficult to predict (Klaus et al., 1997). Different authors suggested both positive and negative effects of lack of sedimentation in microgravity on bacterial cell growth (Marsh and Odum, 1979; Kacena et al., 1999a). For instance, lack of sedimentation in microgravity could influence continuous diffusional access to nutrients (Kacena et al., 1999a). Nutrient richness could influence the bacterial response to microgravity (Baker et al., 2004; Kim et al., 2013a,b). The theoretical calculations we presented in this study showed that sedimentation could occur in less than the total timeframe (21 days) of the experiment, along the entire length of the chamber, for both 1 × *g* and 0.4 × *g*, while sedimentation in microgravity conditions was estimated to be negligible in our experiment (**Table 2**). Our calculations showed that the cells would not be completely dispersed through the chamber by diffusion alone in 21 days, since the mean square distance traveled by a cell due to Brownian movement in this time was theoretically ∼1.3 mm^2. Consistent with our calculations, no aggregation was observed in the BMRs subject to microgravity while they were visible in 1 × *g* and 0.4 × *g* (**Figure 6**), although aggregation by quorum sensing has been reported in microgravity (Mastroleo et al., 2013; Condori et al., 2016).

Motility should be considered. If sedimentation limited access to nutrients as reported above, motile bacteria would have had an advantage at a higher sedimentation rate as they could have escaped sedimentation. Some authors suggested that, in the absence of convective mixing (i.e., in μ*g*) or in the presence of sedimentation associated with gravity conditions on the Earth, motility is an advantage, as the movement of flagella allows cells to move into a fresh-nutrient area (Benoit and Klaus, 2007; Zea et al., 2017). Yet, the single non-motile microorganisms present in the BioRock experiment, *S. desiccabilis*, exhibited no obvious difference in final cell concentration in microgravity compared to higher gravities, similarly to the motile *B. subtilis* and *C. metallidurans*. Considering the arguments above, a complete lack of gravity-driven effects on bacterial growth is unlikely, and the first explanation provided is therefore implausible.

A second explanation could be that the conditions were indeed different between the gravity regimens, but the diverse factors exactly counteracted each other, leading to similar growth rates and final numbers within each bacterial species. For example, the increase in oxygen availability caused by sedimentation on the gas-semipermeable membrane might have been offset by a lack of cell access to nutrients, and these growth conditions also matched those under the microgravity diffusion-limited regime. However, a perfect counteraction of all the factors seems unlikely.

A third explanation is that, although the different physical environment in each gravity regime could have led to different growth rates and responses, by the end of the experiment all cells had effectively reached stationary phase, resulting in similar cell numbers within each bacterial species. Other space experiments reported comparable final cell concentrations with respect to their ground controls, despite differences in early growth phases (Klaus et al., 1997; Nicholson and Ricco, 2020), and after several days of growth in simulated microgravity compared to normal gravity control (Mastroleo et al., 2013). In our experiment, the bacterial cultures were grown for 21 days (which allowed us to maximize the bioleaching of elements from the rock). This is much longer than most space microbiology experiments, which tend to be on the order of hours or days. Our experiment would have allowed all the species to grow beyond exponential phase into stationary phase (similarly to the ground experiment in **Figure 4**), reaching similar final cell numbers in all conditions. Hence, we suggest the third hypothesis represents the most plausible explanation.

Although direct cell counts in the three organisms showed no significant difference between the different gravities in space, we did observe a significant optical density reduction in *S. desiccabilis* ground control (True 1-*g*) samples compared to samples in microgravity and simulated Mars gravity. Because optical density is influenced by cell shape and size, we cannot exclude that the results were due to a modified cell morphology in microgravity and Mars gravity, an effect shown in at least one other space experiment (Zea et al., 2017). Interestingly, these results were only observed when the optical densities of microgravity and Mars *g* were compared with True-1*g*, but not to simulated Earth *g* (Flight-1*g*) in space. Moreover, *B. subtilis* showed a significant difference in the final cell concentration (but not for optical densities) of Flight 1-*g* compared to True 1-*g*. Although the samples were treated with the same or very similar procedures and conditions (e.g., similar temperatures

as verified using temperature logs), there are still unavoidable differences between spaceflight and ground experiments. For instance, in contrast to real Earth gravity, simulated Earth gravity achieved by centrifugation generates inertial shear and Coriolis forces (Van Loon et al., 2003; van Loon, 2015). The launch and download of spaceflight samples may have added differences such as higher gravity levels and vibration stresses (de Sousa et al., 2020). Although this occurred before and after the bacterial growth period, they may have conditioned sample preservation. In addition to different gravity, an object within a space capsule in LEO is exposed to a higher dose of cosmic radiations compared to an object on Earth (Horneck et al., 2010), however, we did not undertake a biochemical study of radiation effects in this experiment. Although we did not have empirically determined explanations for the discrepancies between simulated and true Earth gravities, they nevertheless showed that using simulated Earth gravity controls in space in addition to ground is important and can greatly improve the comparison and confidence in results.

In conclusion, the results reported here have demonstrated no statistically significant effect of gravity conditions on the final cell concentrations achieved by three microorganisms with different cell characteristics (with respect to motility, spore formation and growth rates), after 21 days of growth. This included simulated Martian gravity, to our knowledge the first experiment to report the effects of Martian gravity on bacteria using a space platform. From the human perspective, microorganisms could represent both enormous advantages and threats in space as on Earth. As the ambitions for future spaceflight missions expand, it is important to understand the long-term effects of low gravity on bacteria (Horneck et al., 2010). BioRock provided a rare example of a microbial growth experiment in space over multiple weeks, a timeframe that resembles those required in bio-industrial processes. Our data suggests that biotechnological applications such as bioproduction, bio-manufacture and life support systems on Mars will be possible, as final cell concentrations would not be deleteriously affected by Mars gravity under similar growth conditions reported here. It has been demonstrated that different partial gravities can lead to diverse results in some organisms, such as plants (Kiss et al., 2012; Kiss, 2014). However, we showed no difference on final cell concentration between microgravity and Mars gravity, suggesting that a similar result might be obtained in Moon and other partial gravities. Follow-up studies should be focused on repetition of the experiment, with the aim to obtain insights on the molecular mechanisms leading the bacterial growth of the microorganisms used. It would also be important to select further natural and artificial substrates for bacterial growth, as well as suitable and bioindustrially relevant microorganisms. Scaling-up the system needs to consider the effects of sedimentation and convective mixing and the specific physical and chemical parameters of a larger bioreactor. In addition to their impact on space exploration, our results could provide useful inputs to applications on Earth, such as bioproduction in space for terrestrial utilization (Benoit et al., 2006; Huang et al., 2018), or employment of controlled shear stress bioreactors in bioindustry (Kacena et al., 1999b; Lange et al., 2001; Jonczyk et al., 2013).

DATA AVAILABILITY STATEMENT

All datasets presented in this study are included in the article/**Supplementary Material**.

ETHICS STATEMENT

Written informed consent was obtained from Luca Parmitano for the publication of any potentially identifiable images or data included in this article.

AUTHOR CONTRIBUTIONS

CSC conceived the BioRock experiment in the framework of ESA topical team. RS and CSC designed the experiments for this manuscript. RS, CSC, and ACW integrated the hardware for spaceflight and ground controls. RS, ACW, and WdW produced the experimental data. RM performed the spore enumeration. CSC and RS calculated the sedimentation rates. RS performed the data analyses. LP performed the procedures onboard the ISS with the supervision of BIOTESC. DLR (FMF, RM, and PR) and SCK CEN (RVH, IC, and NL) provided *B. subtilis* and *C. metallidurans* samples, respectively. RE and JW hosted the ground control experiment. Kayser Italia produced the hardware. ESTEC supervised the whole technical organization and BIOTESC supervised the flight procedures. RS wrote the manuscript. All authors discussed the results and commented on the manuscript, contributed to the article, and approved the submitted version.

FUNDING

CSC and RS have been funded by UK Science and Technology Facilities Council under grant ST/R000875/1. RM, FMF, and PR were supported by the DLR grant "DLR-FuE-Projekt ISS LIFE, Programm RF-FuW, Teilprogramm 475." FMF was also supported by the Helmholtz Space Life Sciences Research School at DLR. RVH and NL received financial support for this study from Belspo and ESA through the PRODEX EGEM/Biorock project contract (PEA 4000011082). ACW was funded by NERC Doctoral Training Partnership grant (NE/L002558/1) and PCDS (Principal's Career Development Scholarship).

ACKNOWLEDGMENTS

We thank the European Space Agency (ESA) for offering the flight opportunity. A special thanks to the dedicated ESA/ESTEC teams, Kayser Italia s.r.l., and the USOC BIOTESC for the development, integration and operation effort and the excellent collaboration. We are thankful to the UK Space Agency (UKSA) for the national support to the project. We also thank NASA Kennedy for their support in the experiment integration prior to

the SpaceX Falcon 9 CSR-18 rocket launch, particularly Kamber Scott and Anne Currin, and NASA Ames for hosting both the ground control experiment and the PI team during the post-flight sample recovering. We are thankful to Hadrien Jouet and Mauro Manzo for creating the BioRock logo.

SUPPLEMENTARY MATERIAL

The Supplementary Material for this article can be found online at: https://www.frontiersin.org/articles/10.3389/fmicb.2020.579156/full#supplementary-material

REFERENCES

Axpe, E., Chan, D., Abegaz, M. F., Schreurs, A.-S., Alwood, J. S., Globus, R. K., et al. (2020). A human mission to mars: predicting the bone mineral density loss of astronauts. *PLoS One* 15:e0226434. doi: 10.1371/journal.pone.0226434

Baker, P. W., Meyer, M. L., and Leff, L. G. (2004). *Escherichia coli* growth under modeled reduced gravity. *Micrograv. Sci. Technol.* 15, 39–44. doi: 10.1007/BF02870967

Bart, M. C., Vet, S. J., De, Bakker, D. M. D., Alexander, B. E., Oevelen, D., et al. (2019). Spiculous skeleton formation in the freshwater sponge *Ephydatia fluviatilis* under hypergravity conditions. *PeerJ* 6, 1–18. doi: 10.7717/peerj.6055

Benoit, M., and Klaus, D. (2005). Can genetically modified *Escherichia coli* with neutral buoyancy induced by gas vesicles be used as an alternative method to clinorotation for microgravity studies? *Microbiology* 151, 69–74. doi: 10.1099/mic.0.27062-0

Benoit, M., Stodieck, L., Ica, B., Relevant, L. L. Y., Nd, E. A., and Teins, P. R. O. (2006). Microbial antibiotic production aboard the International Space Station. *Appl. Microbiol. Biotechnol.* 70, 403–411. doi: 10.1007/s00253-005-0098-3

Benoit, M. R., and Klaus, D. M. (2007). Microgravity, bacteria, and the influence of motility. *Adv. Sp. Res.* 39, 1225–1232. doi: 10.1016/j.asr.2006.10.009

Bouloc, P., and D'Ari, R. (1991). *Escherichia coli* metabolism in space. *J. Gen. Microbiol.* 137, 2839–2843. doi: 10.1099/00221287-137-12-2839

Bryce, C. C., Le Bihan, T., Martin, S. F., Harrison, J. P., Bush, T., Spears, B., et al. (2016). Rock geochemistry induces stress and starvation responses in the bacterial proteome. *Environ. Microbiol.* 18, 1110–1121. doi: 10.1111/1462-2920.13093

Byloos, B., Coninx, I., Van Hoey, O., Cockell, C., Nicholson, N., Ilyin, V., et al. (2017). The impact of space flight on survival and interaction of *Cupriavidus metallidurans* CH34 with basalt, a volcanic moon analog rock. *Front. Microbiol.* 8:671. doi: 10.3389/fmicb.2017.00671

Cavanagh, P. R., Licata, A. A., and Rice, A. J. (2005). Exercise and pharmacological countermeasures for bone loss during long-duration space flight. *Gravitat. Sp. Biol.* 18, 39–58.

Cockell, C. S. (2010). Geomicrobiology beyond earth: microbe-mineral interactions in space exploration and settlement. *Trends Microbiol.* 18, 308–314. doi: 10.1016/j.tim.2010.03.005

Condori, S., Atkinson, S., Leys, N., Wattiez, R., and Mastroleo, F. (2016). Construction and phenotypic characterization of M68, an RruI quorum sensing knockout mutant of the photosynthetic alphaproteobacterium *Rhodospirillum rubrum*. *Res. Microbiol.* 167, 380–392. doi: 10.1016/j.resmic.2016.02.006

de Sousa, N., Caporicci, M., Vandersteen, J., Rojo-Laguna, J. I., Salò, E., Adell, T., et al. (2020). Molecular impact of launch related dynamic vibrations and static hypergravity in planarians. *npj Micrograv.* 6:25.

Fajardo-Cavazos, P., Leehan, J. D., and Nicholson, W. L. (2018). Alterations in the spectrum of spontaneous rifampicin-resistance mutations in the Bacillus subtilis rpoB gene after cultivation in the human spaceflight environment. *Front. Microbiol.* 9:192. doi: 10.3389/fmicb.2018.00192

Fuchs, F. M., Driks, A., Setlow, P., and Moeller, R. (2017). An improved protocol for harvesting *Bacillus subtilis* colony biofilms. *J. Microbiol. Methods* 134, 7–13. doi: 10.1016/j.mimet.2017.01.002

Gasset, G., Tixador, R., Eche, B., Lapchine, L., Moatti, N., Toorop, P., et al. (1994). Growth and division of *Escherichia coli* under microgravity conditions. *Res. Microbiol.* 145, 111–120. doi: 10.1016/0923-2508(94)90004-3

Gòdia, F., Albiol, J., Montesinos, J. L., Pérez, J., Creus, N., Cabello, F., et al. (2002). MELISSA: a loop of interconnected bioreactors to develop life support in Space. *J. Biotechnol.* 99, 319–330. doi: 10.1016/S0168-1656(02)00222-5

Gu, J. D., Roman, M., Esselman, T., and Mitchell, R. (1998). The role of microbial biofilms in deterioration of space station candidate materials. *Int. Biodeterior. Biodegrad.* 41, 25–33. doi: 10.1016/s0964-8305(98)80005-x

Hader, D.-P. (1996). NIZEMI - Experiments on the slow rotating centrifuge microscope during the IML-2 mission. *J. Biotechnol.* 47, 223–234. doi: 10.1016/0168-1656(96)01397-1

Hader, D.-P., Rosum, A., Schafer, J., and Hemmersbach, R. (1996). Graviperception in the flagellate *Euglena gracilis* during a shuttle space flight. *J. Biotechnol.* 47, 261–269. doi: 10.1016/0168-1656(96)01374-0

Hemmersbach, R., Bromeis, B., Block, I., Bräucker, R., Krause, M., Freiberger, N., et al. (2001). Paramecium - a model system for studying cellular graviperception. *Adv. Sp. Res.* 27, 893–898. doi: 10.1016/S0273-1177(01)00155-7

Hemmersbach, R., Voormanns, R., Briegleb, W., Riederb, N., and Hider, D.-P. (1996). Influence of accelerations on the spatial orientation of Loxodes and Paramecium. *J. Biotechnol.* 47, 271–278. doi: 10.1016/0168-1656(96)01337-5

Horneck, G., Klaus, D. M., and Mancinelli, R. L. (2010). Space microbiology. *Microbiol. Mol. Biol. Rev.* 74, 121–156. doi: 10.1128/MMBR.00016-09

Huang, B., Li, D. G., Huang, Y., and Liu, C. T. (2018). Effects of spaceflight and simulated microgravity on microbial growth and secondary metabolism. *Mil. Med. Res.* 5, 1–14. doi: 10.1186/s40779-018-0162-9

Ichijo, T., Yamaguchi, N., Tanigaki, F., Shirakawa, M., and Nasu, M. (2016). Four-year bacterial monitoring in the International Space Station—Japanese Experiment Module "Kibo" with culture-independent approach. *npj Micrograv.* 2:16007. doi: 10.1038/npjmgrav.2016.7

Janssen, P. J., van Houdt, R., Moors, H., Monsieurs, P., Morin, N., Michaux, A., et al. (2010). The complete genome sequence of *Cupriavidus metallidurans* strain CH34, a master survivalist in harsh and anthropogenic environments. *PLoS One* 5:e10433. doi: 10.1371/journal.pone.0010433

Jerez, C. A. (2017). Biomining of metals: how to access and exploit natural resource sustainably. *Microb. Biotechnol.* 10, 1191–1193. doi: 10.1111/1751-7915.12792

Jonczyk, P., Takenberg, M., Hartwig, S., Beutel, S., Berger, R. G., and Scheper, T. (2013). Cultivation of shear stress sensitive microorganisms in disposable bag reactor systems. *J. Biotechnol.* 167, 370–376. doi: 10.1016/j.jbiotec.2013.07.018

Kacena, M., and Todd, P. (1997). Growth characteristics of *E. coli* and *B. subtilis* cultured on an agar substrate in microgravity. *Micrograv. Sci. Technol.* 10, 58–62.

Kacena, M. A., Leonard, P. E., Todd, P., and Luttges, M. W. (1997). Low gravity and inertial effects on the growth of *E. coli* and *B. subtilis* in semi-solid media. *Aviat. Space Environ. Med.* 68, 1104–1108.

Kacena, M. A., Manfredi, B., and Todd, P. (1999a). Effects of space flight and mixing on bacterial growth in low volume cultures. *Micrograv. Sci. Technol.* 12, 74–77.

Kacena, M. A., Merrell, G. A., Manfredi, B., Smith, E. E., Klaus, D. M., and Todd, P. (1999b). Bacterial growth in space flight: logistic growth curve parameters for *Escherichia coli* and *Bacillus subtilis*. *Appl. Microbiol. Biotechnol.* 51, 229–234. doi: 10.1007/s002530051386

Kim, W., Tengra, F. K., Shong, J., Marchand, N., Chan, H. K., Young, Z., et al. (2013a). Effect of spaceflight on *Pseudomonas aeruginosa* final cell density is modulated by nutrient and oxygen availability. *BMC Microbiol.* 13:241. doi: 10.1186/1471-2180-13-241

Kim, W., Tengra, F. K., Young, Z., Shong, J., Marchand, N., Chan, H. K., et al. (2013b). Spaceflight promotes biofilm formation by *Pseudomonas aeruginosa*. *PLoS One* 8:e62437. doi: 10.1371/journal.pone.0062437

Kiss, J. Z. (2014). Plant biology in reduced gravity on the Moon and Mars. *Plant Biol.* 16, 12–17. doi: 10.1111/plb.12031

Kiss, J. Z., Millar, K. D. L., and Edelmann, R. E. (2012). Phototropism of *Arabidopsis thaliana* in microgravity and fractional gravity on the International Space Station. *Planta* 236, 635–645. doi: 10.1007/s00425-012-1633-y

Klaus, D., Simske, S., Todd, P., and Stodieck, L. (1997). Investigation of space flight effects on *Escherichia coli* and a proposed model of underlying physical mechanisms. *Microbiology* 143, 449–455. doi: 10.1099/00221287-143-2-449

Klaus, D. M., Benoit, M., Bonomo, J., Bollich, J., Freeman, J., and Stodieck, L. (2001). "Antibiotic production in space using an automated fed-bioreactor system," in *Proceedings of the 2001 Conference and Exhibit on International Space Station Utilization*, Cape Canaveral, FL, 1–6.

Lange, H., Taillandier, P., and Riba, J. (2001). Effect of high shear stress on microbial viability. *J. Chem. Technol. Biotechnol.* 76, 501–505. doi: 10.1002/jctb.401

Leys, N., Baatout, S., Rosier, C., Dams, A., s'Heeren, C., Wattiez, R., et al. (2009). The response of *Cupriavidus metallidurans* CH34 to spaceflight in the international space station. *Int. J. Gen. Mol. Microbiol.* 96, 227–245. doi: 10.1007/s10482-009-9360-5

Leys, N., Hendrickx, L., de Boever, P., Baatout, S., and Mergeay, M. (2004). Space flight effects on bacterial physiology. *J. Biol. Regul. Homeost. Agents* 18, 193–199.

Loudon, C. M., Nicholson, N., Finster, K., Leys, N., Byloos, B., Van Houdt, R., et al. (2018). BioRock: new experiments and hardware to investigate microbe–mineral interactions in space. *Int. J. Astrobiol.* 17, 303–313. doi: 10.1017/S1473550417000234

Marsh, D. H., and Odum, W. E. (1979). Effect of suspension and sedimentation on the amount of microbial colonization of salt marsh microdetritus. *Estuaries* 2, 184–188. doi: 10.2307/1351733

Mastroleo, F., Houdt, R., Van, Atkinson, S., Mergeay, M., Hendrickx, L., et al. (2013). Modelled microgravity cultivation modulates N-acylhomoserine lactone production in *Rhodospirillum rubrum* S1H independently of cell density. *Microbiology* 159, 2456–2466. doi: 10.1099/mic.0.066415-0

Matía, I., González-Camacho, F., Herranz, R., Kiss, J. Z., Gasset, G., van Loon, J. J. W. A., et al. (2010). Plant cell proliferation and growth are altered by microgravity conditions in spaceflight. *J. Plant Physiol.* 167, 184–193. doi: 10.1016/j.jplph.2009.08.012

Maupin, K. A., Childress, P., Brinker, A., Khan, F., Abeysekera, I., Aguilar, I. N., et al. (2019). Skeletal adaptations in young male mice after 4 weeks aboard the International Space Station. *npj Microgravity* 5:21. doi: 10.1038/s41526-019-0081-4

McCutcheon, G., Kent, R., Paulino-Lima, I., Pless, E., Ricco, A., Mazmanian, E., et al. (2016). "PowerCells payload on EuCROPIS - measuring synthetic biology in space," in *Proceedings of the 29th Annual AIAA/USU Conference on Small Satellites* Logan, UT

Menezes, A. A., Cumbers, J., Hogan, J. A., and Arkin, A. P. (2015a). Towards synthetic biological approaches to resource utilization on space missions. *J. R. Soc. Interface* 12:20140715. doi: 10.1098/rsif.2014.0715

Menezes, A. A., Montague, M. G., Cumbers, J., Hogan, J. A., and Arkin, A. P. (2015b). Grand challenges in space synthetic biology. *J. R. Soc. Interface* 12:20150803. doi: 10.1098/rsif.2015.0803

Milojevic, T., and Weckwerth, W. (2020). Molecular mechanisms of microbial survivability in outer space: a systems biology approach. *Front. Microbiol.* 11:923. doi: 10.3389/fmicb.2020.00923

Monsieurs, P., Mijnendonckx, K., Provoost, A., Venkateswaran, K., Ott, M., Leys, N., et al. (2014). Genome sequences of *Cupriavidus metallidurans* strains NA1, NA4, and NE12, isolated from space equipment. *Genome Announc.* 2:e00719-14. doi: 10.1128/genomeA.00719-14

Mora, M., Wink, L., Kögler, I., Mahnert, A., Rettberg, P., Schwendner, P., et al. (2019). Space Station conditions are selective but do not alter microbial characteristics relevant to human health. *Nat. Commun.* 10:3990. doi: 10.1038/s41467-019-11682-z

Morrison, M. D., Fajardo-Cavazos, P., and Nicholson, W. L. (2019). Comparison of Bacillus subtilis transcriptome profiles from two separate missions to the International Space Station. *npj Microgravity* 5:1. doi: 10.1038/s41526-018-0061-0

Mulders, S. E., Van, Daenen, L., Devreese, B., Siewers, V., Eijsden, R. G. E., et al. (2011). The influence of microgravity on invasive growth in *Saccharomyces cerevisiae*. *Astrobiology* 11, 45–55. doi: 10.1089/ast.2010.0518

Nicholson, W. L., and Ricco, A. J. (2020). Nanosatellites for biology in space: in situ measurement of *Bacillus subtilis* spore germination and growth after 6 months in low earth orbit on the O/OREOS mission. *Life* 10, 1–14. doi: 10.3390/life10010001

Nickerson, C. A., Ott, C. M., Wilson, J. W., Ramamurthy, R., and Pierson, D. L. (2004). Microbial responses to microgravity and other low-shear environments. *Microbiol. Mol. Biol. Rev.* 68, 345–361. doi: 10.1128/mmbr.68.2.345-361.2004

Novikova, N. D. (2004). Review of the knowledge of microbial contamination of the Russian manned spacecraft. *Microb. Ecol.* 47, 127–132. doi: 10.1007/s00248-003-1055-2

Nye, T. M., Schroeder, J. W., Kearns, D. B., and Simmons, L. A. (2017). Complete genome sequence of undomesticated *Bacillus subtilis* strain NCIB 3610. *Genome Announc.* 5, 12–13. doi: 10.1128/genomeA.00364-17

Olsson-Francis, K., Van Houdt, R., Mergeay, M., Leys, N., and Cockell, C. S. (2010). Microarray analysis of a microbe-mineral interaction. *Geobiology* 8, 446–456. doi: 10.1111/j.1472-4669.2010.00253.x

Paul, A. L., Wheeler, R. M., Levine, H. G., and Fer, R. J. (2013). Fundamental plant biology enabled by the space shuttle. *Am. J. Bot.* 100, 226–234. doi: 10.3732/ajb.1200338

Pollard, E. C. (1965). Theoretical studies on living systems in the absence of mechanical stress. *J. Theor. Biol.* 8, 113–123. doi: 10.1016/0022-5193(65)90097-4

Reasoner, D. J., and Geldreich, E. E. (1985). A new medium for the enumeration and subculture of bacteria from potable water. *Appl. Environ. Microbiol.* 49, 1–7. doi: 10.1128/aem.49.1.1-7.1985

Reddy, G. S. N., and Garcia-Pichel, F. (2007). *Sphingomonas mucosissima* sp. nov. and *Sphingomonas desiccabilis* sp. nov., from biological soil crusts in the Colorado Plateau, USA. *Int. J. Syst. Evol. Microbiol.* 57, 1028–1034. doi: 10.1099/ijs.0.64331-0

Reed, D. W., Fujita, Y., Daubaras, D. L., Jiao, Y., and Thompson, V. S. (2016). Bioleaching of rare earth elements from waste phosphors and cracking catalysts. *Hydrometallurgy* 166, 34–40. doi: 10.1016/j.hydromet.2016.08.006

Rosenzweig, J. A., and Chopra, A. K. (2012). The effect of low shear force on the virulence potential of *Yersinia pestis*: new aspects that space-like growth conditions and the final frontier can teach us about a formidable pathogen. *Front. Cell. Infect. Microbiol.* 2:107. doi: 10.3389/fcimb.2012.00107

Ruttley, T. M., Evans, C. A., and Robinson, J. A. (2009). The importance of the International Space Station for life sciences research: past and future. *Gravitat. Sp. Biol.* 22, 67–82.

Santosh, B., Dudhale, R., Dixit, J., Sahasrabuddhe, A., and Vidyasagar, P. B. (2011). Growth of bioluminescent bacteria under modelled gravity of different astronomical bodies in the Solar system. *Arxiv*. Available at: http://arxiv.org/abs/1109.5786

Schippers, A., Hedrich, S., Vasters, J., Drobe, M., Sand, W., and Willscher, S. (2013). "Biomining: metal recovery from ores with microorganisms," in Geobiotechnology I. *Adv. Biochem. Eng. Biotechnol.* 141, 1–47. doi: 10.1007/10

Setlow, P., Wang, S., and Li, Y.-Q. (2017). Germination of spores of the orders bacillales and clostridiales. *Annu. Rev. Microbiol.* 71, 459–477. doi: 10.1146/annurev-micro-090816-093558

Sielaff, A. C., Urbaniak, C., Babu, G., Mohan, M., Stepanov, V. G., Tran, Q., et al. (2019). Characterization of the total and viable bacterial and fungal communities associated with the International Space Station surfaces. *Microbiome* 7:50.

Song, W., Ogawa, N., Oguchi, C. T., Hatta, T., and Matsukura, Y. (2007). Effect of *Bacillus subtilis* on granite weathering: a laboratory experiment. *Catena* 70, 275–281. doi: 10.1016/j.catena.2006.09.003

Stevens, A. H., Childers, D., Fox-powell, M., Nicholson, N., Jhoti, E., and Cockell, C. S. (2019). Growth, viability, and death of planktonic and biofilm *Sphingomonas desiccabilis* in simulated martian brines. *Astrobiology* 19, 87–98. doi: 10.1089/ast.2018.1840

Tahimic, C. G. T., Paul, A. M., Schreurs, A. S., Torres, S. M., Rubinstein, L., Steczina, S., et al. (2019). Influence of social isolation during prolonged simulated weightlessness by hindlimb unloading. *Front. Physiol.* 10:1147. doi: 10.3389/fphys.2019.01147

Taylor, P. W. (2015). Impact of space flight on bacterial virulence and antibiotic susceptibility. *Infect. Drug Resist.* 8, 249–262. doi: 10.2147/IDR.S67275

Todd, P. (1989). Gravity-dependent phenomena at the scale of the single cell. *GSB Bull.* 2, 95–113.

van Loon, J. J. W. A. (2015). *Centrifuges. Generation and Application of Extra-Terrestrial Environments on Earth*. Denmark: River Publishers.

Van Loon, J. J. W. A., Folgering, E. H. T. E., Bouten, C. V. C., Veldhuijzen, J. P., and Smit, T. H. (2003). Inertial shear forces and the use of centrifuges in

gravity research. What is the proper control? *J. Biomech. Eng.* 125, 342–346. doi: 10.1115/1.1574521

Van Ombergen, A., Demertzi, A., Tomilovskaya, E., Jeurissen, B., Sijbers, J., Kozlovskaya, I. B., et al. (2017). The effect of spaceflight and microgravity on the human brain. *J. Neurol.* 264, 18–22. doi: 10.1007/s00415-017-8427-x

Vandecraen, J., Monsieurs, P., Mergeay, M., Leys, N., Aertsen, A., and Van Houdt, R. (2016). Zinc-induced transposition of insertion sequence elements contributes to increased adaptability of *Cupriavidus metallidurans*. *Front. Microbiol.* 7:359. doi: 10.3389/fmicb.2016.00359

Wassersug, R. J., Roberts, L., Gimian, J., Hughes, E., Saunders, R., Devison, D., et al. (2005). The behavioral responses of amphibians and reptiles to microgravity on parabolic flights. *Zoology* 108, 107–120. doi: 10.1016/j.zool.2005.03.001

Wilson, J. W., Ott, C. M., Höner, Zu Bentrup, K., Ramamurthy, R., Quick, L., et al. (2007). Space flight alters bacterial gene expression and virulence and reveals a role for global regulator Hfq. *Proc. Natl. Acad. Sci. U.S.A.* 104, 16299–16304. doi: 10.1073/pnas.0707155104

Zabel, P., Bamsey, M., Schubert, D., and Tajmar, M. (2016). Review and analysis of over 40 years of space plant growth systems. *Life Sci. Sp. Res.* 10, 1–16. doi: 10.1016/j.lssr.2016.06.004

Zaets, I., Burlak, O., Rogutskyy, I., Vasilenko, A., Mytrokhyn, O., Lukashov, D., et al. (2011). Bioaugmentation in growing plants for lunar bases. *Adv. Sp. Res.* 47, 1071–1078. doi: 10.1016/j.asr.2010.11.014

Zea, L., Larsen, M., Estante, F., Qvortrup, K., Moeller, R., de Oliveira, S. D., et al. (2017). Phenotypic changes exhibited by *E. coli* cultured in space. *Front. Microbiol.* 8:1598. doi: 10.3389/fmicb.2017.01598

Zea, L., Prasad, N., Levy, S. E., Stodieck, L., Jones, A., Shrestha, S., et al. (2016). A molecular genetic basis explaining altered bacterial behavior in space. *PLoS One* 2:e0164359. doi: 10.1371/journal.pone.0164359

Conflict of Interest: VZ, MB, AM, SP, FC, and GL were employed by the company Kayser Italia S.r.l.

The remaining authors declare that the research was conducted in the absence of any commercial or financial relationships that could be construed as a potential conflict of interest.

Citation: Santomartino R, Waajen AC, de Wit W, Nicholson N, Parmitano L, Loudon C-M, Moeller R, Rettberg P, Fuchs FM, Van Houdt R, Finster K, Coninx I, Krause J, Koehler A, Caplin N, Zuijderduijn L, Zolesi V, Balsamo M, Mariani A, Pellari SS, Carubia F, Luciani G, Leys N, Doswald-Winkler J, Herová M, Wadsworth J, Everroad RC, Rattenbacher B, Demets R and Cockell CS (2020) No Effect of Microgravity and Simulated Mars Gravity on Final Bacterial Cell Concentrations on the International Space Station: Applications to Space Bioproduction. Front. Microbiol. 11:579156. doi: 10.3389/fmicb.2020.579156

frontiers in Microbiology

ORIGINAL RESEARCH
published: 05 November 2020
doi: 10.3389/fmicb.2020.530661

Prokaryotic and Fungal Characterization of the Facilities Used to Assemble, Test, and Launch the OSIRIS-REx Spacecraft

Aaron B. Regberg[1], Christian L. Castro[2], Harold C. Connolly Jr.[3,4], Richard E. Davis[5], Jason P. Dworkin[6], Dante S. Lauretta[4], Scott R. Messenger[1], Hannah L. Mclain[6], Francis M. McCubbin[1], Jamie L. Moore[7], Kevin Righter[1], Sarah Stahl-Rommel[2] and Sarah L. Castro-Wallace[8]*

[1] Astromaterials Research and Exploration Science Division, National Aeronautics and Space Administration (NASA) Johnson Space Center, Houston TX, United States, [2] JES Tech, Houston, TX, United States, [3] Department of Geology, Rowan University, Glassboro, NJ, United States, [4] Lunar and Planetary Laboratory, University of Arizona, Tucson, AZ, United States, [5] Jacobs@NASA/Johnson Space Center, Houston, TX, United States, [6] Astrochemistry Laboratory, Goddard Space Flight Center, Greenbelt, MD, United States, [7] Lockheed Martin Space Systems, Littleton, CO, United States, [8] Biomedical Research and Environmental Sciences Division, Johnson Space Center, Houston, TX, United States

OPEN ACCESS

Edited by:
Ralf Moeller, German Aerospace Center, Helmholtz Association of German Research Centers (HZ), Germany

Reviewed by:
Brandi Kiel Reese, Dauphin Island Sea Lab, United States
Claudia Coleine, University of Tuscia, Italy

***Correspondence:**
Aaron B. Regberg
aaron.b.regberg@nasa.gov

Specialty section:
This article was submitted to Extreme Microbiology, a section of the journal Frontiers in Microbiology

Received: *29 January 2020*
Accepted: *30 September 2020*
Published: *05 November 2020*

Citation:
Regberg AB, Castro CL, Connolly HC Jr, Davis RE, Dworkin JP, Lauretta DS, Messenger SR, Mclain HL, McCubbin FM, Moore JL, Righter K, Stahl-Rommel S and Castro-Wallace SL (2020) Prokaryotic and Fungal Characterization of the Facilities Used to Assemble, Test, and Launch the OSIRIS-REx Spacecraft. Front. Microbiol. 11:530661. doi: 10.3389/fmicb.2020.530661

To characterize the ATLO (Assembly, Test, and Launch Operations) environment of the OSIRIS-REx spacecraft, we analyzed 17 aluminum witness foils and two blanks for bacterial, archaeal, fungal, and arthropod DNA. Under NASA's Planetary Protection guidelines, OSIRIS-REx is a Category II outbound, Category V unrestricted sample return mission. As a result, it has no bioburden restrictions. However, the mission does have strict organic contamination requirements to achieve its primary objective of returning pristine carbonaceous asteroid regolith to Earth. Its target, near-Earth asteroid (101955) Bennu, is likely to contain organic compounds that are biologically available. Therefore, it is useful to understand what organisms were present during ATLO as part of the larger contamination knowledge effort—even though it is unlikely that any of the organisms will survive the multi-year deep space journey. Even though these samples of opportunity were not collected or preserved for DNA analysis, we successfully amplified bacterial and archaeal DNA (16S rRNA gene) from 16 of the 17 witness foils containing as few as 7 ± 3 cells per sample. Fungal DNA (ITS1) was detected in 12 of the 17 witness foils. Despite observing arthropods in some of the ATLO facilities, arthropod DNA (COI gene) was not detected. We observed 1,009 bacterial and archaeal sOTUs (sub-operational taxonomic units, 100% unique) and 167 fungal sOTUs across all of our samples (25–84 sOTUs per sample). The most abundant bacterial sOTU belonged to the genus *Bacillus*. This sOTU was present in blanks and may represent contamination during sample handling or storage. The sample collected from inside the fairing just prior to launch contained several unique bacterial and fungal sOTUs that describe previously uncharacterized potential for contamination during the final phase of ATLO. Additionally, fungal richness (number of sOTUs) negatively correlates with the number of carbon-bearing particles detected on samples. The total number of fungal sequences

positively correlates with total amino acid concentration. These results demonstrate that it is possible to use samples of opportunity to characterize the microbiology of low-biomass environments while also revealing the limitations imposed by sample collection and preservation methods not specifically designed with biology in mind.

Keywords: tag sequencing, oligotrophs, 16S, ITS, contamination, spacecraft, planetary protection

INTRODUCTION

The OSIRIS-REx (Origins, Spectral Interpretation, Resource Identification, and Security–Regolith Explorer) spacecraft was designed and built to visit, study, and sample the near-Earth asteroid (101955) Bennu (Lauretta et al., 2017). The mission launched in 2016 and reached its target in December 2018. Bennu is a B-type asteroid that is spectrally similar, and therefore expected to be compositionally and mineralogically similar, to carbonaceous chondrites collected on Earth (Hamilton et al., 2019; Lauretta et al., 2019). Carbonaceous chondrites (Weisberg et al., 2006) typically contain a wide variety of organic compounds and are hypothesized to have delivered these prebiotic molecules to Earth early in its history (Lauretta et al., 2015). Some of these compounds, like amino acids (Burton et al., 2012) are easily altered by terrestrial microorganisms; others like large kerogen molecules are more recalcitrant (Kebukawa et al., 2010). Meteorites collected on Earth are often affected by microbial activity (Toporski and Steele, 2007; Steele et al., 2016; Tait et al., 2017). OSIRIS-REx will collect and return samples from Bennu using the pristine TAGSAM (Touch-and-Go Sample Acquisition Mechanism) (Bierhaus et al., 2018). The mission is required to keep these samples pristine and minimally altered during collection and return.

The OSIRIS-REx mission has a strict requirement to mitigate and document organic contamination. An extensive effort was made to characterize potential types and sources of organic and inorganic contamination during assembly, test, and launch operations by placing witness foils inside the cleanrooms where these activities occurred (Dworkin et al., 2018). NASA's Planetary Protection guidelines designate OSIRIS-REx as a Category II outbound, Category V unrestricted sample return mission (Rummel, 2000) so there were no requirements to document biological contamination and thus a campaign of biological or DNA testing was beyond the scope of the mission. However, we had an opportunity to examine surplus witness foils originally prepared for amino acid analysis to characterize the microbiology of the assembly, test, and launch environment. This presents a rare opportunity to study a clean, but not sterilized, spacecraft over time during assembly and testing. Many cleanroom-associated microbes are capable of altering or consuming organic compounds like those we expect to return from Bennu (Balch et al., 2009; Moissl-Eichinger, 2017). Most organisms on Earth are capable of consuming amino acids which is one of the primary compound classes of interest. Even if it is unlikely that any organism will survive the harsh conditions of space for 8 years until the samples are returned to Earth, it is still useful to document microbes that the spacecraft encountered. The knowledge gained by generating a microbial inventory of organically controlled assembly, test, and launch facilities can be used to derive requirements, and develop cleaning protocols for future bioburden-controlled operations. The measurements made on the witness foil from the Atlas V fairing are especially important because every spacecraft is exposed to a similar environment before launch and the microbiological composition of this environment has never been characterized.

The OSIRIS-REx spacecraft was constructed by Lockheed Martin Space Systems at their Waterton facility in Littleton, Colorado. The sample acquisition mechanism (TAGSAM) was assembled inside a small ISO 7 (ISO, 2015) cleanroom in the SSB (Space Science Building) before being attached to the spacecraft in a highbay ISO 7 cleanroom in the same building. The partially assembled spacecraft was then transferred to the ISO 8 RAL (Reverberation and Acoustics Lab) for vibration testing. Following vibration testing, the spacecraft was moved back to the highbay cleanroom in the SSB for further assembly. The fully assembled spacecraft was moved to the RAL, then to the ISO 8 SSL (Space Science Lab) for thermal vacuum testing and back to the highbay in the SSB. The assembled spacecraft was then packed into a N_2 purged shipping container and flown to the Kennedy Space Center in Florida where the batteries were enabled, the sample acquisition mechanism (TAGSAM) was cleaned a final time, and the hydrazine fuel loaded onto the spacecraft. These activities occurred in the ISO 7 highbay cleanroom inside the PHSF (Payload Hazardous Servicing Facility) at the Kennedy Space Center. Finally, the spacecraft was encapsulated in an Atlas V, 4 m. Fairing, or nosecone which protects the spacecraft during launch and ascent. The encapsulated spacecraft was then driven to the launch pad under N_2 purge where it was placed atop the Atlas V 411 launch vehicle. This entire process took 18 months (March 2015–August 2016) and each witness foil was exposed to the assembly, test, and launch environment for about 1 month or at each change in location. This process is summarized in **Table 1** and **Figure 1**.

In this paper, we demonstrate that contamination knowledge samples collected to monitor organic contamination can also be used to characterize microbiological changes, even when those samples are not handled aseptically or stored under conditions ideal for preserving DNA. We refer to these as, "samples of opportunity." We successfully extracted DNA from the majority of these samples, and we describe community shifts that correspond to different portions of the assembly, test, and launch environment. The sample collected from inside the rocket fairing contained several unique organisms not present in any of the other samples. To our knowledge, this is the first time that the microbiology of the fairing environment has been described. We also describe contamination potentially introduced by utilizing samples of opportunity and discuss the

TABLE 1 | Sample information.

Sample	Exposure start	Exposure stop	Location	ATLO processes
OR-CKP-01-1-A,0	3/11/2015	4/14/2015	LM[a]/Denver	SRC[d] assembly. & functional. test; TAGSAM[e] assembly w/clean head
OR-CKP-02-1-A,0	4/14/2015	5/11/2015	LM/Denver	TAGSAM function Development
OR-CKP-03-1-A,0	5/11/2015	6/10/2015	LM/Denver	avionics box/SRC function Post-vibrational;
OR-CKP-04-1-A,0	6/12/2015	7/14/2015	LM/Denver	SARA[f] TVAC[g]/launch container/TAGSAM deploy. function Post-vibrational testing/OVIRS[h]/OTES[i]
OR-CKP-05-1-A,0	7/14/2015	8/19/2015	LM/Denver	TAGSAM installation, deployment.
OR-CKP-06-1-A,0	8/19/2015	9/18/2015	LM/Denver	OCAMS[j] installation/SARA deployment
OR-CKP-07-1-A,0	9/18/2015	11/4/2015	LM/Denver	SARA deployment/move to RAL[k]
OR-CKP-08-1-A,0	11/4/2015	12/9/2015	LM/Denver	RAL vibrational testing/move to SSB[l]
OR-CKP-09-1-A,0	12/9/2015	1/7/2016	LM/Denver	REXIS[m] OLA[n] installation/spacecraft moved/shipping container
OR-CKP-10-1-A,0	1/8/2016	2/5/2016	LM/Denver	Flight. TAGSAM/spacecraft to RAL/EMI-EMC[o]/TVAC pre-certification.
OR-CKP-11-1-A,0	2/5/2016	3/16/2016	LM/Denver	TVAC lid opened/spacecraft to SSL/TVAC pumpdown/lid opened 3/10 move to SSB
OR-CKP-12-1-A,0	3/6/2016	4/26/2016	LM/Denver	launch container/SARA
OR-CKP-13-1-A,0	4/26/2016	4/27/2016	LM/Denver	TAGSAM flight installation
OR-CKP-14-1-A,0	4/27/2016	6/17/2016	KSC[b]	SARA deployment/Flight head test
OR-CKP-15-1-A,0	6/17/2016	7/14/2016	KSC	SRC battery enable/TAGSAM cleaning
OR-CKP-16-1-A,0	7/14/2016	8/26/2016	KSC	He load/prop tests/TAGSAM bottle loads/fuel sampling/cleaning & inspection/pack & shipping preparations
OR-GCKP-17-1-A1			JSC[c]/GSFC[p]	Shipping Blank
ORX Fairing Blank–FB–18			KSC	Fairing Blank
ORX Fairing CK Fck – 19	8/26/2019	9/8/2016	KSC	Fairing contamination knowledge
Swab Blank – Sb 20			JSC	
Kit Blank – Kb -21			JSC	

[a]Lockheed-Martin; [b]Kennedy Space Center, Florida; [c]Johnson Space Center, Texas; [d]Sample Return Capsule; [e]Touch and Go Sample Acquisition Mechanism; [f]Sample Acquisition and Return Assembly; [g]Thermal Vacuum Testing; [h]OSIRIS-REx Visible and Infrared Spectrometer; [i]OSIRIS-REx Thermal Emission Spectrometer; [j]OSIRIS-REx Camera Suite; [k]Reverberation and Acoustics Lab; [l]Space Sciences Building; [m]Regolith X-ray Imaging Spectrometer; [n]OSIRIS-REx Laser Altimeter; [o]electromagnetic interference testing; [p]Goddard Space Flight Center.

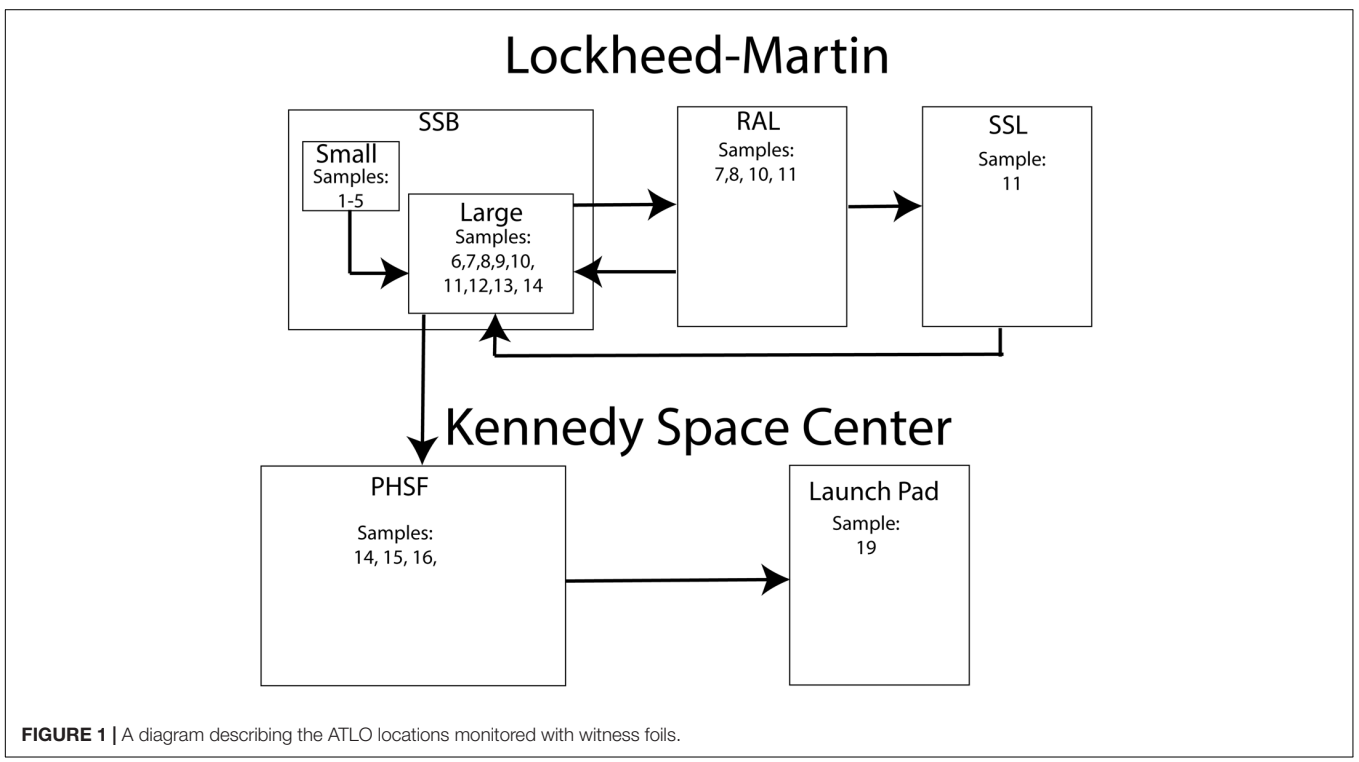

FIGURE 1 | A diagram describing the ATLO locations monitored with witness foils.

limits of short-read amplicon sequencing. For example, it is not possible to definitively characterize the metabolic function of the organisms we identified in these cleanrooms due to the low amount of DNA recovered. This is the first time samples collected for organic contamination have been used for DNA sequencing. The success of this study demonstrates that organically clean contamination knowledge samples can be used for microbial monitoring even when a mission does not have microbial monitoring requirements. These types of samples could be studied from other missions with relatively little cost.

MATERIALS AND METHODS

We collected DNA from 17 witness foils and five blanks/controls. The witness foils were 1 cm^2 squares of aluminum foil (Dworkin et al., 2018). Sixteen of the witness foils were exposed to cleanroom locations where assembly test and launch activities for OSIRIS-REx occurred. One additional foil, a 1 ft^2 piece prepared as described above was exposed to the environment inside the Atlas V rocket fairing just prior to launch. To our knowledge this is the first microbiological measurement inside an Atlas V fairing. We extracted DNA from two control foils that were not exposed to the assembly, test, and launch environment, and three negative process controls (a blank swab, a QIAamp BiOstic Bacteremia DNA Kit with nothing added except for the included reagents, and a PCR (polymerase chain reaction) blank). The foils were organically clean and were prepared as described in Dworkin et al. (2018). Briefly, witness foils were cleaned by baking at 500°C for at least 8 h and were deployed and collected by technicians wearing nylon-free cleanroom suits with nose and mouth coverings. Technicians' gloves were wiped with Fisher Optima 2-propanol prior to handling witness foils. We received aliquots of these witness foils in sealed glass vials (also baked at 500°C) and processed them at the Johnson Space Center microbiology lab using a previously established method. Dworkin et al. (2018), DNA was extracted by swabbing the witness foils with a polyester swab (Puritan, United States). The swab was immersed in DNA-free-water and vortexed for 5 min. A modified version of the QIAamp BiOstic Bacteremia DNA Kit (Qiagen) protocol was used to extract DNA from the swabs. We modified the kit protocol by using zircon beads to mechanically lyse the cells on the swab for 10 min prior to extracting the DNA. We also extracted DNA from the ZymoBIOMICS^{TM} Cellular Microbial Community Standard and a fungal mock community (Bakker, 2018). These mock communities (**Supplementary Table S1**) allowed us to describe any systematic bias in our DNA extraction and sequencing protocols. Potential contaminant sequences were included in subsequent analyses due to ambiguity in the results, which are described below (section "Bacterial and Archaeal Sequencing").

Extracted DNA concentration was measured with a Qubit fluorimeter (Thermo Fisher Scientific) prior to amplification with 35 cycles of PCR. An Agilient 2100 Bioanalzyer was used to check the quality of the amplified product. We used the Earth Microbiome primers (Caporaso et al., 2012; Walters et al., 2015) (515F-806R and 27Fmod-519Rmod) to amplify the V4 region of the 16S rRNA gene in order to identify bacteria and archaea. We used the ITS1f-ITS2 primers to amplify the ITS1 region in order to identify fungi (Walters et al., 2015). Several insect species were observed in the cleanrooms during assembly and testing, so we also amplified the COI gene (mitochondrial cytochrome c oxidase subunit I) to identify any arthropod DNA that may have been present on the witness foils. We used the ZBJ-ArtF1c/ZBJ-ArtR2c primer pair to amplify the COI gene (Zeal et al., 2011; Madden et al., 2016). The amplified products were pooled and purified using Agencourt AMPure XP beads (Beckman Coulter). DNA was normalized and sequenced using an Illumina MiSeq with V2 chemistry for 500 cycles.

The resulting 250 base pair, paired-end reads were demultiplexed on the sequencer and processed using QIIME2 (Caporaso et al., 2010) and the Deblur pipeline (Amir et al., 2017) with a minimal read length of 120 bp and suggested parameters for quality filtering and sOTU (sub-operational taxonomic unit, 100% unique) clustering. sOTUs were identified using the SILVA v132 database and or by using BLASTn (Camacho et al., 2009) to align to the NCBI database. ITS sequences were processed using QIIME2 (Caporaso et al., 2010) and a 120 bp minimal read length in the DADA2 pipeline (Callahan et al., 2016) for quality filtering and sOTU clustering. DADA2 is preferable to Deblur for ITS sequences because it does not require uniform length reads. The length of the ITS region can vary significantly (250–400 bp) from species to species (Lindahl et al., 2013; Nilsson et al., 2019). Therefore, it is preferable to use a pipeline that can accommodate this variation.

In order to quantify the detection limits of our sequencing run, we also extracted and amplified DNA from 12 positive control samples containing 34, 340, 3,400, or 34,000 *Bacillus subtilis* cells. DNA was extracted from these cells using the Bacteremia kit described above and amplified using the 515F-806R and 27Fmod-519Rmod primer pair.

The KatharoSeq method (Minich et al., 2018) uses standards of a known organism to quantify the detection limits for a sequencing run. After sequencing, the standards and identifying sOTUs two plots are generated. **Figure 2A** relates the number of cells in each standard sample to the fraction of the total number of sequences assigned to the standard organism (*Bacillus subtilis*). **Figure 2B** relates the total number of sequences in each sample to the fraction of the total number of sequences assigned to the standard organism. Both plots are fit using an allosteric sigmoidal fitting Eq. (1) of the type

$$Y = V^*_{max} \frac{X^h}{(K^h_{1/2} + X^h)} \quad (1)$$

This equation is adopted from the field of enzyme kinetics (e.g., Childs and Bardsley, 1975). For our data $K_{1/2}$ represents the detection limit. This corresponds to the point at which < 50% of the sequences are identified as *B. subtilis*. This value can be used to determine a detection limit in terms of the minimum number of cells in **Figure 2A** and the number of sequences or reads in **Figure 2B**. $V_{max}$is a fitting parameter that represents the theoretical maximum fraction of sequences that can be

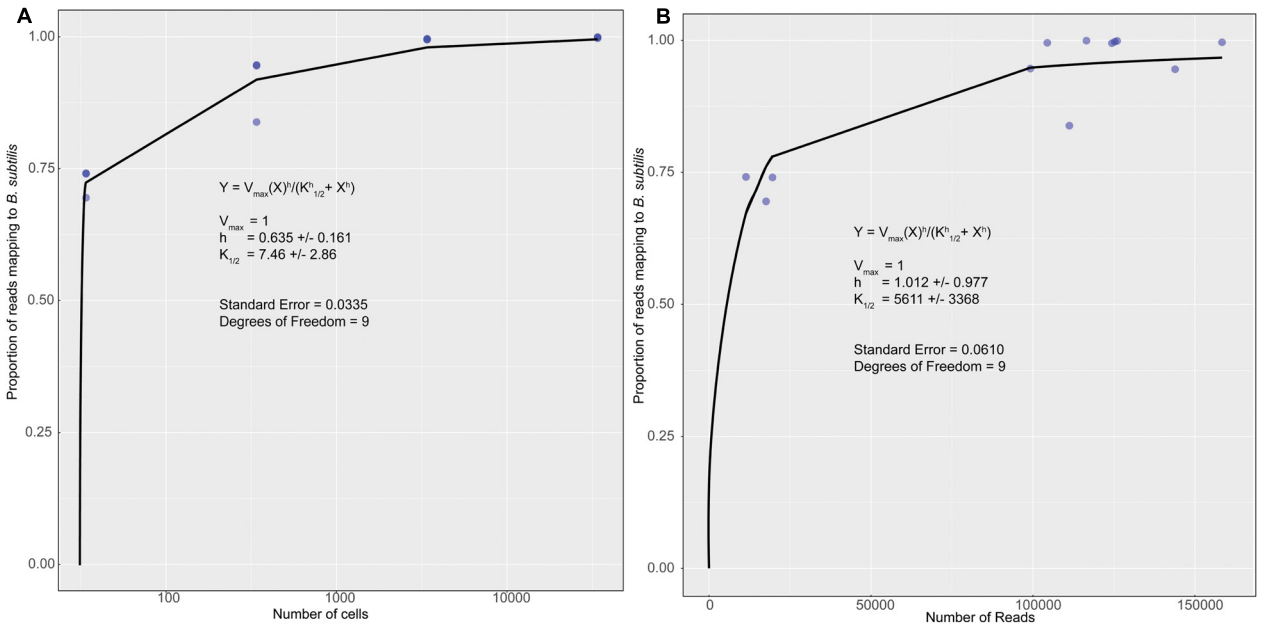

FIGURE 2 | A plot of the fraction of reads for each standard that mapped to the known organism *Bacillus subtilis* vs. the number of cells in each samples **(A)** and the fraction of reads for each standard that mapped to the known organism *Bacillus subtilis* vs. the number of reads or sequences collected for each sample **(B)**. The data was fit using an allosteric sigmoidal equation. The detection limit for this sequencing run was 7 ± 3 cells and 5,611 ± 3,369 reads.

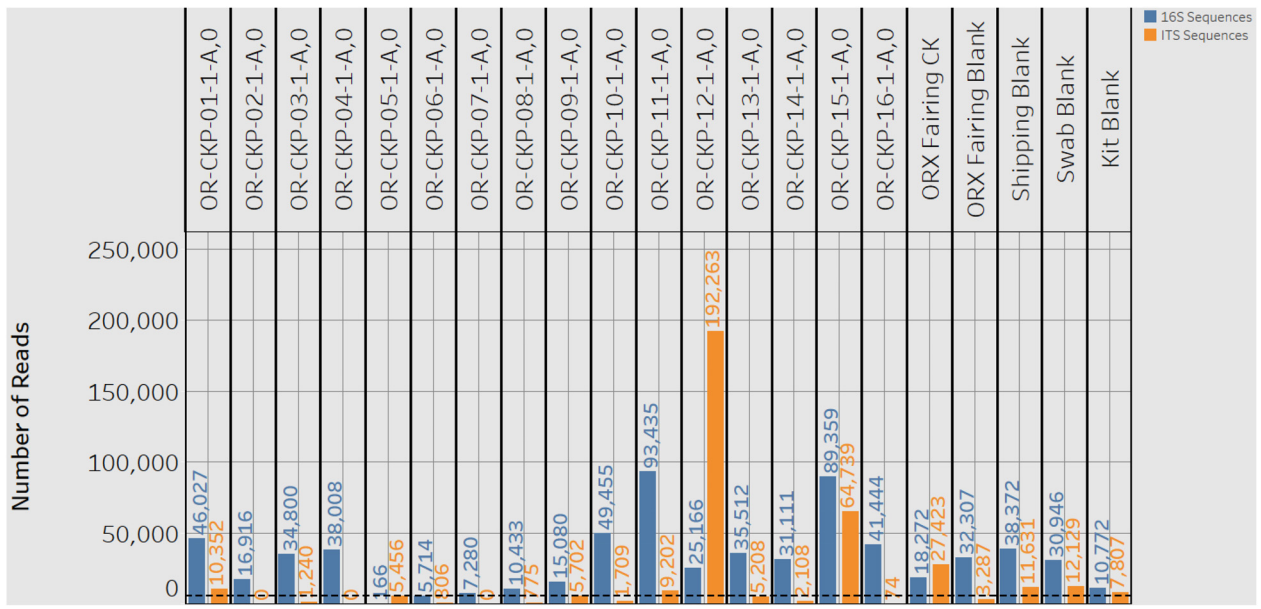

FIGURE 3 | A plot showing the number of 16S rRNA gene (blue bars) and ITS (orange bars) reads or sequences for each sample. A black dashed line marks the detection limit for 16S rRNA gene sequences of 5,611 sequences. One 16S rRNA gene sample (CKP-05) and nine ITS samples fell below this limit of detection.

identified as B. *subtilis*. In the original paper (Minich et al., 2018), this value was allowed to vary freely. However, we were unable to accurately fit our data in **Figure 2B** unless we forced to be one. This is a reasonable value because it is impossible for more than 100% of the reads to be identified as B. *subtilis*. For allosteric enzymes, h is a fitting parameter called the Hill coefficient. Values larger than 1 reflect stronger interactions between enzyme subunits. For our data, h is purely a fitting parameter and was allowed to vary freely. Fitting was performed in the statistical software R (version 3.6.2) using the MINPACK package to implement a Levenber-Marquardt non-linear least-squares algorithm. Fitting the data in **Figure 2A** gave a $K_{1/2}$ value

of 7 ± 3 cells as our detection limit. This corresponds to $K_{1/2}$ value of 5,611 ± 3,369 reads in **Figure 2B**. The large standard deviation is likely reflective of error introduced prior to PCR amplification. Small amounts of contamination introduced prior to this step would have been amplified along with the target DNA and would result in large variability in the number of reads per sample. Using this information, we can assert that the swab from OR-CKP-05-1-A,0 (**Figure 3**) was below our limit of detection for bacterial and archaeal DNA. This sample had fewer than 5,611 reads and therefore presumably had fewer than seven cells. We did not analyze the 16S rRNA gene sequences from this sample any further.

Bacterial and archaeal communities were described using the ecological concepts of alpha and beta diversity. Analyses were chosen based on previous studies of cleanrooms (e.g., Koskinen et al., 2017; Lax et al., 2017; Minich et al., 2018) so that we could easily compare results. Alpha diversity is a measure of the number of different organisms present in a sample as well as relative abundance or "evenness" of these organisms. We chose to represent alpha diversity using the Shannon index (Shannon and Weaver, 1949). The Shannon index is an alpha diversity statistic that summarizes the number of sOTUs present in each sample and the relative abundance with which they occur. Larger numbers indicate that a sample is more diverse. Beta diversity statistics are often used to distinguish samples with many common sOTUs. Beta diversity compares the presence, absence and relative abundance of sOTUs between samples. The weighted UNIFRAC metric (Lozupone and Knight, 2005) calculates the distance between samples as a function of sOTU: presence/absence, relative abundance, and phylogeny. These distances are then analyzed using PCOA (principle coordinate analysis), a method used to explain the variance in multivariate data sets. Samples that have a similar composition cluster together on a PCOA plot. Samples with a different composition appear as outliers. Diversity indices and PCOA values were calculated using QIIME2 (Caporaso et al., 2010).

$$Y = V^*_{max} \frac{X^h}{(K^h_{1/2} + X^h)} V_{max} V_{max}$$

We investigated correlations between sequencing results, previously published amino acid concentrations, and microscopic observations of carbon-bearing particles (Dworkin et al., 2018) using a linear regression as implemented in the Tableau software package.

RESULTS

Bacterial and Archaeal DNA Sequencing

Extracted DNA ranged from 0.13 and 1.11 ng/μl of in our samples. After cleanup and amplification we did not observe any evidence of contamination. We observed 1,009 sOTUs across all of our samples. Most of these sOTUs were only identified in a few samples. Individual samples contained 23–72 sOTUs (**Figure 4**). The sample with the highest number of sOTUs (72) was the shipping blank that we used to document contamination from the sample preparation and analysis labs at Johnson Space Center and Goddard Space Flight Center. This result implies that a large portion of the bacterial diversity may be attributable to contamination from sample handling for amino acid measurements. Sample OR-CKP-04-1-A,0-CKP had the second highest number of sOTUs (64). This sample was collected while the TAGSAM was vacuum tested. The number of sOTUs does not appear to systematically change with time. The Zymo mock community was sequenced as a positive control and we were able to detect all the included bacterial species at relative abundances < 10% different than the expected abundance.

Most of the samples are composed of a few dominant sOTUs (**Figures 5A,B**). These sOTUs map to human associated genera like *Bacillus, Listeria, Enterococcus,* and *Staphylococcus*. Because we were able to detect all the species included in the Zymo mock community at relative abundances < 10% different than those expected we conclude that our DNA amplification and sequencing methods did not impart any undue biases and that it is appropriate to apply alpha and beta diversity parameters. Shannon indices range from 3.2 for OR-CKP-11-1-A,0, which is dominated by *Micrococcus* sp., to 4.7 for sample OR-CKP-09-1-A, which has a more even distribution of sOTUs. The shipping blank, OR-CKP-17-1-A,0 had the highest Shannon index (5.0), which again indicates that sample handling may have artificially increased diversity. Overall, these are low diversity scores and a narrow range indicating that the samples have low diversity (**Figure 6**). For comparison, samples collected from the Jet Propulsion Laboratory's Spacecraft Assembly Facility have Shannon indices as high as 6.6 (Mahnert et al., 2015) which represents a sixfold increase in diversity from a score of 4.7 because the Shannon index is on a natural log scale. The PCOA plot of the weighted UNIFRAC (**Figure 7**) metric contained one cluster and two outliers. The cluster contained all the blanks and control samples as well as most of the contamination knowledge samples. The two outliers were OR-CKP-11-1-A,0, exposed during thermal vacuum testing and the fairing contamination knowledge sample.

Fungal and Arthropod Sequencing Results

We observed 87 fungal sOTUs across all our samples. As with the 16S rRNA gene sequencing most of these sOTUs only occurred in a few samples. We observed 1–16 sOTUs per sample (**Figure 4**). We sequenced the ZymoBIOMICS Microbial Community Standard, which contained two fungal isolates, and a mock community from the USDA (Bakker, 2018) containing 19 isolates as positive controls. We were able to detect both fungal isolates in the ZymoBIOMICS Microbial Community Standard, but the relative abundance of *Cryptococcus neoformans* was only 4.4%. The theoretical abundance in this mock community is 26% implying we are under-sampling this organism. We only detected six of the 19 isolates in the USDA mock community. These six isolates belonged to three different divisions. We did not detect organisms belonging to the *Chytridiomycota* or *Glomermomycota* divisions even though they were present in the USDA mock community.

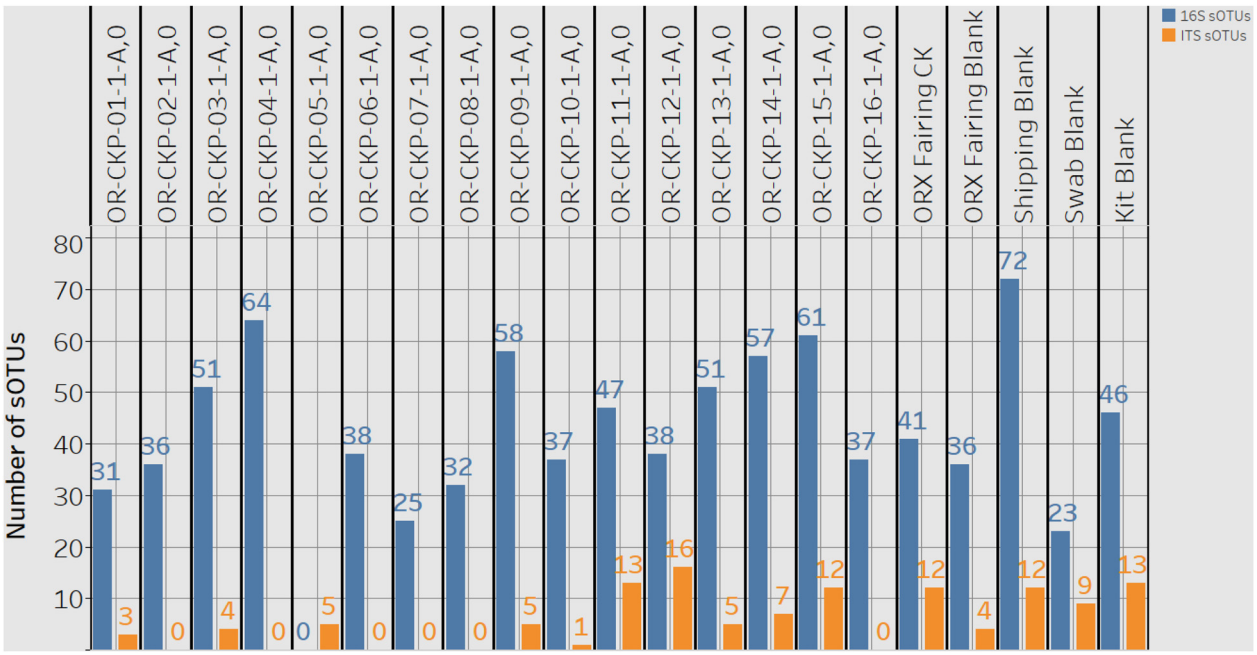

FIGURE 4 | A plot detailing the number of 16S rRNA gene or bacterial sOTUs (blue bars) and ITS or fungal sOTUs identified in each sample. 16S rRNA gene samples with < 5,611 16S rRNA gene sequences are listed as having zero sOTUs. ITS samples with zero sequences also have zero sOTUs.

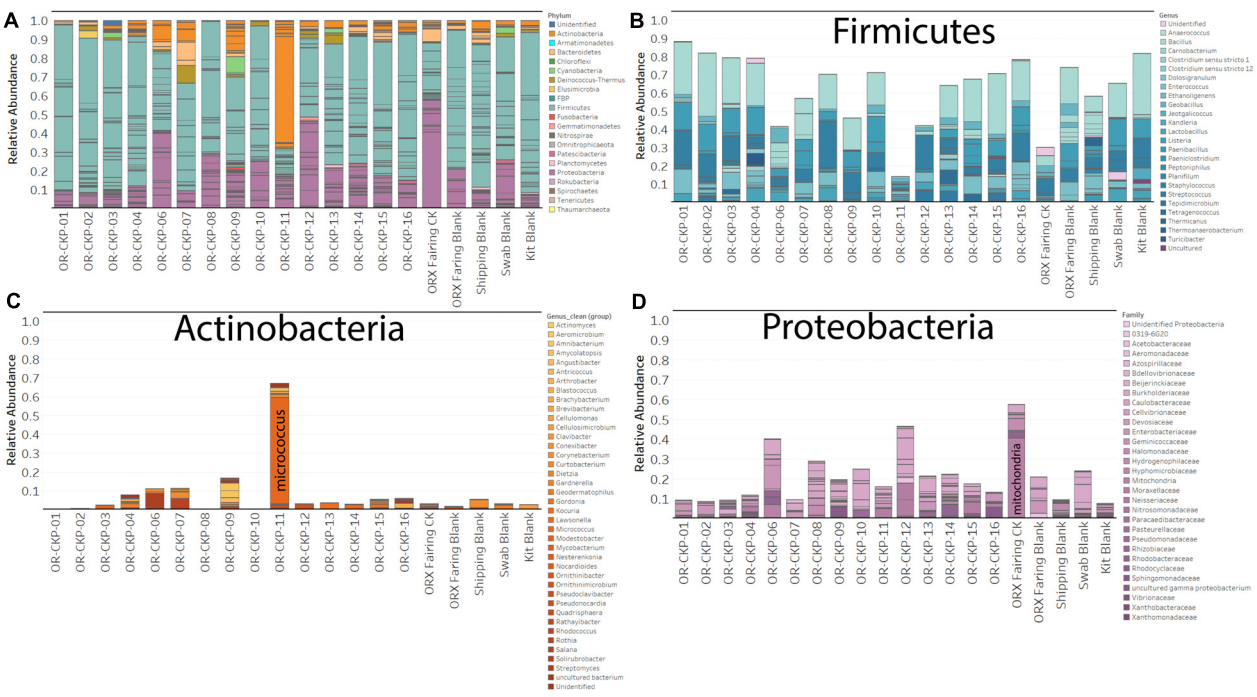

FIGURE 5 | Bar charts detailing bacterial and archaeal sOTUs identified in each sample. Bars are colored by phyla in **(A)**. Abundant phyla are presented with genus level identifications **(B,C)** or family level identifications **(D)**. The most abundant phylum in most samples is Firmicutes (Blue bars; **A,B**).

Sample 12 had the largest number of fungal OTUs (16) (**Figure 4**) and the largest number of ITS sequences (**Figure 4**) (192,263). This sample was collected in the SSB while the launch container was being installed. In general, the samples collected after thermal vacuum testing (OR-CKP-11-1-A,0) appear to have more fungal OTUs than those collected prior to this procedure

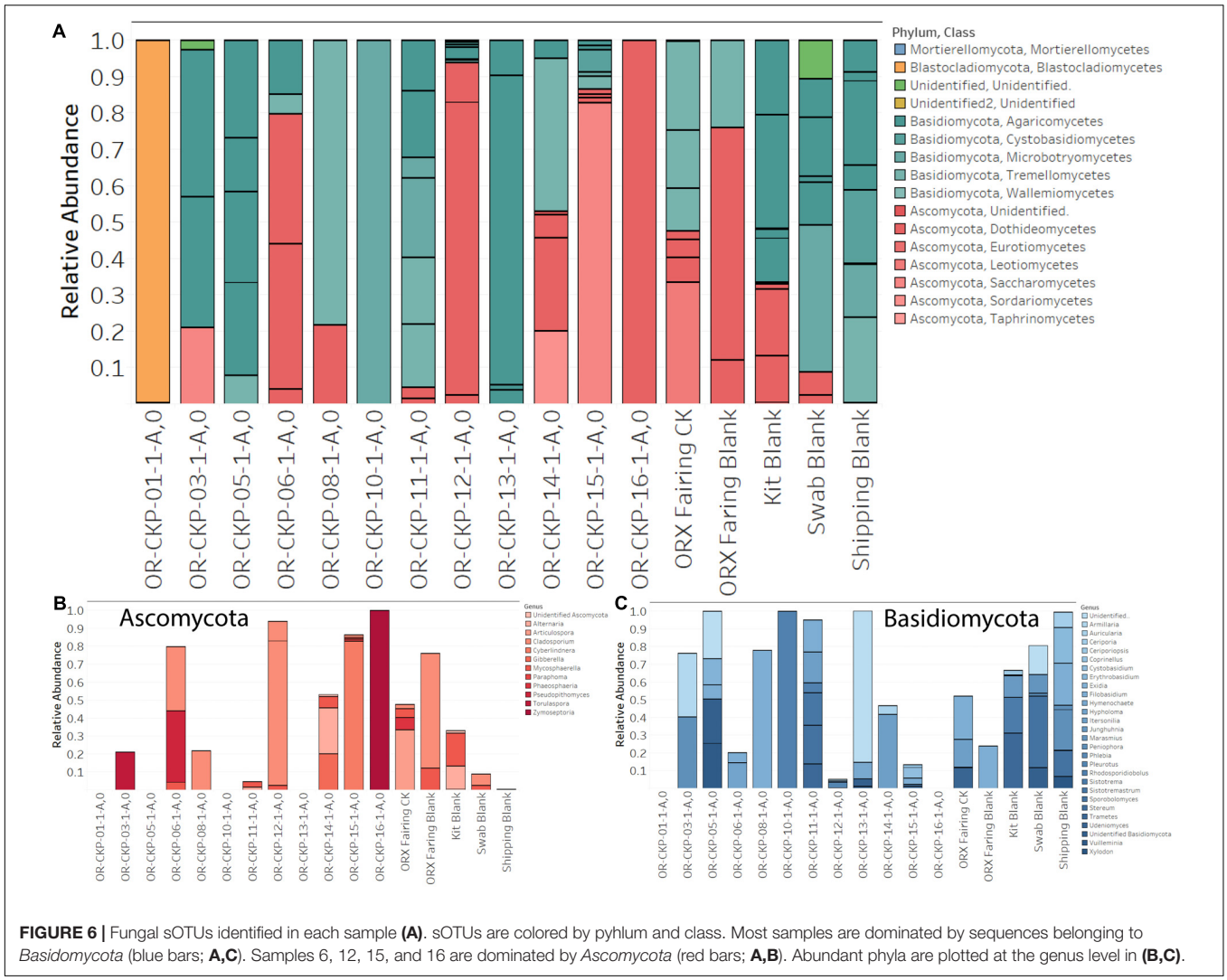

FIGURE 6 | Fungal sOTUs identified in each sample **(A)**. sOTUs are colored by pyhlum and class. Most samples are dominated by sequences belonging to *Basidomycota* (blue bars; **A,C**). Samples 6, 12, 15, and 16 are dominated by *Ascomycota* (red bars; **A,B**). Abundant phyla are plotted at the genus level in **(B,C)**.

(**Figure 4**). Sequences belonging to the genus's *Filobasidium* and *Cladosporium* are the most commonly occurring sequences in our samples, but they each only occur in five of the seventeen samples (**Figure 8**).

We were unable to detect arthropod DNA in any of our samples except for the positive controls.

DISCUSSION

Bacterial and Archaeal Sequencing

We observed low numbers of sOTUs per sample (23–72) even for a cleanroom environment. For example, samples collected from the Spacecraft Assembly Facility at the Jet Proposal Laboratory contained about 100 sOTUs (Minich et al., 2018).

In general our results from sequencing the 16S rRNA gene are consistent with those reported in Dworkin et al. (2018). In that paper, six bacterial species and one archaea were detected using 16S rRNA gene sequencing. We detected the same archaeal species (*Natronococcus amylolyticus)* in our samples and two of the same bacterial species (*L. fermentum* and *Sphingobium* sp.). We detected other members of the *Pseudomonas* genus and species from the same family as *Brevibacterium* and *Reyranella*. Dworkin et al. (2018) also reported detecting *Eubacterium* sp. We did not identify any close relatives of this organism but did detect members of the same taxonomic order. The minor differences in what we were able to detect are likely due to the fact that we analyzed our samples several years after the sample reported in Dworkin et al. (2018). Since the samples were stored at room temperature, DNA from low abundance species may have degraded during that time.

The most abundant sOTU in the entire dataset was present in almost every sample, and maps to the genus *Bacillus*. The presence of this sOTU in the shipping blank suggests that it represents contamination from sample handling and storage. However, the sOTU for *Bacillus* as well as other abundant sOTUs for *Listeria, Staphyloccocus*, and *Enterococcus* are not capable of distinguishing individual species from these genera. We used BLASTn to compare the 250 base pair sequence of the *Bacillus* sOTU to the NCBI database. This sOTU was a 100%

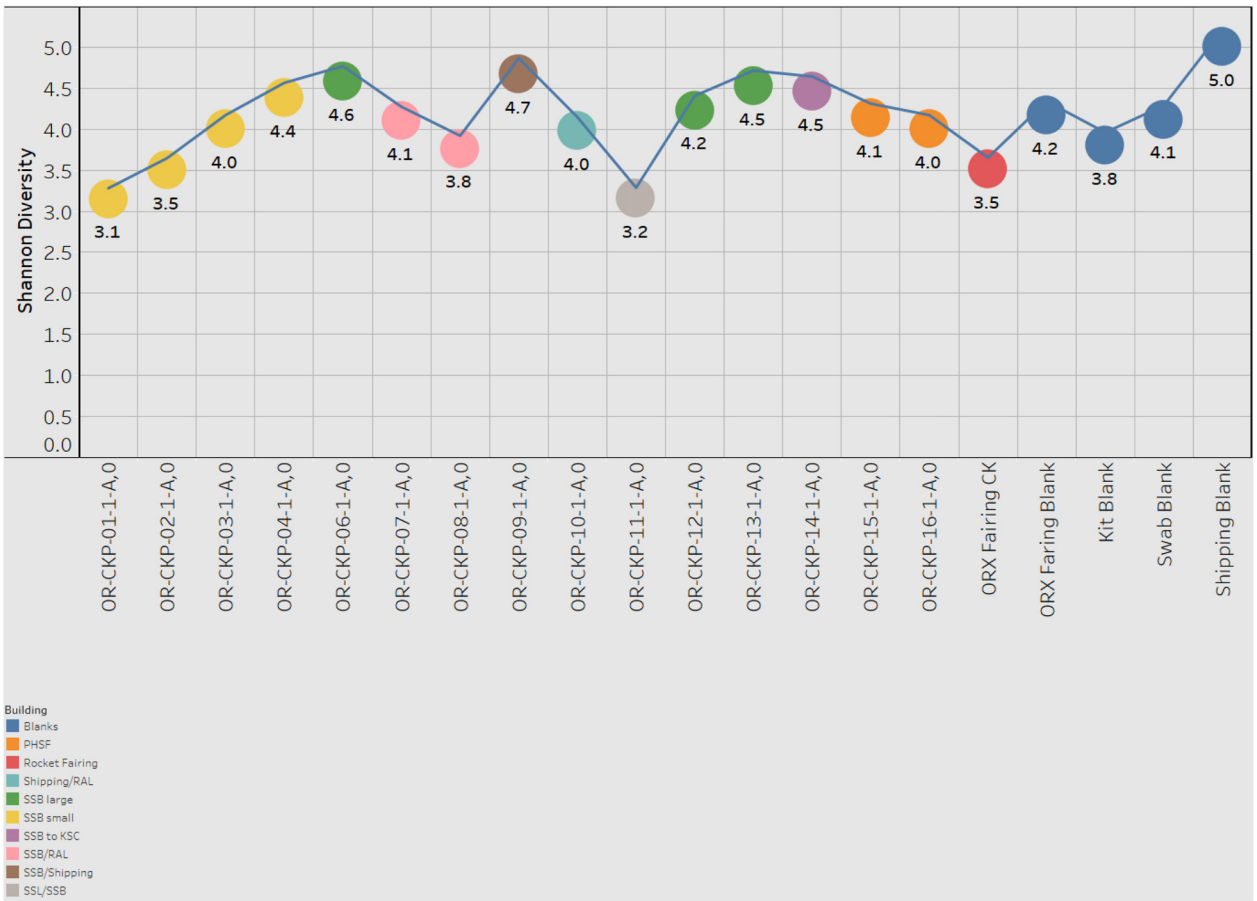

FIGURE 7 | Shannon index for each sample. Samples are colored according to the building in which the witness foil was exposed.

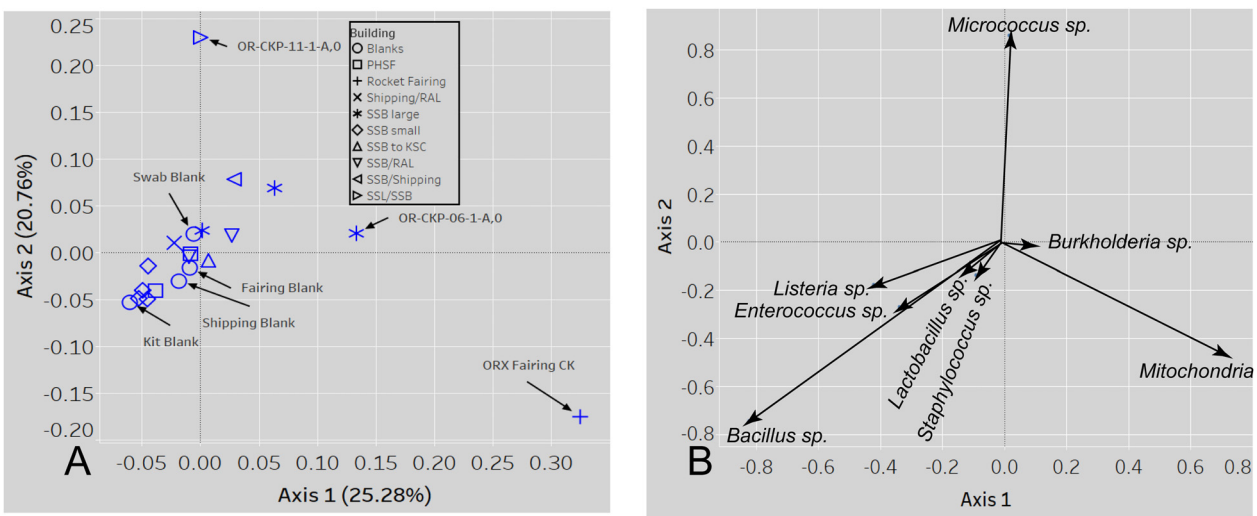

FIGURE 8 | A PCOA plot of the weighted UNIFRAC beta diversity metric **(A)** shows that samples 11 and the fairing CK sample are outliers. Samples are colored by location A biplot **(B)** shows which sOTUs/organisms affect the distribution of the data. The length of the arrow is proportional to the strength of the effect.

match to six different *Bacillus* species. *Listeria, Enterococcus,* and *Staphylococcus* sOTUs matched five, four, and nine different species, respectively (**Table 2**). These ubiquitous sOTUs could contain multiple species that are not contaminants. We do not believe these sequences represent contamination from DNA extraction or PCR amplification because the relative abundance of sequences in the Zymo mock community matched the expected values ± 2%, and because we did not observe any evidence of contamination in the bioanalyzer data collected post-PCR. The sOTUs present in most of our samples were not present in samples from a different study sequenced during the same run, which implies that cross contamination between samples during sequencing did not occur. The low concentration of extractable DNA prevented us from reamplifying and resequencing a different region of the 16S rRNA gene to better resolve these sOTUs. This is a limitation imposed by working with samples of opportunity that were not originally collected for microbiological analysis.

The largest variations in the weighted UNIFRAC metric (**Figure 7**) appear to correspond to times when the spacecraft was moved to a less clean environment. Sample 11 was exposed to the room containing the thermal vacuum testing apparatus. It was not possible to place a witness foil inside the test chamber. Sample 11 has a large proportion (56.2%) of *Micrococcus* reads (OTU ID: 6c891abaa8f2147383dd332e601800eb). Using BLAST (Camacho et al., 2009) this sequence matches eight different Micrococcus species: *M. aloeverae, M. yunnanensis, M. luteus, M. endophyticus, M.* sp. *KBS0714, M.* sp. *MZ2688K, M.* sp. *MZ0397G*, and *M. flavus* in the NCBI database. It is likely that this is a signal from the room where the vacuum testing occurred. *Micrococcus* species, especially *Micrococcus luteus*, are common bacteria associated with human skin and are often detected in the built environment including pharmaceutical (Utescher et al., 2007; Pacheco and Pinto, 2010) and aerospace (Puleo et al., 1973; La Duc et al., 2004; Schwendner et al., 2013; Moissl-Eichinger et al., 2015; Yang et al., 2018; Zhang et al., 2018) cleanrooms. While *Micrococcus* species are not commonly considered extremophiles *Micrococcus luteus* has been isolated from a pharmaceutical ISO 7 cleanroom maintained at 2–8°C (Sandle and Skinner, 2013). *Micrococcus* are Gram-positive cocci capable of aerobically reducing nitrate and oxidizing a variety of carbohydrates to CO_2 and water. On human, skin these bacteria survive by consuming organic compounds in human sweat. *Micrococcus* is more prevalent on human skin during, cold winter months (Kloos and Musselwhite, 1975), which is consistent with when sample OR-CKP-11-1-A,0 was collected (February–March, 2016). We also detected a sOTU unique to this sample that belonged to the genus *Enhydrobacter* (OTU ID: 8c8598245ea67244fb156b6f31192a41) and comprised 5% of the total sequences. *Enhydrobacter aerosaccus* is the only cultivated member of this genus. This species is a Gram-negative facultative anaerobe capable of fermenting sugars and growing on a wide variety of organic compounds aerobically. It was isolated from a eutrophic lake (Staley et al., 1987). However, the genus has been detected using both culture-based and molecular methods on the International Space Station (Mora et al., 2019) and in the cleanrooms used to assemble the ExoMars 2016 mission (Koskinen et al., 2017). It is not clear what ecological niche *Enhydrobacter* is filling in the cleanroom environment, but this genus is common in aerospace cleanrooms and controlled environments like the International Space Station. We hypothesize that these organisms were shed from the skin of workers outside the test chamber and were not actively growing in the cleanroom. It is unlikely that these microbes interacted with the spacecraft given that it was isolated inside the thermal vacuum chamber, but it is encouraging that we can detect a change in the microbiome associated with moving the spacecraft to a different building in these samples of opportunity.

The samples from the small cleanroom in SSB form a very tight cluster on the PCOA plot (**Figure 7A**), which implies that they are highly similar. This cleanroom was used to assemble the sample return capsule and the TAGSAM portions of the spacecraft. It was one of the most stringently controlled rooms during the entire ATLO process. These four samples are dominated by the four sOTUs that occur in almost every sample, which map to the genera: *Bacillus, Listeria, Enterococcus*, and *Staphylococcus*. As discussed above, we cannot resolve these sOTUs so this may be a contamination signal from sample handling that is especially apparent in low-biomass samples. However, the sample with the lowest number of sequences (OR-CKP-06) does not cluster with these samples and, in fact, appears to have a unique bacterial signature.

Sample six has one of the highest Shannon indices of any sample analyzed (4.6) (**Figure 6**). The most abundant sOTU comprises 12% of the total number of sequences and is unique to sample six. The sOTU (OTU ID: f2e4355abb553aed0f53a97b59f2acf2) maps to family *Enterobacteriaceae*. Using BLASTn to compare this sequence to the NCBI database suggests that this sOTU may be from the genus *Citrobacter*, a human associated microbe commonly found in the intestinal tract that has been reported in other aerospace cleanrooms (Schwendner et al., 2013). Strains of this bacteria are capable of reducing nitrate as well as anaerobically oxidizing Fe(II) (Li et al., 2014). The other abundant, unique sOTU (OTU ID: ca3429ecc56580a91a143253d556e498) represents 7.5% of the total sequences and maps to the family *Solirubrobacter*. Despite having a smaller number of total sequences, this sample does not contain many sequences from the sOTUs that are abundant in most of the samples. It is unclear why this sample should be an outlier, as it does not correspond to any moves between buildings or extra activity during the ATLO process. The foil was exposed while the Sample Acquisition and Return Assembly was being installed and special care was taken to avoid organic contamination.

In the fairing contamination knowledge sample, 40.3% of the sequences correspond to mitochondrial (OTU ID: 12c056b5ee8cf31ff032dab1bbd2d1a4) DNA. In most microbiome samples, these sequences would be discarded as contaminants because we were specifically trying to amplify ribosomal DNA from bacteria and archaea. However, the sOTU from this sample was not present in any of our blanks or control samples indicating that it may be a legitimate signal. We used the BLASTn algorithm to compare this sequence to the NCBI database and discovered that it was a ≥ 97% match

TABLE 2 | sOTUs occurring in every sample and organisms with identical sequences in the NCBI database.

sOTU	Sequence	Organism	Blast Name	Score[a]	Number of Hits
82595768ab5e2e41 50162ed4f0d9885a	TACGTAGGTGGCAAGCGTTGTCCGGAATTATTGGGCGTAAAGGGCTCGCAGGCGGTTCCTTAAGTCTGATGTGAAAGCCCCCGGCTCAA CCGGGGAGGGTCATTGGAAACTGGGGAACTTGAGTGCAGAAGAGGAGAGTGGAATTCCACGTGTAGCGGTGAAATGCGTAGAGATGTG GAGGAACACCAGTGGCGAAGGCGACTCTCTGGTCTGTAACTGACGCTGAGGAGCGAAAGCGTGGGGAGCGAAC				
		Bacillus subtilis	Firmicutes	452	20
		Bacillus subtilis subsp. spizizenii	Firmicutes	452	2
		Bacillus mojavensis	Firmicutes	452	15
		Bacillus halotolerans	Firmicutes	452	17
		Bacillus tequilensis	Firmicutes	452	2
		Bacillus subtilis subsp. spizizenii ATCC 6633	Firmicutes	452	1
		Bacillus subtilis subsp. stercoris	Firmicutes	452	1
		Bacillus sp. (in: Bacteria)	Firmicutes	452	32
		Bacillus safensis	Firmicutes	452	1
		Bacillus endophyticus	Firmicutes	452	1
		Bacillaceae bacterium	Firmicutes	452	2
		Uncultured bacterium	Bacteria	452	1
		Uncultured prokaryote	Unclassified	452	5
e336f37a27cbd76d b5b0040a8c078e20	TACGTAGGTGGCAAGCGTTGTCCGGATTTATTGGGCGTAAAGCGCGCGCAGGCGGTCTTTTAAGTCTGATGTGAAAGCCCCCGGCTTA ACCGGGGAGGGTCATTGGAAACTGGAAGACTGGAGTGCAGAAGAGGAGAGTGGAATTCCACGTGTAGCGGTGAAATGCGTAGATATG TGGAGGAACACCAGTGGCGAAGGCGACTCTCTGGTCTGTAACTGACGCTGAGGCGCGAAAGCGTGGGGAGCAAAC				
		Listeria monocytogenes	Firmicutes	452	36
		Listeria seeligeri	Firmicutes	452	4
		Listeria ivanovii	Firmicutes	452	2
		Listeria welshimeri	Firmicutes	452	1
		Listeria innocua	Firmicutes	452	1
		Listeria ivanovii subsp. londoniensis	Firmicutes	452	1
		Listeria sp.	Firmicutes	452	4
		Uncultured *Listeria* sp.	Firmicutes	452	51
a1a3200b76bcd600 0a0914892d370b6e	TACGTAGGTGGCAAGCGTTGTCCGGATTTATTGGGCGTAAAGCGAGCGCAGGCGGTTTCTTAAGTCTGATGTGAAAGCCCCCGGCTCAAC CGGGGAGGGTCATTGGAAACTGGGAGACTTGAGTGCAGAAGAGGAGAGTGGAATTCCATGTGTAGCGGTGAAATGCGTAGATATATGG AGGAACACCAGTGGCGAAGGCGGCTCTCTGGTCTGTAACTGACGCTGAGGCTCGAAAGCGTGGGGAGCAAAC				
		Enterococcus faecalis	Firmicutes	452	59
		Enterococcus faecium	Firmicutes	452	23
		Enterococcus hirae	Firmicutes	452	6
		Enterococcus sp.	Firmicutes	452	6
		Enterococcus sp. DA9	Firmicutes	452	1
		Enterococcus durans	Firmicutes	452	3
		Enterococcus faecalis EnGen0107	Firmicutes	452	1
		Uncultured bacterium	Bacteria	452	1
d23fbef2f31d48ed a40876cdbc49933a	TACGTAGGTGGCAAGCGTTATCCGGAATTATTGGGCGTAAAGCGCGCGTAGGCGGTTTTTTAAGTCTGATGTGAAAGCCCACGGCTCAAC CGTGGAGGGTCATTGGAAACTGGAAAACTTGAGTGCAGAAGAGGAAAGTGGAATTCCATGTGTAGCGGTGAAATGCGCAGAGATATGGA GGAACACCAGTGGCGAAGGCGACTTTCTGGTCTGTAACTGACGCTGATGTGCGAAAGCGTGGGGATCAAAC				
		Staphylococcus aureus	Firmicutes	452	35
		Staphylococcus hominis	Firmicutes	452	8
		Uncultured *Staphylococcus* sp.	Firmicutes	452	1
		Staphylococcus sp.	Firmicutes	452	9
		Staphylococcus epidermidis	Firmicutes	452	14
		Staphylococcus haemolyticus	Firmicutes	452	5
		Staphylococcus argenteus	Firmicutes	452	1
		Staphylococcus warneri	Firmicutes	452	9
		Staphylococcus caprae	Firmicutes	452	2
		Staphylococcus pasteuri	Firmicutes	452	4
		Staphylococcus capitis	Firmicutes	452	5
		Uncultured bacterium	Bacteria	452	4
		Stenotrophomonas maltophilia	G-proteobacteria	452	1
		Uncultured prokaryote	Unclassified	452	2

[a] *Calculated value representing the quality of the alignment see https://www.ncbi.nlm.nih.gov/books/NBK62051/ for definition.*

to mitochondrial DNA from the genus *Pseudoperonospora*. Specifically, the sequence matched *P. humuli* and *P. cubensis*. These eukaryotes belong to the Class *Oomycetes*. *Oomycetes*, commonly called water molds or downy mildew are fungus-like plant pathogens. *P. humuli* and *P. cubensis* are obligate parasites that infect members of the gourd family including squash, pumpkin, melon, and cucumber (Choi et al., 2005), which are grown in the areas surrounding the launch site in Florida. We also identified sequences from the genus *Pedobacter* (OTU ID: 5984c840c5cdeabb6540d4863e81270a) and *Halomonas* (OTU ID: cb49d9d1556e1d334127cfa72e508340) that were completely unique to the fairing and comprised > 5% of the total number of sequences for that sample. *Pedobacter* is a ubiquitous genus of soil bacteria that has been isolated from all over the world. These microbes may be especially relevant because some members of this genus are capable of crude oil degradation (Chang et al., 2017). Microbes that can degrade crude oil may be more able to degrade complex organic molecules like cyclo-alkanes in carbonaceous chondrites. Any of these organisms are likely capable of consuming amino acids and simple sugars like ribose (Furukawa et al., 2019). The *Halomonas* genus consists of bacteria from high salt environments like the estuaries and marine environments surrounding the launch site (e.g., Gunde-Cimerman et al., 2018). Detecting unique sOTUs in the fairing sample that are likely to have come directly from the environment surrounding the launch site implies that conditions inside the fairing prior to launch were not completely pristine. We hypothesize that (1) these microbes are indicative of contamination from the surrounding environment, and (2) they were not actively growing inside the fairing.

Although the fairing was cleaned to UV clean-highly sensitive levels prior to use and kept under a positive-pressure nitrogen purge encapsulation, then under flowing filtered air with gowned technicians working generally downstream of the witnesses (Dworkin et al., 2018), it seems likely that some amount of exchange with the surrounding environment occurred. Finding evidence for a unique microbiome inside the fairing is significant because this microbiome has never been characterized despite being an environment that every robotic spacecraft launched from Kennedy Space Center experiences. Missions with strict planetary protection requirements may need to monitor this environment to ensure that these requirements are met going forward.

Fungal Sequencing

Previous sequencing of a contamination knowledge witness plate identified six fungal species (Dworkin et al., 2018). We detected organisms from the genus *Fusarium* but not *F. cerealis* specifically. We did not detect any *Penicillium*, but we did detect other organisms from the same class and members of the same order as *C. intermedia* and *Phoma* sp. We were unable to detect any organism closely related to *Malassezia restricta*. These differences are likely due to sample degradation caused by non-ideal storage conditions. It appears that this effect was more pronounced for ITS amplicons than it was for 16S rRNA gene sequences.

Our failure to detect 13 of the 19 species present in the USDA mock community (Bakker, 2018), indicates that there was significant bias imparted by our workflow. It is possible that the primers we chose are inappropriate. Although we chose primers validated by the Earth Microbiome Project (Walters et al., 2015) and used to characterize the USDA mock community (Bakker, 2018), several researchers have suggested that there are better suited primer sets available for ITS sequencing that produce less biased results (Bokulich and Mills, 2013; Lindahl et al., 2013; Tedersoo and Lindahl, 2016; Usyk et al., 2017). Unfortunately, we do not have enough remaining material to re-amplify our DNA with different primers. It is also possible that aggressive bead-beating to attack bacterial spores damaged the fungal DNA, or that we are eliminating valid sequences during our analysis process. Bakker (2018) reported such problems in his own analysis although to a much lesser extent. He was able to detect 17 of the 19 species in the mock community. In order to determine if our bioinformatics pipeline was responsible for our results, we processed the data using several different tools. Amplifying the ITS1 region inevitably captures some of the proceeding SSU (small sub unit) and following 5.8S genes (Nilsson et al., 2019). Some researchers suggest that better results are obtained by removing this overhang and only analyzing the ITS region (e.g., Lindahl et al., 2013; Nilsson et al., 2019). We attempted this method using ITSxpress in QIIME2 (Rivers et al., 2018), and independently using ITSx (Bengtsson-Palme et al., 2013) as implemented in the PIPITS pipeline (Gweon et al., 2015) with little success. All of these tools produced results that had even fewer species present in the mock community sample than directly processing the sequences using the DADA2 pipeline (Callahan et al., 2016) without extracting the ITS region. Due to the bias in our dataset, we chose not to employ standard ecological analysis methods like alpha and beta diversity. These calculations rely on a fully accurate measurement of the type and abundance of organisms present. The results obtained by sequencing the mock communities suggest that we did not obtain this result.

Even though our fungal sequencing results are biased, it is still useful to examine them especially when we have evidence from the bacterial and archaeal sequencing or from previous chemical measurements that changes in the assembly, test, and launch environment were occurring. For example, the fairing sample contained DNA from several unique bacterial species that are likely from the surrounding environment. We also identified several unique fungal species in this sample. The most abundant sequences (33% of the total) in the sample map to *Articulospora proliferata*. *A. proliferata* is a hyphomycete or mold. It has been isolated from leaf litter in freshwater environments. Sequences mapping to *Udeniomyces pyricola* were also abundant (11.7% of the total sequences) and unique to the fairing sample. *U. pyricola* is also a leaf degrader, but it is classified as a yeast due to its ability to reproduce by budding. *U. pyricola* has been isolated from glacial ice in Patagonia (de Garcia et al., 2012) and so is reported to be cold-tolerant. *Itersonilia pannonica* was also unique and represented 15.8% of the total sequences. The *Udeniomyces and Itersonilia*

genuses are capable of producing teliospores, a unique type of spore that contains two cells per spore (Weiss et al., 2014). Sequences mapping to *Phaeosphaeria caricicola* (another leaf degrading fungi) represented 6.8% of the total sequences and were also unique to the fairing. Again, we hypothesize that these organisms are indicative of contamination from the launch environment in Florida and not indicative of fungal growth inside the fairing.

Sample 11 only contained one sOTU that was unique to the sample. The sOTU maps to the genus *Sistotremastrum* and represents 13.3% of the sequences. This is a genus of saprophytic fungi associated with white rot and lignin degradation (Nguyen et al., 2016). Samples 1, 12, and 16 appear to be dominated by individual sOTUs. Sample one is dominated by an unidentified *Blastocladiales*. The closest relative is *Brunneoporus minutus* (97% similar), which is also known as *Antrodia minuta,* a lignin degrading fungi responsible for cellulose degradation or brown rot (Spirin, 2007). Sample 12 is dominated by *Cladosporium deliculatulum* (72.5%), a more common type of indoor fungi (Yang et al., 2016). This species was also found in sample six (36%), the fairing sample (2.5%), the swab blank (6.3%), and the fairing blank (64%), which suggests that it may be contamination due to sample handling. Sample 16 is dominated by a sOTU mapping to the genus *Zymoseptoria,* which contains mostly plant pathogens (Quaedvlieg et al., 2011).

In general, our samples are dominated by the phyla *Ascomyctoa* and *Basidiomycota*. Genus *Itersonilia* found in samples 11 (17.3%), sample 12 (0.7%), sample 14 (42%), and the fairing sample (16%) belongs to the class *Tremellomycetes*. Other species from this class were also identified in sample five and sample eight (7 of 14 samples). This class is composed of wood degrading fungi, micro-fungi, gelatinous fruiting fungi, opportunistic pathogens, and parasitic fungi that live inside other fungi. These fungi are ubiquitous in the environment and have even been cultivated in samples from the Antarctic Dry Valleys (Weiss et al., 2014). Class *Agaricomycetes* is found in 8 of the 13 samples (3, 5, 6, 11, 12, 13, 14, and 15). This class includes plant pathogens and saprotrophs associated with lignin degradation or white rot (Hibbett et al., 2014). Both classes have been detected in Jet Propulsion Laboratory cleanrooms used to assemble spacecraft (La Duc et al., 2012; Checinska et al., 2015). However, their ecological function in the built environment remains uncharacterized (Samson, 2011). Perhaps the sample to sample variation represents a seasonal pattern as described by Weikl et al. (2016). Sample 12 has the highest largest number of fungal sequences and corresponds to a month with above average rainfall in the Denver area. Even in cleanrooms fungi, from the surrounding environment seems to predominate over fungi associated with human activity (Adams et al., 2013). Fungal ecology in the built environment is poorly described in the literature and further research is needed to understand how these organisms survive in cleanroom environments.

In natural environments, fungi are well adapted to utilizing recalcitrant carbon compounds like lignin. In the built environment, different fungal species have been reported growing on and degrading: wood, paper, and gypsum based plaster, polyethylene, polyvinyl chloride, and even formaldehyde based resin used in fiberglass ceiling tiles (Yang et al., 2016). Although it is unlikely that any fungal spores survived the journey to Bennu, fungi in cleanrooms on Earth are some of the best suited organisms to degrade organic compounds like kerogen (e.g., Wong et al., 2015). Kerogen along with many other organics, is expected to be a component of the returned samples (Kebukawa et al., 2010). Interestingly, we observed a weak negative correlation between the number of fungal sOTUs identified in the samples and relative abundance of carbon-bearing particles as previously identified with a scanning electron microscope on the witness plates (Dworkin et al., 2018; **Supplementary Figure S1**). One explanation for this observation is that fungi in the cleanroom were consuming carbon and lowering the relative abundance on witness plates. The number of bacterial sOTUs did not show this negative correlation, which is surprising considering that many members of the *Bacillus* genus are also capable of degrading recalcitrant carbon (e.g., da Cunha et al., 2006). Unfortunately, we were not able to analyze these particles to determine whether the carbon was biologically available. Additional research is required to test this hypothesis. The number of fungal ITS sequences are weakly correlated with the measured amino acid concentration (**Supplementary Figure S2A**). It is possible that samples with higher amino acid concentrations also had higher levels of microbial activity and thus larger amounts of detectable DNA. Amino acids can serve as a carbon source for most types of bacteria and fungi and thus prevalent organic contamination could exacerbate biological contamination. An alternate explanation is that fungal ingress into the lab was weakly correlated with lapses in cleaning or gowning procedures. Things like air leaks, missed wipe downs, and incorrectly donning and doffing cleanroom garments could have introduced amino acids and fungi. This is consistent with the observations of Adams et al. (2013) that most fungi are not endemic to cleanrooms but are introduced from the external environment. We were unable to correlate any other aspect of this dataset with amino acid concentration (**Supplementary Figure S2B**).

We successfully used samples of opportunity to extract and sequence bacterial, archaeal, and fungal DNA from witness foils present during assembly test and launch operations for the OSIRIS-REx spacecraft. Bacterial sequences were dominated by human associated microbes and appear to vary slightly from cleanroom to cleanroom. While it was not possible to conclusively describe the ecological niches occupied by these bacteria, it is plausible that they survive in the cleanrooms by consuming cleaning products like isopropyl alcohol (Mogul et al., 2018). Sequencing standards allowed us to quantify the minimum number of bacterial cells that we were able to detect at seven cells per sample. Fungal sequences were dominated by two fungal phyla commonly reported in cleanrooms, but these results are likely biased due to inherent limitations in DNA sequencing and data processing technologies. Further research is needed on fungal metabolism in cleanrooms. A witness foil from inside the rocket fairing contained bacterial, fungal, and other eukaryotic DNA from organisms that were not detected anywhere else during assembly or testing.

This is the first time that the microbiology of a rocket fairing has been studied and demonstrates that microbial contamination of outbound spacecraft is possible even when the fairing is visibly cleaned and subsequently maintained with a positive pressure nitrogen purge.

Many of the potential contamination issues we encountered were caused by low biomass and were exacerbated by limited sample quantity and sample handling protocols that were not designed with DNA sequencing or any type of microbiological analysis in mind. Although using samples of opportunity for microbiology is possible and has generated important information about organisms present in the assembly, test, and launch environment, we recommend collecting dedicated contamination knowledge samples for DNA sequencing if microbial contamination is of interest (McCubbin et al., 2019). Dedicated samples should be frozen to preserve DNA and would allow potential contamination due to sample handling to be addressed by reanalyzing samples to amplify different genetic regions that are more discriminatory for the species we detected (e.g., *Bacillus*). Our inability to distinguish individual species of the *Bacillus, Listeria, Staphyloccocus,* and *Enterococcus* genuses demonstrates the limitations of "universal" PCR primers. The V4 region of the 16S rRNA gene amplified by the Earth Microbiome primers does not appear to be useful for distinguishing members of the genuses at the species level. If we had collected and stored samples specifically for DNA sequencing, we may have had enough material to reanalyze these samples using different primers that better discriminate these organisms, but for this study we were limited to small samples of opportunity. Collecting dedicated samples with the intent of microbiological analysis would be especially useful for missions with strict planetary protection requirements. Our results from inside the rocket fairing should also prompt more detailed study of this environment as it is unclear whether the signal that we detected represents microbial incursion from the launch environment or microbes that remain on the inside of the fairing after cleaning.

The Astromaterials Acquisition and Curation Office at Johnson Space Center is already taking precautions to limit microbial contamination in curation facilities. Routine microbial monitoring of existing curation cleanrooms is ongoing, and the results will inform new sterilization and cleaning protocols for the OSIRIS-REx lab that is currently under construction. Astromaterials curators will also collect soil from the landing sight of the Sample Return Capsule in Utah to characterize the microbes present there. Finally, it may be beneficial to try to detect DNA inside the Sample Return Capsule after the samples have been removed. The presence of identifiable DNA inside the Sample Return Capsule could indicate the microorganisms survived the trip to and from Bennu. Further research is needed to describe how bacterial and fungal growth could alter returned samples. We recommend using carbonaceous chondrites as analog materials for this work so that cleaning protocols designed to limit inorganic, organic, and biological contamination can be developed prior to the return of samples from Bennu (McCubbin et al., 2019).

DATA AVAILABILITY STATEMENT

The datasets generated for this study can be found in the SRA database https://www.ncbi.nlm.nih.gov/sra/PRJNA602955 under accession number PRJNA602955.

AUTHOR CONTRIBUTIONS

AR assisted with DNA extraction, processed the sequencing data, and prepared the manuscript for publication. CC, RD, SS-R, and SC-W extracted and sequenced the DNA and provided input on the manuscript. SM prepared the witness foils. HM and JD collected the witness foils, performed the amino acid analysis, and provided input on the manuscript. KR oversaw witness foil deployment, coordinated additional witness foil measurements, and provided input on the manuscript. HC, DL, and FM participated in discussions and provided substantive input on the manuscript. JM operated the facilities used to construct the spacecraft and provided input on the manuscript. All authors contributed to the article and approved the submitted version.

FUNDING

This material is based upon work supported by the National Aeronautics and Space Administration under Contracts NNH09ZDA007O, NNM10AA11C, and NNG12FD66C issued through the New Frontiers Program.

ACKNOWLEDGMENTS

We acknowledge NASA, Lockheed-Martin, and ULA for allowing us to characterize their facilities, Cat Wolner and Beau Bierhaus for assisting with the manuscript and Dr. Matthew G. Bakker for providing us with a sample of his fungal mock community.

SUPPLEMENTARY MATERIAL

The Supplementary Material for this article can be found online at: https://www.frontiersin.org/articles/10.3389/fmicb.2020.530661/full#supplementary-material

Supplementary Figure 1 | The number of fungal sOTUs (orange symbols) displays a weak inverse correlation to the proportion of carbon-bearing particles on the witness foils. The number of bacterial sOTUs (blue symbols) displays a weak positive correlation to the proportion of carbon bearing particles. Symbol shape corresponds to the building in which the sample was collected.

Supplementary Figure 2 | The number of fungal ITS sequences (orange symbols) is correlated with the amino acid concentration **(A)**. The number of 16S rRNA gene bacterial and archaeal sequences (blue symbols) is weakly correlated with amino acid concentration. The number of sOTUs observed does not appear to correlate to amino acid concentration **(B)**. Symbol shape corresponds to the building in which the sample was collected.

REFERENCES

Adams, R. I., Miletto, M., Taylor, J. W., and Bruns, T. D. (2013). The diversity and distribution of fungi on residential surfaces. *PLoS One* 8:e78866. doi: 10.1371/journal.pone.0078866

Amir, A., McDonald, D., Navas-Molina, J. A., Kopylova, E., Morton, J. T., Zech Xu, Z., et al. (2017). Deblur rapidly resolves single-nucleotide community sequence patterns. *mSystems* 2:e00191-16. doi: 10.1128/mSystems.00191-16

Bakker, M. G. (2018). A fungal mock community control for amplicon sequencing experiments. *Mol. Ecol. Resour.* 18, 541–556. doi: 10.1111/1755-0998.12760

Balch, W. E., Wolfe, R. S., Kminek, G., and Moissl-Eichinger, C. (2009). Cultivation of anaerobic and facultatively anaerobic bacteria from spacecraft-associated clean rooms. *Appl. Environ. Microbiol.* 7532, 781–791. doi: 10.1128/aem.02565-08

Bengtsson-Palme, J., Ryberg, M., Hartmann, M., Branco, S., Wang, Z., Godhe, A., et al. (2013). Improved software detection and extraction of ITS1 and ITS2 from ribosomal ITS sequences of fungi and other eukaryotes for analysis of environmental sequencing data. *Methods Ecol. Evol.* 4, 914–919. doi: 10.1111/2041-210X.12073

Bierhaus, E. B., Clark, B. C., Harris, J. W., Payne, K. S., Dubisher, R. D., Wurts, D. W., et al. (2018). The OSIRIS-REx Spacecraft and the Touch-and-Go Sample Acquisition Mechanism (TAGSAM). *Space Sci. Rev.* 214:107. doi: 10.1007/s11214-018-0521-6

Bokulich, N. A., and Mills, D. A. (2013). Improved selection of internal transcribed spacer-specific primers enables quantitative, ultra-high-throughput profiling of fungal communities. *Appl. Environ. Microbiol.* 79, 2519–2526. doi: 10.1128/AEM.03870-12

Burton, A. S., Stern, J. C., Elsila, J. E., Glavin, D. P., Dworkin, J. P., Huss, G. R., et al. (2012). Understanding prebiotic chemistry through the analysis of extraterrestrial amino acids and nucleobases in meteorites. *Chem. Soc. Rev.* 41:5459. doi: 10.1039/c2cs35109a

Callahan, B. J., McMurdie, P. J., Rosen, M. J., Han, A. W., Johnson, A. J. A., and Holmes, S. P. (2016). DADA2: high-resolution sample inference from Illumina amplicon data. *Nat. Methods* 13, 581–583. doi: 10.1038/nmeth.3869

Camacho, C., Coulouris, G., Avagyan, V., Ma, N., Papadopoulos, J., Bealer, K., et al. (2009). BLAST+: architecture and applications. *BMC Bioinformatics* 10:421. doi: 10.1186/1471-2105-10-421

Caporaso, J. G., Kuczynski, J., Stombaugh, J., Bittinger, K., Bushman, F. D., Costello, E. K., et al. (2010). QIIME allows analysis of high-throughput community sequencing data. *Nat. Methods* 7, 335–336. doi: 10.1038/nmeth.f.303

Caporaso, J. G., Lauber, C. L., Walters, W. A., Berg-Lyons, D., Huntley, J., Fierer, N., et al. (2012). Ultra-high-throughput microbial community analysis on the Illumina HiSeq and MiSeq platforms. *ISME J.* 6, 1621–1624. doi: 10.1038/ismej.2012.8

Chang, S., Zhang, G., Chen, X., Long, H., Wang, Y., Chen, T., et al. (2017). The complete genome sequence of the cold adapted crude-oil degrader: *Pedobacter steynii* DX4. *Stand. Genomic Sci.* 12, 1–8. doi: 10.1186/s40793-017-0249-z

Checinska, A., Probst, A. J., Vaishampayan, P., White, J. R., Kumar, D., Stepanov, V. G., et al. (2015). Microbiomes of the dust particles collected from the International Space Station and Spacecraft Assembly Facilities. *Microbiome* 3:50. doi: 10.1186/s40168-015-0116-3

Childs, R. E., and Bardsley, W. G. (1975). Allosteric and related phenomena: an analysis of sigmoid and non-hyperbolic functions. *J. Theor. Biol.* 50, 45–58. doi: 10.1016/0022-5193(75)90023-5

Choi, Y.-J., Hong, S.-B., and Shin, H.-D. (2005). A re-consideration of *Pseudoperonospora cubensis* and P. *humuli* based on molecular and morphological data. *Mycol. Res.* 109, 841–848. doi: 10.1017/S0953756205002534

da Cunha, C., Rosado, A., Sebastián, G., Seldin, L., and von der Weid, I. (2006). Oil biodegradation by Bacillus strains isolated from the rock of an oil reservoir located in a deep-water production basin in Brazil. *Appl. Microbiol. Biotechnol.* 73, 949–959. doi: 10.1007/s00253-006-0531-2

de Garcia, V., Brizzio, S., and van Broock, M. R. (2012). Yeasts from glacial ice of Patagonian Andes, Argentina. *FEMS Microbiol. Ecol.* 82, 540–550. doi: 10.1111/j.1574-6941.2012.01470.x

Dworkin, J. P., Adelman, L. A., Ajluni, T., Andronikov, A. V., Aponte, J. C., Bartels, A. E., et al. (2018). OSIRIS-REx Contamination Control Strategy and Implementation. *Space Sci. Rev.* 214:19. doi: 10.1007/s11214-017-0439-4

Furukawa, Y., Chikaraishi, Y., Ohkouchi, N., Ogawa, N. O., Glavin, D. P., Dworkin, J. P., et al. (2019). Extraterrestrial ribose and other sugars in primitive meteorites. *Proc. Natl. Acad. Sci. U.S.A.* 116:201907169. doi: 10.1073/pnas.1907169116

Gunde-Cimerman, N., Plemenitaš, A., and Oren, A. (2018). Strategies of adaptation of microorganisms of the three domains of life to high salt concentrations. *FEMS Microbiol. Rev.* 42, 353–375. doi: 10.1093/femsre/fuy009

Gweon, H. S., Oliver, A., Taylor, J., Booth, T., Gibbs, M., Read, D. S., et al. (2015). PIPITS: an automated pipeline for analyses of fungal internal transcribed spacer sequences from the Illumina sequencing platform. *Methods Ecol. Evol.* 6, 973–980. doi: 10.1111/2041-210X.12399

Hamilton, V. E., Simon, A. A., Christensen, P. R., Reuter, D. C., Clark, B. E., Barucci, M. A., et al. (2019). Evidence for widespread hydrated minerals on asteroid (101955) Bennu. *Nat. Astron.* 3, 332–340. doi: 10.1038/s41550-019-0722-2

Hibbett, D., Bauer, R., Binder, M., Giachini, A. J., Hosaka, K., Justo, A., et al. (2014). "Agaricomycetes," in *Systematics and Evolution: Part A: Second Edition The Mycota VII Part A*, eds D. J. Mclaughlin and J. W. Spatafora (Berlin: Springer-Verlag), 373–429. doi: 10.1007/978-3-642-55318-9_14

ISO (2015). *14644-1:2015 - Cleanrooms and Associated Controlled Environments – Part 1: Classification of air Cleanliness by Particle Concentration*. Available online at: https://www.iso.org/standard/53394.html?browse=tc (accessed February 4, 2018).

Kebukawa, Y., Nakashima, S., and Zolensky, M. E. (2010). Kinetics of organic matter degradation in the Murchison meteorite for the evaluation of parent-body temperature history. *Meteorit. Planet. Sci.* 45, 99–113. doi: 10.1111/j.1945-5100.2009.01008.x

Kloos, W. E., and Musselwhite, M. S. (1975). *Distribution and Persistence of Staphylococcus and Micrococcus Species and Other Aerobic Bacteria on Human Skin'*. Available online at: http://aem.asm.org/ (accessed June 28, 2020).

Koskinen, K., Rettberg, P., Pukall, R., Auerbach, A., Wink, L., Barczyk, S., et al. (2017). Microbial biodiversity assessment of the European Space Agency's ExoMars 2016 mission. *Microbiome* 5:143. doi: 10.1186/s40168-017-0358-3

La Duc, M., Kern, R., and Venkateswaran, K. (2004). Microbial monitoring of spacecraft and associated environments. *Microb. Ecol.* 47, 150–158. doi: 10.1007/s00248-003-1012-0

La Duc, M. T., Vaishampayan, P., Nilsson, H. R., Torok, T., and Venkateswaran, K. (2012). Pyrosequencing-derived bacterial, archaeal, and fungal diversity of spacecraft hardware destined for mars. *Appl. Environ. Microbiol.* 78, 5912–5922. doi: 10.1128/AEM.01435-12

Lauretta, D. S., Balram-Knutson, S. S., Beshore, E., Boynton, W. V., Drouet d'Aubigny, C., DellaGiustina, D. N., et al. (2017). OSIRIS-REx: sample Return from Asteroid (101955) Bennu. *Space Sci. Rev.* 212, 925–984. doi: 10.1007/s11214-017-0405-1

Lauretta, D. S., Bartels, A. E., Barucci, M. A., Bierhaus, E. B., Binzel, R. P., Bottke, W. F., et al. (2015). The OSIRIS-REx target asteroid (101955) Bennu: constraints on its physical, geological, and dynamical nature from astronomical observations. *Meteorit. Planet. Sci.* 50, 834–849. doi: 10.1111/maps.12353

Lauretta, D. S., DellaGiustina, D. N., Bennett, C. A., Golish, D. R., Becker, K. J., Balram-Knutson, S. S., et al. (2019). The unexpected surface of asteroid (101955) Bennu. *Nature* 568, 55–60. doi: 10.1038/s41586-019-1033-6

Lax, S., Sangwan, N., Smith, D., Larsen, P., Handley, K. M., Richardson, M., et al. (2017). Bacterial colonization and succession in a newly opened hospital. *Sci. Transl. Med.* 9:eaah6500. doi: 10.1126/SCITRANSLMED.AAH6500

Li, B., Tian, C., Zhang, D., and Pan, X. (2014). Anaerobic Nitrate-Dependent Iron (II) Oxidation by a Novel Autotrophic Bacterium, Citrobacter freundii Strain PXL1. *Geomicrobiol. J.* 31, 138–144. doi: 10.1080/01490451.2013.816393

Lindahl, B. D., Nilsson, R. H., Tedersoo, L., Abarenkov, K., Carlsen, T., Kjøller, R., et al. (2013). Fungal community analysis by high-throughput sequencing of amplified markers - a user's guide. *New Phytol.* 199, 288–299. doi: 10.1111/nph.12243

Lozupone, C., and Knight, R. (2005). UniFrac: a New Phylogenetic Method for Comparing Microbial Communities. *Appl. Environ. Microbiol.* 71, 8228–8235. doi: 10.1128/AEM.71.12.8228-8235.2005

Madden, A. A., Barberán, A., Bertone, M. A., Menninger, H. L., Dunn, R. R., and Fierer, N. (2016). The diversity of arthropods in homes across the United States as determined by environmental DNA analyses. *Mol. Ecol.* 25, 6214–6224. doi: 10.1111/mec.13900

Mahnert, A., Vaishampayan, P., Probst, A. J., Auerbach, A., Moissl-Eichinger, C., Venkateswaran, K., et al. (2015). Cleanroom maintenance significantly reduces abundance but not diversity of indoor microbiomes. *PLoS One* 10:e0134848. doi: 10.1371/journal.pone.0134848

McCubbin, F. M., Herd, C. D. K., Yada, T., Hutzler, A., Calaway, M. J., Allton, J. H., et al. (2019). Advanced Curation of Astromaterials for Planetary Science. *Space Sci. Rev.* 215:48. doi: 10.1007/s11214-019-0615-9

Minich, J. J., Zhu, Q., Janssen, S., Hendrickson, R., Amir, A., Vetter, R., et al. (2018). KatharoSeq enables high-throughput microbiome analysis from low-biomass samples. *mSystems* 3:e00218-17. doi: 10.1128/mSystems.00218-17

Mogul, R., Barding, G. A., Lalla, S., Lee, S., Madrid, S., Baki, R., et al. (2018). Metabolism and biodegradation of spacecraft cleaning reagents by strains of spacecraft-associated acinetobacter. *Astrobiology* 18, 1517–1527. doi: 10.1089/ast.2017.1814

Moissl-Eichinger, C. (2017). "Extremophiles in Spacecraft Assembly Cleanrooms," in *Adaption of Microbial Life to Environmental Extremes*, eds H. Stan-Lotter and S. Fendrihan (Cham: Springer), 253–281. doi: 10.1007/978-3-319-48327-6_10

Moissl-Eichinger, C., Auerbach, A. K., Probst, A. J., Mahnert, A., Tom, L., Piceno, Y., et al. (2015). Quo vadis? Microbial profiling revealed strong effects of cleanroom maintenance and routes of contamination in indoor environments. *Sci. Rep.* 5:9156. doi: 10.1038/srep09156

Mora, M., Wink, L., Kögler, I., Mahnert, A., Rettberg, P., Schwendner, P., et al. (2019). Space Station conditions are selective but do not alter microbial characteristics relevant to human health. *Nat. Commun.* 10:3990. doi: 10.1038/s41467-019-11682-z

Nguyen, N. H., Song, Z., Bates, S. T., Branco, S., Tedersoo, L., Menke, J., et al. (2016). FUNGuild: an open annotation tool for parsing fungal community datasets by ecological guild. *Fungal Ecol.* 20, 241–248. doi: 10.1016/j.funeco.2015.06.006

Nilsson, R. H., Anslan, S., Bahram, M., Wurzbacher, C., Baldrian, P., and Tedersoo, L. (2019). Mycobiome diversity: high-throughput sequencing and identification of fungi. *Nat. Rev. Microbiol.* 17, 95–109. doi: 10.1038/s41579-018-0116-y

Pacheco, F. L. C., and Pinto, T. D. J. A. (2010). The bacterial diversity of pharmaceutical clean rooms analyzed by the Fatty Acid methyl ester technique. *PDA J. Pharm. Sci. Technol.* 64, 156–166.

Puleo, J. R., Oxborrow, G. S., Fields, N. D., Herring, C. M., and Smith, L. S. (1973). Microbiological profiles of four Apollo spacecraft. *Appl. Microbiol.* 26, 838–845. doi: 10.1128/aem.26.6.838-845.1973

Quaedvlieg, W., Kema, G. H. J., Groenewald, J. Z., Verkley, G. J. M., Seifbarghi, S., Razavi, M., et al. (2011). *Zymoseptoria* gen. nov.: a new genus to accommodate Septoria-like species occurring on graminicolous hosts. *Persoonia* 26, 57–69. doi: 10.3767/003158511X571841

Rivers, A. R., Weber, K. C., Gardner, T. G., Liu, S., and Armstrong, S. D. (2018). ITSxpress: Software to rapidly trim internally transcribed spacer sequences with quality scores for marker gene analysis. *F1000Res.* 7:1418. doi: 10.12688/f1000research.15704.1

Rummel, J. D. (2000). Implementing planetary protection requirements for sample return missions. *Adv. Space Res.* 26, 1893–1899. doi: 10.1016/S0273-1177(00)00157-5

Samson, R. A. (2011). "Ecology and general characteristics of indoor fungi," in *Fundamentals of Mold Growth in Indoor Environments and Strategies for Healthy Living*, eds O. C. G. Adan and R. A. Samson (Wageningen: Wageningen Academic Publishers), 101–116. doi: 10.3920/978-90-8686-722-6_5

Sandle, T., and Skinner, K. (2013). Study of psychrophilic and psychrotolerant micro-organisms isolated in cold rooms used for pharmaceutical processing. *J. Appl. Microbiol.* 114, 1166–1174. doi: 10.1111/jam.12101

Schwendner, P., Moissl-Eichinger, C., Barczyk, S., Bohmeier, M., Pukall, R., and Rettberg, P. (2013). Insights into the Microbial Diversity and Bioburden in a South American Spacecraft Assembly Clean Room. *Astrobiology* 13, 1140–1154. doi: 10.1089/ast.2013.1023

Shannon, C. E., and Weaver, W. (1949). *The Mathematical Theory of Communication*. Urbana, IL: University of Illinois Press.

Spirin, W. (2007). New and noteworthy Antrodia species (Polyporales, Basidiomycota) in Russia. *Mycotaxon* 101, 149–156.

Staley, J. T., Irgens, R. L., and Brenner, D. J. (1987). *Enhydrobacter aerosaccus* gen. nov., sp. nov., a Gas-Vacuolated, Facultatively Anaerobic, Heterotrophic Rod. *Int. J. Syst. Bacteriol.* 37, 289–291. doi: 10.1099/00207713-37-3-289

Steele, A., McCubbin, F. M., and Fries, M. D. (2016). The provenance, formation, and implications of reduced carbon phases in Martian meteorites. *Meteorit. Planet. Sci.* 51, 2203–2225. doi: 10.1111/maps.12670

Tait, A. W., Gagen, E. J., Wilson, S. A., Tomkins, A. G., and Southam, G. (2017). Microbial populations of stony meteorites: substrate controls on first colonizers. *Front. Microbiol.* 8:1227. doi: 10.3389/fmicb.2017.01227

Tedersoo, L., and Lindahl, B. (2016). Fungal identification biases in microbiome projects. *Environ. Microbiol. Rep.* 8, 774–779. doi: 10.1111/1758-2229.12438

Toporski, J., and Steele, A. (2007). Observations from a 4-year contamination study of a sample depth profile through Martian Meteorite Nakhla. *Astrobiology* 7, 389–401. doi: 10.1089/ast.2006.0009

Usyk, M., Zolnik, C. P., Patel, H., Levi, M. H., and Burk, R. D. (2017). Novel ITS1 Fungal Primers for Characterization of the Mycobiome. *mSphere* 2:e00488-17. doi: 10.1128/mSphere.00488-17

Utescher, C. L., de, A., Franzolin, M. R., Trabulsi, L. R., and Gambale, V. (2007). Microbiological monitoring of clean rooms in development of vaccines. *Braz. J. Microbiol.* 38, 710–716. doi: 10.1590/S1517-83822007000400023

Walters, W., Hyde, E. R., Berg-Lyons, D., Ackermann, G., Humphrey, G., Parada, A., et al. (2015). Improved bacterial 16S rRNA Gene (V4 and V4-5) and fungal internal transcribed spacer marker gene primers for microbial community surveys. *mSystems* 1:e00009-15.

Weikl, F., Tischer, C., Probst, A. J., Heinrich, J., Markevych, I., Jochner, S., et al. (2016). Fungal and bacterial communities in indoor dust follow different environmental determinants. *PLoS One* 11:e0154131. doi: 10.1371/journal.pone.0154131

Weisberg, M. K., Mccoy, T. J., and Krot, A. N. (2006). "Systematics and Evaluation of Meteorite Classification," in *Meteorites and the Early Solar System II*, eds D. S. Lauretta and H. Y. McSween (Tucson, AZ: University of Arizona Press), 19–52.

Weiss, M., Bauer, R., Sampaio, J. P., and Oberwinkler, F. (2014). "12 Tremellomycetes and Related Groups," in *Systematics and Evolution: Part A*, eds D. J. McLaughlin and J. W. Spatafora (Berlin: Springer), 331–355. doi: 10.1007/978-3-642-55318-9_12

Wong, M.-L., An, D., Caffrey, S. M., Soh, J., Dong, X., Sensen, C. W., et al. (2015). Roles of Thermophiles and fungi in bitumen degradation in mostly cold oil sands outcrops. *Appl. Environ. Microbiol.* 81, 6825–6838. doi: 10.1128/AEM.02221-15

Yang, C., Pakpour, S., Klironomos, J., and Li, D.-W. (2016). "Microfungi in Indoor Environments: What Is Known and What Is Not," in *Biology of Microfungi*, ed. D. W. Li (Cham: Springer), 373–412. doi: 10.1007/978-3-319-29137-6_15

Yang, J., Thornhill, S. G., Barrila, J., Nickerson, C. A., Ott, C. M., and McLean, R. J. C. (2018). Microbiology of the Built Environment in Spacecraft Used for Human Flight. *Methods Microbiol.* 45, 3–26. doi: 10.1016/bs.mim.2018.07.002

Zeal, M. R. K., Butlin, R. K., Barker, G. L. A., Lees, D. C., and Jones, G. (2011). Taxon-specific PCR for DNA barcoding arthropod prey in bat faeces. *Mol. Ecol. Resour.* 11, 236–244. doi: 10.1111/j.1755-0998.2010.02920.x

Zhang, Y., Xin, C., Wang, X., and Deng, Y.-L. (2018). Detection of microorganism from China's spacecraft assembly cleanroom. *Acta Astronaut.* 166, 545–547. doi: 10.1016/J.ACTAASTRO.2018.08.024

Conflict of Interest: CC and SS-R were employed by the company JES Tech. RD was employed by Jacobs@NASA/Johnson Space Center. JM was employed by Lockheed Martin Space Systems.

The remaining authors declare that the research was conducted in the absence of any commercial or financial relationships that could be construed as a potential conflict of interest.

frontiers in Microbiology

ORIGINAL RESEARCH
published: 06 November 2020
doi: 10.3389/fmicb.2020.566412

Assessing the Risk of Transfer of Microorganisms at the International Space Station Due to Cargo Delivery by Commercial Resupply Vehicles

*Snehit Mhatre[1†], Jason M. Wood[1†], Aleksandra Checinska Sielaff[1], Maximilian Mora[2], Stefanie Duller[2], Nitin Kumar Singh[1], Fathi Karouia[3,4‡], Christine Moissl-Eichinger[2,5] and Kasthuri Venkateswaran[1]**

[1] Biotechnology and Planetary Protection Group, Jet Propulsion Laboratory, California Institute of Technology, Pasadena, CA, United States, [2] Department of Internal Medicine, Medical University of Graz, Graz, Austria, [3] Space Bioscience Division, NASA Ames Research Center, Moffett Field, CA, United States, [4] Department of Pharmaceutical Chemistry, University of California, San Francisco, San Francisco, CA, United States, [5] BioTechMed-Graz, Graz, Austria

Background: With increasing numbers of interplanetary missions, there is a need to establish robust protocols to ensure the protection of extraterrestrial planets being visited from contamination by terrestrial life forms. The current study is the first report comparing the commercial resupply vehicle (CRV) microbiome with the International Space Station (ISS) microbiome to understand the risks of contamination, thus serving as a model system for future planetary missions.

Results: Samples obtained from the internal surfaces and ground support equipment of three CRV missions were subjected to various molecular techniques for microbial diversity analysis. In total, 25 samples were collected with eight defined locations from each CRV mission prior to launch. In general, the internal surfaces of vehicles were clean, with an order of magnitude fewer microbes compared to ground support equipment. The first CRV mission had a larger microbial population than subsequent CRV missions, which were clean as compared to the initial CRV locations sampled. Cultivation assays showed the presence of *Actinobacteria*, *Proteobacteria*, *Firmicutes*, and *Bacteroidetes* and members of *Ascomycota* and *Basidiomycota*. As expected, shotgun metagenome analyses revealed the presence of more microbial taxa compared to cultivation-based assays. The internal locations of the CRV microbiome reportedly showed the presence of microorganisms capable of tolerating ultraviolet radiation (e.g., *Bacillus firmus*) and clustered separately from the ISS microbiome.

Conclusions: The metagenome sequence comparison of the CRV microbiome with the ISS microbiome revealed significant differences showing that CRV microbiomes were a negligible part of the ISS environmental microbiome. These findings suggest that the maintenance protocols in cleaning CRV surfaces are highly effective in controlling the contaminating microbial population during cargo transfer to the ISS via the CRV route.

Keywords: forward contamination, microbial diversity, commercial resupply vehicle, viability, International Space Station

OPEN ACCESS

Edited by:
Rakesh Mogul, California State Polytechnic University, Pomona, United States

Reviewed by:
Henrik R. Nilsson, University of Gothenburg, Sweden
Marta Filipa Simões, Macau University of Science and Technology, China
Aaron Benjamin Regberg, Astromaterials Acquisition and Curation Office, Johnson Space Center (NASA), United States

****Correspondence:***
Kasthuri Venkateswaran
kjvenkat@jpl.nasa.gov

† These authors have contributed equally to this work

‡Present address:
Fathi Karouia, Blue Marble Space Institute of Science, Exobiology Branch, NASA Ames Research Center, Moffett Field, CA, United States

Specialty section:
This article was submitted to Extreme Microbiology, a section of the journal Frontiers in Microbiology

Received: *27 May 2020*
Accepted: *08 October 2020*
Published: *06 November 2020*

Citation:
Mhatre S, Wood JM, Sielaff AC, Mora M, Duller S, Singh NK, Karouia F, Moissl-Eichinger C and Venkateswaran K (2020) Assessing the Risk of Transfer of Microorganisms at the International Space Station Due to Cargo Delivery by Commercial Resupply Vehicles. Front. Microbiol. 11:566412. doi: 10.3389/fmicb.2020.566412

INTRODUCTION

Spacefaring nations carrying out interplanetary missions are subject to rules and regulations that were designed and instigated by the Committee on Space Research (COSPAR) in 1967 (COSPAR, 2011). Protocols for cleaning and sterilization are of the highest priority and are regularly practiced and meticulously followed during spacecraft assembly for various missions (Benardini et al., 2014). Cleanrooms are where various spacecraft subsystems, including commercial resupply vehicles (CRV) transporting cargo to the International Space Station (ISS), are assembled. These cleanrooms undergo daily cleaning procedures, including vacuuming and mopping of floors with 70% Isopropanol, high efficiency particulate arrestance (HEPA) air filtration, regular replacement of sticky mats at the entrance, and strict gowning procedures. Utmost care is taken by personal entering these facilities, as they are required to put on face masks, gloves, bodysuits, shoe covers, cleanroom boots, and cover hair and beards with nets (Benardini et al., 2014). These precautionary measures are a part of routine exercises, because humans are the primary source of microbial contamination (Moissl-Eichinger et al., 2015; Checinska Sielaff et al., 2019; Avila-Herrera et al., 2020). On average, humans shed 1.5 million skin cells an hour which carry approximately 15 million bacterial cells, thus becoming a significant source of the indoor microbiome (Jaffal et al., 1997; Lax et al., 2014). Many reports showed transfer of microorganisms via direct contact to indoor surfaces like keyboards (Fierer et al., 2010), restrooms (Flores et al., 2011), offices (Hewitt et al., 2012), kitchens (Flores et al., 2013), airplanes (McManus and Kelley, 2005; Korves et al., 2013), and hospitals (Kembel et al., 2012; Lax et al., 2017). Because of the human presence in these cleanrooms, their surfaces are not expected to be free of microbial burden.

The ISS and CRV assembly cleanrooms, including spacecraft assembly facility (SAF) environments, are strictly controlled and monitored for airflow, water circulation, temperature, and humidity; however, individual differences do exist between the two systems (Checinska et al., 2015). The ISS is a closed system where the air is recirculated after purification, while cleanrooms get a constant supply of fresh air from the outside environment. Additionally, astronauts live and work on the ISS as humans do in a typical household on Earth, while SAF cleanrooms have strict requirements that avoid activities like eating or sleeping. At a given point in time, the ISS harbors around six astronauts with a maximum of around 13 crew, while approximately 50 people can work in a cleanroom every day in a highly regulated manner. Despite high human traffic in SAF, the microbial burden was minimal and ranged between 10^2 and 10^4 cells per m^2 (Hendrickson et al., 2017). It has also been shown that the cleaning procedures followed at SAF significantly decreased the number of microorganisms, but these procedures led to the selection of hardy, robust microorganisms capable of surviving extreme oligotrophic conditions (Gioia et al., 2007; Vaishampayan et al., 2012; Mahnert et al., 2015). Cargos such as food and equipment for scientific experiments are assembled in clean conditions and delivered to the ISS via CRV. All spacefaring nations impose cleanroom requirements when packaging their cargos that are resupplying the ISS.

The objective of this study is to decipher the role of CRV systems in potentially transporting microorganisms to the ISS to understand if CRV could be a source of microbial contamination of the ISS. Sampling of various surfaces of CRV systems (CRV1, CRV2, and CRV3) was carried out prior to launch (∼1 month) and corresponding in-flight sampling of the ISS (Flight 1, Flight 2, and Flight 3) was designed to be within 25–51 days after docking of the respective CRV systems (see **Figure 1** for a timeline). This sampling scheme was implemented to help understand whether CRV1 had any influence on the microbial population of ISS Flight 1, whether CRV2 had any influence on the microbial population of ISS Flight 2, or whether CRV3 had any influence on the microbial population of ISS Flight 3. Microbial burden associated with CRV environmental surface samples were estimated using traditional techniques (e.g., colony counts), and molecular techniques like adenosine triphosphate (ATP) assay and 16S rRNA gene (bacteria) and internal transcribed spacer (ITS) region (fungi) quantification using quantitative polymerase chain reaction (qPCR) assays. In addition to characterizing cultivable microbial diversity using the Sanger sequencing method, the CRV samples were more thoroughly analyzed using a shotgun metagenome sequencing approach. Subsequently, the microbial diversity of the CRV samples was compared with the ISS environmental microbiome (Checinska Sielaff et al., 2019) to understand the potential transfer of biological materials from Earth to the ISS.

MATERIALS AND METHODS

In this study, internal surfaces and external ground support equipment (GSE) of three CRV destined to the ISS were sampled ($N = 22$ and 3 controls; **Table 1**). Samples collected aboard the ISS were done during the berthing period of their respective vehicles, except for CRV1 (see **Figure 1** for a timeline) (Checinska Sielaff et al., 2019). Eight samples were collected in 2014 for CRV1, nine in 2015 for CRV2, and eight in 2016 for CRV3. Since CRV3 vehicle surfaces were extremely clean and all analyses, including traditional microbiology assays, were below detection limits, data pertaining to CRV3 vehicle locations are not presented in this study. Since CRV were not reused during this study, we could not sample from the same capsule multiple times. Efforts were taken to collect samples as close together as possible in subsequent CRV, but due to differences in configuration of each vehicle, it was not always possible to collect samples from the same locations. All CRV sampled were manufactured by the same vendor.

Sampling kits were assembled as detailed in our previous ISS studies (Singh et al., 2018; Checinska Sielaff et al., 2019; Avila-Herrera et al., 2020) to facilitate comparisons between these datasets. Briefly, each polyester wipe (9″ × 9″; ITW Texwipe, Mahwah, NJ, United States) was soaked in 15 mL of sterile molecular grade water (Sigma-Aldrich, St. Louis, MO, United States) for 30 min followed by transfer to a sterile zip lock bag (Venkateswaran et al., 2012). Several locations were sampled on CRV surfaces using polyester wipes, and descriptions of the

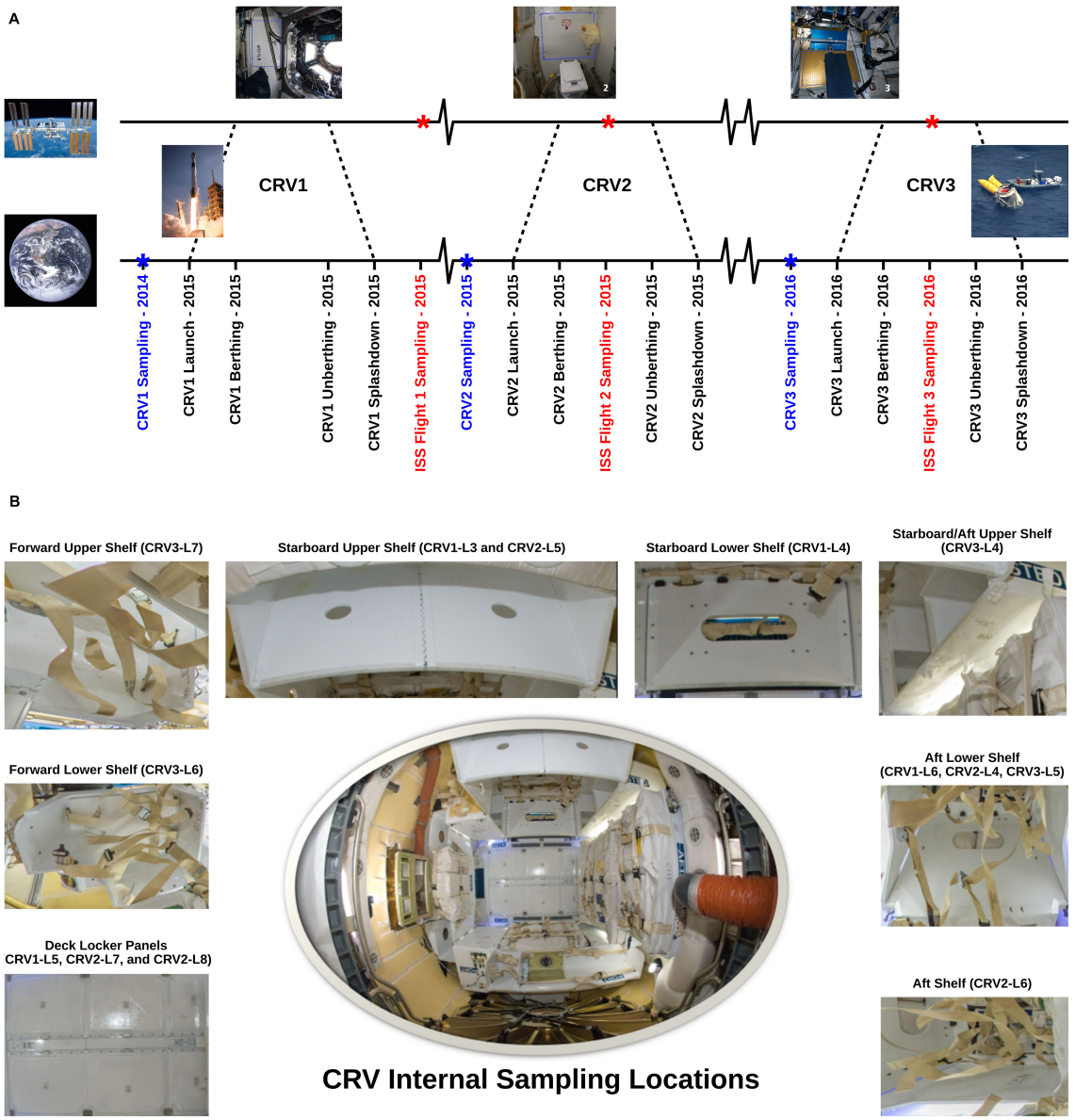

FIGURE 1 | (A) Sampling time line for the CRV and the ISS samples. Blue labels mark sampling events conducted on CRV prior to launch, and red labels mark sampling events on board the ISS. **(B)** Representative sampling locations of internal CRV surfaces. Pictures: NASA/ESA Credit.

locations are summarized in **Table 1**. A single wipe was used for each location by donning sterile gloves (KIMTEC Pure G3 White; Nitrile Clean-room Certified; Cat. HC61190; Fisher Scientific, Waltham, MA, United States) to collect a sample of one-meter square area. The samples were stored at 4°C and shipped to Jet Propulsion Laboratory (JPL, Pasadena, CA, United States) for processing. Microbiological analyses were carried out within 48 h of sampling at JPL. A control wipe (environmental control) was taken out from the zip lock bag, unfolded, waved for 30 s, and packed back inside a new sterile zip lock. One control wipe was included for each CRV sampling session. Similarly, an unused wipe that was flown to the sampling location and brought back to JPL along with the samples served as a negative control for sterility testing. If field controls (wipes that were exposed to the CRV environment but not used in active sampling) showed any signs of microbial growth, then negative controls would be assayed for cultivable counts to check sterility of the wipes used for sampling. However, none of the field controls showed any colony forming units (CFU) for all CRV sampling events.

Sample Collection and Processing

Samples from CRV were processed in the same way as ISS samples from our previous studies (Singh et al., 2018; Checinska Sielaff et al., 2019; Avila-Herrera et al., 2020). Briefly, each wipe was transferred to an individual 500 mL bottle containing 200 mL of sterile phosphate-buffered saline (PBS; Sigma-Aldrich,

TABLE 1 | Descriptions of sampling locations on commercial resupply vehicles.

Sample ID	Description	Category
CRV1-L1	Ladder platform just prior to the vehicle entrance	GSE
CRV1-L2	Clean room floor near the ladder that leads up to the vehicle entrance	GSE
CRV1-L3	Upper shelf in starboard side of the vehicle	Internal
CRV1-L4	Lower shelf in starboard side of the vehicle	Internal
CRV1-L5	Front panels in deck side of the vehicle	Internal
CRV1-L6	Lower shelf in aft side of the vehicle	Internal
CRV1-L7	Ladder steps that leads up to the platform near the vehicle entrance	GSE
CRV1-FC	Control wipe exposed to the air for 30 s inside the vehicle	Control
CRV2-L1	Right leg/side of ladder	GSE
CRV2-L2	Left leg/side of ladder	GSE
CRV2-L3	Left and right rail arms of the ladder above the platform	GSE
CRV2-L4	Lower shelf in aft side of the vehicle	Internal
CRV2-L5	Upper shelf in starboard side of the vehicle	Internal
CRV2-L6	Upper shelf in aft side of the vehicle	Internal
CRV2-L7	Locker panels in deck side of the vehicle	Internal
CRV2-L8	Locker panels in deck side of the vehicle near the aft side	Internal
CRV2-FC	Control wipe exposed to the air for 30 s inside the vehicle	Control
CRV3-L1	Ladder platform just prior to the vehicle entrance	GSE
CRV3-L2	Left rail arm of the ladder above the platform	GSE
CRV3-L3	Right rail arm of the ladder above the platform	GSE
CRV3-L4	Upper shelf in starboard side of the vehicle near the aft side	Internal
CRV3-L5	Lower shelf in aft side of the vehicle	Internal
CRV3-L6	Lower shelf in forward side of the vehicle	Internal
CRV3-L7	Upper shelf in forward side of the vehicle	Internal
CRV3-FC	Control wipe exposed to the air for 30 s inside the vehicle	Control

The nomenclature used to describe the sides of the cargo resupply vehicle are based on the following reference directions, with respect to the +X, +Y, +Z Local Vertical, Local Horizontal, and Velocity Vector.
CRV, commercial resupply vehicle; GSE, ground support equipment.

St. Louis, MO, United States) and vigorously hand shaken for 2 min. The resulting suspension was then concentrated to 4 mL using a CP-150 concentration pipette (Innova Prep, Drexel, MO, United States). Both negative and field controls used in this study were processed the same way as other samples for comparison. The concentrated sample (4 mL) were further aliquoted to four different parts for shotgun metagenome analysis (2 × 1.5 mL; PMA treated and untreated), ATP analysis (900 μL), and for growing microorganisms (100 μL). Due to the measurement of different kinds of microorganisms, that require multiple culture media (3 types) in duplicates, the aliquots kept for growing microorganisms were further diluted (10^{-1} and 10^{-2}) and used.

Culture Based Microbial Diversity

Due to proprietary cleaning regimes, the surfaces of CRV might be oligotrophic. Although most nutrient and carbon sources necessary for microbial growth are presumably lacking or at very-low concentrations, these surfaces may still harbor microorganisms that are either dormant or slowly metabolizing. Furthermore, microorganisms adapted to more stringent conditions may not necessarily grow on normal nutrient media. Therefore, to target the slow-growing microbial population, Reasoner's 2A agar (R2A; Difco, MI, United States) media (Reasoner and Geldreich, 1985) was used. Similarly, as humans are always near the CRV during the assembly and packaging processes, potential opportunistic pathogenic microorganisms may transfer to the CRV surfaces. As a result, the CRV samples were also plated on blood agar media (BA; Difco, MI, United States) to decipher the potentially pathogenic microbial population. Additionally, the samples were also plated on potato dextrose agar (PDA; Difco, MI, United States) medium, thus targeting the fungal population on CRV.

To estimate the bacterial and fungal populations, the concentrated sample was diluted to a suitable serial 10-fold dilution in sterile PBS. A volume of 100 μl of suspension from the serially diluted sample was spread onto R2A media plates and PDA plates with chloramphenicol (100 μg/mL; Sigma-Aldrich, St. Louis, MO, United States), incubated at 25°C for 7 days for bacterial and fungal population enumeration, respectively. For enumeration of human commensal microorganisms, 100 μl of serially diluted sample was also spread onto BA and incubated at 35°C for 2 days. Distinct isolated colonies were transferred to fresh media and subsequently archived in semi-solid R2A media (dilution 1:10) and stored at room temperature.

Strain Identification

Bacterial isolates were identified by amplifying partial 16S rRNA genes using the primers 9bF (5′- GRGTTTGATCCTGG CTCAG-3′) (Huber et al., 2002) and 1406uR (5′- ACGGG CGGTGTGTRCAA-3′) (Lane, 1991) and the following cycling conditions: initial denaturation at 95°C for 2 min, 10 cycles of denaturing at 96°C for 30 s, annealing at 60°C for 30 s and elongation at 72°C for 60 s, followed by another 25 cycles of denaturing at 94°C for 30 s, annealing at 60°C for 30 s and elongation at 72°C for 60 s and a final elongation step at 72°C for 10 min. The template was either a small fraction of a picked colony in a colony-PCR assay or 5–20 ng of DNA purified from culture via the peqGOLD Bacterial DNA Kit (peqlab, Germany). The 16S rRNA gene amplicons were Sanger-sequenced (Eurofins, Germany) and the obtained sequences were classified using the EzTaxon identification service (Yoon et al., 2017).

Fungal isolates were identified by amplifying their ITS region using the primers ITS1F (5′-CTTGGTCATTTAGAGG AAGTAA-3′) and ITS4 (5′-TCCTCCGCTTATTGATATGC-3′) (Manter and Vivanco, 2007) at the following cycling conditions: initial denaturation at 95°C for 10 min, followed by 35 cycles of denaturing at 94°C for 60 s, annealing at 51°C for 60 s, elongation at 72°C for 60 s, and a final elongation step at 72°C for 8 min. The amplicons were Sanger-sequenced (Eurofins, Germany) and the obtained sequences were classified using the curated databases UNITE version 7.2 (Kõljalg et al., 2013) and BOLD version 4 (Ratnasingham and Hebert, 2013).

Molecular Methods for Quantitation of Total and Viable Microorganisms

ATP Assay

To determine the total and intracellular ATP from all samples, a bioluminescence assay was performed using the CheckLite HS Kit (Kikkoman, Japan) and the manufacturer's protocol, as described previously (Venkateswaran et al., 2003). For total ATP assay (dead and viable microbes), four replicates of 100 μl sample were mixed with 100 μl of benzalkonium chloride, a cell lysing reagent and incubated at room temperature for 1 min. To this mixture, 100 μl of luciferin-luciferase reagent was added, and the resulting bioluminescence was measured immediately using a Lumitester K-210 luminometer (Kikkoman, Japan). For intracellular ATP (viable microorganisms), 500 μl of the serially diluted sample was amended with a 50 μl of an ATP-eliminating reagent (apyrase, adenosine deaminase) and incubated for 30 min at room temperature for eliminating extracellular ATP. Following which, the ATP assay was performed as described previously for the total ATP. It has been reported that one relative luminescent unit (RLU), the unit of measurement of ATP, was considered equivalent to approximately one CFU (La Duc et al., 2004).

PMA-Viability Assay

Before DNA extraction, half of the sample was treated with propidium monoazide (PMA; Biotium, Inc., Hayward, CA, United States) so that the microbiome of intact/viable cells (PMA treatment) could be characterized. The PMA-untreated samples yielded information about the total microbial population (including free DNA, dead cells, cells with a compromised cell membrane, intact cells, and viable cells). PMA binds to DNA, making the DNA unavailable for amplification during PCR steps (Nocker et al., 2007). Due to its higher molecular weight and/or charge, PMA cannot penetrate cells that have an intact cell membrane (i.e., viable) but can bind to free floating DNA or DNA inside cells with a compromised cell membrane (i.e., dead cells) (Nocker et al., 2006, 2007). It is in this way that many studies have utilized PMA to distinguish between intact/viable cells and compromised/dead cells (Lin et al., 2011; Vaishampayan et al., 2013; Checinska et al., 2015; Jäger et al., 2018; Singh et al., 2018; Checinska Sielaff et al., 2019; Avila-Herrera et al., 2020).

A 3 mL aliquot of the concentrated sample was split into two halves. One 1.5 mL aliquot was treated with PMA (Biotium, Inc., Hayward, CA, United States) to a final concentration of 25 μM, followed by 5 min incubation in the dark at room temperature. The sample was then exposed to photoactivation for 15 min in a PMA-Lite LED Photolysis Device (Biotium, Inc., Hayward, CA, United States). The other aliquot with no PMA treatment was also incubated in dark for 5 min followed by photoactivation for 15 min like the PMA treated aliquot. Both PMA treated and untreated samples were then each split into half again. One half (750 μl) of each sample was then transferred to Lysing Matrix E tube (MP Biomedicals, Santa Ana, CA, United States) and subjected to bead beating for 60 s to allow cell disruption of hardy cells and spores with a limited loss of microbial diversity. The mechanically disrupted sample was then mixed with the unprocessed counterpart and used for DNA extraction via the Maxwell 16 automated system (Promega, Madison, WI, United States), per the manufacturer's protocol. DNA was extracted in 50 μl volume and stored at −20°C until further processing.

Quantitative PCR Assay

Real-time quantitative polymerase chain reaction (qPCR) assays, targeting the 16S rRNA gene (bacteria) and ITS region (fungi), were performed in triplicate with a SmartCycler (Cepheid, CA, United States) to quantify the bacterial and fungal burden. The following primers were used for targeting the 16S rRNA gene: 1369F (5′-CGGTGAATACGTTCYCGG-3′) and modified 1492R (5′-GGWTACCTTGTTACGACTT-3′) were used for this analysis (Suzuki et al., 2000). Primers targeting the ITS region, were NS91 (5′-GTCCCTGCCCTTTGTACACAC-3′) and ITS51 (5′-ACCTTGTTACGACTTTTACTTCCTC-3′) (Onofri et al., 2012). Each 25 μL reaction consisted of 12.5 μL of 2X iQ SYBR Green Supermix (Bio-Rad, Hercules, CA, United States), 1 μL each of forward and reverse oligonucleotide primers (10 μM each), and 1 μL of template DNA. Purified DNA from Model Microbial Consortium (Kwan et al., 2011) served as the positive control and DNase/RNase free molecular-grade distilled water (Promega, Madison, WI, United States) was used as the negative control. These controls were included in all qPCR runs. The reaction conditions were as follows: a 3 min denaturation at 95°C, followed by 40 cycles of denaturation at 95°C for 15 s, and combined annealing and extension at 55°C for 35 s. The number of gene copies were determined from the standard curve. The 16S rRNA gene of *Bacillus pumilus* SAFR-032 and the ITS region of *Aureobasidium pullulans* 28v1 were synthesized and used for preparing standard curves as described previously (Checinska et al., 2015). The qPCR efficiency was ∼98% for each run. Negative controls yielded similar values (∼100 copies) despite using either 1 or 10 μL of DNA templates.

Metagenome Sequencing

DNA extracted from all CRV samples was quantified using the Qubit® Quant-iT dsDNA High Sensitivity Kit (Invitrogen, Life Technologies, Grand Island, NY, United States) and samples were selected based on the minimum DNA concentration requirement (∼10 pg/μL) for metagenome sequencing. Only two samples from CRV1 and two samples from CRV2, with and without PMA treatment, satisfied this cutoff, resulting in 8 samples proceeding to metagenomics sequencing (2 CRV × 2 samples × 2 treatments = 8). Sample preparation for metagenome sequencing was carried out using the Illumina Nextera Kit (Illumina, San Diego, CA, United States). Each library was assessed for quality and fragment size using the Bioanalyzer 2100 (Agilent, Santa Clara, CA, United States). Adapters were added and ligated to DNA sequences in each library. All libraries were then normalized to 2 mM, pooled together and subjected to denaturation followed by dilution to 1.8 pM concentration, as per the manufacturer's protocol. Sequencing was carried out using the HiSeq 2500 platform (Illumina, San Diego, CA, United States) resulting in 100 bp paired end reads.

Data Processing

Adapter sequences and low-quality ends were trimmed from the 100 bp paired end reads using Trimmomatic (version 0.32) (Bolger et al., 2014) with a quality cutoff value set at minimum Phred score of 20 along the entire read length. Additionally, reads shorter than 80 bp were removed, followed by data normalization based on guidelines provided by Nayfach and Pollard (2016). Using the MEGAN 6 lowest common ancestor (LCA) algorithm (Huson et al., 2016), filtered high quality reads were binned to their respective domain and normalized for semi-quantitative comparative analysis.

Assigning taxonomy and function to the filtered CRV metagenome sequences was performed using the MEGAN 6 tool kit (Huson et al., 2016). We used the NCBI taxonomy database (Sayers et al., 2008) and NCBI-NR protein sequence database with entries from GenPept, SwissProt, PIR, PDB, and RefSeq, to assign taxonomic features to sequences using the sequence comparison tool DIAMOND (version 0.8.29). Assignments were based on the weighted LCA assignment algorithm of MEGAN 6 (Huson et al., 2007). Additionally, filtered DNA sequences were mapped against protein databases like eggnog (Powell et al., 2011), KEGG (Kanehisa and Goto, 2000), and SEED (Overbeek et al., 2005) for functional analysis.

Comparison of CRV and ISS Metagenomes

Metagenome data from a previously reported study (Singh et al., 2018) of samples collected from the ISS were analyzed in tandem with metagenome data for samples collected from the CRV. These ISS metagenome samples were collected shortly after unberthing of CRV1 from the station or while CRV2 was berthed to the station (see **Figure 1** for a timeline). Analyzing ISS and CRV metagenomes together allowed us to focus on microbial dynamics associated with the transfer of materials from CRV to the ISS. Microbial diversity analyses performed on normalized reads were designed to retain a minimum of one unique sequence to avoid the loss of low depth samples or unique sequences. Furthermore, BLAST hits of $\geq$20 amino acids and $\geq$90% nucleotide identity were used for taxonomic and functional studies. Normalized read counts for each sample at multiple taxonomic levels (e.g., domain, family, species, etc.) were exported in matrix form from MEGAN 6 and used in downstream statistical analyses.

Statistical Analyses

To determine the differences in samples collected from the GSE and internal surfaces of both CRV1 and CRV2 and to compare them with samples collected from the ISS, several statistical analyses were performed. The non-parametric Mann–Whitney–Wilcoxon (MWW) test was used to evaluate differences in microbial diversity detected on internal surfaces of CRV and surfaces of their GSE, across CRV sampling events, and with samples collected from the ISS surfaces. The null hypothesis for the MWW test is that the distributions of microorganisms are equal between two conditions tested (e.g., internal or GSE surface), or alternatively these distributions are not equal. Parametric tests were considered for this purpose, but transformation of these data to satisfy assumptions of these tests was not practical. Samples below detection limit were assumed to have a value of 0.01 for all statistical analyses. These analyses were performed using a custom R script[1]. To measure the diversity in the microbial communities residing on the internal and GSE surfaces of CRV1 and CRV2, various statistical indices were used, including the Shannon–Weaver index (Shannon and Weaver, 1949), Simpson's index (Simpson, 1949), and the Chao1 metric (Chao, 1984). To visualize differences in relative species abundance among CRV and ISS metagenome samples, non-metric multidimensional scaling (NMDS) using a Bray-Curtis dissimilarity matrix calculated from the normalized read counts was used. Analyses were performed using the vegan R package[2] and custom R scripts[3,4].

RESULTS

Microbial Burden

Microbial burden assays were aimed at using both cultivation-dependent and independent methods to assess the broad diversity of microorganisms on various locations sampled from CRV1 and CRV2 (see **Table 1** for a description of each sample). Since CRV3 did not show any cultivable counts, such information was not obtained.

Microbial colonies were isolated from all three locations on the GSE surfaces of CRV1 (locations 1, 2, and 7), and only one internal surface (location 4) as shown in **Table 2**. Using the R2A media, bacteria isolated from three GSE surfaces of CRV1 ranged between 1.3×10^5 to 2.8×10^6 CFU per m^2 while 1.8×10^4 CFU per m^2 colonies were isolated from the internal location CRV1-L4, an order of magnitude lower than samples from GSE surfaces. The MWW test of colony counts on R2A media show that the three GSE surfaces of CRV1 harbor a significantly different number of cultivable bacteria than the internal locations ($W = 12$, p-value $= 0.0436$). No colonies were isolated from internal locations of CRV1 on BA media while GSE surfaces (location 2 and 7) showed 1×10^6 CFU per m^2 and location 1 showed 5.1×10^2 CFU per m^2 colonies. Fungal colonies isolated on PDA media from GSE of CRV1 ranged between 3.8×10^4 to 2.9×10^5 CFU per m^2 while 2×10^4 CFU per m^2 were isolated from the internal location CRV1-L4. The MWW test of colony counts on PDA media show that the three GSE surfaces of CRV1 harbor a significantly different amount of cultivable fungi than the internal surfaces ($W = 12$, p-value $= 0.0436$).

CRV2 was clean as compared to CRV1 and microbial colonies were isolated from only three samples (location 1; GSE and locations 7 and 8; internal) as shown in **Table 2**. The microbial colonies isolated from the CRV2-L1 GSE location were 3.7×10^4 and internal locations of CRV2-L7 and CRV2-L8 were 3.3×10^3

[1]https://github.com/sandain/R/blob/master/mw.R
[2]https://cran.r-project.org/web/packages/vegan/
[3]https://github.com/sandain/R/blob/master/diversity.R
[4]https://github.com/sandain/R/blob/master/mds.R

TABLE 2 | Total, viable, and cultivable microbiological characteristics of CRV system surface samples.

	Cultivable bacteria (CFU/m^2)		Cultivable fungi (CFU/m^2)	ATP based microbial population (RLU/m^2)		Bacterial 16S rRNA (copies/m^2)		Fungal ITS (copies/m^2)	
Sample ID	**R2A**	**BA**	**PDA**	**Total**	**Intracellular**	**Untreated**	**PMA-Treated**	**Untreated**	**PMA-Treated**
CRV1-L1	1.3×10^5	5.1×10^2	3.8×10^4	4.9×10^5	6.6×10^5	8.6×10^5	4.3×10^5	7.0×10^5	BDL
CRV1-L2	2.8×10^6	1.0×10^6	2.9×10^5	9.9×10^6	1.2×10^7	1.0×10^{10}	5.6×10^8	1.3×10^6	2.6×10^6
CRV1-L3	BDL	BDL	BDL	2.8×10^1	4.0×10^0	3.7×10^5	2.3×10^5	BDL	BDL
CRV1-L4	1.8×10^4	BDL	2.0×10^4	1.9×10^5	3.1×10^5	7.2×10^5	3.2×10^5	7.2×10^4	6.6×10^4
CRV1-L5	BDL	BDL	BDL	3.1×10^1	5.0×10^0	5.0×10^5	2.3×10^5	BDL	BDL
CRV1-L6	BDL	BDL	BDL	3.1×10^1	9.0×10^0	3.1×10^5	3.3×10^5	BDL	BDL
CRV1-L7	4.0×10^5	1.0×10^6	1.7×10^5	2.3×10^6	2.6×10^6	1.4×10^8	6.0×10^7	7.6×10^5	7.7×10^5
CRV1-FC	BDL	BDL	BDL	1.9×10^1	6.0×10^0	4.3×10^3	2.7×10^3	BDL	6.3×10^2
CRV2-L1	3.7×10^4	5.0×10^2	1.5×10^3	1.3×10^5	9.0×10^4	4.5×10^5	2.8×10^5	6.1×10^5	BDL
CRV2-L2	BDL	BDL	BDL	6.0×10^1	1.5×10^1	1.9×10^5	7.9×10^4	2.6×10^5	1.8×10^5
CRV2-L3	BDL	BDL	BDL	1.8×10^5	1.9×10^1	2.8×10^5	1.0×10^5	1.3×10^5	BDL
CRV2-L4	BDL	BDL	BDL	2.8×10^1	3.0×10^0	3.8×10^4	6.1×10^4	BDL	BDL
CRV2-L5	BDL	BDL	BDL	4.1×10^1	2.0×10^0	7.3×10^4	3.6×10^4	BDL	BDL
CRV2-L6	BDL	BDL	BDL	2.2×10^1	8.0×10^0	5.3×10^4	5.4×10^4	8.1×10^4	BDL
CRV2-L7	3.3×10^3	1.5×10^3	1.5×10^3	8.5×10^1	1.3×10^1	2.8×10^5	9.5×10^4	9.3×10^4	BDL
CRV2-L8	9.5×10^2	BDL	BDL	9.2×10^1	2.4×10^1	2.3×10^5	6.6×10^4	BDL	BDL
CRV2-FC	BDL	BDL	BDL	BDL	BDL	BDL	BDL	BDL	BDL

BDL, below detection limit.

and 9.5×10^2 CFU per m^2, respectively on R2A media. The MWW test of colony counts on R2A media failed to show a significant difference between bacterial counts among the internal and GSE surfaces of CRV2 ($W = 8$, p-value $= 1.0$). About 5.0×10^2 (GSE location 1) and 1.5×10^3 (internal location 7) CFU per m^2 were isolated on the BA media. The MWW test of colony counts on BA media failed to show a significant difference between bacterial counts among the internal and GSE surfaces of CRV2 ($W = 8$, p-value $= 1.0$). About 1.5×10^3 CFU per m^2 of fungi were isolated from both GSE location CRV2-L1 and internal location CRV2-L7 on the PDA media. The MWW test of colony counts on PDA media failed to show a significant difference between fungal counts between the internal and GSE surfaces of CRV2 ($W = 8.5$, p-value $= 0.8437$). The microbial colony counts for the CRV2 were lower by almost an order of magnitude as compared to CRV1. However, the MWW test failed to show a significant difference in colony counts between CRV1 and CRV2 on R2A media ($W = 38.5$, p-value $= 0.2094$), BA media ($W = 35$, p-value $= 0.3698$), or PDA media ($W = 41$, p-value $= 0.1023$). Strikingly, no samples from GSE or internal surfaces of the CRV3 vehicle showed any trace of a microbial population.

Identification of cultured microbes revealed the presence of four bacterial phyla (*Actinobacteria*, *Proteobacteria*, *Firmicutes*, and *Bacteroidetes;* **Supplementary Table S1**) and two fungal phyla (*Ascomycota* and *Basidiomycota*; **Supplementary Table S1**). Almost all the bacterial isolates, besides *Pseudarthrobacter*, *Compostimonas*, and *Mycobacterium*, have also been detected by the metagenome derived diversity analysis, at least at the genus level, whereas half of the fungal isolates (*Bullera/Papiliotrema*, *Cryptococcus/Hannaella/Naganishia*, *Cladosporium*, *Dioszegia*, *Rhodotorula*, *Periconia*, *Phialemoniopsis*, and *Phlebia*) were not detected.

Cultivation-independent methods used to estimate the microbial burden included ATP and qPCR assays. The intracellular ATP assay quantified the content of live cells, and total ATP quantified both dead and live cells to provide an estimate of the viable microbial population in a given sample. In the case of CRV1, the total ATP content for the GSE surfaces ranged between 10^5 to 10^6 RLUs per m^2, while all internal surface locations had ATP content lower by four orders of magnitude, except for the CRV1-L4 location which had 1.9×10^5 RLUs per m^2 (**Table 2** and **Supplementary Figure S1**). The intracellular ATP content for all GSE surfaces and one internal surface (CRV1-L4) were similar to their respective total ATP content, thus indicating that almost 100% of the microorganisms were viable at these locations. However, the intracellular ATP content was considerably lower for other internal locations of CRV1 and indicated that only 15–30% of the total microorganisms were viable. Incidentally, cultivable populations were isolated only from the CRV1-L4 sample. In the case of the CRV2, all GSE surfaces showed total ATP content of 10^5 RLUs per m^2, except for CRV2-L2 which had only 10^1 RLUs per m^2 (**Table 2** and **Supplementary Figure S1**). The total ATP RLU values for all internal locations of CRV2 were similar to CRV1 with only 10^1 RLUs per m^2. The MWW test failed to show a significant difference in total or intracellular ATP content between CRV1 and CRV2 ($W = 45.5$, p-value $= 0.3859$ or $W = 49$, p-value $= 0.2359$). The intracellular ATP content for all internal locations of CRV2 was lower than the respective total ATP content thus indicating that 5–36% of the total microorganisms were viable.

The qPCR-based DNA quantification using the 16S rRNA gene and the ITS region provided an estimate of the bacterial and fungal burden of the CRV1 and CRV2. In the case of CRV1, the PMA treated samples (viable microbes) from the GSE sample locations had very high bacterial density for locations 2 and 7, ranging between 10^7–10^8 16S rRNA gene copies per m^2 (**Table 2** and **Supplementary Figure S2A**). However, location 1 (GSE) and all internal locations of CRV1 showed 10^5 viable bacterial population per m^2. In general, the PMA treated CRV1 samples showed 16S rRNA gene copy numbers lower by one to two orders of magnitude for the intact cells from GSE locations samples, while there was an only minute difference in the intact cell population for all internal CRV surface samples. The percentage of the intact cells for both internal and GSE locations of CRV1 ranged between 40 and 64%, except for the location 2 and 6, which had 5 and 100% of the intact cells, respectively.

Similarly, the fungal density estimated using quantification of the ITS region showed that the ITS gene copies in PMA untreated samples in CRV1 samples were less by three to four orders of magnitude as compared to their bacterial counterpart. The ITS copies for the PMA untreated samples ranged between 10^5 and 10^6 for the GSE locations and 10^4 ITS copies per m^2 for internal locations (**Table 2** and **Supplementary Figure S2B**). The PMA treated samples for both internal and GSE CRV1 locations showed similar ITS copy numbers to the PMA untreated samples, thus making the percentage of intact fungal cells 90–100% for CRV1-L4 and CRV1-L7. However, the GSE location CRV1-L2 showed only 20% of the intact fungal population.

In the case of CRV2, the 16S rRNA gene copy numbers of PMA untreated samples for the GSE and internal locations were 10^5 and 10^4 copies per m^2, respectively. The percentage of the intact bacterial cell numbers determined from the PMA treated samples for both GSE and internal locations were in the range of 36–62% and 34–100%, respectively. The fungal density for the CRV2 samples for both GSE and internal locations for the PMA untreated samples was in the range of 10^5 and 10^4, respectively. Additionally, these fungal cell numbers were higher by an order of magnitude as compared to their bacterial counterpart.

The MWW test of 16S rRNA gene copy numbers of PMA treated samples showed a significant difference in bacterial abundance between CRV1 and CRV2 ($W = 62$, p-value $= 0.01408$). The MWW test of ITS copy numbers of PMA treated samples, however, failed to demonstrated a significant difference in fungal abundance between CRV1 and CRV2 ($W = 50$, p-value $= 0.107$). When comparing 16S rRNA or ITS copy numbers from GSE and internal samples, the MWW test failed to find any significant difference ($M = 43$, p-value $= 0.0675$ or $M = 39$, p-value $= 0.08197$, respectively).

Metagenome Derived Microbial Diversity

Samples were collected from three CRV vehicles (25 samples in total; **Table 1**) and each wipe was either treated with PMA or left untreated, resulting in an analysis of 50 samples, including 6 controls. Among the 50 samples subjected for shotgun library preparation, only 8 samples (4 non-PMA and corresponding 4 PMA treated) yielded shotgun metagenome libraries (none from the controls) and all other 42 samples were below the detection limit (0.01 ng DNA/μL). Subsequently, these low DNA concentration samples (42 samples) did not produce any shotgun metagenome sequences. High quality metagenome reads were obtained for four samples; one each from GSE (CRV1-L2; CRV2-L1) and internal (CRV1-L4; CRV2-L7) locations. Interestingly, the microbial burden (both cultivable and qPCR assays) of these four sites were high when compared to other locations (**Table 2**).

At the domain level, bacteria dominated the microbial diversity detected in the metagenomes sampled from internal and GSE surfaces of CRV1 and CRV2. In the case of CRV1, bacteria at both internal (CRV1-L4) and GSE (CRV1-L2) locations constituted 99 and 88% of the total reads from PMA treated samples, respectively (**Supplementary Figure S3**). PMA treated samples from CRV2 were very similar to CRV1 samples when compared at the domain level, both GSE (CRV2-L1) and internal (CRV2-L7) locations were dominated by bacteria (90 and 94%, respectively). Most of the remaining reads belonged to Eukaryota, constituting <1–12% of the total reads from CRV1 and CRV2 internal and GSE locations. The viral and archaeal reads constituted a very minute fraction of the total reads in PMA treated samples from internal and GSE locations of CRV1 and CRV2.

At the phylum level (**Supplementary Figure S4**), the PMA treated samples showed significant differences between internal and GSE locations of both CRV1 and CRV2. The CRV1 GSE was dominated by Proteobacteria (95%) while the internal locations majorly constituted of Proteobacteria (32%), Firmicutes (29%), Actinobacteria (21%), followed by Ascomycota (8%). The CRV2 GSE also showed dominance of Proteobacteria reads (53%) followed by Actinobacteria (11%), Firmicutes (10%), and Ascomycota (7%). The CRV2 internal location had a different composition as compared to the GSE at the phylum level, which was dominated by Firmicutes (40%), closely followed by Proteobacteria (32%), and Actinobacteria (16%) reads. Also, the internal locations of CRV1 and CRV2 showed relatively similar abundance at the phylum level except for Actinobacteria, Firmicutes, and Ascomycota, as mentioned earlier.

At the class level (**Supplementary Figure S5**), the PMA treated GSE samples of CRV1 were dominated by Betaproteobacteria (73%) followed by Alphaproteobacteria (11%), while the internal location was dominated in descending order by Bacilli (28%), Actinobacteria (21%), Gammaproteobacteria (18%), Alphaproteobacteria (8%), Dothideomycetes (6%), and Betaproteobacteria (4%). In the case of CRV2 PMA treated samples, the GSE showed a high abundance of Gammaproteobacteria (21%), followed by Betaproteobacteria (17%), Actinobacteria (11%), Alphaproteobacteria (10%), and Bacilli (10%). On the other hand, Bacilli (39%) dominated the internal location of CRV2 PMA treated samples, followed by Betaproteobacteria (18%), Actinobacteria (15%), and Alphaproteobacteria (8%). Additionally, significant differences were observed at the class level for the internal locations of both CRV1 and CRV2.

At the order level (**Supplementary Figure S6**), Burkholderiales constituted more than 71% of the reads for the PMA treated samples from the GSE of CRV1, which was distantly followed by Caulobacterales (7%), and Sphingomonadales (3%).

The internal location of CRV1 presented a completely different picture, with only 4% of the reads belonging to Burkholderiales, while the most dominant order was Bacillales (27%), followed by Pseudomonadales (16%), and Propionibacteriales (10%). Furthermore, reads for Caulobacterales and Sphingomonadales were detected at very low levels (<1%) from the internal location of CRV1. The PMA treated samples for CRV2 internal and GSE surfaces showed a similar trend with respect to the order level. Burkholderiales, Bacillales, Pseudomonadales, and Propionibacteriales were the dominant orders detected on both internal and GSE surfaces. However, the only difference between GSE and internal CRV2 samples was that the reads belonging to Bacillales were dominant at the internal location (36%) and Pseudomonadales was dominant for GSE (18%).

At the family level (**Supplementary Figure S7**), large differences were observed on the internal and GSE surfaces of CRV1 for the PMA treated samples. Reads for *Oxalobacteraceae* (33%), *Comamonadaceae* (22%), and *Caulobacteraceae* (6%) dominated the GSE surface of CRV1, followed by *Sphingomonadaceae* (3%) and *Burkholderiaceae* (1%). The internal location for CRV1 showed the complete opposite trend with only 4% of the reads belonging to *Oxalobacteraceae* family, while *Comamonadaceae*, *Caulobacteraceae*, *Sphingomonadaceae*, and *Burkholderiaceae* were detected at very low levels (<1%). Instead, the CRV1 internal location was dominated by *Pseudomonadaceae* (15%), *Bacillaceae* (10%), *Propionibacteriaceae* (10%), and *Aureobasidiaceae* (5%) families. The CRV2 PMA treated samples for both internal and GSE surfaces were relatively similar at the family level, mainly belonging to *Oxalobacteraceae*, *Bacillaceae, Pseudomonadaceae,* and *Propionibacteriaceae*. However, *Bacillaceae* was dominant on the internal surface (13%) while *Oxalobacteraceae* and *Pseudomonadaceae* were dominant on the GSE surface (12 and 11%, respectively) for the PMA treated CRV2 samples. Additionally, reads belonging to a fungal family *Pleosporaceae* was present in abundance at only the GSE surface (3%) of CRV2.

At the genera level (**Supplementary Figure S8**), as observed previously for other taxon levels, the PMA treated samples of CRV1 showed large differences between the GSE and internal surfaces. Human commensal *Massilia* (25%), *Acidovorax* (15%), and *Caulobacter* (6%) were the most dominant genus detected at the GSE surface of CRV1. However, reads for the genus *Acidovorax*, and *Caulobacter* were only detected at low levels (<1%) from the internal location of CRV1 and *Massilia* constituted only 3% of the total reads. The internal location of CRV1 was instead dominated by the bacterial genera *Pseudomonas* (15%) and *Bacillus* (9%), and the fungal genus *Aureobasidium* (5%). On the other hand, both the GSE and internal surfaces of CRV2 presented a relatively similar pattern of genera, including *Massilia*, *Acidovorax*, *Pseudomonas*, *Bacillus*, and *Caulobacter*. Abundances of these genera were different between the GSE and internal surfaces, with *Pseudomonas* (11%) and *Massilia* (8%) being dominant on the GSE surface, while the internal surface showed an abundance of *Bacillus* (12%), *Massilia* (7%), and *Acidovorax* (2%).

At the species level (**Figure 2**), PMA treated samples for the internal and GSE surfaces of both CRV1 and CRV2 presented a clear distinction in terms of species abundance. *Caulobacter vibrioides* is the only microbial species detected in abundance (3%) on the GSE surface of CRV1. The internal location, however, showed a completely different trend with *Pseudomonas aeruginosa* being the most abundant member, comprising 5% of total microbial abundance, followed by *Bacillus firmus* (4%), *Massilia timonae* (2%), *Lentzea waywayandensis* (1%), and the fungus *Aureobasidium melanogenum* (1%). The CRV2 PMA treated samples for the internal location showed the presence of *Bacillus firmus* (5%), *Cutibacterium acnes* (1%), and *Lentzea waywayandensis* (1%). In the sample collected from the GSE surface of CRV2, *Pseudomonas stutzeri* (2%), *Bacillus firmus* (1%), *Cutibacterium acnes* (1%), and *Lentzea waywayandensis* (1%) were present at the outside location of CRV2 samples.

Statistical Significance

To determine the differences at various taxon levels between the PMA treated and untreated samples from the GSE and internal surfaces of both CRV1 and CRV2, several statistical analyses were performed. Based on the Mann–Whitney–Wilcoxon statistics (**Supplementary Table S2**), no significant differences ($p > 0.05$) were observed at the domain and phylum levels between the GSE and internal surfaces of PMA treated samples of CRV1. The class, family, order, genus, and species levels showed significant differences ($p < 0.05$) between the GSE and internal surfaces of PMA treated samples for CRV1. In the case of CRV2, no significant differences ($p > 0.05$) were observed at the domain, phylum, and class levels between the GSE and internal surfaces of PMA treated samples although, family, order, genus, and species levels were significantly different ($p < 0.05$). Similar results were also seen for the PMA untreated samples, except for the CRV2 samples where phylum and class also showed significant difference ($p = 0.0077$ and $p = 0.0004$, respectively) between the internal and GSE surfaces. On comparing the PMA treated samples at internal locations between the CRV1 and CRV2, the Mann–Whitney–Wilcoxon statistics failed to detect any differences at the domain, class, and species level ($p > 0.05$), with phylum, order, family, and genera level being significantly different ($p < 0.05$). On the other hand, the untreated samples were significantly different ($p < 0.05$) between CRV1 and CRV2 at the internal locations except for the domain and species level ($p = 0.1353$ and $p = 0.0918$, respectively). The PMA treated as well as untreated samples for the GSE surfaces were significantly different ($p < 0.05$) for all taxon levels at the CRV1 and CRV2, except for the domain and phylum level ($p = 0.0647$ and $p = 0.2069$, respectively).

Subsequently, to measure the diversity in the microbial communities residing on the internal and GSE surfaces of CRV1 and CRV2, various statistical indices were used (**Figures 3A–C**). The Shannon–Weaver index H values for the PMA treated samples were consistently lower than the PMA untreated samples on the internal and GSE surfaces of both CRV1 and CRV2. The H values can thus be interpreted as an increase in the species richness and evenness of the untreated samples as compared to the PMA treated samples. In the case of CRV1, the internal surface showed higher H values compared to the GSE surface (both PMA treated and untreated) thus indicating high species

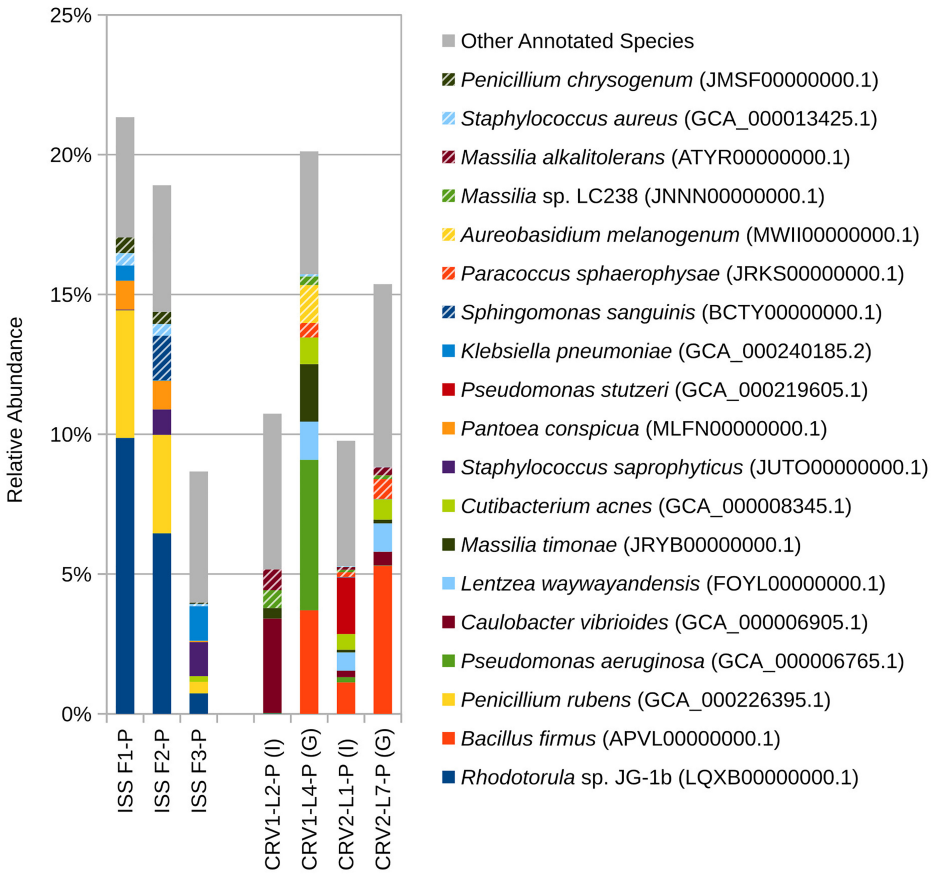

FIGURE 2 | Relative abundance of species based on shotgun metagenomic reads generated from PMA treated samples collected from three sampling events on the ISS and the internal (I) and ground support equipment (G) surfaces of CRV1 and CRV2.

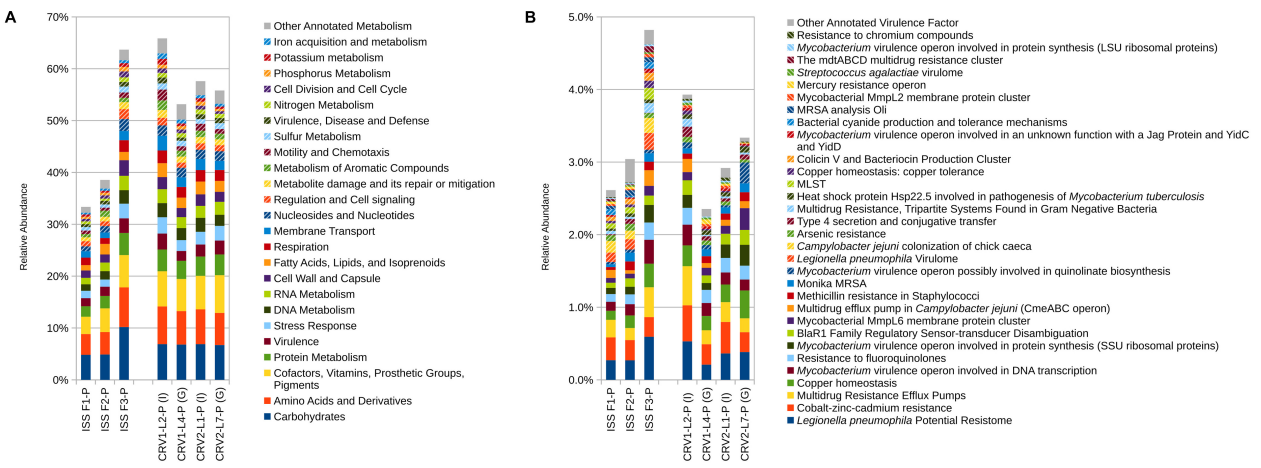

FIGURE 3 | Relative abundance of metagenomic reads associated with **(A)** microbial metabolism and **(B)** virulence. Metagenomic reads were generated from PMA treated samples collected from three sampling events on the ISS and the internal (I) and ground support equipment (G) surfaces of CRV1 and CRV2.

richness at the internal location. However, a completely opposite trend was observed for CRV2 where the GSE surface showed higher species richness and evenness as compared to the internal surface. A similar comparison made between the *H* values of the internal and GSE surfaces of CRV1 and CRV2 PMA treated samples showed that the CRV2 had higher species richness as

compared to CRV1. Diversity analysis carried out using the Simpson index further confirmed the Shannon–Weaver index findings. Another diversity index, the c index, showed that the species diversity increased for the PMA untreated samples as compared to that of the PMA treated samples on the internal and GSE surfaces of both CRV1 and CRV2. Similarly, in the case of CRV2, the untreated samples showed more species diversity compared to PMA treated on both internal and GSE surfaces. Additionally, the comparison of PMA treated samples at internal locations of CRV2 and CRV1 showed that the CRV2 had more species diversity as compared to the CRV1.

Functional Genes

Reads associated with metabolic functions like amino acid derivatives, carbohydrates, cofactors and vitamin metabolism, and protein metabolism were most abundant and relatively equally distributed for all the PMA treated samples on the internal and GSE surfaces of CRV1 and CRV2 as shown in the (**Figure 3A**). However, genes corresponding to other important functions like membrane transport, DNA and RNA metabolism, nucleotide metabolism, cell wall synthesis, and metabolism of aromatic compounds showed major differences between the internal and GSE surfaces of CRV1 and CRV2, and were statistically significant (**Supplementary Table S2**, $p < 0.05$). Furthermore, the MWW analysis (**Supplementary Table S2**) showed significant differences ($p < 0.05$) between the internal locations of CRV1 and CRV2 as well as the GSE surfaces of CRV1 and CRV2.

Virulence Genes

The metagenome reads for internal and GSE surfaces of both CRV1 and CRV2 were also subjected to virulence gene analyses using the virulence factors from the SEED database as reference. A major fraction of the virulence genes belonged to multiple drug resistance (MDR) efflux pump, *Legionella pneumophila* potential resistome, and Cobalt-Zinc-Cadmium resistance genes as shown in **Figure 3B**. Furthermore, these genes showed relatively equal distribution on both internal and GSE surfaces of CRV1 and CRV2. The relative abundance of the reads associated with virulence factors were vastly different on the internal location as compared to the GSE surfaces for both CRV1 and CRV2, and were statistically significant (**Supplementary Table S2**, $p < 0.05$). The MWW method (**Supplementary Table S2**) additionally showed statistically significant differences ($p < 0.05$) between the internal locations of CRV1 and CRV2 as well as the GSE surfaces of CRV1 and CRV2 ($p = 0.05$).

Antimicrobial Resistance

Metagenomic reads of PMA treated samples of internal and GSE surfaces of CRV1 and CRV2 were screened for antimicrobial resistance (AMR) genes. Based on the percent abundance, the AMR genes were sorted into different categories as shown in (**Figure 4**). Beta-lactam resistance, Cationic antimicrobial peptide (CAMP) resistance, and Vancomycin resistance together comprised a major fraction of the reads belonging to AMR genes and were also relatively equally distributed across internal and GSE surfaces of both CRV1 and CRV2. The remaining half of the AMR genes were mainly comprised of penicillin binding protein, multidrug efflux pump, and serine protease genes. Importantly, except for the MDR efflux pump there was no overlap between the virulence and AMR genes. Therefore, an independent analysis was performed for AMR and virulence genes.

Comparative Analyses of ISS and CRV Microbial Diversity

Two bacterial species and one fungal species that were isolated during this study of CRV surfaces (**Supplementary Table S1**) were also isolated from the ISS surfaces by Checinska Sielaff et al. (2019). Strains of the common skin commensal bacterium and opportunistic pathogen, *Staphylococcus epidermidis*, were isolated from CRV ($N = 3$) and ISS ($N = 6$) surfaces. Strains of *Micrococcus yunnanensis*, a bacterium previously detected within plant roots (Zhao et al., 2009), were isolated from CRV ($N = 5$) and ISS ($N = 1$) surfaces. Strains of *Rhodotorula mucilaginosa*, a common environmental saprophytic yeast and opportunistic pathogen, were also isolated from CRV ($N = 1$) and ISS ($N = 33$) surfaces. The other 45 bacterial species and 19 fungal species isolated from CRV surfaces were not isolated from ISS surfaces.

Eight bacterial species and one fungal species were detected in both ISS and CRV microbiome samples, including human commensal and environmental microbes. *Cutibacterium acnes*, a common skin commensal, could be detected at low levels in ISS samples (<2%) and CRV samples (<1%). *Klebsiella pneumoniae*, a common nosocomial pathogen, could be detected at varying levels in ISS samples (0–7%) but at very low levels in CRV samples (≤0.1%). Similarly, *Staphylococcus aureus*, a common commensal bacterium also known to be an opportunistic pathogen, was detected at varying levels in ISS samples (0–3%) but at very low levels in CRV samples (≤0.1%, **Figure 5**). *Streptococcus pneumoniae*, another common commensal bacterium that is also an opportunistic pathogen, was detected at low abundance in ISS and CRV microbiome samples (<1% and <0.2%, respectively). *Methylobacterium* sp. ME121, an environmental bacterium, could be detected at low levels in ISS samples (<1%) and very low levels in CRV samples (<0.1%). *Sphingobium yanoikuyae*, an environmental bacterium known to degrade polycyclic aromatic hydrocarbons, was detected at very low abundance in ISS samples (<0.1%) and low abundance in CRV samples (<0.2%). Environmental bacteria *Sphingomonas* sp. Ag1 and *Sphingomonas* sp. OV641 were also detected at very low abundance in ISS (<0.2%) and CRV (<0.3%) microbiome samples. *Rhodotorula* sp. JG-1b, a psychrophilic fungus, was detected at varying levels in the ISS microbiome samples (0–40%), but at very-low levels in CRV samples (<0.01%).

Although there was some overlap in species detected among ISS and CRV samples, the vast number of species detected did not overlap (309 and 111 species, respectively). Microbial species indices as calculated by Chao1 (**Figure 6A**), Shannon (**Figure 6B**), and Simpson (**Figure 6C**) also supported that microbial diversity was different between CRV and ISS environmental surface samples. When the overall abundance of species detected in each sample is visualized in an NMDS ordination (**Figure 6D**), this relationship becomes apparent.

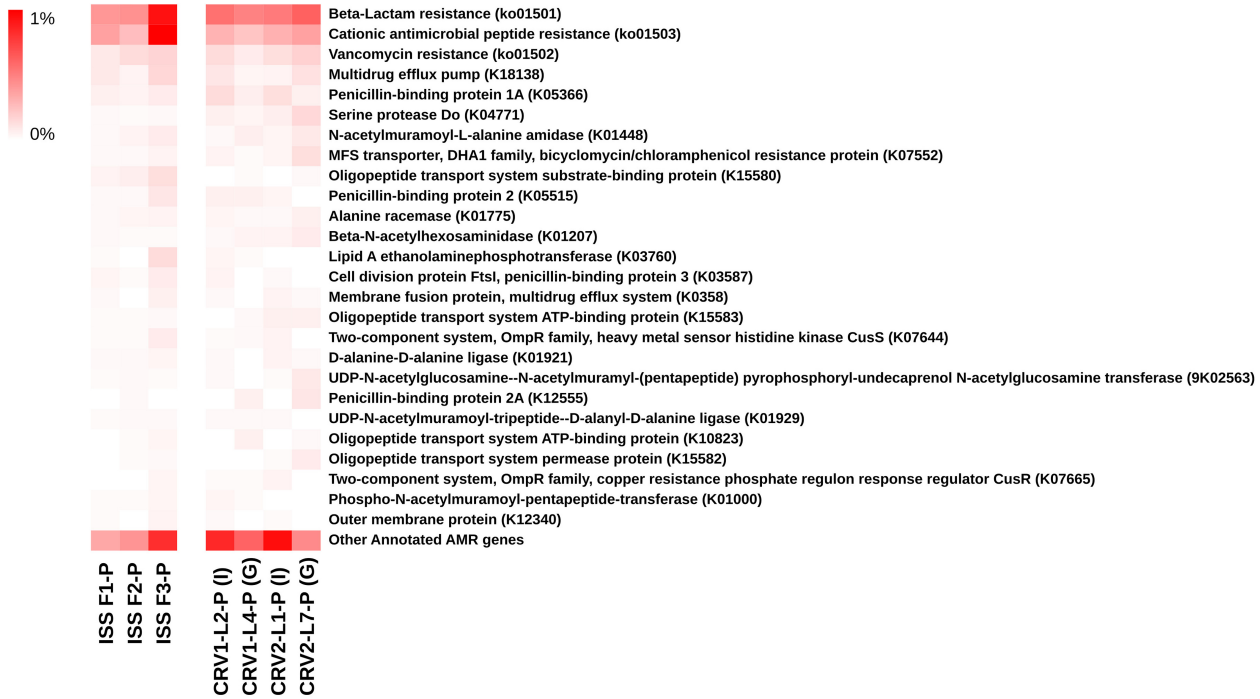

FIGURE 4 | Distribution of the antibiotic resistance genes detected in metagenomes generated from PMA treated samples collected from the internal (I) and ground support equipment (G) surfaces of CRV1 and CRV2 and three sampling events on the ISS.

The microbiomes sampled in the ISS (red, blue, and green glyphs) cluster separately in the ordination from the microbiomes sampled in CRV1 (purple glyphs) and CRV2 (orange glyphs). The MWW test showed a significant difference in species abundance between CRV and ISS samples ($W = 246120$, p-value $= 0.000162$). Significant differences between ISS and CRV microbiomes could also be detected in genes associated with virulence ($W = 4308.5$, p-value $= 1.443e\text{-}07$) and AMR ($W = 30626$, p-value $< 2.2e\text{-}16$). However, no significant difference could be detected in genes associated with metabolism between the ISS and CRV ($W = 1210$, p-value $= 0.4271$).

DISCUSSION

The current study aims at understanding the source of contamination of the ISS by characterizing the microbial diversity of the CRV just before launching. The ISS's robotic Canadarm appendage captures CRV carrying payloads for the ISS crew, after the CRV reaches the orbit of the ISS. As a result, in the current study, we compare the microbial diversity of the CRV with that of the previously reported ISS microbiome (Singh et al., 2018; Checinska Sielaff et al., 2019).

Most of the CRV cultivable isolates were already reported from samples collected from SAF cleanroom environments (Moissl-Eichinger et al., 2013), with the exception of *Compostimonas*. Most of these CRV isolates have been identified as species normally associated with soils, whereas cultivable microorganisms from the ISS were primarily associated with humans (*Staphylococcaceae* and *Enterobacteriaceae*) with the exception of *Bacillus* that was common in both CRV and ISS (Checinska Sielaff et al., 2019). When culturable fungi were compared, most of the CRV fungal members were also present in the ISS (Checinska Sielaff et al., 2019). However, strain specific similarities of these fungal isolates will need to be carried out via a sophisticated strain-tracking molecular method in the future. The CRV isolates that pose a potential health risk for astronauts that may be immunocompromised are *Staphylococcus pasteuri* (e.g., bacteraemia) (Savini et al., 2009), *Exophiala xenobiotica* (e.g., phaeohyphomycosis) (Aoyama et al., 2009), and *Phialemonium dimorphosporum* (e.g., fungemia) (Guarro et al., 1999). The cultivable strains also included members of the genera *Bacillus* and *Paenibacillus*, which are often encountered in SAF environments and can withstand harsh conditions (e.g., desiccation, low nutrients, and radiation) because of their spore formation ability (Vaishampayan et al., 2012). In addition, *Bacillus* and *Sphingomonas* are also known to form biofilms, which may increase various resistance capabilities of these microorganisms, and therefore also lead to an increased contamination risk (Checinska Sielaff et al., 2019).

The metagenome sequence analysis of the GSE and internal surfaces of CRV1 and CRV2 grouped separately when compared with the eight locations from the ISS environment sampled during three flights from a previously reported study by Singh et al. (2018) (**Figure 6**). Furthermore, the microbiome profiles of the internal CRV were different from GSE of the CRV. The PMA treated samples collected from the GSE surface of the CRV1 were dominated by reads belonging to

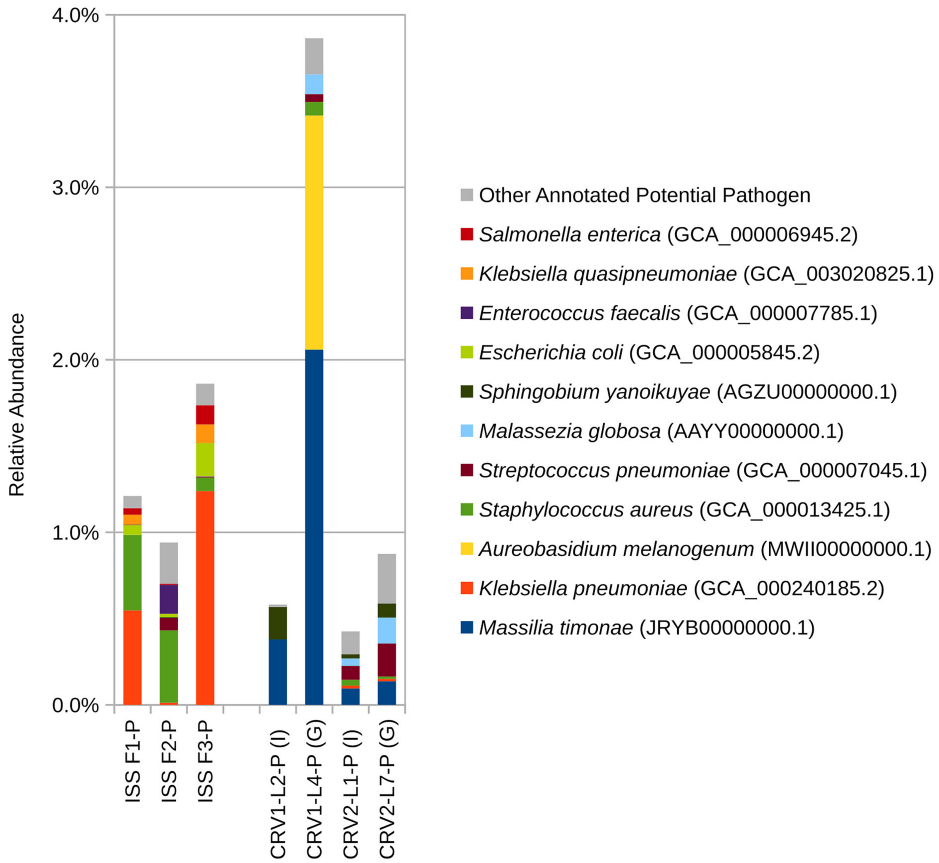

FIGURE 5 | Relative abundance of potential opportunistic pathogenic microorganisms detected in metagenomes generated from PMA treated samples collected from the internal (I) and ground support equipment (G) surfaces of CRV1 and CRV2 and three sampling events on the ISS.

genera *Acidovorax*, *Caulobacter*, and *Massilia* (reclassified as *Naxibacter*), while the CRV2 GSE surface showed *Pseudomonas* and *Bacillus*. These bacteria are known to survive extreme oligotrophic conditions for extended time periods (Wilhelm, 2018; Gray et al., 2019). Additionally, the members of the aforementioned genera are known to tolerate alkaline (Yumoto et al., 2001; Xu et al., 2005) and oxidative stress conditions (Lan et al., 2010), and survive high levels of ultraviolet radiation (Vaishampayan et al., 2012). Similarly, routine maintenance and cleaning procedures could presumably have removed most of the bacterial taxa associated with the SAF cleanrooms, however, spore-forming bacteria and members of Actinobacteria and *Massilia* persist in these environments (Vaishampayan et al., 2013; Mahnert et al., 2015).

The PMA treated samples collected from the internal locations of CRV1 and CRV2 were dominated by *Bacillaceae*, *Pseudomonadaceae*, *Propionibacteriaceae*, and *Oxalobacteraceae*, and were different from the ISS microbiome which was dominated by *Enterobacteriaceae*, *Methylobacteriaceae*, *Staphylococcaceae*, *Aspergillaceae*, and *Sporidiobolaceae*. Furthermore, the CRV microbiomes showed similarities with the SAF microbiome (Vaishampayan et al., 2013; Mahnert et al., 2015). The species level comparison between the ISS and CRV microbiomes (cut off value of minimum 10 reads) showed that only nine microorganisms were common between the two ecosystems. Except for *Methylobacterium*, all other microbes were common skin commensals (e.g., *Cutibacterium acnes*, *Enterobacter cloacae*, *Malassezia globosa*, *Propionibacterium humerusii*, *Staphylococcus aureus*, and *Streptococcus pneumoniae*). Additionally, the CRV also showed the presence of the members of genera belonging to different ecosystems (indoor to aquatic environments), like *Pseudomonas*, *Mycobacterium*, *Massilia*, *Leifsonia*, *Corynebacterium*, *Caulobacter*, *Bacillus*, *Acidovorax*, and *Aureobasidium*. It is also interesting to note that some of the microorganisms that were cultured were not detected in a shotgun metagenome sequencing approach. This might be due to the fact that ITS-based identification of fungi was not always ideal in determining the species accurately. Further research on the WGS of cultured microorganisms would reveal the authentic identification.

In general, most of the species observed in the CRV microbiome could not be observed in the ISS microbiome, potentially because the ISS has a consistent human presence. On the other hand, although the CRV assembly facility has constant human traffic, the cleanrooms are continuously undergoing

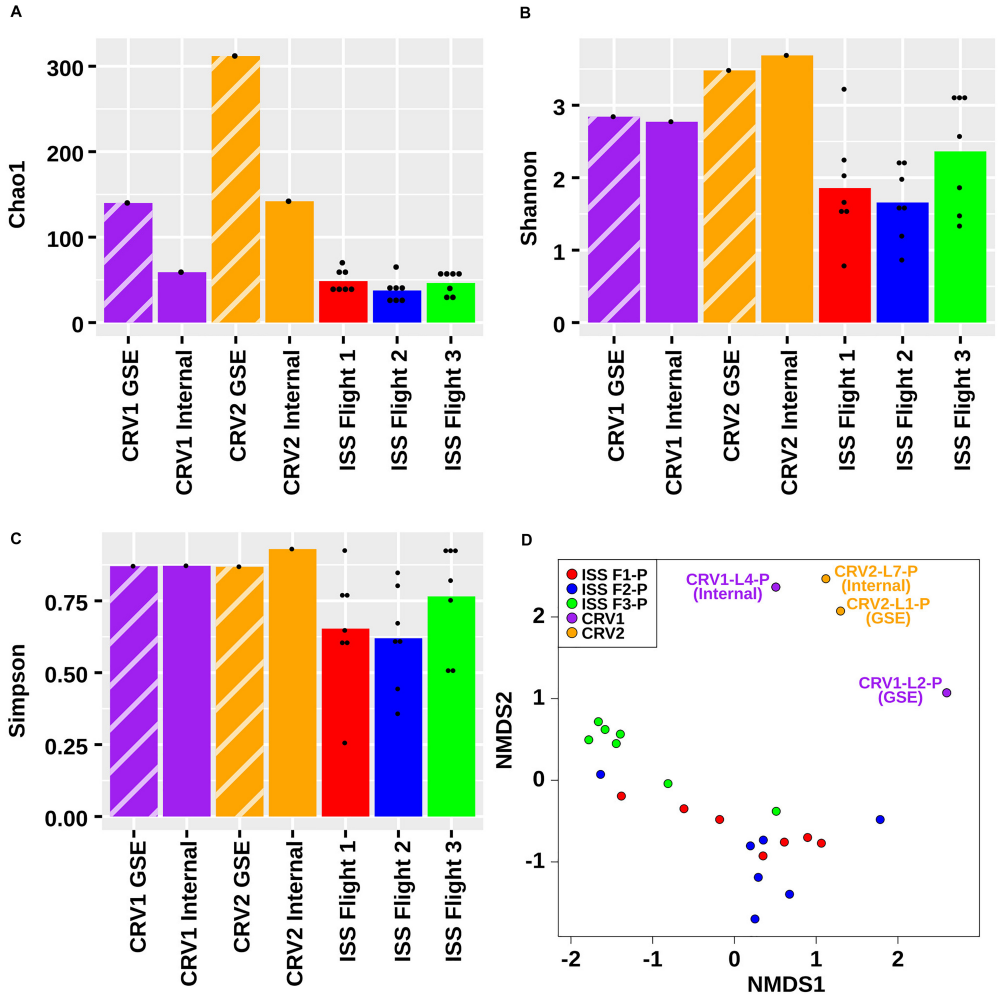

FIGURE 6 | Chao1 **(A)**, Shannon **(B)**, Simpson **(C)**, and NMDS **(D)** plots representing the differences in the microbial diversity detected from metagenomes generated from PMA treated samples collected from the internal (I) and ground support equipment (GSE) surfaces of CRV1, CRV2 and the locations from three sampling events of the ISS.

cleaning and maintenance procedures. It is also important to note that cleaning aboard the ISS occurs sporadically and mainly during the weekend. Whereas daily stringent cleaning regiment occurs inside the CRV assembly facility to maintain a low biomass. Additionally, chemical used to clean inside the CRV are based on wipes with 3% hydrogen peroxide, whereas aboard the ISS the crew use wipes with 0.1% dimethyl ammonium chloride derivatives. Difference seen between the CRV sampled could be also due to differences in the time of the year the samples were collected. Furthermore, it is important to note that cleaning within the CRV1 was done 24 h prior to sampling. Whereas for CRV2 and CRV3, it was done the day of the sampling event and for the latter just prior to our arrival. Another potential reason for the absence of CRV microbiome in the ISS microbiome would be the limitations of the sequencing procedures. Being dominated by the human microbiome, sequences of rare or extremely low abundance microorganisms may not be detected in the ISS microbiome. Therefore, even though a certain low number of microorganisms are carried via CRV to the ISS, most of them will be outcompeted by the existing ISS microbiome, potentially rendering them undetectable in both traditional microbiology assays and state-of-the-art metagenome sequencing. The limitations of this study are related to the extremely low biomass of the CRV samples collected. When examining metagenome positive samples, it is apparent that they harbor more cultivable bacteria and fungi which might require appropriate cultivation conditions.

In conclusion, this is the first report that demonstrates, using both traditional microbiological methods and molecular techniques, that there is a very little risk of transferring microorganisms to the ISS owing to CRV transport. Significant differences were shown between the ISS and the CRV microbiomes using statistical methods. The cleaning protocols for CRV surfaces appear to be highly effective, and continued observance of these protocols is recommended to limit forward contamination of the ISS.

DATA AVAILABILITY STATEMENT

The datasets generated for this study can be found in online repositories. The names of the repository/repositories and accession number(s) can be found below: https://www.ncbi.nlm.nih.gov/, PRJNA448453 and https://genelab.nasa.gov/, GLDS-286.

AUTHOR CONTRIBUTIONS

SM, JW, and KV wrote the manuscript. JW generated all figures in the manuscript. NS processed the shotgun metagenome sequencing data. JW performed all statistical analyses. KV and AS were involved in study design, helped interpret and write the manuscript, processed the samples, and performed culture and qPCR analysis. MM, SD, and CM-E prepared Sanger sequencing data and performed culturable diversity analyses. JW performed a comparative analysis of the ISS surface and CRV microbiomes. FK was instrumental in science payload, metadata generation, and coordinated with CRV institution in sample collection. KV was involved in early organization, study design and planning of the research project, and providing direct feedback to all authors throughout the project and during write-up of the manuscript. All authors read and approved the final manuscript.

FUNDING

The research described in this manuscript was funded by a 2012 Space Biology NNH12ZTT001N grant no. 19-12829-26 under Task Order NNN13D111T award to KV, which also funded post-doctoral fellowship for AS, SM, NS, and JW. FK was supported through the KBRwyle/FILMSS subcontract with the Department of Pharmaceutical Chemistry at the University of California, San Francisco, # NNA14AB82C, at NASA Ames Research Center.

ACKNOWLEDGMENTS

The research described in this manuscript was performed at the Jet Propulsion Laboratory, California Institute of Technology under a contract with NASA. We would like to thank the CRV institution for providing access to their vehicle for sampling purposes.

SUPPLEMENTARY MATERIAL

The Supplementary Material for this article can be found online at: https://www.frontiersin.org/articles/10.3389/fmicb.2020.566412/full#supplementary-material

Supplementary Figure 1 | Total and Intracellular ATP measured in field control (FC) and surface samples collected from CRV1 and CRV2.

Supplementary Figure 2 | Number of copies of **(A)** bacterial 16S and **(B)** fungal ITS detected via qPCR in CRV1 and CRV2 samples with and without PMA treatment. Field controls (FC), no template controls (NTC), extraction controls (Maxwell controls; MC), and positive controls (PC) are included for comparison.

Supplementary Figure 3 | Relative abundance of domain based on shotgun metagenomic reads generated from PMA treated samples collected from three sampling events on the ISS and the internal (I) and ground support equipment (G) surfaces of CRV1 and CRV2.

Supplementary Figure 4 | Relative abundance of phyla based on shotgun metagenomic reads generated from PMA treated samples collected from three sampling events on the ISS and the internal (I) and ground support equipment (G) surfaces of CRV1 and CRV2.

Supplementary Figure 5 | Relative abundance of classes based on shotgun metagenomic reads generated from PMA treated samples collected from three sampling events on the ISS and the internal (I) and ground support equipment (G) surfaces of CRV1 and CRV2.

Supplementary Figure 6 | Relative abundance of orders based on shotgun metagenomic reads generated from PMA treated samples collected from three sampling events on the ISS and the internal (I) and ground support equipment (G) surfaces of CRV1 and CRV2.

Supplementary Figure 7 | Relative abundance of families based on shotgun metagenomic reads generated from PMA treated samples collected from three sampling events on the ISS and the internal (I) ground support equipment (G) surfaces of CRV1 and CRV2.

Supplementary Figure 8 | Relative abundance of genera based on shotgun metagenomic reads generated from PMA treated samples collected from three sampling events on the ISS and the internal (I) and ground support equipment (G) surfaces of CRV1 and CRV2.

REFERENCES

Aoyama, Y., Nomura, M., Yamanaka, S., Ogawa, Y., and Kitajima, Y. (2009). Subcutaneous Phaeohyphomycosis caused by *Exophiala xenobiotica* in a non-Hodgkin lymphoma patient. *Med. Mycol.* 47, 95–99. doi: 10.1080/13693780802526857

Avila-Herrera, A., Thissen, J., Urbaniak, C., Be, N. A., Smith, D. J., Karouia, F., et al. (2020). Crewmember Microbiome may influence microbial composition of ISS habitable surfaces. *PLoS One* 15:e0231838. doi: 10.1371/journal.pone.0231838

Benardini, J. N., La Duc, M. T., Ballou, D., and Koukol, R. (2014). Implementing planetary protection on the atlas V fairing and ground systems used to launch the mars science laboratory. *Astrobiology* 14, 33–41. doi: 10.1089/ast.2013.1011

Bolger, A. M., Lohse, M., and Usadel, B. (2014). Trimmomatic: a flexible trimmer for illumina sequence data. *Bioinformatics* 30, 2114–2120. doi: 10.1093/bioinformatics/btu170

Chao, A. (1984). Nonparametric estimation of the number of classes in a population. *Scand. J. Statist.* 11, 265–270. doi: 10.2307/4615964

Checinska, A., Probst, A. J., Vaishampayan, P., White, J. R., Kumar, D., Stepanov, V. G., et al. (2015). Microbiomes of the dust particles collected from the international space station and spacecraft assembly facilities. *Microbiome* 3:50. doi: 10.1186/s40168-015-0116-3

Checinska Sielaff, A., Urbaniak, C., Mohan, G. B. M., Stepanov, V. G., Tran, Q., Wood, J. M., et al. (2019). Characterization of the total and viable bacterial and fungal communities associated with the international space station surfaces. *Microbiome* 7:50. doi: 10.1186/s40168-019-0666-x

COSPAR (2011). *COSPAR Planetary Protection Policy in World Space Council*. Houston, TX: COSPAR.

Fierer, N., Lauber, C. L., Zhou, N., McDonald, D., Costello, E. K., and Knight, R. (2010). Forensic identification using skin bacterial communities. *Proc. Natl. Acad. Sci. U.S.A.* 107, 6477–6481. doi: 10.1073/pnas.1000162107

Flores, G. E., Bates, S. T., Caporaso, J. G., Lauber, C. L., Leff, J. W., Knight, R., et al. (2013). Diversity, distribution and sources of bacteria in residential kitchens. *Environ. Microbiol.* 15, 588–596. doi: 10.1111/1462-2920.12036

Flores, G. E., Bates, S. T., Knights, D., Lauber, C. L., Stombaugh, J., Knight, R., et al. (2011). Microbial biogeography of public restroom surfaces. *PLoS One* 6:e28132. doi: 10.1371/journal.pone.0028132

Gioia, J., Yerrapragada, S., Qin, X., Jiang, H., Igboeli, O. C., Muzny, D., et al. (2007). Paradoxical DNA repair and peroxide resistance gene conservation in *Bacillus pumilus* SAFR-032. *PLoS One* 2:e928. doi: 10.1371/journal.pone.0000928

Gray, D. A., Dugar, G., Gamba, P., Strahl, H., Jonker, M. J., and Hamoen, L. W. (2019). Extreme slow growth as alternative strategy to survive deep starvation in bacteria. *Nat. Commun.* 10:890. doi: 10.1038/s41467-019-08719-8

Guarro, J., Nucci, M., Akiti, T., Gené, J., Cano, J., Barreiro, M. D. G. C., et al. (1999). *Phialemonium* fungemia: two documented nosocomial cases. *J. Clin. Microbiol.* 37, 2493–2497. doi: 10.1128/jcm.37.8.2493-2497.1999

Hendrickson, R., Lundgren, P., Malli Mohan, G. B., Urbaniak, C., Benardini, J. N., and Venkateswaran, K. (2017). "Comprehensive measurement of microbial burden in nutrient-deprived cleanrooms," in *Proceedings of the 47th International Conference on Environmental Systems. International Conference on Environmental Systems*, Charleston.

Hewitt, K. M., Gerba, C. P., Maxwell, S. L., and Kelley, S. T. (2012). Office space bacterial abundance and diversity in three metropolitan areas. *PLoS One* 7:e37849. doi: 10.1371/journal.pone.0037849

Huber, H., Hohn, M. J., Rachel, R., Fuchs, T., Wimmer, V. C., and Stetter, K. O. (2002). A new phylum of archaea represented by a nanosized hyperthermophilic symbiont. *Nature* 417, 63–67. doi: 10.1038/417063a

Huson, D. H., Auch, A. F., Qi, J., and Schuster, S. C. (2007). MEGAN analysis of metagenomic data. *Genome Res.* 17, 377–386. doi: 10.1101/gr.5969107

Huson, D. H., Beier, S., Flade, I., Górska, A., El-Hadidi, M., Mitra, S., et al. (2016). MEGAN community edition - interactive exploration and analysis of large-scale microbiome sequencing data. *PLoS Comput. Biol.* 12:e1004957. doi: 10.1371/journal.pcbi.1004957

Jaffal, A. A., Banat, I. M., El Mogheth, A. A., Nsanze, H., Bener, A., and Ameen, A. S. (1997). Residential indoor airborne microbial populations in the United Arab Emirates. *Environ. Intern.* 23, 529–533. doi: 10.1016/S0160-4120(97)00055-X

Jäger, T., Alexander, J., Kirchen, S., Dötsch, A., Wieland, A., Hiller, C., et al. (2018). Live-dead discrimination analysis, qPCR assessment for opportunistic pathogens, and population analysis at ozone wastewater treatment plants. *Environ. Pollut.* 232, 571–579. doi: 10.1016/j.envpol.2017.09.089

Kanehisa, M., and Goto, S. (2000). KEGG: kyoto encyclopedia of genes and genomes. *Nucleic Acids Res.* 28, 27–30. doi: 10.1093/nar/28.1.27

Kembel, S. W., Jones, E., Kline, J., Northcutt, D., Stenson, J., Womack, A. M., et al. (2012). Architectural design influences the diversity and structure of the built environment microbiome. *ISME J.* 6, 1469–1479. doi: 10.1038/ismej.2011.211

Kõljalg, U., Nilsson, R. H., Abarenkov, K., Tedersoo, L., Taylor, A. F. S., Bahram, M., et al. (2013). Towards a unified paradigm for sequence-based identification of fungi. *Mol. Ecol.* 22, 5271–5277. doi: 10.1111/mec.12481

Korves, T. M., Piceno, Y. M., Tom, L. M., DeSantis, T. Z., Jones, B. W., Andersen, G. L., et al. (2013). Bacterial communities in commercial aircraft high-efficiency particulate air (HEPA) filters assessed by PhyloChip analysis. *Indoor Air* 23, 50–61. doi: 10.1111/j.1600-0668.2012.00787.x

Kwan, K., Cooper, M., La Duc, M. T., Vaishampayan, P., Stam, C., Benardini, J. N., et al. (2011). Evaluation of procedures for the collection, processing, and analysis of biomolecules from low-biomass surfaces. *Appl. Environ. Microbiol.* 77, 2943–2953. doi: 10.1128/aem.02978-10

La Duc, M. T., Kern, R., and Venkateswaran, K. (2004). Microbial monitoring of spacecraft and associated environments. *Microb. Ecol.* 47, 150–158. doi: 10.1007/s00248-003-1012-0

Lan, L., Murray, T. S., Kazmierczak, B. I., and He, C. (2010). *Pseudomonas aeruginosa* OspR is an oxidative stress sensing regulator that affects pigment production, antibiotic resistance and dissemination during infection. *Mol. Microbiol.* 75, 76–91. doi: 10.1111/j.1365-2958.2009.06955.x

Lane, D. J. (1991). "16S/23S rRNA sequencing," in *Nucleic Acid Techniques in Bacterial Systematics*, eds E. Stackebrandt and M. Goodfellow (New York, NY: John Wiley and Sons).

Lax, S., Sangwan, N., Smith, D., Larsen, P., Handley, K. M., Richardson, M., et al. (2017). Bacterial colonization and succession in a newly opened hospital. *Sci. Transl. Med.* 9:eaah6500. doi: 10.1126/scitranslmed.aah6500

Lax, S., Smith, D. P., Hampton-Marcell, J., Owens, S. M., Handley, K. M., Scott, N. M., et al. (2014). Longitudinal analysis of microbial interaction between humans and the indoor environment. *Science* 345, 1048–1052. doi: 10.1126/science.1254529

Lin, W.-T., Luo, J.-F., and Guo, Y. (2011). Comparison and characterization of microbial communities in sulfide-rich wastewater with and without propidium monoazide treatment. *Curr. Microbiol.* 62, 374–381. doi: 10.1007/s00284-010-9716-0

Mahnert, A., Vaishampayan, P., Probst, A. J., Auerbach, A., Moissl-Eichinger, C., Venkateswaran, K., et al. (2015). Cleanroom maintenance significantly reduces abundance but not diversity of indoor microbiomes. *PLoS One* 10:e0134848. doi: 10.1371/journal.pone.0134848

Manter, D. K., and Vivanco, J. M. (2007). Use of the ITS primers, ITS1F and ITS4, to characterize fungal abundance and diversity in mixed-template samples by qPCR and length heterogeneity analysis. *J. Microbiol. Methods* 71, 7–14. doi: 10.1016/j.mimet.2007.06.016

McManus, C. J., and Kelley, S. T. (2005). Molecular survey of aeroplane bacterial contamination. *J. Appl. Microbiol.* 99, 502–508. doi: 10.1111/j.1365-2672.2005.02651.x

Moissl-Eichinger, C., Auerbach, A. K., Probst, A. J., Mahnert, A., Tom, L., Piceno, Y., et al. (2015). Quo Vadis? microbial profiling revealed strong effects of cleanroom maintenance and routes of contamination in indoor environments. *Sci. Rep.* 5:9156. doi: 10.1038/srep09156

Moissl-Eichinger, C., Pukall, R., Probst, A. J., Stieglmeier, M., Schwendner, P., Mora, M., et al. (2013). Lessons learned from the microbial analysis of the herschel spacecraft during assembly, integration, and test operations. *Astrobiology* 13, 1125–1139. doi: 10.1089/ast.2013.1024

Nayfach, S., and Pollard, K. S. (2016). Toward accurate and quantitative comparative metagenomics. *Cell* 166, 1103–1116. doi: 10.1016/j.cell.2016.08.007

Nocker, A., Cheung, C.-Y., and Camper, A. K. (2006). Comparison of propidium monoazide with ethidium monoazide for differentiation of live vs. dead bacteria by selective removal of dna from dead cells. *J. Microbiol. Methods* 67, 310–320. doi: 10.1016/j.mimet.2006.04.015

Nocker, A., Sossa-Fernandez, P., Burr, M. D., and Camper, A. K. (2007). Use of propidium monoazide for live/dead distinction in microbial ecology. *Appl. Environ. Microbiol.* 73, 5111–5117. doi: 10.1128/aem.02987-06

Onofri, S., de la Torre, R., de Vera, J.-P., Ott, S., Zucconi, L., Selbmann, L., et al. (2012). Survival of rock-colonizing organisms after 1.5 years in outer space. *Astrobiology* 12, 508–516. doi: 10.1089/ast.2011.0736

Overbeek, R., Begley, T., Butler, R. M., Choudhuri, J. V., Chuang, H.-Y., Cohoon, M., et al. (2005). The subsystems approach to genome annotation and its use in the project to annotate 1000 genomes. *Nucleic Acids Res.* 33, 5691–5702. doi: 10.1093/nar/gki866

Powell, S., Szklarczyk, D., Trachana, K., Roth, A., Kuhn, M., Muller, J., et al. (2011). eggNOG v3.0: orthologous groups covering 1133 organisms at 41 different taxonomic ranges. *Nucleic Acids Res.* 40, D284–D289. doi: 10.1093/nar/gkr1060

Ratnasingham, S., and Hebert, P. D. N. (2013). A DNA-based registry for all animal species: the barcode index number (BIN) system. *PLoS One* 8:e66213. doi: 10.1371/journal.pone.0066213

Reasoner, D. J., and Geldreich, E. E. (1985). A new medium for the enumeration and subculture of bacteria from potable water. *Appl. Environ. Microbiol.* 49, 1–7. doi: 10.1128/aem.49.1.1-7.1985

Savini, V., Catavitello, C., Bianco, A., Balbinot, A., and D'Antonio, D. (2009). Epidemiology, pathogenicity and emerging resistances in *Staphylococcus pasteuri*: from mammals and lampreys, to man. *Recent Pat. Anti Infect. Drug Discov.* 4, 123–129.

Sayers, E. W., Barrett, T., Benson, D. A., Bryant, S. H., Canese, K., Chetvernin, V., et al. (2008). Database resources of the national center for biotechnology information. *Nucleic Acids Res.* 37(Suppl._1), D5–D15. doi: 10.1093/nar/gkn741

Shannon, C. E., and Weaver, W. (1949). *The Mathematical Theory of Communication*. Urbana, IL: The University of Illinois Press.

Simpson, E. H. (1949). Measurement of diversity. *Nature* 163:688. doi: 10.1038/163688a0

Singh, N. K., Wood, J. M., Karouia, F., and Venkateswaran, K. (2018). Succession and persistence of microbial communities and antimicrobial resistance genes

associated with international space station environmental surfaces. *Microbiome* 6:214. doi: 10.1186/s40168-018-0609-y

Suzuki, M. T., Taylor, L. T., and DeLong, E. F. (2000). Quantitative analysis of small-subunit rRNA genes in mixed microbial populations via 5'-nuclease assays. *Appl. Environ. Microbiol.* 66, 4605–4614. doi: 10.1128/aem.66.11.4605-4614.2000

Vaishampayan, P. A., Probst, A. J., La Duc, M. T., Bargoma, E., Benardini, J. N., Andersen, G. L., et al. (2013). New perspectives on viable microbial communities in low-biomass cleanroom environments. *ISME J.* 7, 312–324. doi: 10.1038/ismej.2012.114

Vaishampayan, P. A., Rabbow, E., Horneck, G., and Venkateswaran, K. J. (2012). Survival of *Bacillus pumilus* spores for a prolonged period of time in real space conditions. *Astrobiology* 12, 487–497. doi: 10.1089/ast.2011.0738

Venkateswaran, K., Hattori, N., La Duc, M. T., and Kern, R. (2003). ATP as a biomarker of viable microorganisms in clean-room facilities. *J. Microbiol. Methods* 52, 367–377. doi: 10.1016/S0167-7012(02)00192-6

Venkateswaran, K., La Duc, M. T., and Vaishampayan, P. (2012). *Genetic Inventory Task Final Report in Jet Propulsion Laboratory*. Pasadena, CA: California Institute of Technology.

Wilhelm, R. C. (2018). Following the terrestrial tracks of *Caulobacter* - redefining the ecology of a reputed aquatic oligotroph. *ISME J.* 12, 3025–3037. doi: 10.1038/s41396-018-0257-z

Xu, P., Li, W.-J., Tang, S.-K., Zhang, Y.-Q., Chen, G.-Z., Chen, H.-H., et al. (2005). Naxibacter *Alkalitolerans* gen. nov., sp. nov., a novel member of the family 'Oxalobacteraceae' isolated from china. *Intern. J. Syst. Evol. Microbiol.* 55, 1149–1153. doi: 10.1099/ijs.0.63407-0

Yoon, S.-H., Ha, S.-M., Kwon, S., Lim, J., Kim, Y., Seo, H., et al. (2017). Introducing EzBioCloud: a taxonomically united database of 16S rRNA Gene sequences and whole-genome assemblies. *Intern. J. Syst. Evol. Microbiol.* 67, 1613–1617. doi: 10.1099/ijsem.0.001755

Yumoto, I., Yamazaki, K., Hishinuma, M., Nodasaka, Y., Suemori, A., Nakajima, K., et al. (2001). *Pseudomonas alcaliphila* sp. nov., a novel facultatively psychrophilic alkaliphile isolated from seawater. *Intern. J. Syst. Evol. Microbiol.* 51, 349–355. doi: 10.1099/00207713-51-2-349

Zhao, G.-Z., Li, J., Qin, S., Zhang, Y.-Q., Zhu, W.-Y., Jiang, C.-L., et al. (2009). *Micrococcus Yunnanensis* sp. nov., a novel actinobacterium isolated from surface-sterilized *Polyspora axillaris* roots. *Intern. J. Syst. Evol. Microbiol.* 59, 2383–2387. doi: 10.1099/ijs.0.010256-0

Conflict of Interest: The authors declare that the research was conducted in the absence of any commercial or financial relationships that could be construed as a potential conflict of interest.

The reviewer AR declared a shared affiliation with several of the authors SM, JW, AS, NS, and KV.

frontiers in Microbiology

ORIGINAL RESEARCH
published: 24 November 2020
doi: 10.3389/fmicb.2020.587556

Identification of a Stable Hydrogen-Driven Microbiome in a Highly Radioactive Storage Facility on the Sellafield Site

Sharon Ruiz-Lopez[1]†, Lynn Foster[1], Chris Boothman[1], Nick Cole[2], Katherine Morris[1] and Jonathan R. Lloyd[1]**

[1] Department of Earth and Environmental Sciences, University of Manchester (UoM), Manchester, United Kingdom, [2] Sellafield Ltd., Warrington, United Kingdom

OPEN ACCESS

Edited by:
Rakesh Mogul,
California State Polytechnic University,
United States

Reviewed by:
Cynthia B. Silveira,
San Diego State University,
United States
Steven Singer,
Lawrence Berkeley National
Laboratory, United States

***Correspondence:**
Sharon Ruiz-Lopez
sharulo_268@hotmail.com
Jonathan R. Lloyd
Jon.Lloyd@manchester.ac.uk

†Present address:
Sharon Ruiz-Lopez,
Department of Environmental
Microbiology, Manchester
Metropolitan University, Manchester,
United Kingdom

Specialty section:
This article was submitted to
Extreme Microbiology,
a section of the journal
Frontiers in Microbiology

Received: 26 July 2020
Accepted: 26 October 2020
Published: 24 November 2020

Citation:
Ruiz-Lopez S, Foster L,
Boothman C, Cole N, Morris K and
Lloyd JR (2020) Identification of a
Stable Hydrogen-Driven Microbiome
in a Highly Radioactive Storage
Facility on the Sellafield Site.
Front. Microbiol. 11:587556.
doi: 10.3389/fmicb.2020.587556

The use of nuclear power has been a significant part of the United Kingdom's energy portfolio with the Sellafield site being used for power production and more recently reprocessing and decommissioning of spent nuclear fuel activities. Before being reprocessed, spent nuclear fuel is stored in water ponds with significant levels of background radioactivity and in high alkalinity (to minimize fuel corrosion). Despite these challenging conditions, the presence of microbial communities has been detected. To gain further insight into the microbial communities present in extreme environments, an indoor, hyper-alkaline, oligotrophic, and radioactive spent fuel storage pond (INP) located on the Sellafield site was analyzed. Water samples were collected from sample points within the INP complex, and also the purge water feeding tank (FT) that supplies water to the pond, and were screened for the presence of the 16S and 18S rRNA genes to inform sequencing requirements over a period of 30 months. Only 16S rRNA genes were successfully amplified for sequencing, suggesting that the microbial communities in the INP were dominated by prokaryotes. Quantitative Polymerase Chain Reaction (qPCR) analysis targeting 16S rRNA genes suggested that bacterial cells in the order of 10^4–10^6 mL^{-1} were present in the samples, with loadings rising with time. Next generation Illumina MiSeq sequencing was performed to identify the dominant microorganisms at eight sampling times. The 16S rRNA gene sequence analysis suggested that 70% and 91% from of the OTUs samples, from the FT and INP respectively, belonged to the phylum Proteobacteria, mainly from the alpha and beta subclasses. The remaining OTUs were assigned primarily to the phyla Acidobacteria, Bacteroidetes, and, Cyanobacteria. Overall the most abundant genera identified were *Hydrogenophaga*, *Curvibacter*, *Porphyrobacter*, *Rhodoferax*, *Polaromonas*, *Sediminibacterium*, *Roseococcus*, and *Sphingomonas.* The presence of organisms most closely related to *Hydrogenophaga* species in the INP areas, suggests the metabolism of hydrogen as an energy source, most likely linked to hydrolysis of water caused by the stored fuel. Isolation of axenic cultures using a range of minimal

and rich media was also attempted, but only relatively minor components (from the phylum Bacteroidetes) of the pond water communities were obtained, emphasizing the importance of DNA-based, not culture-dependent techniques, for assessing the microbiome of nuclear facilities.

Keywords: spent nuclear fuel, microbial ecology, Sellafield, *Hydrogenophaga*, spent nuclear fuel ponds, hydrogen metabolism

INTRODUCTION

Nuclear power supplies about 11% of the world's electricity (WNA, 2016), and with increasing global energy demands this seems unlikely to decline. Although considered a "low carbon" generating energy source, radioactive waste is produced, including spent fuels that need storage prior to reprocessing and final disposal (Deutch et al., 2009). In the United Kingdom, this task is performed at Sellafield, one of the largest and most complex nuclear sites in Europe. With over 1,400 discrete operations, handling 240 nuclear materials, it is located in Cumbria on the North West coast of England and has been operated by the Nuclear Decommissioning Authority (NDA) since 2005 (Baldwin, 2003; WNA, 2018a). Calder Hall, located on the site, was the world's first commercial nuclear power station, and here, energy was generated from 1956 to 2003. The Sellafield site also contains a range of storage ponds built during the 1950s which were intended to support the production of weapon-grade plutonium, and more recently fuels from the United Kingdom's fleet of nuclear power stations (Reddy et al., 2012; WNA, 2018b). The legacy of activities have left a complex range of nuclear operations at Sellafield, including the decommissioning of redundant facilities associated with the site's early defense work, and spent fuel management including Magnox and Oxide fuel reprocessing (Gov UK, 2018).

Prior to reprocessing, all irradiated fuel delivered to Sellafield is stored for a period of at least 100 days in water-filled reinforced concrete ponds that allow the decay of short-lived radioisotopes. During storage, the degree of corrosion experienced by the fuel is monitored to determine storage life and optimize water chemistry (Shaw, 1990). The temperature within the ponds is controlled by refrigerant chillers to further limit fuel corrosion, while the levels of both radioactive and non-radioactive ions in the pond waters are controlled by purging cycles of demineralised water adjusted to pH 11.1–11.6 with the addition of sodium hydroxide (Howden, 1987). The main pre-reprocessing storage pond at the Sellafield site is the indoor alkaline storage pond (INP), a concrete wall pond filled with demineralised water, responsible for receiving, storing and mechanically processing spent nuclear fuel (SNF). The SNF, defined as nuclear reactor fuel that has been used to the extent that it can no longer effectively sustain a chain reaction, is received and handled in Sellafield from Magnox and Advanced Gas-cooled Reactor (AGR) stations from across the United Kingdom (Sellafield Ltd, 2015).

Although Sellafield's nuclear facilities, including the INP, are considered to be oligotrophic with high background levels of radiation, microorganisms have been shown to colonize these inhospitable environments (MeGraw et al., 2018). The presence of diverse microbial communities may impact on site operations and fuel stability. Microorganisms can also play a significant role in the transformations of radionuclides in the environment by altering their chemical speciation, solubility and sorption properties, ultimately impacting their environmental mobility and bioavailability (Lloyd and Renshaw, 2005; Francis, 2012; Newsome et al., 2014a; MeGraw et al., 2018). For example, the interactions between microbial populations and soluble radionuclides in groundwater can lead to precipitation reactions [e.g., via U (VI) or Tc (VII) bioreduction] and subsequent bioremediation (Newsome et al., 2014b). Of particular note within these pond environments is the fate of ^{90}Sr and ^{137}Cs, which dominate the radionuclide inventory in the water columns in storage ponds at Sellafield (Lang et al., 2019). Previous studies showed that seasonal blooms dominated by the alga *Haematococcus*, have adapted to survive in a circumneutral pH outdoor spent fuel storage pond at Sellafield, and are able to accumulate high levels of these radionuclides (MeGraw et al., 2018).

The accumulation of radionuclides by microbial cells can be driven by a range of processes including biosorption, biomineralization and bioprecipitation (Gadd, 2009), although these are poorly defined in nuclear storage ponds. Biosorption is species-specific and is affected by the chemistry and the pH of the solution, the physiological state of the cells, the cell wall architecture, and the presence of extracellular polymeric substances (EPS) (Comte et al., 2008; Merroun and Selenska-Pobell, 2008). The EPS is especially important, being mainly composed of polysaccharides, proteins, humic substances, uronic acids, nucleic acids, and lipids (Wingender et al., 1999), and containing ionisable functional groups that represent potential binding sites for the sequestration of metal ions (Brown and Lester, 1982; Lawson et al., 1984). Biosorption of divalent cations such as Sr^{2+} is well known (White and Gadd, 1990; Gadd, 2009; Liu et al., 2014), and would be favored in high pH pond systems (Ghorbanzadeh and Mohammad, 2009). Monovalent cations such as Cs^{+} would sorb less strongly than divalent cations (Andrès et al., 2001), although can bioaccumulate in biomass being transported into microbial cells, such as *Rhodococcus*, via potassium transport systems (Tomioka et al., 1992; Avery, 1995a,b). Recent work on a legacy high pH outdoor storage system at Sellafield, identified a *Pseudanabaena* species as the dominant photosynthetic microorganism (Foster et al., 2020a), and lab-based experiments on a culture dominated by a close relative showed increased polysaccharide production following irradiation treatments (Foster et al., 2020b). The polysaccharide production can promote the EPS formation which

eventually can impact on ^{90}Sr sorption-desorption behavior at alkaline environmental conditions under pond water conditions (Ashworth et al., 2018; MeGraw et al., 2018; Foster et al., 2020b).

Biomineralization reactions can also be linked to radionuclide fate (reviewed by Lloyd and Macaskie, 2000), due to local redox changes (e.g., bioreduction of actinides or key fission products) (Lloyd, 2003), localized alkalinisation at the cell surface (Van Roy et al., 1997) or the accumulation of microbially generated ligands (e.g., phosphate, sulfide, oxalate or carbonate) (White and Gadd, 1990; Macaskie et al., 1992; White et al., 1998; Boswell et al., 2001; Lloyd and Macaskie, 2002). For the latter, induced or mediated carbonate mineralization (MICP) (Braissant et al., 2002), can affect the mobility and sequestration of radionuclides in the near-surface environment (Ferris et al., 1994; Reeder et al., 2001), and has been studied widely due to its importance in the remediation on contaminated Sr systems (Mortensen et al., 2011). Additionally, a variety of microorganisms are able to drive MICP via urea hydrolysis (Fujita et al., 2004; Achal et al., 2012; Bhaduri et al., 2016) or via photosynthetic processes (Ferris et al., 1994; Dittrich et al., 2003; Lee et al., 2014; Zhu and Dittrich, 2016).

Finally microorganisms can affect the physical chemistry of the water-fuel interactions, leading to microbial-influenced corrosion (MIC) and hence fuel material degradation and radionuclide release (Shaw, 1990; Springell et al., 2014; Rajala et al., 2017). In open storage systems, the proliferation of microorganisms (together with the accumulation of radioactive sludge as a result of corrosion in spent fuel ponds) can also adversely impact on pond visibility, increasing the costs of fuel storage, hampering decommissioning operations and also increasing the exposure time to personnel (Wolfram et al., 1996; Jackson et al., 2014).

Recent publications have shown the presence of wide diversity of microorganisms living in SNF ponds, mainly bacteria, photosynthetic cyanobacteria and eukaryotic algae (Chicote et al., 2004, 2005; Sarró et al., 2005; Sellafield Ltd, 2011; Tišáková et al., 2013; Karley et al., 2018; MeGraw et al., 2018; Pipíška et al., 2018; Silva et al., 2018). The observed adaptation mechanisms include biofilm formation (Santo Domingo et al., 1998; Sarró et al., 2005; Bruhn et al., 2009), interactions with radionuclides via biosorption (Tomioka et al., 1992; Adam and Garnier-Laplace, 2003; Ghorbanzadeh and Mohammad, 2009; Dekker et al., 2014) and bioprecipitation (Ferris et al., 1994; Achal et al., 2012; Bhaduri et al., 2016; Zhu and Dittrich, 2016; Bagwell et al., 2018). To date, most published work on the Sellafield site has been on legacy outdoor pond systems (MeGraw et al., 2018; Foster et al., 2020a,b) which are open to external energy sources (including daylight, supporting photosynthetic primary colonizers). Indoor pond systems on the Sellafield site, with lower light intensities, and reduced inputs from atmospheric deposition, have not been studied in such detail.

The aim of this study was to characterize microbial communities of an indoor alkaline spent fuel storage pond (INP) on the Sellafield site, to help understand the microbial ecology of this facility, and the potential forms of metabolism that could underpin colonization. An additional goal was to provide baseline microbial community data, so that the impact of receiving new fuels and stored waste material during upcoming and extensive site-wide decommissioning activities across the Sellafield site can be assessed. The findings of this 30-month survey are discussed in relation to microbial survival to extreme environments (including potential energy sources) and how the extant microbiomes may potentially impact pond management. Microbial communities in the feeding tank supplying the pond system were identified and compared to those in the main and subponds containing spent fuel, to determine which organisms were uniquely adapted to the extreme pond chemistry (e.g., high pH) and high background radiation levels. Throughout the sampling campaign, the presence of hydrogen-oxidizing bacteria (affiliated with the genus *Hydrogenophaga*) in the INP, was consistent with the existence of hydrogen-oxidizing ecosystem, potentially linked to radiolysis in the fuel storage pond.

MATERIALS AND METHODS

Indoor Nuclear Fuel Storage Pond

The INP is an indoor pond complex divided into three main ponds and three subponds linked by a transfer channel that enables water flow (**Figure 1**). In order to control the pond-water activity and quality, there is a continuous "once through" purge flow; pond-water from the main ponds flows into the transfer channel and enters the recirculation pump chamber where it is continuously pumped round a closed circulation loop and through a heat exchanger system, which cools the pond-water before it is recycled into the main ponds. Through the control feed, purge and re-circulation flow rates, the water depth is maintained at 7 ± 0.05 m. The purge flow can be either from a donor plant or from other hydraulically linked ponds within the Sellafield complex. The temperature and pH are controlled at 15°C and 11.6, respectively. Analyzed samples were taken from three designated main areas: main ponds (MP2 and MP3), subponds (SP1 and SP2), and from the Feeding tank (FT) of the donor plant, where the demineralised water used to feed the INP is stored.

Samples

Thirty samples were taken from three designated areas resulting on five sampling points (**Table 1**) for a period of 30 months (October 2016–April 2019).

Water samples from the FT were considered non-active and were shipped directly to the University of Manchester in October 2016 and stored in the dark at 10°C. Water samples from the MP 2 and 3 and SP 1 and 2 were radioactive, hence appropriate handling procedures were required. The protocols for these samples were developed and applied under Command and Control regimes by Sellafield Ltd. and NNL, with samples transferred directly from the pond to the NNL Central Laboratory (National Nuclear Laboratory, Cumbria, United Kingdom), where DNA was extracted and the samples were checked for radioactivity in line with the Environmental Permits and Nuclear Site licenses held by Sellafield Ltd. Extracted DNA samples free from significant radionuclide contamination

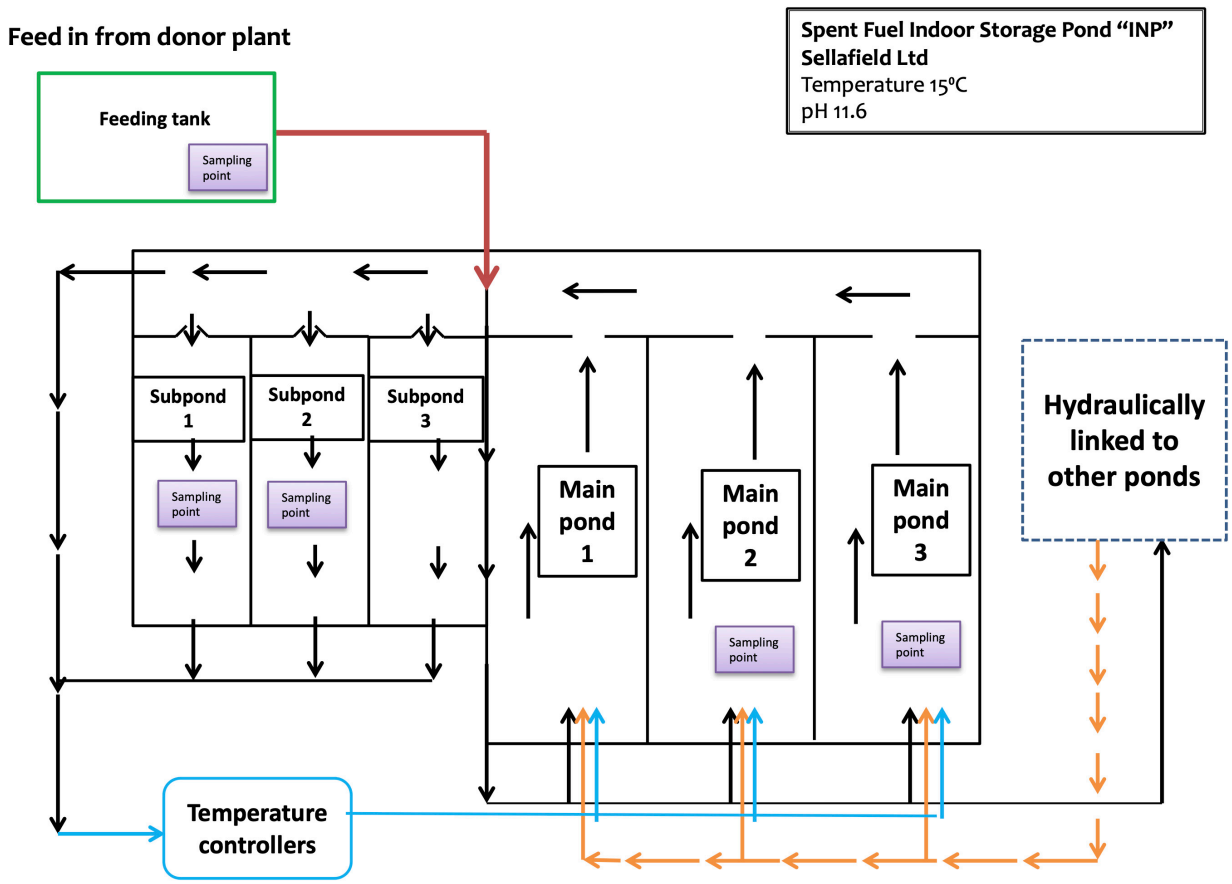

FIGURE 1 | Diagram of the spent fuel indoor storage pond "INP." It consists of 3 main ponds and 3 subponds linked by a transfer channel which enables water flow. The sampling points are located at the main ponds 2 and 3; subponds 1 and 2; and the head feeding tank (at the top of the pond).

were shipped to the University of Manchester and stored in the freezer (−20°C) until use.

In addition to microbial profiling via DNA analyses, a complementary "cultivation-dependent" approach was also adopted to help further characterize the pond microbial community composition. Two low-volume samples (approximately 5 mL) from subponds 1 and 2 (**Figure 1**) were analyzed by traditional culturing techniques. The subponds are more radioactive than the main ponds, but the temperature and pH values are maintained at the same values as the main ponds, 21°C and 11.6, respectively. The typical pond water activities are 1,000 Bq/ml β (**Table 2**).

Cultivation-Independent DNA Analyses of Microbial Communities

DNA Extraction and PCR Amplifications

The MoBio PowerWater DNA isolation kit (MoBio Laboratories, Inc., Carlsbad, CA, United States), was used to extract DNA from water samples of approximately 1 L. The DNA was eluted to a final volume of 100 μL, and stored at 4°C until they were transported to UoM, where it was kept at −20°C to await further analyses.

Polymerase Chain Reaction (PCR) amplification was performed from the extracted DNA using a Techne Thermocycler (Cole-Parmer, Staffordshire, United Kingdom). Primers used for detection of bacterial 16S rRNA gene amplification were the broad-specificity 8F forward primer and the reverse primer 1492R (Eden et al., 1991). The primers used to detect eukaryotic organisms, targeting the 18S rRNA gene, were Euk F forward primer and the reverse primer Euk R (DeLong, 1992) whilst the archaeal primers that targeted the 16S rRNA gene, were forward primer 21F and reverse primer 958R (DeLong, 1992). The PCR reaction mixtures contained; 5 μL 10× PCR buffer, 4 μL 10 mM dNTP solution (2.5 mM each nucleotide), 1 μL of 25 μM forward primer, 1 μL of 25 μM reverse primer, and 0.3 μL Ex Takara Taq DNA Polymerase. The final volume was made up to 50 μL with PCR grade water, which included the addition of 2 μL of sample. The thermal cycling protocol used was as follows for the bacterial 8F and 1492R primers; initial denaturation at 94°C for 4 min, melting at 94°C for 30 s, annealing at 55°C for 30 s, extension at 72°C for 1 min (35 cycles with a final extension at 72°C for 5 min) (Eden et al., 1991). For the eukaryotic 18S rRNA gene amplification, the temperature cycle was; initial denaturation at 94°C for 2 min, melting at 94°C for 30 s, annealing at 55°C for 1.5 min,

TABLE 1 | Distribution of samples taken for a period of 30 months from different areas within the SNF pond, and analyzed using high-throughput (Illumina) DNA microbial profiling.

Main sampling areas	Feeding tank (FT)		Main ponds (MP)			Subponds (SP)			
Sampling points / Date	Feeding tank (FT01)	Number of sequences (after QC)	Main pond 2 (MP2)	Number of sequences (after QC)	Main pond 3 (MP3)	Number of sequences (after QC)	Subpond 1 (SP1)	Number of sequences (after QC)	Subpond 2 (SP2)	Number of sequences (after QC)
October 2016	FT01	183,179	MP2_01	171,186	MP3_01	147,661	–		–	–
	FT02	153,474								
January 2017	–	–	–	–	–	–	SP1_01*	NA	SP2_01*	NA
June 2017	–	–	MP2_02	180,440	MP3_02	170,531	–	–	–	–
October 2017	–	–	MP2_03	110,308	MP3_03	151,014	–	–	–	–
January 2018	–	–	MP2_04	209,292	MP3_04	174,953	SP1_02	178,489	SP2_02	155,145
June 2018	–	–	MP2_05	173,003	MP3_05	163,231	SP1_03	139,082	SP2_03	175,436
November 2018	–	–	MP2_06	138,631	MP3_06	146,546	SP1_04	175,585	SP2_04	133,749
February 2019	–	–	MP2_07	156,500	MP3_07	124,047	SP1_05	150,385	SP2_05	109,585
April 2019	–	–	MP2_08	134,663	MP3_08	148,415	SP1_06	93,102	SP2_06	133,452

Samples SP1_01 and SP2_01 (*) were not sequenced using the Illumina platform but instead were analyzed using culturing techniques (with Sanger sequencing of isolated pure cultures).

extension at 72°C for 1.5 min for a total of 30 cycles, and final extension at 72°C for 5 min (DeLong, 1992). For archaeal 16S rRNA genes the thermal cycle protocol consisted of an initial denaturation step at 94°C for 4 min, melting at 94°C for 45 s, annealing at 55°C for 30 s, extension at 72°C for 1 min (for a total of 30 cycles) and a final extension step at 72°C for 5 min (DeLong, 1992).

The purity of the amplified PCR products were checked by electrophoresis using a 1% (w/v) agarose gel in 1X TAE buffer (Tris-acetic acid-EDTA). DNA was stained with SYBER safe DNA gel stain (Thermofisher), and then viewed under short-wave UV light using a BioRad Geldoc 2000 system (BioRad, Hemel Hempstead, Herts, United Kingdom).

Quantitative Polymerase Chain Reaction

Quantitative Polymerase Chain Reaction (qPCR) of the prokaryotic 16S rRNA gene was performed by using Brilliant II Sybr Green qPCR Master Mix and the MX3000P qPCR System (Agilent Genomics, Headquarters, Santa Clara, CA, United States). The qPCR master mix contained 0.4 μL 8F forward primer (25 μM), and 0.4 μL 519R reverse primer (25 μM) (Turner et al., 1999), 0.4 μL of one in five diluted Rox reference dye, 12.5 μL of 2x qPCR Sybr green master mix, and Roche PCR Grade water to make up a final volume of 23 μL. Finally, 2 μL of sample was added. A standard curve from known serial dilutions of template DNA was constructed by plotting the CT (cycle threshold) values to verify the presence of a single gene-specific peak and the absence of primer dimer. The cycling conditions consisted of one cycle of denaturation at 94°C for 10 min, followed by 35 three-segment cycles of amplification (94°C for 30 s, 50°C for 30 s and 72°C for 45 s). Fluorescence was automatically measured during the PCR amplification, and one three-segment cycle of product melting (94°C for 10 min, 50°C for 30 s and 94°C for 30 s). Gene quantification was achieved by determining the threshold cycle (CT) of the unknown samples compared to the standard curve. The baseline adjustment method for the Mx3000 (Agilent) software was used to determine the Ct in each reaction. All samples were amplified in triplicate, and the mean was used for further analysis. In order to quantify the concentration of target genes, the absolute quantification by the standard-curve (SC) method was used (Brankatschk et al., 2012). To determine the abundance of cells mL^{-1} of sample, the total number of 16S rRNA genes determined by qPCR was adjusted to the approximated number of 16S rRNA gene copy numbers reported for members of the Proteobacteria; specifically for classes alpha and beta the average number of copies is reported to be 4 (Větrovský and Baldrian, 2013). A paired-samples (one-tailed) *t*-test (Sullivan, 2017) was conducted to compare the number of DNA copies over time in the MP and SP areas). Analysis was carried out on MP samples that were collected between 2016 and 2019, whilst the SP samples were collected between 2018 and 2019.

DNA Sequencing

Sequencing of 16S rRNA gene PCR amplicons was conducted using the Illumina MiSeq platform (Illumina, San Diego,

CA, United States) targeting the V4 hyper variable region (forward primer, 515F, 5′-GTGYCAGCMGCCGCGGTAA-3′; reverse primer, 806R, 5′-GGACTACHVGGGTWTCTAAT-3′) for 2 × 250-bp paired-end sequencing (Illumina, San Diego, CA, United States) (Caporaso et al., 2011, 2012). PCR amplification was performed using the Roche FastStart High Fidelity PCR System (Roche Diagnostics Ltd., Burgess Hill, United Kingdom) in 50 μL reactions under the following conditions; initial denaturation at 95°C for 2 min, followed by 36 cycles of 95°C for 30 s, 55°C for 30 s, 72°C for 1 min, and a final extension step of 5 min at 72°C. The PCR products were purified and normalized to ∼20 ng each using the SequalPrep Normalization Kit (Fisher Scientific, Loughborough, United Kingdom). The PCR amplicons from all samples were pooled in equimolar ratios. The run was performed using a 4 pM sample library spiked with 4 pM PhiX to a final concentration of 10% following the method of Schloss and Kozich (Kozich et al., 2013).

Raw sequences were divided into samples by barcodes index I5 and I7 (up to one mismatch was permitted) using a sequencing pipeline. Quality control and trimming (Q score of 20, and a minimum length of 250 base pairs) was performed using Cutadapt (Martin, 2011), FastQC (Bioinformatics, 2018), and Sickle (Joshi and Fass, 2011). MiSeq error correction was performed using SPADes (Nurk et al., 2013). Forward and reverse reads were incorporated into full-length sequences with Pandaseq (Masella et al., 2012). Chimeras were removed using ChimeraSlayer (Edgar et al., 2011), and OTU's were generated with UPARSE (Edgar, 2013). OTUs were classified by Usearch (Edgar, 2010) at the 97% similarity level, and singletons were removed. Rarefaction analysis was conducted using the original detected OTUs in Qiime (Caporaso et al., 2010). The taxonomic assignment was performed by the RDP classifier (Wang et al., 2007). OTU sequences were submitted to the NCBI GenBank repository under the Bioproject number PRJNA660452, detailed accession numbers are indicated in **Supplementary Table 2**.

Culturing and Identification of the Pond Microorganisms

A complementary culture-dependent approach was used to help characterize the microorganisms present. To facilitate this, a series of 10-fold dilutions of water samples from the subponds 1 and 2 were plated onto fresh solid media. A range of complex or semi-defined solid media (at 10, 50, and 100% concentrations) were used (**Supplementary Table 3**) including Luria Bertani (LB) (Sezonov et al., 2007), Nutrient Agar (NA) (Misal et al., 2013), and Minimum medium DL (Lovley et al., 1984) at a range of pH values (7, 10, and 11). The marine medium of Zobell was also selected for isolation of alpha and gammaproteobacteria (Brettar et al., 2004) that had been detected in the pond using cultivation-independent DNA sequencing. Finally the fully defined minimal medium M9 (Neidhart et al., 1974) was also used at a range of concentrations and pH. The M9 medium contained no added carbon, selecting for autotrophic oligotrophs.

The isolated colonies were then resuspended in 10 mL of fresh liquid media and grown aerobically for 48 h. Cells were harvested by centrifuging at 3,500 *g* for 10 min, and supernatant was removed leaving the cell pellet and 100 μL of culture medium. DNA was extracted separately from the cell pellets using the Power Biofilm DNA Isolation Kit (MoBio Laboratories, Inc., Carlsbad, CA, United States). The DNA was eluted to a final volume of 100 μL, and stored at 4°C until use.

The 16S rRNA gene sequences of the isolates were determined by the chain termination sequencing method to facilitate phylogenetic analyses of the pure cultures (Slatko et al., 1999). PCR amplification was performed from the extracted DNA using a Techne Thermocycler (Cole-Parmer, Staffordshire, United Kingdom). Two PCR mixtures were prepared (one for each primer) and contained 3.5 μL 5X PCR buffer, 0.15 μL of 25 μM primer, and 1 μL Terminator BigDye (Thermo Fisher Scientific, Waltham, MA, United States), 1 μL of DNA was added to each tube, and was made to a final volume of 15 μL with PCR grade water. The thermal cycling protocol used was adapted for the primers as follows; initial denaturation at 96°C for 6 min, melting at 94°C for 40 s, annealing at 55°C for 15 s, extension at 60°C for 3 min; 30 cycles, and a final extension at 60°C for 5 min (Lorenz, 2012). The resulting PCR products were purified using the GlycoBlue coprecipitant protocol AM9516 (Thermo Fisher Scientific, Waltham, MA, United States), and the resulting pellets were then sequenced. An ABI Prism BigDye Terminator Cycle Sequencing Kit was used in combination with an ABI Prism 3730XL Capillary DNA Analyzer (Applied Biosystems, Warrington, United Kingdom). The primers 8F and 1592R were used for initial amplification and sequencing: 8F 5′-AGA GTT TGATCC TGG CTC AG-3′, and 1492R 5′-TAC GGY TAC CTT GTTACG ACT T-3′ (Lane et al., 1986). Sequences (typically 950 base pairs in length) were aligned with Muscle (Edgar, 2004) via the MEGA software (Kumar et al., 2016) version X (Kumar et al., 2018), then sequences were compared against the GenBank NCBI database using the BLAST program packages and matched to the most similar known 16S rRNA gene sequences (affiliations are detailed on **Supplementary Figure 1**).

RESULTS

The aim of this study was to characterize the microbial populations living under the inhospitable high pH, oligotrophic and high background radiation conditions within an INP at the Sellafield complex. Duplicate samples of the purge waters of the FT were collected in October 2016. This non-radioactive purge water feeds into the INP, and therefore the analysis set out to determine the microbial community present in these samples that could seed the INP. We received an initial sample from the SP (in duplicate) in which the sole purpose was try to get the microorganisms present in the pond into culture. We were then provided with further samples (January 2018 onward) from this region of the INP facility to carry out next generation sequencing on. Since culture dependent techniques do not reveal the whole microbial community, it was important to use DNA sequencing techniques to better understand what microorganisms inhabit the SP.

Cell Density

In order to get an estimate of the overall cell density of the microorganisms that inhabit this facility, qPCR was carried out. Only the 16S rRNA gene could be detected in the extracted DNA samples, PCR using the eukaryotic 18S rRNA and the archaeal specific 16S rRNA primers did not result in any detectable amplification. Copy numbers were lower in the FT ($\mu = 8.1 \times 10^4$, SE = 3.9×10^4 DNA copies) and SP ($\mu = 2.5 \times 10^5$, SE = 8.8×10^4 DNA copies), while MP values ranged from 2.5×10^5 to 1.5×10^6 DNA copies (**Figure 2**), peaking in MP2_08 and MP3_08 (1.4×10^6 and 1.56×10^6 DNA copies, respectively; April 2019) and in MP3_06 (1.1×10^6 DNA copies, November 2018). The results showed that the number of DNA copies in the MP from the period 2016–2017 ($\mu = 2.9 \times 10^5$, SD = 1.1×10^5) to the period 2018–2019 ($\mu = 1.4 \times 10^5$, SD = 5.5×10^5) increased significantly [$t(16) = 2.09$, $p < 0.05$]. Likewise, the results on the SP showed that the number of DNA copies from 2018 ($\mu = 7.8 \times 10^4$, SD = 5.7×10^4) to 2019 ($\mu = 7.8 \times 10^5$, SD = 2.7×10^5) increased significantly [$t(10) = 2.71$, $p < 0.05$] (detailed statistical data is provided in **Supplementary Table 1**).

Identification of Microorganisms by Next Generation DNA Sequencing

Over a 30-month sampling campaign a total of 30 samples (**Table 1**) from three sampling areas (FT, MP, and SP) were analyzed by 16S rRNA gene sequencing on the Illumina MiSeq. The initial sampling (by duplicate) was taken from the feeding head tank (FT) supplying the pond complex with demineralised water adjusted to pH 11.6 in October 2016, to help identify organisms present in the background waters, and hence (by comparison) help identify the organisms that were exclusively present in the INP main and subponds (**Figure 3**).

DNA extracted from the pond samples were assessed using PCR with 3 primer sets to screen for the presence of the prokaryotic and archaeal 16S rRNA genes and the eukaryotic 18S rRNA gene. However, only prokaryotic 16S rRNA gene amplification products were detected, and it was therefore concluded that eukaryotic and archaeal microorganisms were absent, or below the limit of detection. The 16S rRNA gene was targeted for sequencing using the Illumina MiSeq next generation sequencing platform, and analyzed using a bespoke bioinformatics platform which included comparison to prokaryotic gene sequences deposited in the NCBI databases.

Samples from the main ponds (MP) were dominated [mean ± standard deviation (SD)] by Proteobacteria (92.68 ± 6.26%) and Bacteroidetes (5.25 ± 6.93%). Organisms affiliated with the phylum Cyanobacteria were not detected in the initial samples, but were detected at subsequent times (from October 2017 to April 2019), although at a relative abundance of less than 3%. Samples from the subponds (SP) were also dominated (mean ± SD) by Proteobacteria (90.33 ± 4.01%) and Bacteroidetes (3.67 ± 2.19%), while the relative abundance of Cyanobacteria was again low (0.88 ± 0.52%). In addition, other phyla were detected at higher levels at specific dates in the subponds including organisms affiliated with the Actinobacteria (6.96 ± 2.13%, January 2018), Armatimonadetes (5.54 ± 1.78%, June 2018) and Deinococcus-Thermus groups (3.5 ± 0.95% from November 2018). Samples from the feeding tank (FT) were also dominated (mean ± SD) by Proteobacteria (73.3 ± 3.36%), Bacteroidetes (16.62 ± 3.6%) and Actinobacteria (2.58 ± 1.23%) (**Supplementary Figure 2**).

At the genus level the FT was dominated (mean ± SD) by close relatives of *Curvibacter* (21.4 ± 1.33%, Betaproteobacteria, 1 OTU), *Rhodoferax* (19.97 ± 0.51%, Betaproteobacteria, 1 OTU), *Sediminibacterium* (10.99 ± 0.85 %, Bacteroidetes, 2 OTUs), *Polaromonas* (5.51 ± 5.74%, Betaproteobacteria, 2 OTUs), *Methylotenera* (6.74 ± 6.29%, Betaproteobacteria, 2 OTUs), *Novosphingobium* (3.26 ± 1.87%, Alphaproteobacteria, 2 OTUs), *Flavobacterium* (3.40 ± 3.33%, Bacteroidetes, 2 OTUs), *Unidibacterium* (3.11 ± 0.52%, Betaproteobacteria, 2 OTUs). Approximately 26.25 ± 1.33% of the total OTUs (26) represented unidentified organisms.

Microbial distributions were consistent at all sampling times within the main ponds (MP) (**Figure 3A**). Overall at the genus level the microbial diversity was dominated (mean ± SD) by 1 OTU belonging to genus *Hydrogenophaga* (Betaproteobacteria), representing up to 38.76 ± 10.03% of the total population. The remaining community consisted of *Porphyrobacter* (21.57 ± 8.44%, Alphaproteobacteria, 1 OTU), *Roseococcus* (9.82 ± 4.15%, Alphaproteobacteria, 3 OTUs), *Silanimonas* (9.49 ± 4.50%, Gammaproteobacteria, 1 OTU), *Sphingomonas* (7.84 ± 6.82%, Alphaproteobacteria, 2 OTUs), and *Synechococcus* (0.91 ± 0.49%, Cyanophyceae, 3 OTUs). The exception was one set of samples taken on January 2018 (MP2_04 and MP3_04), where broad microbial diversity was recorded and the abundance of *Hydrogenophaga*, and *Porphyrobacter* dropped to 22.52 ± 4.73% and 7.40 ± 1.19%, respectively. Additionally, representatives of the genera *Methylophilus* (13.61 ± 0.69%, Betaproteobacteria, 1 OTU) and *Mongoliitalea* (9.80 ± 4.37%, Bacteroidetes, 2 OTUs) were exclusively identified at this sampling time. Unidentified (uncultured) sequences, although detected at all sampling times, represented more than 2% of the total community in samples MP2_02 (June 2017, 8.84 ± 6.77%, 24 OTUs), MP2_04 and MP3_04 (January 2018, 8.67 ± 1.08% and 10.19 ± 6.77%, 38 OTUs) and MP3_08 (April 2019, 21.48 ± 6.77%, 47 OTUs).

The microbial profiles of the subponds (SP) were similar to the main ponds (MP), and were dominated (mean ± SD) by representatives of the genera *Hydrogenophaga* (30.55 ± 5.73%, Betaproteobacteria, 1 OTU), *Porphyrobacter* (23.06 ± 7.52%, Alphaproteobacteria, 1 OTU), *Roseococcus* (15.44 ± 3.45%, Alphaproteobacteria, 2 OTUs), *Silanimonas* (8.73 ± 4.34%, Gammaproteobacteria, 2 OTUs), and *Sphingomonas* (2.4 ± 4.21%, Alphaproteobacteria, 3 OTUs). Samples SP1_02 and SP2_02 (January, 2018) showed a few differences with close relatives affiliated to genus *Methylophilus* (13.61 ± 0.69%, Alphaproteobacteria, 1 OTU) detected in these samples only (**Figure 3B**).

When viewed at the phylum level all three sampling areas (5 sampling points in total) showed similar profiles, as they

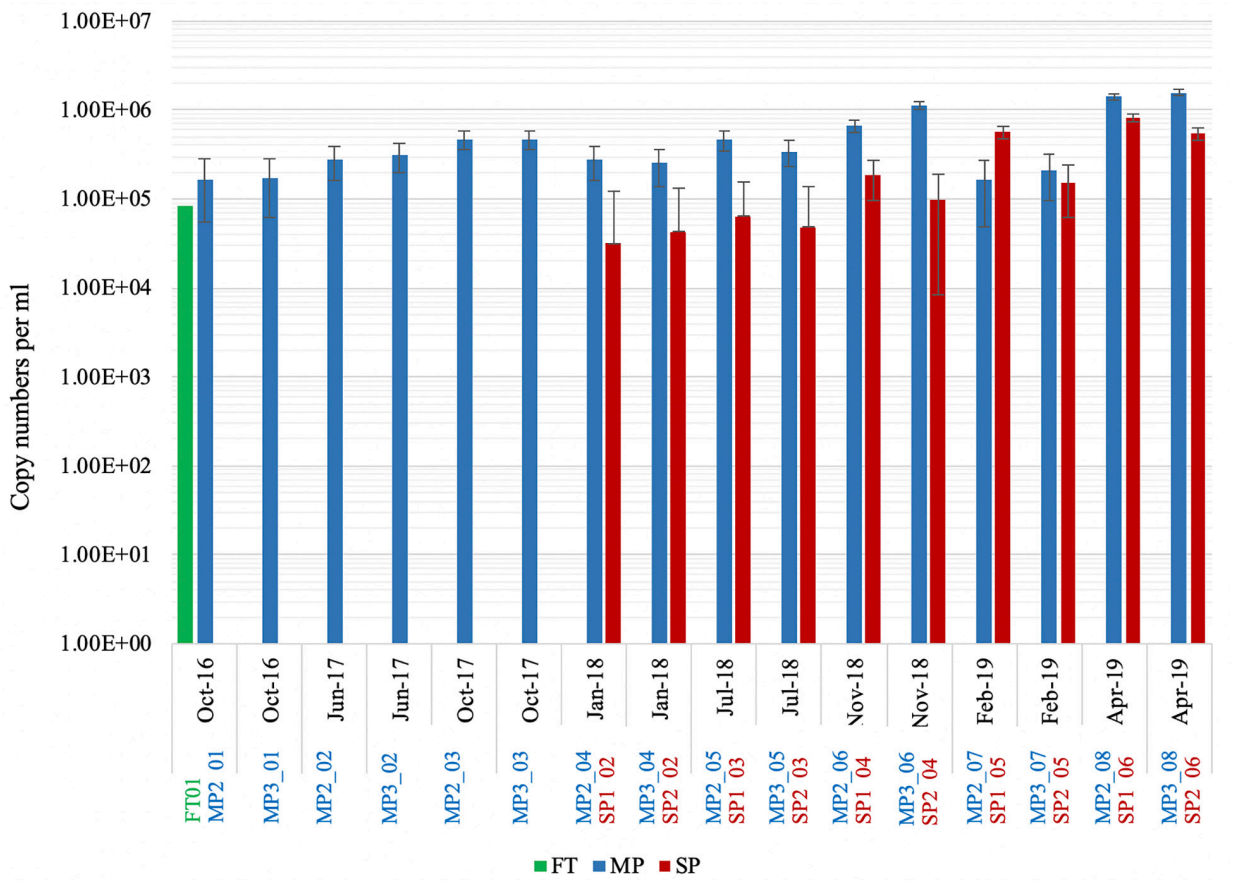

FIGURE 2 | QPCR results show the average number of copies per mL per sampling site and time (FT: feeding tank, MP: main ponds and SP: subponds). Copy numbers are expressed on log scale and error bars represent standard error. Missing bars represent lack of samples for certain sampling dates (FT and SP). A standard curve for QPCR reaction was calculated at concentration ranging from 7.53×10^{-4} to 7.530×10^{3} ng mL^{-1} ($2.8 \times 10^{3} - 2.8 \times 10^{12}$ DNA copies) to estimate the concentration of DNA in the samples.

were dominated by Proteobacteria, however, when looking at the affiliations at the genus level the microbial communities at each sampling point could be seen to differ substantially. Data would seem to suggest that the microbial community compositions in the MP, SP and FT samples represent distinct ecosystems, most likely linked to the impacts of the spent fuel in the INP environment.

Cultivation-Dependent Analysis for Determining Microbial Diversity in the INP

After 7 days of incubation, growth was detected exclusively in the undiluted samples (100) from plates containing non-defined complex media (DL, NA, and Zobell media; **Supplementary Table 3**). CFU mL^{-1} were between 700 and 1,000 mL^{-1} for each medium and eleven distinct colony morphologies were noted. Representative single colonies were isolated and identified by sequencing using the dideoxynucleotide technique. The presence of colonies was not detected on the fully defined media (minimal media M9).

Overall, representatives of four different genera were identified by 16S rRNA gene sequencing. Representatives most closely related to species of the genus *Algoriphagus* (isolates S01, 91.5% similarity; S05, 91% similarity; S06, 91.5% similarity; and S07, 89.5% similarity) were isolated on DL and NA agars, and produced light pink-colored, rod-shaped and raised colonies (1–2 mm diameter). Organisms most closely related to members of *Echinicola* genus (isolates S02, 91% similarity; S08, 88% similarity; and S09, 93.5% similarity) were obtained on the DL and NA agar plates, and produced red-colored colonies, that were rod-shaped with raised elevation (2–3 mm diameter). Strains S03, S10, and S11 were isolated from DL, NA and Zobell plates; were rod-shaped, translucent and had raised colonies (2–3 mm diameter) and were affiliated to an unclassified genus from the family Cyclobacteriaceae (S03, 93.5% similarity; S10, 85% similarity and S11, 91% similarity). Finally, a close relative to genus *Bacteroides* (strain S04, 91.5% similarity) was isolated from the DL plates and produced short round-shaped, bright-orange raised colonies (1–2 mm diameter). All eleven isolated strains belonged to the phylum Bacteroidetes (specific details on similarity and media are shown on **Supplementary Table 4**).

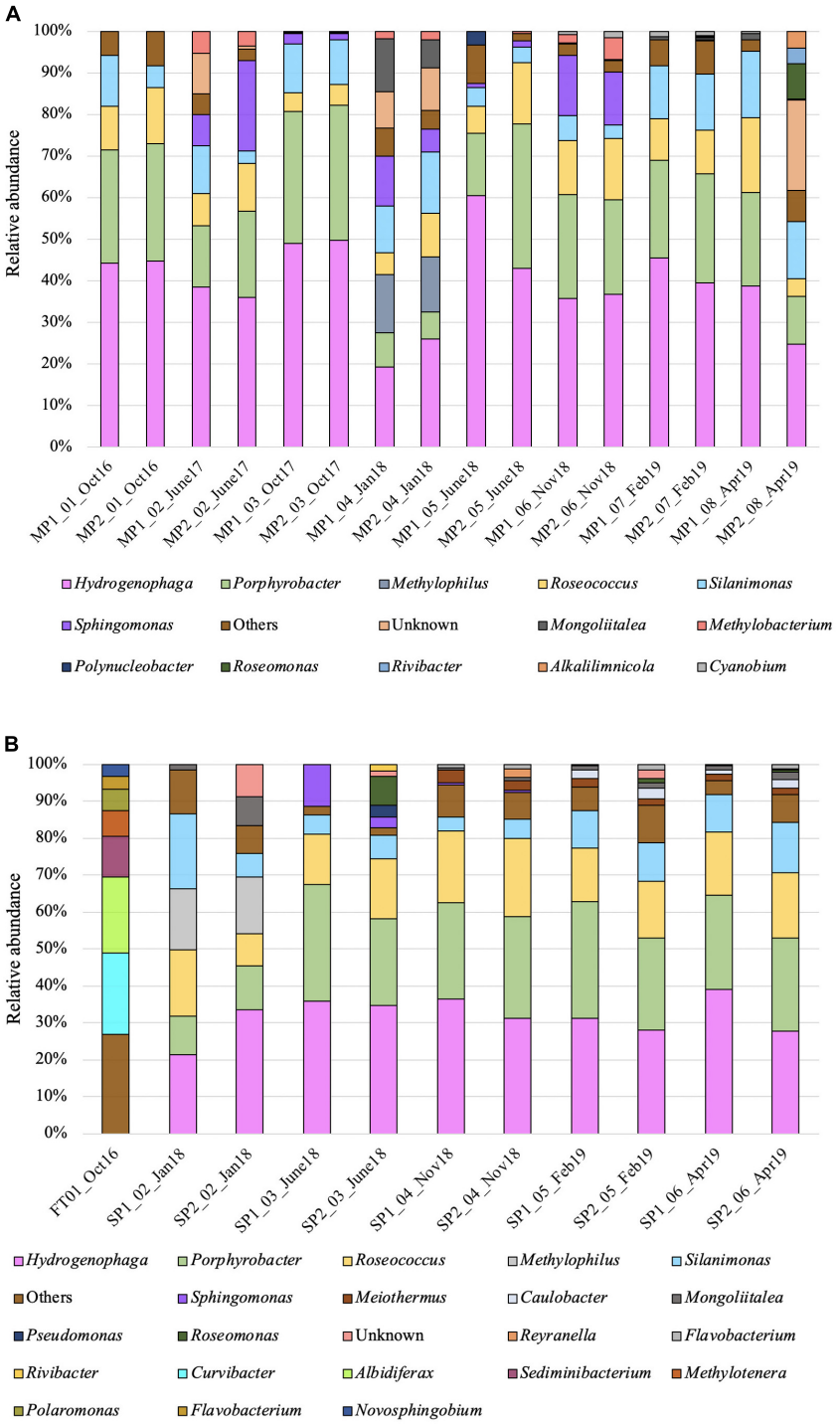

FIGURE 3 | Phylogenetic affiliations (closest known genera) of microorganisms detected in the indoor nuclear pond (INP) at Sellafield: **(A)** microbial community in the main pond (MP); **(B)** microbial community in the feeding tank (FT) and subponds (SP), based on Illumina sequencing of the prokaryote 16S rRNA gene. Only genera that contained more than 1.5% of the total number of sequences are shown.

Members belonging to genus *Echinicola* (phylum Bacteroidetes) were previously detected in the MP and SP samples by DNA-based techniques; however, they did not represent a major component of the community. More precisely, members of the genus *Echinicola* were detected in samples MP2_03 and MP3_03 (October 2017) at a relative abundance of 0.28 and 0.39%, respectively (**Supplementary Table 5**).

TABLE 2 | Parameters measured in the indoor alkaline spent fuel storage pond (INP).

Parameter	Feeding tank (FT)	Main ponds (MP)	Subponds (SP)
pH	11.5124 ± 0.01	11.5779 ± 0.01	11.6 ± 0.02
Temperature (°C)	14.1105 ± 0.04	14.4607 ± 0.04	14.168 ± 0.037
Na^+ (μg/mL)	80.4114 ± 0.41	81.1753 ± 0.35	81.2830 ± 0.38
TOC (μg/mL)	2.11 ± 0.24	2.07 ± 0.23	2.02 ± 0.22
Phosphates PO_4^{-2} (g/mL)	0.00	0.00	0.00
Nitrates NO_3^{-2} (μg/mL)	0.01 ± 0.01	0.01 ± 0.01	0.01 ± 0.01
Beta AC (Bq/mL)	NA	1, 131.6470 ± 28.88	1, 117.44853 ± 30.77

Data provided by Sellafield Ltd. Mean ± standard error is presented for each parameter. NA, not available data.

DISCUSSION

The present research was focused on characterizing the microbial community of a Sellafield INP complex containing main ponds (MP), subponds (SP) and a feeding head tank (FT) over a period of 30 months. The results showed that bacteria affiliated with a range of phylogenetic groups are able to survive and colonize the different areas across the INP complex.

Microbial diversity within the FT, an oligotrophic and hyper-alkaline environment, was dominated by members belonging to the Proteobacteria and Bacteroidetes. Previous studies showed that oligotrophic conditions do not prevent microbial colonization and allow microbial communities to display diverse adaptation mechanisms (Kawai et al., 2002; Kulakov et al., 2002; Chen et al., 2004). Specifically, organisms associated to Proteobacteria and Bacteroidetes have been identified previously in similar oligotrophic environments, including industrial ultrapure water (Galès et al., 2004; Bohus et al., 2011; Proctor et al., 2015). Microbial colonization in such environments has been linked to low levels of residual organic matter in the system, originating from dead microbial cells that and to biofilm formation on the walls, linked to planktonic cells delivered by water recirculation in the pond areas (Bohus et al., 2011). Organisms detected in the FT area are reported to support diverse forms of heterotrophic metabolism, which could occur within the FT. For example, members of the genera *Rhodoferax* (Finneran et al., 2003; Risso et al., 2009), *Curvibacter* and *Sediminibacterium* (Qu and Yuan, 2008; Ding and Yokota, 2010; Kang et al., 2013, 2014; Ma et al., 2016) are able to oxidize a range of complex organic compounds, while *Methylotenera* can utilise reduced one-carbon compounds (methylotrophy) such as methanol as energy sources (Kalyuzhnaya et al., 2006, 2011). However, the source of carbon and the source of energy microorganisms use in the FT remains to be investigated.

Although the INP has a continuous pond purge, the main ponds (MP) and subponds (SP) contained stable microbial populations with similar community profiles, which contrasted with the distinct microbiome of the FT. Key organisms detected in MP and SP samples included species of *Hydrogenophaga*, *Silanimonas*, *Porphyrobacter*, and *Roseococcus*.

In addition to the oligotrophic and hyper-alkaline characteristics of the MP and SP areas, spent nuclear fuel results in high background radioactivity, which further challenges the microbial community in the pond. Despite these adverse conditions, microbial colonization of similar spent fuel storage systems has been documented (Santo Domingo et al., 1998; Galès et al., 2004; Bruhn et al., 2009), and dominated by organisms associated to the phyla Proteobacteria (Chicote et al., 2004; Bagwell et al., 2018; MeGraw et al., 2018; Silva et al., 2018), Firmicutes (Sarró et al., 2005), Actinobacteria (Sarró et al., 2005), Cyanobacteria (MeGraw et al., 2018; Silva et al., 2018; Foster et al., 2020a), and Deinococcus-Thermus (Masurat et al., 2005). Whilst it was not possible to identify any eukaryotic organisms in the INP, other studies have identified fresh water microalgae (Rivasseau et al., 2016; MeGraw et al., 2018) and Fungi (Chicote et al., 2004; Silva et al., 2018) in both indoor and outdoor facilities. Although the energy sources supporting microbial growth in these systems remains largely uncharacterized, it is possible that radiolysis could play a direct role in supporting microbial growth. The presence of alpha, beta and gamma radiation from the spent fuel can promote the radiolysis of water, driving the formation of short-lived, highly oxidizing free radical species, such as -OH and H_2O_2 (Shoesmith, 2000; Jonsson et al., 2007) and also the production of H_2 (Brodie et al., 2006; Libert et al., 2011) that could be utilized by hydrogen-oxidizing bacteria (Knallgas bacteria) (Yu, 2018). The most abundant organism in the MP and SP areas in this study were affiliated with the genus *Hydrogenophaga* (35.61 ± 9.42%), which comprise aerobic, chemoorganotrophic organisms that use hydrogen as an energy source (Willems et al., 1989; Kampfer et al., 2005; Yoon et al., 2008). Members of genus *Hydrogenophaga* are present in a variety of natural and engineered (e.g., waste water) environments (Lambo and Patel, 2006; Fahy et al., 2008; Yoon et al., 2008; Schwartz et al., 2013), including hyper alkaline sites such as Allas Springs, Cyprus where the pH was 11.9, similar to the alkaline conditions to the INP waters (pH 11.6) (Rizoulis et al., 2016) and serpentinizing springs (pH 11.6, The Cedars, Los Angeles, CA, United States) (Suzuki et al., 2014). The presence of *Hydrogenophaga* as a key microbial component during all the sampling times suggests that the metabolism of H_2 may be occurring within the pond, which is of particular interest since oxidation of hydrogen could also be linked to the reduction of a range of electron acceptors, including radionuclides (Lloyd, 2003).

Hydrogen metabolism has not been reported for the remaining microbial community identified in the INP. *Porphyrobacter*, an aerobic anoxygenic phototrophic bacteria (AAP), has the ability to harvest energy photosynthetically

(Hanada et al., 1997; Yoon et al., 2004; Liu et al., 2017); however, given the limited light availability in the pond, it is unlikely to be photosynthetically active in the INP. Members of this genus have been shown to be well-adapted to life in environments with light restrictions using light energy via Bacteriochlorophyll α synthesized in the dark (Fuerst et al., 1993; Yoon et al., 2008; Liu et al., 2017). Members of the *Roseococcus* genus, are obligate aerobes and chemoorganotrophic, they contain Bacteriochlorophyll α and carotenoid pigments (Boldareva et al., 2009; Yurkov, 2015), and are also able to grow in the dark (Yurkov et al., 1994). *Sphingomonas* species are metabolically versatile and can use a wide range of compounds as energy sources (Lee et al., 2001; Feng et al., 2014; Singh et al., 2015) such as polycyclic aromatic hydrocarbons (Leys et al., 2004); and contains ubiquinone Q-10, a molecule involved in respiratory functions (Niharika et al., 2012) where hydrogen, a potentially abundant energy source in the MP and SP areas, is required. *Roseomonas* species also contain ubiquinone Q-10 (Kim et al., 2009; Wang et al., 2016), and have the ability to grow on biofilms to protect themselves from adverse conditions (Diesendorf et al., 2017), such as those present in this radioactive facility. Microorganisms associated with the oxygenic and phototrophic phylum Cyanbacteria (Peschek, 1999), were much less abundant (identified as genera *Synecochoccus* and *Cyanobium*), which is likely to be a result of the low levels of light in the INP. The metabolic pathways utilized in the pond to facilitate their growth are not known yet and further work is required to better understand this.

Finally, agar-based cultivation approaches were tested alongside DNA-based approaches in this study, and resulted in the isolation of bacteria from the family *Cyclobacteriacea*, but proved unsuccessful for targeting organisms that were numerically dominant within the INP complex. Whilst the isolated organisms do not represent the major components of the pond microbial communities identified by NGS techniques, these new findings showed that organisms affiliated with the genera *Algoriphagus* and *Echinicola* were able to tolerate alkaline conditions (and given the source of inocula, presumably high levels of radioactivity and oligotrophic nutrient conditions), in stark contrast to the neutral pH environments they are normally associated with (Tiago et al., 2004; Yoon et al., 2004; Alegado et al., 2013; Kang et al., 2013; Misal et al., 2013; Glaring et al., 2015).

Overall this study reinforces the view that cultivation-independent molecular ecology techniques are crucial first steps in understanding the microbial dynamics in oligotrophic SNPs, offering the benefits of high-throughput sequencing of DNA that has been purified away from contaminating radionuclides present in the pond waters. This opens up the way for more detailed metagenomic analyses which are ongoing in our laboratories, alongside more targeted research on the impact of extant microbiomes within spent nuclear fuel storage ponds on the speciation and fate of key radionuclides present within the pond systems, and also the integrity of stored fuel materials.

DATA AVAILABILITY STATEMENT

The datasets presented in this study can be found in online repositories. The names of the repository/repositories and accession number(s) can be found in the article/ **Supplementary Material**.

AUTHOR CONTRIBUTIONS

SR-L developed the concept, analyzed and interpreted data, and wrote the manuscript. CB performed the DNA sequencing runs. LF performed the DNA extractions at NNL labs. KM contributed to concept development. NC data curation and provision of samples from the facility and reviewed the manuscript. JL developed the concept and extensively reviewed the manuscript. All the authors read and approved the final manuscript.

FUNDING

This work was funded from a Ph.D. program funded by the National Mexican Council of Science and Technology (CONACyT). This work was also supported by funding from Sellafield Limited and the Royal Society to JL. LF was supported by an EPSRC CASE Ph.D. and IAA funding.

ACKNOWLEDGMENTS

The author would like to thank to the National Council of Science and Technology (CONACyT) for providing the funding. In addition to the staff at NNL central laboratory and Sellafield Ltd., for their assistance with handling and transferring the samples.

SUPPLEMENTARY MATERIAL

The Supplementary Material for this article can be found online at: https://www.frontiersin.org/articles/10.3389/fmicb.2020.587556/full#supplementary-material

REFERENCES

Achal, V., Pan, X., and Zhang, D. (2012). Bioremediation of strontium (Sr) contaminated aquifer quartz sand based on carbonate precipitation induced by Sr resistant *Halomonas* sp. *Chemosphere* 89, 764–768. doi: 10.1016/j.chemosphere.2012.06.064

Adam, C., and Garnier-Laplace, J. (2003). Bioaccumulation of silver-110m, cobalt-60, cesium-137, and manganese-54 by the freshwater algae *Scenedesmus obliquus and Cyclotella meneghiana* and by suspended matter collected during a summer bloom event. *Limnol. Oceanogr.* 48, 2303–2313.

Alegado, R. A., Grabenstatter, J. D., Zuzow, R., Morris, A., Huang, S. Y., Summons, R. E., et al. (2013). *Algoriphagus machipongonensis* sp. nov., co-isolated with a colonial choanoflagellate. *Int. J. Syst. Evol. Microbiol.* 63, 163–168.

Andrès, Y., Redercher, S., Gerente, C., and Thouand, G. (2001). Contribution of biosorption to the behavior of radionuclides in the environment. *J. Radioanal. Nucl. Chem.* 247, 89–93. doi: 10.1023/A:1006763030854

Ashworth, H., Abrahamsen-Mills, L., Bryan, N., Foster, L., Lloyd, J. R., Kellet, S., et al. (2018). Effect of humic acid and bacterial exudates on sorption-desorption interactions of ^{90}Sr with brucite. *Environ. Sci. Process. Impacts* 20, 956–964. doi: 10.1039/c8em00073e

Avery, S. V. (1995a). Caesium accumulation by microorganisms: uptake mechanisms, cation competition, compartmentalization and toxicity. *J. Ind. Microbiol.* 14, 76–84. doi: 10.1007/BF01569888

Avery, S. V. (1995b). Microbial interactions with caesium—implications for biotechnology. *J. Chem. Technol. Biotechnol.* 62, 3–16. doi: 10.1002/jctb.280620102

Bagwell, C. E., Noble, P. A., Milliken, C. E., Li, D., and Kaplan, D. I. (2018). Amplicon sequencing reveals microbiological signatures in spent nuclear fuel storage basins. *Front. Microbiol.* 9:377. doi: 10.3389/fmicb.2018.00377

Baldwin, N. D. (2003). "Remediating Sellafield, a new focus for the site," in *Proceedings of the Waste Management Conference*, Tucson, AZ.

Bhaduri, S., Debnath, N., Mitra, S., Liu, Y., and Kumar, A. (2016). Microbiologically induced calcite precipitation mediated by *Sporosarcina pasteurii*. *J. Vis. Exp.* 2016, 1–7. doi: 10.3791/53253

Bioinformatics, B. (2018). *Babraham Bioinformatics - FastQC A Quality Control tool for High Throughput Sequence Data*. Available online at: https://www.bioinformatics.babraham.ac.uk/projects/fastqc/ (accessed December 18, 2019).

Bohus, V., Kéki, Z., Márialigeti, K., Baranyi, K., Patek, G., Schunk, J., et al. (2011). Bacterial communities in an ultrapure water containing storage tank of a power plant. *Acta Microbiol. Immunol. Hung.* 58, 371–382. doi: 10.1556/AMicr.58.2011.4.12

Boldareva, E. N., Tourova, T. P., Kolganova, T. V., Moskalenko, A. A., Makhneva, Z. K., and Gorlenko, V. M. (2009). *Roseococcus suduntuyensis* sp. nov., a new aerobic bacteriochlorophyll a-containing bacterium isolated from a low-mineralized soda lake of Eastern Siberia. *Microbiology* 78, 92–101. doi: 10.1134/S0026261709010123

Boswell, C. D., Dick, R. E., Eccles, H., and Macaskie, L. E. (2001). Phosphate uptake and release by *Acinetobacter johnsonii* in continuous culture and coupling of phosphate release to heavy metal accumulation. *J. Ind. Microbiol. Biotechnol.* 26, 333–340. doi: 10.1038/sj.jim.7000139

Braissant, O., Verrecchia, E. P., and Aragno, M. (2002). Is the contribution of bacteria to terrestrial carbon budget greatly underestimated? *Naturwissenschaften* 89, 366–370. doi: 10.1007/s00114-002-0340-0

Brankatschk, R., Bodenhausen, N., Zeyer, J., and Burgmann, H. (2012). Simple absolute quantification method correcting for quantitative PCR efficiency variations for microbial community samples. *Appl. Environ. Microbiol.* 78, 4481–4489. doi: 10.1128/AEM.07878-11

Brettar, I., Christen, R., and Hofle, M. G. (2004). *Aquiflexum balticum* gen. nov., sp. nov., a novel marine bacterium of the Cytophaga-Flavobacterium-Bacteroides group isolated from surface water of the central Baltic Sea. *Int. J. Syst. Evol. Microbiol.* 54, 2335–2341. doi: 10.1099/ijs.0.63255-0

Brodie, E. L., DeSantis, T. Z., Joyner, D. C., Baek, S. M., Larsen, J. T., Andersen, G. L., et al. (2006). Application of a high-density oligonucleotide microarray approach to study bacterial population dynamics during uranium reduction and reoxidation. *Appl. Environ. Microbiol.* 72, 6288–6298. doi: 10.1128/AEM.00246-06

Brown, M. J., and Lester, J. N. (1982). Role of bacterial extracellular polymers in metal uptake in pure bacterial culture and activate sludge II. Effects of mean cell retention time. *Water Res.* 16, 1549–1560. doi: 10.1016/0043-1354(82)90207-x

Bruhn, D. F., Frank, S. M., Roberto, F. F., Pinhero, P. J., and Johnson, S. G. (2009). Microbial biofilm growth on irradiated, spent nuclear fuel cladding. *J. Nucl. Mater.* 384, 140–145. doi: 10.1016/j.jnucmat.2008.11.008

Caporaso, J. G., Kucynski, J., Stombaugh, J., Bittinger, K., Bushman, F. D., Costello, E., et al. (2010). QIIME allows analysis of high- Intensity normalization improves color. *Nat. Publ. Group* 7, 335–336. doi: 10.1038/nmeth0510-335

Caporaso, J. G., Lauber, C. L., Walters, W. A., Berg-Lyons, D., Huntley, J., Fierer, N., et al. (2012). Ultra-high-throughput microbial community analysis on the Illumina HiSeq and MiSeq platforms. *ISME J.* 6, 1621–1624. doi: 10.1038/ismej.2012.8

Caporaso, J. G., Lauber, C. L., Walters, W. A., Berg-Lyons, D., Lozupone, C. A., Turnbaugh, P. J., et al. (2011). Global patterns of 16S rRNA diversity at a depth of millions of sequences per sample. *Proc. Natl. Acad. Sci. U.S.A.* 108(Suppl. 1), 4516–4522. doi: 10.1073/pnas.1000080107

Chen, C. L., Liu, W. T., Chong, M. L., Wong, M. T., Ong, S. L., Seah, H., et al. (2004). Community structure of microbial biofilms associated with membrane-based water purification processes as revealed using a polyphasic approach. *Appl. Microbiol. Biotechnol.* 63, 466–473. doi: 10.1007/s00253-003-1286-7

Chicote, E., García, A. M., Moreno, D. A., Sarró, M. I., Lorenzo, P. I., and Montero, F. (2005). Isolation and identification of bacteria from spent nuclear fuel pools. *J. Ind. Microbiol. Biotechnol.* 32, 155–162. doi: 10.1007/s10295-005-0216-3

Chicote, E., Moreno, D. A., Garcia, A. M., Sarro, M. I., Lorenzo, P. I., and Montero, F. (2004). Biofouling on the walls of a spent nuclear fuel pool with radioactive ultrapure water. *Biofouling* 20, 35–42. doi: 10.1080/08927010410001662670

Comte, S., Guibaud, G., and Baudu, M. (2008). Biosorption properties of extracellular polymeric substances (EPS) towards Cd, Cu and Pb for different pH values. *J. Hazard. Mater.* 151, 185–193. doi: 10.1016/j.jhazmat.2007.05.070

Dekker, L., Osborne, T. H., and Santini, J. M. (2014). Isolation and identification of cobalt- and caesium-resistant bacteria from a nuclear fuel storage pond. *FEMS Microbiol. Lett.* 359, 81–84. doi: 10.1111/1574-6968.12562

DeLong, E. F. (1992). Archaea in coastal marine environments. *Proc. Natl. Acad. Sci. U.S.A.* 89, 5685–5689. doi: 10.1073/pnas.89.12.5685

Deutch, J. M., Forsberg, C., Kadak, A. C., Kazimi, M. S., Moniz, E. J., and Parsons, J. E. (2009). *Future of Nuclear Power, an Interdisciplinary MIY Study*. Cambridge, MA: Massachusetts Institute of Technology.

Diesendorf, N., Köhler, S., Geißdörfer, W., Grobecker-Karl, T., Karl, M., and Burkovski, A. (2017). Characterisation of *Roseomonas mucosa* isolated from the root canal of an infected tooth. *BMC Res. Notes* 10:212. doi: 10.1186/s13104-017-2538-4

Ding, L., and Yokota, A. (2010). *Curvibacter fontana* sp. nov., a microaerobic bacteria isolated from well water. *J. Gen. Appl. Microbiol.* 56, 267–271. doi: 10.2323/jgam.56.267

Dittrich, M., Müller, B., Mavrocordatos, D., and Wehrli, B. (2003). Induced calcite precipitation by cyanobacterium Synechococcus. *Acta Hydrochim. Hydrobiol.* 31, 162–169. doi: 10.1002/aheh.200300486

Eden, P. A., Schmidt, T. M., Blakemore, R. P., and Pace, N. R. (1991). Phylogenetic analysis of *Aquaspirillum magnetotacticum* Using Polymerase Chain Reaction-Amplified 16s rRNA-Specific DNA. *Int. J. Syst. Bacteriol.* 41, 324–325. doi: 10.1201/b10765-4

Edgar, R. C. (2004). MUSCLE: a multiple sequence alignment method with reduced time and space complexity. *BMC Bioinformatics* 5:113. doi: 10.1186/1471-2105-5-113

Edgar, R. C. (2010). Search and clustering orders of magnitude faster than BLAST. *Bioinformatics* 26, 2460–2461. doi: 10.1093/bioinformatics/btq461

Edgar, R. C. (2013). UPARSE: highly accurate OTU sequences from microbial amplicon reads. *Nat. Methods* 10, 996–998. doi: 10.1038/nmeth.2604

Edgar, R. C., Haas, B. J., Clemente, J. C., Quince, C., and Knight, R. (2011). UCHIME improves sensitivity and speed of chimera detection. *Bioinformatics* 27, 2194–2200. doi: 10.1093/bioinformatics/btr381

Fahy, A., Ball, A. S., Lethbridge, G., Timmis, K. N., and McGenity, T. J. (2008). Isolation of alkali-tolerant benzene-degrading bacteria from a contaminated aquifer. *Lett. Appl. Microbiol.* 47, 60–66. doi: 10.1111/j.1472-765x.2008.02386.x

Feng, G. D., Yang, S. Z., Wang, Y. H., Zhang, X. X., Zhao, G. Z., Deng, M. R., et al. (2014). Description of a Gram-negative bacterium, *Sphingomonas guangdongensis* sp. nov. *Int. J. Syst. Evol. Microbiol.* 64(PART 5), 1697–1702. doi: 10.1099/ijs.0.056853-0

Ferris, F. G., Wiese, R. G., and Fyfe, W. S. (1994). Precipitation of carbonate minerals by microorganisms: implications for silicate weathering and the global carbon dioxide budget. *Geomicrobiol. J.* 12, 1–13. doi: 10.1080/01490459409377966

Foster, L., Boothman, C., Ruiz-Lopez, S., Boshoff, G., Jenkinson, P., Sigee, D., et al. (2020a). Microbial bloom formation in a high pH spent nuclear fuel pond. *Sci. Total Environ.* 720:137515. doi: 10.1016/j.scitotenv.2020.137515

Foster, L., Muhamadali, H., Boothman, C., Sigee, D., Pittman, J. K., Goodacre, R., et al. (2020b). Radiation tolerance of *Pseudanabaena catenata*, a cyanobacterium relevant to the first generation magnox storage pond. *Front. Microbiol.* 11:515. doi: 10.3389/fmicb.2020.00515

Finneran, K. T., Johnsen, C. V., and Lovley, D. R. (2003). *Rhodoferax ferrireducens* sp. nov., a psychrotolerant, facultatively anaerobic bacterium that oxidizes acetate with the reduction of Fe(III). *Int. J. Syst. Evol. Microbiol.* 53, 669–673. doi: 10.1099/ijs.0.02298-0

Francis, A. J. (2012). "Impacts of microorganisms on radionuclides in contaminated environments and waste materials," in *Radionuclide Behaviour in the Natural Environment: Science, Implications and Lessons for the Nuclear Industry,* eds C. Poinssot and H. Geckeis (Cambridge: Woodhead Publishing Limited). doi: 10.1533/9780857097194.1.161

Fuerst, J. A., Hawkins, J. A., Holmes, A., Sly, L. I., Moore, C. J., and Stackebrandt, E. (1993). *Porphyrobacter neustonensis* gen. nov., sp. nov., an aerobic bacteriochlorophyll-synthesizing budding bacterium from fresh water. *Int. J. Syst. Bacteriol.* 43, 125–134. doi: 10.1099/00207713-43-1-125

Fujita, Y., Redden, G. D., Ingram, J. C., Cortez, M. M., Ferris, F. G., and Smith, R. W. (2004). Strontium incorporation into calcite generated by bacterial ureolysis. *Geochim. Cosmochim. Acta* 68, 3261–3270. doi: 10.1016/j.gca.2003.12.018

Gadd, G. M. (2009). Biosorption: critical review of scientific rationale, environmental importance and significance for pollution treatment. *J. Chem. Technol. Biotechnol.* 84, 13–28. doi: 10.1002/jctb.1999

Galès, G., Libert, M. F., Sellier, R., Cournac, L., Chapon, V., and Heulin, T. (2004). Molecular hydrogen from water radiolysis as an energy source for bacterial growth in a basin containing irradiating waste. *FEMS Microbiol. Lett.* 240, 155–162. doi: 10.1016/j.femsle.2004.09.025

Ghorbanzadeh, M. S., and Mohammad, T. G. P. (2009). Biotechnological potential of *Azolla filiculoides* for biosorption of Cs and Sr: application of micro-PIXE for measurement of biosorption. *Bioresour. Technol.* 100, 1915–1921. doi: 10.1016/j.biortech.2008.10.019

Glaring, M. A., Vester, J. K., Lylloff, J. E., Al-Soud, W. A., Soørensen, S. J., and Stougaard, P. (2015). Microbial diversity in a permanently cold and alkaline environment in Greenland. *PLoS One* 10:e0124863. doi: 10.1371/journal.pone.0124863

Gov UK (2018). *Sellafield Ltd*. Available online at: https://www.gov.uk/government/organisations/sellafield-ltd/about (accessed July 6, 2018).

Hanada, S., Kawase, Y., Hiraishi, A., Takaichi, S., Matsuura, K., Shimada, K., et al. (1997). *Porphyrobacter tepidarius* sp. nov., a moderately thermophilic aerobic photosynthetic bacterium isolated from a hot spring. *Int. J. Syst. Bacteriol.* 47, 408–413. doi: 10.1099/00207713-47-2-408

Howden, M. (1987). Radioactive effluent treatment plant - sellafield reprocessing factory. *Proc. Inst. Mech. Eng. A Power Process Eng.* 201, 1–15. doi: 10.1243/pime_proc_1987_201_002_02

Jackson, S. F., Monk, S. D., and Riaz, Z. (2014). An investigation towards real time dose rate monitoring, and fuel rod detection in a First Generation Magnox Storage Pond (FGMSP). *Appl. Radiat. Isot.* 94, 254–259. doi: 10.1016/j.apradiso.2014.08.019

Jonsson, M., Nielsen, F., Roth, O., Ekeroth, E., Nilsson, S., and Hossain, M. M. (2007). Radiation induced spent nuclear fuel dissolution under deep repository conditions. *Environm. Sci. Technol.* 41, 7087–7093. doi: 10.1021/es070832y

Joshi, N., and Fass, J. (2011). *Sickle: A Sliding-Window, Adaptive, Quality-Based Trimming Tool for FastQ Files (Version 1.33*). Available online at: https://github.com/najoshi/sickle (accessed December 18, 2019)

Kalyuzhnaya, M. G., Beck, D. A. C., Vorobev, A., Smalley, N., Kunkel, D. D., Lidstrom, M. E., et al. (2011). Novel methylotrophic isolates from lake sediment, description of *Methylotenera versatilis* sp. nov. and emended description of the genus methylotenera. *Int. J. Syst. Evol. Microbiol.* 62, 106–111. doi: 10.1099/ijs.0.029165-0

Kalyuzhnaya, M. G., Bowerman, S., Lara, J. C., Lidstrom, M. E., and Chistoserdova, L. (2006). *Methylotenera mobilis* gen. nov., sp. nov., an obligately methelamine-utilizing bacterium within the family Methylophilaceae. *Int. J. Syst. Evol. Microbiol.* 56, 2819–2823. doi: 10.1099/ijs.0.64191-0

Kampfer, P., Schulze, R., Jackel, U., Malik, K. A., Amann, R., and Spring, S. (2005). *Hydrogenophaga defluvii* sp. nov and *Hydrogenophaga atypica* sp. nov., isolated from activated sludge. *Int. J. Syst. Evol. Microbiol.* 55, 341–344. doi: 10.1099/ijs.0.03041-0

Kang, H., Kim, H., Lee, B. I., Joung, Y., and Joh, K. (2014). *Sediminibacterium goheungense* sp. nov., isolated from a freshwater reservoir. *Int. J. Syst. Evol. Microbiol.* 64(PART 4), 1328–1333. doi: 10.1099/ijs.0.055137-0

Kang, H., Weerawongwiwat, V., Jung, M. Y., Myung, S. C., and Kim, W. (2013). *Algoriphagus chungangensis* sp. nov., isolated from a tidal flat sediment. *Int. J. Syst. Evol. Microbiol.* 63(PART2), 648–653. doi: 10.1099/ijs.0.039214-0

Karley, D., Shukla, S. K., and Rao, T. S. (2018). Isolation and characterization of culturable bacteria present in the spent nuclear fuel pool water. *Environ. Sci. Pollut. Res.* 25, 20518–20526. doi: 10.1007/s11356-017-0376-5

Kawai, M., Matsutera, E., Kanda, H., Yamaguchi, N., Tani, K., and Nasu, M. (2002). 16S ribosomal DNA-based analysis of bacterial diversity in purified water used in pharmaceutical manufacturing processes by PCR and denaturing gradient gel electrophoresis. *Appl. Environ. Microbiol.* 68, 699–704. doi: 10.1128/AEM.68.2.699-704.2002

Kim, M. S., Baik, K. S., Park, S. C., Rhee, M. S., Oh, H. M., and Seong, C. N. (2009). *Roseomonas frigidaquae* sp. nov., isolated from a water-cooling system. *Int. J. Syst. Evol. Microbiol.* 59, 1630–1634. doi: 10.1099/ijs.0.004812-0

Kozich, J. J., Westcott, S. L., Baxter, N. T., Highlander, S. K., and Schloss, P. D. (2013). Development of a dual-index sequencing strategy and curation pipeline for analyzing amplicon sequence data on the miseq illumina sequencing platform. *Appl. Environ. Microbiol.* 79, 5112–5120. doi: 10.1128/AEM.01043-13

Kulakov, L. A., McAlister, M. B., Ogden, K. L., Larkin, M. J., and O'Hanlon, J. F. (2002). Analysis of bacteria contaminating ultrapure water in industrial systems. *Appl. Environ. Microbiol.* 68, 1548–1555. doi: 10.1128/AEM.68.4.1548-1555.2002

Kumar, S., Stecher, G., Li, M., Knyaz, C., and Tamura, K. (2018). MEGA X: molecular evolutionary genetics analysis across computing platforms. *Mol. Biol. Evol.* 35, 1547–1549. doi: 10.1093/molbev/msy096

Kumar, S., Stecher, G., and Tamura, K. (2016). MEGA7: molecular evolutionary genetics analysis Version 7.0 for bigger datasets. *Mol. Biol. Evol.* 33, 1870–1874. doi: 10.1093/molbev/msw054

Lambo, A. J., and Patel, T. R. (2006). Isolation and characterization of a biphenyl-utilizing psychrotrophic bacterium, *Hydrogenophaga taeniospiralis IA3-A*, that cometabolize dichlorobiphenyls and polychlorinated biphenyl congeners in Aroclor 1221. *J. Basic Microbiol.* 46, 94–107. doi: 10.1002/jobm.200510006

Lane, D. J., Pace, B., Olsen, G. J., Stahl, D. A., Sogin, M. L., and Pace, N. R. (1986). Rapid determination of 16S ribosomal RNA sequences for phylogenetic analyses. *Proc. Natl. Acad. Sci. U.S.A.* 83:4792.

Lang, A. R., Engelberg, D. L., Walther, C., Weiss, M., Bosco, H., Jenkins, A., et al. (2019). Cesium and strontium contamination of nuclear plant stainless steel: implications for decommissioning and waste minimization. *ACS Omega* 4, 14420–14429. doi: 10.1021/acsomega.9b01311

Lawson, P. S., Sterrit, R. M., and Lester, J. N. (1984). Factor affecting the removal of metals during activated sludge wastewater treatment II. The role of mixed liquor biomass. *Arch. Environ. Contam. Toxicol.* 13, 391–402. doi: 10.1007/bf01056254

Lee, J. S., Shin, Y. K., Yoon, J. H., Takeuchi, M., Pyun, Y. R., and Park, Y. H. (2001). *Sphingomonas aquatilis* sp. nov., *Sphingomonas koreensis* sp. nov. and *Sphingomonas taejonensis* sp. nov., yellow-pigmented bacteria isolated from natural mineral water. *Int. J. Syst. Evol. Microbiol.* 51, 1491–1498. doi: 10.1099/00207713-51-4-1491

Lee, S. Y., Jung, K. H., Lee, J. E., Lee, K. A., Lee, S. H., Lee, J. Y., et al. (2014). Photosynthetic biomineralization of radioactive Sr via microalgal CO_2 absorption. *Bioresour. Technol.* 172, 449–452. doi: 10.1016/j.biortech.2014.09.023

Leys, N. M. E. J., Ryngaert, A., Bastiaens, L., Verstraete, W., Top, E. M., Springael, D., et al. (2004). Occurrence and phylogenetic diversity of *Sphingomonas* strains in soils contaminated with polycyclic aromatic hydrocarbons. *Appl. Environ. Microbiol.* 70, 1944–1955. doi: 10.1128/AEM.70.4.1944-1955.2004

Libert, M., Bildstein, O., Esnault, L., Jullien, M., and Sellier, R. (2011). Molecular hydrogen: an abundant energy source for bacterial activity in nuclear waste repositories. *Phys. Chem. Earth* 36, 1616–1623. doi: 10.1016/j.pce.2011.10.010

Liu, M., Dong, F., Kang, W., Sun, S., Wei, H., Zhang, W., et al. (2014). Biosorption of strontium from simulated nuclear wastewater by *Scenedesmus spinosus* under culture conditions: adsorption and bioaccumulation processes and models. *Int. J. Environ. Res. Public Health* 11, 6099–6118. doi: 10.3390/ijerph110606099

Liu, Q., Wu, Y. H., Cheng, H., Xu, L., Wang, C. S., and Xu, X. W. (2017). Complete genome sequence of bacteriochlorophyll-synthesizing bacterium *Porphyrobacter neustonensis* DSM 9434. *Stand. Genomic Sci.* 12:32. doi: 10.1186/s40793-017-0243-5

Lloyd, J. R. (2003). Microbial reduction of metals and radionuclides. *FEMS Microbiol. Rev.* 27, 411–425. doi: 10.1016/S0168-6445(03)00044-5

Lloyd, J. R., and Macaskie, L. E. (2000). "Bioremediation of radionuclide-containing wastewaters," in *Environmental Microbe-metal Interactions*, ed. R. D. Lovley (Washington, DC: ASM Press).

Lloyd, J. R., and Macaskie, L. E. (2002). "Biochemical basis of microbe-radionuclide interactions," in *Interactions of Microorganisms with Radionuclides*, eds M. J. Keith-Roach and F. R. Livens (Amsterdam: Elsevier).

Lloyd, J. R., and Renshaw, J. C. (2005). Bioremediation of radioactive waste: radionuclide-microbe interactions in laboratory and field-scale studies. *Curr. Opin. Biotechnol.* 16, 254-60. doi: 10.1016/j.copbio.2005.04.012

Lorenz, T. C. (2012). Polymerase chain reaction: basic protocol plus troubleshooting and optimization strategies. *J. Vis. Exp.* 63:e3998. doi: 10.3791/3998

Lovley, D. R., Greening, R. C., and Ferry, J. G. (1984). Rapidly growing rumen methanogenic organism that synthesizes coenzyme M and Has a High Affinity for Formate. *Appl. Environ. Microbiol.* 48, 81–87. doi: 10.1128/aem.48.1.81-87.1984

Ma, D., Hao, Z., Sun, R., Bartlam, M., and Wang, Y. (2016). Genome sequence of a typical Ultramicrobacterium, *Curvibacter* sp. Strain PAE-UM, capable of phtalate ester degradation. *Genome Announc.* 4:e01510-15. doi: 10.1128/genomeA.01510-15.Copyright

Macaskie, L. E., Empson, R. M., Cheetham, A. K., Grey, C. P., and Skarnulis, J. (1992). Uranium Bioaccumulation by a *Citrobacter* sp as a result of enzymically mediated growth of polycrystalline HUO2PO4. *Science* 257, 782–784. doi: 10.1126/science.1496397

Martin, M. (2011). Cutadapt removes adapter sequences from high-throughput sequencing reads. *EMBnet.Journal* 7, 10–12. doi: 10.14806/ej.17.1.200

Masella, A. P., Bartram, A. K., Truszkowski, J. M., Brown, D. G., and Neufeld, J. D. (2012). PANDAseq: paired-end assembler for illumina sequences. *BMC Bioinformatics* 13. doi: 10.1016/s0739-5930(09)79285-2

Masurat, P., Fru, E. C., and Pedersen, K. (2005). Identification of *Meiothermus* as the dominant genus in a storage system for spent nuclear fuel. *J. Appl. Microbiol.* 98, 727–740. doi: 10.1111/j.1365-2672.2004.02519.x

MeGraw, V. E., Brown, A. R., Boothman, C., Goodacre, R., Morris, K., Sigee, D., et al. (2018). A novel adaptation mechanism underpinning algal colonization of a nuclear fuel storage pond. *mBio* 9:e02395-17. doi: 10.1128/mBio.02395-17

Merroun, M. L., and Selenska-Pobell, S. (2008). Bacterial interactions with uranium: an environmental perspective. *J. Contam. Hydrol.* 102, 285–295. doi: 10.1016/j.jconhyd.2008.09.019

Misal, S. A., Bajoria, V. D., Lingojwar, D. P., and Gawai, K. R. (2013). Purification and characterization of nitroreductase from red alkaliphilic bacterium *Aquiflexum* sp. DL6. *Appl. Biochem. Microbiol.* 49, 227–232. doi: 10.1134/S0003683813030125

Mortensen, B. M., Haber, M. J., DeJong, J. T., Caslake, L. F., and Nelson, D. C. (2011). Effects of environmental factors on microbial induced calcium carbonate precipitation. *J. Appl. Microbiol.* 111, 338–349. doi: 10.1111/j.1365-2672.2011.05065.x

Neidhart, F. C., Bloch, P. L., and Smith, D. F. (1974). Culture medium for enterobacteria. *J. Bacteriol.* 119, 736–747. doi: 10.1128/jb.119.3.736-747.1974

Newsome, L., Morris, K., and Lloyd, J. R. (2014a). The biogeochemistry and bioremediation of uranium and other priority radionuclides. *Chem. Geol.* 363, 164–184. doi: 10.1016/j.chemgeo.2013.10.034

Newsome, L., Morris, K., Trivedi, D., Atherton, N., and Lloyd, J. R. (2014b). Microbial reduction of uranium(VI) in sediments of different lithologies collected from Sellafield. *Appl. Geochem.* 51, 55–64. doi: 10.1016/j.apgeochem.2014.09.008

Niharika, N., Jindal, S., Kaur, J., and Lal, R. (2012). *Sphingomonas indica* sp. nov., isolated from hexachlorocyclohexane (HCH)-contaminated soil. *Int. J. Syst. Evol. Microbiol.* 62, 2997–3002. doi: 10.1099/ijs.0.033845-0

Nurk, S., Bankevich, A., Antipov, D., Gurevich, A., Korobeynikov, A., Lapidus, A., et al. (2013). "Assembling genomes and mini-metagenomes from highly chimeric reads," in *Research in Computational Molecular Biology. RECOMB 2013. Lecture Notes in Computer Science*, eds M. Deng, R. Jiang, F. Sun, and X. Zhang (Berlin: Springer), 7821, 158–170. doi: 10.1007/978-3-642-37195-0_13

Peschek, G. A. (1999). "Photosynthesis and respiration of cyanobacteria," in *The Phototrophic Prokaryotes*, eds G. A. Peschek, W. Loffelhardt, and G. Schmetterer (Boston, MA: Springer).

Pipíška, M., Trajtešová, Z., Horník, M., and Frišták, V. (2018). Evaluation of Mn bioaccumulation and biosorption by bacteria isolated from spent nuclear fuel pools using 54Mn as a radioindicator. *Radiochim. Acta* 106, 217–228. doi: 10.1515/ract-2017-2836

Proctor, C. R., Edwards, M. A., and Pruden, A. (2015). Microbial composition of purified waters and implications for regrowth control in municipal water systems. *Environ. Sci. Water Res. Technol.* 1, 882–892. doi: 10.1039/c5ew00134j

Qu, J. H., and Yuan, H. L. (2008). *Sediminibacterium salmoneum* gen. nov., sp. nov., a member of the phylum Bacteroidetes isolated from sediment of a eutrophic reservoir. *Int. J. Syst. Evol. Microbiol.* 58, 2191–2194. doi: 10.1099/ijs.0.65514-0

Rajala, P., Bomberg, M., Vepsalainen, M., and Carpen, L. (2017). Microbial fouling and corrosion of carbon steel in deep anoxic alkaline groundwater. *Biofouling* 33, 195–209. doi: 10.1080/08927014.2017.1285914

Reddy, S. F., Monk, S. D., Nye, D. W., Colling, B. R., and Stanley, S. J. (2012). Proposal to characterize legacy Sellafield ponds using SONAR and RadLine. *Appl. Radiat. Isot.* 70, 1162–1165. doi: 10.1016/j.apradiso.2012.04.002

Reeder, J. R., Nugent, M., Tait, C. D., Morris, D. E., Heald, S., Beck, K. M., et al. (2001). Coprecipitation of Uranium (VI) with calcite: XAFS, micro XAS, and luminescence characterization. *Geochim. Cosmochim. Acta* 65, 3491–3503. doi: 10.1016/s0016-7037(01)00647-0

Rivasseau, C., Farhi, E., Compagnon, E., de Gouvion Saint Cyr, D., van Lis, R., Falconet, D., et al. (2016). *Coccomyxa actinabiotis* sp. nov. (Trebouxiophyceae, Chlorophyta), a new green microalga living in the spent fuel cooling pool of a nuclear reactor. *J. Phycol.* 52, 689–703. doi: 10.1111/jpy.12442

Risso, C., Sun, J., Zhuang, K., Mahadevan, R., DeBoy, R., Ismail, W., et al. (2009). Genome-scale comparison and constraint-based metabolic reconstruction of the facultative anaerobic Fe(III)-reducer *Rhodoferax ferrireducens*. *BMC Genomics* 10:447. doi: 10.1186/1471-2164-10-447

Rizoulis, A. E., Morris, K., and Lloyd, J. R. (2016). Bacterial Diversity in the Hyperalkaline Allas Springs (Cyprus), a Natural Analogue for Cementitious Radioactive Waste Repository. *Geomicrobiol. J.* 73–84. doi: 10.1080/01490451.2014.961107

Santo Domingo, J. W., Berry, C. J., Summer, M., and Fliermans, C. B. (1998). Microbiology of spent nuclear fuel storage basins. *Curr. Microbiol.* 37, 387–394. doi: 10.1007/s002849900398

Sarró, M. I., García, A. M., and Moreno, D. A. (2005). Biofilm formation in spent nuclear fuel pools and bioremediation of radioactive water. *Int. Microbiol.* 8, 223–230. doi: 10.2436/im.v8i3.9529

Schwartz, E., Fritsch, J., and Friedrich, B. (2013). "H2-metabolizing prokaryotes," in *The Prokaryotes: Prokaryotic Physiology and Biochemistry*, Vol. 9783642301414, (Berlin: Springer-Verlag), 119–199. doi: 10.1007/978-3-642-30141-4_65

Sellafield Ltd (2011). *Sellafield Plan*. Available online at: https://www.cumbria.gov.uk/eLibrary/Content/Internet/538/755/1929/17716/17720/17722/41333114920.pdf (accessed December 2, 2015).

Sellafield Ltd (2015). *Enablers*. https://webarchive.nationalarchives.gov.uk/20170712124354/http://www.sellafieldsites.com/solution/spent-fuel-management/magnox-reprocessing/enablers/ (accessed November 14, 2015)

Sezonov, G., Joseleau-Petit, D., and D'Ari, R. (2007). *Escherichia coli* physiology in Luria-Bertani broth. *J. Bacteriol.* 189, 8746–8749. doi: 10.1128/jb.01368-07

Shaw, R. D. (1990). Corrosion prevention and control at Sellafield nuclear fuel reprocessing plant. *Br. Corros. J.* 25, 97–107. doi: 10.1179/bcj.1990.25.2.97

Shoesmith, D. W. (2000). Fuel corrosion processes under waste disposal conditions. *J. Nucl. Mater.* 282, 1–31. doi: 10.1016/s0022-3115(00)00392-5

Silva, R., De Almeida, D. M., Cabral, B. C. A., Dias, V. H. G., De Toledo, E., Mello, I. C., et al. (2018). Microbial enrichment and gene functional categories revealed on the walls of a spent fuel pool of a nuclear power plant. *PLoS One* 13:e0205228. doi: 10.1371/journal.pone.0205228

Singh, P., Kim, Y. J., Hoang, V. A., Farh, M. E. A., and Yang, D. C. (2015). *Sphingomonas panacis* sp. nov., isolated from rhizosphere of rusty ginseng. *Antonie van Leeuwenhoek* 108, 711–720. doi: 10.1007/s10482-015-0527-y

Slatko, B. E., Albright, L. M., Tabor, S., and Ju, J. (1999). DNA Sequencing by the Dideoxy Method. *Curr. Protoc. Mol. Biol.* 47, 7.4A.1–7.4A.39. doi: 10.1002/0471142727.mb0704as47

Springell, R., Rennie, S., Costelle, L., Darnbrough, J., Stitt, C., Cocklin, E., et al. (2014). Water corrosion of spent nuclear fuel: radiolysis driven dissolution at the UO2/water interface. *Faraday Discuss.* 180, 301–311. doi: 10.1039/c4fd00254g

Sullivan, L. (2017). *Hypotehsis Testing for Means and Proportions*. Available online at: https://sphweb.bumc.bu.edu/otlt/mph-modules/bs/bs704_hypothesistest-means-proportions/ (accessed September 13, 2020).

Suzuki, S., Kenuen, J. G., Schipper, K., Van de Velde, S., Ishii, S., Sorokin, D. Y., et al. (2014). Physiological and genomic features of highly alkaliphilic hydrogen-utilizing Betaproteobacteria from a continental serpentinizing site. *Nat. Commun.* 5:3900.

Tiago, I., Chung, A. P., and Veríssimo, A. (2004). Bacterial diversity in a nonsaline alkaline environment: heterotrophic aerobic populations. *Appl. Environ. Microbiol.* 70, 7378–7387. doi: 10.1128/AEM.70.12.7378-7387.2004

Tišáková, L., Pipíška, M., Godány, A., Horník, M., Vidová, B., and Augustín, J. (2013). Bioaccumulation of 137Cs and 60Co by bacteria isolated from spent nuclear fuel pools. *J. Radioanal. Nucl. Chem.* 295, 737–748. doi: 10.1007/s10967-012-1932-6

Tomioka, N., Uchiyama, H., and Yagi, O. (1992). Isolation and characterization of cesium-accumulating bacteria. *Appl. Environ. Microbiol.* 58, 1019–1023. doi: 10.1128/aem.58.3.1019-1023.1992

Turner, S., Miao, V. P., and Palmer, J. D. (1999). Investigating deep phylogenetic relationships among cyanobacteria and plastids by small subunit rRNA sequence analysis. *J. Eukaryot. Microbiol.* 46, 327–338. doi: 10.1111/j.1550-7408.1999.tb04612.x

Van Roy, S., Peys, K., Dresselaers, T., and Diels, L. (1997). The use of *Alcaligenes eutrophus* biofilm in a membrane bioreactor for heavy metal recovery. *Res. Microbiol.* 148, 526–528. doi: 10.1016/s0923-2508(97)88356-8

Větrovský, T., and Baldrian, P. (2013). The variability of the 16S rRNA gene in bacterial genomes and its consequences for bacterial community analyses. *PLoS One* 8:e57923. doi: 10.1371/journal.pone.0057923

Wang, C., Deng, S., Liu, X., Yao, L., Shi, C., Jiang, J., et al. (2016). *Roseomonas eburnea* sp. nov., isolated from activated sludge. *Int. J. Syst. Evol. Microbiol.* 66, 385–390. doi: 10.1099/ijsem.0.000728

Wang, Q., Garrity, G. M., Tiedje, J. M., and Cole, J. R. (2007). Naive Bayesian classifier for rapid assignment of rRNA sequences into the new bacterial taxonomy. *Appl. Environ. Microbiol.* 73, 5261–5267. doi: 10.1128/aem.00062-07

White, C., and Gadd, G. M. (1990). Biosorption of radionuclides by fungal biomass. *J. Chem. Technol. Biotechnol.* 49, 331–343. doi: 10.1002/jctb.280490406

White, C., Sharman, A. K., and Gadd, G. M. (1998). An integrated microbial process for the bioremediation of soild contaminated with toxic metals. *Nat. Biotechnol.* 16, 572–575. doi: 10.1038/nbt0698-572

Willems, A., Busse, J., Goor, M., Pot, B., Falsen, E., Jantzen, E., et al. (1989). *Hydrogenophaga*, a new genus of hydrogen-oxidizing bacteria that includes *Hydrogenophaga flava* comb. nov. (formerly *Pseudomonas flava*), *Hydrogenophaga palleronii (*formerly *Pseudomonas palleronii), Hydrogenophaga pseudoflava* (formerly *Pseudomonas pseudoflav*). *Int. J. Syst. Bacteriol.* 39, 319–333. doi: 10.1099/00207713-39-3-319

Wingender, J., Neu, T. R., and Flemming, H.-C. (1999). *Microbial Extracellular Polymeric Substances?: Characterization, Structure, and Function*, eds J. Wingender, T. R. Neu, and H.-C. Flemming (Berlin: Springer).

WNA (2016). *World Nuclear Performance Report 2016*. London: World Nuclear Association.

WNA (2018a). *Nuclear Power in the United Kingdom*. Available online at: http://www.world-nuclear.org/information-library/country-profiles/countries-t-z/united-kingdom.aspx (accessed February 4, 2019).

WNA (2018b). *Radioactive Waste Management*. Available online at: http://www.world-nuclear.org/information-library/nuclear-fuel-cycle/nuclear-wastes/radioactive-waste- (accessed May 25, 2019).

Wolfram, J. H., Mizia, R. E., Jex, R., Nelson, L., and Garcia, K. M. (1996). *The Impact of Microbially Influenced Corrosion on Spent Nuclear Fuel and Storage Life*. Idaho Falls, ID: Idaho National Laboratory.

Yoon, J. H., Lee, M. H., and Oh, T. K. (2004). *Porphyrobacter donghaensis* sp. nov., isolated from sea water of the East Sea in Korea. *Int. J. Syst. Evol. Microbiol.* 54, 2231–2235. doi: 10.1099/ijs.0.63226-0

Yoon, J. H., Tsukada, N., Sakai, Y., Ishii, M., Igarashi, Y., and Nishihara, H. (2008). Isolation and characterization of a new facultatively autotrophic hydrogen-oxidizing *Betaproteobacterium*, *Hydrogenophaga* sp. AH-24. *FEMS Microbiol. Lett.* 278, 94–100. doi: 10.1111/j.1574-6968.2007.00983.x

Yu, J. (2018). Fixation of carbon dioxide by a hydrogen-oxidizing bacterium for value-added products. *World Microbiol. Technol.* 34:89.

Yurkov, V., Stackebrandt, E., Holmes, A., Fuerst, J. A., Hugenholtz, P., Golecki, J., et al. (1994). Phylogenetic positions of novel aerobic, bacteriochlorophyll a-containing bacteria and description of *Roseococcus thiosulfatophilus* gen. nov., sp. nov., *Erythromicrobium ramosum* gen. nov., sp. nov., and *Erythrobacter litoralis* sp. nov. *Int. J. Syst. Bacteriol.* 44, 427–434. doi: 10.1099/00207713-44-3-427

Yurkov, V. V. (2015). "*Roseococcus*," in *Bergey's Manual of Systematics of Archaea and Bacteria*, eds V. Yurkov, E. Stackebrandt, A. Holmes, J. A. Fuerst, P. Hugenholtz, J. Golecki et al. (Hoboken, NJ: John Wiley & Sons, Inc.), 1–4. doi: 10.1002/9781118960608.gbm00887

Zhu, T., and Dittrich, M. (2016). Carbonate precipitation through microbial activities in natural environment, and their potential in biotechnology: a review. *Front. Bioeng. Biotechnol.* 4:4. doi: 10.3389/fbioe.2016.00004

Conflict of Interest: Additional funding was provided by Sellafield. The funder played no role in the study design and analysis, decision to publish, or preparation of the manuscript. Sellafield Ltd., did provide pond samples and detailed pond data was collected as part of routine operations.

NC was employed by Sellafield Ltd.

The remaining authors declare that the research was conducted in the absence of any commercial or financial relationships that could be construed as a potential conflict of interest.

frontiers in Microbiology

ORIGINAL RESEARCH
published: 11 January 2021
doi: 10.3389/fmicb.2020.515319

Genomic and Functional Characterization of *Enterococcus faecalis* Isolates Recovered From the International Space Station and Their Potential for Pathogenicity

*Noelle C. Bryan[1], Francois Lebreton[2,3], Michael Gilmore[2], Gary Ruvkun[4], Maria T. Zuber[1] and Christopher E. Carr[1,4,5]**

[1] Department of Earth, Atmospheric and Planetary Sciences, Massachusetts Institute of Technology, Cambridge, MA, United States, [2] Department of Ophthalmology, Massachusetts Eye and Ear Infirmary, Boston, MA, United States, [3] Walter Reed Army Institute of Research, Silver Spring, MD, United States, [4] Department of Molecular Biology, Massachusetts General Hospital, Boston, MA, United States, [5] Georgia Institute of Technology, Atlanta, GA, United States

OPEN ACCESS

Edited by:
Rakesh Mogul, California State Polytechnic University, Pomona, United States

Reviewed by:
Kasthuri Venkateswaran, NASA Jet Propulsion Laboratory (JPL), United States
Madhan Tirumalai, University of Houston, United States

***Correspondence:**
Christopher E. Carr
chrisc@mit.edu

Specialty section:
This article was submitted to Extreme Microbiology, a section of the journal Frontiers in Microbiology

Received: *27 November 2019*
Accepted: *09 December 2020*
Published: *11 January 2021*

Citation:
Bryan NC, Lebreton F, Gilmore M, Ruvkun G, Zuber MT and Carr CE (2021) Genomic and Functional Characterization of Enterococcus faecalis Isolates Recovered From the International Space Station and Their Potential for Pathogenicity. Front. Microbiol. 11:515319. doi: 10.3389/fmicb.2020.515319

Enterococcus faecalis is a multidrug resistant, opportunistic human pathogen and a leading cause of hospital acquired infections. Recently, isolates have been recovered from the air and surfaces onboard the International Space Station (ISS). Pangenomic and functional analyses were carried out to assess their potential impact on astronaut health. Genomes of each ISS isolate, and both clinical and commensal reference strains, were evaluated for their core and unique gene content, acquired antibiotic resistance genes, phage, plasmid content, and virulence traits. In order to determine their potential survival when outside of the human host, isolates were also challenged with three weeks of desiccation at 30% relative humidity. Finally, pathogenicity of the ISS strains was evaluated in the model organism *Caenorhabditis elegans.* At the culmination of this study, there were no defining signatures that separated known pathogenic strains from the more commensal phenotypes using the currently available resources. As a result, the current reliance on database information alone must be shifted to experimentally evaluated genotypic and phenotypic characteristics of clinically relevant microorganisms.

Keywords: International Space Station (ISS), *Enterococcus faecalis*, pangenome, antibiotic resistance, desiccation tolerance, pathogenicity

INTRODUCTION

Enterococcus faecalis represent a core, yet quantitatively minor portion of the human gut microbiome (Schloissnig et al., 2013) that are well suited to persist outside of the host environment. Evidence recently emerged that the enterococci may have split from their last common ancestor at approximately the time animal life began to colonize terrestrial habitats (∼425 million years ago), and traits that promote survival and transmission in the exposed land environment selected for the characteristic ruggedness of the genus (Lebreton et al., 2017). Supporting that proposition,

enterococci display significantly higher levels of resistance to a variety of antiseptics, salts, organic compounds, desiccation, and starvation than ancestral outgroups (Lebreton et al., 2017).

Because traits contributing to environmental persistence also contribute to persistence in the hospital environment, enterococci rank among leading causes of healthcare associated infections (Weiner et al., 2016). While certain strains of *E. faecalis* are pathogenic for hospitalized patients, *e.g.*, MMH594 (Huycke et al., 1991) and V583 (Sahm et al., 1989), and possess genomes swollen to 3.3 Mb by the accretion of mobile genetic elements (MGEs), the genomes of commensal isolates are 25% smaller, as typified by the strain OG1RF (Bourgogne et al., 2008). In the antibiotic era, loss of CRISPR (clustered regularly interspaced short palindromic repeats) protection of the chromosome further facilitated the accumulation of additional antibiotic resistance by enterococci (Fiore et al., 2019). Several other MGEs have been directly linked to virulence factors (Shankar et al., 2002), however, the selective value of most mobile elements in clinical isolates of enterococci remains to be determined.

The ISS provides a unique opportunity to study the establishment of a microbiome in what originated as a clean, hermetically sealed built environment, where the influx of new microorganisms only occurs periodically with the arrival of new crew and supplies. The microbiome of the ISS has been extensively characterized in recent years by metagenomic (Be et al., 2017; Lang et al., 2017; Singh et al., 2018b; Urbaniak et al., 2018; Blaustein et al., 2019; Mora et al., 2019; Sielaff et al., 2019) and culture-based investigations (Schiwon et al., 2013; Venkateswaran, 2017; Singh et al., 2018a; Blaustein et al., 2019; Mora et al., 2019; Sobisch et al., 2019; Urbaniak et al., 2019), yet only recently have these effort been combined (Mora et al., 2019; Sielaff et al., 2019). The results are divided among those that report similarities to Earth built environments (Schiwon et al., 2013; Mora et al., 2019; Sielaff et al., 2019) including United States based spacecraft assembly cleanrooms (Be et al., 2017), and those that detected significant differences from terrestrial residences, the Human Microbiome Project (Lang et al., 2017), the Japan-based ISS analog module (Ichijo et al., 2016), and a French Guiana-based cleanroom (Mora et al., 2019). Despite the differences in methodologies and results, the detection of opportunistic human pathogens (Schiwon et al., 2013; Be et al., 2017; Lang et al., 2017; Mora et al., 2019; Singh et al., 2018a,b; Sielaff et al., 2019; Sobisch et al., 2019; Urbaniak et al., 2019) including *E. faecalis,* is a common phenomenon. With the exception of Be et al. (2017), the previous metagenomic efforts were limited to characterizing diversity at the genus level or identifying antibiotic resistance or virulence gene content, and thereby lacked the genetic resolution to confidently identify pathogenic bacterial strains. While genome-based pathogenicity analyses have been performed for *Staphylococcus aureus* (Blaustein et al., 2019) and *Enterobacter bugandensis* (Singh et al., 2018a), only a single culture-based report has quantified pathogenicity (*Fusarium oxysporum* isolates from the ISS Urbaniak et al., 2019) in a host model. As a result, the ability to predict how opportunistic pathogens may impact crew health remains unclear.

In addition to characterizing the microbiome of the ISS, understanding the effects of spaceflight on bacterial physiology will be imperative for assessing the impacts on crew health. When *Pseudomonas aeruginosa* was exposed to spaceflight, there was an increase in the total cell viable numbers, biomass, biofilm thickness, and the cells produced a unique biofilm architecture not seen in ground controls of the species (Mclean et al., 2001; Kim et al., 2013). Su et al. (2014) documented growth curve, transcriptomic, and proteomic alterations (related to amino acid transport, metabolism, energy production, and conversion) in *Bacillus cereus* and *Serratia marcescens* during spaceflight (Wang et al., 2014). Carbon utilization profiles were altered among *S. marcescens* clones after flight, and transcriptomic and proteomic data revealed significant changes in metabolic functions (Wang et al., 2014). Additionally, Wilson et al. (2007) utilized proteomic analysis and expression profiles to demonstrate that changes in genomic regulation of *Salmonella typhymurium* were widely distributed, and virulence was increased in response to spaceflight. Although Hammond et al. (2013) report a significant decrease in *E. faecalis* OG1RF virulence when grown under spaceflight conditions, this was inferred by a reduction in the optical density of cultures grown in the presence of adult *Caenorhabditis elegans* rather than worm viability.

In addition to altered microbial physiological responses, astronaut health is also impacted by the spaceflight environment. Factors such as microgravity, physiological stress, isolation, abnormal circadian rhythms, and altered nutrition have been shown to weaken an astronaut's immunity in as little as 10 to 15 days (Crucian et al., 2013), and these effects can persist up to 6 months post mission ISS (Crucian et al., 2015). This weakened immunity, combined with the prevalence of *E. faecalis* strains, or other potential pathogens including viruses (Rooney et al., 2019), could result in severe human health consequences on board the ISS, even in incidences of routine medicinal procedures (*i.e.*, the introduction of a percutaneous catheter Mermel, 2012).

With the detection of enterococci, we sought to determine the risk they posed to residents within the ISS – specifically, do they represent pathogenic lineages commonly associated with infections in hospitals, or do they represent commensals shed into the environment as a consequence of human habitation? In order to determine if the challenging environment of the air and surfaces of the ISS have selected for pathogenic strains of *E. faecalis*, we coupled previously employed genomic data analyses (Singh et al., 2018a) with phenotypic characterization of *E. faecalis* isolates recovered onboard the ISS. By assessing their antibiotic resistance, desiccation tolerance, and pathogenicity in the well-established *C. elegans* model (Garsin et al., 2001), we sought to test existing methods for identification of strains of *E. faecalis* with a high likelihood of causing in-flight infections.

MATERIALS AND METHODS

Strains and Culture Conditions

Bacterial isolates from the ISS (**Figure 1** and **Table 1**) were initially recovered on tryptic soy agar, and preliminary

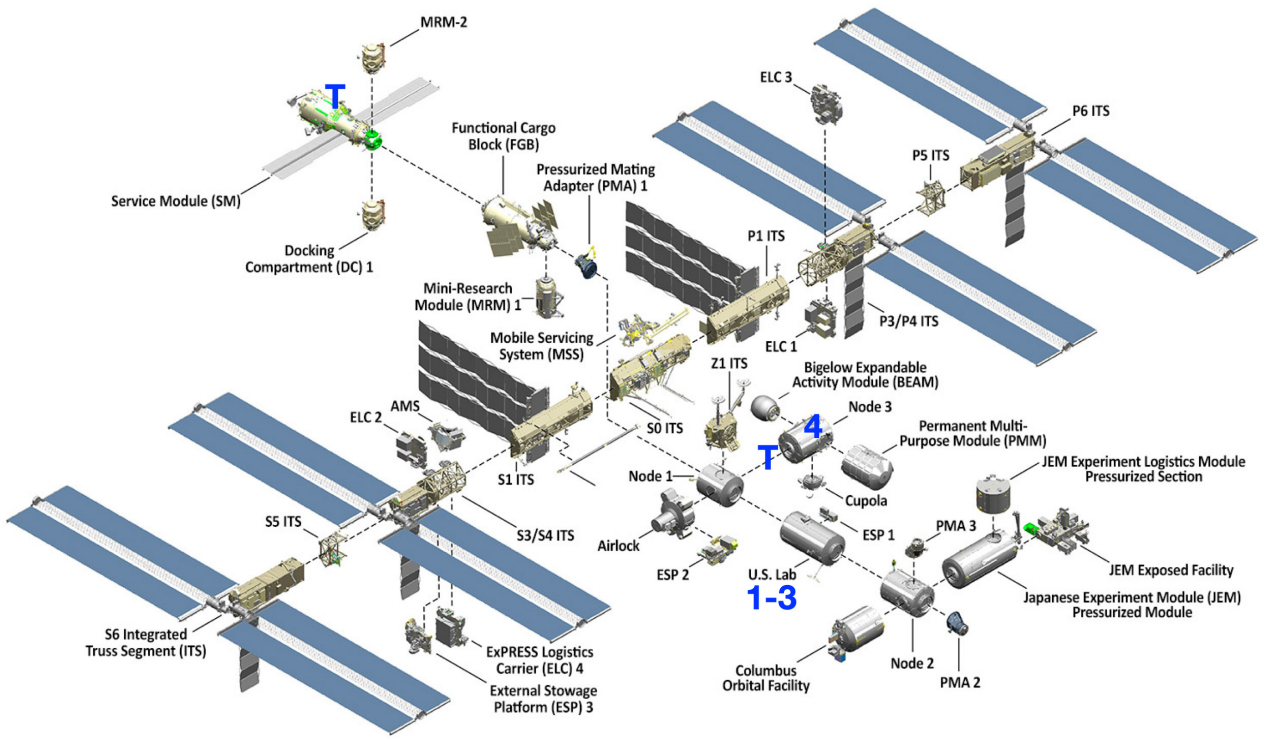

FIGURE 1 | Isolate recovery locations on the International Space Station. Isolates (denoted 1-4) were recovered from the United States Lab and Node 3. Toilets (T) are located in Zvezda (Service Module) and Tranquility (Node 3).

identification was performed using a VITEK identification system (bioMérieux, Hazelwood, MO, United States) as previously described (Castro et al., 2004). *E. faecalis* isolates OG1RF, MMH594, V583, and the genome sequences of *E. faecalis* 5952 and JH-1 were made available from the Gilmore lab strain collection. All additional available whole genomes of *E. faecalis* (N = 44) were obtained from the National Center for Biotechnology Information (NCBI).

Except where described below, cultures of *E. faecalis* OG1RF, MMH594, V583, and the ISS isolates (**Table 1**) were grown aerobically with shaking (250 RPM) at 37°C in brain heart infusion (BHI; Difco™, cat. no: 237500) broth. Growth kinetics for each isolate was assessed using a Synergy 2 microplate reader (Bio-Tek Instruments Inc.), measuring optical density at 620 nm. Minimum inhibitory concentration (MIC) for various antibiotics was evaluated in both Mueller-Hinton (MH) broth or in BHI, as further detailed below. For the desiccation experiments, isolates were grown overnight in a chemically defined medium (CDM; Hussain et al., 1991) and plated onto M9 (Difco™, cat. no: 237500) agar plates amended with 1.0% glucose. To perform the *C. elegans* pathogenicity assays, cultures of *Escherichia coli* OP50 were prepared on nematode growth media (NGM) agar plates as previously described (Powell and Ausubel, 2008).

Genome Sequencing of ISS Strains

For preparation of DNA, isolates were grown overnight in BHI broth. Cells were lysed using lysozyme (50 μg mL^{-1}) and mutanolysin (2500 U mL^{-1}), and the total DNA was isolated using the DNeasy Blood and Tissue Kit (Qiagen©, cat. no: 69504). Purified DNA was used for preparing libraries, which were then sequenced on Illumina HiSeq (250 nucleotide paired end reads) as previously described (**Supplementary Table S1** in Lebreton et al., 2017).

Additionally, a MinION (Oxford Nanopore Technologies©; ONT) library was prepared using the "one-pot" barcoding protocol, as developed by Josh Quick and the Loman Lab[1]. For each isolate, 24 μL of AMPure XP (Beckman Coulter® Life Sciences cat. no.: A63880) eluate was used as input for library preparation. This was incubated at room temperature (RT) for 5 min, 65°C for 5 min, then placed on ice for 30 s. Samples were barcoded using the Rapid Barcoding Kit (ONT cat. no.: SQK-RBK001) and each was incubated at RT for 10 min, 70°C for 5 min, then placed on ice. The reaction product was then pooled with other samples (N = 4 total) in a clean 1.5 mL low-bind Eppendorf tube, before addition of 26.75 μl AMPure XP beads per sample. This was incubated at RT for 5 min, placed on the magnet rack until clear, and the supernatant removed. The beads were washed with 200 μl 70% ethanol, incubated for 30 s, and the supernatant removed (2X) before spinning down and removal of the residual 70% ethanol. After air drying for 1 min, the beads were resuspended in 31 μl elution buffer (EB, 10 mM Tris–HCl pH 8), incubated off the magnet rack for 5 min, returned to

[1]https://lab.loman.net/protocols/

TABLE 1 | Summary of genomic characterization of ISS and control strains of *Enterococcus faecalis*.

Isolate (Accession Number)	Sample Type	Location	Collection Date	Expedition (Duration in days)	Genome size (Mb)	No. Unique Genes	MLST	Predicted Intact Phage	Plasmids	Pathogen Score (%)
ISS_1 (CP046113)	Air	United States LAB	7/15/2009	20 (137)	2.65*	11	875**	No	No	84.4
ISS_2 (CP046112)	Surface	United States LAB	4/15/11	27 (70)	2.93*	39	30	3	No	85.4
ISS_3 (CP046111)	Surface	United States LAB	4/15/11	27 (70)	2.94*	39	30	3	No	85.4
ISS_4 (CP046108-10)	Air	Node 3	10/23/13	37 (61)	2.91*	25	40	1	2	85.4
OG1RF‡	Oral	NA	≤ 1975	NA	2.74	61	1	No	No	81.6
MMH594‡	Blood	NA	1985	NA	3.25	52	6	1	3	82.9
V583‡	Blood	NA	1987	NA	3.36	20	6	1	3	82.9

*Results of hybrid assemblies (See **Supplementary Information**).
**Single nucleotide variant of the nearest ST.
‡McBride et al. (2007).
NA: Not applicable.

the rack. DNA was quantified by fluorescence (ThermoFisher Scientific© Qubit 3.0 with Qubit dsDNA HS Assay Kit; cat. no.: Q32854) and the sequencing adaptors were ligated (ONT cat. no.: SQK-LSK109) following the manufacturer's protocols. This tube was incubated at RT for 10 min, 45.5 μl AMPure XP beads added, incubated for another 5 min, placed on magnet rack until clear, and the supernatant removed. Next, 150 μl ABB was added and the beads resuspended by flicking, before placing the tube back on the magnet rack until clear. The supernatant was removed and the ABB wash repeated before spinning down the tube and removing the residual supernatant. Next, 12 ul EB was added and the bead resuspended by flicking before incubation at RT for 5 min. The tube was placed again on the magnet rack until clear, and the elution library was loaded on to an ONT MinION flow cell (R9.4.1) according to the manufacturer's protocols and sequenced using MinKNOW (v1.11.5) with live basecalling (**Supplementary Table S2**). Output fastq files were concatenated and adaptors were removed and debarcoded with PoreChop (v0.2.3[2]). Reads were quality filtered (≥ Q9) using NanoFilt (v2.2.0), and NanoPlot (v1.13.0) was then used to characterize sequencing datasets (De Coster et al., 2018).

Genome Assembly

Unicycler (v0.4.4) was used for long-read and hybrid assembly using default parameters, with the initial long-read assembly specified via the –existing_long_read_assembly flag for hybrid assembly (Wick et al., 2017). BWA (v0.7.17-r1188 with -x ont2d flag; docker container alexcoppe/bwa:latest) was used to map long reads onto the hybrid assembly to inspect assemblies and verify lack of evidence of mis-assemblies based on coverage. CheckM (v1.0.7) was used to evaluate completeness of final hybrid assemblies described in **Table 1** (Parks et al., 2015).

Pangenomic and Phylogenetic Analysis

Genomes were annotated using Prokka (v.1.14.6; docker container quay.io/biocontainers/prokka:1.14.6–pl526_0 Seemann, 2014), and the pangenome analysis was performed using Roary (v3.12.0; docker container staphb/roary:3.12.0 Page et al., 2015). Genes that were present in a single isolate were defined as unique genes and, for strains utilized in this study, their identities were further examined by BLASTn (Altschul et al., 1990) for comparison to the NCBI non-redundant database. Based on DNA sequence comparison, an *E. faecalis* phylogenetic tree (**Figure 2A**) was constructed from the Roary-determined core gene alignment (1.69 Mb) using FastTree (docker container staphb/fasttree:2.1.11) using the General Time Invariant (GTR) model, and visualized using IcyTree (Vaughan, 2017). For a list of all genomes and gene presence/absence data see **Supplementary Data File S1**.

Comparative Genomic Analysis

Multilocus sequence typing (MLST) was performed by evaluating seven *E. faecalis* genes (*aroE*, *gdh*, *gki*, *gyd*, *pstS*, *xpt*, and *yqiL*) and sequence types (STs) assigned based on the alleles present in each genome (Larsen et al., 2012). The potential presence

[2]https://github.com/rrwick/Porechop

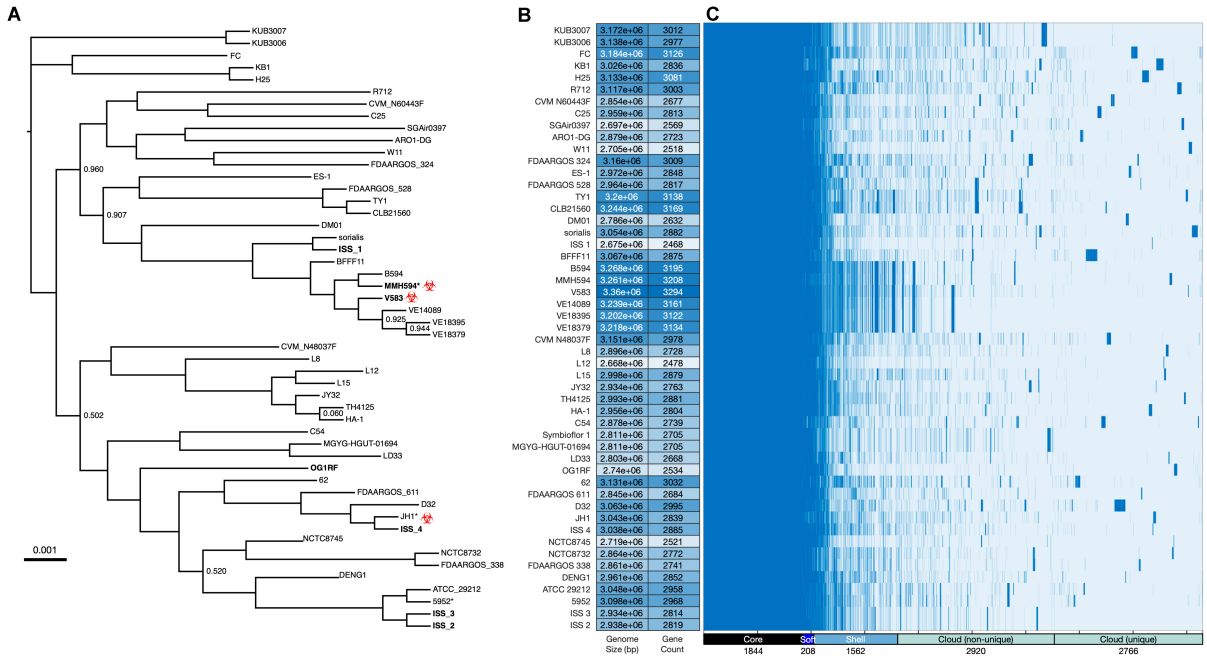

FIGURE 2 | Whole genome analysis of *Enterococcus faecalis*. **(A)** Phylogenetic analysis of *E. faecalis* strains was determined based on FastTree generalized-time-reversible (GTR) analysis of SNPs present in the 1,844 core genes as determined by Roary (Page et al., 2015) and visualized with IcyTree (Vaughan, 2017). The alignment, when corrected for gaps and ambiguous bases, was 1.69 Mb. Branch support was 100% except as indicated. Isolates used in this study are indicated in **bold**. Asterisk (*) denotes an unfinished genome assembly (contigs). Clinical isolates that are phylogenetic neighbors of the ISS isolates are tagged with the biohazard symbol. **(B)** Genome size and gene count, the latter as estimated by Prokka (Seemann, 2014). **(C)** Gene presence/absence as estimated by Roary for the total of 9300 genes identified across the 51 genomes. A histogram of these data is provided as **Supplementary Figure S1**.

of plasmids was assessed using PlasmidFinder (Carattoli et al., 2014). VirFinder was used to detect potential *E. faecalis* virulence factor genes (Joensen et al., 2014), and PathogenFinder provided a predictive score for each strain's potential pathogenicity for humans (Cosentino et al., 2013). Additionally, the web server PHAge Search Tool – Enhanced Release (PHASTER) was used to detect the presence of phage sequences within bacterial genomic data (Arndt et al., 2016), and the Comprehensive Antibiotic Resistance Database (CARD) was used to identify genes potentially associated with antimicrobial resistance (Jia et al., 2016). The presence of CRISPR (clustered regularly interspaced short palindromic repeats) arrays and Cas (CRISPR associated proteins) was detected using the online tool, CRISPRCasFinder (Couvin et al., 2018). Capsule type polymorphisms were determined as described by McBride et al. (2007). Briefly the presence, or absence, of genes in the locus (EF2485 to EF2495) were verified in the genomes of each isolate. CPS type 1 strains are defined as isolates with *cpsA* and *B,* and *hcp1* (EF2484), while CPS type 2 strains consist of the full *cps* locus and *hcp1* (EF2484 to EF2495). CPS type 5 strains are similar to the type 2 gene profile, but do not contain *cpsF* (EF0090).

Minimum Inhibitory Concentration of Antibiotics

Antibiotic MIC was determined by broth microdilution as described (CLSI, 2017). Briefly, overnight cultures of isolates were diluted and 10^4 cells in MH broth were inoculated into each well of 96 well plates containing serial 2-fold dilutions of antibiotics. Maximum concentration tested: penicillin (10 μg mL^{-1}), amoxicillin (10 μg mL^{-1}), ampicillin (10 μg mL^{-1}), oxacillin (256 μg mL^{-1}), erythromycin (50 μg mL^{-1}), and tetracycline (64 μg mL^{-1}). This procedure was repeated in BHI (McBride et al., 2007), and isolates were additionally evaluated for high level aminoglycoside resistance (HLGR) with: gentamicin, streptomycin, and kanamycin (each at a maximum concentration of 2 mg mL^{-1}). Plates were incubated at 37°C and growth was monitored at 24 and 48 h. Wells containing the lowest antibiotic concentration lacking growth after 48 h were designated the MIC for the respective antibiotics.

Desiccation Survival

Survival to desiccation was assessed as previously described (Lebreton et al., 2017; Bryan et al., 2019) with the following modifications. *E. faecalis* isolates were harvested from stationary phase by centrifugation, and washed twice with sterile (autoclaved, 0.22 μm filtered) water (sH_2O). Prior to desiccation, the concentrated cells were resuspended in CDM, and a 10 μL sample was track diluted (Jett et al., 1997) onto M9 medium (M9; Amresco®, cat. no.: J863-500G) amended with 0.1% glucose agar, and incubated at 37°C. After ∼24 h, the number of CFUs recovered from 10 μL track dilutions prepared according to Jett et al. (1997) were used to determine

the original concentration of cells mL^{-1} ($t = -1$). Aliquots of cell suspensions (50 μL) were spotted onto autoclaved coverslips, and placed into the desiccation chamber containing Drierite® (≥ 98% $CaSO_4$, W. A. Hammond Drierite Company, Ltd., cat. no.: 778-18-9) until the liquid evaporated ($t = 0$, 24 h). The relative humidity (RH) in the chamber was monitored using a digital hygrometer, and maintained between 30-40% by adding additional Drierite®. Three replicates were prepared for each isolate at each timepoint. The dried cells were removed from the coverslips by rinsing and resuspending the material with a pipet into 1 mL of sH_2O. To ensure the samples were homogenously resuspended, rehydrated cells were incubated at 37°C for 1 h while shaking (225 RPM), and vortexed for 15 minutes. The cells were then serially diluted into sH_2O and 10 μL track dilutions were plated onto M9 agar. At the $t = 0$ time point, the number of CFUs recovered from the substrate was designated as the starting population size that survived the initial drying on the coverslip (N_0). Subsequent samples were removed from the desiccation chamber every three days and rehydrated as described above to determine the number of surviving CFUs over time (N). The surviving fraction of cells was determined from the ratio of N/N_0. Each time point was evaluated when N was ≥ 30 CFU.

Pathogenicity of *E. faecalis* isolates in a *C. elegans* model

Nematode killing assays were performed as previously described (Yuen and Ausubel, 2018). Briefly, *C. elegans fer-15;fem-1* (CF512) worms were grown on NGM inoculated with *E. coli* strain OP50 and incubated at 15°C until they reached the L4 stage. Approximately 30–40 of the L4 stage worms were then transferred to BHI agar plates (amended with kanamycin, 10 μg mL^{-1}) inoculated with 100 μL aliquots of each log phase *E. faecalis* isolate. The plates were incubated at 25°C and worms were examined for viability. Worms that did not exhibit movement nor respond to physical touch were scored as dead and removed from the plate. Moving worms were scored as alive and also counted.

Statistical Analyses

Statistical analyses for the desiccation experiments were performed using JMP® Pro v.14.3 (JMP®, 2019). Prior to evaluating the data for significant differences, the data were assessed for equal variances. Subsequent one-way ANOVAs were performed to determine the significant differences of desiccation survival at different timepoints and among individual isolates. *Post hoc* comparisons for time were performed using parametric comparisons with a control using Dunnett's method ($N = 18$ for each isolate, with the exception of $t = 12$ d where $N = 17$). The mean N/N_0 for each isolate at $t = 21$ d was evaluated using the non-parametric comparison with a control performed following the Steel method ($N = 3$ for each isolate). Individual comparisons for survival at two timepoints were performed using a homoscedastic Student's *t*- test.

The survival of *C. elegans* on each *E. faecalis* isolate was performed in triplicate. A Kaplan-Meier log rank analysis was performed to evaluate the survival curves using OASIS-2 (Han et al., 2016) as previously described Yuen (Yuen and Ausubel, 2018). The data were determined to follow the normal distribution using the Shapiro-Wilk test (Han et al., 2016), and pairwise comparisons with Bonferroni-corrected p-values < 0.05 were considered significant. Data are reported as the average and the standard error (± SE) of the number of worms scored, and is reported in **Table 2**.

RESULTS

Isolates Recovered From the ISS

The *E. faecalis* isolates recovered from air samples (ISS_1 and ISS_4) were both collected mid-module. ISS_1 was isolated from air samples collected in the United States Lab in 2009, and ISS_4 was recovered from the air in Node 3 in 2013 (**Figure 1**). ISS_2 and ISS_3, were two isolates recovered in 2011 from the same location, United States Lab handrail surfaces, approximately 14 feet apart. One was collected from the aft end of the module (at the interface with Node 1), and the other was recovered mid-module. The United States Lab was launched in 2001, and houses the various science payloads conducting research onboard the ISS (Singh et al., 2018b). Node 3, launched in 2010, and houses the air revitalization and water recovery systems, as well as amenities for crew hygiene, the restrooms, and exercise devices (Singh et al., 2018b). With preliminary identification based solely on the VITEK identification system, the first task for the isolate characterization was to create a fully sequenced genome for each isolate (**Table 1**).

Pangenome Analysis

With the complete genomes for each isolate assembled, several web-based tools were utilized for genomic characterization. First, seven gene loci were evaluated for their respective MLST using the web-based MLST server (**Table 1**; Larsen et al., 2012). ISS_1 was determined to be a single locus variant of sequence type (ST) 875, with a single nucleotide polymorphism (SNP) in the 583 bases of *pstS*. Isolates ISS_2 and ISS_3 were identified as ST30. ISS_4 was classified as ST40, a commonly recovered ST and a member of one of the largest clonal clusters, CC40 (McBride et al., 2007). A clonal cluster is defined as a ST consisting of three or more isolates (McBride et al., 2007). CC40 is comprised of ST40 and ST114, many of which were isolated from clinical sources (McBride et al., 2007).

Based on the ST data described above, representative type strains were chosen for each as a comparator for each ISS ST (McBride et al., 2007), and a core genome of 1,844 genes shared by all 51 strains was defined (Page et al., 2015). An alignment of the core genome was then used to construct the phylogenetic tree (**Figure 2A**). Phylogenetic proximity of the selected type strains to the ISS isolates validated the selection based on ST. Genome size and gene count (**Figure 2B**) show patterns of genomic expansion and loss within clades; for example, within the clade containing V583 a general pattern of larger genome size and higher gene count is evident, yet nearby ISS_1 has a more streamlined genome in comparison to its neighbors. Genes are

TABLE 2 | Analysis of the survival of *Caenorhabditis elegans* infected with the ISS and control strains of *Enterococcus faecalis*.

Isolate	*N**	Restricted Mean			LT_{50}	Pairwise Comparisons**
		Days	SE	95% C.I.		
ISS_1	37.0	9.00	0.66	7.44–10.0	8.13	BC
ISS_2	33.0	13.0	0.53	12.5–14.5	12.9	AB
ISS_3	29.0	13.0	0.59	12.0–14.3	13.1	ABC
ISS_4	35.0	10.0	0.70	9.06–11.8	10.4	BC
OG1RF	42.0	10.0	0.48	9.5–11.3	10.0	BC
MMH594	35.0	9.00	0.50	8.4–10.3	8.88	BC
V583	34.0	11.0	0.91	8.71–12.3	9.00	ABC

*The data are reported as the restricted mean (± SE) of three replicates, with the exception of ISS_1 (N = 2 at t = 9 d). *Starting number of worms. **Pairwise analysis of each Kaplan-Meier survival curve using the log-rank test (Han et al., 2016). Those that were not significantly different from each other are indicated with a capital letter, with A being the least pathogenic ($p > 0.05$).*

classified into core, soft core, shell, and cloud on the basis of the number of isolates sharing each gene (**Figure 2C**; **Supplementary Figure S1**) and the Roary-estimated patterns of gene presence and absence highlight potential patterns of gene loss or gain (**Supplementary Data File S1**).

Unique chromosomal genes, defined as those genes that were present in a single isolate, were non-uniformly distributed across each isolate genome (**Supplementary Data File S1**). ISS_1 (Accession no.: CP046113) contained the fewest number of unique genes (11 genes), 9 of which were designated hypothetical by Prokka (Seemann, 2014) yet had homology with other *E. faecalis* genomes on the basis of BLASTn searches. Seven of the 11 unique genes formed a contiguous region suggestive of an operon, which contained two genes with known annotations, *mazG*, which encodes a nucleoside triphosphate pyrophosphohydrolase involved in survival under nutrient stress, and another that encodes an LPxTG-motif protein cell wall anchor domain protein. Neither ISS_2 (Accession no.: CP046112) nor ISS_3 (Accession no.: CP046111) contained individually unique genes. Consistent with this finding, analysis of the core alignment revealed that isolates ISS_2 and ISS_3 differed by only 14 bases. However, these two isolates shared 39 genes that were not present in any of the other strains analyzed, of which 30 were classified as hypothetical. ISS_4 (Accession no.: CP046108-110) had 25 unique genes, 16 of which were located on a plasmid (pTEF2); no unique genes were found on the second (pAD1) plasmid. Based on BLASTn analysis (**Supplementary Figure S2**), the majority of genes unique to the ISS strains are closely related to genes present in *Enterococcus* species, with all non-*Enterococcus* genera restricted to *Lactococcus*, *Lactobacillus*, and, with lower identity and query coverage, *Listeria* (**Supplementary Figure S3**).

Following the designations of McBride et al. (2007), the capsule type for each ISS strain was determined. All three known capsule type polymorphisms were detected from the ISS strains. ISS_1 contained the full *cps* locus (EF2485 to EF2495) and *hcp1 (*EF2484), and similar to MMH594 and V583, was designated CPS type 2. Isolates ISS_2 and ISS_3 contained the *cps* locus and *hcp1,* but lacked *cpsF* (EF0090). In agreement with previous analysis of two additional ST30 isolates (McBride et al., 2007), these strains were classified as CPS type 5. The strain ISS_4 contained only *cpsA* (EF0095), *cpsB* (EF0094), and *hcp1*, and like the other isolates of CC40 and OG1RF, was classified as CPS type 1 (McBride et al., 2007).

Assessment of Mobile Elements and Defense Systems

The Comprehensive Antibiotic Resistance Database (CARD) database identified the tetracycline resistance gene, *tetW/N/W*, in isolates ISS_2, ISS_3, and ISS_4, which was not present in OG1RF (Jia et al., 2016). The ISS *tetW/N/W* shared 69.3 (ISS_2 and ISS_3) and 69.1% (ISS_4) sequence homology with the reference sequence (Accession no.: ARO:3004442). The reference gene has been detected in 2.70% of the available *E. faecalis* isolates surveyed (Jia et al., 2016). A standard nucleotide BLAST search confirmed the *tetW/N/W* genes present in ISS_2 and ISS_3 shared 100% sequence identity to each other, and differed by three SNPs to the *tetW/N/W* gene present in ISS_4 (Altschul et al., 1990).

PHASTER identified the presence of intact phage in isolates ISS_2, ISS_3, and ISS_4 (**Supplementary Table S3**; Arndt et al., 2016). ISS_2 and ISS_3 each contained three intact phage nucleotide sequences. The CC40 member ISS_4 contained a single intact phage region. No intact phage were detected in either ISS_1 or OG1RF. Thirty two (82%) of the 39 genes shared only by ISS_2 and ISS_3 were associated with intact or incomplete phage (**Supplementary Data File S1**). Plasmid-born genomic elements were only detected in ISS_4 using the tool PlasmidFinder (**Table 1**; Carattoli et al., 2014). Two plasmids were determined to share 96.7% sequence identity, and 99% coverage, to the V583 plasmid pTEF2 (accession number: AE016831; Paulsen et al., 2003), and 96.0% identity, with 100% coverage, to the pheromone responsive plasmid pAD1 (accession number: L01794; Ehrenfeld and Clewell, 1987). Notably, evidence for *Lactobacillus prophage* Lj928 was identified for ISS_2, ISS_3, ISS_4, and V583 (**Supplementary Table S3**). Similarly, evidence for *Enterococcus phage* phiFL4A was identified for ISS_2, ISS_3, ISS_4, and MMH594 (**Supplementary Table S3**). Overall, mobile elements

explained a majority (65%) of the unique genes identified in the ISS isolates. High confidence CRISPR-Cas systems were detected in isolates ISS_1, ISS_4, and OG1RF (**Supplementary Table S4**). CRISPR loci without the Cas genes were detected in the genomes of each of the ISS isolates and OG1RF (**Supplementary Table S4**).

Genome-Based Assessment of the Potential for Pathogenicity

The PathogenFinder server scored each of the ISS isolates and the reference strains as potential human pathogens (**Table 1**; Cosentino et al., 2013). The commensal strain OG1RF had the lowest pathogen score of 81.6%. With pathogen scores > 84%, all of the ISS strains had a higher assigned probability to be pathogenic than the clinical isolates, MMH594 and V583 (each at 82.9%).

By comparing the genomic content of the isolates to known *E. faecalis* genes associated with disease, a second predictor of pathogenicity could be compiled (**Table 3**; Joensen et al., 2014). The genomes of the clinical isolates contained the highest proportion of predicted virulence factors (18/20), while ISS_2 and ISS_3 contained the least (13/20). ISS_1 and OG1RF both contained 15/20 virulence factors, and the genome ISS_4 was positive for 16/20. The clinical isolates and ISS_4 were the only strains to contain *agg*, encoding for the *E. faecalis* aggregation substance involved in biofilm formation, plasmid transfer, and increased virulence in endocarditis models (Bhatty et al., 2015).

MMH594 was the only isolate with *cylA*, one of the genes responsible for the production of cytolysin. Neither OG1RF nor the ISS isolates carried any of the genes in the cytolysin pathway reviewed by Coburn and Gilmore (2003).

Minimum Inhibitory Concentration of Antibiotics

Dilution concentration broth assays were used to determine the MIC for various antibiotics. Optical density measurements revealed there were no significant differences in the growth kinetics between the ISS isolates and the reference strains. Strains were first evaluated in Mueller-Hinton broth for comparison to clinical laboratory standards for antibiotic resistance of *E. faecalis* ATCC® 29212 (CLSI, 2017), and in the commonly used growth media BHI to determine MICs relative to the commensal isolate OG1RF. In MH broth, all strains tested exceeded the resistance levels set forth by ≥ 2-fold for amoxicillin, ampicillin, oxacillin, gentamycin, and kanamycin (CLSI, 2017). ISS_2, ISS_3, and ISS_4 were also categorized as resistant to tetracycline. When evaluated in BHI, all ISS strains exhibited MICs equivalent to OG1RF with the exceptions of oxacillin and tetracycline (**Table 4**). All ISS strains showed ≥ 4-fold more resistance to oxacillin. Isolates ISS_2, ISS_3, and ISS_4, each carrying a *tetW/N/W* gene, displayed an MIC of 64 $\mu g\ mL^{-1}$. These isolates were 4-fold more resistant to tetracycline than OG1RF (MIC of 16 $\mu g\ mL^{-1}$), and displayed resistance levels equivalent to the clinical isolates, MMH594 and V583. Unlike the clinical isolates, the ISS strains did not exhibit HLGR.

Desiccation Tolerance of *E. faecalis* Strains

During the initial 24 h dry down period, the RH in the desiccation chamber spiked to 56%. For the remainder of the experiment, the RH was maintained between 30-40% by adding additional Drierite®. The concentration of cells surviving the drying process (N_0) ranged from 1.2 (± 0.044) x 10^{10} to 5.5 (± 0.091) x 10^7 CFU for ISS-1 and OG1RF, respectively. The average number of survivors (N) after three weeks of desiccation ranged from 0.11 (± 0.024) to 8.5 (± 0.79) x 10^8 CFU for OG1RF and MMH594, respectively. OG1RF demonstrated the greatest loss in viability during dry down with a 2.1-log reduction, and ISS-2 was the only isolate that did not experience a significant loss in viability between t = 0 and t = 3 d (p = 0.11). There was no significant difference in N/N_0 at any of the timepoints evaluated (p = 0.98; **Figure 3**). When the variances of N/N_0 at t = 21 d for each isolate were determined to be significantly different from each other (F = 58, $p < 0.001$), a non-parametric comparison was performed with OG1RF chosen as the control using the Steel method. There was no significant difference in N/N_0 at t = 21 d among the isolates tested when compared to OG1RF (**Figure 3**).

Pathogenicity of Isolates in a *C. elegans* Model

The survival data (**Figure 4**) were determined to follow the normal distribution using the Shapiro-Wilk test (Han et al., 2016). With the exception of ISS_1, all data are reported as the mean (± SE) of three replicates. For ISS_1, one sample became contaminated with fungus on day 9, and all subsequent data are reported as N = 2. *C. elegans* was least susceptible to strains ISS_2, ISS_3, and V583 with mean survival times of 13 (± 0.53), 13 (± 0.59), and 11 (± 0.91) days, respectively (**Table 2**). While the time for 50% of the worm population to die (LT_{50}; Garsin et al., 2001) for these isolates ranged from 9 days (V583) to 14 (ISS_3), the total lifespan of worms challenged with these isolates were not significantly different from each other. For isolates ISS_2 and ISS_3, all worms were deceased by day 18 and 17, respectively. While 90% of worms fed V583 were dead by day 18, some survivors persisted until day 24. Additionally, the lifespan of worms infected with ISS_3 was also statistically similar to those challenged with ISS_4. With a 31% decrease in the mean lifespan, worms infected with ISS_1 were significantly more susceptible than isolates fed ISS_2 or ISS_3 ($p < 0.001$). Based on the survival curves of worms fed ISS_1, ISS_4, OG1RF, MMH594, and V583 there were no significant differences in the pathogenicity profiles for these isolates ($p > 0.05$).

DISCUSSION

While multiple studies have detected the presence of a wide range of opportunistic human pathogens onboard the ISS, the consensus was that additional data was needed to determine if these microorganisms posed an actual threat to crew health (Schiwon et al., 2013; Be et al., 2017; Lang et al., 2017; Singh et al., 2018a,b; Mora et al., 2019; Sielaff et al., 2019Sobisch et al., 2019;

TABLE 3 | The presence, and sequence identity (%), of known virulence factors of *Enterococcus faecalis* present in the ISS and reference genomes (Joensen et al., 2014).

Virulence factor	Identity (%)						
	ISS_1	ISS_2	ISS_3	ISS_4	OG1RF	V583	MMH594
ElrA	99.5	99.72	99.72	100	100	100	100
SrtA	100	100	100	100	100	100	100
ace	98.5	97.71	97.71	96.9	97.5	100	
agg				95.6		100, 96.8*	100
cCF10	99.8	99.9, 99.9*	99.9	99.8, 99.8*	100, 100*		
cOB1	100	100	100	99.9	100	100	100
cad	99.9	100	100	99.8	100	100	100
camE	100	99.6, 99.6*	99.6	100, 100*	100	100	100
cylA							99.8, 99.8*
cylL						100	100
cylM						100	100
ebpA	100	100	100	100	100	100	100
ebpB	100	99.8	99.8			100	100
ebpC	100			100	100	100	100
efaAfs	100	99.9	99.9	100	100	100	100
fsrB	99.9			100	100	100	100
gelE	99.4	99.9	99.9	100	100, 100*	100	100
hylA				99.9	100	100	99.7
hylB	99.9	99.5	99.5	99.6	100	100	100
tpx	100	100	100	100	100	100	100

**Multiple copies were detected.*

TABLE 4 | Minimum inhibitory concentration of antibiotics evaluated in BHI.

Isolate	Antibiotic MIC ($\mu g\ mL^{-1}$)								
	Penicillin	Amoxicillin	Ampicillin	Oxacillin	Erythromycin	Tetracycline	Gentamycin	Streptomycin	Kanamycin
ISS-1	10.0	> 10.0	2.50	256	1.56	16.0	125	500	500
ISS-2	5.00	> 10.0	2.50	128	1.56	64.0	125	500	500
ISS-3	5.00	> 10.0	2.50	128	1.56	64.0	125	500	500
ISS-4	10.0	> 10.0	2.50	128	1.56	> 64.0	62.5	500	250
OG1RF	5.00	> 10.0	2.50	32.0	1.56	16.0	125	500	500
MMH594	10.0	> 10.0	5.00	128	> 50.0	64.0	$> 2.00 \times 10^3$	1.00×10^3	$> 2.00 \times 10^3$
V583	2.50	10.0	2.50	256	> 50.0	64.0	$> 2.00 \times 10^3$	500	$> 2.00 \times 10^3$

Urbaniak et al., 2019). Here, we expanded upon previous genomic analyses in an effort to provide a framework for the determination of the pathogenic potential of *E. faecalis* isolates. For the comparative analyses, the commensal type strain OG1RF and the clinical isolates, MMH594 and V583, were chosen because of their extensive genotypic (Shankar et al., 2002; Paulsen et al., 2003; McBride et al., 2007; Bourgogne et al., 2008) and phenotypic characterization, specifically in regards to *C. elegans* pathogenesis (Garsin et al., 2001; Yuen and Ausubel, 2018). In addition, the *E. faecalis* genomes of strains 5952 and JH-1 were chosen as representative ST strains of the ISS isolates ISS_2 and ISS_3, and ISS_4, respectively.

While the amount of information that can be gleaned from a complete genome is large, the current methodologies (Singh et al., 2018a) are insufficient for the accurate assessment of pathogenicity for *E. faecalis* strains. The scores from the tool, PathogenFinder (Cosentino et al., 2013), predicted each of the ISS isolates as possessing > 84% probability of being pathogenic to humans, placing them above known clinical isolates MMH594 and V583 (**Table 1**). Another tool related to scoring pathogenicity, VirFinder, identified twenty virulence factors among the ISS strains, but fifteen were present in the commensal isolate OG1RF as well (**Table 3**). We cautiously interpret this to mean that ISS isolates do share some of the potentially virulence-related properties found in clinical isolates, but many of these are also shared by prototype commensal strains of *E. faecalis*. Further validation for these predictive algorithms applied to enterococci is needed in order to make more accurate predictions of which strains could impact human health. Predictions from PathogenFinder or its equivalent can be expected to improve if additional training data at the genus or species level is incorporated.

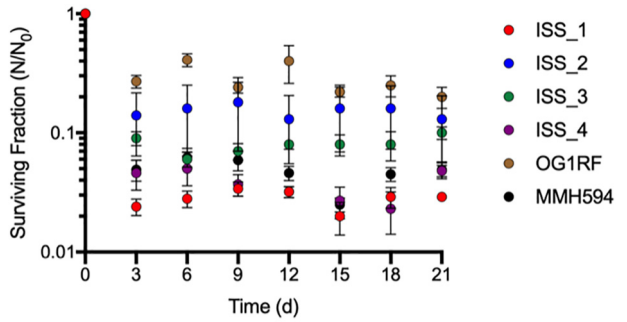

FIGURE 3 | Desiccation survival of *Enterococcus faecalis* strains from the ISS and the control strains, OG1RF and MMH594. The data are presented as the average (± SD) of triplicate measurements. Some error bars have been obscured by the data points.

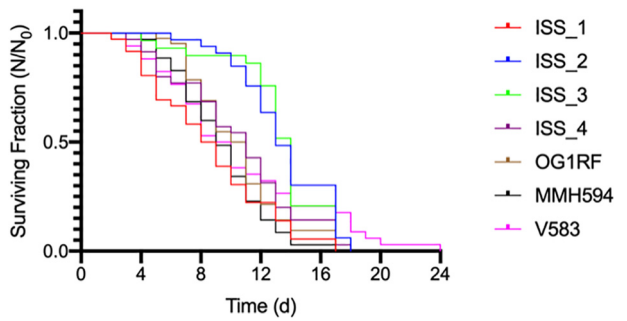

FIGURE 4 | The average survival of *Caenorhabditis elegans* exposed to ISS and control strains of *Enterococcus faecalis*.

Because of the difficulty in interpreting potential pathogenicity of the ISS strains based on genome content alone, we tested them directly in the *C. elegans* infection model (**Figure 4**). Previous studies identified parallels in the pathogenicity profiles of various enterococcal lineages when tested in *C. elegans* (Garsin et al., 2001) and in mice (Bourgogne et al., 2008). In contrast to that report (Garsin et al., 2001), we did not detect significant difference in *C. elegans* survival when exposed to commensal OG1RF, or pathogenic V583 and the cytolytic strain MMH594. *E. faecalis* proliferate in the intestine of *C. elegans* (Garsin et al., 2001) ultimately occluding it (Yuen and Ausubel, 2018). As a result, *C. elegans* infected with *E. faecalis* reach the LT_{50} 33% faster than worms fed a normal diet of *E. coli* OP50 (Garsin et al., 2001). None of the *E. faecalis* strains tested here, including ISS strains, exhibited enhanced *C. elegans* killing (**Figure 4**). Closely related strains ISS_2 and 3, despite possessing a high computed pathogenicity score, were found to be least able to kill *C. elegans* (**Figure 4**).

Additionally, there are currently no validated methods to predict phenotypic responses of enterococci to environmental stressors (*e.g.*, desiccation, starvation, increased cosmic radiation) based on their genomic content alone. Because each of the ISS isolates were recovered from air and surface samples, we examined them specifically for the ability to survive desiccation at RH relevant to the clinical environment (ASHRAE, 2013). In general, members of the genus *Enterococcus* are more desiccation tolerant than closely related microorganisms (Lebreton et al., 2017). Blaustein et al. (2019) demonstrated that the spaceflight environment onboard the ISS did not select for "extremo-tolerant" strains of *B. cereus* and *S. aureus*. Likewise, we found no significant differences in desiccation tolerance between the ISS *E. faecalis* isolates and their representative type strains (**Figure 3**). This indicates that their environmental survival in the ISS was attributable to the previously described intrinsically rugged nature of E. *faecalis* (Lebreton et al., 2017). Tirumalai et al. (2018) compared the genomes of the highly resistant *B. safensis* FO-36b and *B. pumilus* SAFR-032 to over 60 reference strains, and also failed to find genomic signatures for their increased environmental resistances (*e.g.*, desiccation, starvation, increased ultraviolet radiation). Rather, it is more likely the regulation of a suite of genes that confers increased resistance as a generalized stress response. In agreement with Blaustein et al. (2019) we conclude that the interior space environment (*e.g.*, microgravity, increased cosmic radiation) selects for intrinsically rugged species of bacteria, such as *E. faecalis,* but as of yet, there is no evidence suggesting selection for enhanced environmental persistence.

In agreement with previous observations (Schiwon et al., 2013; Sobisch et al., 2019), the *E. faecalis* isolates examined here were resistant to multiple antibiotics. While the detection of multidrug resistant bacteria may sound alarming, much of that resistance is intrinsic to all enterococci, and other genetic signatures indicate that these are largely commensal strains (**Table 3**). However, resistance to tetracycline displayed by ISS_2, ISS_3, and ISS_4 was found to be mediated by an acquired *tetW/N/W* gene, which confers an MIC equivalent to that of clinical isolates (**Table 4**). In addition to harboring genes that make combating infections difficult, *E. faecalis* strains possess the ability to spread antibiotic resistance to genes to other bacterial species, including the commonly isolated ISS inhabitant *S. aureus* (Sobisch et al., 2019). Although there have been no reports of VRE isolated from onboard the ISS at the time of this publication, it is important to note that both vancomycin resistance genes and *E. faecalis* genomic signatures were detected concurrently from the surface of the dining table during expedition 43 (Singh et al., 2018b). During the same mission, *E. faecalis* was also ranked the second most abundant BSL-2 microorganism in the metagenomic analysis of the entire campaign (Singh et al., 2018b). In fact, Mora et al. (2019) determined *Enterococcus* to be one of the ten indicator genera that distinguished the ISS microbiome from the human and indoor samples of the Home Microbiome Project (Mora et al., 2019).

There were several limitations to the data presented above. The desiccation survival experiments were terminated before any significant decrease in viability was observed. Extending the experiment until no surviving cells remained may have revealed a difference in the survival curves among the strains and provide insight to the length of time *E. faecalis* can remain viable. The lack of experimentally validated computational tools for *E. faecalis* led to conflicting results when comparing the genomes known clinical isolates to commensal strains. In addition, *C. elegans* serves as a rudimentary model system for human infection.

However, the challenges presented here provide the foundation for future investigations of *E. faecalis*, on Earth or in space.

As members of the core gut microbiome, *E. faecalis* will continue to be transported to the ISS and the ability to detect pathogenic strains will be beneficial for crew health. Unlike most environmental bacteria (Staley and Konopka, 1985), *E. faecalis* strains are routinely recovered on culture media. Based on the antibiotic resistance profiles presented here, incorporating the above high-level aminoglycosides to the routine onboard culturing activities could serve as the first step toward distinguishing pathogenic from commensal strains of *E. faecalis*. Because of their commonness as survivors on abiotic surfaces, their potential ability to infect, as well as the ability of *E. faecalis* to readily acquire and spread mobile elements conferring antibiotic resistance, continued microbial monitoring and pathogen identification will be important.

Current microbial monitoring of ISS air and surface sampling occurs once a month for the first 90 days of a mission, and decreases to one sample event for every 90 days thereafter (ISS-MORD, 2013). Because these microbial monitoring procedures are culture based, there is an inherent bias toward the small fraction of bacterial species that will form a colony on a plate (Staley and Konopka, 1985). Assessing the total microbial burden, and viable fraction, by combining genomic and culture-based analyses provides a more accurate representation of the ISS microbiome (Be et al., 2017; Mora et al., 2019; Sielaff et al., 2019). However, it is still unclear which, if any, of these microorganisms are relevant to crew health (Schiwon et al., 2013; Be et al., 2017; Lang et al., 2017; Singh et al., 2018a,b; Mora et al., 2019; Sielaff et al., 2019; Sobisch et al., 2019; Urbaniak et al., 2019).

The need for expedient identification of pathogenic microorganisms and their antibiotic resistance profiles is not a challenge unique to the spaceflight environment. Recent advances in rapid diagnostics have helped alleviate the clinical reliance on culture based techniques to identify infectious agents, yet these resources are not always widely available (Maurer et al., 2017). Fortunately, this is not the case for the ISS where the crew have access to Wetlab-2 Cepheid© SmartCycyler that can be used for quantitative PCR (qPCR) analysis of air, surface, water, and clinical samples[3]. Although it is currently configured to detect only a limited number of microbial pathogens, the RAZOR^{TM} EX BioDetection System (Idaho Technology Inc.) is currently being developed for in-flight microbial monitoring and could be modified for a wider range of microbial targets. Another promising technology for pathogen detection is the ONT MinION sequencing device employed above. Castro-Wallace et al. (2017) have previously validated its efficacy in the spacecraft environment. The MinION is currently capable of identifying bacterial species in near real time from metagenomic data (Sanderson et al., 2018) or isolated samples (Gargis et al., 2019) and has been used for the first ever off-Earth identification of bacteria cultured and sequenced in flight (Burton et al., 2020).

Due to the inability for the existing tools to distinguish pathogenic from commensal strains of *E. faecalis*, we make the following recommendations: Rather than continuing to wait for sample return and analysis using the current unvalidated databases, we suggest performing an initial screen for HLGR. Then, any isolates exhibiting HLGR should be sequenced using the MinION and evaluated for the presence of the type 2 capsule (McBride et al., 2007), the vancomycin resistance operon observed in V583 (Paulsen et al., 2003), components of the pathogenicity island (*e.g.*, cytolysin production loci and the enterococcal surface protein, Esp), and the absence of functional CRISPR-Cas arrays (Van Tyne et al., 2019). This information would then provide near real-time information for the crew regarding the need for additional decontamination procedures. These advancements would not be limited to *E. faecalis* isolates, however more accurate genomic targets for additional pathogen detection will need to be experimentally validated (Chiu and Miller, 2019). With the development of such targets, multiple pathogens (including bacteria, fungi, and viruses) can quickly be identified within a single sample (Miller et al., 2019).

[3]https://www.nasa.gov/spacebio/microbiology/hardware

DATA AVAILABILITY STATEMENT

The datasets generated for this study can be found in the NCBI BioProject website (https://www.ncbi.nlm.nih.gov/bioproject) using the BioProject ID: PRJNA587161 and the accession numbers SAMN13182395–SAMN13182398.

AUTHOR CONTRIBUTIONS

NB designed the experiments, performed the research, analyzed the data, and wrote the manuscript. CC assembled the genomes and advised on bioinformatic analysis and experimental design. MG advised on experimental design. FL advised on bioinformatic analysis and experimental design. GR and MZ advised and reviewed the manuscript. All authors contributed to the manuscript.

FUNDING

NB was supported by a NASA Space Biology Fellowship, award 80NSSC17K0688. CC was supported by NASA award NNX15AF85G.

ACKNOWLEDGMENTS

The authors would like to thank members of the Ruvkun, Ausubel, and Gilmore labs for their guidance during the experimental design. We also thank M. Ott for his input regarding the ISS samples.

SUPPLEMENTARY MATERIAL

The Supplementary Material for this article can be found online at: https://www.frontiersin.org/articles/10.3389/fmicb.2020.515319/full#supplementary-material

Supplementary Figure 1 | Gene membership of the 51 *Enterococcus faecalis* isolate genomes analyzed. Counts and categories as estimated by Roary analysis of presence/absence as described in the methods.

Supplementary Figure 2 | Sequence similarity of *Enterococcus faecalis* genes unique to ISS_1, ISS_2/ISS_3, and ISS_4. Query coverage and percentage sequence identity from BLASTn searches across all isolates (upper left) and for each isolate, respectively. Because ISS_2 and ISS_3 have no individually unique genes, and differ in their core gene alignment by only 14 bases, but have genes that are not represented in any of the other 49 genomes studied, ISS_3 was excluded from this analysis. **Supplementary Data File 1** contains details of each BLASTn hit.

Supplementary Figure 3 | Sequence similarity of *Enterococcus faecalis* genes unique to ISS_1, ISS_2/ISS_3, and ISS_4 segmented by the genus of the hit subject. Query coverage and percentage sequence identity from BLASTn searches are as in **Supplementary Figure S2** (upper left) after eliminating all hits associated with *Enterococcus* (upper left) and further segmenting by genus (there were only three remaining genera).

Supplementary Table 1 | Illumina HiSeq short read coverage estimates.

Supplementary Table 2 | Nanopore long read coverage estimates.

Supplementary Table 3 | Predicted intact phage content as determined by PHASTER for ISS and control *E. faecalis* isolates (Arndt et al., 2016).

Supplementary Table 4 | CRISPR-Cas system detection in the genomes of ISS and reference strains (Couvin et al., 2018).

Supplementary Data File 1 | Excel file listing all genomes used in the project, the detected presence/absence of each annotated gene for all genomes, and BLASTn hits for genes unique to the ISS isolates.

REFERENCES

Altschul, S. F., Gish, W., Miller, W., Myers, E. W., and Lipman, D. J. (1990). Basic local alignment search tool. *J. Mol. Biol.* 215, 403–410.

Arndt, D., Grant, J. R., Marcu, A., Sajed, T., Pon, A., Liang, Y., et al. (2016). PHASTER: a better, faster version of the PHAST phage search tool. *Nucleic Acids Res.* 44, W16–W21.

ASHRAE (2013). *ANSI/ASHRAE Standard 170-2013, Ventilation of Health Care Facilities*. Atlanta, GA: American Society of Heating, Inc.

Be, N. A., Avila-Herrera, A., Allen, J. E., Singh, N., Checinska Sielaff, A., Jaing, C., et al. (2017). Whole metagenome profiles of particulates collected from the International Space Station. *Microbiome* 5:81.

Bhatty, M., Cruz, M. R., Frank, K. L., Laverde Gomez, J. A., Andrade, F., Garsin, D. A., et al. (2015). *Enterococcus faecalis* pCF 10-encoded surface proteins PrgA, PrgB (aggregation substance) and PrgC contribute to plasmid transfer, biofilm formation and virulence. *Mol. Microbiol.* 95, 660–677. doi: 10.1111/mmi.12893

Blaustein, R. A., Mcfarland, A. G., Maamar, S. B., Lopez, A., Castro-Wallace, S., and Hartmann, E. M. (2019). Pangenomic approach to understanding microbial adaptations within a model built environment, the International Space Station, relative to human hosts and soil. *mSystems* 4: e00281-18.

Bourgogne, A., Garsin, D. A., Qin, X., Singh, K. V., Sillanpaa, J., Yerrapragada, S., et al. (2008). Large scale variation in *Enterococcus faecalis* illustrated by the genome analysis of strain OG1RF. *Genome Biol.* 9: R110.

Bryan, N. C., Christner, B. C., Guzik, T. G., Granger, D. J., and Stewart, M. F. (2019). Abundance and survival of microbial aerosols in the troposphere and stratopshere. *ISME J.* 13, 2789–2799. doi: 10.1038/s41396-019-0474-0

Burton, A. S., Stahl, S. E., John, K. K., Jain, M., Juul, S., Turner, D. J., et al. (2020). Off earth identification of bacterial populations using 16S rDNA Nanopore Sequencing. *Genes* 11:76. doi: 10.3390/genes11010076

Carattoli, A., Zankari, E., Garcìa-Fernandez, A., Larsen, M. V., Lund, O., Villa, L., et al. (2014). PlasmidFinder and pMLST: *in silico* detection and typing of plasmids. *Antimicrob. Agents Chemother.* 58, 2412–2414.

Castro, V., Thrasher, A. N., Healy, M., Ott, C. M., and Pierson, D. L. (2004). Microbial characterization during the early habitation of the International Space Station. *Microb. Ecol.* 47, 119–126. doi: 10.1007/s00248-003-1030-y

Castro-Wallace, S. L., Chiu, C. Y., John, K. K., Stahl, S. E., Rubins, K. H., Mcintyre, A. B., et al. (2017). Nanopore DNA sequencing and genome assembly on the International Space Station. *Sci. Rep.* 7:18022.

Chiu, C. Y., and Miller, S. A. (2019). Clinical metagenomics. *Nat. Rev. Genet.* 20, 341–355.

CLSI (2017). *Performance Standards for Antimicrobial Susceptibility Testing*. Wayne, PA: Clinical and Laboratory Standards Institute.

Coburn, P. S., and Gilmore, M. S. (2003). The *Enterococcus faecalis* cytolysin: a novel toxin active against eukaryotic and prokaryotic cells. *Cell. Microbiol.* 5, 661–669. doi: 10.1046/j.1462-5822.2003.00310.x

Cosentino, S., Larsen, M. V., Aarestrup, F. M., and Lund, O. (2013). PathogenFinder-distinguishing friend from foe using bacterial whole genome sequence data. *PLoS One* 8:e77302. doi: 10.1371/journal.pone.0077302

Couvin, D., Bernheim, A., Toffano-Nioche, C., Touchon, M., Michalik, J., Néron, B., et al. (2018). CRISPRCasFinder, an update of CRISRFinder, includes a portable version, enhanced performance and integrates search for Cas proteins. *Nucleic Acids Res.* 46, W246–W251.

Crucian, B., Stowe, R., Mehta, S., Uchakin, P., Quiriarte, H., Pierson, D., et al. (2013). Immune system dysregulation occurs during short duration spaceflight on board the space shuttle. *J. Clin. Immunol.* 33, 456–465. doi: 10.1007/s10875-012-9824-7

Crucian, B., Stowe, R. P., Mehta, S., Quiriarte, H., Pierson, D., and Sams, C. (2015). Alterations in adaptive immunity persist during long-duration spaceflight. *NPJ Microgravity* 1:15013.

De Coster, W., D'hert, S., Schultz, D. T., Cruts, M., and Van Broeckhoven, C. (2018). NanoPack: visualizing and processing long-read sequencing data. *Bioinformatics* 34, 2666–2669. doi: 10.1093/bioinformatics/bty149

Ehrenfeld, E., and Clewell, D. (1987). Transfer functions of the *Streptococcus faecalis* plasmid pAD1: organization of plasmid DNA encoding response to sex pheromone. *J. Bacteriol.* 169, 3473–3481. doi: 10.1128/jb.169.8.3473-3481.1987

Fiore, E., Van Tyne, D., and Gilmore, M. S. (2019). Pathogenicity of Enterococci. *Microbiol. Spectr.* 7:10.1128/microbiolspec.GPP3-0053-2018.

Gargis, A. S., Cherney, B., Conley, A. B., Mclaughlin, H. P., and Sue, D. (2019). Rapid detection of genetic engineering, structural variation, and antimicrobial resistance markers in bacterial biothreat pathogens by Nanopore sequencing. *Sci. Rep.* 9:13501.

Garsin, D. A., Sifri, C. D., Mylonakis, E., Qin, X., Singh, K. V., Murray, B. E., et al. (2001). A simple model host for identifying Gram-positive virulence factors. *Proc. Natl. Acad. Sci. U.S.A.* 98, 10892–10897. doi: 10.1073/pnas.191378698

Hammond, T. G., Stodieck, L., Birdsall, H. H., Becker, J. L., Koenig, P., Hammond, J. S., et al. (2013). Effects of microgravity on the virulence of *Listeria monocytogenes*, *Enterococcus faecalis*, *Candida albicans*, and methicillin-resistant *Staphylococcus aureus*. *Astrobiology* 13, 1081–1090.

Han, S. K., Lee, D., Lee, H., Kim, D., Son, H. G., Yang, J.-S., et al. (2016). OASIS 2: online application for survival analysis 2 with features for the analysis of maximal lifespan and healthspan in aging research. *Oncotarget* 7, 56147–56152. doi: 10.18632/oncotarget.11269

Hussain, M., Hastings, J. G. M., and White, P. J. (1991). A chemically defined medium for slime production by coagulase-negative staphylococci. *J. Med. Microbiol.* 34, 143–147. doi: 10.1099/00222615-34-3-143

Huycke, M. M., Spiegel, C. A., and Gilmore, M. S. (1991). Bacteremia caused by hemolytic, high-level gentamicin-resistant *Enterococcus faecalis*. *Antimicrob. Agents Chemother.* 35, 1626–1634. doi: 10.1128/aac.35.8.1626

Ichijo, T., Yamaguchi, N., Tanigaki, F., Shirakawa, M., and Nasu, M. (2016). Four-year bacterial monitoring in the International Space Station—Japanese Experiment Module "Kibo" with culture-independent approach. *NPJ Microgravity* 2:16007.

ISS-MORD (2013). *International Space Station Medical Operatinos Requirements Documents*, Revision B Edn, ed. I. S. S. Program (Houston, TX: National Aeronautics and Space Administration).

Jett, B. D., Hatter, K. L., Huycke, M. M., and Gilmore, M. S. (1997). Simplified agar plate method for quantifying viable bacteria. *Biotechniques* 23, 648–650. doi: 10.2144/97234bm22

Jia, B., Raphenya, A. R., Alcock, B., Waglechner, N., Guo, P., Tsang, K. K., et al. (2016). CARD 2017: expansion and model-centric curation of the comprehensive antibiotic resistance database. *Nucleic Acids Res.* 45, D566–D573.

JMP® (2019). *JMP® Pro*, 14.3 Edn. Cary, NC: SAS Institute Inc.

Joensen, K. G., Scheutz, F., Lund, O., Hasman, H., Kaas, R. S., Nielsen, E. M., et al. (2014). Real-time whole-genome sequencing for routine typing, surveillance, and outbreak detection of verotoxigenic *Escherichia coli*. *J. Clin. Microbiol.* 52, 1501–1510. doi: 10.1128/jcm.03617-13

Kim, W., Tengra, F. K., Young, Z., Shong, J., Marchand, N., Chan, H. K., et al. (2013). Spaceflight promotes biofilm formation by *Pseudomonas aeruginosa*. *PloS One* 8:e62437.

Lang, J. M., Coil, D. A., Neches, R. Y., Brown, W. E., Cavalier, D., Severance, M., et al. (2017). A microbial survey of the International Space Station (ISS). *PeerJ* 5:e4029.

Larsen, M. V., Cosentino, S., Rasmussen, S., Friis, C., Hasman, H., Marvig, R. L., et al. (2012). Multilocus sequence typing of total-genome-sequenced bacteria. *J. Clin. Microbiol.* 50, 1355–1361. doi: 10.1128/jcm.06094-11

Lebreton, F., Manson, A. L., Saavedra, J. T., Straub, T. J., Earl, A. M., and Gilmore, M. S. (2017). Tracing the Enterococci from Paleozoic origins to the hospital. *Cell* 169, 849. doi: 10.1016/j.cell.2017.04.027

Maurer, F. P., Christner, M., Hentschke, M., and Rohde, H. (2017). Advances in rapid identification and susceptibility testing of bacteria in the clinical microbiology laboratory: implications for patient care and antimicrobial stewardship programs. *Infect. Dis. Rep.* 9, 6839–6839.

McBride, S. M., Fischetti, V. A., Leblanc, D. J., Moellering, R. C. Jr., and Gilmore, M. S. (2007). Genetic diversity among *Enterococcus faecalis*. *PLoS One* 2:e582. doi: 10.1371/journal.pone.0000582

Mclean, R. J., Cassanto, J. M., Barnes, M. B., and Koo, J. H. (2001). Bacterial biofilm formation under microgravity. *FEMS Microbiol. Lett.* 195, 115–119.

Mermel, L. A. (2012). Infection prevention and control during prolonged human space travel. *Clin. Infect. Dis.* 56, 123–130. doi: 10.1093/cid/cis861

Miller, S., Naccache, S. N., Samayoa, E., Messacar, K., Arevalo, S., Federman, S., et al. (2019). Laboratory validation of a clinical metagenomic sequencing assay for pathogen detection in cerebrospinal fluid. *Genome Res.* 29, 831–842. doi: 10.1101/gr.238170.118

Mora, M., Wink, L., Kögler, I., Mahnert, A., Rettberg, P., Schwendner, P., et al. (2019). Space Station conditions are selective but do not alter microbial characteristics relevant to human health. *Nat. Commun.* 10:3990.

Page, A. J., Cummins, C. A., Hunt, M., Wong, V. K., Reuter, S., Holden, M. T., et al. (2015). Roary: rapid large-scale prokaryote pan genome analysis. *Bioinformatics* 31, 3691–3693. doi: 10.1093/bioinformatics/btv421

Parks, D. H., Imelfort, M., Skennerton, C. T., Hugenholtz, P., and Tyson, G. W. (2015). CheckM: assessing the quality of microbial genomes recovered from isolates, single cells, and metagenomes. *Genome Res.* 25, 1043–1055. doi: 10.1101/gr.186072.114

Paulsen, I. T., Banerjei, L., Myers, G., Nelson, K., Seshadri, R., Read, T. D., et al. (2003). Role of mobile DNA in the evolution of vancomycin-resistant *Enterococcus faecalis*. *Science* 299, 2071–2074. doi: 10.1126/science.1080613

Powell, J. R., and Ausubel, F. M. (2008). "Models of *Caenorhabditis elegans* infection by bacterial and fungal pathogens," in *Innate Immunity*, ed. E. V. J. Ewbank (Totowa, NJ: Humana Press Inc), 403–427. doi: 10.1007/978-1-59745-570-1_24

Rooney, B. V., Crucian, B. E., Pierson, D. L., Laudenslager, M. L., and Mehta, S. K. (2019). Herpes virus reactivation in astronauts during spaceflight and its application on earth. *Front. Microbiol.* 10:16. doi: 10.3389/fmicb.2019.00016

Sahm, D. F., Kissinger, J., Gilmore, M. S., Murray, P. R., Mulder, R., Solliday, J., et al. (1989). In vitro susceptibility studies of vancomycin-resistant *Enterococcus faecalis*. *Antimicrob. Agents Chemother.* 33, 1588–1591. doi: 10.1128/aac.33.9.1588

Sanderson, N. D., Street, T. L., Foster, D., Swann, J., Atkins, B. L., Brent, A. J., et al. (2018). Real-time analysis of nanopore-based metagenomic sequencing from infected orthopaedic devices. *BMC Genomics* 19:714. doi: 10.1186/s12864-018-5094-y

Schiwon, K., Arends, K., Rogowski, K. M., Furch, S., Prescha, K., Sakinc, T., et al. (2013). Comparison of antibiotic resistance, biofilm formation and conjugative transfer of *Staphylococcus* and *Enterococcus* isolates from International Space Station and Antarctic Research Station Concordia. *Microb. Ecol.* 65, 638–651. doi: 10.1007/s00248-013-0193-4

Schloissnig, S., Arumugam, M., Sunagawa, S., Mitreva, M., Tap, J., Zhu, A., et al. (2013). Genomic variation landscape of the human gut microbiome. *Nature* 493, 45–50. doi: 10.1038/nature11711

Seemann, T. (2014). Prokka: rapid prokaryotic genome annotation. *Bioinformatics* 30, 2068–2069. doi: 10.1093/bioinformatics/btu153

Shankar, N., Baghdayan, A. S., and Gilmore, M. S. (2002). Modulation of virulence within a pathogenicity island in vancomycin-resistant *Enterococcus faecalis*. *Nature* 417, 746–750. doi: 10.1038/nature00802

Sielaff, A. C., Urbaniak, C., Mohan, G. B. M., Stepanov, V. G., Tran, Q., Wood, J. M., et al. (2019). Characterization of the total and viable bacterial and fungal communities associated with the International Space Station surfaces. *Microbiome* 7:50.

Singh, N. K., Bezdan, D., Sielaff, A. C., Wheeler, K., Mason, C. E., and Venkateswaran, K. (2018a). Multi-drug resistant *Enterobacter bugandensis* species isolated from the International Space Station and comparative genomic analyses with human pathogenic strains. *BMC Microbiol.* 18:175. doi: 10.1186/s12866-018-1325-2

Singh, N. K., Wood, J. M., Karouia, F., and Venkateswaran, K. (2018b). Succession and persistence of microbial communities and antimicrobial resistance genes associated with International Space Station environmental surfaces. *Microbiome* 6:204.

Sobisch, L.-Y., Rogowski, K. M., Fuchs, J., Schmieder, W., Vaishampayan, A., Oles, P., et al. (2019). Biofilm forming antibiotic resistant Gram-positive pathogens isolated from surfaces on the International Space Station. *Front. Microbiol.* 10:543. doi: 10.3389/fmicb.2019.00543

Staley, J. T., and Konopka, A. (1985). Measurement of in situ activities of nonphotosynthetic microorganisms in aquatic and terrestrial habitats. *Annu. Rev. Microbiol.* 39, 321–346. doi: 10.1146/annurev.mi.39.100185.001541

Su, L., Zhou, L., Liu, J., Cen, Z., Wu, C., Wang, T., et al. (2014). Phenotypic, genomic, transcriptomic and proteomic changes in *Bacillus cereus* after a short-term space flight. *Adv. Space Res.* 53, 18–29. doi: 10.1016/j.asr.2013.08.001

Tirumalai, M. R., Stepanov, V. G., Wünsche, A., Montazari, S., Gonzalez, R. O., Venkateswaran, K., et al. (2018). *Bacillus safensis* FO-36b and *Bacillus pumilus* SAFR-032: a whole genome comparison of two spacecraft assembly facility isolates. *BMC Microbiol.* 18:57. doi: 10.1186/s12866-018-1191-y

Urbaniak, C., Sielaff, A. C., Frey, K., Allen, J., Singh, N., Jaing, C., et al. (2018). Detection of antimicrobial resistance genes associated with the International Space Station environmental surfaces. *Sci. Rep.* 8:814.

Urbaniak, C., Van Dam, P., Zaborin, A., Zaborina, O., Gilbert, J. A., Torok, T., et al. (2019). Genomic characterization and virulence potential of two *Fusarium oxysporum* isolates cultured from the International Space Station. *mSystems* 4:e345-18.

Van Tyne, D., Manson, A. L., Huycke, M. M., Karanicolas, J., Earl, A. M., and Gilmore, M. S. (2019). Impact of antibiotic treatment and host innate immune pressure on enterococcal adaptation in the human bloodstream. *Sci. Transl. Med.* 11:eaat8418. doi: 10.1126/scitranslmed.aat8418

Vaughan, T. G. (2017). IcyTree: rapid browser-based visualization for phlogenetic trees and networks. *Bioinformatics*. 33, 2392–2394. doi: 10.1093/bioinformatics/btx155

Venkateswaran, K. (2017). "Microbial Characteristics of ISS Environmental Surfaces," in *Proceedings of the 47th International Conference on Environmental Systems*, Charleston, SC.

Wang, Y., Yuan, Y., Liu, J., Su, L., Chang, D., Guo, Y., et al. (2014). Transcriptomic and proteomic responses of *Serratia marcescens* to spaceflight conditions involve large-scale changes in metabolic pathways. *Adv. Space Res.* 53, 1108–1117. doi: 10.1016/j.asr.2014.01.018

Weiner, L. M., Webb, A. K., Limbago, B., Dudeck, M. A., Patel, J., Kallen, A. J., et al. (2016). Antimicrobial-resistant pathogens associated with healthcare-associated infections: summary of data reported to the National Healthcare Safety Network at the Centers for Disease Control and Prevention, 2011–2014. *Infect. Control Hosp. Epidemiol.* 37, 1288–1301. doi: 10.1017/ice.2016.174

Wick, R. R., Judd, L. M., Gorrie, C. L., and Holt, K. E. (2017). Unicycler: resolving bacterial genome assemblies from short and long sequencing reads. *PLoS Comput. Biol.* 13:e1005595. doi: 10.1371/journal.pcbi.1005595

Wilson, J., Ott, C., Zu Bentrup, K. H., Ramamurthy, R., Quick, L., Porwollik, S., et al. (2007). Space flight alters bacterial gene expression and virulence and reveals a role for global regulator Hfq. *Proc. Natl. Acad. Sci. U.S.A.* 104, 16299–16304. doi: 10.1073/pnas.0705175104

Yuen, G. J., and Ausubel, F. M. (2018). Both live and dead Enterococci activate *Caenorhabditis elegans* host defense via immune and stress pathways. *Virulence* 9, 683–699. doi: 10.1080/21505594.2018.1438025

Conflict of Interest: The authors declare that the research was conducted in the absence of any commercial or financial relationships that could be construed as a potential conflict of interest.

frontiers in Microbiology

ORIGINAL RESEARCH
published: 29 July 2021
doi: 10.3389/fmicb.2021.608478

Characterization of Spacesuit Associated Microbial Communities and Their Implications for NASA Missions

David Danko[1,2†], Ganesh Babu Malli Mohan[3†], Maria A. Sierra[1,4], Michelle Rucker[5], Nitin K. Singh[1], Aaron B. Regberg[6], Mary S. Bell[7], Niamh B. O'Hara[2], Rachid Ounit[8], Christopher E. Mason[2,4,9,10] and Kasthuri Venkateswaran[3*]*

[1] Tri-Institutional Computational Biology & Medicine Program, Weill Cornell Medicine of Cornell University, Manhattan, NY, United States, [2] The HRH Prince Alwaleed Bin Talal Bin Abdulaziz Alsaud Institute for Computational Biomedicine, Weill Cornell Medicine, New York, NY, United States, [3] Biotechnology and Planetary Protection Group, Jet Propulsion Laboratory, California Institute of Technology, Pasadena, CA, United States, [4] Department of Physiology and Biophysics, Weill Cornell Medicine, New York, NY, United States, [5] Exploration Mission Planning Office, Johnson Space Center, Houston, TX, United States, [6] Astromaterials Research and Exploration Science Division, Johnson Space Center, Houston, TX, United States, [7] Jacobs@NASA/Johnson Space Center, Houston, TX, United States, [8] Department of Computer Science and Engineering, University of California, Riverside, Riverside, CA, United States, [9] The WorldQuant Initiative for Quantitative Prediction, Weill Cornell Medicine, New York, NY, United States, [10] The Feil Family Brain and Mind Research Institute, Weill Cornell Medicine, New York, NY, United States

Background: Crewed National Aeronautics and Space Administration (NASA) missions to other solar system bodies are currently being planned. One high-profile scientific focus during such expeditions would be life detection, specifically the discovery of past or present microbial life, if they exist. However, both humans and associated objects typically carry a high microbial burden. Thus, it is essential to distinguish between microbes brought with the expedition and those present on the exploring planets. Modern spacesuits are unique, customized spacecraft which provide protection, mobility and life support to crew during spacewalks, yet they vent, and the mobility of microbes through spacesuits has not been studied.

Results: To evaluate the microbial colonization of spacesuits, NASA used an Extravehicular Activity swab kit to examine viable microbial populations of 48 samples from spacesuits using both traditional microbiological methods and molecular sequencing methods. The cultivable microbial population ranged from below the detection limit to 9×10^2 colony forming units per 25 cm^2 of sample and also significantly varied by the location. The cultivable microbial diversity was dominated by members of *Bacillus, Arthrobacter,* and *Ascomycota.* However, 16S rRNA-based viable bacterial burden ranged from 10^5 to 10^6 copies per 25 cm^2 of sample. Shotgun metagenome sequencing revealed the presence of a diverse microbial population on the spacesuit surfaces, including *Curtobacterium* and *Methylobacterium* from across all sets of spacesuits in high abundance. Among bacterial species identified, higher abundance of *Cutibacterium acnes*, *Methylobacterium oryzae,* and *M. phyllosphaerae* reads were documented.

OPEN ACCESS

Edited by:
Andreas Teske, University of North Carolina at Chapel Hill, United States

Reviewed by:
Tim Sandle, The University of Manchester, United Kingdom
Rakesh Mogul, California State Polytechnic University, Pomona, United States

***Correspondence:**
Christopher E. Mason
chm2042@med.cornell.edu
Kasthuri Venkateswaran
kjvenkat@jpl.nasa.gov

† These authors have contributed equally to this work and share first authorship

Specialty section:
This article was submitted to Extreme Microbiology, a section of the journal Frontiers in Microbiology

Received: *20 September 2020*
Accepted: *16 June 2021*
Published: *29 July 2021*

Citation:
Danko D, Malli Mohan GB, Sierra MA, Rucker M, Singh NK, Regberg AB, Bell MS, O'Hara NB, Ounit R, Mason CE and Venkateswaran K (2021) Characterization of Spacesuit Associated Microbial Communities and Their Implications for NASA Missions. Front. Microbiol. 12:608478. doi: 10.3389/fmicb.2021.608478

Conclusion: The results of this study provide evidence that identical microbial strains may live on the wrist joint, inner gauntlet, and outer gauntlet of spacesuits. This raises the possibility, but does not confirm that microbial contaminants on the outside of the suits could contaminate planetary science operations unless additional measures are taken. Overall, these data provide the first estimate of microbial distribution associated with spacesuit surfaces, which will help future mission planners develop effective planetary protection strategies.

Keywords: spacesuit, microbial diversity, ISS, metagemonic, metagenome assembled genomes (MAGs), microbial ecology

INTRODUCTION

Several spacefaring nations and private corporations are planning to send humans and spacecraft to other planets such as Mars, to search for evidence of habitats that could support life (NRC, 2014). Planetary Protection research efforts at National Aeronautics and Space Administration (NASA) seek to develop technologies to minimize any terrestrial microbial contamination to ensure the safety and health of astronauts, while also preserving scientific integrity of exoplanetary samples (NASA, 2019a). Planetary Protection aims involve the study and prevention of forward and back contamination, meaning the interchange of microbes and organic materials from Earth to other solar system bodies and vice versa (Debus and Arnould, 2008).

When astronauts will be sent to search for life on other planets, it will be necessary to understand what microorganisms they may bring with them. It is estimated that 85% of all microbial isolates recovered from spacecraft and supported facilities are microorganisms associated with the human microbiota (Nicholson et al., 2009). Accordingly, a team at the Johnson Space Center (JSC) at NASA has developed a prototype Extravehicular Activity (EVA) swab kit that is suitable for handling by the astronauts in spacesuits to collect microbial samples aseptically, aiming to profile microorganisms associated with spacesuits (Rucker et al., 2018). In this communication, a microbial characterization associated with wrist joints of flight Extravehicular Mobility Unit (EMU), Modified Advanced Crew Escape System and Orion Crew Survival System (MACES/OCSS) spacesuits was carried out to evaluate the form, fit and function of the EVA swab tool; that functional testing provided an opportunity to characterize the typical microbial contamination on spacesuits.

To explore and work in space, crew members must take their environment with them because there is no atmospheric pressure and no oxygen to sustain life. Inside the human crew vehicle, the atmosphere can be controlled so that special clothing is not necessary, but when outside exploring in space, astronauts need protection (Schwartz et al., 2002). Since various materials including fabrics and clothing are known to harbor specific microbiomes (Breuker et al., 2003; Cappitelli and Sorlini, 2008; Cataño et al., 2012; Callewaert et al., 2014; Sterndorff et al., 2020), it is of the highest interest to the NASA scientific community to explore the microbiome of the spacesuit (National Academies of Sciences, Engineering and Medicine, 2018). This study is not designed to understand the indigenous microbiome of the spacesuit when manufactured; instead spacesuit microbiome was measured when crew wear them after nominal handling and use to see how microorganisms might persist on the suits. Thorough characterization of spacesuit microbiome will enable the design of appropriate spacesuit architecture to minimize human commensal microorganism, which cannot be sterilized, from leaking into the external environment thus compromising life detection missions. Currently, all NASA spacesuits are designed to be flexible and which could lead to leakage. However, leak paths are not well-characterized, and it remains unclear what fraction of leakage occurs through mechanisms that would transport microbes. Characterization of spacesuits will also allow NASA to better understand cleaning process effectiveness for the spacesuits.

Since 2006, the field of genomics has been revolutionized by the development of next-generation sequencing technologies, enabling the comprehensive understanding of the microbial ecology of built environments such as offices (Chase et al., 2016), hospitals (Westwood et al., 2014), and transportation system environments (Hsu et al., 2016; Danko et al., 2021a) where humans spend a significant fraction of their time. Subsequently, molecular microbial community analyses were implemented to monitor the International Space Station (ISS) (Singh et al., 2018; Checinska Sielaff et al., 2019) and spacecraft assembly cleanrooms (Danko et al., 2021b) but this is the first report measuring spacesuit microbiome. While these technologies for microbial detection have elucidated the prevalence of microbial species, it was not until recently significant efforts have been pointed at developing sampling methods that enable sample collection in microgravity or a vacuum, that are simple to handle by crew members donned with large gloves, and that could preserve samples appropriately before performing subsequent molecular methods (Sandle, 2011; Rucker et al., 2018).

Since bulky EVA suits can restrict movement and limit visibility through the helmet visor, the primary objective was aimed to evaluate the interface between a fully suited test subject handling the EVA swab tool by the crew. Fully suited testing is important for identifying tool design issues prior to flight. At exploration destinations, such as Mars, suited crew may be required to periodically sample their suits as part of an environmental monitoring protocol. In addition, a benefit of this test was an opportunity to characterize the microorganisms found on or near selected suit pressure joints under vacuum and when the spacesuits were positively pressured, enabling NASA

to assess exploration mission operations and hardware design to mitigate microbial leakage.

In this study EVA swab tools were used to collect several samples from variety of spacesuits ($n = 7$ sets; 48 samples) in a JSC training session. Spacesuit samples were treated with (allowing measurement of viable/intact cells) or without propidium monoazide (PMA, dead and alive cells) (48 samples each of PMA and no PMA; total $n = 98$ samples), a DNA intercalating dye before utilizing molecular technologies (Vaishampayan et al., 2013). The viable microbial burden targeting 16S rRNA gene (for bacteria/archaea) and internal transcribed region (ITS; for fungi) were estimated using quantitative polymerase chain reaction (qPCR) assay and shotgun metagenome sequencing (Singh et al., 2018). Furthermore, culturable microbial burden associated with spacesuits was measured using the traditional culture-based colony counts. This study will provide NASA with the ability to evaluate the spectrum of microbial diversity associated with spacesuits.

MATERIALS AND METHODS

EVA Swab Material Selection

Validation of the macrofoam swabs (EVA swab tool material) to collect microorganisms from various material types was not a part of this study. However, a comprehensive study was performed previously to understand the suitable swab materials (cotton, polyester, and macrofoam) in the efficient removal of the microorganisms from the aluminum and titanium surfaces (Kwan et al., 2011). Briefly, a model microbial community comprised 11 distinct species of bacterial, archaeal, and fungal lineages, was used to examine the effects of variables in sampling matrices, target cell density/molecule concentration, and cryogenic storage on the overall efficacy of the sampling regimen. The biomolecules and cells/spores recovered from each collection device were assessed by cultivable and microscopic enumeration, and quantitative and species-specific PCR assays. rRNA gene-based quantitative PCR analysis showed that cotton swabs were superior to nylon-flocked swabs and macrofoam swabs significantly outperformed polyester wipes. Furthermore, macrofoam swab materials were found to withstand extreme temperature fluctuations of the space conditions including varying pressure, and vacuum (Rucker et al., 2018).

EVA Swab Sample Kit Preparation and Sample Collection

Three different kinds of spacesuits were sampled (**Figure 1**). Briefly, the EMU suits are currently used for EVA on ISS, but are not designed for use in planetary missions. We sampled stainless steel wrist joints and cloth gauntlets covering the joints on these suits. The outer fabric of the EMU is made of Ortho-Fabric, which is a blend of Gortex (ePTFE), Kevlar (a para-aramid type fiber related to nylon) and Nomex (a meta-aramid type fiber) (Newman et al., 2000). The MACES and OCSS suits designed for internal cabin use, such as inside Orion during launch and reentry through Earth's atmosphere, use similar wrist joint as the EMU but without a gauntlet to cover it. The outer layer of the MACES and OCSS suits is comprised of orange Nomex (Watson, 2014; NASA, 2019b). NASA has conducted a series of ground tests intended to evaluate the EVA swab kit's form, fit, and function under mission operations scenarios, in preparation for eventual sample collection from outside the ISS (Rucker et al., 2018). For samples collected from the EMU, EVA swabbing was an add-on to a routine suit familiarization test that all flight crew are required to perform. Familiarization involves suit fit and functional checks, followed by a 4-h prebreathe protocol (to mitigate potential for decompression sickness) before exposure to vacuum in the Space Station Airlock Test Article chamber. Spacesuit samples were collected during the prebreathe protocol, when the crew member was breathing pure oxygen at a suit internal pressure 4.3 psi higher than ambient external pressure, but not yet at external vacuum pressure. Although standard laboratory swabs could have been used under these conditions, this test provided an opportunity for suited crew to practice self-swabbing with the flight-like EVA swab kit, which will be necessary in future studies where samples will be taken under external vacuum conditions. A second series of tests was conducted with the MACES and OCSS suits. In these tests, four test subjects sampled their own suits (two MACES suits and two OCSS suits) inside the 11-foot vacuum chamber while the chamber was at vacuum (0.01 torr). The internal pressure inside the suits was 4.3 psi. Samples collected during these tests were exposed to a maximum of 4 h of vacuum.

Sample kit cleaning, sterilization, and assembly were performed at JSC according to a purpose-developed protocol. Each sample canister (assembled with filter and ball plungers) and swab end effector assembly was placed into separate autoclave bags. Bagged components were placed into Steris LV 250 laboratory steam sterilizer and sterilized using a gravity cycle of 45 min at 121°C (250°F) and 103.4 kPa (15 psi). Note that neither the sample caddy itself nor the tool handle which was never in contact with the swab head were autoclaved. Bagged components were allowed up to 1 h of cool-down time at approximately 22°C (71.6°F) for safe handling. Following autoclaving, bagged components were transferred to a Labconco Horizontal Clean Bench (Model # 36100000, ISO Class 5). With the commercial swab inside its sterile packaging, the swab stem was cut to optimal length [approximately 6.0 cm (2.4 in)] using sterilized wire cutters, making sure the swab head remained inside its packaging until the final assembly step. The cut end of the swab was then inserted into the end effector slot, and set screws were tightened to hold the swab in place. Sterile packaging was removed from the swab head immediately before inserting each swab assembly into its sterile container. Each container/swab assembly was then mounted into the tool caddy, wiped clean with isopropanol and placed into bonded storage until the test.

During swab assembly, technicians wore sterile gloves, and both the gloves and assembly tools (Allen wrench, scissors, and forceps) were sprayed with 70% ethanol surface disinfectant. All parts were handled either with sterile forceps or the autoclave bags, with no contact between the gloves and tool areas that must remain sterile. After assembly, the EVA sample kits were

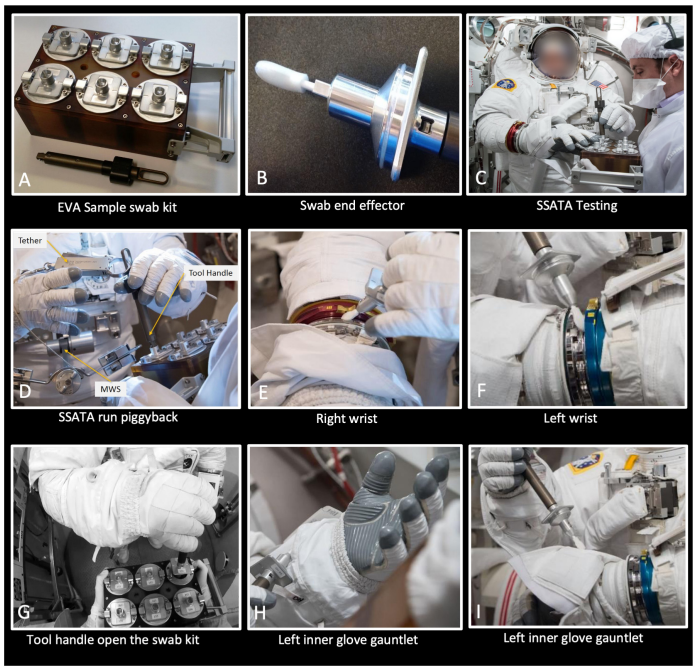

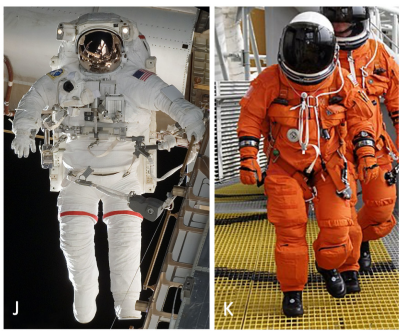

	EMU	MACES
Wrist Joint	12	11
Inner Flap	9	N/A
Outer Flap	11	N/A
Control	4	1
Total Samples	36	12

FIGURE 1 | Photographs showing collection of various types of samples from different spacesuit types. **(A–I)** Images of sample collection and associated equipment, intended for use in flight. **(J)** An image of an Extravehicular Mobility Unit (EMU) suit. **(K)** An image of an Advanced Crew Escape Suit (ACES). Total number of samples collected are tabulated. N/A: Not available.

transported to the test site packed inside hard-sided storage cases. Once at the test site, the analog crew were briefed on tool usage and were given an opportunity to practice with a spare handle and sample caddy assembly. Over a period of 7 months between December 2016 and June 2017, 176 spacesuits, environmental control, and floor samples were collected during eight sampling time periods at JSC. **Figure 1** shows sample collection from various parts of the spacesuits, EVA sampling kits, and number of samples associated with various spacesuits. The specific location for each sampling event of these 48 samples, surface area, and collection dates are given in Table 1 and detailed metadata about spacesuit types used, fabrics composition, microbial burden, cultivable diversity, are given in the **Supplementary Tables 1, 2**.

Controls

Among 48 spacesuit samples including five controls samples were further analyzed for various microbiological characteristics using traditional and shotgun metagenomic sequence analyses. Environmental controls were the swabs that were removed from the canister during testing but not touched to any surface. Negative controls were swabs that were not opened at all during testing. Among these 48 samples, 36 were from EMU and 12 were from MACES spacesuits.

Sample Processing

After sample collection, sample processing took place in an ISO 7 (10K class) cleanroom at JPL. Under ISO 5 certified biosafety cabinet, each swab was aseptically severed with a sterile cutter and transferred to a 50 mL Falcon tube containing 15 mL of sterile phosphate-buffered saline (PBS; pH 7.4). The tube with the swab was shaken for 2 min followed by concentration with a Concentrating Pipette (Innova Prep, Drexel, MO, United States) using 0.22 μm Hollow Fiber Polysulfone tips (Cat #: CC08022) and PBS as elution fluid. Each sample was concentrated to 5 mL. A 100 μL concentrated aliquots were plated on various agar plates to estimate cultivable population using traditional plate count methods (described below). One mL of the diluted solution (200 μL plus 1.8 mL PBS) was used to conduct an ATP assay (Kikkoman Corp., Noda, Japan) to rapidly measure total and viable microbial population (Venkateswaran et al., 2003), enabling appropriate serial dilutions. Furthermore, 3 mL of each concentrated sample was split into two 1.5 mL- aliquots and one aliquot was treated with PMA to assess viability (Vaishampayan et al., 2013), while the second aliquot was handled similarly but without the addition of PMA. Briefly, 18.25 μL of 2 mM PMA was added to one half of the 3-mL sample (final concentration 25 μM) followed by 5 min incubation at room temperature in the dark and 15 min exposure to the activation system (PMA LED device, Biotium, Hayward, CA, United States). Each sample was then split into two 0.75 mL aliquots. One aliquot was transferred to bead beating tubes containing Lysing Matrix E (MP Biomedicals, Santa Ana, CA, United States), followed by bead beating for 60 s using the vortex sample holder (MO Bio, Carlsbad, CA, United States). The bead-beaten aliquot and the aliquot without bead beating were combined for their corresponding PMA-treated and non-treated samples. DNA extraction was accomplished with the Maxwell 16 automated system (Promega, Madison, WI, United States), in accordance

with manufacturer instructions. A Maxwell control (MC) without any sample added in its cartridge was run concurrently with each flight sample set to account for microbial contamination associated with reagents (kitome) used in the automated DNA extraction. The extracted DNA was eluted in 50 μL of water and stored at −20°C and processed with the rest of the samples later.

Estimation and Identification of Cultivable Microbial Population

The 100 μl of each concentrated sample were plated on Reasoner's 2A agar (R2A for environmental microbes), Potato Dextrose Agar with chloramphenicol (100 μg/mL; PDA for fungi), and blood agar (BA for human commensals; Hardy Diagnostics, Santa Maria, CA, United States) in duplicate. R2A and PDA plates were incubated at 25°C for 7 days and BA plates at 37°C for 2 days at which time colony forming units (CFU) were counted. All colonies were picked from each plate and from each suit sampling location. The isolates were then archived in semisolid R2A or PDA slants (agar media diluted 1:10) and stored at room temperature. Once a culture was confirmed to be pure, two cryobead stocks (Copan Diagnostics, Murrieta, CA, United States) were prepared for each isolate and stored at –80°C. A loopful of purified microbial culture was directly subjected to PCR, and the targeted fragment was amplified (colony PCR), or DNA was extracted with the UltraClean DNA kit (MO Bio, Carlsbad, CA, United States) or Maxwell 16 instrument. The extracted DNA was used for PCR to amplify the 1.5 kb 16S rRNA gene to identify bacterial strains. The following primers were used for the 16S rRNA gene amplification to estimate bacterial population. The forward primer, 27F (5′-AGA GTT TGA TCC TGG CTC AG-3′) and the reverse primer, 1492R (5′-GGT TAC CTT GTT ACG ACT T-3′) (Lane, 1991; Turner et al., 1999). The PCR conditions were as follows: denaturation at 95°C for 5 min, followed by 35 cycles consisting of denaturation at 95°C for 50 s, annealing at 55°C for 50 s, and extension at 72°C for 1 min 30 s and finalized by extension at 72°C for 10 min. For fungal population estimation, the forward primer ITS 1F (5′-TTG GTC ATT TAG AGG AAG TAA-3′) (Lai et al., 2007) and reverse primer Tw13 (5′-GGT CCG TGT TTC AAG ACG-3′) (Taylor and Bruns, 1999) were used to obtain ∼1.2 kb ITS product. The PCR conditions were as follows: Initial denaturation at 95°C for 3 min followed by 25 cycles of 95°C for 50 s, annealing at 58°C for 30 s, and extension at 72°C for 2 min, followed by a final extension at 72°C for 10 min. The amplicons were inspected by gel electrophoresis in 1% agarose gel. When bands for products were visible, amplification products were treated with Antarctic phosphatase and exonuclease to remove 5′- and 3′- phosphates from unused dNTPs before sequencing. The sequencing was performed (Rockville, MD, United States) using 27F and 1492R primers for *Bacteria*, and ITS1F and Tw13 primers for fungi. The sequences were assembled using SeqMan Pro from DNAStar Lasergene Package (DNASTAR Inc., Madison, WI, United States). The bacterial sequences were searched against EzTaxon-e database (Kim et al., 2012) and the fungal sequences against the UNITE database (Koljalg et al., 2013). The identification was based on the closest percentage similarity (>97%) to previously identified microbial type strains.

qPCR Assay

Following the DNA extraction, quantitative polymerase chain reaction (qPCR), targeting the partial 16S rRNA gene (bacteria) or partial ITS region (fungi), was performed with SmartCycler (Cepheid, CA, United States) to quantify the microbial burden as previously established (Checinska Sielaff et al., 2019). Each 25-μL reaction consisted of 12.5 μL of 2X iQ SYBR Green Supermix (BioRad, Hercules, CA, United States), 1 μL each of forward and reverse oligonucleotide primers (10 μM each), and 1 μL of template DNA (PMA treated and non-treated samples). Each sample was run in triplicate; the average and standard deviation were calculated based on these results. Purified DNA from a model microbial community (Kwan et al., 2011) served as the positive control and DNase/RNase free molecular-grade distilled water (Promega, Madison, WI, United States) was used as the negative control in each run. The number of gene copies was determined from the standard curve as described previously with a modification where synthetic fragments of *B. pumilus* (1.4 kb 16S rRNA gene) or *Aureobasidium pullulans* (1-kb ITS region) were used instead of genomic DNA (Checinska et al., 2015). The qPCR efficiency was ∼98%. The negative control values were not deducted since the values were at ∼100 copies per 1 or 10 μL and not scalable (yielded the same results despite using 1 μL and 10 μL of DNA templates).

Illumina Based DNA Sequencing and Analysis

The initial DNA yield and metagenome library quantitation of all 96 samples tested (48 samples PMA treated and 48 samples PMA untreated) were measured by Qbit (Thermo Fisher Scientific Inc., United States). DNA libraries for all 96 samples were prepared for shotgun metagenome sequencing using the Nextera DNA Library Preparation Kit from Illumina. The quality and fragment size of each library were assessed on a Bioanalyzer 2100 (Agilent). Separate adapters were added to the DNA from each library, normalized to 2 nM, pooled, denatured, and diluted to 1.8 pM according to the standard recommendations by Illumina. The HiSeq4000 platform (Illumina) was used for sequencing, resulting in 100-bp paired-end reads.

Bioinformatics Analysis

Bioinformatic analyses were performed on Weill Cornell Medicine's Athena compute cluster, a typical high-performance grid compute (Slurm) system. The secondary analysis was performed on Linux and MacOS systems. Unless otherwise noted programs were run with default settings.

Data Quality Control and Filtering

Sequence data were processed with AdapterRemoval (v2.17) to remove low-quality reads and reads with ambiguous bases. Subsequently, reads were aligned to the human genome (hg38, including alternate contigs) using Bowtie2 (v2.3.0, fast preset). Read pairs where both ends mapped to the human genome were

separated from read pairs where neither mate mapped. Read pairs where only one mate mapped were discarded. Hereafter, we refer to these read sets as human reads and non-human reads. We did not process human reads beyond counting the total fraction of DNA from our samples which mapped to the human genome.

Taxonomic Profiling and Analysis

Taxonomic profiles were generated by processing non-human reads KrakenUniq (v0.3.2) with a database based on all draft and reference genomes in RefSeq Microbial (bacteria, fungi, virus, and archaea) ca. March 2017. KrakenUniq uses a *k*-mer based approach to identify reads. Reads are broken into *k*-mers of 31 bases. Each *k*-mer is mapped to a database that lists the lowest common ancestor of all genomes which contained the *k*-mer. Each read is classified by identifying the best supported path in the taxonomic tree of markers. Finally, the taxonomic makeup of a sample is given by concatenating annotations for reads without further processing. KrakenUniq counts the number of unique marker *k*-mers assigned to each taxa, and we filtered taxa with fewer than 512 unique markers. Differential abundance estimation (where applicable) using the ALDEx2 R package was performed (Fernandes et al., 2013). Briefly, ALDEx2 transforms read count matrices using a centered log ratio transformation that models samples as Dirichlet-Multinomial distributions over taxa then compares taxonomic abundances across groups. If two groups are given, comparison is done with a Wilcoxon rank sum test, more than two groups are tested via a generalized linear model. All *p*-values are multiple hypotheses corrected using Benjamini-Hochberg. We considered a taxon to have differential abundance in a given condition if its corrected p-value was less than or equal to $p = 0.05$.

Dimensionality reduction of taxonomic profiles was performed with Uniform Manifold Approximation and Projection UMAP (McInnes et al., 2018) based on a matrix of Jensen-Shannon Divergences (JSD) between samples. Analysis of intersample diversity (beta-diversity) was achieved using the same matrix of JSD. Intrasample diversity (alpha-diversity) was measured by taking Shannon's Entropy of the total sum normalized taxonomic profile of each sample. Rarefaction analysis of taxa was performed by grouping samples by location and setting and selecting 16 uniform random groups for each value. A curve of best fit was found by fitting a logarithmic model to the series.

Profile of Eukaryotic species were generated using CLARK-S (v1.2.5) (Ounit and Lonardi, 2016) using sequences classified with high confidence (i.e., confidence score > 0.75, and gamma score > 0.10) as defined in the CLARK manual. Identification of taxa was further restricted to species with relative abundance at least 0.01% of the total sequences.

Samples were compared to eight representative samples of human body sites selected from the Human Microbiome Project (HMP) (Turnbaugh et al., 2007) for each of five body sites: oral, skin, airways, gastrointestinal, and urogenital. Using MetaPhlAn2 (v2.2) (Truong et al., 2015), we generated taxonomic profiles for HMP samples and our samples and compared profiles using Cosine Similarity.

Functional Profiling and Analysis

HUMANn2 (Franzosa et al., 2018) was used to generate functional metabolic profiles of the genes in our samples. Non-human reads were aligned to Uniref90 (ca. March 2017) using the DIAMOND aligner (v0.8.6) (Buchfink et al., 2015). Subsequently, alignments were processed using HUMANn2 (v0.11.1) to produce profiles of pathway abundance. Pathways were tested for differential expression using the Wilcoxon rank sum corrected by Benjamini Hochberg. Dimensionality reduction of pathways was performed using PCoA over normalized pathway abundances.

Profiling Antimicrobial Resistance Genes

Profiles of antimicrobial resistance (AMR) genes using MegaRes (v1.0.1) (Lakin et al., 2017) were created. To generate profiles from MegaRes, we mapped non-human reads to the database using Bowtie2 (v2.3.0, very-sensitive presets) (Langmead and Salzberg, 2012). Subsequently, alignments were analyzed using ResistomeAnalyzer (commit 15a52dd) (Dean, 2018) and normalized by total reads per sample and gene length to give Reads per kilo base per million mapped reads (RPKMs). MegaRes includes an ontology grouping resistance genes into, gene classes, AMR mechanisms, and gene groups.

Identification of Genomes and Strains

We assembled contigs from all PMA treated samples using MegaHIT (v1.1.3) (Li et al., 2015) then clustered the resulting contigs into draft genomes using MetaBAT2 (Kang et al., 2019). Draft genomes were quality controlled and assigned a rough taxonomic rank using CheckM (Parks et al., 2015). Genomes with less than 50% completeness or more than 20% contamination were discarded. We aligned all genomes to one another to using Nucleotide MUMmer (Delcher et al., 2003) and processed the results to generate an Average Nucleotide Identity (ANI) between all pairs of draft genomes. We discarded all alignments that covered less than half the average lengths of the genomes being aligned. We further discarded alignments with less than 99% ANI so that we would only be left with pairs of nearly identical genomes. We grouped these alignments into connected components and analyzed the sites where each component was found.

RESULTS

Microbial Abundance

A total of 48 samples (36 EMU and 12 MACES) were collected from six different surfaces of the spacesuits or environmental controls. Sampling surfaces include: left wrist joint (12 samples), left inner glove gauntlet (5 samples), left outer glove gauntlet (5 samples), right wrist joint (11 samples), right inner glove gauntlet (4 samples), right outer glove gauntlet (6 samples). All controls were analyzed for all microbiological and molecular biological examinations (5 samples, **Table 1**). All these 48 samples were categorized into sets ($n = 7$ sets) based on the suit types or sample collection dates (**Table 1**). In addition, metadata such as locations, type of suits, materials of spacesuits, and date of collection are given in **Supplementary Table 1**.

TABLE 1 | Characteristics of various spacesuites sampled during this study and associated metadata.

Set #	Sampled locations	Metagenome sample ID	Sampling date	Suit types sampled	Material type sampled	Sample pressure	PMA or no PMA
SET-1	Control Swab – Not removed from canister	JC-044	12/28/2016	EMU	N/A	760	No PMA
SET-1	Control Swab – Not removed from canister	JC-092	12/28/2016	EMU	N/A	760	PMA
SET-1	Outside, left wrist gauntlet	JC-018	12/28/2016	EMU	Beta cloth	760	No PMA
SET-1	Outside, left wrist gauntlet	JC-066	12/28/2016	EMU	Beta cloth	760	PMA
SET-1	Inside, left wrist gauntlet	JC-013	12/28/2016	EMU	Beta cloth	760	No PMA
SET-1	Inside, left wrist gauntlet	JC-061	12/28/2016	EMU	Beta cloth	760	PMA
SET-1	Left wrist joint groove	JC-001	12/28/2016	EMU	Stainless Steel	760	No PMA
SET-1	Left wrist joint groove	JC-049	12/28/2016	EMU	Stainless Steel	760	PMA
SET-1	Outside, right wrist gauntlet	JC-038	12/28/2016	EMU	Beta cloth	760	No PMA
SET-1	Outside, right wrist gauntlet	JC-086	12/28/2016	EMU	Beta cloth	760	PMA
SET-1	Inside, right wrist gauntlet	JC-034	12/28/2016	EMU	Beta cloth	760	No PMA
SET-1	Inside, right wrist gauntlet	JC-082	12/28/2016	EMU	Beta cloth	760	PMA
SET-1	Right wrist joint groove	JC-023	12/28/2016	EMU	Stainless Steel	760	No PMA
SET-1	Right wrist joint groove	JC-071	12/28/2016	EMU	Stainless Steel	760	PMA
SET-2	Control Swab – Not removed from canister	JC-045	12/14/2016	EMU	N/A	760	No PMA
SET-2	Control Swab – Not removed from canister	JC-093	12/14/2016	EMU	N/A	760	PMA
SET-2	Outside, left wrist gauntlet	JC-019	12/14/2016	EMU	Beta cloth	760	No PMA
SET-2	Outside, left wrist gauntlet	JC-067	12/14/2016	EMU	Beta cloth	760	PMA
SET-2	Left wrist joint groove	JC-002	12/14/2016	EMU	Stainless Steel	760	No PMA
SET-2	Left wrist joint groove	JC-050	12/14/2016	EMU	Stainless Steel	760	PMA
SET-2	Outside, Right wrist gauntlet	JC-039	12/14/2016	EMU	Beta cloth	760	No PMA
SET-2	Outside, Right wrist gauntlet	JC-087	12/14/2016	EMU	Beta cloth	760	PMA
SET-2	Right wrist joint groove	JC-024	12/14/2016	EMU	Stainless Steel	760	No PMA
SET-2	Right wrist joint groove	JC-072	12/14/2016	EMU	Stainless Steel	760	PMA
SET-4	Long Term Control assembled 2/6 tested 3/16	JC-047	3/15/2017	EMU	N/A	760	No PMA
SET-4	Long Term Control assembled 2/6 tested 3/16	JC-095	3/15/2017	EMU	N/A	760	PMA
SET-3	Exterior, palm-side left wrist gauntlet	JC-020	2/6/2017	EMU	Beta cloth	760	No PMA
SET-3	Exterior, palm-side left wrist gauntlet	JC-068	2/6/2017	EMU	Beta cloth	760	PMA
SET-3	Left wrist joint groove	JC-003	2/6/2017	EMU	Stainless Steel	760	No PMA
SET-3	Left wrist joint groove	JC-051	2/6/2017	EMU	Stainless Steel	760	PMA
SET-3	Interior, left wrist gauntlet	JC-014	2/6/2017	EMU	Beta cloth	760	No PMA
SET-3	Interior, left wrist gauntlet	JC-062	2/6/2017	EMU	Beta cloth	760	PMA
SET-3	Right wrist joint groove	JC-025	2/6/2017	EMU	Stainless Steel	760	No PMA
SET-3	Right wrist joint groove	JC-073	2/6/2017	EMU	Stainless Steel	760	PMA
SET-3	Control Swab – Not removed from canister	JC-046	2/6/2017	EMU	N/A	760	No PMA
SET-3	Control Swab – Not removed from canister	JC-094	2/6/2017	EMU	N/A	760	PMA
SET-4	Left wrist outer gauntlet	JC-021	3/15/2017	EMU	Beta cloth	760	No PMA
SET-4	Left wrist outer gauntlet	JC-069	3/15/2017	EMU	Beta cloth	760	PMA
SET-4	Left wrist inner gauntlet	JC-015	3/15/2017	EMU	Beta cloth	760	No PMA
SET-4	Left wrist inner gauntlet	JC-063	3/15/2017	EMU	Beta cloth	760	PMA
SET-4	Left glove/lower arm groove	JC-004	3/15/2017	EMU	Stainless Steel	760	No PMA
SET-4	Left glove/lower arm groove	JC-052	3/15/2017	EMU	Stainless Steel	760	PMA
SET-4	Right wrist outer gauntlet	JC-040	3/15/2017	EMU	Beta cloth	760	No PMA
SET-4	Right wrist outer gauntlet	JC-088	3/15/2017	EMU	Beta cloth	760	PMA
SET-4	Right wrist inner gauntlet	JC-035	3/15/2017	EMU	Beta cloth	760	No PMA
SET-4	Right wrist inner gauntlet	JC-083	3/15/2017	EMU	Beta cloth	760	PMA
SET-4	Right glove/lower arm groove	JC-026	3/15/2017	EMU	Stainless Steel	760	No PMA
SET-4	Right glove/lower arm groove	JC-074	3/15/2017	EMU	Stainless Steel	760	PMA
SET-5	Control Swab – Not removed from canister	JC-048	3/16/2017	MACES/OCCS	N/A	0.01	No PMA
SET-5	Control Swab – Not removed from canister	JC-096	3/16/2017	MACES/OCCS	N/A	0.01	PMA

(Continued)

TABLE 1 | Continued

Set #	Sampled locations	Metagenome sample ID	Sampling date	Suit types sampled	Material type sampled	Sample pressure	PMA or no PMA
SET-5	Left wrist	JC-005	5/16/2017	OCCS	Stainless Steel	0.01	No PMA
SET-5	Left wrist	JC-053	5/16/2017	OCCS	Stainless Steel	0.01	PMA
SET-5	Right wrist	JC-027	5/16/2017	OCCS	Stainless Steel	0.01	No PMA
SET-5	Right wrist	JC-075	5/16/2017	OCCS	Stainless Steel	0.01	PMA
SET-5	Left wrist	JC-006	5/30/2017	MACES	Stainless Steel	0.01	No PMA
SET-5	Left wrist	JC-054	5/30/2017	MACES	Stainless Steel	0.01	PMA
SET-5	Right wrist	JC-028	5/30/2017	MACES	Stainless Steel	0.01	No PMA
SET-5	Right wrist	JC-076	5/30/2017	MACES	Stainless Steel	0.01	PMA
SET-6	Left wrist outer gauntlet	JC-022	5/30/2017	EMU	Beta cloth	760	No PMA
SET-6	Left wrist outer gauntlet	JC-070	5/30/2017	EMU	Beta cloth	760	PMA
SET-6	Left wrist inner gauntlet	JC-016	5/30/2017	EMU	Beta cloth	760	No PMA
SET-6	Left wrist inner gauntlet	JC-064	5/30/2017	EMU	Beta cloth	760	PMA
SET-6	Left glove/lower arm groove	JC-007	5/30/2017	EMU	Stainless Steel	760	No PMA
SET-6	Left glove/lower arm groove	JC-055	5/30/2017	EMU	Stainless Steel	760	PMA
SET-6	Right wrist outer gauntlet	JC-041	5/30/2017	EMU	Beta cloth	760	No PMA
SET-6	Right wrist outer gauntlet	JC-089	5/30/2017	EMU	Beta cloth	760	PMA
SET-6	Right wrist inner gauntlet	JC-036	5/30/2017	EMU	Beta cloth	760	No PMA
SET-6	Right wrist inner gauntlet	JC-084	5/30/2017	EMU	Beta cloth	760	PMA
SET-6	Right glove/lower arm groove	JC-029	5/30/2017	EMU	Stainless Steel	760	No PMA
SET-6	Right glove/lower arm groove	JC-077	5/30/2017	EMU	Stainless Steel	760	PMA
SET-6	Right wrist outer gauntlet	JC-042	6/14/2017	EMU	Beta cloth	760	No PMA
SET-6	Right wrist outer gauntlet	JC-090	6/14/2017	EMU	Beta cloth	760	PMA
SET-6	Left Wrist Crew 3	JC-008	6/8/2017	MACES	Stainless Steel	0.01	No PMA
SET-6	Left Wrist Crew 3	JC-056	6/8/2017	MACES	Stainless Steel	0.01	PMA
SET-6	Right Wrist Crew 3	JC-030	6/8/2017	MACES	Stainless Steel	0.01	No PMA
SET-6	Right Wrist Crew 3	JC-078	6/8/2017	MACES	Stainless Steel	0.01	PMA
SET-6	L Wrist Crew 4	JC-009	6/8/2017	MACES	Stainless Steel	0.01	No PMA
SET-6	L Wrist Crew 4	JC-057	6/8/2017	MACES	Stainless Steel	0.01	PMA
SET-6	Left wrist crew 3	JC-010	6/12/2017	OCCS	Stainless Steel	0.01	No PMA
SET-6	Left wrist crew 3	JC-058	6/12/2017	OCCS	Stainless Steel	0.01	PMA
SET-6	Right wrist crew 3	JC-031	6/12/2017	OCCS	Stainless Steel	0.01	No PMA
SET-6	Right wrist crew 3	JC-079	6/12/2017	OCCS	Stainless Steel	0.01	PMA
SET-6	Left wrist crew 4	JC-011	6/12/2017	MACES	Stainless Steel	0.01	No PMA
SET-6	Left wrist crew 4	JC-059	6/12/2017	MACES	Stainless Steel	0.01	PMA
SET-6	Right wrist crew 4	JC-032	6/12/2017	MACES	Stainless Steel	0.01	No PMA
SET-6	Right wrist crew 4	JC-080	6/12/2017	MACES	Stainless Steel	0.01	PMA
SET-7	Right wrist outer gauntlet	JC-043	6/26/2017	EMU	Beta cloth	760	No PMA
SET-7	Right wrist outer gauntlet	JC-091	6/26/2017	EMU	Beta cloth	760	PMA
SET-7	Right wrist inner gauntlet	JC-037	6/26/2017	EMU	Beta cloth	760	No PMA
SET-7	Right wrist inner gauntlet	JC-085	6/26/2017	EMU	Beta cloth	760	PMA
SET-7	Right glove/lower arm groove	JC-033	6/26/2017	EMU	Stainless Steel	760	No PMA
SET-7	Right glove/lower arm groove	JC-081	6/26/2017	EMU	Stainless Steel	760	PMA
SET-7	Left wrist inner gauntlet	JC-017	6/26/2017	EMU	Beta cloth	760	No PMA
SET-7	Left wrist inner gauntlet	JC-065	6/26/2017	EMU	Beta cloth	760	PMA
SET-7	Left glove/lower arm groove	JC-012	6/26/2017	EMU	Stainless Steel	760	No PMA
SET-7	Left glove/lower arm groove	JC-060	6/26/2017	EMU	Stainless Steel	760	PMA

N/A, Not applicable; PMA, Propidium monoazide treated to measure viable microorganisms and no-PMA are the samples constitute both dead and live microbes; EMU, Extravehicular Mobility Unit; MACES, Modified Advanced Crew Escape System; OCCS, Onboard Complex Control System.

Our samples contained viable bacterial populations which were estimated by culture-dependent and independent analyses and are summarized in **Supplementary Table 1** and **Figure 2A**. We cultured various microorganisms from our samples on three different types of media: blood agar, R2A, and PDA. The number of cultivable bacterial counts on R2A plates ranged from no growth to 9.0×10^2 CFU per 25 cm^2 (**Figure 2A**). The bacterial counts on blood agar were ranged from no growth to 3.5×10^2 CFU per 25 cm^2. No bacterial colonies were observed in any of the controls during this study. The phylogenetic affiliation of the bacterial strains isolated in this study was shown in **Supplementary Figure 1A**. Among 24 bacterial strains isolated and identified, the microorganisms belonged to the members of the phyla *Firmicutes* (13 strains), *Actinobacteria* (10 strains) and *Proteobacteria* (1 strain). *Bacillus* species represented the highest number of isolates, followed by *Arthrobacter* species. Comparatively, fungal isolates were not abundant and only six strains belonging to six different species were isolated. The ITS-based sequence analyses identified them as *Epicorum nigrum, Alternaria* sp., *Penicillium fagi, Aureobasidium pullulans, Naganishia adeliensis,* and *Neonectria* sp. The results of ATP-assay were not shown but ATP contents were used to estimate the microbial burden which further helped to determine appropriate serial dilutions.

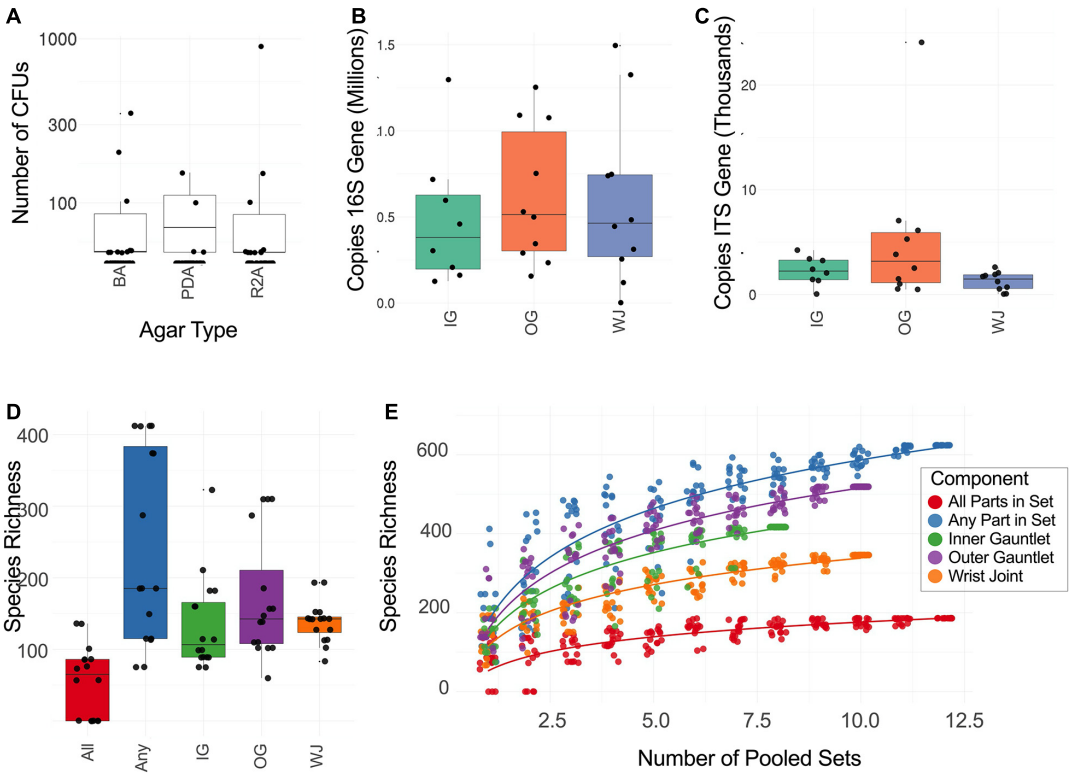

FIGURE 2 | (A) Number of CFU found when plating samples on three different media. R2A, Reasoner's 2A agar (for environmental bacteria); PDA, potato dextrose agar with chloramphenicol (100 μg/mL; for fungi); BA, blood agar (for human commensals). **(B)** Number of copies of the 16S rRNA gene found on different suit component: inner gauntlet (IG), outer gauntlet (OG), and wrist joint (WJ). **(C)** Number of copies of the ITS gene found on different components. **(D)** Total number of species detected by metagenomics on different components. *All* refers to microbes which were found in all components from a given set while *Any* refers to species on at least one component in a set. **(E)** Rarefaction curves showing the diversity of different numbers of components pooled together.

A qPCR assay of the 16S and ITS genes was performed to measure the absolute microbial population of both viable (PMA treated) and total (PMA-untreated) microorganisms. This assay did not show a statistically significant difference in the microbial load among various locations sampled on spacesuits tested nor in various sets categorized. Viable bacterial load (PMA treated samples) was estimated at approximately 10^5 to 10^6 16S rRNA copies per 25 cm^2, **Figure 2B**. Viable bacterial population was an order of magnitude less abundant than total bacterial burden that include both dead and live microorganisms (**Supplementary Table 1**). Viable fungal population was measured at approximately 10^2 to 10^4 ITS copies per 25 cm^2, **Figure 2C**. No significant difference was observed between EMU and MACES suits in either cultivable and culture-independent microbial burden assays.

Molecular Microbial Diversity

Spacesuits are modular, each set refers to a single assembled set of components operated and sampled on a given day. The 48 samples including five controls were either treated with PMA or left untreated, resulting in an analysis of 96 samples. Among the 96 samples subjected for shotgun library preparation, all samples yielded enough DNA fragments except four PMA-treated samples and one non-PMA treated sample, hence 91 samples were subsequently assayed for shotgun metagenome sequencing. The PMA treated samples that did not yield any shotgun metagenome reads were SET-2 outside, left wrist gauntlet; SET-3 interior, left wrist gauntlet; SET-3 right wrist joint groove; and SET-7 left glove/lower arm groove.

In total, 319M reads were generated from all 91 samples. Human (∼38.2%) and animal (∼30%) associated reads were removed from the analyses. The PMA (49.8M) and non-PMA (54.7M) reads were ∼30% of the total reads. Approximately 104.5M reads associated with microorganisms were generated after high quality trimming from PMA (44 samples) and non-PMA treated (47 samples) samples. Dimensionality reduction comparing microbial taxonomic profiles between PMA treated and untreated samples showed an average shift based on PMA treatment (**Supplementary Figure 2**) suggesting that some types of microbes may be present on spacesuits as non-viable detritus. PMA treated samples were the focus of this study as they represent the intact/viable cells and information about PMA untreated samples were presented in supplementary datasets (**Supplementary Tables 2, 3**). The PMA-based analyses revealed that there were no microbial diversity differences among the EMU and MACES suits.

For all PMA treated samples, at domain level, the majority of the reads were assigned to bacteria (98.6%), followed by eukaryotes (0.9%), then archaea (0.24%), and viral signatures were 0.17%. For samples not treated with PMA, these reads were assigned to bacteria (98.6%), followed by eukaryotes (0.9%), archaea (0.5%), and viruses (0.1%). The proportional abundance of bacteria and fungi were similar in both PMA treated and non-PMA treated samples. When the relative abundance of all metagenomics reads was summed, ∼80% of the reads were attributed to the species whose reads were >100K.

None of the control samples yielded microbes that could be cultured in the media employed during this study which confirms that the EVA tool kit prepared for this study was sterile. But when all samples were considered for molecular analyses, ∼5% of the total metagenomics reads associated with bacteria, fungi, and viruses were present in control samples (n = 5). Among 993 microbial species observed in all spacesuits including control during this study (**Supplementary Table 2**), 13 bacterial taxa of control samples exhibited >10K reads and they were identified as *Bacillus pumilus, Cutibacterium acnes, Janthinobacterium* species (n = 3), *Micrococcus luteus, Negativicoccus massiliensis, Pseudomonas* species (n = 5), and *Ralstonia insidiosa.* Among them, *C. acnes, Janthinobacterium* species, *Pseudomonas* species, and *R. insidiosa* members were present in all five control samples. The bacterial species associated with controls that exhibited >100K reads were *N. massiliensis* (512K reads), *C. acnes* (448K reads), and *Pseudomonas* sp. NC02 (347K reads). Hence, few contaminant species were found as "kitomes" during this study and our finding is based on identifying microbial species/strains that are not in controls.

When various sets of spacesuits were compared, some differences were observed. Set #7 samples consist of members of the genera *Methylobacterium* and *Curtobacterium* whereas *Pseudomonas* species were prevalent in samples collected from set #5. Among 350 bacterial genera constituting 660 bacterial taxa identified, sequences of the members of the genera *Curtobacterium* and *Methylobacterium* were retrieved across all sets of spacesuits in high abundance. The compositional analysis showed a higher abundance of *Curtobacterium, Methylobacterium, Negativicoccus,* and *Pseudomonas* that exhibited more than two million reads. Among bacterial species identified (60 species > 100K reads; 239 species > 10K reads), higher abundance (>2M reads) of *Curtobacterium acnes* (8.9M reads), *Methylobacterium oryzae* (4.4M reads), and *M. phyllosphaerae* (4.2M reads) sequences were observed. Low fungal, archaeal, and viral reads were retrieved during this study and their sequence abundances and taxa characteristics are presented in **Supplementary Tables 2–4**.

Molecular Microbial Diversity Indices

The total number of microbial species (species richness) found on each type of component (Inner Glove Gauntlet, Outer Glove Gauntlet, and Wrist Joint) was similar and typically between 100 and 200 (**Figure 2C**). A subset of these species could be found on all components in a set (typically 50–100 species found in all three components of either the left or right side of the suit) establishing a shared community. The inner and outer suit gauntlet had higher richness than the wrist joint ($p < 2^{-16}$, one-way ANOVA).

To establish the total number of microbial species in the entire study (**Figure 2D**), a rarefaction analysis was performed (**Figure 2E**). Suits were considered as a whole and separately by component. A total of 660 microbial species were observed across all samples but a curve fit to the subsamples did not flatten which suggests that more microbial diversity would be seen with more samples collected. However, an analogous curve fit to subsets of species that occurred in all part in set did flatten, suggesting there may be a core community of 100–200 organisms common to spacesuits. Individual component types necessarily had more species than were found in all parts in set but fewer than were found in any part of a set.

To address the study design of collecting multiple samples from the same suit, we conducted a nested analysis using a regression Generalized Linear Mixed Model, and found that alpha diversity (Shannon Index) varied significantly across spacesuits for the PMA untreated group ($F_{5,35} = 4.84$, $P = 0.002$) but did not vary significantly for the PMA treated group. This may be due to the higher power demands of nested models and the limited number of samples collected.

Taxonomic Analysis of Spacesuits

Microbial taxa were categorized based on a number of different conditions (1) differential abundance between PMA treated samples and untreated samples (determined by ALDEx2), (2) high prevalence taxa found in 31 out of 32 PMA treated EMU samples (excluding controls), (3) increased abundance in MACES suits compared to EMU suits for PMA treated samples (determined by ALDEx2), (4) differential abundance between suit components (wrist, inner, and outer gauntlets) in EMU samples treated with PMA (determined by ALDEx2). Differential abundance was defined as a Benjamini–Hochberg corrected q-value of 0.05 or less based on ALDEx2. Among PMA treated EMU samples one species *Corynebacterium kroppenstedtii* was identified as being significantly (q = 0.031) less abundant in wrist joint samples compared to other microbial species. Ninety-nine species were identified as differentially abundant in samples treated with PMA and untreated samples.

UMAP plot on the taxonomic profiles of samples (**Supplementary Figure 2**) and PMA treated samples only are depicted in **Figure 3A**. As expected, PMA treated sample clearly separated from untreated samples. This shows that there is a distinct likely viable set of microbes present on the sampled spacesuits. Within PMA treated samples, generally samples from the same suit clustered together with Sets 1 and 7 as notably tight clusters. Set 7 (all EMU suit sampled on June 26, 2017) was a definite outlier in relative abundance matching the pattern observed for alpha diversity.

Beta Diversity and Sample Differentiation

The distance between taxonomic profiles of PMA treated samples of EMU suites was compared using JSD analysis. Dimensionality reduction of these distances using UMAP showed limited clustering by suit (**Figure 3A**). EMU suits were subdivided

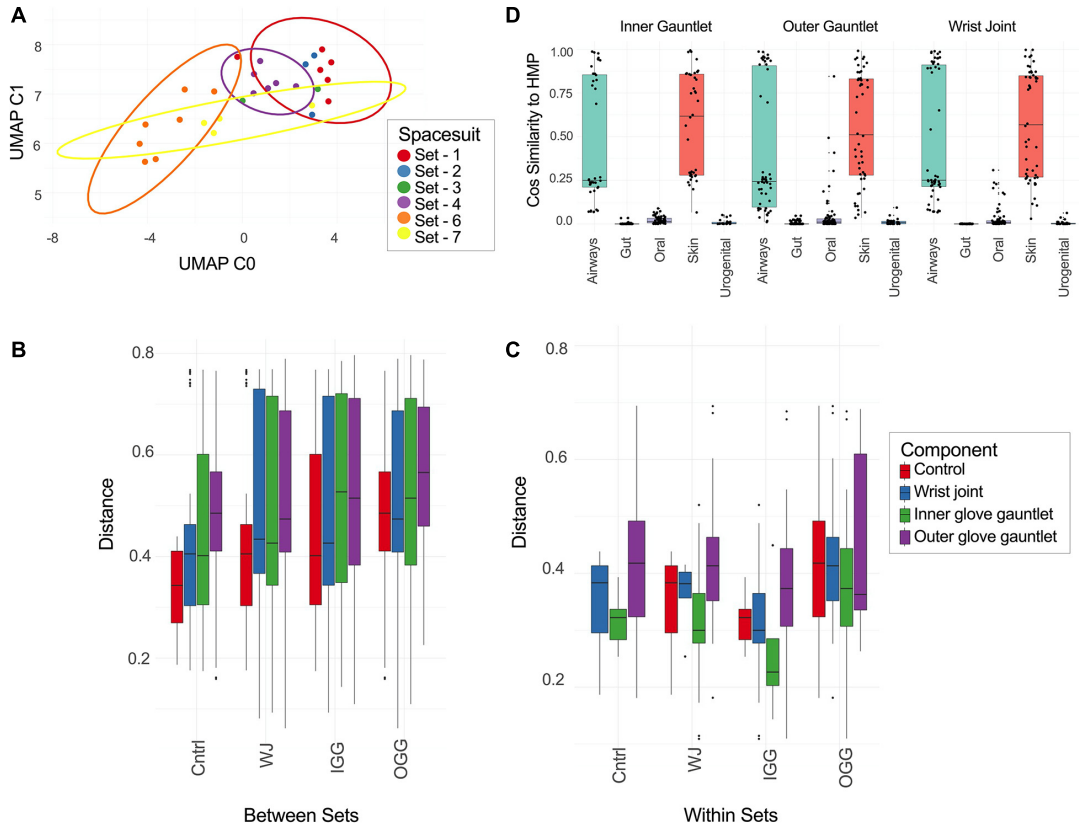

FIGURE 3 | (A) UMAP of taxonomic profiles from PMA treated samples from EMU suits. Color indicates the set a sample came from. **(B,C)** Distance between different types of suit components [inner gauntlet (IG), outer gauntlet (OG), wrist joint (WJ), and controls (cntrl)] and samples from different sets **(B)** or the same set **(C)**. **(D)** The similarity of taxa from different components to representative samples from the Human Microbiome Project.

into eight triplets of samples that contained precisely one wrist, inner gauntlet, and outer gauntlet from the same suit. These triplets were in physical proximity to one another when sampled. We then compared two distributions: the distribution of distances between components in the same set and the distribution of distances between components in different sets (**Figures 3B,C**). The average JSD between components in the same set was 0.355 compared to 0.542 between components in different sets. A two-sided Welch's *t*-test showed that these distributions did not share the same mean with *p*-value less than 2.0^{-16}.

We also compared these distributions to distance distributions for control samples. The mean JSD between suit components and control samples collected at the same time was 0.365 while the mean distance between control samples and suit components from other sets was 0.470. The distance between components from different sets was larger than the difference between controls and components from other sets based on a two-sided Welch's *t*-test with p of 1.01^{-4}. Analogously, the distances between components from the same set were less than controls with a p of 2.17^{-7}.

Taxonomic profiles of PMA treated samples during this study were compared to exemplar samples from the HMP. Spacesuit samples were found to be most similar to HMP skin and airway samples, suggesting that spacesuit microbiomes could originate from human skin or airway communities (**Figure 3D**). Notably the similarity to human body sites was not found to significantly vary by suit component or by which suit was being tested (one-way ANOVA), suggesting all components of all suits are exposed to human skin and airways microbiomes.

Antimicrobial Resistance Genes

Sequences of EMU PMA samples were mapped to known AMR genes and performed a rarefaction analysis of potential AMR genes (**Figure 4A**). Suits were considered as a whole and separately by component. Left and right gauntlet samples from the same component of the same suit were grouped together. A total observed richness of 40 AMR genes was noticed, but a curve fit to subsamples did not flatten, suggesting more diversity of AMR genes could be found. Samples from the outer gauntlet had more abundance than samples taken from the wrist, which in turn showed more AMR genes from the inner gauntlet. We grouped identified AMR genes by resistance class according to the MegaRes ontology. Five samples contained genes from the macrolide, lincosamide and streptogramin (MLS) class, 3 from the elfamycins, and just one sample contained a resistance gene from the beta-lactams (**Figure 4B**).

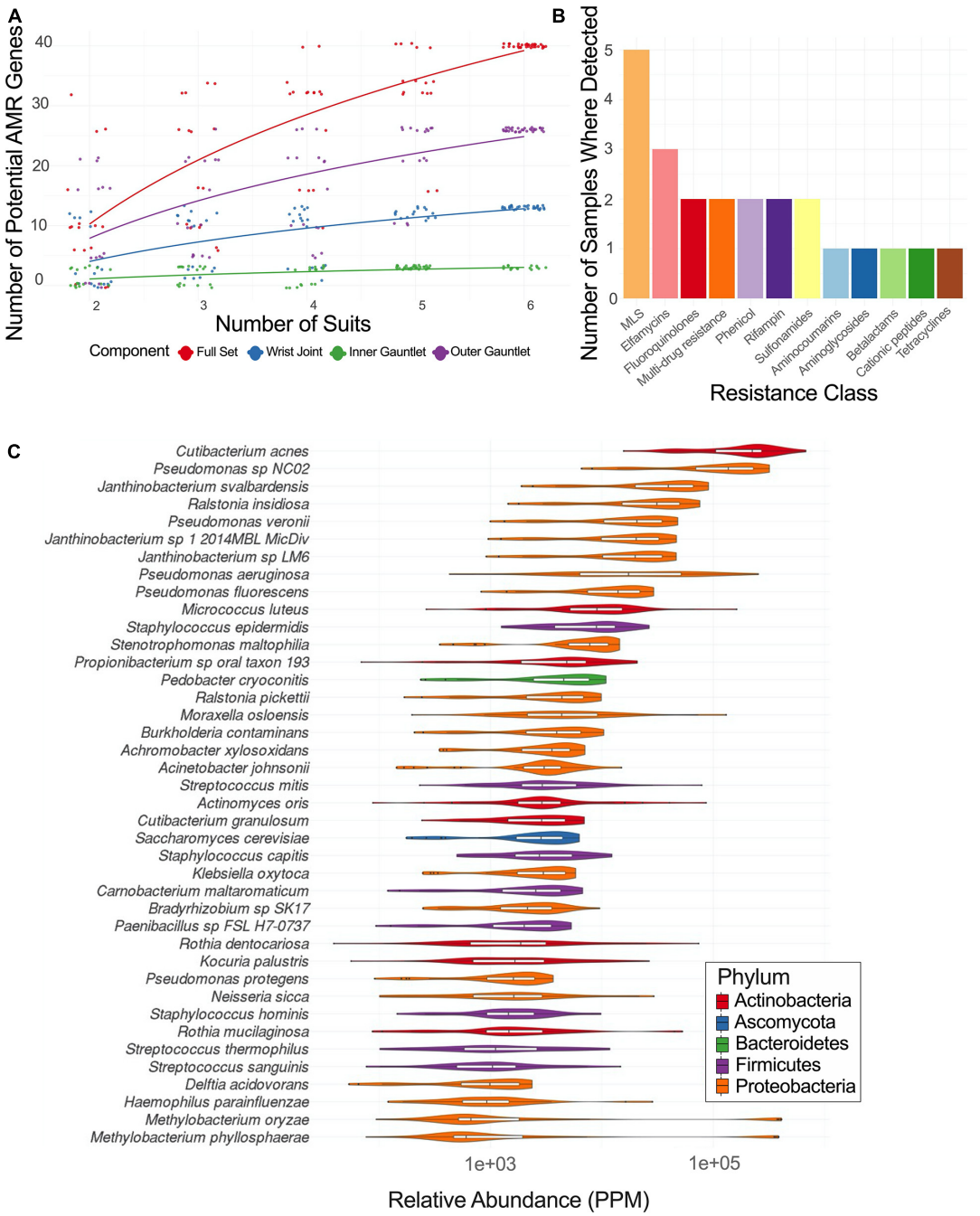

FIGURE 4 | (A) Rarefaction plot of the number of AMR genes in different suit subsets. **(B)** Plot of the number of samples with AMR genes from a given resistance class. MLS stands for macrolide-lincosamide-streptogramin. **(C)** Relative abundance of major taxa in parts per million (PPM) across PMA treated samples from EMU suits.

Identified Microbial Species

Among the viable microbial species, *Pseudomonas* species were abundant in spacesuits studied. A core microbiome (occurring in 90% of samples or more) of 40 species in EMU samples treated with PMA was determined with several species in *Staphylococcus*, *Streptococcus, Pseudomonas,* and *Burkholderiales*. The distribution of abundances for microbial species with the highest median relative abundances was identified. *Cutibacterium acnes* was the most abundant taxa followed by several *Pseudomonas, Janthinobacterium,* and *Ralstonia insidiosa* (**Figure 4C**).

Fungal species (identified using CLARK-S, see methods) were also prevalent with 13 species identified in two or more samples. These include *Malassezia restricta* (found in all samples) which

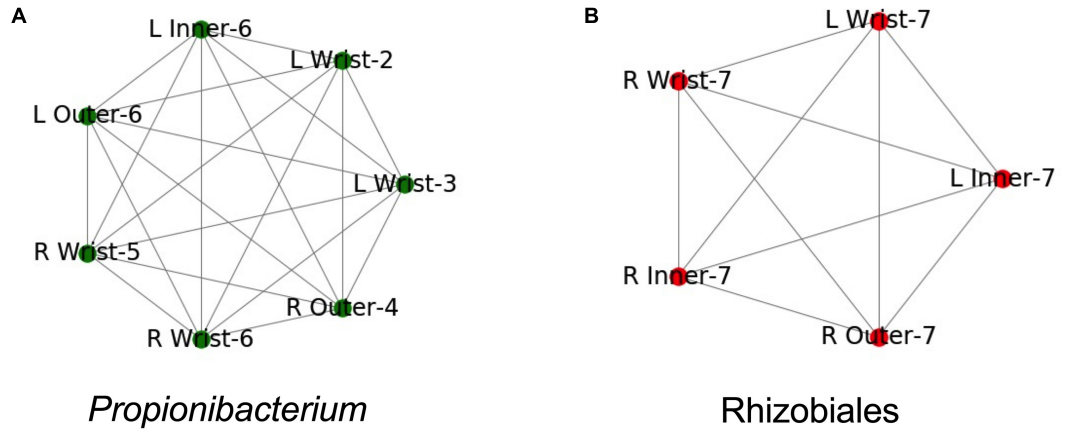

FIGURE 5 | Both samples where identical taxa were assembled. Names are structured as Left (L) or Right (R), the suit component, and the set number. Edges indicate identical assemblies based on 99.5% ANI. **(A)** Samples where a *Propionibacterium* taxa was found. **(B)** Samples where a *Rhizobiales* taxa was found.

was associated with the skin microbiome of astronauts after their missions on the ISS by Sugita et al. (2016) and a number of other human commensal species. The full list of fungal species identified is given in **Supplementary Table 3**.

Strain Specific Metagenome Assembled Genomes

We built Metagenome Assembled Genomes (MAGs) from assemblies of all PMA treated samples, including controls. We identified MAGs that were found in more than one sample (99% ANI, see methods). These MAGs corresponded to two groups. One group of draft genomes was found in seven samples and was roughly categorized as a *Propionibacterium* species, the other group was found in five samples and was categorized as a member of *Rhizobiales* (**Figures 5A,B**). Both genome groups were fully connected, each draft genome from each sample had 99% ANI to each other sample in the group.

Both genomes were found in multiple samples from the same spacesuit. The *Propionibacterium* group was found in three samples from Set 6: the right wrist, and the inner and outer left gauntlets (**Figure 5A**). The *Rhizobiales* group was found in five samples from Set 7: the right wrist, inner and outer gauntlets and the left wrist and inner gauntlet (**Figure 5B**). Neither genome was found in any control sample. Since the samples where the genomes were found were treated with PMA, we further conclude that these microorganisms were likely viable.

The incidence of multiple examples of the same genome at wrist, inner, and outer gauntlets of two suits is consistent with the possibility that viable bacteria might have migrated from the inside to the outside of a spacesuit, but could also have been deposited in all three locations during the suit donning process. For crew health, surfaces inside the space suits were cleaned using stericide wipes; however exterior surfaces (including the surfaces that were sampled), were not cleaned. The stericide wipes chemical components were: 1.5% *n*-alkyl dimethyl benzyl ammonium chloride (60% C_{14}, 30% C_{16}, 5% C_{12}, 5% C_{18}) and 1.5% *n*-alkyl ethylbenzyl ammonium chloride (50% C_{12}, 30% C_{14}, 17% C_{16}, 5% C_{18}) as maintenance procedure. Since neither MAG was found in any control it is concluded that presence of these genomes is not due to contamination but might be due to migration from one location to another location of the spacesuit.

DISCUSSION

In this study, we established that viable microbes (and their MAGs) are present on the wrist assemblages of spacesuits, that certain microbial strains can survive on all three components of the wrist assembly without being found in corresponding controls, and that these microbes broadly resemble those of human commensal skin microbiomes.

Microorganisms associated with fabrics have not historically been studied in detail (Buschle-Diller et al., 1994; Cappitelli and Sorlini, 2008; Linacre et al., 2010; Daly et al., 2012; Lee et al., 2016), whereas microbiome of human (Turnbaugh et al., 2007; Nelson et al., 2010; Jensen, 2013; Shafquat et al., 2014) and built environments (Danko et al., 2021a), including closed habitat of ISS environment (Singh et al., 2018; Checinska Sielaff et al., 2019), has received much attention (Westwood et al., 2014; Kettleson et al., 2015; Chase et al., 2016; Lax et al., 2017). One of the objectives of this study was determining if a human within a spacesuit could act as a source for the unintentional microbial contamination and pass on microbial signatures out of the spacesuits. Future in-depth sampling and testing of various spacesuit components are necessary to conclude the transmission route. A detailed microbiome analyses of spacesuit before crew occupation should be carried out and such samples are not available for this study.

Microorganisms might escape through the clothing fibers via adherence, growth, and damage to the fibers. When synthetic fabrics were evaluated for microbial composition, micrococci were predominantly isolated both via culture and molecular methods (Callewaert et al., 2014). Prior studies have also revealed abundance of staphylococci on both cotton and synthetic fabrics, but corynebacteria were not enriched on any textile

TABLE 2 | Potential transmission of viable microorganisms among various locations of space suits.

Taxa	Number of PMA reads* retrieved from:		
	Wrist joint (n=23)	Inner gauntlet (n=10)	Outer gauntlet (n=10)
Acinetobacter baumannii	1,364	1,088	
Enterobacter cloacae	402	736	
Corynebacterium kroppenstedtii	9,987	1,102	630
Rothia dentocariosa	1,132	804	6,972
Kocuria rhizophila	1,022	7,258	534
Pseudomonas stutzeri	1,917	763	214,233
Methylobacterium radiotolerans	102,052	214,816	110,274
Methylobacterium extorquens	12,163	26,274	12,994
Methylobacterium nodulans	1,245	2,710	1,335
Methylobacterium populi	2,274	4,842	2,413
Methylobacterium sp 4-46	2,221	4,709	2,306
Streptococcus thermophilus	2,200	1,027	625

**The shotgun metagenome reads generated after PMA treatment andretrieved from various locations were pooled to generate potential transmission of the viable microorganisms from one location to another.*

types, indicating that clothing fiber composition might promote differential growth of distinct microbes. Similarly, the spacesuits examined during the study revealed isolation of actinobacteria and staphylococci, but members of corynebacteria were not isolated using traditional methods (**Supplementary Figure 1A**). However, the culture-independent analyses showed presence of corynebacteria (**Figure 4C**).

Characterization of microorganisms degrading the synthetic polymers such as polyvinyl chloride (PVC), polyurethane, nylon, and acrylics and their mode of action have been reviewed (Cappitelli and Sorlini, 2008). As shown in this study black fungi were isolated (**Supplementary Figure 1B**), however colonization of PVCs by these fungi and their degrading capabilities of plasticizers should be assessed before their concluding potential polymer degradation (Roberts and Davidson, 1986; Webb et al., 2000). The sequences associated with *Candida albicans*, a common skin microbiota, were not retrieved during this study, but retrieval of sequence from taxonomically related *Candida dubliniensis* was found from the majority of suit samples and not from controls.

The composition of the fabrics and particles associated with them might determine the interaction of the microbes and fiber, but such phenomenon is not always uniform and large discrepancies exist. Fabric materials that are plant-based (e.g., cotton) might provide nutrients for microorganisms to degrade and also cotton fabrics were reported to adsorb sweat components thus promotes growth of microorganisms (Szostak-Kotowa, 2004). Several enzymes were reported to degrade fibers like cellulose and notably fungi secreting cellulolytic enzymes (Buschle-Diller et al., 1994). Even though synthetic fibers last longer than natural fabrics like cotton, they collect moisture between the fibers and become nutrients source for microorganisms (Szostak-Kotowa, 2004). However, during this study, no differences in microbial burden was noticed when EMU and MACES/OCCS suits were compared.

When all PMA-treated samples were pooled into various locations of the spacesuit such as wrist joint (n = 23), inner gauntlet (n = 10), and outer gauntlet (n = 10), opportunistic pathogens were found to be associated with wrist joint rather than the inner or outer gauntlet samples (**Table 2**). Notably, *C. kroppenstedtii*, an opportunistic pathogen, has a high relative abundance in wrist joints (∼10K reads) compared to inner gauntlets (∼1K reads) and outer gauntlets (630 reads). *Rothia dentocariosa,* an oral cavity microbe, was found more in outer gauntlet. Similarly, the microbiome of outer and inner gauntlets appeared to harbor microorganisms associated with soil (*Pseudomonas stutzeri*) as well as the radiation-resistant *Methylobacterium radiotolerans*. The possibility of microbes surviving harsh conditions associated with space by migrating on or through spacesuits should be explored with controlled experiment before drawing the movement of microbes from one location to another location.

Detecting microbes that were reported to be potentially harmful to astronaut health might be a concern. Members of *Methylobacterium* (12 species) dominated microbial communities on set #7 suits in this study, were reported to be opportunistic pathogens and might cause infections to immunocompromised patients (Kovaleva et al., 2014). Moreover, since astronauts are in close contact with suits while in use and shared suits present a hypothetical route for pathogen transmission, these measures can help inform potential risk. Though our work was limited to the exterior of suits, this study documented that spacesuit could harbor viable microbes. None of the microbes discovered are thought to present a health risk, but some belong to clades that contain potential pathogens. All of them represent organisms that may be relevant for NASA planetary protection (NASA, 2019a), since they may persist on the suit.

CONCLUSION

The microbial characterization of spacesuits examined during this study established the following scenarios. (1) Viable microbes are present on the exterior of spacesuits. (2) Certain microbes exist on suit joints and gauntlets. (3) The microbiomes on suit surfaces resemble those of human skin and airways.

More sophisticated approaches can help to conclusively establish whether microbes do migrate from the interior to the exterior of pressurized suits in space.

Additional work to better determine microbial origin and evaluate microbial contamination mitigation techniques is warranted. This report is a first step in establishing a catalog of microbial sequences known to occur on spacesuits and equipment. Gene specific marker, single nucleotide polymorphism (gene property), single nucleotide variation, and with deep coverage (×100) should be performed to track the source of microbial passage between the exterior and interior of currently existing spacesuits.

DATA AVAILABILITY STATEMENT

The datasets presented in this study can be found in online repositories. The names of the repository/repositories and accession number(s) can be found below: https://www.ncbi.nlm.nih.gov/genbank/, PRJNA545796.

AUTHOR CONTRIBUTIONS

MR developed EVA tool, collected samples, coordinated and designed the study with input from KV. MR, MB, and AR collected samples at JSC. MB and AR wrote the cleaning, sterilization, and assembly protocol for the EVA Swab Kit. GM contributed to sample processing, traditional microbiology assays, extracted DNA, assayed molecular microbial burden, generated corresponding figures, tables, and text associated with these analyses. CM group generated shotgun metagenome sequencing. DD designed, coordinated, and carried out computational analyses. NO'H and RO assisted with strain level analyses. NS conducted metagenome-based phylogenetic and functional analyses and interpreted the results. KV, DD, and MS drafted the manuscript and responsible for data analysis and interpretation. CM edited the manuscript. All authors read and approved the final manuscript.

FUNDING

This research was supported by the JPL Advanced Concept Development fund awarded to KV that funded a fellowship for GM. DD was supported by the Tri-Institutional Training Program in Computational Biology and Medicine (CBM) funded by the NIH grant 1T32GM083937. We thank XSEDE and Philip Blood for their support of this project. AR and MB were supported by the Astromaterials Acquisition and Curation Office at NASA's Johnson Space Center. EVA Swab Kit development and spacesuit testing was funded via a Johnson Space Center Independent Research and Development award for MR.

ACKNOWLEDGMENTS

Part of the research described in this publication was carried out at the Jet Propulsion Laboratory (JPL), California Institute of Technology, under a contract with NASA. Government sponsorship acknowledged.

SUPPLEMENTARY MATERIAL

The Supplementary Material for this article can be found online at: https://www.frontiersin.org/articles/10.3389/fmicb.2021.608478/full#supplementary-material

Supplementary Figure 1 | Phylogenetic tree of cultivated strains (bacteria **[A]** and fungi **[B]**) isolated from spacesuit surfaces.

Supplementary Figure 2 | UMAP of taxonomic profiles from all samples colored by whether the samples were treated with PMA or not.

Supplementary Table 1 | Metadata for samples including what suit they were taken from and when.

Supplementary Table 2 | Bacterial abundances (in number of reads) from metagenomics for all samples.

Supplementary Table 3 | Eukaryote abundances (in number of reads) from metagenomics for all samples.

Supplementary Table 4 | Percentage of reads assigned to different major groups.

REFERENCES

Breuker, M., McNamara, C., Young, L., Perry, T., Young, A., and Mitchell, R. (2003). Fungal growth on synthetic cloth from Apollo spacesuits. *Ann. Microbiol.* 53, 47–54.

Buchfink, B., Xie, C., and Huson, D. H. (2015). Fast and sensitive protein alignment using DIAMOND. *Nat. Methods* 12, 59–60. doi: 10.1038/nmeth.3176

Buschle-Diller, G., Zeronian, S. H., Pan, N., and Yoon, M. Y. (1994). Enzymatic hydrolysis of cotton, linen, ramie, and viscose rayon fabrics. *Text. Res. J.* 64, 270–279. doi: 10.1177/004051759406400504

Callewaert, C., De Maeseneire, E., Kerckhof, F.-M., Verliefde, A., Van de Wiele, T., and Boon, N. (2014). Microbial odor profile of polyester and cotton clothes after a fitness session. *Appl. Environ. Microbiol.* 80, 6611–6619. doi: 10.1128/AEM.01422-14

Cappitelli, F., and Sorlini, C. (2008). Microorganisms attack synthetic polymers in items representing our cultural heritage. *Appl. Environ. Microbiol.* 74, 564–569. doi: 10.1128/aem.01768-07

Cataño, J. C., Echeverri, L. M., and Szela, C. (2012). Bacterial contamination of clothes and environmental items in a third-level hospital in Colombia. *Interdiscipl. Perspect. Infect. Dis.* 2012:507640. doi: 10.1155/2012/507640

Chase, J., Fouquier, J., Zare, M., Sonderegger, D. L., Knight, R., Kelley, S. T., et al. (2016). Geography and location are the primary drivers of office microbiome composition. *mSystems* 1:e0022-16. doi: 10.1128/mSystems.00022-16

Checinska, A., Probst, A. J., Vaishampayan, P., White, J. R., Kumar, D., Stepanov, V. G., et al. (2015). Microbiomes of the dust particles collected from the international space station and spacecraft assembly facilities. *Microbiome* 3:50. doi: 10.1186/s40168-015-0116-3

Checinska Sielaff, A., Urbaniak, C., Mohan, G. B. M., Stepanov, V. G., Tran, Q., Wood, J. M., et al. (2019). Characterization of the total and viable bacterial and fungal communities associated with the International Space Station surfaces. *Microbiome* 7:50. doi: 10.1186/s40168-019-0666-x

Daly, D. J., Murphy, C., and McDermott, S. D. (2012). The transfer of touch DNA from hands to glass, fabric and wood. *Forens. Sci. Int. Genet.* 6, 41–46. doi: 10.1016/j.fsigen.2010.12.016

Danko, D., Bezdan, D., Afshin, E. E., Ahsanuddin, S., Bhattacharya, C., Butler, D. J., et al. (2021a). A global metagenomic map of urban microbiomes and

antimicrobial resistance. *Cell* 184, 3376–3393e17. doi: 10.1016/j.cell.2021.05.002

Danko, D. C., Sierra, M. A., Benardini, J. N., Guan, L., Wood, J. M., Singh, N., et al. (2021b). A comprehensive metagenomics framework to characterize organisms relevant for planetary protection. *Microbiome* 9, 1–15.

Dean, C. (2018). *Resistome Analyzer*. Available online at: https://github.com/cdeanj/resistomeanalyzer

Debus, A., and Arnould, J. (2008). Planetary protection issues related to human missions to Mars. *Adv. Space Res.* 42, 1120–1127. doi: 10.1016/j.asr.2007.10.005

Delcher, A. L., Salzberg, S. L., and Phillippy, A. M. (2003). Using MUMmer to identify similar regions in large sequence sets. *Curr. Protoc. Bioinform.* 10:Unit10.3.

Fernandes, A. D., Macklaim, J. M., Linn, T. G., Reid, G., and Gloor, G. B. (2013). ANOVA-like differential expression (ALDEx) analysis for mixed population RNA-Seq. *PLoS One* 8:e67019. doi: 10.1371/journal.pone.0067019

Franzosa, E. A., McIver, L. J., Rahnavard, G., Thompson, L. R., Schirmer, M., Weingart, G., et al. (2018). Species-level functional profiling of metagenomes and metatranscriptomes. *Nat. Methods* 15, 962–968. doi: 10.1038/s41592-018-0176-y

Hsu, T., Joice, R., Vallarino, J., Abu-Ali, G., Hartmann, E. M., Shafquat, A., et al. (2016). Urban transit system microbial communities differ by surface type and interaction with humans and the environment. *mSystems* 1:e0018-16. doi: 10.1128/mSystems.00018-16

Jensen, G. L. (2013). *The Human Microbiome, Diet, and Health: Workshop Summary*. Washington, DC: National Academies Press.

Kang, D. D., Li, F., Kirton, E., Thomas, A., Egan, R., An, H., et al. (2019). MetaBAT 2: an adaptive binning algorithm for robust and efficient genome reconstruction from metagenome assemblies. *PeerJ* 7:e7359. doi: 10.7717/peerj.7359

Kettleson, E. M., Adhikari, A., Vesper, S., Coombs, K., Indugula, R., and Reponen, T. (2015). Key determinants of the fungal and bacterial microbiomes in homes. *Environ. Res.* 138, 130–135. doi: 10.1016/j.envres.2015.02.003

Kim, O.-S., Cho, Y.-J., Lee, K., Yoon, S.-H., Kim, M., Na, H., et al. (2012). Introducing EzTaxon-e: a prokaryotic 16S rRNA gene sequence database with phylotypes that represent uncultured species. *Intern. J. Syst. Evol. Microbiol.* 62, 716–721. doi: 10.1099/ijs.0.038075-0

Koljalg, U., Nilsson, R. H., Abarenkov, K., Tedersoo, L., Taylor, A. F., Bahram, M., et al. (2013). Towards a unified paradigm for sequence-based identification of fungi. *Mol. Ecol.* 22, 5271–5277. doi: 10.1111/mec.12481

Kovaleva, J., Degener, J. E., and van der Mei, H. C. (2014). *Methylobacterium* and its role in health care-associated infection. *J. Clin. Microbiol.* 52, 1317–1321. doi: 10.1128/jcm.03561-13

Kwan, K., Cooper, M., La Duc, M. T., Vaishampayan, P., Stam, C., Benardini, J. N., et al. (2011). Evaluation of procedures for the collection, processing, and analysis of biomolecules from low-biomass surfaces. *Appl. Environ. Microbiol.* 77, 2943–2953. doi: 10.1128/aem.02978-10

Lai, X., Cao, L., Tan, H., Fang, S., Huang, Y., and Zhou, S. (2007). Fungal communities from methane hydrate-bearing deep-sea marine sediments in South China See. *ISME J.* 1, 756–762. doi: 10.1038/ismej.2007.51

Lakin, S. M., Dean, C., Noyes, N. R., Dettenwanger, A., Ross, A. S., Doster, E., et al. (2017). MEGARes: an antimicrobial resistance database for high throughput sequencing. *Nucleic Acids Res.* 45, D574–D580.

Lane, D. J. (1991). "Nucleic acid techniques in bacterial systematics," in *Nucleic Acid Techniques in Bacterial Systematics*, Vol. 1, eds E. Stackebrandt and M. Goodfellow (New York, NY: Wiley), 115–175.

Langmead, B., and Salzberg, S. L. (2012). Fast gapped-read alignment with Bowtie 2. *Nat. Methods* 9:357. doi: 10.1038/nmeth.1923

Lax, S., Sangwan, N., Smith, D., Larsen, P., Handley, K. M., Richardson, M., et al. (2017). Bacterial colonization and succession in a newly opened hospital. *Sci. Transl. Med.* 9:eaah6500. doi: 10.1126/scitranslmed.aah6500

Lee, S.-Y., Woo, S.-K., Lee, S.-M., and Eom, Y.-B. (2016). Forensic analysis using microbial community between skin bacteria and fabrics. *Toxicol. Environ. Health Sci.* 8, 263–270. doi: 10.1007/s13530-016-0284-y

Li, D., Liu, C.-M., Luo, R., Sadakane, K., and Lam, T.-W. (2015). MEGAHIT: an ultra-fast single-node solution for large and complex metagenomics assembly via succinct de Bruijn graph. *Bioinformatics* 31, 1674–1676. doi: 10.1093/bioinformatics/btv033

Linacre, A., Pekarek, V., Swaran, Y. C., and Tobe, S. S. (2010). Generation of DNA profiles from fabrics without DNA extraction. *Forens. Sci. Int. Genet.* 4, 137–141. doi: 10.1016/j.fsigen.2009.07.006

McInnes, L., Healy, J., and Melville, J. (2018). Umap: Uniform manifold approximation and projection for dimension reduction. *arXiv* [Preprint]. Available online at: https://arxiv.org/abs/1802.03426

NASA (2019a). *NASA Policy Instruction-8020.7G: NASA Policy on Planetary Protection Requirements for Human Extraterrestrial Missions*. Washington, DC: NASA.

NASA (2019b). *Orion Suit Equipped to Expect the Unexpected on Artemis Missions*. Washington, DC: NASA.

National Academies of Sciences, Engineering and Medicine (2018). *A Midterm Assessment of Implementation of the Decadal Survey on Life and Physical Sciences Research at NASA*. Washington, DC: The National Academies Press.

Nelson, K. E., Weinstock, G. M., Highlander, S. K., Worley, K. C., Creasy, H. H., Wortman, J. R., et al. (2010). A catalog of reference genomes from the human microbiome. *Science* 328, 994–999.

Newman, D., Schmidt, P., and Rahn, D. (2000). *Modeling the Extravehicular Mobility Unit (EMU) Space Suit: Physiological Implications for Extravehicular Activity (EVA) (0148-7191)*. Available online at: http://web.mit.edu/aeroastro/www/people/dnewman/pdfs/DJN_ICES2000-3.26.pdf

Nicholson, W. L., Schuerger, A. C., and Race, M. S. (2009). Migrating microbes and planetary protection. *Trends Microbiol.* 17, 389–392. doi: 10.1016/j.tim.2009.07.001

NRC (2014). *Pathways to Exploration: Rationales and Approaches for a U.S. Program of Human Space Exploration*. Washington, DC: The National Academies Press.

Ounit, R., and Lonardi, S. (2016). Higher classification sensitivity of short metagenomic reads with CLARK-S. *Bioinformatics* 32, 3823–3825. doi: 10.1093/bioinformatics/btw542

Parks, D. H., Imelfort, M., Skennerton, C. T., Hugenholtz, P., and Tyson, G. W. (2015). CheckM: assessing the quality of microbial genomes recovered from isolates, single cells, and metagenomes. *Genome Res.* 25, 1043–1055. doi: 10.1101/gr.186072.114

Roberts, W. T., and Davidson, P. M. (1986). Growth characteristics of selected fungi on polyvinyl chloride film. *Appl. Environ. Microbiol.* 51, 673–676. doi: 10.1128/aem.51.4.673-676.1986

Rucker, M. A., Hood, D., Walker, M., Venkateswaran, K. J., and Schuerger, A. C. (2018). EVA swab tool to support planetary protection and astrobiology evaluations. *Paper Presented at the 2018 IEEE Aerospace Conference*, New York, NY.

Sandle, T. (2011). A review of cleanroom microflora: types, trends, and patterns. *PDA J. Pharm. Sci. Technol.* 65, 392–403. doi: 10.5731/pdajpst.2011.00765

Schwartz, S. J., Hoffman, J. A., Hodgson, E., and Ronzani, P. A. (2002). Is there space for wearables?. *Paper Presented at the Proceedings of the Sixth International Symposium on Wearable Computers*, London.

Shafquat, A., Joice, R., Simmons, S. L., and Huttenhower, C. (2014). Functional and phylogenetic assembly of microbial communities in the human microbiome. *Trends Microbiol.* 22, 261–266. doi: 10.1016/j.tim.2014.01.011

Singh, N. K., Wood, J. M., Karouia, F., and Venkateswaran, K. (2018). Succession and persistence of microbial communities and antimicrobial resistance genes associated with International Space Station environmental surfaces. *Microbiome* 6:214. doi: 10.1186/s40168-018-0609-y

Sterndorff, E. B., Russel, J., Jakobsen, J., Mortensen, M. S., Gori, K., Herschend, J., et al. (2020). The T-shirt microbiome is distinct between individuals and shaped by washing and fabric type. *Environ. Res.* 185:109449. doi: 10.1016/j.envres.2020.109449

Sugita, T., Yamazaki, T., Makimura, K., Cho, O., Yamada, S., Ohshima, H., et al. (2016). Comprehensive analysis of the skin fungal microbiota of astronauts during a half-year stay at the International Space Station. *Sabouraudia* 54, 232–239. doi: 10.1093/mmy/myv121

Szostak-Kotowa, J. (2004). Biodeterioration of textiles. *Intern. Biodeteriorat. Biodegrad.* 53, 165–170. doi: 10.1016/S0964-8305(03)00090-8

Taylor, D. L., and Bruns, T. D. (1999). Community structure of ectomycorrhizal fungi in a *Pinus muricata* forest: minimal overlap between the mature forest and resistant propagule communities. *Mol. Ecol.* 8, 1837–1850. doi: 10.1046/j.1365-294x.1999.00773.x

Truong, D. T., Franzosa, E. A., Tickle, T. L., Scholz, M., Weingart, G., Pasolli, E., et al. (2015). MetaPhlAn2 for enhanced metagenomic taxonomic profiling. *Nat. Methods* 12, 902–903. doi: 10.1038/nmeth.3589

Turnbaugh, P. J., Ley, R. E., Hamady, M., Fraser-Liggett, C. M., Knight, R., and Gordon, J. I. (2007). The human microbiome project. *Nature* 449, 804–810. doi: 10.1038/nature06244

Turner, S., Pryer, K. M., Miao, V. P., and Palmer, J. D. (1999). Investigating deep phylogenetic relationships among cyanobacteria and plastids by small subunit rRNA sequence analysis. *J. Eukaryot. Microbiol.* 46, 327–338. doi: 10.1111/j.1550-7408.1999.tb04612.x

Vaishampayan, P., Probst, A. J., La Duc, M. T., Bargoma, E., Benardini, J. N., Andersen, G. L., et al. (2013). New perspectives on viable microbial communities in low-biomass cleanroom environments. *ISME J.* 7, 312–324. doi: 10.1038/ismej.2012.114

Venkateswaran, K., Hattori, N., La Duc, M. T., and Kern, R. (2003). ATP as a biomarker of viable microorganisms in clean-room facilities. *J. Microbiol. Methods* 52, 367–377. doi: 10.1016/s0167-7012(02)00192-6

Watson, R. D. (2014). *Modified Advanced Crew Escape Suit Intravehicular Activity Suit for Extravehicular Activity Mobility Evaluations*. Available online at: http://hdl.handle.net/2346/59685

Webb, J. S., Nixon, M., Eastwood, I. M., Greenhalgh, M., Robson, G. D., and Handley, P. S. (2000). Fungal colonization and biodeterioration of plasticized polyvinyl chloride. *Appl. Environ. Microbiol.* 66, 3194–3200. doi: 10.1128/aem.66.8.3194-3200.2000

Westwood, J., Burnett, M., Spratt, D., Ball, M., Wilson, D. J., Wellsteed, S., et al. (2014). The hospital microbiome project: meeting report for the UK science and innovation network UK-USA workshop 'beating the superbugs: hospital microbiome studies for tackling antimicrobial resistance', October 14th 2013. *Stand. Genom. Sci.* 9:12. doi: 10.1186/1944-3277-9-12

Conflict of Interest: The authors declare that the research was conducted in the absence of any commercial or financial relationships that could be construed as a potential conflict of interest.

Advantages of publishing in Frontiers

OPEN ACCESS
Articles are free to read for greatest visibility and readership

FAST PUBLICATION
Around 90 days from submission to decision

HIGH QUALITY PEER-REVIEW
Rigorous, collaborative, and constructive peer-review

TRANSPARENT PEER-REVIEW
Editors and reviewers acknowledged by name on published articles

Frontiers
Avenue du Tribunal-Fédéral 34
1005 Lausanne | Switzerland

Visit us: www.frontiersin.org
Contact us: frontiersin.org/about/contact

REPRODUCIBILITY OF RESEARCH
Support open data and methods to enhance research reproducibility

DIGITAL PUBLISHING
Articles designed for optimal readership across devices

FOLLOW US
@frontiersin

IMPACT METRICS
Advanced article metrics track visibility across digital media

EXTENSIVE PROMOTION
Marketing and promotion of impactful research

LOOP RESEARCH NETWORK
Our network increases your article's readership